



PhD-FSTC-2018-64
The Faculty of Sciences, Technology and Communication

DISSERTATION

Defence held on 05/10/2018 in Luxembourg

to obtain the degree of



DOCTEUR DE L'UNIVERSITÉ DU LUXEMBOURG EN PHYSIQUE

by

Riccardo RAO

Born on 23 April 1989 in Naples (Italy)

CONSERVATION LAWS IN NONEQUILIBRIUM THERMODYNAMICS: STOCHASTIC PROCESSES, CHEMICAL REACTION NETWORKS, AND INFORMATION PROCESSING

Dissertation defence committee

Dr Massimiliano Esposito, dissertation supervisor
Professor, Université du Luxembourg

Dr Pierre Gaspard
Professor, Université Libre de Bruxelles

Dr Ludger Wirtz, Chairman
Professor, Université du Luxembourg

Dr Thomas E. Ouldridge
Imperial College London

Dr Alexander Skupin, Vice Chairman
Université du Luxembourg

to Ann

The scientist worthy of his name . . . experiences in front of his work the same feeling as the artist; his pleasure is as great and of the same nature.

— Henri Poincaré

ABSTRACT

Thermodynamics has a long history. It was established during the 19th century as a phenomenological theory grasping the principles underlying heat engines. In the 20th and 21st centuries its range of applicability was extended to nonequilibrium stochastic and chemical processes. However a systematic procedure to identify the thermodynamic forces at work in these systems was lacking. In this thesis, we provide one by making use of conservation laws. Of particular importance are the conservation laws which are broken when putting the system in contact with different reservoirs (thermostats or chemostats). These laws depend on the internal structure of the system and are specific to each system. We introduce a systematic procedure to identify them and show how they shape the entropy production (*i.e.* the dissipation) into fundamental contributions. Each of these provides precious insight on how to drive and control the system out of equilibrium. We first present our results at the level of phenomenological thermodynamics. We then show that they can be systematically derived for various dynamics: Markov jump processes used in stochastic thermodynamics, also including the chemical master equation, and deterministic chemical rate equations with and without diffusion, which are used to describe chemical reaction networks. Generalized nonequilibrium Landauer principles ensue from our theory. They predict that the minimal thermodynamic cost necessary to transform the system from an arbitrary nonequilibrium state to another can be expressed in terms of information metrics such as relative entropies between the equilibrium and nonequilibrium states of the system.

CONTENTS

Introduction	1
I THERMODYNAMIC SYSTEMS FAR FROM EQUILIBRIUM 13	
1 PHENOMENOLOGICAL DESCRIPTION 15	
1.1 Equilibrium States 15	
1.2 Fundamental Laws of Thermodynamics 16	
1.2.1 The First Law 17	
1.2.2 The Second Law 17	
1.3 Conservation Laws: Illustrative Examples 18	
1.3.1 Example 1. System in contact with one reservoir 18	
1.3.2 Example 1+1/2. Driven System in contact with one reservoir 19	
1.3.3 Example 2. System in contact with multiple reservoirs 20	
1.3.4 Example 3: System-specific description: conservation laws 21	
1.4 Systems in contact with multiple reservoirs 22	
1.5 System-specific Thermodynamics 24	
1.5.1 Cyclic Transformations and Broken Conservation Laws 24	
1.5.2 System-specific Energy and Entropy balance 25	
1.5.3 Isothermal Processes 27	
1.5.4 Adiabatic Processes 28	
1.6 Nonequilibrium Landauer Principle 28	
1.7 Equilibrium States of Extensive Systems 29	
2 STOCHASTIC DESCRIPTION 31	
Article: [New Journal of Physics 20, 023007 (2018)] 37	
Article: [Entropy 20, 635 (2018)] 71	
II CHEMICALLY REACTING SYSTEMS FAR FROM EQUILIBRIUM 99	
3 PHENOMENOLOGICAL DESCRIPTION 101	
3.1 Chemical Reaction Networks 101	
3.2 Thermodynamics 102	
3.3 System-specific Thermodynamics 103	
3.3.1 Stoichiometric Cycles and Broken Conservation Laws 104	
3.4 Example 105	
4 STOCHASTIC DESCRIPTION 107	
Preprint: [arXiv 1805:12077] 111	
5 DETERMINISTIC DESCRIPTION 139	
5.1 Spatially Homogeneous Processes 139	
5.2 Spatially Inhomogeneous Processes 140	
5.3 Coarse-grained Processes 141	
Article: [Physical Review X 6, 041064 (2016)] 145	
Article: [The Journal of Chemical Physics 143, 244903 (2015)] 171	
Article: [Physical Review Letters 121, 108301 (2018)] 185	
Article: [New Journal of Physics 20, 042002 (2018)] 201	
Conclusions 219	
Author Contributions 221	
Acknowledgements 223	

Thermodynamics is a funny subject. The first time you go through it, you do not understand it at all. The second time you go through it, you think you understand it, except for one or two points. The third time you go through it, you know you do not understand it, but by that time you are so used to the subject, it doesn't bother you anymore.

— Arnold Sommerfeld

INTRODUCTION

Understanding the detailed functioning of life and its distinctive features is one of the greatest challenges of contemporary science. This is clearly the consequence of the enormous complexity that living systems have achieved through billions of years of evolution. It is also clear, however, that the functioning of these systems is based on energy and information processing. The former allows living organisms to sustain themselves, the latter to evolve. We aim at understanding these processings, as we believe it is important to understand life. To do so, nonequilibrium thermodynamics is the well suited, but systematic and rigorous descriptions are necessary to tame the complexity of living organisms.

In this thesis, we provide a generic and systematic description of arbitrary nonequilibrium processes. This is achieved using conservation laws, as they carry information about the topological structure of the process and allow more informative descriptions. This framework is also specialized to two relevant classes of processes: stochastic Markov jump processes, and chemical processes modelled as chemical reaction networks. We also demonstrate how thermodynamics of information processing naturally fits in our description.

We start by introducing thermodynamics and its recent developments from a historical perspective, and then summarize and motivate further the contributions of this thesis.

THERMODYNAMICS: A HISTORICAL PERSPECTIVE

The development of heat engines, namely machines able to perform work by extracting power from heat, indisputably triggered the industrial revolution [1]. The major improvement regarding their performances was made by J. Watt, who had the idea of spatially separating the cooling system (the cold reservoir) from the heat source (the hot reservoir). Hence, at the turn of the 19th century, engines had reached a high level of sophistication, but the fundamental principles underlying their functioning were still unknown. In 1824, S. Carnot publishes his celebrated work *Reflections on the Motive Power of Fire and on Machines Fitted to Develop that Power* [2], thus overturning the

situation. Rarely in the history of science, technological innovation was the spark of a new scientific theory: *thermodynamics*, as it would have been later called by W. Thomson.

Carnot managed to abstract the functioning of heat engines, by conceiving an ideal set of operations, the *Carnot cycle*, describing a systematic extraction of work. He realized that this extraction requires the *transfer* of heat between two reservoirs, at least: a heat source (the hot reservoir) and a heat sink (the cold reservoir), as they produce the necessary fall of *caloric*, akin to a fall of water powering hydraulic engines. We recall that his argument was based on the theory of caloric, according to which heat is a mass-less, indestructible, and hence *conserved* substance exchanged by systems at different temperatures. Driving his engine in a *reversible* manner, *i.e.* quasi-statically between equilibrium states, he derived the maximum efficiency that any heat engine can achieve: that in which no caloric flows in the sink without performing work, the *Carnot's efficiency*. Notably, his derivation was based mainly on one uncontested observation: it must be impossible to create perpetual motion of any kind.

The First Law

At Carnot's times, the most endorsed theory of heat was that of caloric, which was put forward by Lavoisier and Laplace during the prior century. In the past, some people questioned this theory in favour of kinetic theories of heat, according to which mechanical energy and heat are equivalent and can be *converted* one into the other¹. However, their argument were merely based on empirical observations, *e.g.* the heat continuously produced by friction during the boring of cannons. In contrast, the caloric theory could still qualitatively, and somehow quantitatively, explain many phenomena like that of latent heat or the expansion of materials when their temperature is increased.

It was thanks to the subtle but sound theoretical argument put forward by J.R. von Mayer, and the exceptional experimental measurements obtained by J.P. Joule that equivalence between mechanical energy and heat was finally recognized. Like many before him, Mayer was guided to his conclusion by empirical observations, the most intriguing of which regarded the heat which had to be produced by animals to keep their body temperature constant. In contrast to others, he put his argument in a mathematical framework and derived a quantitative value for the mechanical equivalent of one unit of heat: it was calculated as the difference between the specific heat at constant pressure and that at constant volume. On the other hand, Joule quantitatively measured this value. His idea was to evaluate the increase of temperature of some system when some controlled and reproducible amount of mechanical work was spent to *heat* the system. In his first experiment, work was spent to produce an electric current which subsequently heated a surrounding vessel filled with water. In his second experiment, work was spent to produce motion in a vessel of water, and the heat was released by friction.

H. von Helmholtz theoretically extended the equivalence of mechanical energy and heat to electromagnetic phenomena, thus establishing the principle of conservation of energy [3], *i.e.* the *first law of thermodynamics*

$$\Delta U = Q + W \tag{1}$$

¹ The most prominent scholar sustaining this novel theory Count Rumford.

where ΔU are internal energy changes of a thermodynamic system, W is the work that the system does on its environment, *e.g.* lifting a weight or charging a battery, whereas Q is the heat exchanged with the environment.

The Second Law

It thus became clear that Carnot's idea of work production in terms of caloric transfer had to be revised and reconciled with the equivalence of heat and mechanical energy. W. Thomson, also known as Lord Kelvin, made the first step by unveiling a subtle constraint on the overall flow of heat in reversible cyclic operations

$$\sum_r \frac{Q_r}{T_r} = 0, \quad (2)$$

where Q_r is the heat reversibly exchanged with the r -th reservoir. In doing so, he introduced the *absolute scale of temperatures*, $T > 0$, *i.e.* a scale which is independent from any property of the working substance. Using Thomson's results, R. Clausius made the two decisive steps. First, he understood that heat transfer between reservoirs and heat conversion into work happen at the same time in heat engine, and can be both regarded as heat *transformation*. In irreversible cyclic processes, the heat transferred between reservoirs always exceeds that converted in work, and he called the difference between the two *uncompensated heat*, nowadays called *total entropy change* or *entropy production*. Second, he introduced the concept of *entropy* S to describe the thermal content and the molecular arrangement of the thermodynamic system. In this way he could go beyond cyclic transformations, and generalize Eq. (2) to

$$\Delta S = \sum_r \frac{Q_r}{T_r} + \Sigma, \quad (3)$$

where $\Sigma \geq 0$ is the entropy production, which vanishes solely for reversible transformations. This equation is a mathematical formulation of the *second law of thermodynamics*,

Heat can never pass from a colder to a warmer body without some other change, connected therewith, occurring at the same time.

Chemical and Irreversible Processes

During the early development of thermodynamics, chemical processes were left quite aside. J.W. Gibbs first introduced the *chemical potential* to quantify the energetic content of a molecule in a mixture of chemicals, and used it to define the thermodynamic potentials ruling these mixtures [4]. Several decades later, this enabled T. de Donder to approach the study of chemical reacting mixtures from a thermodynamic standpoint. He proposed the concept of *affinity* to characterize the chemical force irreversibly driving chemical reactions and related it to the uncompensated heat established by Clausius [5]. In the meantime, L. Onsager gave a first formulation of nonequilibrium thermodynamics for small perturbations close to equilibrium, the so called *linear regime*. He thus established his celebrated *reciprocal relations*, which are universal symmetries that the phenomenological coefficients coupling currents to thermodynamic forces (*e.g.* electrical currents to

voltage drops, chemical currents to affinities, heat currents to thermal gradients) must obey [6, 7]. These relationships and the ensuing theory of irreversible processes, were later extended by H. Casimir, J. Meixner, P. Mazur, S. de Groot, and I. Prigogine [8]. The last, who perpetuated the Brussels School founded by de Donder, introduced the assumption of *local equilibrium* to describe irreversible processes in terms of equilibrium quantities [9, 10]. In doing so, he pioneered the connections between thermodynamics and kinetics of chemical reacting mixtures [11].

Thermodynamics of Computation

The development of thermodynamics was clearly followed by new questions and paradoxes. Among the most remarkable, J.C. Maxwell conceived the existence of an intelligent being who was able to exploit thermal fluctuations to violate the second law of thermodynamics. For a gas in two boxes separated by a tiny gate, this *demon* would do so by opening the gate in such a way that fast—and thus *hot*—molecules are gathered on one side and slow ones—*cold* molecules—on the other. Later, L. Szilard designed an *engine* in which Maxwell’s demon could extract work from a single heat reservoir. But he also realized that the acquisition of information regarding the fluctuating state of the system should come at the same cost as that extracted by the engine, hence not violating the second law [12]. L.N. Brillouin indeed conceived a measurement apparatus which would work at the same cost as that extracted, but he used a specific model rather than an abstract argument [13]. The crucial intuition of Szilard and Brillouin was that information is not unrelated from thermodynamics.

In 1961, R. Landauer showed that information processing has an intrinsic thermodynamics cost [14, 15]. He demonstrated that the erasure of a bit of information changes the system entropy and hence entails a release of heat. Therefore, in agreement with the first law, erasure must have an intrinsic thermodynamic cost—at least for isoenergetic bit states. This principle was named after Landauer, as well as the aforementioned bound. Several decades later, C. Bennett revisited the Szilard’s engine at the light of Landauer’s result [16] and argued that: since the demon needs to erase the information previously acquired in order perform the next one, the work spent in the erasure compensates for that acquired, and the second law is not violated. His argument was based on the fact that he could conceive some specific conditions for which measurement was costless.

Chemical Reaction Network Theory and Stochastic Thermodynamics

During the second half of the 20th century, biological processes drew a significant part of the attention, which increased and diversified the studies on chemical kinetics and thermodynamics.

One the one hand, the first unsuccessful attempt to establish general dynamical and thermodynamic principles for systems of reacting chemical species [17, 18] triggered the interest of mathematicians. Feinberg [19], and Horn and Jackson [20], formulated a rigorous mathematical description of *deterministic chemical reaction networks*, *i.e.* systems of arbitrary number of chemically reacting species whose concentrations are described by deterministic rate equations. In doing so they established *chemical reaction network theory*, an applied mathematical theory which aims at modelling chemical processes and understanding what are the connection between the topo-

logical properties of the network of reactions and its dynamical behaviour. Indeed, their major result was the discovery of a large class of chemical networks whose dynamics is completely determined by their topology, which they called *complex-balanced networks*.

On the other side, the interest toward bio-chemical processes also required the development of stochastic descriptions, since many of these processes involve low number of molecules, and hence they are highly fluctuating. These are well described in terms of *master equation* or *chemical master equation* [21–23], which describe, for instance, the probability of observing a molecule in a certain chemical state or the probability of observing a certain population of molecules. Among the first, T.L. Hill and coworkers investigated bio-catalysts as small fluctuating machines and introduced the concept of *free energy transduction* to describe the average work performed by a chemical force to drive another flow of chemicals against its spontaneous direction [24, 25]. Networks of bio-chemical reactions were investigated by Oster and coworkers [26–28], but all these studies were limited to steady-state processes described in terms of linear chemical reaction networks. The stochastic as well as the deterministic dynamics of these networks is described by linear rate equations for either probabilities or concentrations.

Inspired by these seminal works, J. Schnakenberg understood the crucial role played by cycles—*i.e.* cyclic sets of transitions or reactions—for characterizing the steady-state thermodynamics of generic Markov jump processes. Based on a graph-theoretical approach, he provided the first systematic cycle decomposition of the average entropy production rate [29]—which has been recently extended to nonsteady-state regimes in Ref. [30]. Beyond linear networks, the Brussels school, as well as many others, addressed the thermodynamics of nonlinear chemical reaction networks described by chemical master equation [31, 32]. Yet, they were mainly focused on steady states and on the relationship between the stochastic and deterministic description [33–35].

Nevertheless, these works played a seminal role during the first decade of the 21st century for the development of Stochastic Thermodynamics [36–39], which is a rigorous nonequilibrium thermodynamic description for systems obeying Markovian stochastic dynamics. Within this framework, the first and second law of thermodynamics could be formulated for stochastic trajectories of systems subject to large fluctuations [40–42]. Remarkably, the entropy production need not be always positive at this level [43, 44]. This is manifest in *fluctuation theorems*, for which stochastic thermodynamics provided a unifying framework, see *e.g.* Ref. [38, 45, 46] and references therein. These relations express fundamental symmetries that the fluctuations of some thermodynamic observables satisfy arbitrarily far from equilibrium. For instance, the detailed fluctuation theorem for the entropy production reads

$$\frac{P(\Sigma)}{P^\dagger(-\Sigma)} = \exp \Sigma, \quad (4)$$

where $P(\Sigma)$ is the probability of observing Σ entropy production in a given process, and $P^\dagger(-\Sigma)$ is that of observing $-\Sigma$ in a conjugated process, *e.g.* the time-reversed one, see Sec. [3.4, p. 78]. Hence, observing negative entropy production is possible, but these fluctuations are exponentially hard to observe.

Stochastic thermodynamics also provided a fresh view on many aspects of thermodynamics. It enabled to formulate the first thermodynamic descriptions of stochastic chemical reaction networks [47–49], as well as to study

their fluctuations at the steady state [50, 51]. The performance of molecular machines like pumps, motors, enzymes, and information-handling systems could be systematically analysed [52–56], thus extending the seminal works by Hill. The fluctuations of efficiency in generic stochastic processes were addressed, thus showing that Carnot’s efficiency can be reached in nonreversible processes, but its probability is the smallest among all possible values [57–60]. Since stochastic thermodynamics naturally encompasses information theory, thermodynamics of computation found the ideal framework in which its concept could be systematically formulated [61–69]. In this way, clearer—if not definite—answers could be given to the apparent violation of the second law of Szilard’s engine [70]. General thermodynamic principles of information processing at the cellular level could also be investigated [71–75].

CONSERVATION LAWS AND THERMODYNAMICS

Despite these huge advances, the role of conservation laws in nonequilibrium thermodynamics remained thus far ignored. Conservation laws identify quantities which are conserved during the interaction between the system and its environment. These globally conserved quantities are *specific* for each thermodynamic system, and carry information about how the system *globally* exchanges system quantities, *e.g.* energy and particles, with its environment. In other words, they carry information about the detailed *topological structure* of the system plus reservoirs. As we will show, their importance is manifold. On a theoretical level, they enable to formulate generic yet *system-specific* nonequilibrium thermodynamic descriptions. Indeed, by combining conservation laws with the first and second law of thermodynamics one can provide informative descriptions about the way in which the system exchanges energy and dissipates. These laws allow to identify the maximal set of independent nonconservative forces, which are gradients of intensive fields created by the coupling with multiple reservoirs, *e.g.* differences of temperature or chemical potential. These forces are the fingerprint of nonequilibrium processes, *i.e.* processes not relaxing to thermodynamic equilibrium. When these forces vanish, conservation laws determine the potential which is maximized at equilibrium. On a practical level, the analysis of conservation laws for specific systems fosters a deeper understanding of these. For instance, let us regard a thermodynamic system as an engine fuelled by some forces, *e.g.* temperature or chemical potential gradients, and performing work against other *load* forces. A clearer comprehension of the fundamental thermodynamic forces coupled to the system thus simplifies the recognition of fuel and load forces, and hence simplifies performance analyses. This is especially important for large biochemical processes, *e.g.* metabolic ones, whose complexity prevents a first-sight understanding.

In this thesis, we introduce a systematic procedure to identify conservation laws, we reformulate nonequilibrium thermodynamics by making use of them, and we demonstrate their importance. This program will be first carried out at a phenomenological level of description, and then for two classes of systems: generic systems described by Markov jump processes and chemical reaction networks. The phenomenological level will enable us to appreciate the role of conservation laws in absolute terms, since no specific dynamics will be considered. This level provides the fundamental theoretical structure that any thermodynamic system must be compatible with.

Markov jump processes allow us to introduce conservation laws in the large class of systems described by stochastic thermodynamics: *e.g.* molecular motors, pumps, and small quantum devices. For chemical reaction networks, we will show that conservation laws are necessary to establish a rigorous nonequilibrium thermodynamic description, and to relate this description to chemical reaction network theory.

We have already mentioned that information processing can be regarded as a thermodynamic process. Since our description is highly general, we will be able to generalize Landauer’s bound to arbitrary information processing and for arbitrary dynamics. For chemical reaction networks, this paves the way for thermodynamics of information in chemical computing, namely chemical systems designed for computational purposes [76–78].

This thesis is structured in two parts. In the first one, we address the role of conservation laws in generic nonequilibrium thermodynamic processes. In Ch. 1, we introduce the fundamental laws of thermodynamics as well as a *phenomenological* thermodynamic description based on conservation laws. In Ch. 2, we consider stochastic Markov jump processes. This chapter consists of two reprinted Articles: Refs. [79, 80]. In the second part of this thesis, we specialize the aforementioned description to chemical reaction networks. In Chs. 3, 4, and 5, we formalize the phenomenological, stochastic, and several form of deterministic descriptions, respectively. The last two chapters consists of several reprinted Articles: Refs. [81–85].

REFERENCES

- [1] D. CARDWELL, *From Watt to Clausius: The Rise of Thermodynamics in the Early Industrial Age*, Iowa State University Press, 1989.
- [2] S. CARNOT, *Réflexions sur la puissance motrice du feu et sur les machines propres à développer cette puissance*, Bachelier, 1824.
- [3] H. von HELMHOLTZ, *Über die Erhaltung der Kraft*, Reimer, 1847.
- [4] J. GIBBS, *The Scientific Papers of J. Willard Gibbs, Vol.1: Thermodynamics*, Dover, 1961.
- [5] T. de DONDER, *L'affinité*, Gauthier-Villars, 1927.
- [6] L. ONSAGER, “**Reciprocal Relations in Irreversible Processes. I.**” *Phys. Rev.* **37.4** (1931), 405–426.
- [7] L. ONSAGER, “**Reciprocal Relations in Irreversible Processes. II.**” *Phys. Rev.* **38.12** (1931), 2265–2279.
- [8] S. R. de GROOT and P. MAZUR, *Non-equilibrium Thermodynamics*, Dover, 1984.
- [9] I. PRIGOGINE, *Etude Thermodynamique des Phénomènes Irréversibles*, Desoer, 1947.
- [10] I. PRIGOGINE, *Introduction to thermodynamics of irreversible processes*, John Wiley & Sons, 1967.
- [11] I. PRIGOGINE and R. DEFAY, *Chemical Thermodynamics*, Longmans, Green & Co., 1954.
- [12] L. SZILARD, “On the reduction of entropy in a thermodynamic system by the interference of an intelligent being”, *Z. Phys.* **53.** (1929), 840–856.

- [13] L. BRILLOUIN, “Maxwell’s Demon Cannot Operate: Information and Entropy. I”, *J. Appl. Phys.* **22**.3 (1951), 334–337.
- [14] R. LANDAUER, “Irreversibility and heat generation in the computing process”, *IBM J. Res. Dev.* **44**.1.2 (2000), 261–269.
- [15] C. H. BENNETT, “Notes on Landauer’s principle, reversible computation, and Maxwell’s Demon”, *Stud. Hist. Philos. M. P.* **34**.3 (2003), 501–510.
- [16] C. H. BENNETT, “The thermodynamics of computation—a review”, *Int. J. Theor. Phys.* **21**.12 (1982), 905–940.
- [17] D. SHEAR, “An analog of the Boltzmann H-theorem (a Liapunov function) for systems of coupled chemical reactions”, *J. Theor. Biol.* **16**.2 (1967), 212–228.
- [18] J. HIGGINS, “Some remarks on Shear’s Liapunov function for systems of chemical reactions”, *J. Theor. Biol.* **21**.3 (1968), 293–304.
- [19] M. FEINBERG, “Complex balancing in general kinetic systems”, *Arch. Ration. Mech. An.* **49**.3 (1972), 187–194.
- [20] F. HORN and R. JACKSON, “General mass action kinetics”, *Arch. Ration. Mech. An.* **47**.2 (1972), 81–116.
- [21] D. A. MCQUARRIE, “Stochastic Approach to Chemical Kinetics”, *J. Appl. Probab.* **4**.3 (1967), 413.
- [22] D. T. GILLESPIE, “A rigorous derivation of the chemical master equation”, *Physica A* **188**.1–3 (1992), 404–425.
- [23] N. G. van KAMPEN, *Stochastic Processes in Physics and Chemistry*, Elsevier, 2007.
- [24] T. L. HILL, *Free energy transduction in biology, the steady-state kinetic and thermodynamic formalism*, Academic Press, 1977.
- [25] T. L. HILL, *Free Energy Transduction and Biochemical Cycle Kinetics*, Dover, 2005.
- [26] G. F. OSTER, A. S. PERELSON and A. KATCHALSKY, “Network Thermodynamics: dynamic modelling of biophysical systems”, *Q. Rev. Biophys.* **6**. (1973), 1–134.
- [27] G. F. OSTER and A. S. PERELSON, “Chemical Reaction Networks”, *IEEE T. Circuits. Syst.* **21**.6 (1974), 709–721.
- [28] A. S. PERELSON and G. F. OSTER, “Chemical Reaction Dynamics. Part II: Reaction networks”, *Arch. Ration. Mech. Anal.* **57**.1 (1974), 31–98.
- [29] J. SCHNAKENBERG, “Network theory of microscopic and macroscopic behavior of master equation systems”, *Rev. Mod. Phys.* **48**.4 (1976), 571–585.
- [30] M. POLETTINI, “Cycle/Cocycle Oblique Projections on Oriented Graphs”, *Lett. Math. Phys.* **105**.1 (2014), 89–107.
- [31] J.-l. LUO, C. VAN DEN BROECK and G. NICOLIS, “Stability criteria and fluctuations around nonequilibrium states”, *Z. Phys. B* **56**.2 (1984), 165–170.
- [32] M. O. VLAD and J. ROSS, “Fluctuation–dissipation relations for chemical systems far from equilibrium”, *J. Chem. Phys.* **100**.10 (1994), 7268–7278.

- [33] C. VAN DEN BROECK, "Stochastic Thermodynamics", *Selforganization by Nonlinear Irreversible Processes*, ed. by W. EBELING and H. ULRICH, Springer Berlin Heidelberg, 1986, pp. 57–61.
- [34] C. Y. MOU, J.-L. LUO and G. NICOLIS, "Stochastic thermodynamics of nonequilibrium steady states in chemical reaction systems", *J. Chem. Phys.* **84**.12 (1986), 7011–7017.
- [35] Q. ZHENG and J. ROSS, "Comparison of deterministic and stochastic kinetics for nonlinear systems", *J. Chem. Phys.* **94**.5 (1991), 3644–3648.
- [36] K. SEKIMOTO, *Stochastic Energetics*, Springer-Verlag Berlin Heidelberg, 2010.
- [37] C. JARZYNSKI, "Equalities and Inequalities: Irreversibility and the Second Law of Thermodynamics at the Nanoscale", *Annu. Rev. Condens. Matter Phys.* **2**.1 (2011), 329–351.
- [38] U. SEIFERT, "Stochastic thermodynamics, fluctuation theorems and molecular machines", *Rep. Prog. Phys.* **75**.12, 126001 (2012), 126001.
- [39] C. VAN DEN BROECK and M. ESPOSITO, "Ensemble and trajectory thermodynamics: A brief introduction", *Physica A* **418**. (2015), 6–16.
- [40] K. SEKIMOTO, "Langevin Equation and Thermodynamics", *Prog. Theor. Phys. Supp.* **130**. (1998), 17–27.
- [41] U. SEIFERT, "Entropy Production along a Stochastic Trajectory and an Integral Fluctuation Theorem", *Phys. Rev. Lett.* **95**.4 (2005), 040602.
- [42] U. SEIFERT, "Stochastic thermodynamics: principles and perspectives", *Eur. Phys. J. B* **64**.3–4 (2008), 423–431.
- [43] D. J. EVANS and D. J. SEARLES, "Equilibrium microstates which generate second law violating steady states", *Phys. Rev. E* **50**.2 (1994), 1645–1648.
- [44] I. NERI, É. ROLDÁN and F. JÜLICHER, "Statistics of Infima and Stopping Times of Entropy Production and Applications to Active Molecular Processes", *Phys. Rev. X* **7**.1 (2017), 011019.
- [45] D. J. EVANS and D. J. SEARLES, "The Fluctuation Theorem", *Advances in Physics* **51**.7 (2002), 1529–1585.
- [46] R. J. HARRIS and G. M. SCHÜTZ, "Fluctuation theorems for stochastic dynamics", *J. Stat. Mech. Theor. Exp.* **07** (2007), P07020.
- [47] T. SCHMIEDL, T. SPECK and U. SEIFERT, "Entropy Production for Mechanically or Chemically Driven Biomolecules", *J. Stat. Phys.* **128**.1–2 (2007), 77–93.
- [48] T. SCHMIEDL and U. SEIFERT, "Stochastic thermodynamics of chemical reaction networks", *J. Chem. Phys.* **126**.4 (2007), 044101.
- [49] M. POLETTINI, A. WACHTEL and M. ESPOSITO, "Dissipation in noisy chemical networks: The role of deficiency", *J. Chem. Phys.* **143**.18, 184103 (2015), 184103.
- [50] P. GASPARD, "Fluctuation theorem for nonequilibrium reactions", *J. Chem. Phys.* **120**.19 (2004), 8898–8905.
- [51] D. ANDRIEUX and P. GASPARD, "Fluctuation theorem and Onsager reciprocity relations", *J. Chem. Phys.* **121**.13 (2004), 6167.
- [52] A. W. C. LAU, D. LACOSTE and K. MALLICK, "Nonequilibrium Fluctuations and Mechanochemical Couplings of a Molecular Motor", *Phys. Rev. Lett.* **99**.15 (2007), 158102.

- [53] U. SEIFERT, “Stochastic thermodynamics of single enzymes and molecular motors”, *Eur. Phys. J. E* **34**.3 (2011), 26.
- [54] E. ZIMMERMANN and U. SEIFERT, “Efficiencies of a molecular motor: a generic hybrid model applied to the F₁-ATPase”, *New J. Phys.* **14**.10 (2012), 103023.
- [55] B. ALTANER, A. WACHTEL and J. VOLLMER, “Fluctuating currents in stochastic thermodynamics. II. Energy conversion and nonequilibrium response in kinesin models”, *Phys. Rev. E* **92**.4 (2015), 042133.
- [56] R. RAO and L. PELITI, “Thermodynamics of accuracy in kinetic proof-reading: dissipation and efficiency trade-offs”, *J. Stat. Mech. Theor. Exp.* **6** (2015), P06001.
- [57] M. ESPOSITO, K. LINDENBERG and C. VAN DEN BROECK, “Universality of Efficiency at Maximum Power”, *Phys. Rev. Lett.* **102**.13 (2009), 130602.
- [58] G. VERLEY et al., “The unlikely Carnot efficiency”, *Nat. Commun.* **5** (2014), 4721.
- [59] M. POLETTINI, G. VERLEY and M. ESPOSITO, “Efficiency Statistics at All Times: Carnot Limit at Finite Power”, *Phys. Rev. Lett.* **114**. (2015), 050601.
- [60] K. PROESMANS, B. CLEUREN and C. VAN DEN BROECK, “Power-Efficiency-Dissipation Relations in Linear Thermodynamics”, *Phys. Rev. Lett.* **116**.22 (2016), 220601.
- [61] T. SAGAWA and M. UEDA, “Minimal Energy Cost for Thermodynamic Information Processing: Measurement and Information Erasure”, *Phys. Rev. Lett.* **102**.25 (2009), 250602.
- [62] M. ESPOSITO and C. VAN DEN BROECK, “Second law and Landauer principle far from equilibrium”, *Europhys. Lett.* **95**.4 (2011), 40004.
- [63] P. STRASBERG et al., “Thermodynamics of a Physical Model Implementing a Maxwell Demon”, *Phys. Rev. Lett.* **110**.4 (2013), 040601.
- [64] T. SAGAWA, “Thermodynamic and logical reversibilities revisited”, *J. Stat. Mech. Theor. Exp.* **3** (2014), P03025.
- [65] A. C. BARATO and U. SEIFERT, “Unifying Three Perspectives on Information Processing in Stochastic Thermodynamics”, *Phys. Rev. Lett.* **112**.9 (2014), 090601.
- [66] J. M. HOROWITZ and M. ESPOSITO, “Thermodynamics with Continuous Information Flow”, *Phys. Rev. X* **4**.3 (2014), 031015.
- [67] J. M. R. PARRONDO, J. M. HOROWITZ and T. SAGAWA, “Thermodynamics of information”, *Nature Phys.* **11**. (2015), 131–139.
- [68] B. ALTANER, “Nonequilibrium thermodynamics and information theory: basic concepts and relaxing dynamics”, *J. Phys. A: Math. Theor.* **50**.45 (2017), 454001.
- [69] A. KOLCHINSKY and D. H. WOLPERT, “Dependence of dissipation on the initial distribution over states”, *J. Stat. Mech. Theor. Exp.* **8** (2017), 083202.
- [70] T. SAGAWA, *Thermodynamics of Information Processing in Small Systems*, Springer Japan, 2013.
- [71] D. ANDRIEUX and P. GASPARD, “Nonequilibrium generation of information in copolymerization processes”, *Proc. Natl. Acad. Sci. U.S.A.* **105**.28 (2008), 9516–9521.

- [72] P. SARTORI and S. PIGOLOTTI, “Kinetic versus energetic discrimination in biological copying”, *Phys. Rev. Lett.* **110**.18 (2013), 188101.
- [73] P. SARTORI and S. PIGOLOTTI, “Thermodynamics of Error Correction”, *Phys. Rev. X* **5**.4 (2015), 041039.
- [74] T. E. OULD RIDGE, C. C. GOVERN and P. R. ten WOLDE, “Thermodynamics of Computational Copying in Biochemical Systems”, *Phys. Rev. X* **7**.2 (2017), 021004.
- [75] T. E. OULD RIDGE and P. R. ten WOLDE, “Fundamental Costs in the Production and Destruction of Persistent Polymer Copies”, *Phys. Rev. Lett.* **118**.15 (2017), 158103.
- [76] A. HJELMFELT, E. WEINBERGER and J. Ross, “Chemical implementation of neural networks and Turing machines”, *Proc. Natl. Acad. Sci. U.S.A.* **88**.24 (1991), 10983–10987.
- [77] A. HJELMFELT, E. WEINBERGER and J. Ross, “Chemical implementation of finite-state machines”, *Proc. Natl. Acad. Sci. U.S.A.* **89**.1 (1992), 383–387.
- [78] D. SOLOVEICHIK et al., “Computation with finite stochastic chemical reaction networks”, *Nat. Comp.* **7**.4 (2008), 615–633.
- [79] R. RAO and M. ESPOSITO, “Conservation laws shape dissipation”, *New J. Phys.* **20**.2 (2018), 023007.
- [80] R. RAO and M. ESPOSITO, “Detailed Fluctuation Theorems: A Unifying Perspective”, *Entropy* **20**.9 (2018), 635.
- [81] R. RAO and M. ESPOSITO, “Conservation Laws and Work Fluctuation Relations in Chemical Reaction Networks” (arXiv 1805.12077).
- [82] R. RAO and M. ESPOSITO, “Nonequilibrium Thermodynamics of Chemical Reaction Networks: Wisdom from Stochastic Thermodynamics”, *Phys. Rev. X* **6**.4 (2016), 041064.
- [83] R. RAO, D. LACOSTE and M. ESPOSITO, “Glucans monomer-exchange dynamics as an open chemical network”, *J. Chem. Phys.* **143**.24 (2015), 244903.
- [84] G. FALASCO, R. RAO and M. ESPOSITO, “Information Thermodynamics of Turing Patterns”, *Phys. Rev. Lett.* **121**.10 (2018), 108301.
- [85] A. WACHTEL, R. RAO and M. ESPOSITO, “Thermodynamically Consistent Coarse Graining of Biocatalysts beyond Michaelis–Menten”, *New J. Phys.* **20**.4 (2018), 042002.

Part I

THERMODYNAMIC SYSTEMS FAR FROM EQUILIBRIUM

1

PHENOMENOLOGICAL
DESCRIPTION

In this chapter, we establish a phenomenological formulation of nonequilibrium thermodynamics that accounts for conservation laws. This formulation provides the fundamental structure that we will recover in the stochastic description discussed in the next chapter.

The plan of this chapter is as follows, we first review equilibrium thermodynamics, Sec. 1.1, the fundamental laws of thermodynamics, Sec. 1.2, and illustrate the importance of conservation laws using a series of very simple examples, Sec. 1.3. In Sec. 1.4, we describe systems coupled to multiple reservoirs without using conservation laws, while in Sec. 1.5, we introduce a systematic procedure to identify these laws and reformulate our thermodynamic description. In Sec. 1.6, we provide the connection between thermodynamics and information processing by generalizing the Landauer's bound to arbitrary isothermal processes. Finally, in Sec. 1.7, we discuss equilibrium states in extensive systems.

NOTATION All nonexact one-forms are denoted using \mathbf{d} . The Boltzmann constant k_B as well as the gas constant R are set to 1 throughout the thesis.

1.1 EQUILIBRIUM STATES

Equilibrium states of thermodynamic systems are completely determined by the values of some *system quantities*, U and $\{X^\kappa\}$ for $\kappa = 1, \dots, N_\kappa$, and do not depend at all by the history of the system. Among these quantities, the internal energy U plays a prominent role in our discussion, whereas typical instances of others system quantities are the volume V and number of particles N . In addition to U and $\{X^\kappa\}$, we postulate the existence of a quantity, the *entropy* S , which takes its maximum value at equilibrium. Its equilibrium value, denoted by S , is solely determined by the system quantities, $S = S(U, \{X^\kappa\})$, and has the following property: Equilibrium entropy changes due to internal energy changes at fixed $\{X^\kappa\}$ are always positive and define *inverse temperatures*:

$$\frac{1}{T} \equiv \beta := \left. \frac{\partial S}{\partial U} \right|_{\{X^\kappa\}} > 0. \quad (5)$$

This property allows us to write the entropy as function of the internal energy, $U = U(S, \{X^\kappa\})$. The thermodynamic description having S , resp. U , as main quantity is referred to as the *entropy representation*, resp. *energy representation*, of thermodynamics [1]. We will use both in this chapter, as we will see that the former better describes the phenomenology related to the first law whereas the latter that related to the second law.

We now imagine that the equilibrium system undergoes a *process* which infinitesimally changes its system quantities. The changes of internal energy

system quantity, X^κ	energetic intensive field, g_κ
volume, V	(negative) pressure, $-p$
particles number, N	chemical potential, μ
magnetization, M	magnetic field, H

Table 1: Examples of system quantity–intensive field conjugated pairs.

(resp. equilibrium entropy) define the energetic (resp. entropic) *intensive fields* $\{g_\kappa\}$ (resp. $\{-\beta g_\kappa\}$):

$$dS = \beta dU - \beta \sum_\kappa g_\kappa dX^\kappa \quad (6)$$

$$dU = TdS + \sum_\kappa g_\kappa dX^\kappa, \quad (7)$$

where

$$g_\kappa := \frac{\partial U}{\partial X^\kappa} \Big)_{S, \{X^{\kappa'}\}_{\kappa' \neq \kappa}} = -T \frac{\partial S}{\partial X^\kappa} \Big)_{U, \{X^{\kappa'}\}_{\kappa' \neq \kappa}}. \quad (8)$$

They quantify the amount of energy (resp. entropy) that needs to be supplied externally to vary X^κ while keeping all other system quantities unchanged. Table 1 summarizes some g_κ – X^κ conjugated pairs.

1.2 FUNDAMENTAL LAWS OF THERMODYNAMICS

We now introduce the phenomenological laws of thermodynamics. To do so, we consider a system exchanging energy U and $\{X^\kappa\}$ with N_r reservoirs, which we label by r . Reservoirs are regarded as large equilibrium system whose properties are unaffected by the coupling with the system. The system is not necessarily at equilibrium, but the conservation of system quantities requires that the following *balance equations* hold

$$dU = \partial U + \dot{d}_i U + \sum_r \dot{d}_r U \quad (9a)$$

$$dX^\kappa = \partial X^\kappa + \dot{d}_i X^\kappa + \sum_r \dot{d}_r X^\kappa, \quad \text{for all } \kappa. \quad (9b)$$

where the exact derivative, $d\cdot$, denotes the overall changes in the system. For each balance, the first term on the rhs, $\partial\cdot$, quantifies the variations due to *external driving*, namely purely mechanical manipulations. The second term, $\dot{d}_i\cdot$, denote the changes due *internal transformations*, which transform some system quantities into some other, *e.g.* chemical reactions. Finally, the third term, $\dot{d}_r\cdot$, are the variations due to the exchange with the r -th reservoir.

The first contribution in the internal energy balance is the work due to the external driving,

$$\partial U = \partial W, \quad (10)$$

which might also be determined by the manipulations of some other system quantities. For instance, in macroscopic systems, the *mechanical work* follows from controlled changes of volume, $\partial W_{\text{mech}} = \{\partial U / \partial V\} \partial V = p_{\text{mech}} \partial V$. We will refer to this type of work as *driving work contributions*.

Regarding the reservoirs, their thermodynamic properties in the intensive fields, β_r (or equivalently T_r) and $\{g_{(\kappa, r)}\}$. They may possibly change due to *external driving*, and their variations are denoted using ∂ . Processes occurring without any form of external driving, $\partial\cdot = 0$, are said *undriven*.

1.2.1 The First Law

Since each reservoir is at equilibrium, Eq. (7) holds for the changes of system quantities in the reservoirs,

$$d_r U = d_r Q + \sum_{\kappa} g_{\kappa} d_r X^{\kappa} \quad (11)$$

where

$$d_r Q = T_r d_r S \quad (12)$$

is minus the *heat flow* in the r -th reservoir. Inserting this equation in the energy balance (9a) we obtain the traditional expression of the first law of thermodynamics

$$dU = \partial W + \sum_{r,\kappa} d_r W^{\kappa} + dQ \quad (13)$$

where

$$dQ := \sum_r d_r Q \quad (14)$$

is the overall heat flow, and

$$d_r W^{\kappa} := g_{(\kappa,r)} d_r X^{\kappa} \quad (15)$$

are *autonomous work contributions* [2]. This type of work accounts for energy changes due to autonomous exchanges of system quantities with the reservoirs. The *chemical work* is a contribution of this type, $dW_{\text{chem}} = \sum_r \mu_r d_r N$, see Ch. 3, [1, Eq. 2.9]. We also emphasize that in our general setting dQ does not account solely for thermal heat (*i.e.* the heat exchanged with thermal reservoirs), but also other form of heat exchanged with other types of reservoirs, see for instance Eq. [(64) and (65), p. 118] in the context of chemical reaction networks. In this respect, we remark that the common identification of heat as solely the thermal energy exchanged with a thermal reservoir is no more than a point of view. On the one hand, it is already clear that the definition of heat flow in nonequilibrium thermodynamics is not unique [3, Sec. III.3]. On the other hand, if one conceive thermodynamics as a science of symmetries rather than of mere transformation of energy, one can build thermodynamic systems in which internal energy plays no role and nonetheless heat is well defined [4].

1.2.2 The Second Law

In addition to the balance of system quantities, thermodynamics establishes the *unbalance* of entropy,

$$d\Sigma = dS - \partial S - \sum_r \beta_r d_r Q = dS - \partial S + \sum_r d_r S \geq 0, \quad (16)$$

where $d\Sigma$ is the *entropy production*. It is the sum of the entropy change in the system not due to driving, $(d - \partial)S$, plus the sum of heat flows in the reservoirs times their inverse temperatures. Similar to the internal energy, entropy changes due to driving might be caused by manipulations of other system quantities. According to the *second law of thermodynamics*, $d\Sigma$ is always non-negative and vanishes only for reversible processes. Since all reservoirs are constantly at equilibrium, we can use Eq. (11)—or equivalently (6)—to recast the last term

$$d\Sigma = dS - \partial S - \sum_r \left[\beta_r d_r U - \beta_r \sum_{\kappa} g_{(\kappa,r)} d_r X^{\kappa} \right] \geq 0. \quad (17)$$

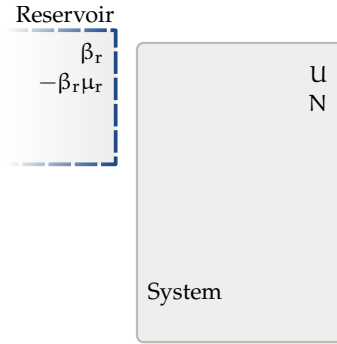


Figure 1: Schematic illustration of the system considered in the Example 1.

In this form, the dissipation is related to the changes of system quantities in the reservoirs.

1.3 CONSERVATION LAWS: ILLUSTRATIVE EXAMPLES

We now introduce and illustrate the role of conservation laws using a series of three examples.

1.3.1 Example 1. System in contact with one reservoir

Let us consider an undriven system exchanging internal energy and particles with a reservoir at inverse temperature β_r and chemical potential μ_r , see Fig. 1. For the sake of simplicity, the related system quantities U and N are subject to neither internal transformations nor external driving, and hence their balance equations read

$$dU = \dot{d}_r U, \text{ and } dN = \dot{d}_r N. \quad (18)$$

By combining these balances and using the equilibrium properties of the reservoir, Eq. (11), we obtain

$$d\mathcal{H} = \dot{d}_r Q \quad (19)$$

where

$$\mathcal{H} := U - \mu_r N \quad (20)$$

is reminiscent of the thermodynamic potential obtained as a Legendre transform of U wrt N . It is however a nonequilibrium potential, since the system is not necessarily at equilibrium. This potential can be understood as the portion of internal energy which is not attributed to its chemical composition, and its changes quantify the heat flow during the process [2].

Dissipation is quantified by the entropy production, Eq. (17),

$$d\Sigma = dS - \beta_r (\dot{d}_r U - \mu_r \dot{d}_r N), \quad (21)$$

which combined with the other balances, Eq. (18), gives

$$\dot{d}\Sigma = d\Phi, \quad (22)$$

where

$$\Phi := \delta - \beta_r (U - \mu_r N) , \quad (23)$$

is reminiscent of the Massieu potential corresponding to the grand potential. We recall that Massieu potentials are thermodynamic potentials in the entropy representation [1, Secs. 5-4 and 19-1] [5, Sec. 3.13]. In our case, Φ can be regarded as the part of entropy which is attributed to neither its thermal nor chemical composition. In other words, it quantify the entropy *freely produced*, as its variations determine the entropy production.

At equilibrium, $d\Sigma = 0$ implies that $d\Phi_{eq} = 0$. Since the system is at equilibrium, its entropy changes reads as in Eq. (6), and we obtain

$$0 = d\Phi_{eq} = (\beta - \beta_r) dU - (\mu - \mu_r) dN . \quad (24)$$

Since the changes of U and N are independent, this equation requires that $\beta = \beta_r$ and $\mu = \mu_r$, namely the system temperature and chemical potential equal those of the reservoirs.

In this first example, we recovered traditional equilibrium thermodynamics from a nonequilibrium description.

1.3.2 Example 1+1/2. Driven System in contact with one reservoir

For the sake of illustrating the effect of driving, let us imagine that the internal energy and the chemical potential of the reservoirs are manipulated by an (not clearly identified) external agent: $\partial U \neq 0$, $\partial \delta \neq 0$, and $\partial \mu_r \neq 0$. The balance of energy now reads

$$dU = \partial U + d_r U , \quad (25)$$

and by combining it with the balance for N and Eq. (11) we obtain

$$d\mathcal{H} = \partial \mathcal{H} + d_r Q , \quad (26)$$

where we have used Eq. (20) and the identity $d(\mu_r N) = \partial \mu_r N + \mu_r dN$. The second term on the rhs is distinctive of driving,

$$\partial \mathcal{H} = \partial U - \partial \mu_r N , \quad (27)$$

as it accounts for the manipulation of energy and chemical potential of the reservoir. It is clear, though, that these contributions have completely different nature: The first accounts for direct changes of energy, while the second changes the energy indirectly by changing the thermodynamic properties of the reservoir. Despite this important difference, we will refer to both terms as driving work.

Analogously, for the entropy balance we obtain

$$d\Sigma = d\Phi - \partial \Phi , \quad (28)$$

where Φ is given as in Eq. (23) and the second term on the rhs reads

$$\partial \Phi = \partial \delta - \beta_r \partial U + \partial \mu_r N . \quad (29)$$

The latter term accounts for the dissipation due the driving mechanisms.

In this example we showed that driving introduces a new work and dissipative contributions. It is clear that they must vanish at equilibrium, else the entropy production would be different from zero.

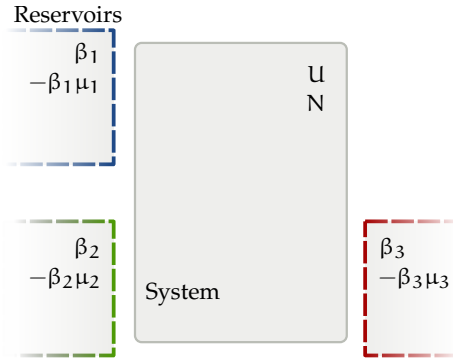


Figure 2: Schematic illustration of the system considered in the Example 2.

1.3.3 Example 2. System in contact with multiple reservoirs

Let us consider the same system as in Example 1 (no driving), but now exchanging energy and matter with three reservoirs, each with its own fields, as in see Fig. 2. The balance equations for these quantities read

$$dU = \sum_{r=1}^3 d_r U, \text{ and } dN = \sum_{r=1}^3 d_r N. \quad (30)$$

By combining these equations and using the equilibrium properties of the reservoirs, we get

$$d\mathcal{H} = \sum_{r=2}^3 (\mu_r - \mu_1) d_r N + dQ \quad (31)$$

where

$$\mathcal{H} := U - \mu_1 N. \quad (32)$$

is a nonequilibrium potential similar to those discussed in the previous example. We used the first reservoir as a reference, and its chemical potential appears in this potential. The first term on the rhs of Eq. (31) vanishes in presence of only one reservoir, *cf.* Eq. (19), and quantifies the energetic cost of transferring particles between the first and the other two reservoirs. In Eq. (31), $dQ = \sum_r d_r Q$ is the total heat flow.

Concerning the entropy balance, the entropy production now reads

$$d\Sigma = dS - \sum_{r=1}^3 \beta_r (d_r U - \mu_r d_r N), \quad (33)$$

which combined with the other balances gives

$$d\Sigma = d\Phi + \sum_{r=2}^3 (\beta_1 - \beta_r) d_r U + \sum_{r=2}^3 (\beta_r \mu_r - \beta_1 \mu_1) d_r N, \quad (34)$$

where

$$\Phi := S - \beta_1 (U - \mu_1 N), \quad (35)$$

is the nonequilibrium Massieu potential corresponding to the grand potential. The first term is the dissipative contribution due to overall changes of

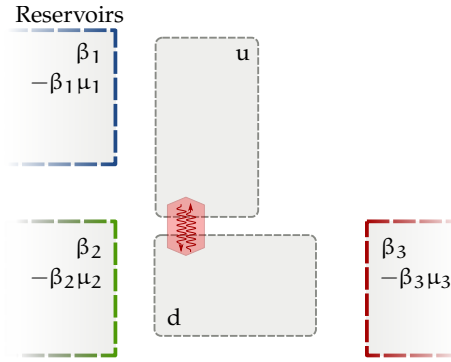


Figure 3: Schematic illustration of the system considered in the Example 3.

system quantities and uses the thermodynamic properties of first reservoirs as a reference. Since the system is coupled to three reservoirs and each of them tries to impose its own equilibrium, four nonconservative force–flow contributions arise. They quantify the dissipation due to the flow of thermal and chemical energy between the first reservoir and the other two.

For the system to be at equilibrium, $d\Sigma = 0$, all nonconservative forces need to vanish independently, which follows when $\beta_1 = \beta_2 = \beta_3$ and $\mu_1 = \mu_2 = \mu_3$. The changes of Massieu potential also need to vanish, which entails that the system intensive fields equal those of the reservoirs: $\beta = \beta_1$ and $\mu = \mu_1$.

In this second example we saw that in presence of multiple reservoirs, energetic and dissipative contributions due to exchanges of system quantities with the reservoirs arise. We now remark that we said nothing about the properties of the system, which has been treated as a *black box*. The question which we will answer in the next section is in which way the knowledge of its specifications improves this thermodynamic description.

1.3.4 Example 3: System-specific description: conservation laws

We now consider the system described in the previous example, but a detailed inspection inform us that the system is divided into an upper and a lower part, see Fig. 3. The former exchanges energy and particles with the first reservoir, while the latter with the other two reservoirs. Only thermal energy can be transferred between these parts as particle transfers are forbidden. This revealed constraint introduces a new balance equation since the number of particles in the upper and lower part of the system, N^u and N^d respectively, are now separately conserved:

$$dN^u = d_1 N^u, \text{ and } dN^d = \sum_{r=2}^3 d_r N^d. \quad (36)$$

The total number of particles is clearly recovered as $N = N^u + N^d$. Upon combination of these balances with the energy balance and the first law of thermodynamics, Eq. (13), we obtain

$$d\mathcal{H} = (\mu_3 - \mu_2) d_3 N + d_r Q, \quad (37)$$

where

$$\mathcal{H} := U - \mu_1 N^u - \mu_2 N^d \quad (38)$$

is a system-specific nonequilibrium potential. Notice that we have now used the chemical potentials of the first and the second reservoir as a reference. The first term on the rhs is the energetic cost associated to the transfer of particle between the second and the third reservoirs.

Analogously, the knowledge of the additional balance allows to recast the entropy production into

$$\dot{\Sigma} = d\Phi - \partial\Phi + \sum_{r=2}^3 (\beta_1 - \beta_r) \dot{d}_r U + (\beta_3 \mu_3 - \beta_2 \mu_2) \dot{d}_3 N, \quad (39)$$

where

$$\Phi := S - (\beta_1 U - \beta_1 \mu_1 N^u - \beta_2 \mu_2 N^d), \quad (40)$$

is the nonequilibrium Massieu potential corresponding to a system-specific grand potential. By comparing Eqs. (34) and (39) we notice that the Massieu potential contains an additional term, which comes from the additional balance. In contrast, the number of nonconservative dissipative contributions is decreased by one, since the additional constraint prevents some particle flows. In summary, one nonconservative contribution is recognized as a conservative one and it is included in the potential.

For the system to be at equilibrium, the three nonconservative forces must independently vanish, which implies that: $\beta_1 = \beta_2 = \beta_3 =: \beta_r$ and $\mu_2 = \mu_3$. Notice that now that we have more information about the system, we learn that μ_1 need not be equal to μ_2 and μ_3 . Finally, $d\Phi_{eq} = 0$, implies that $\beta = \beta_1$, $\mu_u = \mu_1$ and $\mu_d = \mu_2$. In other words, the system temperature equals that of the reservoirs, the upper part of the system is characterized by a chemical potential equilibrated with that of the first reservoir, and the lower part by one equilibrated with the second and third reservoir.

We now argue that the system quantities U , N^u , and N^d , can be regarded as a particular class of *conserved quantities* in two respects. First, they are system-specific—not all systems are split in two parts. Second, they do not change due to internal transformations. Hence, if the system were isolated, $\dot{d}_r = \partial \dot{d}_r = 0$, they would be constants, but the driving or the coupling with the reservoirs *breaks* them. We will refer to the conservation laws corresponding to these type of conserved quantities as *broken conservation laws*. The benefit of identifying these laws is clear from this example: they allow us to clearly separate the nonconservative energetic and dissipative contributions from the conservative ones. Additionally, they allow to accurately determine what are the conditions so that the system is at equilibrium.

1.4 SYSTEMS IN CONTACT WITH MULTIPLE RESERVOIRS

We now proceed to construct a formulation of nonequilibrium thermodynamics which generalizes the observations drawn in the previous examples. In this section, we generalize the case of the second example, in which the system is treated as a black box and no system-specific conservation law is used. For the purpose of identifying the different energetic and dissipative contributions, we will combine the balances of system quantities with the first and second law of thermodynamics.

Choosing the first reservoir as a reference, we can rewrite Eq. (9b) as

$$d_1 X^k = dX^k - \partial X^k - d_i X^k - \sum_{r \neq 1} d_r X^k. \quad (41)$$

Since

$$d(g_{(k,r)} X^k) = dg_{(k,r)} X^k + g_{(k,r)} dX^k = \partial g_{(k,r)} X^k + g_{(k,r)} dX^k, \quad (42)$$

the previous equation can be combined with the energy balance, Eq. (9a), to give

$$d\mathcal{H} = d_i \mathcal{H} + \partial \mathcal{H} + \sum_{k,r \neq 1} (g_{(k,r)} - g_{(1,k)}) d_r X^k + dQ. \quad (43)$$

where we introduced the *nonequilibrium generalized enthalpy*,

$$\mathcal{H} := U - \sum_k g_{(k,1)} X^k. \quad (44)$$

Indeed, \mathcal{H} recalls the thermodynamic potential obtained as a Legendre transform of U wrt all other system quantities. It is clearly defined up to a closed zero-form φ , $d\varphi = 0$, which we omit for brevity. Equation (43) combines the changes of all system quantities in one balance. The first term on the rhs quantifies the overall nonequilibrium enthalpy changes due to internal transformations, whereas the second those due to external manipulations. The third term accounts for the transfer of X^k from the first reservoir to the r -th, and the last one is the overall heat flow.

As for the energy balance, we now combine the entropy balance with all other balances. By choosing again the first reservoir as a reference, we obtain

$$d\Sigma = d\Phi - d_i \Phi - \partial \Phi + \sum_r (\beta_1 - \beta_r) d_r U + \sum_{r,k} (\beta_r g_{(k,r)} - \beta_1 g_{(k,1)}) d_r X^k, \quad (45)$$

where

$$\Phi := S - \beta_1 \left(U - \sum_k g_{(k,1)} X^k \right) \equiv S - \beta_1 \mathcal{H} \quad (46)$$

is reminiscent of a Massieu potential obtained as a Legendre transform of the entropy with respect to all other system quantities. In contrast to the terms appearing in Eq. (43), those in Eq. (45) are *dissipative contributions* rather than enthalpic changes. The first two terms quantify the dissipation due to overall changes of system quantities and those due to internal transformations, respectively. The third term characterizes the dissipation corresponding to the external manipulations, whereas the fourth and fifth term quantify that due to the exchange of thermal energy and X^k between the first and the r -th reservoir. These nonconservative force-flow contributions are the distinctive feature of systems coupled to multiple reservoirs. Since each of them tries to impose its own equilibrium the system is in general prevented from reaching equilibrium.

At this level of description, equilibrium ($d\Sigma = 0$) is reached when the following conditions are satisfied. (i) all reservoirs have the same intensive fields, $\beta_r = \beta_1$ and $g_{(k,r)} = g_{(k,1)}$ for all r , since in this way all non-conservative force-flow contribution vanish. (ii) external manipulations are stopped $\partial\Phi = 0$. (iii) the changes of Φ due to internal transformations vanish, $d_i \Phi_{\text{eq}} = 0$. Finally, (iv) the overall changes of Φ vanish, $d\Phi_{\text{eq}} = 0$. At

equilibrium, system entropy changes can be written as in Eq. (6), and hence the latter requirement reads

$$0 = d\Phi_{eq} = (\beta - \beta_1)dU - \sum_{\kappa} (g_{\kappa} - g_{(\kappa,1)}) dX^{\kappa}, \quad (47)$$

where β and $\{g_{\kappa}\}$ are the intensive fields of the system at equilibrium. Since the changes of all system quantities are independent, this equation implies that $\beta = \beta_1$, and $g_{\kappa} = g_{(\kappa,1)}$ for all κ . In other words, all system fields become well defined and equal to those of the reservoirs. We notice that the requirement (iii) is not written in terms of properties of the intensive fields—as for the conditions (i) and (iv)—, but rather as a condition on the internal state of the system, which cannot be elucidate further. This is a consequence of treating the system as a black box.

We described in this section a *black-box* description of nonequilibrium thermodynamics: we made no mention of the properties of the system. Combining the balances of system quantities give us incomplete information about both the nature of the different energetic and dissipative contributions, and the conditions for equilibrium, which cannot be completely characterized in terms of properties of the reservoirs.

1.5 SYSTEM-SPECIFIC THERMODYNAMICS

In this section, we will reconsider the problem of identifying the energetic and dissipative contributions characterizing a given process, but we will make use of the properties of the system. These properties are encoded in its topological structure and determine its broken conservation laws. We will thus introduce a systematic procedure to identify them. But to do so, we first rewrite the laws of thermodynamics in a more compact way.

We define the index $y := (r, \bar{\kappa})$ as that labelling *the system quantity $\bar{\kappa}$ exchanged with the reservoir r* . The index $\bar{\kappa}$ labels all system quantities including the internal energy. The changes of each system quantity due to each reservoir can be thus encoded in a vector of *exchange one-forms* $\{dX^y := d_r X^{\bar{\kappa}}\}$. Similarly, we collect all intensive fields in a vector, $\{g_y := g_{(r, \bar{\kappa})}\}$, where $g_{(r, U)} = -1$. We denote by β_y the inverse temperature of the reservoir corresponding to y : $\beta_y = \beta_r$ for $y = (r, \bar{\kappa})$. First and second law, Eqs. (13) and (16), can be thus recast into

$$0 = dQ + \partial W + \sum_y g_y dX^y \quad (48)$$

$$d\Sigma = dS - \partial S + \sum_y \beta_y g_y dX^y \geq 0. \quad (49)$$

1.5.1 Cyclic Transformations and Broken Conservation Laws

We define *instantaneous cyclic transformations*, denoted by γ , as any system transformation which does not involve driving, $\partial \cdot = 0$, and in which the microscopic state of the system is overall unchanged. It is clear that all exact one-forms vanish along these transformations, *i.e.*

$$\oint_{\gamma} d\mathcal{O} = 0, \quad \text{for any state observable } \mathcal{O}. \quad (50)$$

For instance, a cyclic transformation for the system in Sec. 1.3.4 is one in which n molecules enter in the lower part of the system from the second

reservoir and then exit from the third one. Notice that cyclic transformations encode the topological structure of the system.

We introduce *broken conservation laws*, as y -space vectors ℓ_y , satisfying

$$\sum_y \ell_y \oint_\gamma dX^y = 0, \quad \text{for all } \gamma. \quad (51)$$

Broken conservation laws identify *broken conserved quantities*, whose balance is given by

$$dL = \partial L + \sum_y \ell_y dX^y. \quad (52)$$

These equations can be understood as follows. Equation (51) identifies a combination of exchange terms which leaves the internal state of the system unchanged upon any instantaneous cyclic transformation. This combination must correspond to an exact one-form, $dL := \sum_y \ell_y dX^y$, which generalizes to Eq. (52) when L is externally manipulated. Clearly, L is defined up to a zero-form. Notice that the changes of L are due to either external manipulations or the coupling with the reservoirs, and not to internal transformations. If the system were isolated, L would be conserved in the system, $dL = 0$, which motivates *a posteriori* the name *broken conserved quantity*.

A complete set of broken conservation laws is defined as a maximal set of independent vectors in the y -space which satisfy Eq. (51), and we denote it by $\{\ell_y^\lambda\}$, for $\lambda = 1, \dots, N_\lambda$. The corresponding conserved quantities are denoted by $\{L_\lambda\}$. System quantities that are not subject to internal transformations are trivial cases of broken conserved quantities. Their balance is recovered for $\ell_{(r, \bar{r})}^{\bar{r}'} = \delta_{\bar{r}}^{\bar{r}'}$.

1.5.2 System-specific Energy and Entropy balance

We now proceed to reformulate the laws of thermodynamics using the broken conserved quantities. Since $\{\ell^\lambda\}$ are linearly independent, it is always possible to identify N_λ exchanged quantities, labelled by y_p , such that the matrix whose row vectors are $\{\ell_{y_p}^\lambda\}$, for $\lambda = 1, \dots, N_\lambda$, is nonsingular. We denote by $\{\bar{\ell}_\lambda^{y_p}\}$, for $\lambda = 1, \dots, N_\lambda$, the column vector of the corresponding inverse matrix. All other exchanged quantities are denoted by y_f . Therefore, Eq. (52) can be recast into

$$dX^{y_p} = \sum_\lambda \bar{\ell}_\lambda^{y_p} (dL_\lambda - \partial L_\lambda) - \sum_\lambda \bar{\ell}_\lambda^{y_p} \sum_{y_f} \ell_{y_f}^\lambda dX^{y_f}, \quad (53)$$

i.e. the changes of y_p can be related to the changes of the set of conserved quantities, $\{dL_\lambda\}$ and $\{\partial L_\lambda\}$, and the remaining exchange terms, $\{dX^{y_f}\}$. Using this equation, the first law, Eq. (48), can be recast into

$$d\mathcal{H} = \partial \mathcal{H} + \sum_{y_f} \mathcal{K}_{y_f} dX^{y_f} + dQ, \quad (54)$$

where

$$\mathcal{H} := - \sum_\lambda g_\lambda L_\lambda \quad (55)$$

is a system-specific nonequilibrium generalized enthalpy,

$$g_\lambda := \sum_{y_p} g_{y_p} \bar{\ell}_\lambda^{y_p} \quad (56)$$

are the energetic intensive fields conjugated to the conservation laws, and

$$\mathcal{K}_{y_f} := g_{y_f} - \sum_\lambda g_\lambda \ell_{y_f}^\lambda. \quad (57)$$

are differences of intensive fields. Concerning the second law, Eq. (49), using Eq. (53), we obtain

$$d\Sigma = d\Phi - \partial\Phi + \sum_{y_f} \mathcal{F}_{y_f} dX^{y_f} \quad (58)$$

where

$$\Phi := \mathcal{S} - \sum_{\lambda} f_{\lambda} L_{\lambda} \quad (59)$$

is a system-specific nonequilibrium Massieu potential, and

$$f_{\lambda} := -\sum_{y_p} \beta_{y_p} g_{y_p} \bar{\ell}_{\lambda}^{y_p} \quad (60)$$

are the entropic intensive fields conjugated to the conservation laws. The nonconservative forces read

$$\mathcal{F}_{y_f} := \beta_{y_f} g_{y_f} + \sum_{\lambda} f_{\lambda} \ell_{y_f}^{\lambda}. \quad (61)$$

Equations (54) and (58) are the main result of this chapter. The fundamental enthalpic and dissipative contributions, *i.e.* internal, driving, and transport between reservoirs, are completely separated, thanks to the use of conservation laws. The *driving* term $\partial\mathcal{H}$ (resp. $-\partial\Phi$) quantifies the enthalpic cost (resp. dissipation) of external manipulations, and vanish in nondriven systems. The *nonconservative* force-flow terms $\mathcal{K}_{y_f} dX^{y_f}$ (resp. $\mathcal{F}_{y_f} dX^{y_f}$) quantify the enthalpic cost (resp. the dissipation) of transporting system quantities from some reservoir to some other. Finally the *conservative* term $d\Phi$ appearing in the entropy balance accounts for the dissipation due to internal transformations. Wrt Eq. (43) and (45) we notice that: (i) the contributions due to internal transformation are disappeared; (ii) the terms appearing in the potentials \mathcal{H} and Φ now account for broken conservation laws, which are invariant under internal transformations; (iii) the nonconservative forces now account for both the presence of constraints preventing the flow between some reservoirs (as seen in the illustrative example) and the possibility that internal transformations create pathways between reservoirs of different system quantities (see example in Part ii). In this respect, $\{\mathcal{F}_{y_f}\}$ is a set of *fundamental nonconservative forces* as they are maximal and independent: if and only if they all vanish, the system can relax to equilibrium when undriven. Indeed, since all contributions in Eq. (58) are independent one another, they must independently vanish at thermodynamic equilibrium, $d\Sigma = 0$. Specifically, $\mathcal{F}_{y_f} = 0$ for all y_f , means that the reservoirs do not develop gradients of intensive fields which create flows across the system. $\partial\Phi = 0$ requires that the system is not manipulated, and $d\Phi_{eq} = 0$ implies that all system intensive fields $\{f_{\lambda}^s\}$ are well defined and equilibrated with those of the reservoirs $\{f_{\lambda}\}$.

We point out that the relationship between the fundamental forces $\{\mathcal{F}_{y_f}\}$ and $\{\mathcal{K}_{y_f}\}$, Eqs. (57) and (61), is nontrivial:

$$\mathcal{F}_{y_f} = \sum_{y_p} \left[\beta_{y_f} - \beta_{y_p} \right] g_{y_p} \sum_{\lambda} \bar{\ell}_{\lambda}^{y_p} \ell_{y_f}^{\lambda} + \beta_{y_f} \mathcal{K}_{y_f}. \quad (62)$$

This entails that $\mathcal{F}_{y_f} = 0 \Leftrightarrow \mathcal{K}_{y_f} = 0$, and therefore $\{\mathcal{K}_{y_f}\}$ cannot be interpreted as fundamental forces: they could vanish in a system prevented from reaching equilibrium, as well as be finite in a system relaxing to equilibrium.

We finally emphasize that Eqs. (54) and (58) hold for arbitrary systems and arbitrarily far from equilibrium. They are based on the laws of thermodynamics, on the fact that the reservoirs are at equilibrium, and on the

possibility of attributing system quantities and entropy to the overall system. In Chs. 2, 4, and 5 we will discuss several classes of micro- and macroscopic dynamics for which these results are recovered.

We conclude our main discussion with two important remarks and then consider some specific classes of processes.

REMARK The decompositions in Eqs. (54) and (58) are not unique since they depend on the partitioning of y in y_p and y_f . We recall that not all partitioning are allowed since $\ell_{y_p}^\lambda$ needs to be nonsingular, but $N_{y_p} = N_\lambda$ and $N_{y_f} = N_y - N_\lambda$.

REMARK A detailed inspection of the system could reveal that the system is characterized by some *constants of motion*, or *unbroken* conservation laws, namely a set of closed zero-forms $\{L_v\}$ for $v = 1, \dots, N_v$, such that $dL_v = 0$. We have already mentioned that all conservation laws are defined up to a closed zero-form. Let us therefore consider the following *gauge transformation* of the conserved quantities

$$L_\lambda \rightarrow L_\lambda + \sum_v \Omega_v^\lambda L_v \quad (63)$$

where $\{\Omega_v^\lambda\}$ are real coefficients. It is clear that

$$dL_\lambda \rightarrow dL_\lambda, \quad (64)$$

but the changes of system-specific potentials are not left unchanged

$$\begin{aligned} d\mathcal{H} &\rightarrow d\mathcal{H} - \sum_\lambda \partial g_\lambda \sum_v \Omega_v^\lambda L_v \\ d\Phi &\rightarrow d\Phi - \sum_\lambda \partial f_\lambda \sum_v \Omega_v^\lambda L_v. \end{aligned} \quad (65)$$

Crucially, the extra gauge terms appearing on the rhs disappear in the energy and entropy balances, Eqs. (54) and (58), since it cancels with term arising from the driving terms. We have thus shown that the potentials and the related driving terms are defined up to a gauge, which overall does not affect any balance equation. Notice also that the gauge term disappears from the energy and entropy balances, Eqs. (54) and (58), for nondriven systems as well as under cyclic transformations.

1.5.3 Isothermal Processes

For isothermal processes all reservoirs are characterized by the same inverse temperature, β_r , and hence the entropy balance, Eq. (49), can be written as

$$d\Sigma = dS + \beta_r \sum_y g_y dX^y \geq 0. \quad (66)$$

By making use of conservation laws, we obtain

$$d\Sigma = d\Phi - \partial\Phi + \beta_r \sum_{y_f} \mathcal{K}_{y_f} dX^{y_f}, \quad (67)$$

where the system-specific Massieu potential becomes

$$\Phi = S - \beta_r \mathcal{H}. \quad (68)$$

Indeed, the entropic intensive fields conjugated to conservation laws can be written in terms of the energetic ones,

$$f_\lambda = -\beta_r g_\lambda, \quad (69)$$

and Eq. (62) guarantees that $\mathcal{F}_{y_f} = \beta_r \mathcal{K}_{y_f}$. Therefore, only for isothermal processes $\mathcal{F}_{y_f} = 0 \Leftrightarrow \mathcal{K}_{y_f} = 0$, which implies that also $\{\mathcal{K}_{y_f}\}$ can be regarded as fundamental forces.

1.5.4 Adiabatic Processes

In adiabatic processes no heat is exchanged, $dQ = 0$, and hence the energy balance reads

$$\sum_y g_y dX^y = d\mathcal{H} - \partial\mathcal{H} - \sum_{y_f} \mathcal{K}_{y_f} dX^{y_f} = 0 \quad (70)$$

whereas the entropy one

$$d\Sigma = dS. \quad (71)$$

Since heat is not exchanged, all kind of thermal and chemical reservoirs do not appear. The exchanged system quantities are restricted to purely mechanical ones like for instance the volume.

1.6 NONEQUILIBRIUM LANDAUER PRINCIPLE

We now reconsider Eq. (58) from an information theoretical perspective, and for the sake of simplicity we consider isothermal processes, Eq. (67). We have already mentioned that when all fundamental forces vanish and the variations of intensive fields are stopped, the overall dissipation is $d\Sigma = d\Phi \geq 0$ and it vanishes at equilibrium, $d\Phi_{eq} = 0$. Therefore, we can assume that Φ is maximized at equilibrium, and we rewrite it as

$$\Phi = \Phi_{eq} - \mathcal{D}, \quad (72)$$

where Φ_{eq} is the equilibrium potential maximizing Φ , and the *generalized relative entropy* $\mathcal{D} \geq 0$ quantifies the deviation of Φ from equilibrium: the larger \mathcal{D} is, the further the system is from equilibrium, and it vanishes solely at equilibrium. By combining this equation with Eq. (67), we can recast the latter into

$$-\partial\Phi_{irr} + \beta_r \sum_{y_f} \mathcal{K}_{y_f} dX^{y_f} = d\mathcal{D} + d\Sigma \geq d\mathcal{D}, \quad (73)$$

where

$$-\partial\Phi_{irr} = d\Phi_{eq} - \partial\Phi = \partial(\Phi_{eq} - \Phi) \quad (74)$$

is an *irreversible driving dissipative contribution*—notice its gauge invariance. In the last equality, $d\Phi_{eq} = \partial\Phi_{eq}$, accounts for the fact that the equilibrium state changes because of the external manipulation.

Equation (73) is an important result which relates the dissipative cost of transforming the system via either external driving or nonconservative forces, to its deviation from equilibrium, \mathcal{D} . Since the total entropy change is always positive, $d\mathcal{D}$ determines the minimal dissipative cost of this transformation. It is negative (entropy released by the system) when approaching equilibrium, and positive (entropy flowing in the system) when moving away from it. If we multiply both sides by T_r , and integrate Eq. (73) over a process, we obtain

$$-T_r \int \partial\Phi_{irr} + \sum_{y_f} \int \mathcal{K}_{y_f} dX^{y_f} = T_r \Delta\mathcal{D} + T_r \int d\Sigma \geq T_r \Delta\mathcal{D}. \quad (75)$$

In this form, the lhs represents the work, either due to driving or nonconservative mechanisms, that is spent to transform the system from two arbitrary nonequilibrium states. The difference $T_r \Delta\mathcal{D}$ thus quantifies the minimal

thermodynamic cost of transforming the system. For systems starting at equilibrium, $T_r \Delta D = T_r D_{\text{final}} \geq 0$ quantifies the minimal cost of structuring the final nonequilibrium state. In contrast, for system relaxing to equilibrium, $T_r \Delta D = -T_r D_{\text{initial}} \leq 0$ quantifies the maximum amount of work that can be extracted during the relaxation. For transformations between equilibrium states ($\mathcal{K}_{y_f} = 0$ for all y_f), we recover the classic result, $-T_r \int \partial \Phi_{\text{irr}} \geq 0$.

We will refer to the bound on the work contributions expressed in Eq. (75) as *nonequilibrium Landauer principle*, but we postpone the justification for this name to the next chapter, where we specialize it to stochastic processes. We finally remark that a generalization of this principle to nonisothermal processes is possible but requires care, as we explain in the reprinted article at p. 37.

1.7 EQUILIBRIUM STATES OF EXTENSIVE SYSTEMS

We conclude this section by discussing the equilibrium Massieu potential for those systems whose equilibrium entropy is extensive: if the system is scaled by α , then the equilibrium entropy scales by α as well. In other words, S satisfies *Euler equation*

$$S(\{\alpha L_\lambda\}, \{\alpha L_\nu\}) = \alpha S(\{L_\lambda\}, \{L_\nu\}), \quad \text{for any } \alpha. \quad (76)$$

where $\{L_\nu\}$ is a set of unbroken conserved quantities, *i.e.* system quantities which are not exchanged with the reservoirs: $dL_\nu = 0$. Taking the derivative wrt α and imposing $\alpha = 1$, we recover *Euler theorem*,

$$S(\{L_\lambda\}, \{L_\nu\}) = \sum_\lambda f_\lambda^S L_\lambda + \sum_\nu f_\nu^S L_\nu. \quad (77)$$

Since the system is at equilibrium with its reservoirs, $\{f_\lambda^S\}$ must be equal to those in Eq. (60). We can thus write the system-specific equilibrium Massieu potential as

$$\Phi_{\text{eq}} = \sum_\nu f_\nu^S L_\nu. \quad (78)$$

In conclusions, when assuming that the equilibrium entropy is extensive the equilibrium Massieu potential becomes a combination of unbroken conserved quantities.

REFERENCES FOR CHAPTER 1

- [1] H. CALLEN, *Thermodynamics and an Introduction to Thermostatistics*, Wiley, 1985.
- [2] B. ALTANER, “Nonequilibrium thermodynamics and information theory: basic concepts and relaxing dynamics”, *J. Phys. A: Math. Theor.* **50**.45 (2017), 454001.
- [3] S. R. de GROOT and P. MAZUR, *Non-equilibrium Thermodynamics*, Dover, 1984.
- [4] H. CALLEN, “Thermodynamics as a science of symmetry”, *Found. Phys.* **4**.4 (1974), 423–443.
- [5] L. PELITI, *Statistical Mechanics in a Nutshell*, Princeton University Press, 2011.

2 | STOCHASTIC DESCRIPTION

In Ch. 1 we established a phenomenological description of generic thermodynamic systems far from equilibrium. We made no mention of the microscopic dynamics which determines the evolution of the system. Nonetheless, conservation laws enabled us to clearly separate the various types of energetic and dissipative contributions.

We have already introduced stochastic thermodynamics as a nonequilibrium thermodynamic description for systems whose stochastic dynamics is Markovian. In the following reprinted Article, we present the first general formulation of stochastic thermodynamics for Markov jump processes which makes full use of conservation laws. In this setting, the microscopic configurations of the system are described as *states* $\{n\}$ whereas the transitions from one state to another, $\{e\}$, are stochastic events. The evolution in time of the probability of finding the system in the state n , p_n , is ruled by the master equation, Eqs. [(1), p. 38] and [(5), 73], whose *timeless* expression reads

$$dp_n = \sum_e D_e^n d\zeta_e, \quad (79)$$

where the incidence matrix D encodes how the states are connected by transitions, and $\{d\zeta_e\}$ are the *extent* of transitions that count their occurrence. At an average level, the values of the system quantities are replaced by their averages, *e.g.* $X^k = \sum_n X_n^k p_n$, where X_n^k is the value of the system quantity in the state n . Their balance equations, Eq. (9), can be thus written as

$$\begin{aligned} dX^k &= \sum_n dX_n^k p_n + \sum_e \sum_n X_n^k D_e^n d\zeta_e \\ &= \sum_n \partial X_n^k p_n + \sum_e (\delta_i X_e^k + \sum_r \delta_r X_e^k) d\zeta_e \end{aligned} \quad (80)$$

where $dX_n^k = \partial X_n^k$ are changes due to driving, while $\delta_i X_e^k$ and $\delta_r X_e^k$ encode the changes due to internal transformations and exchanges with the reservoir r along the transition e , see Eqs. [(5), p. 39] and [(62), p. 83]. The average system entropy is given by *Gibbs–Shannon* expression

$$S = \sum_n p_n (S_n - \ln p_n), \quad (81)$$

where S_n is the internal entropy of the state n , Eq. [(78), p. 87]. The connection between the stochastic dynamics (79) and thermodynamics (80) lies the *local detailed balance* property, Eqs. [(6) and (7), p. 40] and [(65) and (66), p. 84]. In its timeless formulation, it relates the ratio of forward and backward extent of transition to the entropy production along the latter, *i.e.* the *affinity*, see Eqs. (17) and (49),

$$\ln \frac{d\zeta_e}{d\zeta_{-e}} = \sum_y \beta_y g_y \delta X_e^y + \sum_n (S_n - p_n) D_e^n = \delta \Sigma_e \equiv A_e, \quad (82)$$

where $\delta X_e^y := \delta_r X_e^y$ follows the notation introduced in Sec. 1.5. Once the fundamental laws of thermodynamics are built on top of the stochastic dynamics, we can use the procedure described in Sec. 1.5.1 to identify broken conservation laws, Eqs. [(10) and (11), p. 41] and [(63) and (64), p. 84]. Using the balances of the corresponding conserved quantities we are thus

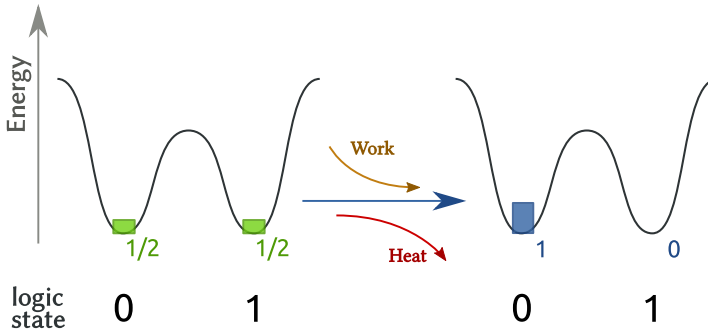


Figure 4: Schematic illustration of the erasure of one bit of information. The bit is modeled as a double-well potential, in which each well corresponds to a logic state. We have no prior knowledge of the information stored in the bit, and hence the probability to find it in 0 or 1 is equally likely. Since the wells have the same energy and shape, the system is at equilibrium. At the end of the erasure procedure, the system is in a nonequilibrium state, as it is in 0 (or equivalently 1) with probability 1.

able to reproduce the phenomenological description discussed in Sec. 1.5, see Sec. [5.1–2 p. 49]. Importantly, our stochastic formulation provides us with a clearer understanding of the dissipative entropy production contributions in Eq. (58). Indeed, we show that each of them is distinctive for a class of processes: $d\Phi$ for relaxation to equilibrium, $-\partial\Phi$ for time-dependently driven processes, and $\{\mathcal{F}_{y_f} dX^{y_f}\}$ for nonequilibrium steady states, see Tab. [3, p. 46].

The stochastic thermodynamic formulation of the nonequilibrium Landauer principle discussed in Sec. 1.6 is also derived, Sec. [5.3–4 p 50]. Here, the generalized relative entropy introduced in Eq. (72) assumes an information theoretical significance, as we show it to be a *relative entropy* [1]

$$\mathcal{D} \equiv \mathcal{D}(p \| p^{\text{ref}}) = \sum_n p_n \ln \frac{p_n}{p_n^{\text{eq}}} \geq 0. \quad (83)$$

This quantity can be regarded a measure of the dissimilarity between the nonequilibrium probability mass function p_n and p_n^{eq} , which is the equilibrium probability mass function obtained when turning off the fundamental forces, $\mathcal{F}_{y_f} = 0$ for all y_f , stopping the driving, $-\partial\Phi = 0$, and letting the system relax to equilibrium.

We now mention that the specialization of Eq. (75) to closed isothermal stochastic processes (no matter exchange) first appeared in the framework of stochastic thermodynamics as a generalization to nonequilibrium conditions of the Landauer principle [2, 3]. In its original formulation, this principle quantifies the minimal cost of erasing a bit of information, which can be regarded as a process of transforming a bit from an equilibrium state (bit equally likely to be found in 0 or 1) to a nonequilibrium state (bit found with probability one in 0), see Fig. 4. Equations (73) and (75), generalize this principle to any form of isothermal information processing, and for this reason we keep calling it *nonequilibrium Landauer principle*. In Eqs. [(74) and (76), p. 50], this principle is specialized to arbitrary isothermal stochastic processes.

We also formulate our nonequilibrium thermodynamic description at the level of single stochastic trajectories. At this level, all thermodynamic quantities described in Ch. 1 can be regarded as fluctuating quantities rather than averages Sec. [3.1–2, p. 45]. The importance of our entropy production de-

composition, Eqs. (58) and [(36), p. 45], will be emphasized as we show that the fluctuating expressions of $-\partial\Phi$ and $\{\mathcal{F}_{y_f}dX^{y_f}\}$ satisfy a fluctuation theorem, Eq. [(55), p. 47]. We recall that these relations are symmetries that the fluctuations of some thermodynamic observables obey arbitrarily far from equilibrium, see Eq. (4).

We further elaborate on fluctuation theorems in the second reprinted Article, p. 71, in which a unifying perspective on several of these relations is presented. This unification hinges on the following entropy production decomposition

$$d\Sigma = \underbrace{\sum_e A_e^{\text{ref}} d\zeta_e}_{=: d\Sigma_{\text{nc}}} + \underbrace{\sum_n p_n \partial \psi_n^{\text{ref}}}_{=: d\Sigma_d} - d\mathcal{D}(p||p^{\text{ref}}) \quad (84)$$

[(14)–(19), pp. 75–76], which is achieved when introducing a reference probability mass function, $p_n^{\text{ref}} = \exp -\psi_n^{\text{ref}}$, and the related affinities

$$A_e^{\text{ref}} := \ln \frac{d\zeta_e^{\text{ref}}}{d\zeta_{-e}^{\text{ref}}} = \ln \frac{d\zeta_e}{d\zeta_{-e}} + \sum_n (\psi_n^{\text{ref}} - \ln p_n) D_e^n \quad (85)$$

[(12) and (13), p. 74]. As we demonstrate, several known entropy production decompositions follow when considering specific references, p_n^{ref} . For instance, the decompositions in Eqs. (16) and (49) ensue when choosing the equilibrium probability mass function of the isolated and open system, Secs. [7–8, pp. 86–89]. As a major result, we show that when (i) the system is initially prepared in p_n^{ref} , and (ii) p_n^{ref} is determined solely by the parameters controlling the dynamics, then $d\Sigma_d$ and $d\Sigma_{\text{nc}}$ satisfy a fluctuation theorem, Eq. [(32), p. 77]. The fluctuation theorem for $-\partial\Phi$ and $\{\mathcal{F}_{y_f}dX^{y_f}\}$ Eq. [(55), p. 47] is recovered as a special case.

REFERENCES FOR CHAPTER 2

- [1] T. M. COVER and J. A. THOMAS, *Elements of Information Theory*, Wiley-Interscience, 2006.
- [2] K. TAKARA, H.-H. HASEGAWA and D. DRIEBE, “Generalization of the second law for a transition between nonequilibrium states”, *Phys. Lett. A* **375**.2 (2010), 88–92.
- [3] M. ESPOSITO and C. VAN DEN BROECK, “Second law and Landauer principle far from equilibrium”, *Europhys. Lett.* **95**.4 (2011), 40004.

The following article is reprinted from
[R. RAO and M. ESPOSITO, *New J. Phys.* **20**.2 (2018), 023007]
under the conditions of the Creative Commons Attribution 3.0 Unported
Licence¹.

The page numbers placed in the outer margins provide a continuous pagination throughout the thesis.

¹ <https://creativecommons.org/licenses/by/3.0/>

New Journal of Physics

The open access journal at the forefront of physics

Deutsche Physikalische Gesellschaft 

IOP Institute of Physics

Published in partnership with: Deutsche Physikalische Gesellschaft and the Institute of Physics



OPEN ACCESS

RECEIVED
7 September 2017

REVISED
3 December 2017

ACCEPTED FOR PUBLICATION
13 December 2017

PUBLISHED
5 February 2018

Original content from this work may be used under the terms of the Creative Commons Attribution 3.0 licence.

Any further distribution of this work must maintain attribution to the author(s) and the title of the work, journal citation and DOI.



PAPER

Conservation laws shape dissipation

Riccardo Rao  and Massimiliano Esposito 

Complex Systems and Statistical Mechanics, Physics and Materials Science Research Unit, University of Luxembourg, L-1511, Luxembourg

E-mail: riccardo.rao@uni.lu and massimiliano.esposito@uni.lu

Keywords: stochastic thermodynamics, network, fluctuation theorem, conservation law, entropy production, cycles, graph theory

Abstract

Starting from the most general formulation of stochastic thermodynamics—i.e. a thermodynamically consistent nonautonomous stochastic dynamics describing systems in contact with several reservoirs—we define a procedure to identify the conservative and the minimal set of nonconservative contributions in the entropy production. The former is expressed as the difference between changes caused by time-dependent drivings and a generalized potential difference. The latter is a sum over the minimal set of flux-force contributions controlling the dissipative flows across the system. When the system is initially prepared at equilibrium (e.g. by turning off drivings and forces), a finite-time detailed fluctuation theorem holds for the different contributions. Our approach relies on identifying the complete set of conserved quantities and can be viewed as the extension of the theory of generalized Gibbs ensembles to nonequilibrium situations.

1. Introduction

Stochastic thermodynamics provides a rigorous formulation of nonequilibrium thermodynamics for open systems described by Markovian dynamics [1–4]. Thermodynamic quantities fluctuate and the first and second law of thermodynamics can be formulated along single stochastic trajectories. Most notably, entropy-production fluctuations exhibit a universal symmetry, called fluctuation theorem (FT). This latter implies, among other things, that the average entropy production is non-negative. Besides being conceptually new, this framework has been shown experimentally relevant in many different contexts [5]. It also provides a solid ground to analyze energy conversion [3, 6, 7], the cost of information processing [8–12], and speed-accuracy trade-offs [13, 14] in small systems operating far from equilibrium.

In stochastic thermodynamics, the dynamics is expressed in terms of Markovian rates describing transition probabilities per unit time between states. The thermodynamics, on the other hand, assigns conserved quantities to each system state (e.g. energy and particle number). This means that transitions among states entail an exchange of these conserved quantities between the system and the reservoirs. The core assumption providing the connection between dynamics and thermodynamics is local detailed balance. It states that the log ratio of each forward and backward transition rate corresponds to the entropy changes in the reservoirs caused by the exchange of the conserved quantities (divided by the Boltzmann constant). These changes are expressed as the product of the entropic intensive fields characterizing the reservoirs (e.g. inverse temperature, chemical potential divided by temperature) and the corresponding changes of conserved quantities in the reservoirs, in accordance to the fundamental relation of equilibrium thermodynamics in the entropy representation.

Microscopically, the local detailed balance arises from the assumption that the reservoirs are at equilibrium [15].

In this paper, we ask a few simple questions which lie at the heart of nonequilibrium thermodynamics. We consider a system subject to time-dependent drivings—i.e. nonautonomous—and in contact with multiple reservoirs. What is the most fundamental representation of the EP for such a system? In other words, how many independent nonconservative forces multiplied by their conjugated flux appear in the EP? Which thermodynamic potential is extremized by the dynamics in absence of driving when the forces are set to zero? How do generic time-dependent drivings affect the EP? Surprisingly, up to now, no systematic procedure exists to answer these questions. We provide one in this paper based on a systematic identification of conserved

quantities. While some of them are obvious from the start (e.g. energy and particle number) the others are system specific and depend on the way in which reservoirs are coupled to the system and on the topology of the network of transitions.

The main outcome of our analysis is a rewriting of the EP, equation (36), which identifies three types of contributions: a driving contribution caused by the nonautonomous mechanisms, a change of a generalized Massieu potential, and a flow contribution made of a sum over a fundamental set of flux-force contributions. For autonomous systems relaxing to equilibrium—all forces must be zero—the first and the third contributions vanish and the dynamics maximizes the potential. This amounts to a dynamical realization of the maximization of the Shannon entropy under the constraints of conserved quantities, which is commonly done by hand when deriving generalized Gibbs distributions. For (autonomous) steady-state dynamics, the first two contributions vanish and we recover the results of [16], showing that conservation laws reduce the number of forces created by the reservoirs. The key achievement of this paper is to demonstrate that conservation laws are essential to achieve a general and systematic treatment of stochastic thermodynamics.

Important results ensue. We show that system-specific conservation laws can cause the forces to depend on system quantities and not only on intensive fields. We derive the most general formulation of finite-time detailed FTs expressed in terms of measurable quantities. This result amounts to make use of conservation laws on the FT derived in [17]. We identify the minimal cost required for making a transformation from one system state to another one. In doing so we generalize to multiple reservoirs the nonequilibrium Landauer's principle derived in [18–20]. We also apply our method to four different models which reveal different implications of our theory.

This paper is organized as follows. In section 2 we derive an abstract formulation of stochastic thermodynamics. We then describe the procedure to identify all conserved quantities, which we use to rewrite the local detailed balance in terms of potential and (nonconservative) flow contributions. In section 3 we use the above decomposition to establish balance equations along stochastic trajectories, which allow us to formulate our finite-time detailed FT, section 4. In section 5 we discuss the ensemble average description of our EP decompositions, as well as the nonequilibrium Landauer's principle. Four detailed applications conclude our analysis in section 6. The first is referenced systematically throughout the paper to illustrate our results. It describes two quantum dots coupled to three reservoirs. The second describes a quantum point contact tightly coupled to a quantum dot and shows that thermodynamic forces can depend on system features. The third is a molecular motor exemplifying the differences between conservative and nonconservative forces in relation to the topology of the network used to model it. The last one is a randomized grid illustrating that our formalism becomes essential when analyzing more complex systems.

2. Edge level description

After formulating stochastic thermodynamics for continuous-time Markov jump processes from a graph-theoretical perspective, we describe the general procedure to identify conservative and nonconservative contributions to the local detailed balance.

2.1. Stochastic dynamics

We consider an externally driven open system characterized by a discrete number of states, which we label by n . Allowed transitions between pairs of states, $n \xleftarrow{\nu} m$, are described by directed edges, $e \equiv (nm, \nu)$. The index $\nu = 1, \dots$ labels different types of transitions between the same pair of states, e.g. transitions due to different reservoirs. The time evolution of the probability of finding the system in the state n , $p_n \equiv p_n(t)$, is governed by the master equation

$$d_t p_n = \sum_e D_e^n \langle J^e \rangle, \quad (1)$$

which is here written as a continuity equation. Indeed, the *incidence matrix* D ,

$$D_e^n := \begin{cases} +1 & \text{if } \xrightarrow{e} n \\ -1 & \text{if } \xleftarrow{e} n \\ 0 & \text{otherwise} \end{cases}, \quad (2)$$

associates each edge to the pair of states that it connects. It thus encodes the *network topology*. On the graph identified by $\{n\}$ and $\{e\}$, it can be thought of as a (negative) divergence operator when acting on edge-space vectors—as in the master equation (1)—or as a gradient operator when acting on state-space vectors. The ensemble averaged edge probability currents,

$$\langle J^e \rangle = w_e p_{o(e)}, \quad (3)$$

Table 1. Summary of the indices used throughout the paper and the object they label.

Index	Label for	Number
n	State	N_n
e	Transition	N_e
κ	System quantity	N_κ
r	Reservoir	N_r
$y \equiv (\kappa, r)$	Conserved quantity Y^κ from reservoir r	N_y
α	Cycle	N_α
λ	Conservation law and conserved quantity	N_λ
y_p	'Potential' y	N_λ
y_f	'Force' y	$N_y - N_\lambda$
ρ	Symmetry	N_ρ
η	Fundamental cycle	$N_\alpha - N_\rho$ $= N_y - N_\lambda$

Table 2. Examples of system quantity-intensive field conjugated pairs in the entropy representation [21, sections 2 and 3]. $\beta_r := 1/T_r$ denotes the inverse temperature of the reservoir. Since charges are carried by particles, the conjugated pair $(Q_{nr} - \beta_r V_r)$ is usually embedded in $(N_{nr} - \beta_r \mu_r)$, see e.g. [22, section 1.7.2, 23].

System quantity Y^κ	Intensive field $f_{(\kappa, r)}$
Energy, E_n	Inverse temperature, β_r
Particles number, N_n	Chemical potential, $-\beta_r \mu_r$
Charge, Q_n	Electric potential, $-\beta_r V_r$
Displacement, X_n	Generic force, $-\beta_r k_r$
Angle, θ_n	Torque, $-\beta_r \tau_r$

are expressed in terms of the transition rates, $\{w_e \equiv w_e(t)\}$, which describe the probability per unit time of observing a transition along the edge e . The function

$$o(e) := m, \quad \text{for } \xleftarrow{e} m, \quad (4)$$

maps each edge into the state from which it originates. For thermodynamic consistency, each transition $e \equiv (nm, \nu)$ with finite rate w_e has a corresponding backward transition $-e \equiv (mn, \nu)$ with a finite rate w_{-e} . The stochastic dynamics is assumed to be ergodic at any time.

Notation. From now on, upper-lower indices and Einstein summation notation will be used: repeated upper-lower indices implies the summation over all the allowed values for those indices. The meaning of all the indices that will be used is summarized in table 1. Time derivatives are denoted by 'd_t' or 'd_t' whereas the overdot '·' is reserved for rates of change of quantities that are not exact time derivatives. We also take the Boltzmann constant k_B equal to 1.

2.2. Stochastic thermodynamics

Physically, each system state, n , is characterized by given values of some *system quantities*, $\{Y_n^\kappa\}$, for $\kappa = 1, \dots, N_\kappa$, which encompass the internal energy, E_n , and possibly additional ones, see table 2 for some examples. These must be regarded as *conserved quantities* in the total system, as their change in the system is always balanced by an opposite change in the reservoirs. Indeed, when labeling the reservoirs with $\{r\}$, for $r = 1, \dots, N_r$, the balance equation for Y^κ can be written as

$$\underbrace{Y_n^\kappa - Y_m^\kappa}_{\text{system}} \equiv \underbrace{Y_{n'}^\kappa D_e^{n'}}_r = \sum_r \underbrace{\delta Y_e^{(\kappa, r)}}_{\text{reservoir } r}. \quad (5)$$

where $\delta Y_e^{(\kappa, r)}$ quantifies the flow of Y^κ supplied by the reservoir r to the system along the transition e . For the purpose of our discussion, we introduce the index $y = (\kappa, r)$, i.e. the *conserved quantity* Y^κ exchanged with the reservoir r , and define the matrix δY whose entries are $\{\delta Y_e^y \equiv \delta Y_e^{(\kappa, r)}\}$. Enforcing microscopic reversibility, one concludes that $\delta Y_e^y = -\delta Y_{-e}^y$. As a first remark, more than one reservoir may be involved in each transition, see

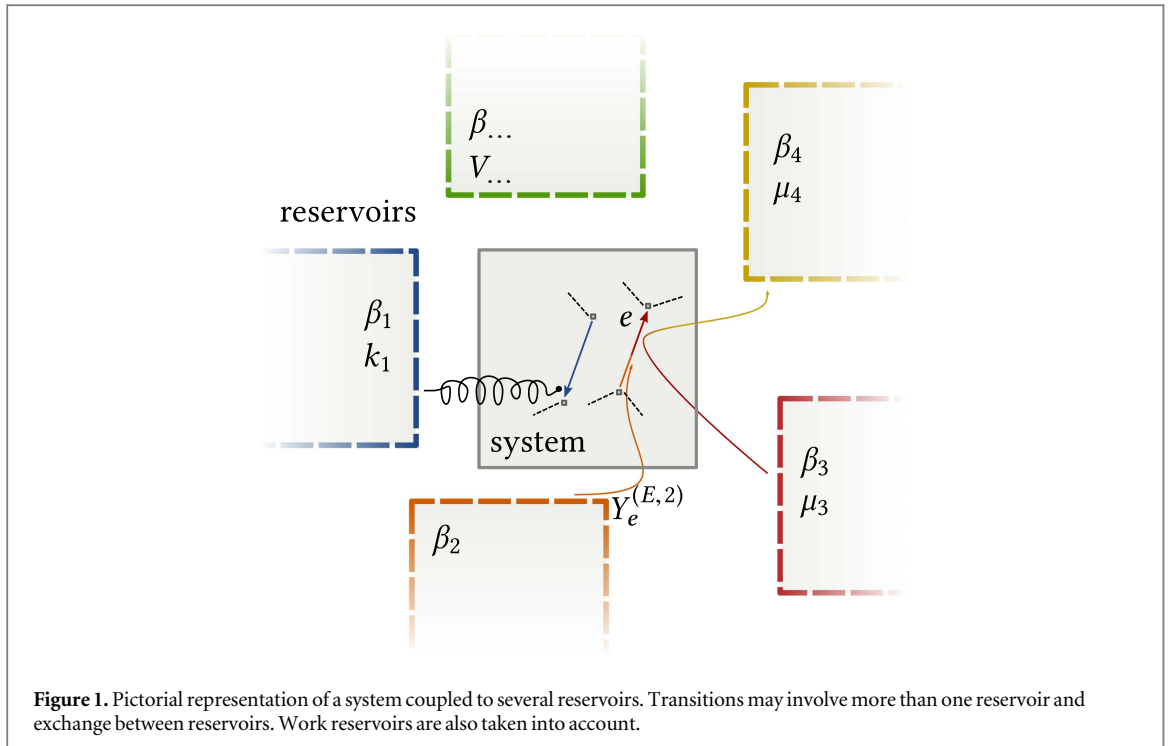


figure 1 and the application in section 6.2. As a second remark, the conserved quantities may not be solely $\{Y^\kappa\}$, since additional ones may arise due to the topological properties of the system, as we will see in the next subsection.

Each reservoir r is characterized by a set of *entropic intensive fields*, $\{f_{(\kappa, r)}\}$ for $\kappa = 1, \dots, N_r$, which are conjugated to the exchange of the system quantities $\{Y^\kappa\}$ [21, sections 2 and 3]. A short list of $Y^\kappa - f_{(\kappa, r)}$ conjugated pairs is reported in table 2. The thermodynamic consistency of the stochastic dynamics is ensured by the *local detailed balance property*,

$$\ln \frac{w_e}{w_{-e}} = -f_y \delta Y_e^\kappa + S_n D_e^n. \quad (6)$$

It relates the log ratio of the forward and backward transition rates to the entropy change generated in the reservoirs, i.e. minus the entropy flow $\{-f_y \delta Y_e^\kappa\}$. The second term on the rhs is the internal entropy change occurring during the transition, since S_n denotes the internal entropy of the state n . This point is further evidenced when writing the entropy balance along a transition

$$\ln \frac{w_e p_{o(e)}}{w_{-e} p_{o(-e)}} = \sum_r \left\{ - \sum_\kappa f_{(\kappa, r)} \delta Y_e^{(\kappa, r)} \right\} + [S_n - \ln p_n] D_e^n, \quad (7)$$

which expresses the edge EP, the lhs, as the entropy change in each reservoir r plus the system entropy change, the rhs. See section 6.1.1 for explicit examples of δY and $\{f_y\}$.

In the most general formulation, the internal entropy S , the conserved quantities $\{Y^\kappa\}$ (hence $\{\delta Y_e^\kappa\}$), and their conjugated fields $\{f_y\}$, change in time. Physically, this modeling corresponds to two possible ways of controlling a system: either through $\{Y^\kappa\}$ or S which characterize the system states, or through $\{f_y\}$ which characterize the properties of the reservoirs. Throughout the paper, we use the word ‘driving’ to describe any of these time-dependent controls, while we refer to those systems that are not time-dependently driven as *autonomous*.

2.3. Network-specific conserved quantities

We now specify the procedure to identify the complete set of conserved quantities of a system. In doing so, we extend the results of [16]. For this purpose, let $\{C_\alpha\}$ for $\alpha = 1, \dots, N_\alpha$, be an independent set of network *cycles*. Algebraically, $\{C_\alpha\}$ is a maximal set of independent vectors in $\ker D$,

$$D_e^n C_\alpha^e = 0, \quad \text{for all } n, \quad (8)$$

in which at most one entry in each forward–backward transition pair is nonzero. Since D is $\{-1, 0, 1\}$ -valued, $\{C\}_\alpha$ can always be chosen in such a way that their entries are $\{0, 1\}$. In this representation, their 1-entries

identify sets of transitions forming loops. In the examples, we will represent cycles using the set of forward transitions only, and negative entries denote transitions along the backward direction. We denote the matrix whose columns are $\{C_\alpha\}$ by $C \equiv \{C_\alpha^e\}$.

By multiplying the matrices δY and C , we obtain the M -matrix [16]:

$$M_\alpha^y := \delta Y_e^y C_\alpha^e. \quad (9)$$

This fundamental matrix encodes the *physical topology* of the system. It describes the ways in which the conserved quantities $\{Y^\kappa\}$ are exchanged between the reservoirs across the system, as its entries quantify the influx of $\{y\}$ along each cycle, α . The physical topology is clearly built on top of the network topology encoded in C .

The basis vectors of the coker M , are defined as the system conservation laws. They are denoted by $\{\ell^\lambda\}$ for $\lambda = 1, \dots, N_\lambda$ where $N_\lambda := \dim \text{coker } M$ and satisfy

$$\ell_y^\lambda \delta Y_e^y C_\alpha^e = \ell_y^\lambda M_\alpha^y = 0, \quad \text{for all } \alpha. \quad (10)$$

From (8), this implies that $\ell^\lambda \delta Y \in (\ker D)^\perp$. Since $(\ker D)^\perp \equiv \text{coim } D$, one can introduce a set of states-space vectors $\{L^\lambda\}$ —i.e. state variables in the states space—which are mapped into $\{\ell^\lambda \delta Y\}$ by the transpose of D :

$$L_n^\lambda D_e^n = \ell_y^\lambda \delta Y_e^y \equiv \sum_r \left\{ \sum_\kappa \ell_{(\kappa, r)}^\lambda \delta Y_e^{(\kappa, r)} \right\}. \quad (11)$$

The properties of the incidence matrix guarantee that each L^λ is defined up to a reference value, see e.g. [24, section 6.2]. We thus confirm that $\{L^\lambda\}$ are *conserved quantities* since equation (11) are their balance equations: the lhs identifies the change of $\{L^\lambda\}$ in the system, while the rhs expresses their change in the reservoirs. The thermodynamic implications of shifting the reference values of $\{L^\lambda\}$ are discussed in section 3.

Importantly, the vector space spanned by the conserved quantities, $\{L^\lambda\}$, encompasses the system quantities $\{Y^\kappa\}$. They correspond to $\ell_y^\kappa \equiv \ell_{(\kappa', r)}^\kappa = \delta_{\kappa'}^\kappa$, so that the balance equation (5) are recovered. The remaining conservation laws arise from the interplay between the *specific* topology of the network, C , and its coupling with the reservoirs, δY , and we will refer to them as *nontrivial*. Only for these, the row vector ℓ may depend on time since M is a function of time, see section 6.1.2 and the application in section 6.2.

Variations in time of the system quantities $\{Y^\kappa\}$ induce changes in the matrix M . If these changes cause a modification of the size of its cokernel, i.e. a change in the number of conserved quantities, we say that the physical topology was altered. We emphasize that these changes are not caused by changes in the network topology since this latter remains unaltered. An example of physical topology transformation is given in section 6.1.2 and in the application in section 6.4, while one of network topology is discussed in section 6.3.

Remark. The introduction of the conserved quantities is akin to that of scalar potentials for irrotational fields in continuous space. Indeed, the vector $\ell^\lambda \delta Y$ replaces the field, D^T plays the role of the gradient operator, and L^λ becomes the potential. The condition expressed by equation (10) is that of irrotational fields, as it tells us that $\ell^\lambda \delta Y$ vanishes along all loops.

2.4. Network-specific local detailed balance

We now make use of the conserved quantities, $\{L^\lambda\}$, to separate the conservative contributions in the local detailed balance (6) from the nonconservative ones. This central result will provide the basis for our EP decomposition in section 3.

We start by splitting the set $\{y\}$ into two groups: a ‘potential’ one $\{y_p\}$, and a ‘force’ one $\{y_f\}$. The first must be constructed with N_λ elements such that the matrix whose entries are $\{\ell_{y_p}^\lambda\}$ is nonsingular. We denote the entries of the inverse of the latter matrix by $\{\bar{\ell}_\lambda^{y_p}\}$. Crucially, since the rank of the matrix whose rows are $\{\ell^\lambda\}$ is N_λ , it is always possible to identify a set of $\{y_p\}$. However, it may not be unique and different sets have different physical interpretations, see sections 6.1.3 and 6.1.6 as well as the following sections. The second group, $\{y_f\}$, is constructed with the remaining $N_y - N_\lambda$ elements of $\{y\}$.

With the above prescription, we can write the entries $\{\delta Y_e^{y_p}\}$ as functions of $\{\delta Y_e^{y_f}\}$ and $\{L_n^\lambda\}$ by inverting $\{\ell_{y_p}^\lambda\}$ in equation (11),

$$\delta Y_e^{y_p} = \bar{\ell}_\lambda^{y_p} L_n^\lambda D_e^n - \bar{\ell}_\lambda^{y_p} \ell_{y_f}^\lambda \delta Y_e^{y_f}. \quad (12)$$

The local detailed balance (6) can thus be rewritten as

$$\ln \frac{w_e}{w_{-e}} = \phi_n D_e^n + \mathcal{F}_{y_f} \delta Y_e^{y_f}. \quad (13)$$

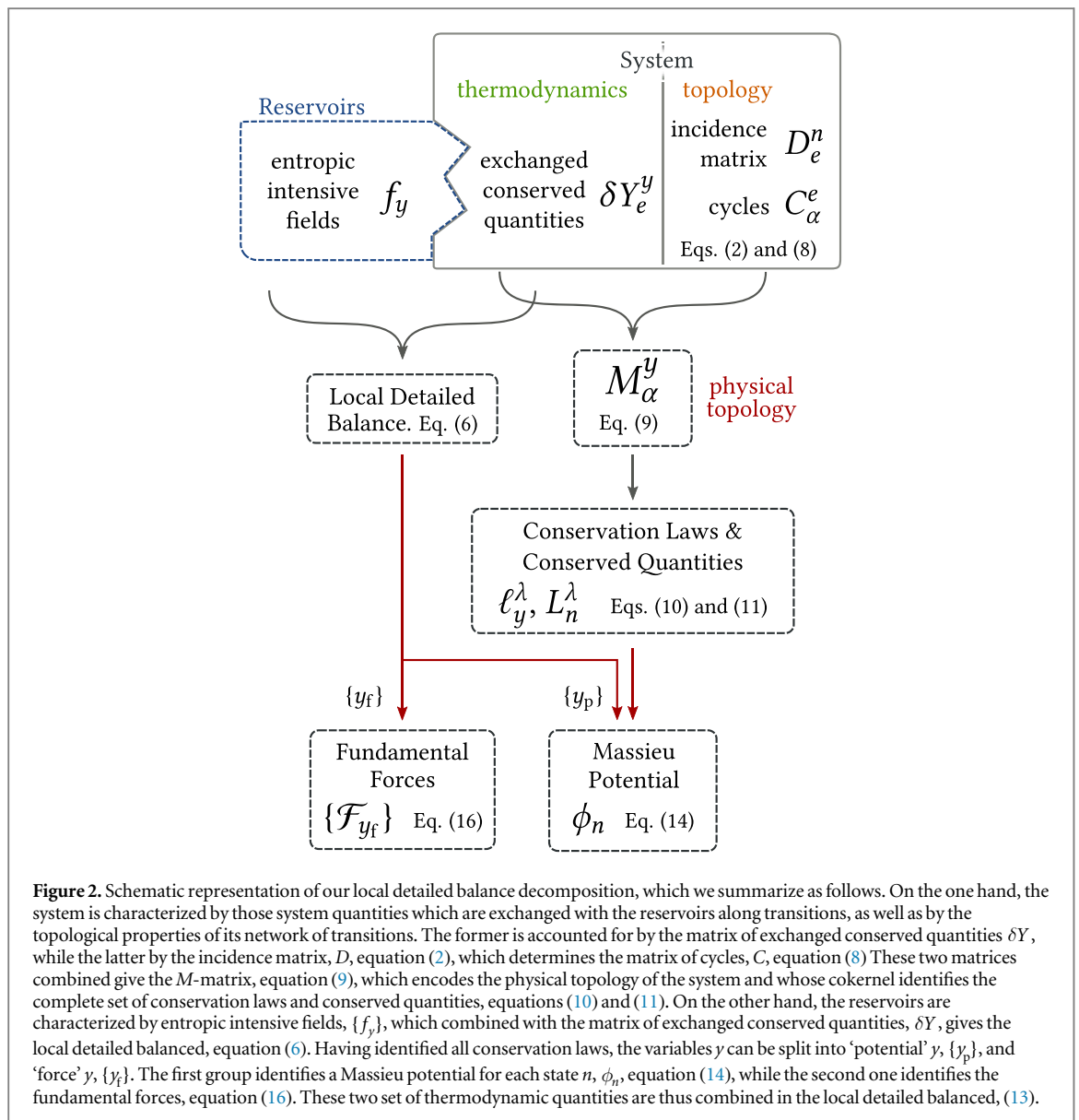


Figure 2. Schematic representation of our local detailed balance decomposition, which we summarize as follows. On the one hand, the system is characterized by those system quantities which are exchanged with the reservoirs along transitions, as well as by the topological properties of its network of transitions. The former is accounted for by the matrix of exchanged conserved quantities δY , while the latter by the incidence matrix, D , equation (2), which determines the matrix of cycles, C , equation (8). These two matrices combined give the M -matrix, equation (9), which encodes the physical topology of the system and whose cokernel identifies the complete set of conservation laws and conserved quantities, equations (10) and (11). On the other hand, the reservoirs are characterized by entropic intensive fields, $\{f_y\}$, which combined with the matrix of exchanged conserved quantities, δY , gives the local detailed balanced, equation (6). Having identified all conservation laws, the variables y can be split into ‘potential’ y_p , $\{y_p\}$, and ‘force’ y_f , $\{y_f\}$. The first group identifies a Massieu potential for each state n , ϕ_n , equation (14), while the second one identifies the fundamental forces, equation (16). These two set of thermodynamic quantities are thus combined in the local detailed balanced, (13).

The first contribution is conservative since it derives from the *potential*

$$\phi_n := S_n - F_\lambda L_n^\lambda, \quad (14)$$

where

$$F_\lambda := f_{y_p} \bar{\ell}_\lambda^{y_p} \quad (15)$$

is a linear combination of entropic intensive fields. Since ϕ_n is the entropy of the state n minus a linear combination of conserved quantities, it can be viewed as the Massieu potential of the state n . (We recall that Massieu potentials are the thermodynamic potentials of the entropy representation, see e.g. [21, section 5-4]. In contrast, the nonconservative *fundamental forces*,

$$\mathcal{F}_{y_f} := f_{y_f} \bar{\ell}_\lambda^{y_p} \ell_{y_f}^\lambda - f_{y_f}, \quad (16)$$

are caused by the presence of multiple reservoirs. As we will show, they control the currents of system quantities through the system. Importantly, ‘fundamental’ must be understood as a property of the set of these forces, since they are independent and in minimal number.

The identification of ϕ_n and $\{\mathcal{F}_{y_f}\}$ and their relation with the local detailed balance, equation (13), is the key result of our paper and we summarize the procedure we used in figure 2. The complete set of conservation laws played an essential role in this identification.

We saw that driving in the system quantities $\{Y^\kappa\}$, may induce changes in the physical topology, whereas the driving in the reservoir properties, $\{f_y\}$ —as well as in the entropy, S —is unable to do so. Since these changes modify the cokernel of M , ϕ_n and $\{\mathcal{F}_{y_f}\}$ are modified as well: when conservation laws are broken new

fundamental forces emerge, and vice versa the emergence of conservation laws breaks some fundamental forces and creates additional terms in ϕ_n , see section 6.1.3.

Even in absence of topological changes, the form of ϕ_n and $\{\mathcal{F}_{\gamma_i}\}$ may change in presence of driving. It is clear that ϕ_n changes when S , $\{Y^\kappa\}$, or $\{f_{\gamma_p}\}$ change, see equation (14). In turn, each fundamental force \mathcal{F}_{γ_i} depends on both f_{γ_i} and $\{f_{\gamma_p}\}$, see equation (16). But in presence of nontrivial conservation laws, they may also depend on the system quantities $\{Y^\kappa\}$ via the vectors $\{\mathcal{C}^\lambda\}$, see section 6.1.3 and the application in section 6.2. Notice that while driving not caused by temperatures solely affects a given intensive field, driving via temperature, say $\beta_{r'}$, affects all the fields associated to r' , namely $\{f_{(\kappa, r')}\}$ for $\kappa = 1, \dots, N_\kappa$, see table 2.

2.5. Fundamental cycles

We now express our conservative–nonconservative forces decomposition of the local detailed balance in terms of cycle affinities. This provides the basis on which our potential–cycle affinities EP decomposition hinges on, section 3.3.

The thermodynamic forces acting along cycles are referred to as *cycle affinities*. Using the local detailed balance (13), they read

$$\mathcal{A}_\alpha := C_\alpha^e \ln \frac{w_e}{w_{-e}} = \mathcal{F}_{\gamma_i} M_{\alpha}^{\gamma_i}. \quad (17)$$

As observed in [16], different cycles may be connected to the same set of reservoirs, thus carrying the same cycle affinity. These are regarded as *symmetries* and they correspond to bases of $\ker M$, $\{\psi_\rho\}$ for $\rho = 1, \dots, N_\rho := \dim \ker M$,

$$M_\alpha^\gamma \psi_\rho^\alpha = 0, \quad \text{for all } \gamma, \quad (18)$$

as their entries identify sets of cycles which, once completed, leave the state of the reservoirs unchanged. A notable consequence is that the affinities corresponding to these sets of cycles are zero irrespective of the fields $\{f_\gamma\}$. The rank-nullity theorem applied to the matrix M allows us to relate the number of symmetries to the number of conservation laws [16]

$$N_y - N_\lambda = N_\alpha - N_\rho. \quad (19)$$

Notice that, while the N_y and N_α are fixed for a given system, N_λ , and hence N_ρ , can change due to changes in the physical topology. From equation (19) we thus learn that for any broken (resp. created) conservation law, a symmetry must break (resp. be created), see section 6.1.4 and the application in section 6.4.

The symmetries given by equation (18) lead us to identify $N_\eta := N_\alpha - N_\rho$ cycles, labeled by η , which correspond to linearly independent columns of M . These cycles can be thought of as physically independent, since they cannot be combined to form cycles that leave the reservoirs unchanged upon completion. In other words, they are the minimal subset of cycles whose affinity is nonzero for a generic choice of the fields $\{f_\gamma\}$ (specific choices of $\{f_\gamma\}$ can always make any cycle affinity equal to zero). We refer to these cycles as *fundamental cycles* and to their affinities as *fundamental affinities*. The fact that the matrix whose entries are $\{M_{\eta}^{\gamma_i}\}$ is square and nonsingular, see appendix A, allows us to see the one-to-one correspondence between fundamental forces, equation (16), and these affinities,

$$\mathcal{F}_{\gamma_i} = \mathcal{A}_\eta \bar{M}_{\gamma_i}^\eta, \quad (20)$$

where $\{\bar{M}_{\gamma_i}^\eta\}$ are the entries of the inverse matrix of that having $\{M_{\eta}^{\gamma_i}\}$ as entries. In terms of $\{\mathcal{A}_\eta\}$, the local detailed balance, equation (13), reads

$$\ln \frac{w_e}{w_{-e}} = \phi_n D_e^n + \mathcal{A}_\eta \zeta_e^\eta, \quad (21)$$

where

$$\zeta_e^\eta := \bar{M}_{\gamma_i}^\eta \delta Y_e^{\gamma_i} \quad (22)$$

quantifies the contribution of each transition e to the current along the fundamental cycle η as well as all those cycles which are physically dependent on η . Algebraically, the row vectors of ζ , $\{\zeta^\eta\}$, are dual to the physically independent cycles, $\{C_\eta\}$,

$$\zeta_e^\eta C_{\eta'}^e = \bar{M}_{\gamma_i}^\eta \delta Y_e^{\gamma_i} C_{\eta'}^e = \bar{M}_{\gamma_i}^\eta M_{\eta'}^{\gamma_i} = \delta_{\eta'}^\eta. \quad (23)$$

Equation (21) is another key result of our paper, which expresses the conservative–nonconservative local detailed balance decomposition in terms of fundamental affinities. Importantly, the affinities $\{\mathcal{A}_\eta\}$ depend on time both via $\{f_\gamma\}$ and $\{Y^\kappa\}$, where the latter originates from the M -matrix, equation (17). Differently from $\{\mathcal{F}_{\gamma_i}\}$, they always have the dimension of an entropy.

Remark. Our set of fundamental cycles differs from that constructed with spanning trees and discussed by Schnakenberg in [25]. Algebraically, our set is not merely in $\ker D$, but rather in $\ker D \setminus \ker M$. Furthermore, it is not constructed from the spanning trees of the graph.

2.6. Detailed-balanced networks

We now focus on a specific class of dynamics called *detailed balanced*. These dynamics are such that either there are no forces ($\{y_f\} = \emptyset$) or these are zero,

$$\mathcal{F}_{y_f} = f_{y_p} \bar{\ell}_\lambda^{y_p} \ell_\lambda^y - f_{y_f} = 0, \quad (24)$$

—equivalently the affinities are zero, see equation (17). A driven detailed-balanced dynamics implies that the driving must keep the forces equal to zero at all times, while changing the potential ϕ_n . An autonomous detailed-balanced dynamics will always relax to an equilibrium distribution [26, 27]

$$p_n^{\text{eq}} = \exp\{\phi_n - \Phi_{\text{eq}}\}, \quad (25)$$

defined by the detailed balance property: $w_e p_{o(e)}^{\text{eq}} = w_{-e} p_{o(-e)}^{\text{eq}}$, for all e . The last term, Φ_{eq} , is the logarithm of the partition function

$$\Phi_{\text{eq}} := \ln \left\{ \sum_m \exp\{\phi_m\} \right\}, \quad (26)$$

and can be identified as an *equilibrium Massieu potential* [21, sections 5-4 and 19-1, 28, section 3.13].

We now point out that one can transform a nondetailed-balance dynamics with the potential ϕ_n into a detailed-balanced dynamics with the same potential, if one can turn off the forces—set them to zero—without changing the potential. This is always possible through an appropriate choice of the fields $\{f_{y_f}\}$, viz.

$f_{y_f} = f_{y_p} \bar{\ell}_\lambda^{y_p} \ell_\lambda^y$, except for the following cases: when there are f_{y_f} such that $f_{y_f} = \beta_{r'}$ (i.e. f_{y_f} is the field conjugated with the exchange of energy with the reservoir r') and r' is among the reservoirs involved in $\{y_p\}$, then turning off the corresponding force \mathcal{F}_{y_f} via f_{y_f} will modify $\{f_{y_p}\}$ and in turn ϕ_n . Due to their importance for our FT, section 4, we label these fields by $\{y_f'\}$, to discriminate them from the other ones, denoted by $\{y_f''\}$. We finally observe that for isothermal processes all thermal gradients vanish beforehand, and one realizes that $\mathcal{F}_{y_f'} = 0$ for all y_f' , see e.g. sections 6.3 and 6.4. Therefore, turning off the forces never changes the potential.

Remark. The equilibrium distribution, equation (25), is clearly the same one would obtain using a maximum entropy approach [28, section 3.17, 29]. Indeed, the distribution maximizing the entropy functional constrained by given values of the average conserved quantities $\{\langle L^\lambda \rangle = L^\lambda\}$,

$$\mathcal{S}[p] = \sum_n p_n [S_n - \ln p_n] - a \left(\sum_n p_n - 1 \right) - a_\lambda \left(\sum_n p_n L_n^\lambda - L^\lambda \right), \quad (27)$$

is given by

$$p_n^* = \exp\{S_n - a_\lambda L_n^\lambda - a\}. \quad (28)$$

This is the equilibrium distribution, equation (25), when the Lagrange multipliers are given by $a = \Phi_{\text{eq}}$ and $a_\lambda = F_\lambda$, see equations (14) and (26).

3. Trajectory level description

We now bring our description from the level of edges to trajectories. A stochastic *trajectory* of duration t , \mathbf{n}_t , is defined as a set of transitions $\{e_i\}$ sequentially occurring at times $\{t_i\}$ starting from n_0 at time 0. If not otherwise stated, the transitions index i runs from $i = 1$ to the last transition prior to time t , N_t , whereas the state at time $\tau \in [0, t]$ is denoted by n_τ . The values of S , $\{Y^\kappa\}$, and $\{f_y\}$ between time 0 and an arbitrary time t are all encoded in the *protocol* π_τ , for $\tau \in [0, t]$.

We first derive the balance for the conserved quantities, equation (11). The conservative and nonconservative contributions identified at the level of single transitions via the local detailed balance, equations (13) and (21), are then used to decompose the trajectory EP into its three fundamental contributions.

3.1. Balance of conserved quantities

Since the conserved quantities are state variables their change along a trajectory for a given protocol reads

$$\Delta L^\lambda[\mathbf{n}_t] = L_{n_t}^\lambda(t) - L_{n_0}^\lambda(0) = \int_0^t d\tau \{\partial_\tau L_n^\lambda(\tau)|_{n=n_\tau} + L_n^\lambda(\tau) D_e^n J^e(\tau)\}. \quad (29)$$

The first term on the rhs accounts for the instantaneous changes due to the time-dependent driving, while the second accounts for the finite changes due to stochastic transitions, since

$$J^e(\tau) := \sum_i \delta_{e_i}^e \delta(\tau - t_i) \quad (30)$$

are the trajectory-dependent instantaneous currents at time τ . Using the edge-wise balance, equation (11), we can recast the above equation into

$$\Delta L^\lambda[\mathbf{n}_t] = \int_0^t d\tau \{\partial_\tau L_n^\lambda(\tau)|_{n=n_\tau} + \ell_y^\lambda(\tau) I^y(\tau)\}, \quad (31)$$

where the physical currents

$$I^y(\tau) := \delta Y_e^y(\tau) J^e(\tau), \quad (32)$$

quantify the instantaneous influx of y at time t .

3.2. Entropy balance

The trajectory entropy balance is given by

$$\Sigma[\mathbf{n}_t] = \int_0^t d\tau J^e(\tau) \ln \frac{w_e(\tau)}{w_{-e}(\tau)} - \ln \frac{p_{n_t}(t)}{p_{n_0}(0)} = - \int_0^t d\tau f_y(\tau) \delta Y_e^y(\tau) J^e(\tau) + \left[(S_{n_t} - S_{n_0}) - \ln \frac{p_{n_t}(t)}{p_{n_0}(0)} \right]. \quad (33)$$

As for the edge-wise balance, equation (7), the lhs is the EP, while the first and second term on the rhs are the entropy change of the reservoirs and the entropy change of the system [25, 30]. Using our decomposition of the local detailed balance, equation (13), we can recast the latter equality into

$$\Sigma[\mathbf{n}_t] = - \ln \frac{p_{n_t}(t)}{p_{n_0}(0)} + \int_0^t d\tau \{\phi_n(\tau) D_e^n J^e(\tau) + \mathcal{F}_{y_f}(\tau) I^{y_f}(\tau)\}. \quad (34)$$

Since ϕ_n is a state variable, its variations along the trajectory can be written as

$$\Delta\phi[\mathbf{n}_t] = \phi_{n_t}(t) - \phi_{n_0}(0) = \int_0^t d\tau \{\phi_n(\tau) D_e^n J^e(\tau) + \partial_\tau \phi_n(\tau)|_{n=n_\tau}\}. \quad (35)$$

By combining equations (34) and (35), we can recast the trajectory EP in

$$\Sigma[\mathbf{n}_t] = \nu[\mathbf{n}_t] + \Delta\Phi[\mathbf{n}_t] + \sum_{y_f} \sigma_{y_f}[\mathbf{n}_t], \quad (36)$$

where

$$\nu[\mathbf{n}_t] := - \int_0^t d\tau \partial_\tau \phi_n(\tau)|_{n=n_\tau}, \quad (37)$$

$$\Delta\Phi[\mathbf{n}_t] = \Phi_{n_t}(t) - \Phi_{n_0}(0), \quad (38)$$

$$\sigma_{y_f}[\mathbf{n}_t] := \int_0^t d\tau \mathcal{F}_{y_f}(\tau) I^{y_f}(\tau), \quad (39)$$

with

$$\Phi_n := \phi_n - \ln p_n. \quad (40)$$

Equation (36), is the major result of our paper. It shows the EP decomposed into a time-dependent driving contribution, a potential difference, and a minimal set of flux-force terms. The first term only arises in presence of time-dependent driving. It quantifies the entropy dissipated when ϕ_n is modified and we refer to it as the *driving contribution*. The second term is entirely conservative as it involves a difference between the final and initial *stochastic Massieu potential*, equation (40). The last terms are nonconservative and prevent the systems from reaching equilibrium. Each $\sigma_{y_f}[\mathbf{n}_t]$ quantifies the entropy produced by the flow of $\{y_f\}$, and we refer to them as *flow contributions*.

To develop more physical intuition of each single term, we now discuss them separately and consider some specific cases. When writing the rate of driving contribution explicitly, equation (37), one obtains

$$-\partial_\tau \phi_n = -\partial_\tau S_n + \partial_\tau F_\lambda L_n^\lambda + F_\lambda \partial_\tau L_n^\lambda. \quad (41)$$

Table 3. Entropy production for common processes. ‘0’ denotes vanishing or negligible contribution, NESS is the acronym of *nonequilibrium steady state*.

Dynamics	ν	$\Delta\Phi$	σ
Autonomous	0		
NESS	0	0	
Driven detailed-balanced			0
Autonomous detailed-balanced	0		0

When all $\{\mathcal{C}^\lambda\}$ are independent from system quantities, the terms, $\{\partial_\tau F_\lambda L_{\lambda,n}\}$, account for the entropy dissipated during the manipulation of the intensive fields $\{f_{\gamma_p}\}$, equation (15). In contrast, $\{F_\lambda \partial_\tau L_{\lambda,n}\}$ and $-\partial_\tau S_n$ characterize the dissipation due to the direct manipulation of the system quantities. Clearly, the changes of those fields that do not appear in ϕ_n do not contribute to $\nu[\mathbf{n}_t]$.

For autonomous processes, the EP becomes

$$\Sigma[\mathbf{n}_t] = \Delta\Phi[\mathbf{n}_t] + \mathcal{F}_{\gamma_f} \mathcal{I}^{\gamma_f}[\mathbf{n}_t], \quad (42)$$

where

$$\mathcal{I}^{\gamma_f}[\mathbf{n}_t] := \int_0^t d\tau I^{\gamma_f}(\tau), \quad (43)$$

are the currents of $\{\gamma_f\}$ integrated along the trajectory. The difference between the final and initial stochastic Massieu potential captures the dissipation due to changes of the internal state of the system. For finite-dimensional autonomous processes, it is typically subextensive in time and negligible with respect to the nonconservative terms for long trajectories

$$\Sigma[\mathbf{n}_t] \xrightarrow{t \rightarrow \infty} \mathcal{F}_{\gamma_f} \mathcal{I}^{\gamma_f}[\mathbf{n}_t]. \quad (44)$$

The nonconservative flow contributions, equations (39) and (44), quantify the dissipation due to the flow of conserved quantities across the network. Finally, for autonomous detailed-balanced systems, the nonconservative terms vanish, in agreement with the fact that these systems exhibit no net flows, and the EP becomes

$$\Sigma[\mathbf{n}_t] = \Delta\Phi[\mathbf{n}_t]. \quad (45)$$

Table 3 summarizes the contributions of the EP for these common processes. We now proceed with three remarks.

Remark. We have already discussed the possibility of physical topology modifications due to driving, which consequently alter ϕ_n and $\{\mathcal{F}_{\gamma_p}\}$. For protocols crossing points in which these modifications occur, the trajectory must be decomposed into subtrajectories characterized by the same physical-topology. For each of these, our decomposition (36) applies.

Remark. The contributions of the EP in equation (36) depend on the choice of $\{\gamma_p\}$ and $\{\gamma_f\}$. When aiming at quantifying the dissipation of a physical system, some choices may be more convenient than others depending on the experimental apparatus, see e.g. section 6.1.6. This freedom can be thought of as a gauge of the EP. In the long time limit, it only affects the flow contributions and it can be understood as a particular case of the gauge freedoms discussed in [31, 32], which hinge on graph-theoretical arguments.

Remark. The driving contribution ν and the nonequilibrium Massieu potential Φ_n are defined up to a gauge. This is evidenced when transforming the state variables $\{L^\lambda\}$ according to

$$L_n^\lambda(t) \rightarrow U_{\lambda'}^\lambda L_n^{\lambda'}(t) + u^\lambda 1_n, \quad (46)$$

where $\{U_{\lambda'}^\lambda\}$ identify a nonsingular matrix, $\{u^\lambda\}$ are finite coefficients, and $\{1_n\}$ a vector whose entries are 1. The first term can be considered as a basis change of $\text{coker}M$,

$$\ell_y^\lambda \rightarrow U_{\lambda'}^\lambda \ell_y^{\lambda'}, \quad (47)$$

while the second as a *reference shift* of L^λ . Under the transformation (47), the fields (15) transform as

$$F_\lambda(t) \rightarrow F_\lambda(t) \bar{U}_\lambda^{\lambda'}, \quad (48)$$

where $U_\lambda^{\lambda'} \bar{U}_{\lambda''}^{\lambda'} = \bar{U}_\lambda^{\lambda'} U_{\lambda''}^{\lambda'} = \delta_{\lambda''}^{\lambda'}$, thus guaranteeing that scalar products are preserved. As a consequence, the stochastic Massieu potential, equation (40), and the rate of driving contribution, equation (41), transform as

$$\Phi_n(t) \rightarrow \Phi_n(t) - \mathfrak{f}(t) \mathbf{1}_n, \text{ and } -\partial_t \phi_n(t) \rightarrow -\partial_t \phi_n(t) + \partial_t \mathfrak{f}(t) \mathbf{1}_n, \quad (49)$$

where

$$\mathfrak{f}(t) := F_{\lambda'}(t) \overline{U}_{\lambda}^{\lambda'} u^{\lambda}. \quad (50)$$

Crucially, neither the local detailed balance (13) nor the EP (69) are affected, as the physical process is not altered. If only a basis change is considered, $\{u^{\lambda} = 0\}$, then $\mathfrak{f}(t) = 0$, and both Φ_n and v are left unvaried. Finally, for cyclic protocols, one readily sees that the driving work over a period is gauge invariant, since $\mathfrak{f}(t)$ is nonfluctuating.

The above gauge is akin to that affecting the potential-work connection and which led to several debates, see [33] and references therein. The problem is rooted in what is experimentally measured, as different experimental set-ups constrain to different gauge choices [33]. We presented a general formulation of the gauge issue, by considering reference shifts of any conserved quantity, and not only of energy.

3.3. Entropy balance along fundamental cycles

An equivalent decomposition of the EP, equation (33), can be achieved using the potential-affinities decomposition of the local detailed balance, equation (21)

$$\Sigma[\mathbf{n}_t] = v[\mathbf{n}_t] + \Delta\Phi[\mathbf{n}_t] + \sum_{\eta} \gamma_{\eta}[\mathbf{n}_t]. \quad (51)$$

Here,

$$\gamma_{\eta}[\mathbf{n}_t] := \int_0^t d\tau \mathcal{A}_{\eta}(\tau) \zeta_{\eta,e} J^e(\tau), \quad (52)$$

quantify the dissipation along the fundamental cycles, as $\{\zeta_{\eta,e} J^e(\tau)\}$, for $\eta = 1, \dots, N_{\eta}$, are the corresponding instantaneous currents, equation (22). For autonomous processes, the EP becomes

$$\Sigma[\mathbf{n}_t] = \Delta\Phi[\mathbf{n}_t] + \mathcal{A}_{\eta} \mathcal{Z}^{\eta}[\mathbf{n}_t], \quad (53)$$

where

$$\mathcal{Z}^{\eta}[\mathbf{n}_t] := \int_0^t d\tau \zeta_{\eta}^{\eta} J^e(\tau) \quad (54)$$

measure the total circulation along $\{\eta\}$.

4. Finite-time detailed FT

The driving and flow contributions of the EP, equation (36), are now shown to satisfy a finite-time detailed FT. This constitutes another crucial result of our paper which generalizes previous FT formulations expressed in terms of physical currents.

We consider a *forward process* of duration t defined as follows. The system is initially prepared in an equilibrium state characterized by ϕ_n^{eq} , equation (25). The latter state corresponds to the equilibrium protocol π_i in which $\phi_n(\pi_i) = \phi_n^{\text{eq}}$ and naturally $\{\mathcal{F}_{\gamma_i}(\pi_i) = 0\}$. At time $\tau = 0$ the protocol π_{τ} , for $0 \leq \tau \leq t$, is activated. It is arbitrary except at the boundaries, $\tau = 0$ and t , where the following requirements must be satisfied: at time 0, the Massieu potential corresponding to π_0 must be the same as that of the initial equilibrium state, i.e. $\phi_n(\pi_0) = \phi_n^{\text{eq}}$. As a consequence, the fields $\{f_{\gamma_i''}(\pi_0)\}$ can take arbitrarily values (i.e. they can be different from $\{f_{\gamma_i''}(\pi_i)\}$), while the other ones cannot: $\{f_{\gamma_i'}(\pi_0) = f_{\gamma_i'}(\pi_i)\}$. This implies that $\{\mathcal{F}_{\gamma_i''}(\pi_0)\}$ can be nonzero while $\{\mathcal{F}_{\gamma_i'}(\pi_0) = 0\}$. Analogously, the protocol at time t must be such that $\mathcal{F}_{\gamma_f}(\pi_t) = 0$ for all γ_f while $\{\mathcal{F}_{\gamma_f'}(\pi_t) \neq 0\}$. This condition guarantees that the Massieu potential $\phi_n(\pi_t)$ identifies the equilibrium state corresponding to the equilibrium protocol π_f : $\phi_n(\pi_f) = \phi_n^{\text{eq}} = \phi_n(\pi_t)$ and vanishing forces $\{\mathcal{F}_{\gamma_f}(\pi_f) = 0\}$. We can thus introduce the *backward process* as that in which the system is initially prepared in the equilibrium state given by π_f , and which is driven by the time-reversed protocol, $\pi_t^{\dagger} := \pi_{t-\tau}$, see figure 3.

The *finite-time detailed FT* states that the forward and backward process are related by

$$\frac{P_t(v, \{\sigma_{\gamma_i}\})}{P_t^{\dagger}(-v, \{-\sigma_{\gamma_i}\})} = \exp \left\{ v + \sum_{\gamma_i} \sigma_{\gamma_i} + \Delta\Phi_{\text{eq}} \right\}, \quad (55)$$

where $P_t(v, \{\sigma_{\gamma_i}\})$ is the probability of observing a driving contribution of the EP equal to v , and flow ones $\{\sigma_{\gamma_i}\}$ along the forward process. Instead, $P_t^{\dagger}(-v, \{-\sigma_{\gamma_i}\})$ is the probability of observing a driving contribution equal to $-v$, and flow ones $\{-\sigma_{\gamma_i}\}$ along the backward process. The difference of equilibrium Massieu potentials, equation (26),

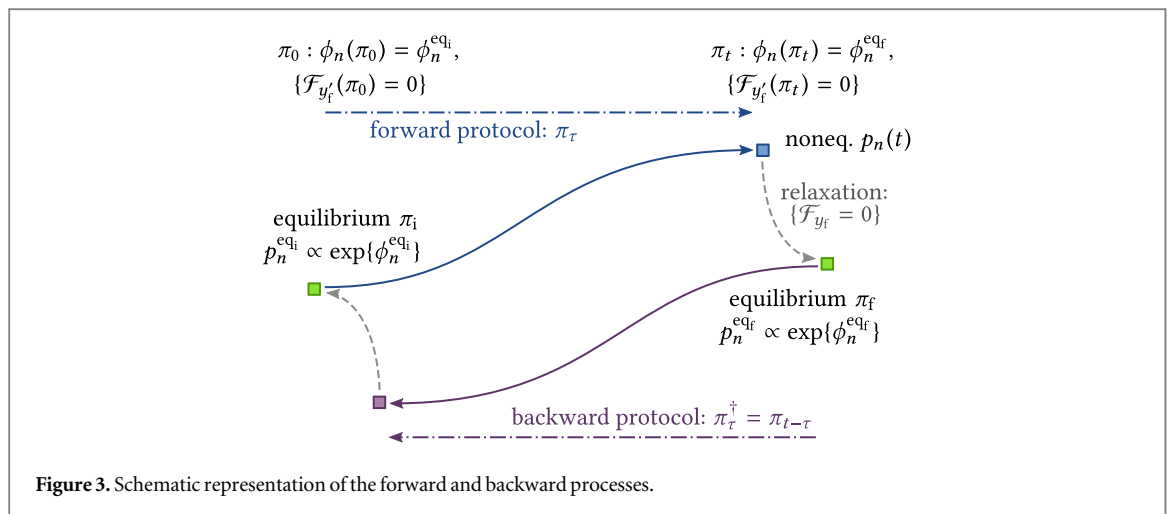


Figure 3. Schematic representation of the forward and backward processes.

$$\Delta\Phi_{\text{eq}} = \Phi_{\text{eq}_f} - \Phi_{\text{eq}_i}, \quad (56)$$

refers to the final and initial equilibrium distributions. When averaging over all possible values of v and $\{\sigma_{y_f}\}$, the integral FT ensues

$$\left\langle \exp \left\{ -v - \sum_{y_f} \sigma_{y_f} \right\} \right\rangle = \exp \{ \Delta\Phi_{\text{eq}} \}. \quad (57)$$

We prove equation (55) in appendix B using a generating function technique which is new to our knowledge.

We now discuss insightful special cases of our general FTs. We first consider those processes in which $\mathcal{F}_{y_f'} = 0$ for all y_f' and at all times—isothermal processes are a notable instance—the protocol can terminate without restrictions since $\phi_n(\pi_\tau)$ always identifies an equilibrium state. If, in addition, the protocol keeps the potential ϕ_n constant, viz. $v = 0$, the FT (55) reads

$$\frac{P_t(\{\sigma_{y_f}\})}{P_t^d(\{-\sigma_{y_f}\})} = \exp \left\{ \sum_{y_f} \sigma_{y_f} \right\}. \quad (58)$$

Yet a more detailed case is when the process is autonomous, for which we have

$$\frac{P_t(\{\mathcal{I}^{y_f}\})}{P_t(\{-\mathcal{I}^{y_f}\})} = \exp \{ \mathcal{F}_{y_f} \mathcal{I}^{y_f} \}, \quad (59)$$

written in terms of integrated currents of $\{y_f\}$, equation (43). The latter FT can be seen as the result of having a constant protocol with nonvanishing the fundamental forces $\{\mathcal{F}_{y_f''}\}$ —but vanishing $\{\mathcal{F}_{y_f'}\}$ —operating on a system initially prepared at equilibrium. Since nothing distinguishes the forward process from the backward one, the lhs is the ratio of the same probability distribution but at opposite values of $\{\mathcal{I}^{y_f}\}$, see application in section 6.3.

Instead, for detailed-balanced systems we recover a Jarzynski–Crooks-like FT [34, 35] generalized to any form of time-dependent driving

$$\frac{P_t(v)}{P_t^d(-v)} = \exp \{ v + \Delta\Phi_{\text{eq}} \}. \quad (60)$$

To provide a physical interpretation of the argument of the exponential on the rhs of equation (55), let us observe that once the protocol terminates, all fundamental forces can be switched off and the system relaxes to the equilibrium initial condition of the backward process. During the relaxation, neither v nor $\{\sigma_{y_f}\}$ evolve and the EP is equal to $\Phi_{\text{eq}_f} - \Phi_{n_i}$, equation (45). Therefore, the argument of the exponential can be interpreted as the dissipation of the fictitious composite process ‘forward process + relaxation to equilibrium’.

Remark. As we discussed in equation (41), the driving contribution consists of several subcontributions, one for each time-dependent parameter appearing in ϕ_n . We formulated the finite-time FT (55) for the whole v , but it can be equivalently expressed for the single subcontributions, see section 6.1.8.

FT for flow contributions along fundamental cycles

The FT (55) can also be expressed in terms of the flow contributions along the fundamental cycles $\{y_\eta\}$ instead of $\{\sigma_{y_f}\}$

$$\frac{P_t(\nu, \{\gamma_\eta\})}{P_t^\dagger(-\nu, \{-\gamma_\eta\})} = \exp \left\{ \nu + \sum_\eta \gamma_\eta + \Delta \Phi_{\text{eq}} \right\}. \quad (61)$$

Its proof is discussed in appendix B. The restrictions on π_0 and π_t that we expressed in terms of $\{\mathcal{F}_{\gamma_f}\}$ can be re-expressed in terms of $\{\mathcal{A}_\eta\}$ via equation (20). For autonomous processes one can write the FT for the integrated currents along fundamental cycles, equation (54),

$$\frac{P_t(\{\mathcal{Z}^\eta\})}{P_t(\{-\mathcal{Z}^\eta\})} = \exp \{\mathcal{A}_\eta \mathcal{Z}^\eta\}, \quad (62)$$

see equation (59).

5. Ensemble average level description

We now discuss our results at the ensemble average level and derive a general formulation of the nonequilibrium Landauer's principle.

5.1. Balance of conserved quantities

Using the master equation (1) and the edge-wise balance (11), the balance equation for the average rates of changes of conserved quantities reads

$$d_t \left[\sum_n L_n^\lambda p_n \right] \equiv d_t \langle L^\lambda \rangle = \langle \dot{L}^\lambda \rangle + \ell_y^\lambda \langle I^y \rangle, \quad (63)$$

where $\langle \dot{L}^\lambda \rangle := \sum_n \partial_t L_n^\lambda p_n$ is the average change due to the driving, and

$$\langle I^y \rangle := \delta Y_e^y \langle J^e \rangle \quad (64)$$

are the average currents of $\{y\}$, see equations (3) and (32). Hence, the second term in equation (63),

$$\ell_y^\lambda \langle I^y \rangle = \sum_r \left\{ \sum_\kappa \ell_{(\kappa, r)}^\lambda \delta Y_e^{(\kappa, r)} \langle J^e \rangle \right\}, \quad (65)$$

accounts for the average flow of the conserved quantities in the reservoirs. Obviously, the balances (63) can also be obtained by averaging the trajectory balances (31) along all stochastic trajectories.

5.2. Entropy balance

In contrast to conserved quantities, entropy is not conserved. The EP rate measures this nonconservation and is always non-negative

$$\langle \dot{\Sigma} \rangle = \sum_e w_e p_{o(e)} \ln \frac{w_e p_{o(e)}}{w_{-e} p_{o(-e)}} \geq 0. \quad (66)$$

The EP decomposition in driving, conservative and flow contributions at the ensemble level, can be obtained by averaging equation (36). Alternatively, one can rewrite equation (66) as

$$\langle \dot{\Sigma} \rangle = -f_y \langle I^y \rangle + [S_n - \ln p_n] D_e^n \langle J^e \rangle, \quad (67)$$

where we used the local detailed balance property (6) and the definition of average physical current (64). The first term is the average entropy flow rate, while the second is the rate of change of the average system entropy. Using the splitting of the set $\{y\}$ explained in section 2, the physical currents of $\{y_p\}$ can be expressed as

$$\langle I^{y_p} \rangle = \bar{\ell}_\lambda^{y_p} [d_t \langle L^\lambda \rangle - \langle \dot{L}^\lambda \rangle - \ell_{y_f}^\lambda \langle I_{y_f} \rangle], \quad (68)$$

where we partially inverted equation (63). When combined with equation (67), the EP rate can be written as

$$\langle \dot{\Sigma} \rangle = \langle \dot{v} \rangle + d_t \langle \Phi \rangle + \sum_{y_f} \langle \dot{\sigma}_{y_f} \rangle, \quad (69)$$

where $\langle \dot{v} \rangle = -\sum_n \partial_t \phi_n p_n$ is the driving contribution, $\langle \dot{\sigma}_{y_f} \rangle = \mathcal{F}_{y_f} \langle I_{y_f} \rangle$ the flow contributions, and

$$\langle \Phi \rangle = \sum_n p_n \Phi_n \quad (70)$$

the *nonequilibrium Massieu potential*.

Following a similar reasoning, and using the local detailed balance decomposition in terms of fundamental affinities, equation (21), we obtain the EP rate decomposed as

$$\langle \dot{\Sigma} \rangle = \langle \dot{v} \rangle + d_t \langle \Phi \rangle + \sum_{\eta} \langle \dot{\gamma}_{\eta} \rangle, \quad (71)$$

where $\langle \dot{\gamma}_{\eta} \rangle = \mathcal{A}_{\eta} \zeta_{\eta, e} \langle J^e \rangle$ are the flow contributions along the fundamental cycles.

5.3. Nonequilibrium massieu potential

In detailed-balanced systems, the nonequilibrium Massieu potential takes its maximum value at equilibrium, equation (25), where it becomes the equilibrium Massieu potential, equation (26). Indeed,

$$\Phi_{\text{eq}} - \langle \Phi \rangle = \langle \Phi_{\text{eq}} - \Phi \rangle = \mathcal{D}(p \| p^{\text{eq}}) \geq 0, \quad (72)$$

where

$$\mathcal{D}(p \| p^{\text{eq}}) := \sum_n p_n \ln \frac{p_n}{p_n^{\text{eq}}} \quad (73)$$

is the relative entropy between the nonequilibrium distribution and the equilibrium one which quantifies the distance from equilibrium.

Remark. For autonomous detailed-balanced networks, the difference of equilibrium and nonequilibrium initial Massieu potential, equation (72), gives the average dissipation during the relaxation to equilibrium, $\langle \dot{\Sigma} \rangle = \mathcal{D}(p(t_0) \| p_{\text{eq}}) \geq 0$. On the one hand, this shows how the MaxEnt principle mentioned in section 2.6 is embedded in the stochastic thermodynamic description (see also [36]). On the other hand, it underlines that its validity is limited to detailed-balanced systems.

5.4. Nonequilibrium Landauer's principle

We now express equation (69) in terms of a well defined equilibrium distribution, obtained by turning off the forces without modifying the potential ϕ_n . We already discussed that this procedure is always well defined for isothermal systems but requires more care for nonisothermal systems. Combining equations (69) and (72), one finds that

$$\langle \dot{\Sigma} \rangle = \langle \dot{v}_{\text{irr}} \rangle - d_t \mathcal{D}(p \| p^{\text{eq}}) + \sum_{\gamma_f} \langle \dot{\sigma}_{\gamma_f} \rangle, \quad (74)$$

where we introduced the average *irreversible driving contribution*

$$\langle \dot{v}_{\text{irr}} \rangle := \langle \dot{v} \rangle + d_t \Phi_{\text{eq}}. \quad (75)$$

Notice that the above contribution is not affected by the gauge discussed in section 3. Integrating equation (74) over time we get

$$\langle v_{\text{irr}} \rangle + \sum_{\gamma_f} \langle \sigma_{\gamma_f} \rangle = \Delta \mathcal{D}(p \| p_{\text{eq}}) + \langle \Sigma \rangle. \quad (76)$$

This relation generalizes the nonequilibrium Landauer's principle, which is typically derived for driven detailed-balance systems, $\langle \sigma_{\gamma_f} \rangle = 0$, [20]—see also [18, 19, 36]—and which is used as the basis to study thermodynamics of information processing [11]. It shows that not only driving but also flow EP must be consumed to move a system away from equilibrium, as depicted in figure 4, and that the minimal cost for doing so is precisely measured by the change in relative entropy. For driven detailed-balanced protocols connecting two equilibrium states, we recover the classical result that $\langle \dot{v}_{\text{irr}} \rangle = \langle \Sigma \rangle \geq 0$.

5.5. Relation with previous EP decompositions

We now briefly comment on the differences between our EP rate decomposition and other decompositions found in the literature.

In [17], the obvious conserved quantities $\{Y^{\kappa}\}$ are used to express the EP rate in terms of a driving, a conservative, and a nonconservative term. The first two are expressed in terms of a Massieu potential based on the N_{κ} obvious conserved quantities, $\{Y^{\kappa}\}$, while the last is a sum of $N_y - N_{\kappa}$ flux-force contributions. A finite-time FT solely expressed in terms of physical observable ensues. In our work, by taking all N_{λ} conserved quantities—trivial and nontrivial—into account, the nonconservative term is reduced to a sum of $N_y - N_{\lambda}$ fundamental flux-force contributions, and the new Massieu potential entering the driving and conservative contribution takes all conservation laws into account. This has two crucial consequences for the ensuing FT: (i) our class of equilibrium distributions is broader since it is determined imposing a lower number of constraints, equation (24) (i.e. $N_y - N_{\lambda}$ vanishing forces instead of $N_y - N_{\kappa}$); (ii) the final value of the protocol must be

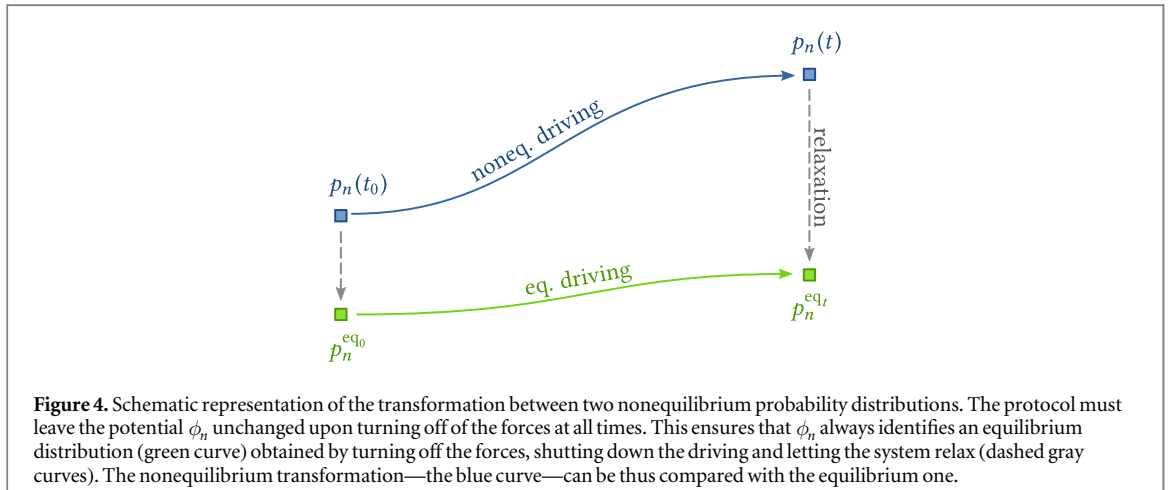


Figure 4. Schematic representation of the transformation between two nonequilibrium probability distributions. The protocol must leave the potential ϕ_n unchanged upon turning off of the forces at all times. This ensures that ϕ_n always identifies an equilibrium distribution (green curve) obtained by turning off the forces, shutting down the driving and letting the system relax (dashed gray curves). The nonequilibrium transformation—the blue curve—can be thus compared with the equilibrium one.

constrained as discussed in section 4 since the new Massieu potential does not always identifies an equilibrium distribution.

In [16] the authors analyzed the reduction of flux-force contributions for systems at steady state, where the conservative contribution is absent. Our decomposition (69) generalizes these results to nonautonomous systems in transient regimes.

In [25, 37], decompositions based on graph-theoretic techniques are proposed, and the ensuing FTs are studied in [38, 39], respectively. The nonconservative term of the EP rate is expressed as the sum of N_α cycle flux-affinity contributions. These are typically in large number, see e.g. sections 6.3 and 6.4. Our decomposition (71) demonstrates that only a subset of $N_\alpha - N_\rho = N_y - N_x$ fundamental cycle flux-affinity contributions are necessary and sufficient to characterize the aforementioned term, where N_ρ is the number of symmetries.

Yet a different EP decomposition is the *adiabatic–nonadiabatic* one [40–44]. Here, the driving and conservative terms arise from the stochastic potential $\Psi_i := -\ln\{p_i/p_i^{ss}\}$, which accounts for the mismatch between the actual and the steady-state probability distribution. Instead, the nonconservative contribution quantifies the break of detailed balance of the steady state. Hence, the steady-state probability distribution plays the role of a reference distribution in the same way that the equilibrium one (obtained by setting the forces to zero) does for our decomposition. This is particularly clear when comparing [40, equation (21)] to equation (74). Naturally, the equilibrium distribution is much more accessible than the steady-state one and implies that our decomposition is expressed in terms of physically measurable quantities.

6. Applications

We now analyze four model-systems: a double quantum dot (QD), a QD coupled to a quantum point contact (QPC), a molecular motor, and a randomized grid.

6.1. Double QD

This model has been extensively used in the past [45–47] and we will analyze it step by step following the order of the main text to illustrate of our formalism and our main results.

6.1.1. Setup

The two single-level QDs is depicted in figure 5(a), whereas the energy landscape and the network of transitions are shown in figures 5(b) and (c), respectively. Electrons can enter empty dots from the reservoirs but cannot jump from one dot to the other. When the two dots are occupied, an interaction energy, u , arises.

The network topology is encoded in the incidence matrix, whose representation in terms of the forward transitions reads

$$D = \begin{matrix} & \begin{matrix} +1 & +2 & +3 & +4 & +5 & +6 \end{matrix} \\ \begin{matrix} 00 \\ 10 \\ 01 \\ 11 \end{matrix} & \begin{pmatrix} -1 & -1 & -1 & 0 & 0 & 0 \\ 1 & 0 & 0 & 0 & -1 & -1 \\ 0 & 1 & 1 & -1 & 0 & 0 \\ 0 & 0 & 0 & 1 & 1 & 1 \end{pmatrix} \end{matrix} \quad (77)$$

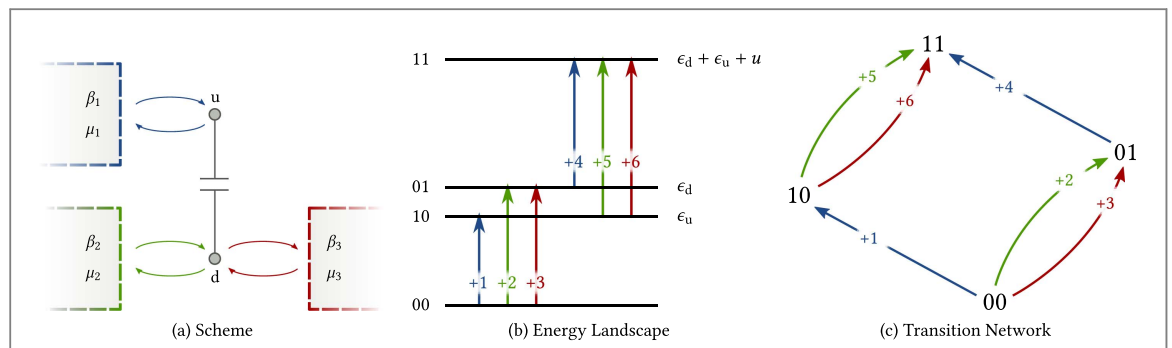


Figure 5. Double QD coupled to three reservoirs and coupled with each other via a capacitor. Transitions related to the first reservoir are depicted in blue while those related to the second and third one by green and red, respectively. (a) Pictorial representation of the system. The upper dot u is coupled to the first reservoir, while the lower dot d is coupled to the second and third reservoir. The reservoirs exchange energy and electrons with the dots, which cannot host more than one electron. (b) Energy landscape of the dot. Importantly, when both dots are occupied, 11, a repulsive energy u adds to the occupied dots energies, ϵ_u and ϵ_d . (c) Transition network of the model.

Energy, E_n , and total number of electrons, N_n , characterize each system state:

$$\begin{aligned} E_{00} &= 0, & N_{00} &= 0, \\ E_{01} &= \epsilon_d, & N_{01} &= 1, \\ E_{10} &= \epsilon_u, & N_{10} &= 1, \\ E_{11} &= \epsilon_u + \epsilon_d + u, & N_{11} &= 2, \end{aligned} \quad (78)$$

where the first entry in n refers to the occupancy of the upper dot while the second to the lower. The entries of the matrix δY corresponding to the forward transitions are

$$\delta Y = \begin{pmatrix} +1 & +2 & +3 & +4 & +5 & +6 \\ (E, 1) & \left(\begin{array}{cccccc} \epsilon_u & 0 & 0 & \epsilon_u + u & 0 & 0 \\ 1 & 0 & 0 & 1 & 0 & 0 \\ 0 & \epsilon_d & 0 & 0 & \epsilon_d + u & 0 \\ 0 & 1 & 0 & 0 & 1 & 0 \\ 0 & 0 & \epsilon_d & 0 & 0 & \epsilon_d + u \\ 0 & 0 & 1 & 0 & 0 & 1 \end{array} \right) \\ (N, 1) & \\ (E, 2) & \\ (N, 2) & \\ (E, 3) & \\ (N, 3) & \end{pmatrix}, \quad (79)$$

see figure 5(c), whereas the entries related to backward transition are equal to the negative of the forward. For instance, along the first transition the system gains ϵ_u energy and 1 electron from the reservoir 1. The vector of entropic intensive fields is given by

$$f = (E, 1) \quad (N, 1) \quad (E, 2) \quad (N, 2) \quad (E, 3) \quad (N, 3) \\ f = (\beta_1 - \beta_1 \mu_1 \quad \beta_2 - \beta_2 \mu_2 \quad \beta_3 - \beta_3 \mu_3). \quad (80)$$

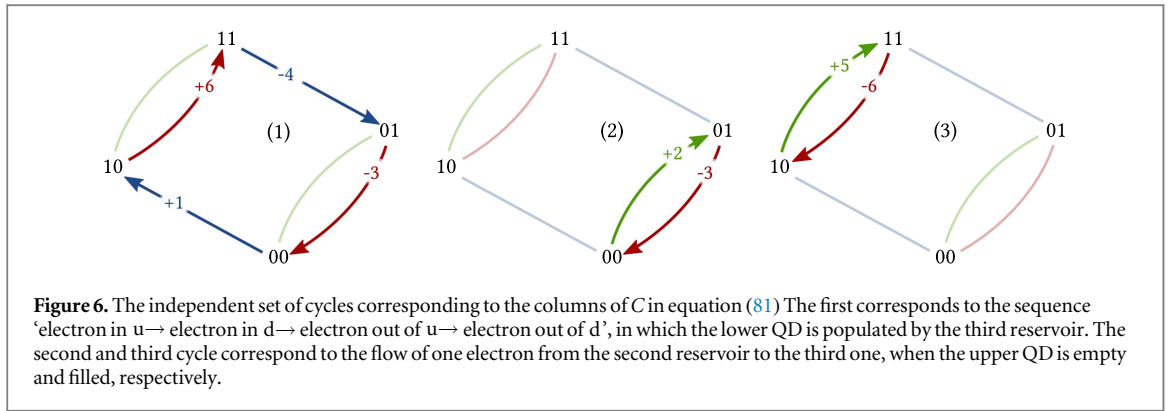
Since the QDs and the electrons have no internal entropy, $S_n = 0$ for all n , the local detailed balance property, equation (6), can be easily recovered from the product $-\delta Y$. From a stochastic dynamics perspective, the latter property arises when considering fermionic transition rates: $w_e = \Gamma_e (1 + \exp\{f_e \delta Y_e^y\})^{-1}$ and $w_{-e} = \Gamma_e \exp\{f_e \delta Y_e^y\} (1 + \exp\{f_e \delta Y_e^y\})^{-1}$ for electrons entering and leaving the dot.

6.1.2. Conservation laws

We now illustrate the identification of the full set of conservation laws. An independent set of cycles of this network, figure 5(c), is stacked in the matrix

$$C = \begin{pmatrix} 1 & 2 & 3 \\ +1 & \left(\begin{array}{ccc} 1 & 0 & 0 \\ 0 & 1 & 0 \\ -1 & -1 & 0 \\ -1 & 0 & 0 \\ 0 & 0 & 1 \\ 1 & 0 & -1 \end{array} \right) \\ +2 & \\ +3 & \\ +4 & \\ +5 & \\ +6 & \end{pmatrix}, \quad (81)$$

and corresponds to the cycles depicted in figure 6. The negative entries denote transitions performed in the backward direction. The matrix encoding the physical topology, M , readily follows from the product of δY and C ,



$$M = \begin{pmatrix} 1 & 2 & 3 \\ (E, 1) & \begin{pmatrix} -u & 0 & 0 \\ 0 & 0 & 0 \end{pmatrix} \\ (N, 1) & \begin{pmatrix} 0 & 0 & 0 \\ 0 & 0 & 0 \end{pmatrix} \\ (E, 2) & \begin{pmatrix} 0 & \epsilon_d & \epsilon_d + u \\ 0 & 1 & 1 \end{pmatrix} \\ (N, 2) & \begin{pmatrix} 0 & 1 & 1 \\ 0 & 0 & 0 \end{pmatrix} \\ (E, 3) & \begin{pmatrix} u & -\epsilon_d & -\epsilon_d - u \\ 0 & -1 & -1 \end{pmatrix} \\ (N, 3) & \begin{pmatrix} 0 & -1 & -1 \\ 0 & 0 & 0 \end{pmatrix} \end{pmatrix}. \quad (82)$$

Its cokernel is spanned by

$$\mathcal{C}^E = (1 \quad 0 \quad 1 \quad 0 \quad 1 \quad 0), \quad (83a)$$

$$\mathcal{C}^u = (0 \quad 1 \quad 0 \quad 0 \quad 0 \quad 0), \quad (83b)$$

$$\mathcal{C}^d = (0 \quad 0 \quad 0 \quad 1 \quad 0 \quad 1). \quad (83c)$$

The first vector identifies the energy state variable, E_n ,

$$\mathcal{C}^E \delta Y = (\epsilon_u \quad \epsilon_d \quad \epsilon_d \quad \epsilon_u + u \quad \epsilon_d + u \quad \epsilon_d + u) \equiv \{E_n D_e^n\}. \quad (84)$$

The other two, instead, give the occupancy of the upper and lower dots, N_n^u and N_n^d ,

$$\begin{aligned} \mathcal{C}^u \delta Y &= (1 \quad 0 \quad 0 \quad 1 \quad 0 \quad 0) \equiv \{N_n^u D_e^n\}, \\ \mathcal{C}^d \delta Y &= (0 \quad 1 \quad 1 \quad 0 \quad 1 \quad 1) \equiv \{N_n^d D_e^n\}. \end{aligned} \quad (85)$$

A posteriori, we see that these conservation laws arise from the fact that no electron transfer from one dot to the other is allowed. The total occupancy of the system, N_n , is recovered from the sum of the last two vectors. Despite \mathcal{C}^u and \mathcal{C}^d are nontrivial conservation laws, they do not depend on any system quantity, equation (78)¹.

Let us now imagine that the interaction energy between the two dots is switched off, i.e. $u \rightarrow 0$. Two conservation laws emerge in addition to those in equation (83):

$$\mathcal{C}^{(E,d)} = (0 \quad 0 \quad 1 \quad 0 \quad 1 \quad 0), \quad (86a)$$

$$\mathcal{C}^t = (0 \quad 0 \quad -1 \quad \epsilon_d \quad 0 \quad 0). \quad (86b)$$

The first is related to the upper–lower QD decoupling, as it corresponds to the conservation of energy of the lower dot

$$\mathcal{C}^{(E,d)} \delta Y = (0 \quad \epsilon_d \quad \epsilon_d \quad 0 \quad \epsilon_d \quad \epsilon_d) \equiv \{E_n^d D_e^n\}. \quad (87)$$

The conservation of energy in the upper dot is obtained as the difference between equations (83a) and (86a), and reads

¹ One may argue that the above statement might be due the fact that we fixed the electron occupancy of each QD to one, equation (78). However, the same conclusion is reached when assuming: $N_{00} = 0$, $N_{01} = \nu_d$, $N_{10} = \nu_u$, and $N_{11} = \nu_u + \nu_d$, for some positive integer values ν_u and ν_d .

$$\mathcal{C}^{(E,u)} \delta Y = \begin{pmatrix} +1 & +2 & +3 & +4 & +5 & +6 \\ \epsilon_u & 0 & 0 & \epsilon_u & 0 & 0 \end{pmatrix} \equiv \{E_n^u D_e^n\}. \quad (88)$$

The second one, equation (86b), arises from the tight coupling between the transport of energy and matter through the second dot. Since \mathcal{C}^t is in $\text{coker} \delta Y$,

$$\mathcal{C}^t \delta Y = \begin{pmatrix} +1 & +2 & +3 & +4 & +5 & +6 \\ 0 & 0 & 0 & 0 & 0 & 0 \end{pmatrix} \equiv \{L_n^t D_e^n\}, \quad (89)$$

the conserved quantity L_n^t is a constant for all n , which can be chosen arbitrarily. Notice the dependence on the system quantity ϵ_d of the nontrivial conservation law (86b). We thus showed that changes of system quantities (u in our case) can modify the properties of M , and hence the set of conservation laws—without changing the network topology.

6.1.3. Massieu potential and fundamental forces

We now provide the expressions of ϕ_n and \mathcal{F}_{γ_f} for the generic case $u \neq 0$. Therefore, we split the set $\{\gamma\}$ in $\{\gamma_p\} = \{(E, 1), (N, 1), (N, 2)\}$ and $\{\gamma_f\} = \{(E, 2), (E, 3), (N, 3)\}$. From equation (83) we see the validity of this splitting, as the matrix whose entries are $\{\mathcal{C}_{\gamma_p}^{\lambda}\}$ is an identity matrix. The fields conjugated with the complete set of conservation laws, equation (15), are

$$F_E = \beta_1, \quad F_u = -\beta_1 \mu_1, \quad F_d = -\beta_2 \mu_2, \quad (90)$$

from which the Massieu potential of the state n , equation (14), follows

$$\phi_n = -\beta_1 E_n + \beta_1 \mu_1 N_n^u + \beta_2 \mu_2 N_n^d. \quad (91)$$

Instead, the fundamental forces, equation (16), are given by

$$\mathcal{F}_{(E,2)} = \beta_1 - \beta_2, \quad (92a)$$

$$\mathcal{F}_{(E,3)} = \beta_1 - \beta_3, \quad (92b)$$

$$\mathcal{F}_{(N,3)} = \beta_3 \mu_3 - \beta_2 \mu_2. \quad (92c)$$

The first two forces rule the energy flowing into the first reservoir from the second and third one, respectively, whereas the third force rules the electrons flowing from the third to the second reservoir.

Concerning the way the changes of ϕ_n and $\{\mathcal{F}_{\gamma}\}$ are intertwined, we see that the former depends on β_1, μ_1, μ_2 , and β_2 , which arises from $f_{(N,2)}$. Therefore, while the changes of $f_{(E,3)} = \beta_3$ and $f_{(N,3)} = -\beta_3 \mu_3$ only affect the related forces, the changes of $f_{(E,2)} = \beta_2$ affect both $\mathcal{F}_{(E,2)}$ and ϕ_n . Since the vectors of conservation laws (83c) do not depend on either E_n or N_n , see section 6.1.2, the forces do not depend on system quantities.

Alternatively, one may split the set $\{\gamma\}$ in $\{\gamma_p\} = \{(N, 1), (E, 2), (N, 3)\}$ and $\{\gamma_f\} = \{(E, 1), (N, 2), (E, 3)\}$. With this choice, we obtain

$$\phi_n = -\beta_2 E_n + \beta_1 \mu_1 N_n^u + \beta_3 \mu_3 N_n^d, \quad (93)$$

and

$$\mathcal{F}_{(E,1)} = \beta_2 - \beta_1, \quad (94a)$$

$$\mathcal{F}_{(N,2)} = \beta_2 \mu_2 - \beta_3 \mu_3, \quad (94b)$$

$$\mathcal{F}_{(E,3)} = \beta_2 - \beta_3. \quad (94c)$$

With respect to the previous decomposition, we here consider the forces ruling the energy flow from the first and third reservoir, and the electrons flow from the second reservoir.

Let us now reconsider the case of vanishing interaction energy, $u = 0$, as in section 6.1.2. The five conservation laws that we consider are $E_n, E_n^d, N_n^u, N_n^d, L_n^t$, and we choose to split $\{\gamma\}$ as $\{\gamma_p\} = \{(E, 1), (N, 1), (E, 2), (N, 2), (E, 3)\}$ and $\{\gamma_f\} = \{(N, 3)\}$. The potential follows

$$\tilde{\phi}_n = -\beta_1 E_n + \beta_1 \mu_1 N_n^u + [\beta_2 \mu_2 - (\beta_2 - \beta_3) \epsilon_d] N_n^d - (\beta_3 - \beta_1) E_n^d - (\beta_3 - \beta_2) L_n^t, \quad (95)$$

whereas the only force is

$$\tilde{\mathcal{F}}_{(N,3)} = \beta_3 (\mu_3 - \epsilon_d) - \beta_2 (\mu_2 - \epsilon_d). \quad (96)$$

We see that the creation of two conservation laws destroyed two nonconservative forces, equations (92a) and (92b), whose expression can be spotted in the new potential, equation (95). Notice also how the emergence of the nontrivial conservation law (86b) makes the fundamental force dependent on the system quantity ϵ_d .

6.1.4. Symmetries and fundamental cycles

The two single-level QD has no symmetries for $u \neq 0$, since its M -matrix (82) has empty kernel. Its three cycle affinities, equations (81) and (17), are thus fundamental and read

$$\mathcal{A}_1 = \beta_1 u - \beta_3 u, \quad (97a)$$

$$\mathcal{A}_2 = \beta_3(\epsilon_d - \mu_3) - \beta_2(\epsilon_d - \mu_2), \quad (97b)$$

$$\mathcal{A}_3 = \beta_3(\epsilon_d + u - \mu_3) - \beta_2(\epsilon_d + u - \mu_2), \quad (97c)$$

while the matrix relating fundamental cycles to edges, equation (22), is given by

$$\zeta_e^\eta = \begin{matrix} & +1 & +2 & +3 & +4 & +5 & +6 \\ \begin{matrix} 1 \\ 2 \\ 3 \end{matrix} & \begin{pmatrix} 0 & \epsilon_d & \epsilon_d & 0 & \epsilon_d + u & \epsilon_d + u \\ 0 & -\epsilon_d & -\epsilon_d - u & 0 & -\epsilon_d - u & -\epsilon_d - u \\ 0 & \epsilon_d & \epsilon_d & 0 & \epsilon_d + u & \epsilon_d \end{pmatrix} \frac{1}{u} \end{matrix} \quad (98)$$

In sharp contrast with the fundamental forces, equation (92), the fundamental affinities depend both on the fields and the system quantities.

As the interaction energy is turned off, two symmetries emerge:

$$\psi_1 = \begin{pmatrix} 1 & 2 & 3 \\ 1 & 0 & 0 \end{pmatrix}, \quad (99a)$$

$$\psi_2 = \begin{pmatrix} 1 & 2 & 3 \\ 0 & 1 & -1 \end{pmatrix}, \quad (99b)$$

in agreement with the creation of two conservation laws, see equations (19) and (86). They inform us that since the QDs are decoupled: (i) the cycle 1 does not produce changes in the reservoirs, i.e. its affinity is zero irrespective of the entries of f ; (ii) the cycle 2 and 3 are physically dependent since the flow of electrons from the second to the third reservoir is the same with empty and filled upper dot. Choosing the third cycle as the fundamental one, its affinity reads as $\tilde{\mathcal{F}}_{(N,3)}$ in equation (96), whereas the matrix of cycle contributions, see equation (22) and section 6.1.3, becomes

$$\zeta_e^3 = \begin{pmatrix} +1 & +2 & +3 & +4 & +5 & +6 \\ 0 & 0 & -1 & 0 & 0 & -1 \end{pmatrix}. \quad (100)$$

Notice that both the transition +3—which belongs to the cycle 2—and +6—which belongs to the cycle 3—contribute to the current along the fundamental cycle 3.

6.1.5. Detailed-balance dynamics

From equation (92), we see that the dynamics of the two QDs is detailed balanced when $\beta_1 = \beta_2 = \beta_3$ and $\mu_2 = \mu_3$. In this case the Massieu potential of state n , equation (91), is given by

$$\phi_n = -\beta_1(E_n - \mu_1 N_n^u - \mu_2 N_n^d). \quad (101)$$

The only element distinguishing the latter from that in equation (91) is the fact that $\beta_2 = \beta_1$, which arises from $\mathcal{F}_{(E,2)} = 0$. Therefore, a nondetailed-balanced dynamics described by the decomposition (91) and (92) can become detailed-balance without changing ϕ_n as long as $\mathcal{F}_{(E,2)} = 0$. Instead, the decomposition in equations (93) and (94c) requires both $\mathcal{F}_{(E,1)}$ and $\mathcal{F}_{(E,3)}$ to be zero.

6.1.6. EP decomposition

For the sake of illustrating our EP decomposition let us assume that only E_n , μ_2 , and β_3 change in time. According to the expressions of ϕ_n and $\{\mathcal{F}_{\mathcal{Y}_i}\}$ derived in section 6.1.3, we can distinguish two driving contributions of the EP, equations (37) and (41):

$$\nu[\mathbf{n}_t] = \nu_E[\mathbf{n}_t] + \nu_{(N,2)}[\mathbf{n}_t], \quad (102)$$

where the first term,

$$\nu_E[\mathbf{n}_t] := \beta_1 \int_0^t d\tau \partial_\tau E_n(\tau)|_{n_\tau}, \quad (103)$$

is usually referred to as mechanical work in stochastic thermodynamics (up to β_1), while the second,

$$\nu_{(N,2)}[\mathbf{n}_t] := -\beta_2 \int_0^t d\tau \partial_\tau \mu_2(\tau) N_{n_\tau}^d, \quad (104)$$

is the entropy dissipated due to the change of the chemical potential of the second reservoir. The flow contributions, equation (39), are instead given by

$$\sigma_{(E,2)}[\mathbf{n}_t] = \mathcal{F}_{(E,2)} \int_0^t d\tau I_{(E,2)}(\tau), \quad (105a)$$

$$\sigma_{(E,3)}[\mathbf{n}_t] = \int_0^t d\tau \mathcal{F}_{(E,3)}(\tau) I_{(E,3)}(\tau), \quad (105b)$$

$$\sigma_{(N,3)}[\mathbf{n}_t] = \int_0^t d\tau \mathcal{F}_{(N,3)}(\tau) I_{(N,3)}(\tau), \quad (105c)$$

where, the forces are given in equation (92), while the instantaneous currents of γ_f are

$$I_{(E,2)} = \epsilon_d [J^{+2} - J^{-2}] + (\epsilon_d + u) [J^{+5} - J^{-5}], \quad (106a)$$

$$I_{(E,3)} = \epsilon_d [J^{+3} - J^{-3}] + (\epsilon_d + u) [J^{+6} - J^{-6}], \quad (106b)$$

$$I_{(N,3)} = J^{+3} - J^{-3} + J^{+6} - J^{-6}. \quad (106c)$$

We thus see that the first and the second flow contribution, equations (105a) and (105b), quantify the dissipation due to the energy flowing from the second and third reservoir to the first, respectively. Analogously, the third contribution, equation (105c), characterizes the EP due to the flow of electrons from the third reservoir to the second. The EP is thus the sum of the terms in equations (102) and (105) plus a difference of stochastic Massieu potential, equations (91) and (40). We notice that the change in time of β_3 is accounted for by the second and third flows, equations (105b) and (105c), while not by a driving contribution, as β_3 does not contribute to ϕ_n , equation (91).

It is worth noting that, from an experimental point of view, the driving contribution demands information on the states of the trajectory. Instead, the flow contributions require the measurement of the energy flow in the second and third reservoir and the electron flow in the third. Let us now compare the above decomposition with that based on a different choice of $\{\gamma_p, \gamma_f\}$, e.g. the second one made in section 6.1.3. In this case the driving contribution reads,

$$\nu[\mathbf{n}_t] = \nu_E[\mathbf{n}_t] + \nu_{(E,3)}[\mathbf{n}_t], \quad (107)$$

where

$$\nu_{(E,3)}[\mathbf{n}_t] := -\mu_3 \int_0^t d\tau \partial_\tau \beta_3(\tau) N_{n_\tau}^d. \quad (108)$$

The flow contributions read as in equation (102) with forces given in equation (94c) and other expressions for the currents. Now, the measurement of the energy flow in the first and third reservoir, as well as the electron flow in the second reservoir, are required to quantify these terms in experiments.

To make the difference between the two choices even sharper, one can easily see that if the only quantity changing in time is μ_2 , the driving contribution of the second choice vanishes while that of the first does not. Therefore, depending on the physical system and the experimental apparatus, one choice may be more convenient than another when it comes to estimating the dissipation.

6.1.7. EP decomposition along fundamental cycles

For the scenario described in the previous subsection, section 6.1.6, the flow contributions along fundamental cycles (52) read

$$\gamma_1[\mathbf{n}_t] = \int_0^t d\tau \mathcal{A}_1(\tau) \zeta_{1,e} J^e(\tau), \quad (109a)$$

$$\gamma_2[\mathbf{n}_t] = \int_0^t d\tau \mathcal{A}_2(\tau) \zeta_{2,e} J^e(\tau), \quad (109b)$$

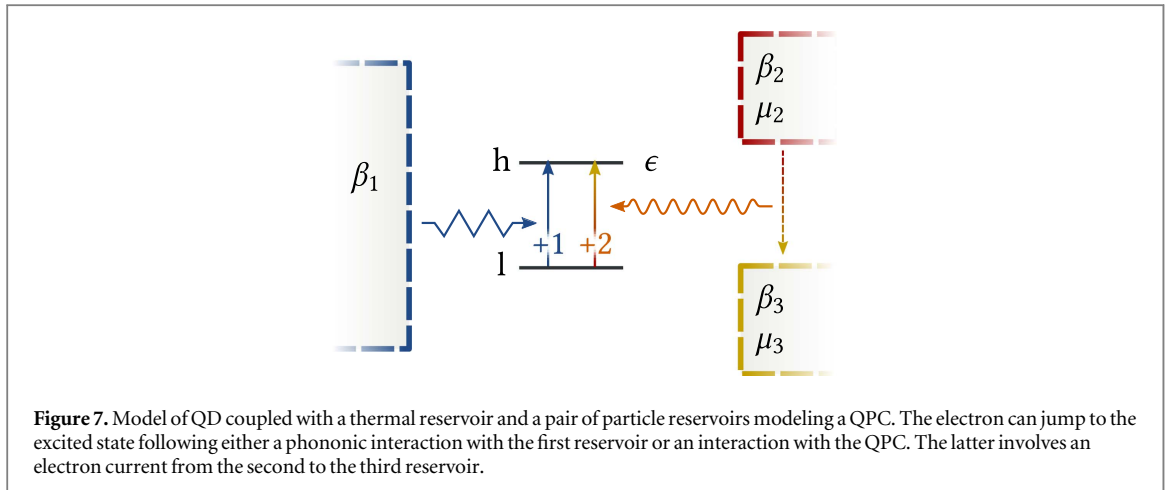
$$\gamma_3[\mathbf{n}_t] = \int_0^t d\tau \mathcal{A}_3(\tau) \zeta_{3,e} J^e(\tau), \quad (109c)$$

where the affinities are given in equation (97) and the cycle-edge coupling matrix ζ in equation (98). Concerning their physical interpretation, the first contribution corresponds to the flow of energy from the third reservoir to the first, while the last two to the entropy dissipated when transferring electrons from the second reservoir to the third with empty and filled upper dot, respectively.

6.1.8. Finite-time detailed FT

We now illustrate the conditions under which our FT applies to the coupled QDs. The process must start from equilibrium, equation (25): all forces vanish and the potential is given in equation (101). As the protocol is activated, it must leave the fields appearing in ϕ_n , equation (91), $(\beta_1, \beta_2 (= \beta_1), \mu_1, \text{ and } \mu_2)$ unchanged, but all the others can be set to arbitrary values. Subsequently, all fields and system quantities controlled by π_τ , for $0 < \tau < t$, can change arbitrarily, until time t , in which the force in equation (92a) must be turned off. This condition guarantees that the potential at time t is of the form in equation (101), thus identifying a new equilibrium state. When the above force vanishes at all times, one can formulate FTs like those in equations (58) and (59).

To simplify the application of the FT let us consider the conditions described in section 6.1.6, with the further simplification that all temperatures are equal and constant: only E_n and μ_2 change in time. Since $\beta_2 = \beta_1$



at all times, we do not need to worry about how the protocol terminates and the FT reads

$$\frac{P_t(v_E, v_{(N,2)}, \sigma_{(N,3)})}{P_t^\dagger(-v_E, -v_{(N,2)}, -\sigma_{(N,3)})} = \exp\{v_E + v_{(N,2)} + \sigma_{(N,3)} + \Delta\Phi_{\text{eq}}\}, \quad (110)$$

where the different contributions are given in equations (103), (104), and (105c). Notice that the contributions of v appear separately in the above expression, but one can equivalently express the FT in terms of the full driving work v , equation (102), as in the main discussion.

6.1.9. FT for flow contributions along fundamental cycles

We saw in the previous example that the force $\mathcal{F}_{(E,2)}$, equation (92a), must be zero at time 0 and t for the validity of the FT (55), and at all times for the FTs (58) and (59). Using equation (20) in combination with the inverse of the submatrix of (82) whose entries are $\{M_{\eta}^{Y_i}\}$,

$$\overline{M} = \begin{smallmatrix} (E, 2) & (E, 3) & (N, 3) \\ 1 & 1 & 0 \\ 2 & -1 & -\epsilon_d - u \\ 3 & 1 & \epsilon_d \end{smallmatrix} \frac{1}{u}, \quad (111)$$

we conclude that the above requirement becomes

$$\mathcal{A}_1 - \mathcal{A}_2 + \mathcal{A}_3 = 0, \quad (112)$$

in terms of fundamental affinities, equation (97). Once identified the above condition, the application of the FT readily follows.

6.2. QD coupled to a QPC

We now consider a simplified description of a two levels QD coupled to a thermal reservoir and a QPC, figure 7. For a detailed analysis of this class of systems we refer to [48]. The interest of this model is twofold, it shows how single transitions can trigger exchanges involving multiple reservoir, and it also provides a further instance of a fundamental force which depends on system quantities due to nontrivial conservation laws.

The two states of the QD, l for 'low' and h for 'high', are characterized by different energies but the same number of electrons

$$E_l = 0, \quad E_h = \epsilon, \quad N_l = 1, \quad N_h = 1. \quad (113)$$

The transition between these states can occur following either a phononic interaction with the first reservoir, ± 1 , or following electron tunneling from the second to the third reservoir, ± 2 . Along the latter transition, an electron with energy $u + \epsilon$ leaves the second reservoir and enters the third with energy u . The matrix of exchanged conserved quantities, δY , thus reads

$$\delta Y = \begin{smallmatrix} (E, 1) & (E, 2) & (N, 2) & (E, 3) & (N, 3) \\ +1 & 0 & 0 & 0 & 0 \\ 0 & u + \epsilon & 1 & -u & -1 \end{smallmatrix}, \quad (114)$$

while the vector of intensive fields is

$$\mathbf{f} = \begin{pmatrix} (E, 1) & (E, 2) & (N, 2) & (E, 3) & (N, 3) \\ \beta_1 & \beta_2 & -\beta_2\mu_2 & \beta_3 & -\beta_3\mu_3 \end{pmatrix}. \quad (115)$$

The nontrivial local detailed balance property for the second transition follows from $-\mathbf{f} \delta Y$, and reads

$$\ln \frac{w_{+2}}{w_{-2}} = -\beta_2(u + \epsilon - \mu_2) + \beta_3(u - \mu_3). \quad (116)$$

The M -matrix,

$$M = \begin{pmatrix} (E, 1) & & & & 1 \\ (E, 2) & & & & \epsilon \\ (N, 2) & & -u - \epsilon & & \\ (E, 3) & & -1 & & \\ (N, 3) & & u & & \\ & & & 1 & \end{pmatrix} \quad (117)$$

follows from the product of δY , equation (114), and the matrix of cycles,

$$C = \begin{pmatrix} & & & 1 \\ & & & \epsilon \\ & & & -u - \epsilon \\ & & & -1 \\ & & & u \\ & & & 1 \end{pmatrix} \quad (118)$$

Its four-dimensional cokernel is spanned by

$$\mathcal{C}^E = \begin{pmatrix} (E, 1) & (E, 2) & (N, 2) & (E, 3) & (N, 3) \\ 1 & 1 & 0 & 1 & 0 \end{pmatrix}, \quad (119a)$$

$$\mathcal{C}^N = \begin{pmatrix} (E, 1) & (E, 2) & (N, 2) & (E, 3) & (N, 3) \\ 0 & 0 & 1 & 0 & 1 \end{pmatrix}, \quad (119b)$$

$$\mathcal{C}^3 = \begin{pmatrix} (E, 1) & (E, 2) & (N, 2) & (E, 3) & (N, 3) \\ 0 & 1 & -u - \epsilon & 0 & 0 \end{pmatrix}, \quad (119c)$$

$$\mathcal{C}^4 = \begin{pmatrix} (E, 1) & (E, 2) & (N, 2) & (E, 3) & (N, 3) \\ 0 & 0 & u & 1 & 0 \end{pmatrix}. \quad (119d)$$

The first two conservation laws are clearly the energy and the number of particles, equation (113), since $\mathcal{C}^E \delta Y = (\epsilon, \epsilon)$ and $\mathcal{C}^N \delta Y = (0, 0)$. For the other two, $\mathcal{C}^3 \delta Y = \mathcal{C}^4 \delta Y = (0, 0)$ implies that the related conserved quantities are constants, i.e. they do not depend on n . Mindful of the gauge freedom described in section 3 we can set the conserved quantities related to \mathcal{C}^N , \mathcal{C}^3 , and \mathcal{C}^4 to zero. When $(E, 1)$ is set as ‘force’ y , the field related to the energy conservation law

$$F_E = [(\epsilon + u - \mu_2)\beta_2 - (u - \mu_3)\beta_3]/\epsilon, \quad (120)$$

determine the values of the nonequilibrium Massieu potential, $\phi_n = -F_E E_n$. Concerning the nonconservative contributions, the fundamental force and the fundamental affinity read

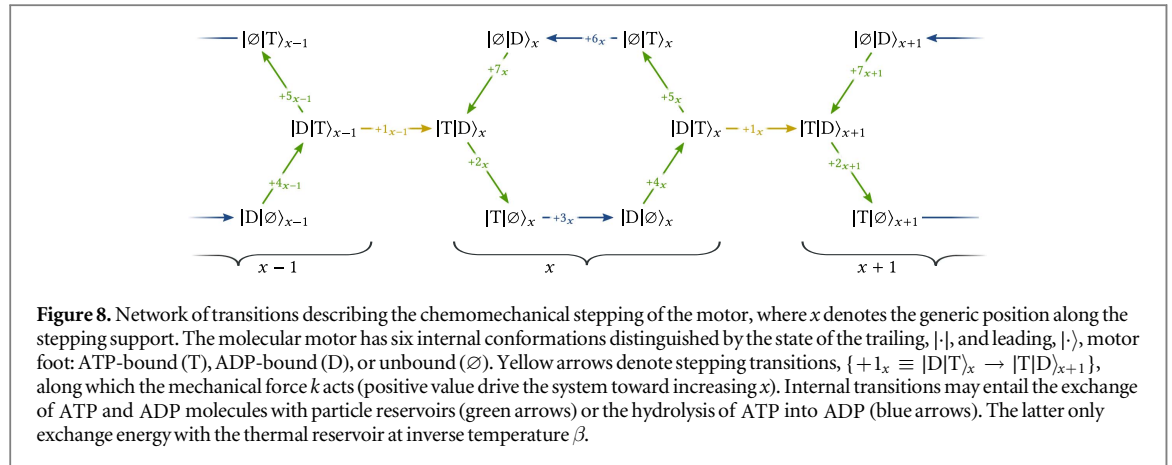
$$\mathcal{F}_{(E,1)} = F_E - \beta_1 = \epsilon \mathcal{A}_l. \quad (121)$$

Due to the emergence of nontrivial conservation laws, equations (119c) and (119d), the fundamental force depends on a system quantity. In detailed balance dynamics, $\mathcal{F}_{(E,1)} = 0$, and we readily recover $\phi_n = -\beta_1 E_n$.

6.3. Molecular motor

We now turn to the thermodynamic description of a molecular motor moving along a single dimension, see [49, 50]. Beside providing an instance of a work reservoir, this model also illustrates how changes in the topology of the network can convert a conservative force into a nonconservative one.

The motor conformations and transitions are described in figure 8. It can step against a mechanical force k thanks to the chemical force produced by the hydrolysis of ATP into ADP, which are exchanged with reservoirs at chemical potential μ_{ATP} and μ_{ADP} . We label each state of the process by $n = (m, x)$, while each transition by e_x , where $e \in \{1, 2, 3, 4, 5, 6, 7\}$ refers to the transitions at a given position $x \in \mathbb{Z}$. The system quantities are the internal energy, $E_n = \epsilon_m$, the total number of ATP plus ADP molecules attached to the motor, $N_n = N_m$, and the position, $X_n = xl$ where l is the size of a step. Importantly, each internal state is characterized by an internal entropy $S_n = s_m$.



The matrix of exchanged conserved quantities for the transitions at given position x is written as

$$\delta Y_x = \begin{pmatrix} (E) & +1_x & +2_x & +3_x & +4_x & +5_x & +6_x & +7_x \\ (N, \text{ATP}) & \epsilon_{TD} - \epsilon_{DT} & \epsilon_{T\emptyset} - \epsilon_{TD} & \epsilon_{D\emptyset} - \epsilon_{T\emptyset} & \epsilon_{DT} - \epsilon_{D\emptyset} & \epsilon_{\emptyset T} - \epsilon_{DT} & \epsilon_{\emptyset D} - \epsilon_{\emptyset T} & \epsilon_{TD} - \epsilon_{\emptyset D} \\ (N, \text{ADP}) & 0 & 0 & 0 & 1 & 0 & 0 & 1 \\ (X) & 0 & -1 & 0 & 0 & -1 & 0 & 0 \\ & 1 & 0 & 0 & 0 & 0 & 0 & 0 \end{pmatrix}, \quad (122)$$

whereas the full matrix is given by $\delta Y = (\dots \delta Y_{x-1} \delta Y_x \delta Y_{x+1} \dots)$. On the other side, the row vector of intensive variables reads

$$\mathbf{f} = \begin{pmatrix} (E) (N, \text{ATP}) & (N, \text{ADP}) & (X) \\ \beta & -\beta\mu_{\text{ATP}} & -\beta\mu_{\text{ADP}} & -\beta k \end{pmatrix}. \quad (123)$$

Differently from all previous cases, the local detailed balance of the step transitions involves the *work reservoir*, $(X, -\beta k)$,

$$\ln \frac{w_{+1x}}{w_{-1x}} = -\beta[(\epsilon_{TD} - \epsilon_{DT}) - kl] + (s_{TD} - s_{DT}). \quad (124)$$

Notice that the interpretation of the first term as minus entropy flow still holds: $q_{+1x} := (\epsilon_{TD} - \epsilon_{DT}) - kl$ is the heat of transition, since the last term is minus the work that the mechanical force exerts on the system [51, 52].

It is easily shown that the subnetwork at given x contains exactly one cycle c_x ,

$$C_x = \begin{pmatrix} c_x \\ +1_x & 0 \\ +2_x & 1 \\ +3_x & 1 \\ +4_x & 1 \\ +5_x & 1 \\ +6_x & 1 \\ +7_x & 1 \end{pmatrix}, \quad (125)$$

which entails the intake of two ATP molecules and the release of two ADP ones

$$M_x := \delta Y_x C_x = \begin{pmatrix} (E) & (N, \text{ATP}) & (N, \text{ADP}) & (X) \\ (N, \text{ATP}) & 0 & 2 & -2 \\ (N, \text{ADP}) & -2 & 0 & 0 \\ (X) & 0 & 0 & 0 \end{pmatrix}, \quad (126)$$

irrespective of the position x . The full M -matrix has thus an infinite-number of columns equal to equation (126), and its three-dimensional cokernel is spanned by

$$\mathbf{e}^E = (1 \quad 0 \quad 0 \quad 0), \quad (127a)$$

$$\mathbf{e}^N = (0 \quad 1 \quad 1 \quad 0), \quad (127b)$$

$$\mathcal{C}^X = \begin{pmatrix} (E) & (N, \text{ATP}) & (N, \text{ADP}) & (X) \\ (0 & 0 & 0 & 1) \end{pmatrix}, \quad (127c)$$

which clearly corresponds to the three system quantities, E_n , N_n , and X_n , respectively. As far as the symmetries are concerned, the intersection between its infinite-dimensional column vector space and its (infinite-dimensional) kernel is one-dimensional, in agreement with the observation that all cycles $\{c_x\}$ are physically dependent on one. In other words, there is an infinity of symmetries and all cycles carry the same cycle affinity

$$\mathcal{A} = 2\beta(\mu_{\text{ATP}} - \mu_{\text{ADP}}), \quad (128)$$

which is thus regarded as the fundamental one.

To illustrate our EP decomposition, we use (N, ATP) as set of γ_f , while leaving $\{(E), (N, \text{ADP}), (X)\}$ as γ_p . Guided by equations (14) and (15), the potential reads

$$\phi_n = \omega_n + \beta k X_n, \quad (129)$$

where

$$\omega_n := S_n - \beta E_n + \beta \mu_{\text{ADP}} N_n, \quad (130)$$

is the Massieu potential corresponding to the grand potential. The fundamental forces, equation (16), consist solely of

$$\mathcal{F}_{(N, \text{ATP})} = \beta(\mu_{\text{ATP}} - \mu_{\text{ADP}}). \quad (131)$$

The EP along a stochastic trajectory with autonomous protocol, equation (36), is

$$\Sigma[\mathbf{n}_t] = \beta(\mu_{\text{ATP}} - \mu_{\text{ADP}})\mathcal{I}_{\text{ATP}}[\mathbf{n}_t] + \Delta\Phi[\mathbf{n}_t], \quad (132)$$

where

$$\mathcal{I}_{\text{ATP}}[\mathbf{n}_t] := \int_0^t d\tau \delta Y_e^{(N, \text{ATP})} J^e(\tau) = \sum_{x=-\infty}^{\infty} \int_0^t d\tau [J^{+4_x}(\tau) - J^{-4_x}(\tau) + J^{+7_x}(\tau) - J^{-7_x}(\tau)] \quad (133)$$

is the total number of ATP molecules flowing into the system, while Φ is the stochastic Massieu potential related to equation (129). Since there is only one fundamental force, the EP in terms of fundamental affinities reads exactly as equation (132)

To illustrate the finite-time detailed FT, let us imagine a system with a finite number of positions $x = 1, \dots, N_x$. The potential (129) thus defines a physical equilibrium state, equation (25), achieved when the force is turned off: $\mu_{\text{ATP}} = \mu_{\text{ADP}}$. At time 0, the autonomous protocol with $\mu_{\text{ATP}} \neq \mu_{\text{ADP}}$ (but with the same μ_{ADP} as at equilibrium) is activated and the system moves far from equilibrium. Notice that any change of μ_{ATP} leaves ϕ_n unaltered and the process can be stopped at any time. Hence, the probability of observing the intake of \mathcal{I}_{ATP} ATP molecules up to time t satisfies

$$\frac{P_t(\mathcal{I}_{\text{ATP}})}{P_t(-\mathcal{I}_{\text{ATP}})} = \exp\{\beta(\mu_{\text{ATP}} - \mu_{\text{ADP}})\mathcal{I}_{\text{ATP}}\}, \quad (134)$$

see equation (59).

To formulate a FT which explicitly counts the number of steps, we have to make a step backward and regard the conservative term $\beta k l$ in the local detailed balance, equation (124), as an additional force contribution, rather than as part of the potential one. Under this condition the EP can be recast into

$$\Sigma[\mathbf{n}_t] = \beta(\mu_{\text{ATP}} - \mu_{\text{ADP}})\mathcal{I}_{\text{ATP}}[\mathbf{n}_t] + \beta k \mathcal{X}[\mathbf{n}_t] + \Delta\Omega[\mathbf{n}_t], \quad (135)$$

where

$$\Omega_n = \omega_n - \ln p_n \quad (136)$$

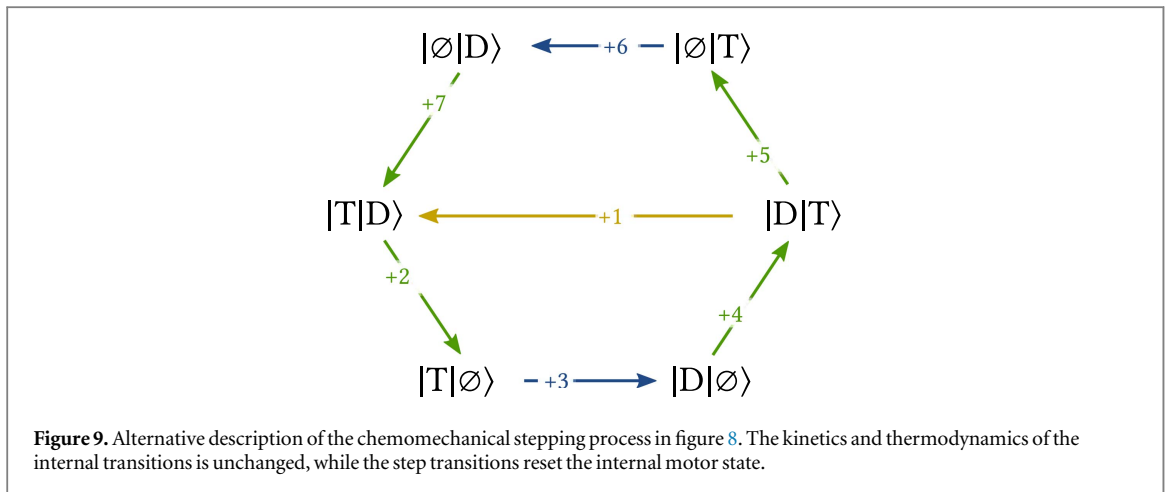
is the stochastic Massieu potential corresponding to equation (130), while

$$\mathcal{X}[\mathbf{n}_t] := X_{n_t} - X_{n_0} \quad (137)$$

the total distance traveled by the motor. If the system is initially prepared in the grandcanonical equilibrium state —achieved by turning off both the external force k and the fundamental force $\mathcal{F}_{(N, \text{ATP})}$ —the FT reads

$$\frac{P_t(\mathcal{I}_{\text{ATP}}, \mathcal{X})}{P_t(-\mathcal{I}_{\text{ATP}}, -\mathcal{X})} = \exp\{\beta(\mu_{\text{ATP}} - \mu_{\text{ADP}})\mathcal{I}_{\text{ATP}} + \beta k \mathcal{X}\}. \quad (138)$$

Tightly coupled model. As an example of change of network topology, we now consider the tightly coupled description in which the transitions $\{5, 6, 7\}$ are absent, and the network becomes a one-dimensional chain of states. Since there are no cycles the whole row space of δY spans the conservation laws, which can thus be written as



$$\mathcal{C}^E = \begin{pmatrix} (E) & (N, ATP) & (N, ADP) & (X) \\ 1 & 0 & 0 & 0 \end{pmatrix}, \quad (139a)$$

$$\mathcal{C}^{ATP} = \begin{pmatrix} (E) & (N, ATP) & (N, ADP) & (X) \\ 0 & 1 & 0 & 0 \end{pmatrix}, \quad (139b)$$

$$\mathcal{C}^{ADP} = \begin{pmatrix} (E) & (N, ATP) & (N, ADP) & (X) \\ 0 & 0 & 1 & 0 \end{pmatrix}, \quad (139c)$$

$$\mathcal{C}^X = \begin{pmatrix} (E) & (N, ATP) & (N, ADP) & (X) \\ 0 & 0 & 0 & 1 \end{pmatrix}. \quad (139d)$$

With respect to the previous model, the number of ATP and ADP molecules are separately conserved quantities, equations (139b) and (139c). The set of fundamental forces is empty while the potential reads

$$\phi_n = S_n - \beta(E_n - \mu_{ATP}N_n^{ATP} - \mu_{ADP}N_n^{ADP} - kX_n), \quad (140)$$

thus making the dissipation equal to

$$\Sigma[\mathbf{n}_t] = \Delta\Phi[\mathbf{n}_t]. \quad (141)$$

Therefore, the change of network topology achieved by removing transitions creating cycles, prevents the reservoirs from creating forces. The potential will be thus described with the maximum amount of conserved quantities, one for each y .

Alternative description. An alternative description of the chemomechanical process is obtained when periodic boundary conditions are imposed, figure 9. One additional cycle is created,

$$C = \begin{pmatrix} c & a \\ +1 & \begin{pmatrix} 0 & 1 \\ 1 & 1 \end{pmatrix} \\ +2 & \begin{pmatrix} 1 & 1 \\ 1 & 1 \end{pmatrix} \\ +3 & \begin{pmatrix} 1 & 1 \\ 1 & 1 \end{pmatrix} \\ +4 & \begin{pmatrix} 1 & 1 \\ 1 & 0 \end{pmatrix} \\ +5 & \begin{pmatrix} 1 & 0 \\ 1 & 0 \end{pmatrix} \\ +6 & \begin{pmatrix} 1 & 0 \\ 1 & 0 \end{pmatrix} \\ +7 & \begin{pmatrix} 1 & 0 \\ 1 & 0 \end{pmatrix} \end{pmatrix}, \quad (142)$$

see equation (125), and the M -matrix now reads

$$M := \begin{pmatrix} (E) & & \\ (N, ATP) & \begin{pmatrix} c & a \\ 0 & 0 \end{pmatrix} & \\ (N, ADP) & & \\ (X) & & \begin{pmatrix} c & a \\ 2 & 1 \\ -2 & -1 \\ 0 & l \end{pmatrix} \end{pmatrix}, \quad (143)$$

As a consequence, the spatial conservation law, (127c), is lost and the nonequilibrium Massieu potential becomes ω_n , equations (130) and (136). However, the set of fundamental forces gains one element,

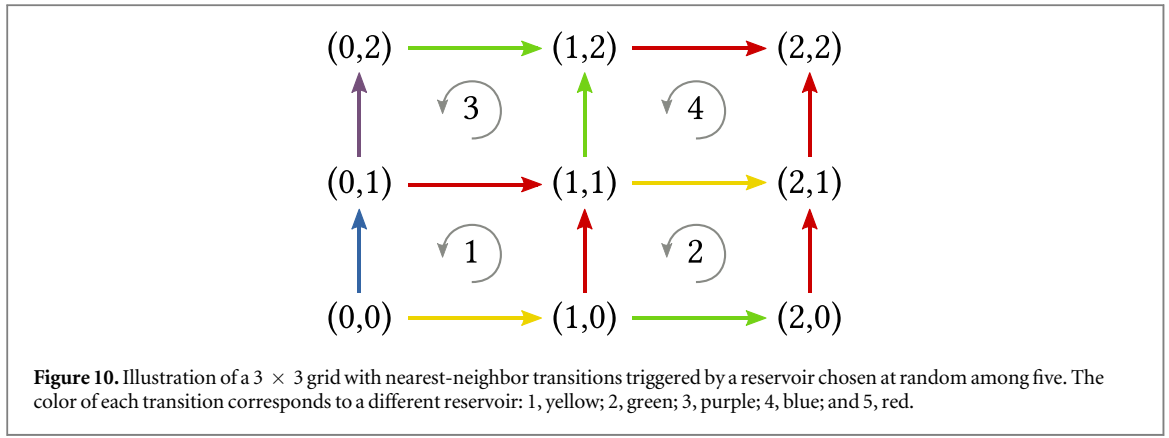


Figure 10. Illustration of a 3×3 grid with nearest-neighbor transitions triggered by a reservoir chosen at random among five. The color of each transition corresponds to a different reservoir: 1, yellow; 2, green; 3, purple; 4, blue; and 5, red.

$$\mathcal{F}_{(X)} = \beta k, \quad (144)$$

which is conjugated to the traveled distance:

$$\mathcal{X}[\mathbf{n}_t] := \int_0^t d\tau \delta Y_e^{(X)} J^e(\tau) = l \int_0^t d\tau [J^{+1_x}(\tau) - J^{-1_x}(\tau)]. \quad (145)$$

Hence, the expression of the EP and the formulation of the finite-time detailed FT read as in equations (135) and (138), respectively.

In conclusion, the periodic boundary condition can be viewed as a change of network topology in which one conservation law is lost and a fundamental force emerges.

6.4. Randomized grid

As a final illustration, we consider a particle hopping between states positioned at the nodes of a two-dimensional grid, $n = (x, z)$ for $x, z = 1, \dots, N$. The transitions along the edges are triggered by randomly distributed work reservoirs. This model provides an example of systems which could not be analyzed thermodynamically without resorting to our systematic procedure. It also shows how physical topological alterations may give rise to symmetry changes which in turn affects the thermodynamics.

The states are characterized by a spatial coordinate $X_n = a_x x + a_z z$, and jumps are only allowed between nearest neighbors: $x \rightarrow x \pm 1$ or $z \rightarrow z \pm 1$. The system is isothermal and each transition is ruled by a force $f_{(X,r)} = -\beta k_r$, which is initially drawn randomly from a set of N_r reservoirs. The δY -matrix relating transitions to reservoirs is given by

$$\delta Y_e^r = \begin{cases} \pm a_x & \text{if } e = x \xrightarrow{r} x \pm 1 \\ \pm a_z & \text{if } e = z \xrightarrow{r} z \pm 1 \\ 0 & \text{otherwise} \end{cases} \quad (146)$$

i.e. if e is triggered by the work reservoir r , then δY_e^r is equal to $\pm a_x$ or $\pm a_z$ depending on the direction of the transition.

As an example, we consider the 3×3 grid coupled to 5 reservoirs depicted in figure 10. We omit to report the matrices δY and C as they can be easily inferred from equation (146) and the picture, and move on to the M -matrix, which reads

$$M = \begin{pmatrix} & 1 & 2 & 3 & 4 \\ (X, 1) & a_x & -a_x & 0 & a_x \\ (X, 2) & 0 & a_x & a_z - a_x & -a_z \\ (X, 3) & 0 & 0 & -a_z & 0 \\ (X, 4) & -a_z & 0 & 0 & 0 \\ (X, 5) & a_z - a_x & 0 & a_x & a_z - a_x \end{pmatrix}. \quad (147)$$

Its one-dimensional cokernel is spanned by the vector

$$\mathcal{C}^X = (1 \quad 1 \quad 1 \quad 1 \quad 1) \quad (X, 1) \quad (X, 2) \quad (X, 3) \quad (X, 4) \quad (X, 5) \quad (148)$$

which corresponds to the global conserved quantity X_n . In contrast, its kernel is empty denoting the absence of symmetries. Setting $-\beta k_l$ as ‘potential’ field, y_p , the nonequilibrium potential reads

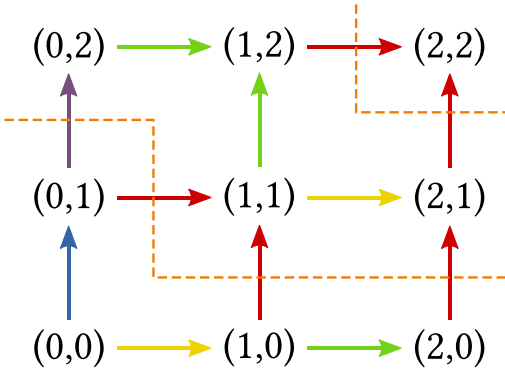


Figure 11. Illustration of the randomized grid in figure 10 for $a_x = a_z = a$. The grid is split into three groups of states by the transitions corresponding to the third (purple) and fifth (red) reservoir: $\{(0, 0), (1, 0), (0, 1), (2, 0)\}$, $\{(1, 1), (0, 2), (2, 1)\}$, and $\{(2, 2)\}$.

$$\phi_n = \beta k_l X_n, \quad (149)$$

while the fundamental forces are equal to

$$\mathcal{F}_{(X,r)} = \beta(k_r - k_l), \quad \text{for } r = 2, \dots, 5. \quad (150)$$

The trajectory EP can be thus expressed as

$$\Sigma[\mathbf{n}_t] = \nu[\mathbf{n}_t] + \sum_{r=2}^5 \sigma_r[\mathbf{n}_t] + \Delta\Phi[\mathbf{n}_t], \quad (151)$$

where

$$\nu[\mathbf{n}_t] := -\beta \int_0^t d\tau \partial_\tau [k_l(\tau) X_n(\tau)]|_{n=n_\tau}, \quad (152a)$$

$$\sigma_r[\mathbf{n}_t] := \beta \int_0^t d\tau [k_r(\tau) - k_l(\tau)] I_r(\tau). \quad (152b)$$

In order to show the emergence of a symmetry following a change of physical topology, let us now assume that $a_x = a_z = a$ and carry on the same analysis as before. The M -matrix now becomes,

$$M = \begin{pmatrix} (X, 1) & 1 & 2 & 3 & 4 \\ (X, 2) & a & -a & 0 & a \\ (X, 3) & 0 & a & 0 & -a \\ (X, 4) & 0 & 0 & -a & 0 \\ (X, 5) & -a & 0 & 0 & 0 \\ (X, 6) & 0 & 0 & a & 0 \end{pmatrix}. \quad (153)$$

whose kernel and cokernel are one and two-dimensional, respectively. The symmetries are given by

$$\psi = \begin{pmatrix} 1 & 2 & 3 & 4 \\ 0 & 1 & 0 & 1 \end{pmatrix}, \quad (154)$$

and tell us that the second and fourth cycles are not physically independent, as they are coupled to the same reservoirs and all displacements are the same. The basis of $\text{coker } M$,

$$\mathcal{C}^X = \begin{pmatrix} (X, 1) & (X, 2) & (X, 3) & (X, 4) & (X, 5) \\ (1 & 1 & 1 & 1 & 1) \end{pmatrix}, \quad (155a)$$

$$\mathcal{C}^V = \begin{pmatrix} (X, 1) & (X, 2) & (X, 3) & (X, 4) & (X, 5) \\ (0 & 0 & 1 & 0 & 1) \end{pmatrix} \quad (155b)$$

identifies two state variables, the first of which is the global conserved quantity, X_n , whereas the second is

$$V_n = \begin{pmatrix} (0, 0) & (1, 0) & (0, 1) & (2, 0) & (1, 1) & (0, 2) & (2, 1) & (1, 2) & (2, 2) \\ (0 & 0 & 0 & 0 & a & a & a & a & 2a) \end{pmatrix} \quad (156)$$

whose interpretation is not obvious. It arises from the fact that x - and z -transitions are indistinguishable and the reservoirs 3 and 5 split the states into three groups, see figure 11, which are identified by different values of V_n , equation (156). We can set $(X, 1)$ and $(X, 3)$ as the reservoirs of the set $\{y_p\}$, according to which the Massieu potential of the state n reads

$$\phi_n = \beta [k_l X_n + (k_3 - k_l) V_n]. \quad (157)$$

The number of fundamental forces is thus reduced,

$$\mathcal{F}_{(X,2)} = \beta k_2 - \beta k_1, \quad (158a)$$

$$\mathcal{F}_{(X,4)} = \beta k_4 - \beta k_1, \quad (158b)$$

$$\mathcal{F}_{(X,5)} = \beta k_5 - \beta k_3. \quad (158c)$$

The EP can be easily written.

This model exemplifies the emergence of nontrivial conservation laws whose identification is not straightforward, and motivates the need for a systematic procedure capable of separating the conservative contributions to the EP from the nonconservative ones.

7. Conclusions and perspectives

The central achievement of this paper is to show that the EP of an open system described by stochastic thermodynamics is shaped by the way conserved quantities constrain the exchanges between the system and the reservoirs. Some of these conserved quantities are the obvious ones which do not depend on the system details (e.g. energy, particle number). But we provide a systematic procedure to identify the nontrivial ones which depend on the system topology. As a result, we can split the EP into three fundamental contributions, one solely caused by the time-dependent drivings, another expressed as the change of a nonequilibrium Massieu potential, and a third one which contains the fundamental set of flux and forces. Table 3 indicates which of these contributions play a role in different known processes. We also showed how to make use of this decomposition to derive a finite-time detailed FT solely expressed in terms of physical quantities, as well as to assess the cost of manipulating nonequilibrium states via time-dependent driving and nonconservative forces.

We believe that this work provides a comprehensive formulation of stochastic thermodynamics. Our framework can be systematically used to study any specific model (as we illustrated on several examples) and demonstrates the crucial importance of conservation laws in thermodynamics, at, as well as out of, equilibrium.

Acknowledgments

We thank G. Bulnes Cuetara for advises on the FT proof. This work was funded by the National Research Fund of Luxembourg (AFR PhD Grant 2014-2, No. 9114110) and the European Research Council project NanoThermo (ERC-2015-CoG Agreement No. 681456).

Appendix A. Proof of the one-to-one correspondence between fundamental forces and fundamental affinities

We need to prove that the matrix whose entries are $\{M_{\eta}^{y_f}\}$ is nonsingular given the following hypotheses: (i) the vectors labeled by η whose entries are $\{M_{\eta}^y\}$, for $y = 1, \dots, N_y$, are linearly independent; (ii) $\ell_{y_f}^{\lambda} M_{\alpha}^{y_f} + \ell_{y_p}^{\lambda} M_{\alpha}^{y_p} = 0$ for all λ and α , where the matrix whose entries are $\{\ell_{y_f}^{\lambda}\}$ is nonsingular. Let us now assume by contradiction that $\{M_{\eta}^{y_f}\}$ is singular, and let us denote by $\{x^{\eta}\}$ the entries of a non-null vector such that $M_{\eta}^{y_f} x^{\eta} = 0$ for all y_f . We can thus construct a vector $\{x^{\alpha}\}$ having as entries corresponding to η , $\{x^{\eta}\}$, and zero for the others. Hence, $M_{\alpha}^{y_f} x^{\alpha} = 0$ for all y_f . From the equation in the second hypothesis, we get

$$\ell_{y_p}^{\lambda} M_{\alpha}^{y_p} x^{\alpha} + \ell_{y_f}^{\lambda} M_{\alpha}^{y_f} x^{\alpha} = \ell_{y_p}^{\lambda} M_{\eta}^{y_p} x^{\eta} = 0.$$

Since the matrix whose entries are $\{\ell_{y_p}^{\lambda}\}$ is nonsingular, we must conclude that $M_{\eta}^{y_p} x^{\eta} = 0$ for all y_p , and thus $M_{\eta}^y x^{\eta} = 0$ for all y , in contradiction with the hypothesis (i).

Appendix B. Proof of the finite-time detailed FTs

We now give the proof of the finite time detailed FTs (55) using moment generating functions. Alternatively, it can be proved using the approach developed in [53]. For our purposes, we change our notation for a bracket operatorial one.

Let $P_t(n, \nu, \{\sigma_{\gamma_i}\})$ be the joint probability of observing a trajectory ending in the state n along which the driving contribution is ν while the flow ones are $\{\sigma_{\gamma_i}\}$. The above probabilities, one for each n , are stacked in the ket $|P_t(\nu, \{\sigma_{\gamma_i}\})\rangle$. The time evolution of the moment generating function of the above probabilities,

$$|\Lambda_t(\xi_d, \{\xi_{\gamma_i}\})\rangle := \int d\nu \prod_{\gamma_i} d\sigma_{\gamma_i} \exp\{-\xi_d \nu - \xi_{\gamma_i} \sigma_{\gamma_i}\} |P_t(\nu, \{\sigma_{\gamma_i}\})\rangle, \quad (\text{B1})$$

is ruled by the biased stochastic dynamics

$$d_t |\Lambda_t(\xi_d, \{\xi_{\gamma_i}\})\rangle = \mathcal{W}_t(\xi_d, \{\xi_{\gamma_i}\}) |\Lambda_t(\xi_d, \{\xi_{\gamma_i}\})\rangle, \quad (\text{B2})$$

where the entries of the biased generator are given by

$$\mathcal{W}_{nm,t}(\xi_d, \{\xi_{\gamma_i}\}) = \sum_e w_e \{ \exp\{-\xi_{\gamma_e} \mathcal{F}_{\gamma_e} \delta Y_{\gamma_e, e}\} \delta_{n,o(-e)} \delta_{m,o(e)} + \delta_{n,m} \delta_{m,o(e)} \} + \xi_d \partial_t \phi_m \delta_{n,m}. \quad (\text{B3})$$

Because of the local detailed balance (13), the stochastic generator satisfies the following symmetry

$$\mathcal{W}_t^T(\xi_d, \{\xi_{\gamma_i}\}) = \mathcal{B}_t^{-1} \mathcal{W}_t(\xi_d, \{1 - \xi_{\gamma_i}\}) \mathcal{B}_t, \quad (\text{B4})$$

where the entries of \mathcal{B}_t are given by

$$\mathcal{B}_{nm,t} := \exp\{\phi_m\} \delta_{n,m}. \quad (\text{B5})$$

Also, the initial condition is given by the equilibrium distribution (25), which reads

$$|\Lambda_0(\xi_d, \{\xi_{\gamma_i}\})\rangle = |p_{\text{eq}_i}\rangle = \mathcal{B}_0/Z_0|1\rangle, \quad (\text{B6})$$

where $Z_0 := \exp\{\Phi_{\text{eq}_i}\}$ is the partition function. The ket $|1\rangle$ refers to the vector in the state space whose entries are all equal to one.

In order to proceed further, it is convenient to first prove a preliminary result. Let us consider the generic biased dynamics, e.g. equation (B2),

$$d_t |\Lambda_t(\xi)\rangle = \mathcal{W}_t(\xi) |\Lambda_t(\xi)\rangle, \quad (\text{B7})$$

whose initial condition is $|\Lambda_0(\xi)\rangle = |p(0)\rangle$. A formal solution of equation (B7) is $|\Lambda_t(\xi)\rangle = \mathcal{U}_t(\xi) |p(0)\rangle$, where the time-evolution operator reads $\mathcal{U}_t(\xi) = \mathcal{T}_+ \exp\left\{\int_0^t d\tau \mathcal{W}_\tau(\xi)\right\}$, \mathcal{T}_+ being the time-ordering operator. We clearly have $d_t \mathcal{U}_t(\xi) = \mathcal{W}_t(\xi) \mathcal{U}_t(\xi)$. Let us now consider the following transformed evolution operator

$$\tilde{\mathcal{U}}_t(\xi) := \mathcal{X}_t^{-1} \mathcal{U}_t(\xi) \mathcal{X}_0, \quad (\text{B8})$$

\mathcal{X}_t being a generic invertible operator. Its dynamics is ruled by the following biased stochastic dynamics

$$d_t \tilde{\mathcal{U}}_t(\xi) = d_t \mathcal{X}_t^{-1} \mathcal{U}_t(\xi) \mathcal{X}_0 + \mathcal{X}_t^{-1} d_t \mathcal{U}_t(\xi) \mathcal{X}_0 = \{d_t \mathcal{X}_t^{-1} \mathcal{X}_t + \mathcal{X}_t^{-1} \mathcal{W}_t(\xi) \mathcal{X}_t\} \tilde{\mathcal{U}}_t(\xi) \equiv \tilde{\mathcal{W}}_t(\xi) \tilde{\mathcal{U}}_t(\xi), \quad (\text{B9})$$

which allows us to conclude that the transformed time-evolution operator is given by

$$\tilde{\mathcal{U}}_t(\xi) = \mathcal{T}_+ \exp\left\{\int_0^t d\tau \tilde{\mathcal{W}}_\tau(\xi)\right\}. \quad (\text{B10})$$

From equations (B8)–(B10) we deduce that

$$\mathcal{X}_t^{-1} \mathcal{U}_t(\xi) \mathcal{X}_0 = \mathcal{T}_+ \exp\left\{\int_0^t d\tau [\mathcal{X}_\tau^{-1} \mathcal{X}_\tau + \mathcal{X}_\tau^{-1} \mathcal{W}_\tau(\xi) \mathcal{X}_\tau]\right\}. \quad (\text{B11})$$

We can now come back to our specific biased stochastic dynamics (B2). The moment generating function of $P_t(\nu, \{\sigma_{\gamma_i}\})$ is thus given by

$$\Lambda_t(\xi_d, \{\xi_{\gamma_i}\}) = \langle 1 | \Lambda_t(\xi_d, \{\xi_{\gamma_i}\}) \rangle = \langle 1 | \mathcal{U}_t(\xi_d, \{\xi_{\gamma_i}\}) \mathcal{B}_0 / Z_0 | 1 \rangle = \left\langle 1 \left| \frac{\mathcal{B}_t}{Z_t} \mathcal{B}_t^{-1} \mathcal{U}_t(\xi_d, \{\xi_{\gamma_i}\}) \mathcal{B}_0 \right| 1 \right\rangle \frac{Z_t}{Z_0}, \quad (\text{B12})$$

where $\mathcal{U}_t(\xi_d, \{\xi_{\gamma_i}\})$ is the time-evolution operator of the biased stochastic dynamics (B2). The requirement imposed on π_t —discussed in the main text—ensures that $\langle 1 | \mathcal{B}_t / Z_t$ with $Z_t := \exp\{\Phi_{\text{eq}_i}\}$ is the equilibrium initial distribution of the backward process $\langle p_{\text{eq}_i} \rangle$. Using the relation in equation (B11), the above term can be rewritten as

$$= \left\langle p_{\text{eq}_i} \left| \mathcal{T}_+ \exp\left\{\int_0^t d\tau [\partial_\tau \mathcal{B}_\tau^{-1} \mathcal{B}_\tau + \mathcal{B}_\tau^{-1} \mathcal{W}_\tau(\xi_d, \{\xi_{\gamma_i}\}) \mathcal{B}_\tau]\right\} \right| 1 \right\rangle \exp\{\Delta \Phi_{\text{eq}}\}, \quad (\text{B13})$$

where $\Delta \Phi_{\text{eq}} \equiv \ln Z_t / Z_0$. Since $\partial_\tau \mathcal{B}_\tau^{-1} \mathcal{B}_\tau = \text{diag}\{-\partial_\tau \phi_n\}$ the first term in square bracket can be added to the diagonal entries of the second term, thus giving

$$= \left\langle p_{\text{eq}_f} \left| \mathcal{T}_+ \exp \left\{ \int_0^t d\tau [\mathcal{B}_\tau^{-1} \mathcal{W}_\tau(\xi_d - 1, \{\xi_{y_f}\}) \mathcal{B}_\tau] \right\} \right| 1 \right\rangle \exp \{\Delta \Phi_{\text{eq}}\}. \quad (\text{B14})$$

The symmetry (B4) allow us to recast the latter into

$$= \left\langle p_{\text{eq}_f} \left| \mathcal{T}_+ \exp \left\{ \int_0^t d\tau \mathcal{W}_\tau^T(\xi_d - 1, \{1 - \xi_{y_f}\}) \right\} \right| 1 \right\rangle \exp \{\Delta \Phi_{\text{eq}}\}. \quad (\text{B15})$$

The crucial step comes as we transform the integration variable from τ to $\tau^\dagger = t - \tau$. Accordingly, the time-ordering operator, \mathcal{T}_+ , becomes an anti-time-ordering one \mathcal{T}_- , while the diagonal entries of the biased generator, equation (B3), become

$$\begin{aligned} \mathcal{W}_{mm, t - \tau^\dagger}(\xi_d, \{\xi_{y_f}\}) &= \sum_e w_e(t - \tau^\dagger) \delta_{m,o(e)} + \xi_d \partial_{(t - \tau^\dagger)} [\phi_m(t - \tau^\dagger)] \\ &= \sum_e w_e(t - \tau^\dagger) \delta_{m,o(e)} - \xi_d \partial_{\tau^\dagger} [\phi_m(t - \tau^\dagger)], \end{aligned} \quad (\text{B16})$$

from which we conclude that

$$\mathcal{W}_{nm, t - \tau^\dagger}(\xi_d, \{\xi_{y_f}\}) = \mathcal{W}_{nm, t - \tau^\dagger}(-\xi_d, \{\xi_{y_f}\}) =: \mathcal{W}_{nm, \tau^\dagger}^*(-\xi_d, \{\xi_{y_f}\}). \quad (\text{B17})$$

Above, $\mathcal{W}_{\tau^\dagger}^*(-\xi_d, \{\xi_{y_f}\})$ is the biased generator of the dynamics subject to the time-reversed protocol, π^\dagger , i.e. the dynamics of the backward process. Equation (B15) thus becomes

$$= \left\langle p_{\text{eq}_f} \left| \mathcal{T}_- \exp \left\{ \int_0^t d\tau^\dagger \mathcal{W}_{\tau^\dagger}^T(1 - \xi_d, \{1 - \xi_{y_f}\}) \right\} \right| 1 \right\rangle \exp \{\Delta \Phi_{\text{eq}}\}. \quad (\text{B18})$$

Upon a global transposition, we can write

$$= \left\langle 1 \left| \mathcal{T}_+ \exp \left\{ \int_0^t d\tau^\dagger \mathcal{W}_{\tau^\dagger}^T(1 - \xi_d, \{1 - \xi_{y_f}\}) \right\} \right| p_{\text{eq}_f} \right\rangle \exp \{\Delta \Phi_{\text{eq}}\}, \quad (\text{B19})$$

where we also used the relationship between transposition and time-ordering

$$\mathcal{T}_+ \left(\prod_i A_{t_i}^T \right) = \left(\mathcal{T}_- \prod_i A_{t_i} \right)^T, \quad (\text{B20})$$

in which A_t is a generic operator. From the last expression, we readily obtain

$$= \langle 1 | \mathcal{U}_t^\dagger(1 - \xi_d, \{1 - \xi_{y_f}\}) | p_{\text{eq}_f} \rangle \exp \{\Delta \Phi_{\text{eq}}\} = \Lambda_t^\dagger(1 - \xi_d, \{1 - \xi_{y_f}\}) \exp \{\Delta \Phi_{\text{eq}}\}, \quad (\text{B21})$$

where $\Lambda_t^\dagger(\xi_d, \{\xi_{y_f}\})$ is the moment generating function of $P^\dagger(\nu, \{\sigma_{y_f}\})$. Summarizing, we have the following symmetry

$$\Lambda_t(\xi_d, \{\xi_{y_f}\}) = \Lambda_t^\dagger(1 - \xi_d, \{1 - \xi_{y_f}\}) \exp \{\Delta \Phi_{\text{eq}}\}, \quad (\text{B22})$$

whose inverse Laplace transform gives the FT

$$\frac{P_t(\nu, \{\sigma_{y_f}\})}{P_t^\dagger(-\nu, \{-\sigma_{y_f}\})} = \exp \left\{ \nu + \sum_{y_f} \sigma_{y_f} + \Delta \Phi_{\text{eq}} \right\}. \quad (\text{B23})$$

B.1. Fundamental cycles

The finite-time detailed FT for flow contributions along fundamental cycles, equation (61), follows the same logic and mathematical steps described above. The moment generating function which now must be taken into account is

$$|\Lambda_t(\xi_d, \{\xi_\eta\})\rangle := \int d\nu \prod_\eta d\gamma_\eta \exp \{-\xi_d \nu - \xi_\eta \gamma_\eta\} |P_t(\nu, \{\gamma_\eta\})\rangle, \quad (\text{B24})$$

which is ruled by the biased generator whose entries are

$$\mathcal{W}_{nm,t}(\xi_d, \{\xi_\eta\}) = \sum_e w_e \{ \exp \{-\xi_\eta \mathcal{A}_\eta \zeta_{\eta,e}\} \delta_{n,o(-e)} \delta_{m,o(e)} + \delta_{n,m} \delta_{m,o(e)} \} + \xi_d \partial_t \phi_m \delta_{n,m}. \quad (\text{B25})$$

The symmetry of the latter generator—on top of which the proof is constructed—is based on the expression of the local detailed balance given in equation (13),

$$\mathcal{W}_t^T(\xi_d, \{\xi_\eta\}) = \mathcal{B}_t^{-1} \mathcal{W}_t(\xi_d, \{1 - \xi_\eta\}) \mathcal{B}_t, \quad (\text{B26})$$

where the entries of \mathcal{B}_t are given in equation (B5). Following the steps from equation (B12) to equation (B22), with the above definitions and equations, equations (B24)–(B26), proves the FT in equation (61).

ORCID iDs

Riccardo Rao  <https://orcid.org/0000-0003-0040-6783>
Massimiliano Esposito  <https://orcid.org/0000-0002-2249-4035>

References

- [1] Sekimoto K 2010 *Stochastic Energetics* (Berlin: Springer)
- [2] Jarzynski C 2011 *Annu. Rev. Condens. Matter Phys.* **2** 329
- [3] Seifert U 2012 *Rep. Prog. Phys.* **75** 126001
- [4] Van den Broeck C and Esposito M 2015 *Physica A* **418** 6
- [5] Ciliberto S 2017 *Phys. Rev. X* **7** 021051
- [6] Verley G, Willaert T, Van den Broeck C and Esposito M 2014 *Phys. Rev. E* **90** 052145
- [7] Proesmans K, Dreher Y, Gavrilov M, Bechhoefer J and Van den Broeck C 2016 *Phys. Rev. X* **6** 041010
- [8] Berut A, Arakelyan A, Petrosyan A, Ciliberto S, Dillenschneider R and Lutz E 2012 *Nature* **483** 187
- [9] Horowitz J M and Esposito M 2014 *Phys. Rev. X* **4** 031015
- [10] Jun Y, Gavrilov M and Bechhoefer J 2014 *Phys. Rev. Lett.* **113** 190601
- [11] Parrondo J M R, Horowitz J M and Sagawa T 2015 *Nat. Phys.* **11** 131
- [12] Ouldridge T E, Govern C C and ten Wolde P R 2017 *Phys. Rev. X* **7** 021004
- [13] Rao R and Peliti L 2015 *J. Stat. Mech.* **P06001**
- [14] Barato A C and Seifert U 2016 *Phys. Rev. X* **6** 041053
- [15] Esposito M 2012 *Phys. Rev. E* **85** 041125
- [16] Polettini M, Bulnes Cuetara G and Esposito M 2016 *Phys. Rev. E* **94** 052117
- [17] Bulnes Cuetara G, Esposito M and Imparato A 2014 *Phys. Rev. E* **89** 052119
- [18] Hasegawa H-H, Ishikawa J, Takara K and Driebe D 2010 *Phys. Lett. A* **374** 1001
- [19] Takara K, Hasegawa H-H and Driebe D 2010 *Phys. Lett. A* **375** 88
- [20] Esposito M and Van den Broeck C 2011 *Europhys. Lett.* **95** 40004
- [21] Callen H 1985 *Thermodynamics and an Introduction to Thermostatistics* (New York: Wiley)
- [22] Beard D A and Qian H 2008 *Chemical Biophysics: Quantitative Analysis of Cellular Systems* (Cambridge: Cambridge University Press)
- [23] Rutten B, Esposito M and Cleuren B 2009 *Phys. Rev. B* **80** 235122
- [24] Knauer U 2011 *Algebraic Graph Theory: Morphisms, Monoids and Matrices* (Berlin: de Gruyter & Co)
- [25] Schnakenberg J 1976 *Rev. Mod. Phys.* **48** 571
- [26] Kolmogoroff A 1936 *Math. Ann.* **112** 155
- [27] Kelly F P 1979 *Reversibility and Stochastic Networks* (New York: Wiley)
- [28] Peliti L 2011 *Statistical Mechanics in a Nutshell* (Princeton, NJ: Princeton University Press)
- [29] Jaynes E T 1957 *Phys. Rev.* **106** 620
- [30] Seifert U 2005 *Phys. Rev. Lett.* **95** 040602
- [31] Polettini M 2012 *Europhys. Lett.* **97** 30003
- [32] Wachtel A, Vollmer J and Altaner B 2015 *Phys. Rev. E* **92** 042132
- [33] Campisi M, Hänggi P and Talkner P 2011 *Rev. Mod. Phys.* **83** 771
- [34] Jarzynski C 1997 *Phys. Rev. Lett.* **78** 2690
- [35] Crooks G E 1998 *J. Stat. Phys.* **90** 1481
- [36] Altaner B 2017 *J. Phys. A: Math. Theor.* **50** 454001
- [37] Polettini M 2014 *Lett. Math. Phys.* **105** 89
- [38] Andrieux D and Gaspard P 2007 *J. Stat. Phys.* **127** 107
- [39] Polettini M and Esposito M 2014 *J. Stat. Mech.* **P10033**
- [40] Esposito M, Harbola U and Mukamel S 2007 *Phys. Rev. E* **76** 031132
- [41] Harris R J and Schütz G M 2007 *J. Stat. Mech.* **7** P07020
- [42] Esposito M and Van den Broeck C 2010 *Phys. Rev. Lett.* **104** 090601
- [43] Esposito M and Van den Broeck C 2010 *Phys. Rev. E* **82** 011143
- [44] Ge H and Qian H 2010 *Phys. Rev. E* **81** 051133
- [45] Sánchez R and Büttiker M 2012 *Europhys. Lett.* **100** 47008
- [46] Strasberg P, Schaller G, Brandes T and Esposito M 2013 *Phys. Rev. Lett.* **110** 040601
- [47] Thierschmann H, Sánchez R, Sothmann B, Arnold F, Heyn C, Hansen W, Buhmann H and Molenkamp L W 2015 *Nat. Nanotechnol.* **10** 854
- [48] Bulnes Cuetara G and Esposito M 2015 *New J. Phys.* **17** 095005
- [49] Liepelt S and Lipowsky R 2007 *Phys. Rev. Lett.* **98** 258102
- [50] Altaner B, Wachtel A and Vollmer J 2015 *Phys. Rev. E* **92** 042133
- [51] Seifert U 2011 *Eur. Phys. J. E* **34** 26
- [52] Horowitz J M and Esposito M 2016 *Phys. Rev. E* **94** 020102
- [53] García-García R, Domínguez D, Lecomte V and Kolton A B 2010 *Phys. Rev. E* **82** 030104

The following article is reprinted from
[R. RAO and M. ESPOSITO, *Entropy* **20**.9 (2018), 635]
under the conditions of the Creative Commons Attribution 4.0 Unported
Licence².

The page numbers placed in the outer margins provide a continuous pagination throughout the thesis.

² <https://creativecommons.org/licenses/by/4.0/>

Article

Detailed Fluctuation Theorems: A Unifying Perspective

Riccardo Rao  **and Massimiliano Esposito**  
¹ Complex Systems and Statistical Mechanics, Physics and Materials Science Research Unit, University of Luxembourg, L-1511 Luxembourg, Luxembourg; riccardo.rao@uni.lu

² Kavli Institute for Theoretical Physics, University of California, Santa Barbara, 93106 CA, USA

* Correspondence: massimiliano.esposito@uni.lu

Received: 24 July 2018; Accepted: 15 August 2018; Published: 24 August 2018



Abstract: We present a general method to identify an arbitrary number of fluctuating quantities which satisfy a detailed fluctuation theorem for all times within the framework of time-inhomogeneous Markovian jump processes. In doing so, we provide a unified perspective on many fluctuation theorems derived in the literature. By complementing the stochastic dynamics with a thermodynamic structure (i.e., using stochastic thermodynamics), we also express these fluctuating quantities in terms of physical observables.

Keywords: stochastic thermodynamics; fluctuation theorem; Markov jump process; entropy production; graph theory; conservation laws

PACS: 02.50.Ga; 05.70.Ln

1. Introduction

The discovery of different fluctuation theorems (FTs) over the last two decades constitutes a major progress in nonequilibrium physics [1–6]. These relations are exact constraints that some fluctuating quantities satisfy arbitrarily far from equilibrium. They have been verified experimentally in many different contexts, ranging from biophysics to electronic circuits [7]. However, they come in different forms: detailed fluctuation theorems (DFTs) or integral fluctuation theorems (IFTs), and concern various types of quantities. Understanding how they are related and to what extent they involve mathematical quantities or interesting physical observables can be challenging.

The aim of this paper is to provide a simple yet elegant method to identify a class of finite-time DFTs for time-inhomogeneous Markovian jump processes. The method is based on splitting the entropy production (EP) in three contributions by introducing a reference probability mass function (PMF). The latter is parametrized by the time-dependent driving protocol, which renders the dynamics time-inhomogeneous. The first contribution quantifies the EP as if the system were in the reference PMF, the second the extent to which the reference PMF changes with the driving protocol, and the last the mismatch between the actual and the reference PMF. We show that when the system is initially prepared in the reference PMF, the joint probability distribution for the first two terms always satisfies a DFT. We then show that various known DFTs can be immediately recovered as special cases. We emphasize at which level our results make contact with physics and also clarify the nontrivial connection between DFTs and EP fluctuations. Our EP splitting is also shown to be connected to information theory. Indeed, it can be used to derive a generalized Landauer principle identifying the minimal cost needed to move the actual PMF away from the reference PMF. While unifying, we emphasize that our approach by no means encompasses all previously derived FTs and that other FT generalizations have been made (e.g., [5,8–11]).

The plan of this paper is as follows. Time-inhomogeneous Markov jump processes are introduced in Section 2. Our main results are presented in Section 3: We first introduce the EP as a quantifier of detailed balance breaking, and we then show that by choosing a reference PMF, a splitting of the EP ensues. This enables us to identify the fluctuating quantities satisfying a DFT and an IFT when the system is initially prepared in the reference PMF. While IFTs hold for arbitrary reference PMFs, DFTs require reference PMFs to be solely determined by the driving protocol encoding the time dependence of the rates. The EP decomposition is also shown to lead to a generalized Landauer principle. The remaining sections are devoted to selecting specific reference PMFs and showing that they give rise to interesting mathematics or physics: In Section 4 the steady-state PMF of the Markov jump process is chosen, giving rise to the adiabatic–nonadiabatic split of the EP [12]. In Section 5 the equilibrium PMF of a spanning tree of the graph defined by the Markov jump process is chosen, and gives rise to a cycle–cocycle decomposition of the EP [13]. Physics is introduced in Section 6, and the properties that the Markov jump process must satisfy to describe the thermodynamics of an open system are described. In Section 7 the microcanonical distribution is chosen as the reference PMF, leading to the splitting of the EP into system and reservoir entropy change. Finally, in Section 8, the generalized Gibbs equilibrium PMF is chosen as a reference and leads to a conservative–nonconservative splitting of the EP [14]. Conclusions are finally drawn, and some technical proofs are discussed in the appendices.

2. Markov Jump Process

We introduce time-inhomogeneous Markovian jump processes and set the notation.

We consider an externally driven open system described by a finite number of states, which we label by n . Allowed transitions between pairs of states are identified by directed edges,

$$e \equiv (nm, \nu), \quad \text{for } n \xleftarrow{\nu} m, \quad (1)$$

where the label ν indexes different transitions between the same pair of states (e.g., transitions due to different reservoirs). The evolution in time of the probability of finding the system in the state n , $p_n \equiv p_n(t)$, is ruled by the *master equation* (ME):

$$d_t p_n = \sum_m W_{nm} p_m, \quad (2)$$

where the elements of the *rate matrix* are represented as

$$W_{nm} = \sum_e w_e \left\{ \delta_{n,t(e)} \delta_{m,o(e)} - \delta_{n,m} \delta_{m,o(e)} \right\}. \quad (3)$$

The latter is written in terms of stochastic transition rates, $\{w_e\}$, and the functions

$$o(e) := m, \quad \text{and} \quad t(e) := n, \quad \text{for } e = (nm, \nu), \quad (4)$$

which map each transition to the state from which it originates (origin) and to which it leads (target), respectively. The off-diagonal entries of the rate matrix (the first term in brackets) give the probability per unit time to transition from m to n . The diagonal ones (second term in brackets) are the escape rates denoting the probability per unit time of leaving the state m . For thermodynamic consistency, we assume that each transition $e \equiv (nm, \nu)$ is reversible, namely if w_e is finite, the corresponding backward transition $-e \equiv (mn, \nu)$ is allowed and additionally has a finite rate w_{-e} . For simplicity, we also assume that the rate matrix is irreducible at all times, so that the stochastic dynamics is ensured to be ergodic. The Markov jump process is said to be *time-inhomogeneous* when the transition rates depend on time. The driving *protocol value* π_t determines the values of all rates at time t , $\{w_e \equiv w_e(\pi_t)\}$.

The ME (2) can be rewritten as a continuity equation:

$$d_t p_n = \sum_e D_e^n \langle j^e \rangle, \quad (5)$$

where we introduced the averaged transition *probability fluxes*,

$$\langle j^e \rangle = w_e p_{\sigma(e)}, \quad (6)$$

and the *incidence matrix* D ,

$$D_e^n := \delta_{n,t(e)} - \delta_{n,\sigma(e)} = \begin{cases} +1 & \text{if } \xrightarrow{e} n, \\ -1 & \text{if } \xleftarrow{e} n, \\ 0 & \text{otherwise,} \end{cases} \quad (7)$$

which couples each transition to the pair of states that it connects, and hence encodes the *network topology*. On the graph identified by the vertices $\{n\}$ and the edges $\{e\}$, it can be viewed as a (negative) divergence operator when acting on edge-space vectors—as in the ME (5)—or as a gradient operator when acting on vertex-space vectors. It satisfies the symmetry $D_{-e}^n = -D_e^n$.

Example

Let us consider the Markov jump process on the network in Figure 1, in which only the six forward transitions are depicted. It is characterized by four states, $\{00, 01, 10, 11\}$, connected by transitions as described by the incidence matrix:

$$D = \begin{pmatrix} & +1 & +2 & +3 & +4 & +5 & +6 \\ 00 & -1 & -1 & -1 & 0 & 0 & 0 \\ 10 & 1 & 0 & 0 & 0 & -1 & -1 \\ 01 & 0 & 1 & 1 & -1 & 0 & 0 \\ 11 & 0 & 0 & 0 & 1 & 1 & 1 \end{pmatrix}. \quad (8)$$

Backward transitions are obtained from $D_{-e}^n = -D_e^n$.

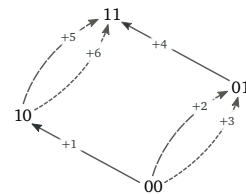


Figure 1. Illustration of a network of transitions.

Notation

From now on, upper-lower indices and Einstein summation notation will be used: repeated upper-lower indices implies the summation over all the allowed values for those indices. Time derivatives are denoted by “ d_t ” or “ ∂_t ”, whereas the overdot “ \cdot ” is reserved for rates of change of quantities that are not exact time derivatives of state functions. We also take the Boltzmann constant k_B equal to 1.

3. General Results

This section constitutes the core of the paper. The main results are presented in their most general form.

3.1. EP Decomposition at the Ensemble Average Level

After defining the ensemble-averaged EP, we will show how to generically decompose it in terms of a reference PMF.

A PMF p_n satisfies the *detailed-balance* property if and only if

$$w_e p_{\sigma(e)} = w_{-e} p_{\sigma(-e)}, \quad \text{for all transitions } e. \quad (9)$$

This implies that all net transition probability currents vanish: $\langle j^e \rangle - \langle j^{-e} \rangle = 0$. The central quantity that we will consider is the *EP rate*:

$$\langle \dot{\Sigma} \rangle = \frac{1}{2} A_e [\langle j^e \rangle - \langle j^{-e} \rangle] = A_e \langle j^e \rangle \geq 0, \quad (10)$$

where the *affinities* are given by

$$A_e = \ln \frac{w_e p_{\sigma(e)}}{w_{-e} p_{\sigma(-e)}}. \quad (11)$$

It is a measure of the amount by which the system breaks detailed balance or, equivalently, time-reversal symmetry. Indeed, its form ensures that it is always non-negative and vanishes if and only if Equation (9) holds. Notice that $A_{-e} = -A_e$. As we will see in Section 7, in physical systems the EP quantifies the total entropy change in the system plus environment [15].

We now decompose the EP rate into two contributions using a generic PMF $p_n^{\text{ref}} \equiv p_n^{\text{ref}}(t)$ as a *reference*. We make no assumption about the properties of p_n^{ref} at this stage, and define the reference potential and the reference affinities as

$$\psi_n^{\text{ref}} := -\ln p_n^{\text{ref}} \quad (12)$$

and

$$A_e^{\text{ref}} := \ln \frac{w_e p_{\sigma(e)}^{\text{ref}}}{w_{-e} p_{\sigma(-e)}^{\text{ref}}} = \ln \frac{w_e}{w_{-e}} + \psi_n^{\text{ref}} D_e^n, \quad (13)$$

respectively. The former can be thought of as the entropy associated to p_n^{ref} —i.e., its *self-information*—, whereas the latter measures the extent by which p_n^{ref} breaks detailed balance. By merely adding and subtracting $\psi_n^{\text{ref}} D_e^n$ from the EP rate, the latter can be formally decomposed as

$$\langle \dot{\Sigma} \rangle = \langle \dot{\Sigma}_{\text{nc}} \rangle + \langle \dot{\Sigma}_{\text{c}} \rangle \geq 0, \quad (14)$$

where the *reference nonconservative contribution* is an EP with affinities replaced by reference affinities:

$$\langle \dot{\Sigma}_{\text{nc}} \rangle := A_e^{\text{ref}} \langle j^e \rangle, \quad (15)$$

and the *reference conservative contribution* is

$$\langle \dot{\Sigma}_{\text{c}} \rangle := -\sum_n d_t p_n \ln \left\{ p_n / p_n^{\text{ref}} \right\}. \quad (16)$$

Using the ME (5), it can be further decomposed as

$$\langle \dot{\Sigma}_{\text{c}} \rangle = -d_t \mathcal{D}(p \| p^{\text{ref}}) + \langle \dot{\Sigma}_{\text{d}} \rangle, \quad (17)$$

where the first term quantifies the change in time of the *dissimilarity* between p_n and p_n^{ref} , since

$$\mathcal{D}(p \| p^{\text{ref}}) := \sum_n p_n \ln \left\{ p_n / p_n^{\text{ref}} \right\} \quad (18)$$

is a *relative entropy*, whereas the second term,

$$\langle \dot{\Sigma}_d \rangle := -\sum_n p_n d_t \ln p_n^{\text{ref}} = \sum_n p_n d_t \psi_n^{\text{ref}}, \quad (19)$$

accounts for possible time-dependent changes of the reference state, and we name it the *driving contribution*. The reason for this name will become clear later, as we will request p_n^{ref} to depend parametrically on time only via the driving protocol (i.e., $p_n^{\text{ref}}(t) = p_n^{\text{ref}}(\pi_t)$).

Using these equations, one can easily rearrange Equation (14) into

$$\langle \dot{\Sigma}_d \rangle + \langle \dot{\Sigma}_{\text{nc}} \rangle \geq d_t \mathcal{D}(p \| p^{\text{ref}}). \quad (20)$$

When $p_n^{\text{ref}}(t) = p_n^{\text{ref}}(\pi_t)$, one can interpret this equation as follows. The lhs describes the EP contribution due to the time-dependent protocol, $\langle \dot{\Sigma}_d \rangle$, and to the break of detailed balance required to sustain the reference PMF, $\langle \dot{\Sigma}_{\text{nc}} \rangle$. When positive, the rhs thus represents the minimal cost (ideally achieved at vanishing EP) to move the PMF further away from the reference PMF. When negative, its absolute value becomes the maximal amount by which the two EP contributions can decrease, as the PMF approaches the reference PMF. This result can be seen as a *mathematical generalization of the Landauer principle*, as it provides a connection between an information-theoretical measure of the dissimilarity between two PMFs and the driving and break of detailed balance needed to achieve it. Its precise physical formulation, discussed in detail in [14], is obtain when expressing Equation (20) in terms of the reference PMF used in Section 8.

3.2. EP Decomposition at the Trajectory Level

We now perform the analogue of the EP decomposition (14) at the level of single stochastic trajectories.

A stochastic *trajectory* of duration t , \mathbf{n}_t , is defined as a set of transitions $\{e_i\}$ sequentially occurring at times $\{t_i\}$ starting from n_0 at time 0. If not stated otherwise, the transitions index i runs from $i = 1$ to the last transition prior to time t , N_t , whereas the state at time $\tau \in [0, t]$ is denoted by n_τ . The whole trajectory is encoded in the *instantaneous fluxes*,

$$j^e(\tau) := \sum_i \delta_{e,e_i} \delta(\tau - t_i), \quad (21)$$

as they encode the transitions that occur and their timing. Its corresponding trajectory probability measure is given by

$$\mathfrak{P}[\mathbf{n}_t; \pi_t] = \prod_{i=1}^{N_t} w_{e_i}(\pi_{t_i}) \prod_{i=0}^{N_t} \exp \left\{ - \int_{t_i}^{t_{i+1}} d\tau \sum_e w_e(\pi_\tau) \delta_{n_\tau, \mathbf{o}(e)} \right\}, \quad (22)$$

where the first term accounts for the probability of transitioning along the edges, while the second accounts for the probability that the system spends $\{t_{i+1} - t_i\}$ time in the state $\{n_{t_i}\}$. When averaging Equation (21) over all stochastic trajectories, we obtain the averaged fluxes, Equation (6),

$$\langle j^e(\tau) \rangle = \int \mathcal{D}\mathbf{n}_t \mathfrak{P}[\mathbf{n}_t; \pi_t] p_{n_0}(0) j^e(\tau), \quad (23)$$

where $\int \mathcal{D}\mathbf{n}_t$ denotes the integration over all stochastic trajectories.

The change along \mathbf{n}_t of a state function like ψ_n^{ref} can be expressed as

$$\Delta \psi^{\text{ref}}[\mathbf{n}_t] = \psi_{n_t}^{\text{ref}}(t) - \psi_{n_0}^{\text{ref}}(0) = \int_0^t d\tau \left\{ \left[d_\tau \psi_n^{\text{ref}}(\tau) \right] \Big|_{n=n_\tau} + \psi_n^{\text{ref}}(\tau) D_e^n j^e(\tau) \right\}. \quad (24)$$

The first term on the rhs accounts for the instantaneous changes of p_n^{ref} , while the second accounts for its finite changes due to stochastic transitions. Analogously, the trajectory EP—which is not a state function—can be written as

$$\Sigma[\mathbf{n}_t; \pi_t] = \int_0^t d\tau j^e(\tau) \ln \frac{w_e(\pi_\tau)}{w_{-e}(\pi_\tau)} - \ln \frac{p_{n_t}(t)}{p_{n_0}(0)}. \quad (25)$$

Adding and subtracting the terms of Equation (24) from the EP, we readily obtain the fluctuating expressions of the nonconservative and conservative contributions of the EP,

$$\Sigma[\mathbf{n}_t; \pi_t] = \Sigma_{\text{nc}}[\mathbf{n}_t; \pi_t] + \Sigma_{\text{c}}[\mathbf{n}_t]. \quad (26)$$

The former reads

$$\Sigma_{\text{nc}}[\mathbf{n}_t; \pi_t] = \int_0^t d\tau A_e^{\text{ref}}(\tau) j^e(\tau), \quad (27)$$

while for the latter

$$\Sigma_{\text{c}}[\mathbf{n}_t] = -\Delta\mathcal{D}[\mathbf{n}_t] + \Sigma_{\text{d}}[\mathbf{n}_t], \quad (28)$$

where

$$\Delta\mathcal{D}[\mathbf{n}_t] := \ln \frac{p_{n_t}(t)}{p_{n_t}^{\text{ref}}(t)} - \ln \frac{p_{n_0}(0)}{p_{n_0}^{\text{ref}}(0)} \quad (29)$$

and

$$\Sigma_{\text{d}}[\mathbf{n}_t] := \int_0^t d\tau \left[d_\tau \psi_n^{\text{ref}}(\tau) \right] \Big|_{n=n_\tau}. \quad (30)$$

We emphasize that Equation (26) holds for any reference PMF p_n^{ref} exactly as it was for its ensemble-averaged rate counterpart, Equation (14).

3.3. Fluctuation Theorems

We proceed to show that a class of FTs ensue from the decomposition (14)–(26). To do so, we now need to assume that the reference PMF depends instantaneously *solely* on the protocol value $p_n^{\text{ref}}(\tau) = p_n^{\text{ref}}(\pi_\tau)$. In other words, p_n^{ref} at time τ is completely determined by $\{w_e(\pi_\tau)\}$. This justifies a posteriori the name driving contribution for Equation (19). Various instances of such PMFs will be provided in the following sections. We define a *forward process* where the system is initially prepared in $p_n(0) = p_n^{\text{ref}}(\pi_0)$ at a value of the protocol π_0 and then evolves under the Markov jump process driven by a protocol π_τ , for $\tau \in [0, t]$. The corresponding *backward process*, denoted with “ † ”, is defined as follows: the system is initially prepared in the reference PMF corresponding to the final value of the forward process, $p_n^\dagger(0) = p_n^{\text{ref}}(\pi_t)$, and then evolves under the Markov jump process driven by the forward protocol reversed in time,

$$\pi_\tau^\dagger := \pi_{t-\tau}, \quad \text{for } \tau \in [0, t], \quad (31)$$

see Figure 2.

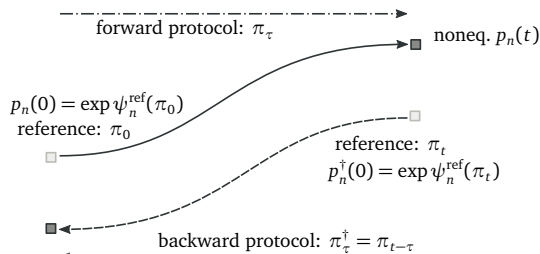


Figure 2. Schematic representation of the forward and backward processes related by our detailed fluctuation theorem (DFT).

Our main result is that the forward and backward process are related by the following *finite-time DFT*:

$$\frac{P_t(\Sigma_d, \Sigma_{nc})}{P_t^\dagger(-\Sigma_d, -\Sigma_{nc})} = \exp \{ \Sigma_d + \Sigma_{nc} \}. \quad (32)$$

Here $P_t(\Sigma_d, \Sigma_{nc})$ is the probability of observing a driving contribution to the EP Σ_d and a nonconservative one Σ_{nc} along the forward process. Instead, $P_t^\dagger(-\Sigma_d, -\Sigma_{nc})$ is the probability of observing a driving contribution equal to $-\Sigma_d$, and a nonconservative one $-\Sigma_{nc}$ along the backward process.

We now mention two direct implications of our DFT. First, by marginalizing the joint probability, one easily verifies that the sum of nonconservative and driving EP contributions also satisfies a DFT:

$$\frac{P_t(\Sigma_d + \Sigma_{nc})}{P_t^\dagger(-\Sigma_d - \Sigma_{nc})} = \exp \{ \Sigma_d + \Sigma_{nc} \}. \quad (33)$$

Second, when averaging Equation (32) over all possible values of Σ_d and Σ_{nc} , an IFT ensues:

$$\langle \exp \{ -\Sigma_d - \Sigma_{nc} \} \rangle = 1. \quad (34)$$

The proofs of Equations (32)–(34) are given in Appendix A, and use the generating function techniques developed in References [12,14].

We note that the IFT holds for any reference PMF regardless of the requirement that $p_n^{\text{ref}}(\tau) = p_n^{\text{ref}}(\pi_\tau)$ (see Appendix A). In contrast, this requirement must hold for the DFT, else the probability $P_t^\dagger(\Sigma_d, \Sigma_{nc})$ would no longer describe a physical backward process in which solely the protocol function is time reversed. Indeed, if one considers an arbitrary p_n^{ref} , the backward process corresponds to not only reversing the protocol, but also the stochastic dynamics itself (see Equation (A23)).

Another noteworthy observation is that the fluctuating quantity $\Sigma_d + \Sigma_{nc}$ can be seen as the ratio between the probabilities to observe a trajectory \mathbf{n}_t along the forward process, Equation (22), and the probability to observe the time-reversed trajectory along the backward process:

$$\Sigma_{nc}[\mathbf{n}_t; \pi_t] + \Sigma_d[\mathbf{n}_t; \pi_t] = \ln \frac{\mathfrak{P}[\mathbf{n}_t; \pi_t] p_{n_0}^{\text{ref}}(\pi_0)}{\mathfrak{P}[\mathbf{n}_t^\dagger; \pi_t^\dagger] p_{n_t}^{\text{ref}}(\pi_t)}. \quad (35)$$

The latter trajectory is denoted by \mathbf{n}_t^\dagger . It starts from n_t , and it is defined by:

$$j^{\dagger e}(\tau) := \sum_i \delta_{e_i, -e_i} \delta(t - \tau - t_i). \quad (36)$$

This result follows using Equation (22) and the observation that the contribution due to the waiting times vanish in the ratio on the rhs. It can also be used to prove the DFT in two alternative ways, the first inspired by Reference [16] and the second using trajectory probabilities (see Appendix B). These proofs rely on the fact that both the driving and the nonconservative EP contributions satisfy the *involution* property:

$$\Sigma_{nc}[\mathbf{n}_t^\dagger; \pi_t^\dagger] = -\Sigma_{nc}[\mathbf{n}_t; \pi_t], \text{ and } \Sigma_d[\mathbf{n}_t^\dagger; \pi_t^\dagger] = -\Sigma_d[\mathbf{n}_t; \pi_t], \quad (37)$$

viz. the change of Σ_d and Σ_{nc} for the backward trajectory along the backward process is minus the change along the forward trajectory of the forward process. This result follows from direct calculation on Equations (27) and (30) (see Appendix B).

Finally, let us get back to the generalized Landauer principle for systems initially prepared in the reference state, as we did in this subsection for the FTs to hold. Using Equation (20), we see that the arguments of the FTs (33) and (34) (i.e., the driving and the nonconservative contribution to the EP) can be interpreted, on average, as the cost to generate a dissimilarity (or a lag) between the actual

and the reference PMF at the end of the forward protocol. A special case of this result is discussed in Reference [17].

3.4. EP Fluctuations

We now discuss the properties of the fluctuating EP and its relation to the previously derived FTs.

An IFT for the EP always holds

$$\langle \exp \{-\Sigma\} \rangle = 1, \quad (38)$$

regardless of the initial condition [18]. In our framework, this can be seen as the result of choosing the actual $p_n(\tau)$ as the reference for the IFT (34).

In contrast, a general DFT for the EP does not hold. This can be easily understood at the level of trajectory probabilities. Indeed, the fluctuating EP can be written as the ratio of forward and backward probabilities as in (35), but the initial condition of the forward process is arbitrary and that of the backward process is the final PMF of the forward process,

$$\Sigma[\mathbf{n}_t; \pi_t] = \ln \frac{\mathfrak{P}[\mathbf{n}_t; \pi_t] p_{n_0}(0)}{\mathfrak{P}[\mathbf{n}_t^\dagger; \pi_t^\dagger] p_{n_t}(t)}. \quad (39)$$

As a result, the involution property is generally lost, $\Sigma[\mathbf{n}_t^\dagger; \pi_t^\dagger] \neq -\Sigma[\mathbf{n}_t; \pi_t]$, since $p_{n_0}^\dagger(t) \neq p_{n_0}(0)$, and hence the DFT is also lost [18].

However, in special cases the fluctuating quantity $\Sigma_d + \Sigma_{nc}$ which satisfies a DFT can be interpreted as an EP. This happens if at the end of the forward (respectively backward) process, the protocol stops changing in time in such a way that the system relaxes from p_{n_t} to an equilibrium $p_{n_t}^{\text{ref}}$ (respectively from $p_n^\dagger(t)$ to an equilibrium $p_n^{\text{ref}}(\pi_0)$) and thus without contributing to either Σ_d or to Σ_{nc} (even at the trajectory level). In such cases, $\Sigma_d + \Sigma_{nc}$ can be seen as the EP of the *extended* process including the relaxation. On average, it is greater or equal than the EP of the same process without the relaxation, since the non-negative EP during the relaxation is given by $\mathcal{D}(p(t) \| p^{\text{ref}}(\pi_t)) \geq 0$.

3.5. A Gauge Theory Perspective

We now show that the decomposition in Equation (14) can be interpreted as the consequence of the gauge freedom discussed by Polettini in Reference [19]. Indeed, in this reference he shows that the following gauge transformation leaves the stochastic dynamics (5) and the EP rate (10) unchanged:

$$p_n \rightarrow p_n \exp \psi_n, \quad w_e \rightarrow w_e \exp -\psi_{o(e)}, \quad D_e^n \rightarrow D_e^n \exp \psi_n, \text{ and} \quad \Sigma_n \rightarrow \Sigma_n \exp -\psi_n. \quad (40)$$

When considering a gauge term ψ_n changing in time, one needs also to shift the time derivative as:

$$d_t \rightarrow d_t - \partial_t, \quad (41)$$

where ∂_t behaves as a normal time derivative but it acts only on ψ_n . Let us now consider the EP rate rewritten as

$$\langle \dot{\Sigma} \rangle = \langle j^e \rangle \ln \frac{w_e}{w_{-e}} + d_t \sum_n p_n [-\ln p_n]. \quad (42)$$

One readily sees that the transformation (40)–(41) changes the first term into the nonconservative term, Equation (15), whereas the second into the conservative one, Equation (16). We finally note that connections between gauge transformations and FTs were also discussed in References [8,20].

This concludes the presentation of our main results. In the following, we will consider various specific choices for p_n^{ref} which solely depend on the driving protocol and thus give rise to DFTs. Each of them will provide a specific meaning to Σ_{nc} and Σ_c . Table 1 summarizes the reference potential, affinity, and conservative contribution for these different choices.

Table 1. Summary of the reference potentials, affinities, and conservative EP contributions for the specific references discussed in the text. The nonconservative EP contribution follows from $\langle \dot{\Sigma}_{\text{nc}} \rangle = A_e^{\text{ref}} \langle j^e \rangle$, whereas the driving one from $\langle \dot{\Sigma}_{\text{d}} \rangle = \sum_n p_n \text{d}_t \psi_n^{\text{ref}}$. Overall, $\langle \dot{\Sigma} \rangle = \langle \dot{\Sigma}_{\text{nc}} \rangle + \langle \dot{\Sigma}_{\text{c}} \rangle = \langle \dot{\Sigma}_{\text{nc}} \rangle + \langle \dot{\Sigma}_{\text{d}} \rangle - \text{d}_t \mathcal{D}(p \| p^{\text{ref}})$, where \mathcal{D} is the relative entropy.

Decomposition	ψ_n^{ref}	A_e^{ref}	$\langle \dot{\Sigma}_{\text{c}} \rangle$
adiabatic–nonadiabatic	$-\ln p_n^{\text{ss}}$	$\ln \frac{w_e p_{\text{o}(e)}^{\text{ss}}}{w_{-e} p_{\text{o}(-e)}^{\text{ss}}}$	$-\langle j^e \rangle D_e^n \ln \{p_n / p_n^{\text{ss}}\}$
cycle–cocycle	$-\ln \{\prod_{e \in \mathcal{T}_n} w_e - Z\}$	$\begin{cases} 0, & \text{if } e \in \mathcal{T}, \\ \mathcal{A}_e, & \text{if } e \in \mathcal{T}^* \end{cases}$	$\sum_{e \in \mathcal{T}} \langle \mathcal{J}_e \rangle A_e$
system–reservoir	$S_{\text{mc}} - S_n$	$\delta S_e^{\text{r}} = -f_y \delta X_e^y$	$[S_n - \ln p_n] D_e^n \langle j^e \rangle$
conservative–nonconservative	$\Phi_{\text{gg}} - [S_n - F_\lambda L_n^\lambda]$	$F_{y_t} \delta X_e^{y_t}$	$[S_n - F_\lambda L_n^\lambda - \ln p_n] D_e^n \langle j^e \rangle$

4. Adiabatic–Nonadiabatic Decomposition

We now provide a first instance of reference PMF based on the fixed point of the Markov jump process.

The Perron–Frobenius theorem ensures that the ME (5) has, at all times, a unique instantaneous steady-state PMF

$$\sum_m W_{nm}(\pi_t) p_m^{\text{ss}}(\pi_t) = 0, \quad \text{for all } n \text{ and } t. \quad (43)$$

When using this PMF as the reference, $p_n^{\text{ref}} = p_n^{\text{ss}}$, we recover the *adiabatic–nonadiabatic EP rate* decomposition [12,16,21–24]. More specifically, the nonconservative term gives the *adiabatic* contribution which is zero only if the steady state satisfies detailed balance, and the conservative term gives the *nonadiabatic* contribution which characterizes transient and driving effects. A specific feature of this decomposition is that both terms are non-negative, as proved in Appendix C: $\langle \dot{\Sigma}_{\text{nc}} \rangle \geq 0$ and $\langle \dot{\Sigma}_{\text{c}} \rangle \geq 0$. In turn, the nonadiabatic contribution decomposes into a relative entropy term and a driving one.

Provided that the forward and backward processes start in the steady state corresponding to the initial value of the respective protocol, the general DFT and IFT derived in Equation (32) and Equation (34) hold for the adiabatic and driving contributions of the adiabatic–nonadiabatic EP decomposition [12,21].

In detailed-balanced systems, the adiabatic contribution is vanishing, $\langle \dot{\Sigma}_{\text{a}} \rangle = 0$, and we obtain a FT for the sole driving contribution:

$$\frac{P_t(\Sigma_{\text{d}})}{P_t^{\dagger}(-\Sigma_{\text{d}})} = \exp \Sigma_{\text{d}}. \quad (44)$$

The celebrated Crooks' DFT [25–27] and Jarzynski's IFT [28] are of this type.

4.1. Additional FTs

Due to the particular mathematical properties of the steady-state PMF, additional FTs for the adiabatic and driving terms ensue. These are not covered by our main DFT, Equation (32), and their proofs are discussed in Appendix D.

For the former, the forward process is produced by the original dynamics initially prepared in an arbitrary PMF. The backward process instead has the same initial PMF and the same driving protocol as the forward process, but the dynamics is governed by the rates

$$\hat{w}_e := w_{-e} p_{\text{o}(-e)}^{\text{ss}} / p_{\text{o}(e)}^{\text{ss}}. \quad (45)$$

At any time, the following DFT relates the two processes,

$$\frac{P_t(\Sigma_a)}{\hat{P}_t(-\Sigma_a)} = \exp \Sigma_a, \quad (46)$$

where $\hat{P}_t(-\Sigma_a)$ is the probability of observing $-\Sigma_a$ adiabatic EP during the backward process. The Speck–Seifert IFT for the housekeeping heat is the IFT version of this DFT [29].

For the driving term, the forward process is again produced by the original dynamics, but now initially prepared in a steady state. The backward process is instead produced by the rates (45) with time-reversed driving protocol and the system must initially be prepared in a steady state. Under these conditions, one has

$$\frac{P_t(\Sigma_d)}{\hat{P}_t^*(-\Sigma_d)} = \exp \Sigma_d, \quad (47)$$

where $\hat{P}_t^*(-\Sigma_d)$ is the probability of observing $-\Sigma_d$ driving EP during the backward process. The Hatano–Sasa IFT [30] is the IFT version of this DFT.

5. Cycle–Cocycle Decomposition

We proceed by providing a second instance of reference PMF based on the equilibrium PMF for a spanning tree of the graph defined by the incidence matrix of the Markov jump process.

We partition the edges of the graph into two disjoint subsets: \mathcal{T} and \mathcal{T}^* . The former identifies a *spanning tree*, namely a minimal subset of paired edges, $(e, -e)$, that connects all states. These edges are called *cochords*. All the other edges form \mathcal{T}^* , and are called *chords*. Equivalently, \mathcal{T} is a maximal subset of edges that does not enclose any cycle—the trivial loops composed by forward and backward transitions, $(e, -e)$, are not regarded as cycles. The graph obtained by combining \mathcal{T} and $e \in \mathcal{T}^*$ identifies one and only one cycle, denoted by \mathcal{C}_e , for $e \in \mathcal{T}^*$. Algebraically, cycles are characterized as:

$$\sum_{e' \in \mathcal{C}_e} D_{e'}^n = \sum_{e'} D_{e'}^n \mathcal{C}_e^{e'} = 0, \quad \text{for all } n, \quad (48)$$

where $\{\mathcal{C}_e^{e'}\}$, for $e \in \mathcal{T}^*$, represent the vectors in the edge space whose entries are all zero except for those corresponding to the edges of the cycle, which are equal to one.

We now note that if \mathcal{T} were the sole allowed transitions, the PMF defined as follows would be an equilibrium steady state [15]:

$$p_n^{\text{st}}(\pi_t) := \frac{1}{Z} \prod_{e \in \mathcal{T}_n} w_e(\pi_t), \quad (49)$$

where $Z = \sum_m \prod_{e \in \mathcal{T}_m} w_e$ is a normalization factor, and \mathcal{T}_n denotes the spanning tree *rooted* in n , namely the set of edges of \mathcal{T} that are oriented towards the state n . Indeed, p_n^{st} would satisfy the property of detailed balance, Equation (9):

$$w_e p_{\sigma(e)}^{\text{st}} = \frac{w_e}{Z} \prod_{e' \in \mathcal{T}_{\sigma(e)}} w_{e'} = \frac{w_{-e}}{Z} \prod_{e' \in \mathcal{T}_{\sigma(-e)}} w_{e'} = w_{-e} p_{\sigma(-e)}^{\text{st}}, \quad \text{for all } e \in \mathcal{T}. \quad (50)$$

We now pick this equilibrium PMF as a reference for our EP decomposition, $p_n^{\text{ref}} = p_n^{\text{st}}$. However, in order to derive the specific expressions for $\langle \dot{\Sigma}_{\text{nc}} \rangle$ and $\langle \dot{\Sigma}_{\text{c}} \rangle$, the following result is necessary: the edge probability fluxes can be decomposed as

$$\langle j^e \rangle = \sum_{e' \in \mathcal{T}} \langle \mathcal{J}_{e'} \rangle \mathcal{E}_{e'}^e + \sum_{e' \in \mathcal{T}^*} \langle \mathcal{J}_{e'} \rangle \mathcal{C}_{e'}^e, \quad (51)$$

where $\{\mathcal{E}_e\}$ denotes the canonical basis of the edge vector space: $\mathcal{E}_e^{e'} = \delta_e^{e'}$ [31]. Algebraically, this decomposition hinges on the fact that the set $\{\mathcal{C}_e\}_{e \in \mathcal{T}^*} \cup \{\mathcal{E}_e\}_{e \in \mathcal{T}}$ is a basis of the edge vector

space [13]. Note that for $e \in \mathcal{T}^*$, the only nonvanishing contribution in Equation (51) comes from the cycle identified by e , and hence $\langle j^e \rangle = \langle \mathcal{J}_e \rangle$. The coefficients $\{ \langle \mathcal{J}_e \rangle \}$ are called *cocycle fluxes* for the cochords, $e \in \mathcal{T}$, and *cycle fluxes* for the chords, $e \in \mathcal{T}^*$. They can be understood as follows [13]: removing a pair of edges, e and $-e$, from the spanning tree ($e, -e \in \mathcal{T}$) disconnects two blocks of states. The cocycle flux $\{ \langle \mathcal{J}_e \rangle \}$ of that edge is the probability flowing from the block identified by the origin of e , $\mathbf{o}(e)$, to that identified by the target of e , $\mathbf{t}(e)$. Instead, the cycle flux $\{ \langle \mathcal{J}_e \rangle \}$ of an edge, $e \in \mathcal{T}^*$, quantifies the probability flowing along the cycle formed by adding that edge to the spanning tree. Graphical illustrations of cocycle and cycle *currents*, $\langle \mathcal{J}^e \rangle - \langle \mathcal{J}^{-e} \rangle$, can be found in Reference [13].

We can now proceed with our main task. Using Equations (48) and (49), we verify that

$$\psi_n^{\text{ref}} D_e^n = \begin{cases} -\ln \{w_e / w_{-e}\}, & \text{if } e \in \mathcal{T}, \\ -\ln \{w_e / w_{-e}\} + \mathcal{A}_e, & \text{if } e \in \mathcal{T}^*, \end{cases} \quad (52)$$

where

$$\mathcal{A}_e = \sum_{e'} \mathcal{C}_e^{e'} \ln \{w_{e'} / w_{-e'}\}, \quad \text{for } e \in \mathcal{T}^* \quad (53)$$

is the cycle affinity related to \mathcal{C}_e . It follows that

$$A_e^{\text{ref}} = \ln \frac{w_e}{w_{-e}} + \psi_n^{\text{ref}} D_e^n = \begin{cases} 0, & \text{if } e \in \mathcal{T}, \\ \mathcal{A}_e, & \text{if } e \in \mathcal{T}^*, \end{cases} \quad (54)$$

from which the nonconservative contribution readily follows:

$$\langle \dot{\Sigma}_{\text{nc}} \rangle = \sum_{e \in \mathcal{T}^*} \mathcal{A}_e \langle j_e \rangle = \sum_{e \in \mathcal{T}^*} \mathcal{A}_e \langle \mathcal{J}_e \rangle. \quad (55)$$

In the last equality, we used the property of cycle fluxes discussed after Equation (51). Hence, the nonconservative contribution accounts for the dissipation along network cycles. In turn, combining Equation (16) with Equations (51) and (52), one obtains the conservative contribution

$$\langle \dot{\Sigma}_{\text{c}} \rangle = \sum_{e \in \mathcal{T}} A_e \langle \mathcal{J}_e \rangle, \quad (56)$$

which accounts for the dissipation along cocycles. Using these last two results, the EP decomposition (14) becomes the *cycle–cocycle* decomposition found in Reference [13]:

$$\langle \dot{\Sigma} \rangle = \sum_{e \in \mathcal{T}^*} \mathcal{A}_e \langle j_e \rangle + \sum_{e \in \mathcal{T}} A_e \langle \mathcal{J}_e \rangle. \quad (57)$$

As for all decompositions, the conservative contribution—here the cocycle one—vanishes at steady state in the absence of driving. The cycle contribution instead disappears in detailed-balanced systems, when all the cycle affinities vanish. This statement is indeed the *Kolmogorov criterion* for detailed balance [32,33].

The fluxes decomposition Equation (51) is also valid at the trajectory level, where the cycle and cocycle fluxes become fluctuating instantaneous fluxes, $\{ \mathcal{J}_e \}$. Obviously, the same holds true for the cycle–cocycle EP decomposition. Therefore, if the system is in an equilibrium PMF of type (49) at the beginning of the forward and the backward process, a DFT and an IFT hold by applying Equations (32) and (34). Note that the fluctuating quantity appearing in the DFT, $\Sigma_d + \Sigma_{\text{nc}}$, can be interpreted as the EP of the extended process in which, at time t , the driving is stopped, all transitions in \mathcal{T}^* are shut down, and the system is allowed to relax to equilibrium—which is the initial PMF of the backward process.

It is worth mentioning that one can easily extend the formulation of our DFT by considering the joint probability distribution for each subcontribution of Σ_d and Σ_{na} antisymmetrical under time reversal. This can be shown using either the proof in Appendix B [16], or that in Appendix A [14]. In the case of the cycle–cocycle decomposition, it would lead to

$$\frac{P_t(\Sigma_d, \{ \mathcal{A}_e (j_e - j_{-e}) \}_{e \in \mathcal{T}^*})}{P_t^\dagger(-\Sigma_d, \{ -\mathcal{A}_e (j_e - j_{-e}) \}_{e \in \mathcal{T}^*})} = \exp \left\{ \Sigma_d + \sum_{e \in \mathcal{T}^*} \mathcal{A}_e j_e \right\}, \quad (58)$$

which is a generalization of the DFT derived in Reference [34] to time-inhomogeneous systems. In turn, the latter is a generalization of the steady-state DFT derived by Andrieux and Gaspard in Reference [35] to finite times.

Example

A spanning tree for the network in Figure 1 is depicted in Figure 3a. The cycles defined by the corresponding chords are depicted in Figure 3b. Algebraically, these cycles are represented as

$$\mathcal{C} = \begin{pmatrix} -4 & +2 & +5 \\ +1 & 1 & 0 & 0 \\ +2 & 0 & 1 & 0 \\ +3 & -1 & -1 & 0 \\ +4 & -1 & 0 & 0 \\ +5 & 0 & 0 & 1 \\ +6 & 1 & 0 & -1 \end{pmatrix}, \quad (59)$$

where the negative entries must be regarded as transitions performed in the backward direction. The corresponding affinities, which determine the nonconservative contribution (55), hence read:

$$\mathcal{A}_{-4} = \ln \frac{w_{+1}w_{+6}w_{-4}w_{-3}}{w_{-1}w_{-6}w_{+4}w_{+3}}, \quad \mathcal{A}_{+2} = \ln \frac{w_{+2}w_{-3}}{w_{-2}w_{+3}}, \quad \text{and} \quad \mathcal{A}_{+5} = \ln \frac{w_{+5}w_{-6}}{w_{-5}w_{+6}}. \quad (60)$$

The affinities corresponding to the cycles taken in the backward direction follow from $\mathcal{A}_{-e} = -\mathcal{A}_e$. Regarding the expression of the cocycle fluxes, it can be checked that they are equal to

$$\begin{aligned} \langle \mathcal{J}_{+1} \rangle &= \langle j_{+1} \rangle - \langle j_{-4} \rangle, & \langle \mathcal{J}_{+3} \rangle &= \langle j_{+3} \rangle - \langle j_{-2} \rangle - \langle j_{+4} \rangle, & \langle \mathcal{J}_{+6} \rangle &= \langle j_{+6} \rangle - \langle j_{-5} \rangle - \langle j_{-4} \rangle, \\ \langle \mathcal{J}_{-1} \rangle &= \langle j_{-1} \rangle - \langle j_{+4} \rangle, & \langle \mathcal{J}_{-3} \rangle &= \langle j_{-3} \rangle - \langle j_{+2} \rangle - \langle j_{-4} \rangle, & \langle \mathcal{J}_{-6} \rangle &= \langle j_{-6} \rangle - \langle j_{+5} \rangle - \langle j_{+4} \rangle \end{aligned} \quad (61)$$

by expanding Equation (57) into Equation (10).

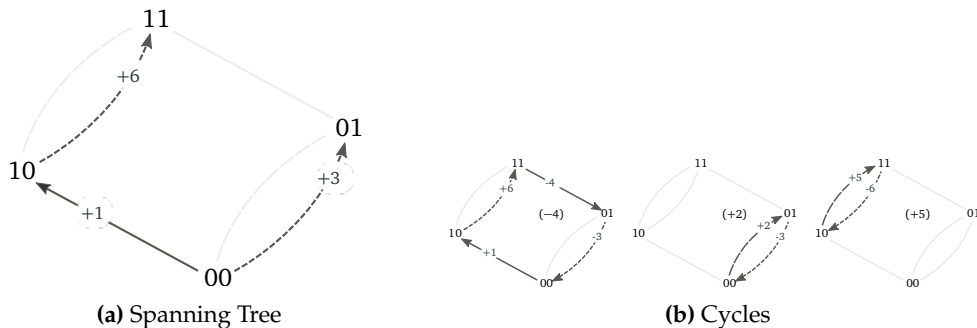


Figure 3. (a) Spanning tree, and (b) corresponding cycles for the network in Figure 1.

6. Stochastic Thermodynamics

The results obtained until this point are mathematical and have a priori no connection to physics. We now specify the conditions under which a Markov jump process describes the dynamics of an open physical system in contact with multiple reservoirs. This will enable us to introduce physically motivated decompositions and derive DFTs with a clear thermodynamic interpretation.

Each system state, n , is now characterized by given values of some *system quantities*, $\{X_n^\kappa\}$, for $\kappa = 1, \dots, N_\kappa$, which include the internal energy, E_n , and possibly additional ones (see Table 2 for some examples). These must be regarded as globally *conserved quantities*, as their change in the system is always balanced by an opposite change in the reservoirs. When labeling the reservoirs with $\{r\}$, for $r = 1, \dots, N_r$, the *balance equation* for X^κ along the transition e can be written as:

$$X_{n'}^\kappa D_e^{n'} = \delta_i X_e^\kappa + \sum_r \delta X_e^{(\kappa, r)}. \quad (62)$$

Table 2. Examples of system quantity–intensive field conjugated pairs in the entropy representation. $\beta_r := 1/T_r$ denotes the inverse temperature of the reservoir. Since charges are carried by particles, the conjugated pair $(Q_n, -\beta_r V_r)$ is usually embedded in $(N_n, -\beta_r \mu_r)$.

System Quantity X^κ	Intensive Field $f_{(\kappa, r)}$
energy, E_n	inverse temperature, β_r
particles number, N_n	chemical potential, $-\beta_r \mu_r$
charge, Q_n	electric potential, $-\beta_r V_r$
displacement, X_n	generic force, $-\beta_r k_r$
angle, θ_n	torque, $-\beta_r \tau_r$

The lhs is the overall change in the system, whereas $\delta_i X_e^\kappa$ denotes the changes due to internal transformations (e.g., chemical reactions [36,37]), and $\delta X_e^{(\kappa, r)}$ quantifies the amount of X^κ supplied by the reservoir r to the system along the transition e . For the purposes of our discussion, we introduce the index $y = (\kappa, r)$ —i.e., the *conserved quantity X^κ exchanged with the reservoir r* —and define the matrix δX whose entries are $\{\delta X_e^y \equiv \delta X_e^{(\kappa, r)}\}$. All indices used in the following discussion are summarized in Table 3. Microscopic reversibility requires that $\delta X_e^y = -\delta X_{-e}^y$. Note that more than one reservoir may be involved in each transition (see Figure 4).

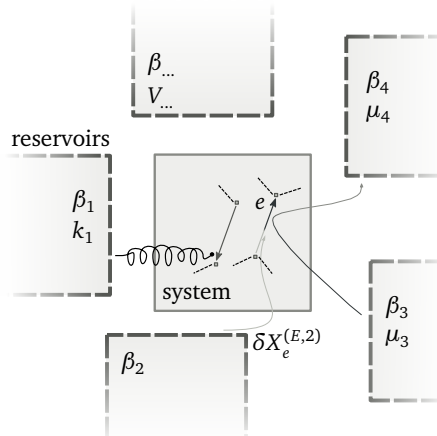


Figure 4. Pictorial representation of a system coupled to several reservoirs. Transitions may involve more than one reservoir and exchange between reservoirs. Work reservoirs are also taken into account.

Table 3. Summary of the indices used throughout the paper and the object they label.

Index	Label for	Number
n	state	N_n
e	transition	N_e
κ	system quantity	N_κ
r	reservoir	N_r
$y \equiv (\kappa, r)$	conserved quantity X^κ from reservoir r	N_y
λ	conservation law and conserved quantity	N_λ
y_p	“potential” y	N_λ
y_f	“force” y	$N_y - N_\lambda$

In addition to the trivial set of conserved quantities $\{X^\kappa\}$, the system may be characterized by some additional ones, which are *specific* for each system. We now sketch the systematic procedure to identify these quantities and the corresponding conservation laws [14,38]. Algebraically, conservation laws can be identified as a maximal set of independent vectors in the y -space, $\{\ell^\lambda\}$, for $\lambda = 1, \dots, N_\lambda$, such that

$$\ell_y^\lambda \delta X_{e'}^y \mathcal{C}_e^{e'} = 0, \quad \text{for all cycles, i.e., for all } e \in \mathcal{T}^*. \quad (63)$$

Indeed, the quantities $\{\ell_y^\lambda \delta X_e^y\}$, for $\lambda = 1, \dots, N_\lambda$, are combinations of exchange contributions $\{\delta X_e^y\}$, for $y = 1, \dots, N_y$, which vanish along all cycles. They must therefore identify some state variables, $\{L^\lambda\}$, for $\lambda = 1, \dots, N_y$, in the same way curl-free vector fields are conservative and identify scalar potentials:

$$L_n^n D_e^n = \ell_y^\lambda \delta X_e^y \equiv \sum_r \left\{ \sum_{\kappa} \ell_{(\kappa, r)}^\lambda \delta X_e^{(\kappa, r)} \right\}. \quad (64)$$

This equation can be regarded as the balance equation for the conserved quantities. In the absence of internal transformations, $\delta_i X_e^\kappa$, trivial conservation laws correspond to $\ell_y^\kappa \equiv \ell_{(\kappa', r)}^\kappa = \delta_{\kappa'}^\kappa$, so that the balance Equations (62) are recovered. Notice that each L^λ is defined up to a reference value.

Each reservoir r is characterized by a set of *entropic intensive fields* conjugated to the exchange of the system quantities $\{X^\kappa\}$, $\{f_{(\kappa, r)}\}$ for $\kappa = 1, \dots, N_\kappa$ (e.g., [39] § 2-3). A short list of X^κ - $f_{(\kappa, r)}$ conjugated pairs is reported in Table 2. The thermodynamic consistency of the stochastic dynamics is ensured by the *local detailed balance*,

$$\ln \frac{w_e}{w_{-e}} = -f_y \delta X_e^y + S_n D_e^n. \quad (65)$$

It relates the log ratio of the forward and backward transition rates to the entropy change in the reservoirs resulting from the transfer of system quantities during that transition. This entropy change is evaluated using equilibrium thermodynamics (in the reservoirs), and reads $\{\delta S_e^r = -f_y \delta X_e^y\}$. The second term on the rhs is the internal entropy change occurring during the transition, as S_n quantifies the internal entropy of the state n . This term can be seen as the outcome of a coarse-graining procedure over a finer description in which multiple states with the same system quantities are collected in one single n [40]. Using Equation (65), the affinities, Equation (11), can be rewritten as:

$$A_e = \sum_r \left[-\sum_{\kappa} f_{(\kappa, r)} \delta X_e^{(\kappa, r)} \right] + [S_n - \ln p_n] D_e^n. \quad (66)$$

This relation shows that the affinity is the entropy change in all reservoirs plus the system entropy change. In other words, while Equation (64) characterizes the balance of the conserved quantities along the transitions, Equation (66) characterizes the corresponding lack of balance for entropy, namely the second law.

As for the transition rates, the changes in time of the internal entropy S , the conserved quantities $\{X^\kappa\}$ (hence $\{\delta X_e^y\}$), and their conjugated fields $\{f_y\}$, are all encoded in the protocol function π_t . Physically, this modeling describes the two possible ways of controlling a system: either through

$\{X^\kappa\}$ or S which characterize the system states, or through $\{f_y\}$ which characterize the properties of the reservoirs.

Example

We illustrate the role of system-specific conservation laws by considering the double quantum dot (QD) depicted in Figure 5a [41–43], whose network of transition and energy landscape are drawn in Figures 1 and 5b, respectively. Electrons can enter empty dots from the reservoirs, but cannot jump from one dot to the other. When the two dots are occupied, an interaction energy, u , arises. Energy, E_n , and total number of electrons, N_n , characterize each state of the system:

$$\begin{aligned} E_{00} &= 0, & E_{10} &= \epsilon_u, & E_{01} &= \epsilon_d, & E_{11} &= \epsilon_u + \epsilon_d + u, \\ N_{00} &= 0, & N_{10} &= 1, & N_{01} &= 1, & N_{11} &= 2, \end{aligned} \quad (67)$$

where the first entry in n refers to the occupancy of the upper dot, and the second to the lower. The entries of the matrix δX for the forward transitions are:

$$\delta X = \begin{pmatrix} & +1 & +2 & +3 & +4 & +5 & +6 \\ (E,1) & \epsilon_u & 0 & 0 & \epsilon_u + u & 0 & 0 \\ (N,1) & 1 & 0 & 0 & 1 & 0 & 0 \\ (E,2) & 0 & \epsilon_d & 0 & 0 & \epsilon_d + u & 0 \\ (N,2) & 0 & 1 & 0 & 0 & 1 & 0 \\ (E,3) & 0 & 0 & \epsilon_d & 0 & 0 & \epsilon_d + u \\ (N,3) & 0 & 0 & 1 & 0 & 0 & 1 \end{pmatrix} \quad (68)$$

(see Figure 1), whereas the entries related to backward transition follow from $\delta X_{-e}^y = -\delta X_e^y$. For instance, along the first transition the system gains ϵ_u energy and 1 electron from the reservoir 1. The vector of entropic intensive fields is given by

$$f = \begin{pmatrix} (E,1) & (N,1) & (E,2) & (N,2) & (E,3) & (N,3) \\ \beta_1 & -\beta_1\mu_1 & \beta_2 & -\beta_2\mu_2 & \beta_3 & -\beta_3\mu_3 \end{pmatrix}. \quad (69)$$

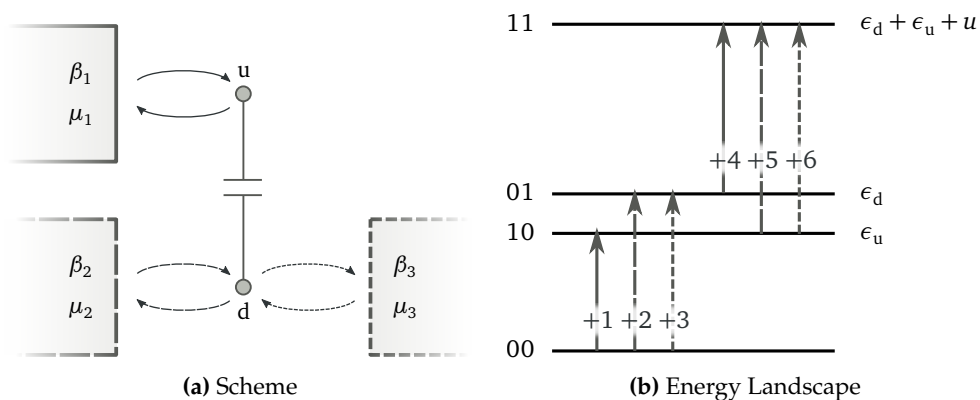


Figure 5. Double coupled quantum dot (QD) in contact with three reservoirs. Transitions related to the first reservoir are depicted using solid lines, while those related to the second and third ones using dashed and dotted lines, respectively. The graphical rule was applied to the network of transitions in Figure 1. (a) Pictorial representation of the system. The upper dot u is in contact with the first reservoir, while the lower dot d with the second and third reservoirs. Energy and electrons are exchanged, but the dots cannot host more than one electron. (b) Energy landscape of the dot. When both dots are occupied, 11 , a repulsive energy u adds to the occupied dots energies, ϵ_u and ϵ_d .

Since the QDs and the electrons have no internal entropy, $S_n = 0$ for all n , the local detailed balance property, Equation (65), can be easily recovered from the product $-f\delta X$. From a stochastic dynamics perspective, this property arises when considering fermionic transition rates, namely $w_e = \Gamma_e(1 + \exp\{f_y\delta X_e^y\})^{-1}$ and $w_{-e} = \Gamma_e \exp\{f_y\delta X_e^y\}(1 + \exp\{f_y\delta X_e^y\})^{-1}$ for electrons entering and leaving the dot.

A maximal set of independent vectors in y -space satisfying Equation (63) is composed of

$$\begin{aligned}\ell^E &= \begin{pmatrix} (E,1) & (N,1) & (E,2) & (N,2) & (E,3) & (N,3) \\ 1 & 0 & 1 & 0 & 1 & 0 \end{pmatrix}, \\ \ell^u &= \begin{pmatrix} (E,1) & (N,1) & (E,2) & (N,2) & (E,3) & (N,3) \\ 0 & 1 & 0 & 0 & 0 & 0 \end{pmatrix}, \\ \ell^d &= \begin{pmatrix} (E,1) & (N,1) & (E,2) & (N,2) & (E,3) & (N,3) \\ 0 & 0 & 0 & 1 & 0 & 1 \end{pmatrix}.\end{aligned}\quad (70)$$

The first vector identifies the energy state variable, E_n :

$$\ell^E \delta X = \begin{pmatrix} +1 & +2 & +3 & +4 & +5 & +6 \\ \epsilon_u & \epsilon_d & \epsilon_d & \epsilon_u + u & \epsilon_d + u & \epsilon_d + u \end{pmatrix} \equiv \{E_n D_e^n\}. \quad (71)$$

The other two instead give the occupancy of the upper and lower dots, N_n^u and N_n^d :

$$\begin{aligned}\ell^u \delta X &= \begin{pmatrix} +1 & +2 & +3 & +4 & +5 & +6 \\ 1 & 0 & 0 & 1 & 0 & 0 \end{pmatrix} \equiv \{N_n^u D_e^n\}, \\ \ell^d \delta X &= \begin{pmatrix} +1 & +2 & +3 & +4 & +5 & +6 \\ 0 & 1 & 1 & 0 & 1 & 1 \end{pmatrix} \equiv \{N_n^d D_e^n\}.\end{aligned}\quad (72)$$

A posteriori, we see that these conservation laws arise from the fact that no electron transfer from one dot to the other is allowed. The total occupancy of the system, N_n , is recovered from the sum of the last two vectors.

Now that a nonequilibrium thermodynamics has been built on top of the Markov jump process, we can proceed by considering two physical relevant p_n^{ref} .

7. System–Reservoirs Decomposition

We start by considering a microcanonical PMF as reference:

$$p_n^{\text{ref}} = p_n^{\text{mc}} := \exp\{S_n - S_{\text{mc}}\}, \quad (73)$$

where

$$S_{\text{mc}} = \ln \sum_m \exp S_m \quad (74)$$

is the *Boltzmann's equilibrium entropy*. With this choice, the reference affinities become sums of entropy changes in the reservoirs

$$A_e^{\text{ref}} = \delta S_e^{\text{r}} = -f_y \delta X_e^y, \quad (75)$$

and hence the nonconservative contribution becomes the rate of entropy change in all reservoirs

$$\langle \dot{\Sigma}_{\text{nc}} \rangle = \langle \dot{S}_{\text{r}} \rangle = -f_y \delta X_e^y \langle j^e \rangle. \quad (76)$$

For the conservative contribution, one instead obtains:

$$\langle \dot{\Sigma}_c \rangle = [S_n - \ln p_n] D_e^n \langle j^e \rangle. \quad (77)$$

Using Equation (17), it can be rewritten in terms of the Gibbs–Shannon entropy,

$$\langle \mathcal{S} \rangle = \sum_n p_n [S_n - \ln p_n] \quad (78)$$

and the Boltzmann entropy. Indeed,

$$\mathcal{D}(p \| p^{\text{mc}}) = \mathcal{S}_{\text{mc}} - \langle \mathcal{S} \rangle \quad (79)$$

and

$$\langle \dot{\Sigma}_d \rangle = d_t \mathcal{S}_{\text{mc}} - \sum_n p_n d_t S_n, \quad (80)$$

so that

$$\langle \dot{\Sigma}_c \rangle = d_t \langle \mathcal{S} \rangle - \sum_n p_n d_t S_n. \quad (81)$$

The conservative contribution thus contains changes in the system entropy caused by the dynamics and the external drive.

The EP decomposition (14) with Equations (76) and (81) is thus the well-known *system–reservoir* decomposition (i.e., the traditional *entropy balance*). Since the same decomposition holds at the trajectory level, if the initial PMF of the forward and backward processes are microcanonical, the DFT and IFT hold by applying Equations (32) and (34). When the driving does not affect the internal entropy of the system states $\{S_n\}$, the DFT and IFT hold for the reservoir entropy alone. Finally, the fluctuating quantity appearing in the DFT, $\Sigma_d + \Sigma_{\text{nc}}$, can be interpreted as the EP of the extended process in which, at time t , the driving is stopped, all temperatures are raised to infinity, $\beta_r \rightarrow 0$, and the system is allowed to relax to equilibrium—the initial PMF of the backward process.

8. Conservative–Nonconservative Decomposition

We now turn to a reference PMF which accounts for conservation laws: the *generalized Gibbs PMF*.

To characterize this PMFs, we observe that since $\{\ell^\lambda\}$ are linearly independent (otherwise we would have linearly dependent conserved quantities), one can always identify a set of y 's, denoted by $\{y_p\}$, such that the matrix whose rows are $\{\ell_{y_p}^\lambda\}$, for $\lambda = 1, \dots, N_\lambda$, is nonsingular. We denote by $\{\bar{\ell}_\lambda^{y_p}\}$ for $\lambda = 1, \dots, N_\lambda$, the columns of the inverse matrix. All other y 's are denoted by $\{y_f\}$. Using the splitting $\{y_p\} - \{y_f\}$ and the properties of $\{\ell_{y_p}^\lambda\}$, in combination with the balance equation for conserved quantities, Equation (64), the local detailed balance (65) can be decomposed as

$$\ln \frac{w_e}{w_{-e}} = \mathcal{F}_{y_f} \delta X_e^{y_f} + \left[S_n - F_\lambda L_n^\lambda \right] D_e^n, \quad (82)$$

where

$$F_\lambda = f_{y_p} \bar{\ell}_\lambda^{y_p} \quad (83)$$

are the system-specific intensive fields conjugated to the conserved quantities, and

$$\mathcal{F}_{y_f} := F_\lambda \ell_{y_f}^\lambda - f_{y_f} \quad (84)$$

are differences of intensive fields called nonconservative *fundamental forces*. Indeed, these nonconservative forces are responsible for breaking detailed balance. When they all vanish, $\mathcal{F}_{y_f} = 0$ for all y_f , the system is indeed detailed balanced and the PMF

$$p_n^{\text{gg}} := \exp \left\{ S_n - F_\lambda L_n^\lambda - \Phi_{\text{gg}} \right\}, \quad (85)$$

with $\Phi_{\text{gg}} := \ln \sum_n \exp \{ S_n - F_\lambda L_n^\lambda \}$, satisfies the detailed balance property (9). The potential corresponding to Equation (85), ψ_n^{gg} , is minus the *Massieu potential* which is constructed by using all conservation laws (e.g. [39] §§ 5-4 and 19-1, [44] § 3.13). Choosing the PMF (85) as a reference, $p_n^{\text{ref}} = p_n^{\text{gg}}$, the reference affinity straightforwardly ensues from Equation (82),

$$A_e^{\text{ref}} = A_e^{\text{gg}} = \mathcal{F}_{y_f} \delta X_e^{y_f}. \quad (86)$$

Hence,

$$\langle \dot{\Sigma}_{\text{nc}} \rangle = \mathcal{F}_{y_f} \langle I^{y_f} \rangle, \quad (87)$$

where

$$\langle I^{y_f} \rangle = \delta X_e^{y_f} \langle j^e \rangle \quad (88)$$

are the fundamental currents conjugated to the forces. For the conservative contribution, one obtains

$$\langle \dot{\Sigma}_{\text{c}} \rangle = \left[S_n - F_\lambda L_n^\lambda - \ln p_n \right] D_e^n \langle j^e \rangle. \quad (89)$$

When written as in Equation (17), its two contributions are:

$$\mathcal{D}(p \| p^{\text{gg}}) = \Phi_{\text{gg}} - \sum_n p_n \left[S_n - F_\lambda L_n^\lambda - \ln p_n \right], \quad (90)$$

which relates the equilibrium Massieu potential to its averaged nonequilibrium counterpart; and

$$\langle \dot{\Sigma}_{\text{d}} \rangle = d_t \Phi_{\text{gg}} - \sum_n p_n d_t \left[S_n - F_\lambda L_n^\lambda - \ln p_n \right], \quad (91)$$

which quantifies the dissipation due to external manipulations of $\{ S_n \}$, the fields $\{ F_\lambda \}$, and the conserved quantities $\{ L^\lambda \}$. We emphasize that since ψ_n^{gg} encompasses all conserved quantities, $\langle \dot{\Sigma}_{\text{c}} \rangle$ captures all dissipative contributions due to conservative forces. Hence, $\langle \dot{\Sigma}_{\text{nc}} \rangle$ consists of a minimal number, $N_y - N_\lambda$, of purely nonconservative contributions. The EP decomposition Equation (14) with Equations (87) and (89) is the *conservative–nonconservative* decomposition of the EP obtained in Reference [14].

The conservative–nonconservative splitting of the EP can also be made at the trajectory level. Hence, if the initial condition of the forward and backward process is of the form (85), the DFT and IFT given by Equations (32) and (34) hold.

Here too, the fluctuating quantity appearing in the DFT, $\Sigma_{\text{d}} + \Sigma_{\text{nc}}$, can be interpreted as the EP of an extended process including relaxation, but for nonisothermal processes the procedure can be significantly more involved. The details of this discussion can be found in Reference [14].

Example

We now provide the expressions of ψ_n^{ref} and A_e^{ref} for the double QD discussed in the previous example (Figure 5). Therefore, we split the set $\{ y \}$ in $\{ y_p \} = \{ (E, 1), (N, 1), (N, 2) \}$ and $\{ y_f \} = \{ (E, 2), (E, 3), (N, 3) \}$, which is valid since the matrix whose entries are $\{ \ell_{y_p}^\lambda \}$ is an identity matrix (see Equation (70)). The fields conjugated with the complete set of conservation laws, Equation (83), are:

$$F_E = \beta_1, \quad F_u = -\beta_1 \mu_1, \text{ and} \quad F_d = -\beta_2 \mu_2, \quad (92)$$

from which the reference potential of the state n , Equation (85), follows

$$\psi_n^{\text{gg}} = \Phi^{\text{gg}} - \left[-\beta_1 E_n + \beta_1 \mu_1 N_n^u + \beta_2 \mu_2 N_n^d \right]. \quad (93)$$

Instead, the fundamental forces, Equation (84), are given by

$$\mathcal{F}_{(E,2)} = \beta_1 - \beta_2, \quad \mathcal{F}_{(E,3)} = \beta_1 - \beta_3, \text{ and} \quad \mathcal{F}_{(N,3)} = \beta_3 \mu_3 - \beta_2 \mu_2, \quad (94)$$

from which the reference affinities follow (Equation (86)). The first two forces drive the energy flowing into the first reservoir from the second and third ones, respectively, whereas the third force drives the electrons flowing from the third to the second reservoir.

9. Conclusions

In this paper, we presented a general method to construct DFTs for Markov jump processes. The strategy to identify the fluctuating quantities which satisfy the DFT consists of splitting the EP in two by making use of a reference PMF. The choice of the reference PMF is arbitrary for IFTs, but must solely depend on the driving protocol for DFTs. Out of the infinite number of FTs that can be considered, we tried to select those that have interesting mathematical properties or that can be expressed in terms of physical quantities when the Markov jump process is complemented with a thermodynamic structure. Table 1 summarizes the terms of to the EP for each of our choices. We also emphasized that the EP always satisfies an IFT but generically not a DFT. Connections to information theory were also made by formulating a generalized Landauer principle.

We do not claim to have been exhaustive, and many other reference PMFs may be interesting. We can mention at least two more interesting cases. By considering the steady-state PMF which is obtained when removing some edges from the graph (but not all chords as in Section 5), the marginal thermodynamic theory presented in References [45,46] emerges. One can also consider a reference PMF in between the microcanonical PMF, which takes no conserved quantity into account, and the generalized Gibbs one, which takes them all into account. This happens for instance when only the obvious conserved quantities are accounted for, $\{X^\kappa\}$, as discussed in Reference [47]. In this case, one uses the fields of a given reservoir to define the reference equilibrium potential

$$\psi_n^{\text{ref}} = \Phi - \left[S_n - \sum_{\kappa} f_{(\kappa,1)} \delta X_n^\kappa \right],$$

where Φ is determined by the normalization. The number of nonconservative forces appearing in $\langle \dot{\Sigma}_{\text{nc}} \rangle$ will be $N_y - N_\kappa$. However, in case additional conservation laws are present ($N_\lambda > N_\kappa$), some of these forces are dependent on others and their number will be larger than the minimal, $N_y - N_\lambda$.

Author Contributions: All Authors prepared the manuscript and contributed to the concepts and theoretical results exposed in this article. All Authors have read and approved the final manuscript.

Funding: This work was funded by the Luxembourg National Research Fund (AFR PhD Grant 2014-2, No. 9114110), the European Research Council (project NanoThermo, ERC-2015-CoG Agreement No. 681456), and the National Science Foundation (NSF Grant No. PHY-1748958).

Acknowledgments: We thank Artur Wachtel and Alexandre Lazarescu for valuable feedback on the manuscript.

Conflicts of Interest: The authors declare no conflict of interest.

Abbreviations

The following abbreviations are used in this manuscript:

DFT	detailed fluctuation theorem
IFT	integral fluctuation theorem
PMF	probability mass function
EP	entropy production
ME	master equation
MGF	moment generating function

Appendix A. Moment Generating Function Dynamics and Proofs of the FTs

We describe the moment generating function (MGF) technique that we use to prove the finite time DFTs (32) [14].

Appendix A.1. MGF Dynamics

Let $P_t(n, \delta O)$ be the joint probability of observing a trajectory ending in the state n along which the change of a generic observable, O , is δO . The changes of O along edges are denoted as $\{\delta O_e\}$, whereas the changes due to time-dependent driving while in the state n as \dot{O}_n . In order to write an evolution equation for this probability, let us expand it as:

$$P_{t+\mathrm{d}t}(n, \delta O) \simeq \sum_e w_e \delta_{n, t(e)} P_t \left(\mathbf{o}(e), \delta O - \delta O_e - \dot{O}_{\mathbf{o}(e)} \mathrm{d}t \right) \mathrm{d}t + \left[1 - \sum_e w_e \delta_{n, \mathbf{o}(e)} \right] P_t(n, \delta O - \dot{O}_n \mathrm{d}t). \quad (\text{A1})$$

The first term accounts for transitions leading to the state n and completing the change of O , whereas the second describes the probability of completing the change of O while dwelling in the state n (and not leaving it). When keeping only the linear term in $\mathrm{d}t$ and performing the limit $\mathrm{d}t \rightarrow 0$, we get:

$$\mathrm{d}_t P_t(n, \delta O) = \sum_e w_e \delta_{n, t(e)} P_t(\mathbf{o}(e), \delta O - \delta O_e) - \sum_e w_e \delta_{n, \mathbf{o}(e)} P_t(n, \delta O) - \dot{O}_n \partial_{\delta O} P_t(n, \delta O). \quad (\text{A2})$$

Rather than working with this differential equation, it is much more convenient to deal with the bilateral Laplace transform of $p_t(n, \delta O)$, that is, the MGF up to a sign,

$$\Lambda_{n,t}(q) := \int_{-\infty}^{\infty} \mathrm{d} \delta O \exp\{-q \delta O\} P_t(n, \delta O), \quad (\text{A3})$$

since its evolution equation is akin to an ME, Equation (2):

$$\mathrm{d}_t \Lambda_{n,t}(q) = \sum_m W_{nm,t}(q) \Lambda_{m,t}(q), \quad (\text{A4})$$

where the *biased rate matrix* reads

$$W_{nm,t}(q) = \sum_e w_e \left\{ \exp\{-q \delta O_e\} \delta_{n, t(e)} \delta_{m, \mathbf{o}(e)} - \delta_{n, m} \delta_{m, \mathbf{o}(e)} \right\} - q \dot{O}_n \delta_{n, m}. \quad (\text{A5})$$

The field q is usually referred to as a *counting field*. This equation is obtained by combining Equations (A2) and (A3), and its initial condition must be $\Lambda_{n,0}(\delta O) = p_n(0)$. Note that Equation (A4) is not an ME, since $\sum_n \Lambda_{n,t}(\delta O)$ is not conserved.

For later convenience, we recast Equation (A4) into a bracket notation:

$$\mathrm{d}_t |\Lambda_t(q)\rangle = \mathcal{W}_t(q) |\Lambda_t(q)\rangle, \quad (\text{A6})$$

and we proceed to prove a preliminary result. A formal solution of Equation (A4) is $|\Lambda_t(q)\rangle = \mathcal{U}_t(q) |P(0)\rangle$, where the time-evolution operator reads $\mathcal{U}_t(q) = \mathcal{T}_+ \exp \int_0^t \mathrm{d}\tau \mathcal{W}_\tau(q)$, \mathcal{T}_+ being the time-ordering operator. We clearly have $\mathrm{d}_t \mathcal{U}_t(q) = \mathcal{W}_t(q) \mathcal{U}_t(q)$. Let us now consider the following transformed evolution operator:

$$\tilde{\mathcal{U}}_t(q) := \mathcal{X}_t^{-1} \mathcal{U}_t(q) \mathcal{X}_0, \quad (\text{A7})$$

\mathcal{X}_t being a generic time-dependent invertible operator. Its dynamics is ruled by the following biased stochastic dynamics:

$$\mathrm{d}_t \tilde{\mathcal{U}}_t(q) = \mathrm{d}_t \mathcal{X}_t^{-1} \mathcal{U}_t(q) \mathcal{X}_0 + \mathcal{X}_t^{-1} \mathrm{d}_t \mathcal{U}_t(q) \mathcal{X}_0 = \left\{ \mathrm{d}_t \mathcal{X}_t^{-1} \mathcal{X}_t + \mathcal{X}_t^{-1} \mathcal{W}_t(q) \mathcal{X}_t \right\} \tilde{\mathcal{U}}_t(q) \equiv \tilde{\mathcal{W}}_t(q) \tilde{\mathcal{U}}_t(q), \quad (\text{A8})$$

which allows us to conclude that the transformed time-evolution operator is given by

$$\tilde{\mathcal{U}}(q) = \mathcal{T}_+ \exp \int_0^t \mathrm{d}\tau \tilde{\mathcal{W}}_\tau(q). \quad (\text{A9})$$

From Equations (A7), (A8), and (A9), we deduce that

$$\mathcal{X}_t^{-1} \mathcal{U}_t(q) \mathcal{X}_0 = \mathsf{T}_+ \exp \int_0^t d\tau \left[d_\tau \mathcal{X}_\tau^{-1} \mathcal{X}_\tau + \mathcal{X}_\tau^{-1} \mathcal{W}_\tau(q) \mathcal{X}_\tau \right]. \quad (\text{A10})$$

Appendix A.2. Proof of the DFT

To prove the DFT (32), we briefly recall its two assumptions: (i) the reference PMF depends on time solely via the protocol function; (ii) for both the forward and backward processes, the system is initially prepared in a reference PMF. Let $P_t(n, \Sigma_d, \Sigma_{nc})$ be the joint probability of observing a trajectory ending in the state n along which the driving contribution is Σ_d , while the nonconservative one is Σ_{nc} . The above probabilities, one for each n , are stacked in the ket $|P_t(\Sigma_d, \Sigma_{nc})\rangle$. The time evolution of the related MGF,

$$|\Lambda_t(q_d, q_{nc})\rangle := \int_{-\infty}^{\infty} d\Sigma_d d\Sigma_{nc} \exp \{-q_d \Sigma_d - q_{nc} \Sigma_{nc}\} |P_t(\Sigma_d, \Sigma_{nc})\rangle, \quad (\text{A11})$$

is ruled by the biased stochastic dynamics, Equation (A4),

$$d_t |\Lambda_t(q_d, q_{nc})\rangle = \mathcal{W}_t(q_d, q_{nc}) |\Lambda_t(q_d, q_{nc})\rangle, \quad (\text{A12})$$

where the entries of the biased generator are given by

$$W_{nm}(q_d, q_{nc}) = \sum_e w_e \left\{ \exp \left\{ -q_{nc} A_e^{\text{ref}} \right\} \delta_{n, t(e)} \delta_{m, o(e)} - \delta_{n, m} \delta_{m, o(e)} \right\} - q_d d_t \psi_m \delta_{n, m}. \quad (\text{A13})$$

Using the definition of reference affinity, Equation (13), one can see that the rate matrix satisfies the following symmetry:

$$\mathcal{W}_t^T(q_d, q_{nc}) = \mathcal{P}_t^{-1} \mathcal{W}_t(q_d, 1 - q_{nc}) \mathcal{P}_t, \quad (\text{A14})$$

where the entries of \mathcal{P}_t are given by

$$\mathcal{P}_{nm, t} := \exp \left\{ -\psi_m^{\text{ref}}(\pi_t) \right\} \delta_{n, m}, \quad (\text{A15})$$

and “ T ” denotes the transposition. Additionally, the initial condition is given by the reference PMF:

$$|\Lambda_0(q_d, q_{nc})\rangle = |p_0^{\text{ref}}\rangle = \mathcal{P}_0 |1\rangle. \quad (\text{A16})$$

$|1\rangle$ denotes the vector in the state space whose entries are all equal to one.

Using the formal solution of Equation (A12), the MGF of $P_t(\Sigma_d, \Sigma_{nc})$ can be written as:

$$\Lambda_t(q_d, q_{nc}) = \langle 1 | \Lambda_t(q_d, q_{nc}) \rangle = \langle 1 | \mathcal{U}_t(q_d, q_{nc}) \mathcal{P}_0 | 1 \rangle = \langle 1 | \mathcal{P}_t \mathcal{P}_t^{-1} \mathcal{U}_t(q_d, q_{nc}) \mathcal{P}_0 | 1 \rangle, \quad (\text{A17})$$

where $\mathcal{U}_t(q_d, q_{nc})$ is the related time-evolution operator. Using the relation in Equation (A10), the last term can be recast into

$$\Lambda_t(q_d, q_{nc}) = \langle p_t^{\text{ref}} | \mathsf{T}_+ \exp \left\{ \int_0^t d\tau \left[d_\tau \mathcal{P}_\tau^{-1} \mathcal{P}_\tau + \mathcal{P}_\tau^{-1} \mathcal{W}_\tau(q_d, q_{nc}) \mathcal{P}_\tau \right] \right\} | 1 \rangle. \quad (\text{A18})$$

Since $d_\tau \mathcal{P}_\tau^{-1} \mathcal{P}_\tau = \text{diag} \left\{ d_\tau \psi_n^{\text{ref}} \right\}$, the first term in square brackets can be added to the diagonal entries of the second term, thus giving

$$\Lambda_t(q_d, q_{nc}) = \langle p_t^{\text{ref}} | \mathsf{T}_+ \exp \left\{ \int_0^t d\tau \left[\mathcal{P}_\tau^{-1} \mathcal{W}_\tau(q_d - 1, q_{nc}) \mathcal{P}_\tau \right] \right\} | 1 \rangle. \quad (\text{A19})$$

The symmetry (A14) allows us to recast the latter into

$$\Lambda_t(q_d, q_{nc}) = \langle p_t^{\text{ref}} | \mathsf{T}_+ \exp \left\{ \int_0^t d\tau \mathcal{W}_\tau^T(q_d - 1, 1 - q_{nc}) \right\} | 1 \rangle. \quad (\text{A20})$$

The crucial step comes as we time-reverse the integration variable: $\tau \rightarrow t - \tau$. Accordingly, the time-ordering operator, T_+ , becomes an anti-time-ordering one, T_- , while the diagonal entries of the biased generator become

$$\begin{aligned} W_{mm,t-\tau}(q_d, q_{nc}) &= -\sum_e w_e(\pi_{t-\tau}) \delta_{m,o(e)} - q_d d_{t-\tau} \psi_m^{\text{ref}}(\pi_{t-\tau}) \\ &= -\sum_e w_e(\pi_\tau^\dagger) \delta_{m,o(e)} + q_d d_\tau \psi_m^{\text{ref}}(\pi_\tau^\dagger), \end{aligned} \quad (\text{A21})$$

from which we conclude that

$$W_{nm,t-\tau}(q_d, q_{nc}) = W_{nm,\tau}^\dagger(-q_d, q_{nc}). \quad (\text{A22})$$

Crucially, the assumption that ψ_n^{ref} depends on time via π_τ ensures that $\mathcal{W}_\tau^\dagger(q_d, q_{nc})$ can be regarded as the biased generator of the dynamics subject to the time-reversed protocol (i.e., the dynamics of the backward process). If we considered an arbitrary p_n^{ref} (i.e., the forward process would start from an arbitrary PMF), then $\mathcal{W}_\tau^\dagger(q_d, q_{nc})$ would be the rate matrix of the time-reversed stochastic dynamics:

$$0 = \sum_m [\delta_{nm} d_{t-\tau} - W_{nm}(\pi_{t-\tau})] p_m = \sum_m \left[-\delta_{nm} d_\tau - W_{nm}(\pi_\tau^\dagger) \right] p_m, \quad (\text{A23})$$

which is unphysical. Equation (A20) thus becomes

$$\Lambda_t(q_d, q_{nc}) = \langle p_t^{\text{ref}} | T_- \exp \left\{ \int_0^t d\tau \mathcal{W}_\tau^\dagger(1 - q_d, 1 - q_{nc}) \right\} | 1 \rangle. \quad (\text{A24})$$

Upon a global transposition, we can write

$$\Lambda_t(q_d, q_{nc}) = \langle 1 | T_+ \exp \left\{ \int_0^t d\tau \mathcal{W}_\tau^\dagger(1 - q_d, 1 - q_{nc}) \right\} | p_t^{\text{ref}} \rangle, \quad (\text{A25})$$

where we also used the relationship between transposition and time-ordering

$$T_+ \left(\prod_i A_{t_i}^\dagger \right) = (T_- \prod_i A_{t_i})^\dagger, \quad (\text{A26})$$

in which A_t is a generic operator. From the last expression, we readily obtain the symmetry that we are looking for:

$$\Lambda_t(q_d, q_{nc}) = \Lambda_t^\dagger(1 - q_d, 1 - q_{nc}), \quad (\text{A27})$$

where $\Lambda_t^\dagger(q_d, q_{nc})$ is the MGF of $P_t^\dagger(\Sigma_d, \Sigma_{nc})$. Indeed, its inverse Laplace transform gives the DFT in Equation (32).

Appendix A.3. Proof of the DFT for the Sum of Driving and Nonconservative EP

Let us define $\Sigma_s := \Sigma_d + \Sigma_{nc}$ as the sum of the driving and nonconservative EP contributions. A straightforward calculation leads from (32) to the DFT for Σ_s , Equation (33):

$$\begin{aligned} P_t(\Sigma_s) &= \int d\Sigma_d d\Sigma_{nc} P_t(\Sigma_d, \Sigma_{nc}) \delta(\Sigma_s - \Sigma_d - \Sigma_{nc}) = \int d\Sigma_d P_t(\Sigma_d, \Sigma_s - \Sigma_d) \\ &= \exp \Sigma_s \int d\Sigma_d P_t^\dagger(-\Sigma_d, \Sigma_d - \Sigma_s) = P_t^\dagger(-\Sigma_s) \exp \Sigma_s. \end{aligned} \quad (\text{A28})$$

Appendix A.4. Proof of the IFT

We now prove the IFT (34) using the MGF technique developed in Reference [12]. We have already mentioned that the dynamics (A12) does not describe a stochastic process, since the normalization is not preserved. However, for $q_d = q_{nc} = 1$, the biased generator (A13) can be written as:

$$W_{nm}(1, 1) = \left[\sum_e w_e p_{o(e)}^{\text{ref}} \{ \delta_{n,o(e)} \delta_{m,t(e)} - \delta_{n,m} \delta_{m,o(e)} \} + d_t p_n^{\text{ref}} \delta_{n,m} \right] \frac{1}{p_m^{\text{ref}}}, \quad (\text{A29})$$

from which it readily follows that

$$d_t |p^{\text{ref}}\rangle = \mathcal{W}(1, 1) |p^{\text{ref}}\rangle \quad (\text{A30})$$

viz. p_n^{ref} is the solution of the biased dynamics (A12) for $q_d = q_{\text{nc}} = 1$. The normalization condition thus demands that

$$1 = \langle 1 | \Lambda_t(1, 1) \rangle = \int_{-\infty}^{\infty} d\Sigma_d d\Sigma_{\text{nc}} \exp \{-\Sigma_d - \Sigma_{\text{nc}}\} \langle 1 | P_t(\Sigma_d, \Sigma_{\text{nc}}) \rangle \equiv \langle \exp \{-\Sigma_d - \Sigma_{\text{nc}}\} \rangle, \quad (\text{A31})$$

which is the IFT in Equation (34). Note that we do not assume any specific property for p_n^{ref} in this context.

Appendix B. Alternative Proofs of the DFT

We here show two alternative proofs of the DFT (32) which rely on the involution property (37). For the nonadiabatic contribution, this property can be proved as follows. By time-reversing Equation (27), $\tau \rightarrow t - \tau$, we obtain

$$\Sigma_{\text{nc}}[\mathbf{n}_t; \pi_t] = \int_0^t d\tau A_e^{\text{ref}}(\pi_\tau) j^e(\tau) = \int_0^t d\tau A_e^{\text{ref}}(\pi_{t-\tau}) j^e(t - \tau). \quad (\text{A32})$$

Since A_e^{ref} is solely determined by the state of protocol at each instant of time, the reference affinities correspond to those of the backward process, $A_e^{\text{ref}}(\pi_{t-\tau}) = A_e^{\text{ref}}(\pi_\tau^\dagger)$. Using the property that $j^e(t - \tau) = j^{\dagger - e}(\tau)$, see Equation (36), and $A_e^{\text{ref}} = -A_{-e}^{\text{ref}}$, we finally obtain

$$\Sigma_{\text{nc}}[\mathbf{n}_t; \pi_t] = - \int_0^t d\tau A_e^{\text{ref}}(\pi_\tau^\dagger) j^{\dagger e}(\tau) = -\Sigma_{\text{nc}}[\mathbf{n}_t^\dagger; \pi_t^\dagger]. \quad (\text{A33})$$

Concerning the driving contribution, Equation (30), we obtain

$$\Sigma_d[\mathbf{n}_t; \pi_t] = \int_0^t d\tau \left[d_\tau \psi_n^{\text{ref}}(\pi_\tau) \right] \Big|_{n=n_\tau} = \int_0^t d\tau \left[-d_\tau \psi_n^{\text{ref}}(\pi_{t-\tau}) \right] \Big|_{n=n_{t-\tau}}. \quad (\text{A34})$$

It is here again crucial that ψ_n^{ref} depends solely on the protocol value, so that $\psi_n^{\text{ref}}(\pi_{t-\tau}) = \psi_n^{\text{ref}}(\pi_\tau^\dagger)$. Therefore,

$$\Sigma_d[\mathbf{n}_t; \pi_t] = - \int_0^t d\tau \left[d_\tau \psi_n^{\text{ref}}(\pi_\tau^\dagger) \right] \Big|_{n=n_\tau^\dagger} = -\Sigma_d[\mathbf{n}_t^\dagger; \pi_t^\dagger]. \quad (\text{A35})$$

Appendix B.1. Alternative Proof 1

Inspired by Reference [16], we here use an alternative approach to derive the symmetry of the MGF which underlies our DFT, Equation (A27). In terms of trajectory probabilities, the MGF (A11) can be written as:

$$\Lambda_t(q_d, q_{\text{nc}}) = \int \mathfrak{D}\mathbf{n}_t \mathfrak{P}[\mathbf{n}_t; \pi_t] p_{n_0}^{\text{ref}}(\pi_0) \exp \{-q_d \Sigma_d[\mathbf{n}_t; \pi_t] - q_{\text{nc}} \Sigma_{\text{nc}}[\mathbf{n}_t; \pi_t]\}. \quad (\text{A36})$$

Using the relation between the EP contributions and the stochastic trajectories in forward and backward processes, Equation (35), we can recast the MGF into

$$\Lambda_t(q_d, q_{\text{nc}}) = \int \mathfrak{D}\mathbf{n}_t \mathfrak{P}[\mathbf{n}_t^\dagger; \pi_t^\dagger] p_{n_t}^{\text{ref}}(\pi_t) \exp \{(1 - q_d) \Sigma_d[\mathbf{n}_t^\dagger; \pi_t^\dagger] + (1 - q_{\text{nc}}) \Sigma_{\text{nc}}[\mathbf{n}_t^\dagger; \pi_t^\dagger]\}, \quad (\text{A37})$$

so that using the property of involution, Equation (37), we get

$$\Lambda_t(q_d, q_{\text{nc}}) = \int \mathfrak{D}\mathbf{n}_t \mathfrak{P}[\mathbf{n}_t^\dagger; \pi_t^\dagger] p_{n_t}^{\text{ref}}(\pi_t) \exp \left\{ -(1 - q_d) \Sigma_d[\mathbf{n}_t^\dagger; \pi_t^\dagger] - (1 - q_{\text{nc}}) \Sigma_{\text{nc}}[\mathbf{n}_t^\dagger; \pi_t^\dagger] \right\}. \quad (\text{A38})$$

Hence, changing and renaming the integration variable, $\mathbf{n}_t \rightarrow \mathbf{n}_t^\dagger$, and using the fact that the Jacobian determinant of this transformation is one, we finally get

$$\begin{aligned}\Lambda_t(q_d, q_{nc}) &= \int \mathfrak{D}\mathbf{n}_t \mathfrak{P}[\mathbf{n}_t; \pi_t^\dagger] p_{n_t}^{\text{ref}}(\pi_t) \exp \left\{ -(1 - q_d) \Sigma_d[\mathbf{n}_t; \pi_t^\dagger] - (1 - q_{nc}) \Sigma_{nc}[\mathbf{n}_t; \pi_t^\dagger] \right\} \\ &= \Lambda_t^\dagger(1 - q_d, 1 - q_{nc}),\end{aligned}\quad (\text{A39})$$

which proves Equation (A27). With respect to the previous proof, this one is based on Equation (35) and on the property of involution, which follow from the specifications of forward and backward processes.

Appendix B.2. Alternative Proof 2

The joint probability distribution $P_t(\Sigma_d, \Sigma_{nc})$ written in terms of trajectory probabilities, Equation (22), reads

$$P_t(\Sigma_d, \Sigma_{nc}) = \int \mathfrak{D}\mathbf{n}_t \mathfrak{P}[\mathbf{n}_t; \pi_t] p_{n_0}^{\text{ref}}(\pi_0) \delta(\Sigma_d[\mathbf{n}_t; \pi_t] - \Sigma_d) \delta(\Sigma_{nc}[\mathbf{n}_t; \pi_t] - \Sigma_{nc}). \quad (\text{A40})$$

Using Equation (35) and then the involution property (37), we finally obtain the DFT (32):

$$\begin{aligned}P_t(\Sigma_d, \Sigma_{nc}) &= \exp \{ \Sigma_d + \Sigma_{nc} \} \int \mathfrak{D}\mathbf{n}_t \mathfrak{P}[\mathbf{n}_t^\dagger; \pi_t^\dagger] p_{n_t}^{\text{ref}}(\pi_t) \delta(\Sigma_d[\mathbf{n}_t; \pi_t] - \Sigma_d) \delta(\Sigma_{nc}[\mathbf{n}_t; \pi_t] - \Sigma_{nc}) \\ &= \exp \{ \Sigma_d + \Sigma_{nc} \} \int \mathfrak{D}\mathbf{n}_t \mathfrak{P}[\mathbf{n}_t^\dagger; \pi_t^\dagger] p_{n_t}^{\text{ref}}(\pi_t) \delta(-\Sigma_d[\mathbf{n}_t^\dagger; \pi_t^\dagger] - \Sigma_d) \delta(-\Sigma_{nc}[\mathbf{n}_t^\dagger; \pi_t^\dagger] - \Sigma_{nc}) \\ &= \exp \{ \Sigma_d + \Sigma_{nc} \} P_t^\dagger(-\Sigma_d, -\Sigma_{nc}).\end{aligned}\quad (\text{A41})$$

Appendix C. Adiabatic and Nonadiabatic Contributions

We now prove that both the adiabatic and nonadiabatic EP rates are non-negative. Concerning the adiabatic contribution, using the log-inequality, $-\ln x \geq 1 - x$, one obtains

$$\begin{aligned}\langle \dot{\Sigma}_a \rangle &= \sum_e w_e p_{\sigma(e)} \ln \frac{w_e p_{\sigma(e)}^{\text{ss}}}{w_{-e} p_{\sigma(-e)}^{\text{ss}}} \geq \sum_e w_e p_{\sigma(e)} \left[1 - \frac{w_{-e} p_{\sigma(-e)}^{\text{ss}}}{w_e p_{\sigma(e)}^{\text{ss}}} \right] \\ &= \sum_e \left[w_e p_{\sigma(e)}^{\text{ss}} - w_{-e} p_{\sigma(-e)}^{\text{ss}} \right] \frac{p_{\sigma(e)}}{p_{\sigma(e)}^{\text{ss}}} = \sum_{e,n} D_n^e w_e p_{\sigma(e)}^{\text{ss}} \left[-\frac{p_n}{p_n^{\text{ss}}} \right] = 0.\end{aligned}\quad (\text{A42})$$

The last equality follows from the definition of steady-state PMF, Equation (43). For the nonadiabatic, instead, using the same inequality and similar algebraic steps, one obtains:

$$\begin{aligned}\langle \dot{\Sigma}_{na} \rangle &= \sum_e w_e p_{\sigma(e)} \ln \frac{p_{\sigma(e)} p_{\sigma(-e)}^{\text{ss}}}{p_{\sigma(e)}^{\text{ss}} p_{\sigma(-e)}} \geq \sum_e w_e p_{\sigma(e)} \left[1 - \frac{p_{\sigma(e)}^{\text{ss}} p_{\sigma(-e)}}{p_{\sigma(e)} p_{\sigma(-e)}^{\text{ss}}} \right] \\ &= \sum_e \left[w_e p_{\sigma(e)}^{\text{ss}} - w_{-e} p_{\sigma(-e)}^{\text{ss}} \right] \frac{p_{\sigma(e)}}{p_{\sigma(e)}^{\text{ss}}} = 0.\end{aligned}\quad (\text{A43})$$

Appendix D. Proofs of the DFTs for the Adiabatic and Driving EP Contributions

We here prove the DFTs in Equations (46) and (47) using the same MGF technique described in Appendix A.

Appendix D.1. Proof of the DFT for the Adiabatic Contribution

The biased generator ruling the sole adiabatic term reads:

$$W_{nm}(q_a) = \sum_e w_e \left\{ \exp \{ -q_a A_e^{\text{ss}} \} \delta_{n,t(e)} \delta_{m,\sigma(e)} - \delta_{n,m} \delta_{m,\sigma(e)} \right\}. \quad (\text{A44})$$

It satisfies the following symmetry:

$$\mathcal{W}(q_a) = \hat{\mathcal{W}}(1 - q_a), \quad (\text{A45})$$

where $\hat{\mathcal{W}}(q_a)$ is the biased generator of the fictitious dynamics ruled by the rates in Equation (45). Crucially, p_n^{ss} is also the steady state of this dynamics:

$$\sum_e D_e^n \hat{w}_e p_{o(e)}^{\text{ss}} = \sum_m \sum_e \hat{w}_e \left\{ \delta_{n,t(e)} \delta_{m,o(e)} - \delta_{n,m} \delta_{m,o(e)} \right\} p_m^{\text{ss}} = 0, \quad \text{for all } n. \quad (\text{A46})$$

This fact guarantees that the escape rates of the fictitious dynamics coincide with those of the original ones:

$$-\sum_e \hat{w}_e \delta_{n,m} \delta_{m,o(e)} = -\sum_e w_e \delta_{n,m} \delta_{m,o(e)}, \quad \text{for all } n. \quad (\text{A47})$$

We can now proceed to prove the FT (46):

$$\begin{aligned} \Lambda_t(q_a) &= \langle 1 | \Lambda_t(q_a) \rangle = \langle 1 | \mathcal{U}_t(q_a) | p \rangle = \langle 1 | \mathcal{T}_+ \exp \left\{ \int_0^t d\tau \mathcal{W}_\tau(q_a) \right\} | p \rangle \\ &= \langle 1 | \mathcal{T}_+ \exp \left\{ \int_0^t d\tau \hat{\mathcal{W}}_\tau(1 - q_a) \right\} | p \rangle. \end{aligned} \quad (\text{A48})$$

In the last equality, we made use of the symmetry in Equation (A45). Following the same mathematical steps backward, we readily get

$$\Lambda_t(q_a) = \hat{\Lambda}_t(1 - q_a), \quad (\text{A49})$$

from which the DFT in Equation (46) ensues.

Appendix D.2. Proof of the DFT for the Driving Contribution

Concerning the DFT of the driving term, Equation (47), the generator of the related biased dynamics reads:

$$W_{nm}(q_d) = \sum_e w_e \left\{ \delta_{n,t(e)} \delta_{m,o(e)} - \delta_{n,m} \delta_{m,o(e)} \right\} - q_d d_t \psi_m^{\text{ss}} \delta_{n,m}, \quad (\text{A50})$$

and it satisfies the following symmetry:

$$\hat{\mathcal{W}}_t^T(q_d, q_{nc}) = \mathcal{P}_t^{-1} \mathcal{W}_t(q_d, 1 - q_{nc}) \mathcal{P}_t, \quad (\text{A51})$$

where $\mathcal{P}_t := \text{diag} \{ \exp -\psi_m^{\text{ss}} \}$. The finite-time DFT ensues when following the mathematical steps of the main proof and using Equation (A51) at the step at Equation (A20).

References

1. Harris, R.J.; Schütz, G.M. Fluctuation theorems for stochastic dynamics. *J. Stat. Mech. Theor. Exp.* **2007**, *7*, P07020. doi:10.1088/1742-5468/2007/07/p07020.
2. Esposito, M.; Harbola, U.; Mukamel, S. Nonequilibrium fluctuations, fluctuation theorems, and counting statistics in quantum systems. *Rev. Mod. Phys.* **2009**, *81*, 1665–1702. doi:10.1103/RevModPhys.81.1665.
3. Jarzynski, C. Equalities and Inequalities: Irreversibility and the Second Law of Thermodynamics at the Nanoscale. *Annu. Rev. Condens. Matter Phys.* **2011**, *2*, 329–351. doi:10.1146/annurev-conmatphys-062910-140506.
4. Campisi, M.; Hänggi, P.; Talkner, P. Colloquium: Quantum fluctuation relations: Foundations and applications. *Rev. Mod. Phys.* **2011**, *83*, 771–791. doi:10.1103/revmodphys.83.771.
5. Seifert, U. Stochastic thermodynamics, fluctuation theorems and molecular machines. *Rep. Prog. Phys.* **2012**, *75*, 126001. doi:10.1088/0034-4885/75/12/126001.

6. Van den Broeck, C.; Esposito, M. Ensemble and trajectory thermodynamics: A brief introduction. *Phys. A Stat. Mech. Appl.* **2015**, *418*, 6–16. doi:10.1016/j.physa.2014.04.035.
7. Ciliberto, S. Experiments in Stochastic Thermodynamics: Short History and Perspectives. *Phys. Rev. X* **2017**, *7*, 021051. doi:10.1103/PhysRevX.7.021051.
8. Chetrite, R.; Gupta, S. Two Refreshing Views of Fluctuation Theorems through Kinematics Elements and Exponential Martingale. *J. Stat. Phys.* **2011**, *143*, 543. doi:10.1007/s10955-011-0184-0.
9. Pérez-Espigares, C.; Kolton, A.B.; Kurchan, J. Infinite family of second-law-like inequalities. *Phys. Rev. E* **2012**, *85*, 031135. doi:10.1103/PhysRevE.85.031135.
10. Verley, G.; Chétrite, R.; Lacoste, D. Inequalities Generalizing the Second Law of Thermodynamics for Transitions between Nonstationary States. *Phys. Rev. Lett.* **2012**, *108*, 120601. doi:10.1103/physrevlett.108.120601.
11. Baiesi, M.; Falasco, G. Inflow rate, a time-symmetric observable obeying fluctuation relations. *Phys. Rev. E* **2015**, *92*, 042162. doi:10.1103/PhysRevE.92.042162.
12. Esposito, M.; Harbola, U.; Mukamel, S. Entropy fluctuation theorems in driven open systems: Application to electron counting statistics. *Phys. Rev. E* **2007**, *76*, 031132. doi:10.1103/PhysRevE.76.031132.
13. Polettini, M. Cycle/Cocycle Oblique Projections on Oriented Graphs. *Lett. Math. Phys.* **2014**, *105*, 89–107. doi:10.1007/s11005-014-0732-z.
14. Rao, R.; Esposito, M. Conservation laws shape dissipation. *New J. Phys.* **2018**, *20*, 023007. doi:10.1088/1367-2630/aaa15f.
15. Schnakenberg, J. Network theory of microscopic and macroscopic behavior of master equation systems. *Rev. Mod. Phys.* **1976**, *48*, 571–585. doi:10.1103/RevModPhys.48.571.
16. García-García, R.; Domínguez, D.; Lecomte, V.; Kolton, A.B. Unifying approach for fluctuation theorems from joint probability distributions. *Phys. Rev. E* **2010**, *82*, 030104. doi:10.1103/PhysRevE.82.030104.
17. Vaikuntanathan, S.; Jarzynski, C. Dissipation and lag in irreversible processes. *Europhys. Lett.* **2009**, *87*, 60005. doi:10.1209/0295-5075/87/60005.
18. Seifert, U. Entropy Production along a Stochastic Trajectory and an Integral Fluctuation Theorem. *Phys. Rev. Lett.* **2005**, *95*, 040602. doi:10.1103/PhysRevLett.95.040602.
19. Polettini, M. Nonequilibrium thermodynamics as a gauge theory. *Europhys. Lett.* **2012**, *97*, 30003. doi:10.1209/0295-5075/97/30003.
20. Garrahan, J.P. Classical stochastic dynamics and continuous matrix product states: Gauge transformations, conditioned and driven processes, and equivalence of trajectory ensembles. *J. Stat. Mech. Theory Exp.* **2016**, *2016*, 073208. doi:10.1088/1742-5468/2016/07/073208.
21. Esposito, M.; Van den Broeck, C. Three Detailed Fluctuation Theorems. *Phys. Rev. Lett.* **2010**, *104*, 090601. doi:10.1103/PhysRevLett.104.090601.
22. Esposito, M.; Van den Broeck, C. Three faces of the second law. I. Master equation formulation. *Phys. Rev. E* **2010**, *82*, 011143. doi:10.1103/PhysRevE.82.011143.
23. Ge, H.; Qian, H. Physical origins of entropy production, free energy dissipation, and their mathematical representations. *Phys. Rev. E* **2010**, *81*, 051133. doi:10.1103/physreve.81.051133.
24. García-García, R.; Lecomte, V.; Kolton, A.B.; Domínguez, D. Joint probability distributions and fluctuation theorems. *J. Stat. Mech. Theor. Exp.* **2012**, *2012*, P02009. doi:10.1088/1742-5468/2012/02/P02009.
25. Crooks, G.E. Nonequilibrium Measurements of Free Energy Differences for Microscopically Reversible Markovian Systems. *J. Stat. Phys.* **1998**, *90*, 1481–1487. doi:10.1023/a:1023208217925.
26. Crooks, G.E. Entropy production fluctuation theorem and the nonequilibrium work relation for free energy differences. *Phys. Rev. E* **1999**, *60*, 2721–2726. doi:10.1103/physreve.60.2721.
27. Crooks, G.E. Path-ensemble averages in systems driven far from equilibrium. *Phys. Rev. E* **2000**, *61*, 2361–2366. doi:10.1103/physreve.61.2361.
28. Jarzynski, C. Equilibrium free-energy differences from nonequilibrium measurements: A master-equation approach. *Phys. Rev. E* **1997**, *56*, 5018–5035. doi:10.1103/PhysRevE.56.5018.
29. Speck, T.; Seifert, U. Integral fluctuation theorem for the housekeeping heat. *J. Phys. A Math. Gen.* **2005**, *38*, L581. doi:10.1088/0305-4470/38/34/L03.
30. Hatano, T.; Sasa, S.I. Steady-State Thermodynamics of Langevin Systems. *Phys. Rev. Lett.* **2001**, *86*, 3463–3466. doi:10.1103/PhysRevLett.86.3463.

31. Knauer, U. *Algebraic Graph Theory: Morphisms, Monoids and Matrices*; Walter de Gruyter: Berlin, Germany, 2011; Volume 41.
32. Kolmogoroff, A. Zur Theorie der Markoffschen Ketten. *Math. Ann.* **1936**, *112*, 155–160. doi:10.1007/bf01565412.
33. Kelly, F.P. *Reversibility and Stochastic Networks*; John Wiley & Sons: New York, NY, USA, 1979.
34. Polettini, M.; Esposito, M. Transient fluctuation theorems for the currents and initial equilibrium ensembles. *J. Stat. Mech. Theor. Exp.* **2014**, *2014*, P10033. doi:10.1088/1742-5468/2014/10/p10033.
35. Andrieux, D.; Gaspard, P. Fluctuation Theorem for Currents and Schnakenberg Network Theory. *J. Stat. Phys.* **2007**, *127*, 107–131. doi:10.1007/s10955-006-9233-5.
36. Schmiedl, T.; Seifert, U. Stochastic thermodynamics of chemical reaction networks. *J. Chem. Phys.* **2007**, *126*, 044101. doi:10.1063/1.2428297.
37. Rao, R.; Esposito, M. Conservation Laws and Work Fluctuation Relations in Chemical Reaction Networks. 2018. Available online: <https://arxiv.org/abs/1805.12077> (accessed on 22 August 2018).
38. Polettini, M.; Bulnes Cuetara, G.; Esposito, M. Conservation laws and symmetries in stochastic thermodynamics. *Phys. Rev. E* **2016**, *94*, 052117. doi:10.1103/PhysRevE.94.052117.
39. Callen, H. *Thermodynamics and an Introduction to Thermostatistics*; John Wiley & Sons: New York, NY, USA, 1985.
40. Esposito, M. Stochastic thermodynamics under coarse graining. *Phys. Rev. E* **2012**, *85*, 041125. doi:10.1103/PhysRevE.85.041125.
41. Sánchez, R.; Büttiker, M. Detection of single-electron heat transfer statistics. *Europhys. Lett.* **2012**, *100*, 47008. doi:10.1209/0295-5075/100/47008.
42. Strasberg, P.; Schaller, G.; Brandes, T.; Esposito, M. Thermodynamics of a Physical Model Implementing a Maxwell Demon. *Phys. Rev. Lett.* **2013**, *110*, 040601. doi:10.1103/physrevlett.110.040601.
43. Thierschmann, H.; Sánchez, R.; Sothmann, B.; Arnold, F.; Heyn, C.; Hansen, W.; Buhmann, H.; Molenkamp, L.W. Three-terminal energy harvester with coupled quantum dots. *Nat. Nanotechnol.* **2015**, *10*, 854–858. doi:10.1038/nnano.2015.176.
44. Peliti, L. *Statistical Mechanics in a Nutshell*; Princeton University Press: Princeton, NJ, USA, 2011.
45. Polettini, M.; Esposito, M. Effective Thermodynamics for a Marginal Observer. *Phys. Rev. Lett.* **2017**, *119*, 240601. doi:10.1103/PhysRevLett.119.240601.
46. Polettini, M.; Esposito, M. Effective Fluctuation and Response Theory. 2018. Available online: <https://arxiv.org/abs/1803.03552> (accessed on 22 August 2018).
47. Bulnes Cuetara, G.; Esposito, M.; Imparato, A. Exact fluctuation theorem without ensemble quantities. *Phys. Rev. E* **2014**, *89*, 052119. doi:10.1103/PhysRevE.89.052119.



© 2018 by the authors. Licensee MDPI, Basel, Switzerland. This article is an open access article distributed under the terms and conditions of the Creative Commons Attribution (CC BY) license (<http://creativecommons.org/licenses/by/4.0/>).

Part II

CHEMICALLY REACTING SYSTEMS FAR FROM EQUILIBRIUM

3 | PHENOMENOLOGICAL DESCRIPTION

We now specialize the phenomenological description discussed in Ch. 1 to chemical reactions networks. As for the previous part, this description provides the theoretical structure underlying the thermodynamics of any chemical reaction networks. This structure will indeed be recovered in the stochastic and deterministic dynamics introduced in the following chapters.

The plan of the chapter is as follows. In Sec. 3.1, chemical reaction networks are introduced, while in Sec. 3.2, we present a *black-box* thermodynamic description. Broken conservation laws are introduced in Sec. 3.3, which contains the main result of this chapter. We conclude with an example, Sec. 3.4.

3.1 CHEMICAL REACTION NETWORKS

We consider an isobaric and isothermal dilute solution of reacting chemical species, which we label by σ and whose abundances are denoted by $\{N^\sigma\}$. The chemical reaction network is described by

$$\sum_{\sigma} S_{+\rho}^{\sigma} \sigma \xrightleftharpoons[-\rho]{+\rho} \sum_{\sigma} S_{-\rho}^{\sigma} \sigma, \quad (86)$$

where the *stoichiometric coefficients* $S_{+\rho}^{\sigma}$ and $S_{-\rho}^{\sigma}$ quantify the amount of species participating in each reaction. Notice that all reactions are *reversible*, and for each pair $\xrightleftharpoons[-\rho]{+\rho}$, $+\rho$ (resp. $-\rho$) denotes the forward (resp. backward) reaction. Among all species, we distinguish the internal ones, x , from the external ones, also called chemostatted, y : $\sigma \equiv \{x, y\}$. The abundances of the *internal* species can only change due to reactions, and hence their balance equations read

$$dN^x = d_i N^x = \sum_{\rho} S_{\rho}^x d\xi_{\rho}, \quad (87)$$

where

$$S_{\rho}^{\sigma} := S_{-\rho}^{\sigma} - S_{+\rho}^{\sigma} \quad (88)$$

denotes the *stoichiometric matrix* of the chemical reaction network. Crucially, S encodes the coupling between species and reactions, and hence the topological properties of the chemical reaction network. The extent in which each reaction occurs is quantified by the *extents of reaction* $\{d\xi_{\rho}\}$. In contrast to x , each *chemostatted* species y is exchanged with a chemical reservoir, called *chemostat*, and the balance equations for their abundances read

$$dN^y = d_i N^y + d_r N^y = \sum_{\rho} S_{\rho}^y d\xi_{\rho} + d_r N^y, \quad (89)$$

where $\{d_r N^y\}$ quantify the changes due to particle exchanges. We denote by $\{\mu_y\}$ the chemical potentials of the reservoirs, *i.e.* the energetic intensive fields conjugated to N^y . Their variations due to external manipulations are again denoted by $d\mu_y = \partial\mu_y$.

Since the solution is isobaric and isothermal, pressure and temperature do not change, $\partial p_r = \partial T_r = 0$. External driving in internal energy, volume, and particle abundances are also absent, $\partial U = \partial V = \partial N^\sigma = 0$ for all σ . The hypothesis of diluteness guarantees that the changes of abundances do not affect the overall volume, which is determined only by the solvent and can be considered as almost constant, $dV \simeq 0$.

3.2 THERMODYNAMICS

We first discuss a phenomenological nonequilibrium thermodynamic description in which only the balances of energy, volume and chemical abundance are taken into account. Therefore, by combining the balances of energy and volume, the first law, Eq. (13), can be rewritten as

$$dH = dQ + dW_{\text{chem}}, \quad (90)$$

where

$$H = U + pV \quad (91)$$

is the system *enthalpy*, and

$$dW_{\text{chem}} = \sum_y \mu_y d_r N^y \quad (92)$$

is the *chemical work*, which quantifies the free energy exchanged with the chemostats. Concerning the second law, Eq. (16), we obtain

$$d\Sigma = -\beta_r dG + \beta_r dW_{\text{chem}}, \quad (93)$$

where

$$G = H - T_r S \quad (94)$$

is the *Gibbs potential*. By combining these laws with the balances of chemostatted species abundances, we obtain

$$d \left[H - \sum_y \mu_y N^y \right] = - \sum_\rho \left(\sum_y \mu_y S_\rho^y \right) d\xi_\rho - \sum_y \partial \mu_y N^y + d_r Q \quad (95)$$

$$d\Sigma = -\beta d \left[G - \sum_y \mu_y N^y \right] - \beta \sum_\rho \left(\sum_y \mu_y S_\rho^y \right) d\xi_\rho - \beta \sum_y \partial \mu_y N^y \geq 0. \quad (96)$$

We recognize these expressions as special cases of Eqs. (43) and (45), respectively, in which the nonconservative contributions are absent. This is clearly a consequence of considering only one reservoir per chemostatted species, as well as only one thermal and volumetric reservoir. Notice the presence of the terms involving internal reactions, which account for the energy and entropy changes as these occur.

For the system to be at equilibrium, the driving must be stopped $\partial \mu_y = 0$ for all y , and all terms conjugated to the extents of reaction must vanish independently, $\sum_y \mu_y S_\rho^y = 0$ for all ρ . We notice that at this level of description, the internal conditions for equilibrium is specified by N_ρ conditions. As previously done for generic thermodynamic systems, we will reduce the number of this conditions using conservation laws.

3.3 SYSTEM-SPECIFIC THERMODYNAMICS

We now identify the broken conservation laws and derive a system-specific nonequilibrium thermodynamic description for chemical reaction networks, like in Sec. 1.5.

For chemical reaction network, broken conservation laws are defined as a maximal set of independent vectors, $\{\ell_y^\lambda\}$ for $\lambda = 1, \dots, N_\lambda$, satisfying

$$\sum_y \ell_y^\lambda \oint_\gamma d_r N^y = 0, \quad \text{for any instantaneous cyclic transformation } \gamma, \quad (97)$$

see Eq. (51). The fact that $d_r U$ and $d_r V$ do not appear, follows from the fact that we are considering thermal exchanges and volume changes as disentangled from the reaction dynamics. Concerning thermal changes, we are neglecting, for instance, relativistic effects in which chemostatted species disintegrate into thermal energy. Concerning volume changes, we have already mentioned that since the solution is dilute, changes of abundances do not change the volume. Therefore, the related conserved quantities follow from

$$dL_\lambda = \sum_y \ell_y^\lambda d_r N^y \quad (98)$$

as for the general case, Eq. (52).

We now follow the same procedure detailed in Sec. 1.5 and decompose the chemostatted species into *potential* y , $\{y_p\}$, and *force* y , $\{y_f\}$. The first law, Eq. (95), can be thus rewritten as

$$d\mathcal{H} = \partial\mathcal{H} + \mathcal{K}_{y_f} d_r N^{y_f} + dQ, \quad (99)$$

where

$$\mathcal{H} = H - \sum_{y_p} \mu_{y_p} \sum_\lambda \bar{\ell}_\lambda^{y_p} L_\lambda \quad (100)$$

is a *nonequilibrium semi-grand enthalpy*, and

$$\mathcal{K}_{y_f} = \mu_{y_f} - \mu_{y_p} \sum_\lambda \bar{\ell}_\lambda^{y_p} \ell_{y_f}^\lambda \quad (101)$$

are *fundamental nonconservative forces*. The second law, instead, reads

$$d\Sigma = \beta_r \left[-dG + \partial\mathcal{H} + \sum_{y_f} \mathcal{K}_{y_f} d_r N^{y_f} \right] \geq 0, \quad (102)$$

where

$$G = \mathcal{H} - T_r S \quad (103)$$

is a *nonequilibrium semi-grand Gibbs potential* [1]. Semi-grand stands for the fact that the system is open wrt a restricted set of species: the chemostatted.

Equations (99) and (102) specialize Eqs. (54) and (58) to chemical reaction networks. They are the major result of this chapter. In the entropy balance, the conservative contribution, $-\beta_r dG$, quantifies the dissipation due to overall chemical free energy changes in the system. In both balances, instead,

$$\partial\mathcal{H} = -\sum_{y_p} \partial\mu_{y_p} \sum_\lambda \bar{\ell}_\lambda^{y_p} L_\lambda \quad (104)$$

is the chemical free energy spent by the external agent to manipulate the chemical potentials of the chemostatted species, which we called *driving*

work. To fully understand the physical meaning of $\{\mathcal{K}_{y_f} \dot{d}_r N^{y_f}\}$, for $y_f = 1, \dots, N_y - N_\lambda$, we need to observe that chemical reactions may give rise to cyclic transformations which allow some chemostatted species to be transformed into some others. In other words, chemical reactions may create pathways between reservoirs of different external species. The stoichiometry of a maximal independent set of these pathways is captured by the coefficients multiplying the chemical potentials in Eq. (101),

$$v_{y_f}^y := \begin{cases} 1 & \text{if } y = y_f, \\ -\sum_\lambda \bar{\ell}_\lambda^y \ell_{y_f}^\lambda & \text{if } y \in \{y_p\}, \end{cases} \quad (105)$$

where the sign determines whether the species enters (+) or leaves (-) the system. Therefore, $\{\mathcal{K}_{y_f} \dot{d}_r N^{y_f}\}$ quantify the work spent by the reservoirs to sustain flows of chemicals across the system. We emphasize that these nonconservative terms can be identified solely thanks to conservation laws, *cf.* Eq. (96).

At equilibrium, the chemical reaction network is nondriven $\partial\mu_y = 0$ for all y , and all fundamental forces must vanish, which implies that

$$\mu_{y_f} = \mu_{y_p} \sum_\lambda \bar{\ell}_\lambda^{y_p} \ell_{y_f}^\lambda, \quad \text{for all } y_f. \quad (106)$$

These N_{y_f} conditions replace those $N_\rho \geq N_{y_f}$ expressed for internal reactions, Eq. (96). The requirement $dG_{eq} = 0$ and Eq. (6) implies that

$$0 = \sum_{y_p} \left(\mu_{y_p}^s - \mu_{y_p} \right) \sum_\lambda \bar{\ell}_\lambda^{y_p} dL_\lambda, \quad (107)$$

which in turn constrains the chemical potentials of the y_p species in the systems, $\{\mu_{y_p}^s\}$, to be equal to those of the chemostats.

3.3.1 Stoichiometric Cycles and Broken Conservation Laws

The stoichiometric structure of chemical reaction networks allows to identify broken conservation laws in a way simpler than Eq. (97) [2]. We now prove that if and only if $\ell_y \neq 0$ satisfies Eq. (97), than it exists an x -species-space vector ℓ_x such that

$$\sum_y \ell_y S_\rho^y + \sum_x \ell_x S_\rho^x = 0. \quad (108)$$

viz. $(\ell_x, \ell_y) \in \text{coker } S$. In order to do so, we first prove some preliminary results.

We define *stoichiometric cycle* of the instantaneous cyclic transformation γ , denoted by c_γ , as the ρ -space vectors whose entries quantify the overall extent of reactions along γ ,

$$c_\gamma^\rho := \oint_\gamma d\xi_\rho. \quad (109)$$

Let $\{c_\eta\}$ for $\eta = 1, \dots, N_\eta$ be a maximal set of independent stoichiometric cycles. By taking the cyclic transformations of the balance of chemical abundances, Eqs. (87) and (89), along $\{\eta\}$ we obtain

$$\begin{aligned} \sum_\rho S_\rho^x c_\eta^\rho &= 0 \\ \sum_\rho S_\rho^y c_\eta^\rho &= -\oint_\eta d_r N^y, \end{aligned} \quad (110)$$

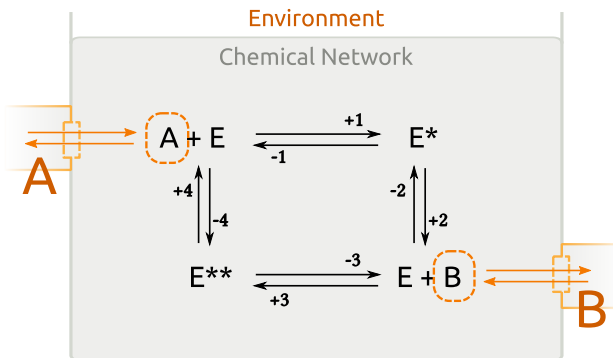


Figure 5: Chemical reaction network taken as an example.

from which we deduce that $\{c_\eta\}$ is a basis of $\ker S^x$ —otherwise the set $\{c_\eta\}$ would not be either maximal or independent. Combining this equation with the definition of broken conservation law, Eq. (97), the latter can be recast into

$$\sum_{y,\rho} \ell_y S_\rho^y c_\eta^\rho = 0, \quad \text{for all } \eta. \quad (111)$$

We can now proceed to prove that Eqs. (97) and (111) are equivalent to Eq. (108).

On the one hand, if $\ell \neq 0$ satisfies Eq. (97)–(111), then the vector $\sum_{y,\rho} \ell_y S_\rho^y$ belongs to $(\ker S^x)^\perp \equiv \text{coim } S^x$. Therefore, there exists a x -species-space vector $\{-\ell_x\}$ such that

$$\sum_y \ell_y S_\rho^y = -\sum_x \ell_x S_\rho^x. \quad (112)$$

which is equivalent to Eq. (108). Clearly, ℓ_x is defined up to a linear combination of vectors in $\text{coker } S^x$.

On the other hand, if Eq. (108) is true, then

$$0 = \sum_{y,\rho} \ell_y S_\rho^y c_\eta^\rho + \sum_{x,\rho} \ell_x S_\rho^x c_\eta^\rho = \sum_{y,\rho} \ell_y S_\rho^y c_\eta^\rho, \quad \text{for all } \eta, \quad (113)$$

as in Eq. (111).

In conclusion, since Eq. (97) and (108) are equivalent, and ℓ_x in Eq. (108) is defined up to a vector in $\text{coker } S^x$, an independent set of broken conservation laws, $\{\ell^\lambda\}$, for $\lambda = 1, \dots, N_\lambda$, can be determined as a basis of the quotient space $\text{coker } S / \text{coker } S^x$.

3.4 EXAMPLE

To illustrate the main results of this chapter, let us consider the enzymatic chemical reaction network in Fig. 5. The chemical species are partitioned into internal, the enzyme complexes $\{E, E^*, E^{**}\}$, and external, the substrates $\{A, B\}$. The stoichiometric matrix reads

$$S = \begin{pmatrix} & +1 & +2 & +3 & +4 \\ E & -1 & 1 & -1 & 1 \\ E^* & 1 & -1 & 0 & 0 \\ E^{**} & 0 & 0 & 1 & -1 \\ A & -1 & 0 & 0 & 1 \\ B & 0 & 1 & -1 & 0 \end{pmatrix}. \quad (114)$$

This chemical reaction network is characterized by one broken conservation law

$$\ell = \begin{pmatrix} A & B \\ 1 & 1 \end{pmatrix}, \quad (115)$$

which can be intuitively understood as follows: for any given amount of A injected along a cyclic transformation, $\oint d_r N^A$, the same amount of B must be expelled, $\oint d_r N^B = -\oint d_r N^A$, see Eq. (97). The related conserved quantity L is the total amount of molecules A and B present in the chemical reaction network, where we need to account for those present in the enzyme complexes E^* and E^{**} , too: $L = N^A + N^B + N^{E^*} + N^{E^{**}}$. Indeed one can readily check using Eq. (114) that $dL = d_i L + d_r L = d_r L = d_r N^A + d_r N^B$.

We mention that broken conservation laws can also be identified from the cokernel of S , as discussed in Sec. 3.3.1, and illustrated in the examples [1 and 3, pp. 113 and 115] and [1, 3, and 4, pp. 146 and 148].

By regarding the species A as y_p whereas B as y_f , the system-specific expression of the first and second law, Eqs. (99) and (102), can be formulated. The nonequilibrium semi-grand enthalpy (100) reads

$$\mathcal{H} = H - \mu_A L, \quad (116)$$

whereas the nonconservative work contribution is

$$\mathcal{K}_B d_r N^B = (\mu_B - \mu_A) d_r N^B. \quad (117)$$

The latter quantifies the cost of maintaining the flow of chemical across the network induced by the gradient of chemical potentials. The driving work $\partial \mathcal{H}$ as well as the nonequilibrium semi-grand Gibbs potential \mathcal{G} readily follow, and the overall entropy production reads

$$d\Sigma = \beta_r \left[-d\mathcal{G} - \partial \mu_A L + \mathcal{K}_B d_r N^B \right]. \quad (118)$$

The illustration of this decomposition for a slightly more complex chemical reaction network is discussed in Sec. [VIII, p. 131].

REFERENCES FOR CHAPTER 3

- [1] R. A. ALBERTY, *Thermodynamics of biochemical reactions*, Wiley-Interscience, 2003.
- [2] M. POLETTINI and M. ESPOSITO, “Irreversible thermodynamics of open chemical networks. I. Emergent cycles and broken conservation laws”, *J. Chem. Phys.* **141**.2 (2014), 024117.

4 STOCHASTIC DESCRIPTION

In the previous chapter, we established a phenomenological thermodynamic description of chemical reaction networks. In the following preprinted article, we will show the connection between this description and a stochastic one based on the chemical master equation [1, 2], which is crucial for describing biochemical processes occurring at low particle numbers, like many cellular processes. From a theoretical point of view, connecting phenomenological and stochastic description shows that the laws of chemical kinetics are consistent with thermodynamics at a very fundamental level of description.

To provide the link between the phenomenological and stochastic description, we observe that timeless expression of the chemical master equation [(11), p. 113] reads

$$dp_n = \sum_{\rho} [\dot{d}\zeta_{+\rho}(n - S_{+\rho}) - \dot{d}\zeta_{-\rho}(n) - \dot{d}\zeta_{+\rho}(n) + \dot{d}\zeta_{-\rho}(n + S_{+\rho})] , \quad (119)$$

where n is a vector counting the number of molecules of each species, p_n is the probability of observing n , and $\{\dot{d}\zeta_{\pm\rho}(n)\}$ are the extents of reaction from each state n . The species abundances, $\{N^\sigma\}$, can be regarded as the average numbers of molecules, which in vectorial form read $\mathbf{N} = \sum_n n p_n$, and their balance, Eqs. (87) and (87), can be recovered as follows. We preliminary observe that using the chemical master equation, one obtains

$$d\mathbf{N} = \sum_n n dp_n = \sum_{\rho} S_{\rho} \sum_n [\dot{d}\zeta_{+\rho}(n) - \dot{d}\zeta_{-\rho}(n)] . \quad (120)$$

We now distinguish those *internal reactions* which do not entail any exchange of chemostatted species, $\{\rho_i\}$, from those *exchange reactions* which model the exchange of each chemostatted species with its corresponding chemostat, $\{\rho_e\}$: $\{\rho\} \equiv \{\rho_i\} \cup \{\rho_e\}$, see Sec. [IIA, p. 112]. We thus recover Eqs. (87) and (89) when replacing

$$\begin{aligned} \dot{d}\xi_{\rho_i} &= \sum_n [\dot{d}\zeta_{+\rho_i}(n) - \dot{d}\zeta_{-\rho_i}(n)] \quad \text{and} \\ \dot{d}_r N^y &= \sum_{\rho_e} S_{\rho}^y \sum_n [\dot{d}\zeta_{+\rho_e}(n) - \dot{d}\zeta_{-\rho_e}(n)] \end{aligned} \quad (121)$$

in the previous equation. As for generic Markov jump processes, the connection between stochastic dynamics and thermodynamics lies in the local detailed balance property, which—in a timeless formulation—relates the ratio of forward and backward stochastic extent of reaction, to the entropy production along the reaction, *i.e.* the affinity. As we will show, this relation is true for elementary reactions, and—in a timeless formulation—can be written either using the Eq. (93) (Eq. [(53) and (56), p. 117]),

$$\ln \frac{\dot{d}\zeta_{+\rho}(n)}{\dot{d}\zeta_{-\rho}(n + S_{+\rho})} = -\beta_r [\Delta_{\rho} G(n) + \sum_y \mu_y S_{\rho}^y] , \quad (122)$$

in terms of differences of Gibbs free energy along reactions $\{\Delta_{\rho} G(n)\}$, see Eq. [(47), p. 117], or using Eq. (16) (Eq. [(75), p. 119])

$$\ln \frac{\dot{d}\zeta_{+\rho}(n)}{\dot{d}\zeta_{-\rho}(n + S_{+\rho})} = -\beta_r \dot{d}Q^{\text{thr}} + \beta_r \dot{d}Q^{\text{chm}} + \Delta_{\rho} S(n) , \quad (123)$$

where dQ^{thr} and dQ^{chm} are the heat exchanged with the thermal and chemical reservoirs, while $\Delta_p S(\mathbf{n})$ is the internal entropy change.

By introducing conservation laws, we will thus reproduce the semigrand enthalpy and entropy balance, Eqs. (99) and (102), both at the level of stochastic trajectories, Eqs. [(101), p. 122] and [(115), p. 123], and ensemble averages, Eqs. [(174), p. 129] and [(175), p. 130]. We further emphasize the importance of our formulation as we show that the driving and nonconservative work contributions, $\partial\mathcal{H}$ and $\{\mathcal{K}_{Y_f} dN^{Y_f}\}$, satisfy a FT, Eq. [(156), p. 128], in contrast to other forms of work like the chemical one, dW_{chem} , Eq. (92), see Sec. [VD, pp. 119–120]. We finally specialize the nonequilibrium Landauer principle to stochastic chemical reaction networks, Eqs. [(178) and (180), p. 130].

REFERENCES FOR CHAPTER 4

- [1] D. A. McQUARRIE, “**Stochastic Approach to Chemical Kinetics**”, *J. Appl. Probab.* **4**.3 (1967), 413.
- [2] D. T. GILLESPIE, “**A rigorous derivation of the chemical master equation**”, *Physica A* **188**.1–3 (1992), 404–425.

The following article is preprinted from
[R. RAO and M. ESPOSITO (arXiv 1805.12077), submitted].

The page numbers placed in the outer margins provide a continuous pagination throughout the thesis.

Conservation Laws and Work Fluctuation Relations in Chemical Reaction Networks

Riccardo Rao and Massimiliano Esposito

Complex Systems and Statistical Mechanics, Physics and Materials Science
Research Unit, University of Luxembourg, L-1511 Luxembourg, G.D. Luxembourg

(Dated: May 20, 2018. Rev. of 69f70)

We formulate a nonequilibrium thermodynamic description for open chemical reaction networks (CRN) described by a chemical master equation. The topological properties of the CRN and its conservation laws are shown to play a crucial role. They are used to decompose the entropy production into a potential change and two work contributions, the first due to time dependent changes in the externally controlled chemostats concentrations and the second due to flows maintained across the system by nonconservative forces. These two works jointly satisfy a Jarzynski and Crooks fluctuation theorem. In absence of work, the potential is minimized by the dynamics as the system relaxes to equilibrium and its equilibrium value coincides with the maximum entropy principle. A generalized Landauer's principle also holds: the minimal work needed to create a nonequilibrium state is the relative entropy of that state to its equilibrium value reached in absence of any work.

PACS numbers: 05.70.Ln, 87.16.Yc

I. INTRODUCTION

Nonequilibrium thermodynamic descriptions of stochastic (bio-)chemical processes have long since been developed. Among the first, T.L. Hill and coworkers studied bio-catalysts as small fluctuating machines operating at steady-state. They introduced the concept of free energy transduction and analyzed how one form of chemical work can drive another one against its spontaneous direction [1, 2]. The importance of decomposing currents into network cycles (*i.e.* cyclic sets of transitions) was already emphasized. These results were however limited to steady-state systems described by linear chemical reaction networks (CRN). The stochastic as well as the deterministic dynamics of these CRNs is described by the same linear rate equations for, respectively, probabilities or concentrations. They model for instance conformational changes of an enzyme or of a membrane transporter. Inspired by these seminal works, J. Schnakenberg formulated a steady-state thermodynamics for generic Markov jump processes and provided a systematic cycle decomposition for the entropy production (EP) rate [3]. He considered in particular the stochastic description in terms of the Chemical Master Equation (CME) [4, 5] of nonlinear chemical reaction networks, *i.e.* CRNs described at the deterministic level by nonlinear rate equations for concentrations. The Brussels school, J. Ross and many others, focused on the connection between the thermodynamic description resulting from the stochastic and the deterministic dynamics [6–9].

With the advent of Stochastic Thermodynamics [10–13], the focus moved to the study of fluctuations, rather than focusing on the first two moments. Gaspard first showed that EP fluctuations in nonlinear CRNs at steady state satisfy a fluctuation theorem (FT) [14]. This result

was later expressed in terms of currents along Schnakenberg cycles [15, 16]. Fluctuations in complex chemical dynamics such as bistability was analyzed, amongst others, by Qian and coworkers [17–19]. A first formulation of stochastic thermodynamics for CRNs beyond steady state was done by Schmiedl and Seifert in Ref. [20].

Despite this long history none of these descriptions made use of the specific topology of the CRN encoded in its stoichiometric matrix. Mathematicians know however that the CRN topology plays an important role on its deterministic [21, 22] as well as stochastic dynamics [23, 24]. But the question of how it affects the thermodynamic description was only studied recently: for deterministic dynamics in Refs. [25, 26], while for stochastic dynamics at steady state in [27]. In this paper we address this question in full generality for CRNs whose dynamics is stochastic. We will do so by presenting a formulation of stochastic thermodynamics for CRNs which systematically makes use of the conservation laws. Doing so leads to a significantly more informative thermodynamic description. In particular, we decompose the EP into three fundamental dissipative contributions: a newly defined potential change, a driving work contribution due to time dependent changes in the externally controlled chemostats concentrations, and a nonconservative work contribution due to a minimal set of flows maintained across the system by nonconservative forces. In contrast to the traditional chemical work given by minus the free energy change in the chemostats, these two new work contributions are shown to jointly satisfy a finite-time detailed and integral FT, when the CRN is initially prepared in an equilibrium state. In turn, the importance of the potential lies in the fact it is minimized by the relaxation dynamics towards equilibrium in absence of the first two work contributions, *i.e.* when the system is detailed-balanced. It can be seen as a Legendre transform with respect to those conservation laws that are bro-

ken by the chemostats. At equilibrium it coincides with the potential obtained from maximizing entropy with broken conservation laws as constrains. We also discuss the connection of our findings to absolute irreversibility [28], to free energy transduction in nonlinear CRNs, and to cycle decompositions of the entropy production. Finally, we derive a nonequilibrium Landauer's principle for the driving and nonconservative work which generalizes the previous ones to nondetailed-balanced dynamics [29, 30].

Outline The paper is organized as follows. In § II (Stochastic Dynamics and CRN Topology) we review the stochastic description of closed and open CRNs and introduce conservation laws and stoichiometric cycles. In § III (Stochastic Thermodynamics) the connection with thermodynamics is made. The stochastic reaction rates are expressed in terms of Gibbs potentials via the equilibrium distribution of the closed CRN. Enthalpy and entropy balance are defined along stochastic trajectories and Jarzynski-like FTs for the chemical work are discussed. In § IV (CRN-Specific Stochastic Thermodynamics) the EP is partitioned into its three contributions. In § V (Semigrand Gibbs Potential) we analyze open detailed balanced CRNs, more specifically their relaxation to equilibrium as chemostats are successively introduced. In § VI (Fluctuation Theorems), finite-time detailed FTs for the driving and nonconservative work are derived. In § VII (Ensemble Average Rates Description) the ensemble averaged description is presented and the nonequilibrium Landauer's principle is derived. Finally in § VIII, our results are applied on a simple model which clarify the importance of our formulation for free energy transduction. Throughout the paper, our formalism is illustrated using a simple enzymatic scheme, whereas some technical derivations are given in appendices.

II. STOCHASTIC DYNAMICS AND CRN TOPOLOGY

A. CRNs

We consider a homogeneous, isobaric, and isothermal *ideal dilute solution* made of N_z chemical species, encoded in a vector \mathbf{z} . Their integer-valued *population* \mathbf{n} changes due to internal reactions which we label by $\{\rho_i\}$ for $\rho_i = \pm 1, \dots, \pm N_i$,

$$\mathbf{v}_{\rho_i} \cdot \mathbf{z} \xrightleftharpoons[k_{-\rho_i}]{k_{\rho_i}} \mathbf{v}_{-\rho_i} \cdot \mathbf{z}. \quad (1)$$

In *open* CRNs, the population of a subset of species, named *exchanged* species and denoted by \mathbf{y} where $\mathbf{z} \equiv (\mathbf{x}, \mathbf{y})$, varies also due to exchanges with external *chemostats* denoted by \mathbf{Y} . Their effect is modeled by exchange reactions, $\{\rho_e\}$ for $\rho_e = \pm 1, \dots, \pm N_y$, see Fig. 1,

	species	symbol	number	abundance
internal	$\{$	\mathbf{x}	N_x	\mathbf{n}_x
exchanged	\mathbf{y}	N_y	\mathbf{n}_y	\mathbf{Y}
chemostatted	\mathbf{Y}	N_y	$[Y]$	

TABLE I. In the second column the symbols used for the various species are listed. The corresponding total number of entries and symbols used to denote their abundance are given in the third and fourth column, respectively. The first column summarizes the name used to refer to these species, while the last one recalls the symbol used to collect the abundances of the internal species. Internal species, \mathbf{x} and \mathbf{y} , are characterized by low populations, \mathbf{n} . The population of \mathbf{x} can change only because of reactions, whereas that of \mathbf{y} are also exchanged with chemostats, which are identified by \mathbf{Y} , Eq. (1).

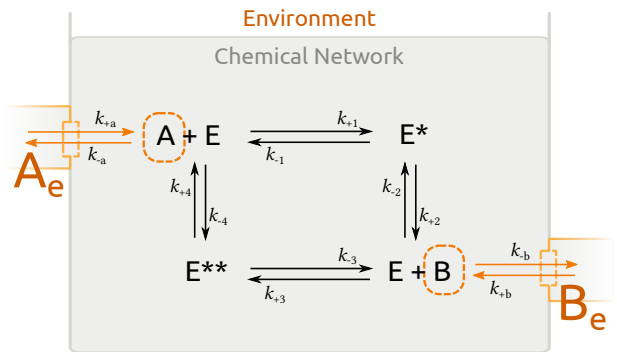


FIG. 1. Pictorial representation of an open CRN modeling an enzymatic scheme. More details are given in Example 1

$$\mathbf{v}_{\rho_e}^y \cdot \mathbf{y} \xrightleftharpoons[k_{-\rho_e}]{k_{\rho_e}} \mathbf{v}_{\rho_e}^Y \cdot \mathbf{Y}. \quad (2)$$

The non-negative integer-valued vectors $\{\mathbf{v}_\rho \equiv (\mathbf{v}_\rho^x, \mathbf{v}_\rho^y)\}$ for $\rho \in \{\rho_i\} \cup \{\rho_e\}$, encode the *stoichiometric coefficients* of each reaction. Note that each entry of $\mathbf{v}_{\rho_e}^y$ and $\mathbf{v}_{\rho_e}^Y$ is nonzero and equal to one only if it corresponds to the species exchanged by ρ_e . Note also that all reactions are assumed *elementary* and *reversible*. The different types of species are summarized in Tab. I.

The topology of the CRN is encoded in its *stoichiometric vectors*,

$$\mathbf{S}_\rho := \mathbf{v}_{-\rho} - \mathbf{v}_\rho, \text{ and } \mathbf{S}_\rho^Y := \mathbf{v}_{-\rho}^Y - \mathbf{v}_\rho^Y. \quad (3)$$

The former quantifies the change of population induced by a give reaction ρ , whereas the latter the corresponding amount of chemostatted species that is exchanged. By definition, $\mathbf{S}_\rho = -\mathbf{S}_{-\rho}$ and $\mathbf{S}_\rho^Y = -\mathbf{S}_{-\rho}^Y$. Collecting the column vectors \mathbf{S}_ρ (resp. \mathbf{S}_ρ^Y) corresponding to arbitrarily-chosen forward reactions defines the internal (resp. external) *stoichiometric matrix* denoted by \mathbf{S} (resp. \mathbf{S}^Y). It is not difficult to see that these can be

decomposed as

$$S \equiv (S_i \ S_e) \equiv \begin{pmatrix} S_i^x & O \\ S_i^y & S_e^y \end{pmatrix}, \quad (4)$$

and

$$S^Y \equiv (S_i^Y \ S_e^Y) \equiv (O \ -S_e^y). \quad (5)$$

In closed CRNs all exchange reactions disappear and the stoichiometric matrix reduces to S_i .

Remark Previous works on thermodynamics of CRNs, *e.g.* Refs. [20, 25, 26, 31], describe open CRNs by assuming that the exchanged species y are so abundant that they can be regarded as particle reservoirs *within* the system. As a result the exchange reactions are disregarded, y are treated as *chemostatted*, and the stoichiometric matrices read

$$S_{\text{alt}} = S_i^x, \text{ and } S_{\text{alt}}^Y = S_i^y. \quad (6)$$

In the closed CRNs, the stoichiometric matrix becomes $(S_{\text{alt}}, S_{\text{alt}}^Y)^\top$. As we will see, the two approach are formally very similar, but the former has the advantage of preserving the number of internal species when the CRN is chemostatted. This makes it more suitable for a stochastic description.

Example 1. For the open CRN in Fig. 1,

$$\begin{aligned} x &= (E, E^*, E^{**}), \\ y &= (A, B), \\ Y &= (A_e, B_e) \end{aligned} \quad (7)$$

and

$$n = (n_E, n_{E^*}, n_{E^{**}}, n_A, n_B)^\top. \quad (8)$$

Internal reactions, $\rho_i = \pm 1, \dots, \pm 4$, are distinguished from the exchange ones, $\rho_e = \pm a, \pm b$. The stoichiometric matrix reads

$$S = \begin{array}{c|ccccc|cc} & +1 & +2 & +3 & +4 & +a & +b \\ \begin{array}{c} E \\ E^* \\ E^{**} \\ A \\ B \end{array} & \left(\begin{array}{ccccc|cc} -1 & 1 & -1 & 1 & 0 & 0 \\ 1 & -1 & 0 & 0 & 0 & 0 \\ 0 & 0 & 1 & -1 & 0 & 0 \\ -1 & 0 & 0 & 1 & 1 & 0 \\ 0 & 1 & -1 & 0 & 0 & 1 \end{array} \right) \end{array}. \quad (9)$$

and

$$S^Y = \begin{array}{c|ccccc|cc} & +1 & +2 & +3 & +4 & +a & +b \\ \begin{array}{c} A_e \\ B_e \end{array} & \left(\begin{array}{ccccc|cc} 0 & 0 & 0 & 0 & -1 & 0 \\ 0 & 0 & 0 & 0 & 0 & -1 \end{array} \right) \end{array}. \quad (10)$$

□

Henceforth, we will use the following notation

$$a! = \prod_i a_i!, \quad a \cdot b = \prod_i a_i^{b_i}, \text{ and } c \cdot b = c^{\sum_i b_i},$$

for generic vectors a and b , and for a generic constant c . “ $\ln a$ ” must be read as a vector whose entries are the logarithm of the entries of a . Finally, 1 denotes a vector whose entries are all equal to 1.

B. Chemical Master Equation

In our stochastic description, n is treated as a fluctuating variable and all reactions are regarded as stochastic events. The probability of finding the CRN in the state n at time t is denoted by $p_n \equiv p_n(t)$ and its evolution is ruled by the CME [4, 5, 32]

$$\begin{aligned} d_t p_n &= \sum_{\rho} \{ w_{-\rho}(n + S_{\rho}) p_{n+S_{\rho}} - w_{\rho}(n) p_n \} \\ &= \sum_m W_{nm} p_m, \end{aligned} \quad (11)$$

where the stochastic generator reads

$$W_{nm} = \sum_{\rho} w_{\rho}(m) \left\{ \delta_{n,m+S_{\rho}} - \delta_{n,m} \right\}. \quad (12)$$

Since all reactions are assumed elementary, we consider *mass-action* stochastic reaction rates

$$w_{\rho}(n) := k_{\rho} \frac{V}{V \cdot v_{\rho}} [Y] \cdot v_{\rho}^Y \frac{n!}{(n - v_{\rho})!}. \quad (13)$$

where $\{k_{\rho}\}$ denote the *rate constants*. The dependence on the volume V ensures the correct scaling when taking the large particle limit and guarantees that $\{k_{\rho}\}$ are the same as in deterministic descriptions [33]. The chemostats concentrations $[Y]$ only appear in exchange reactions ρ_e and quantify the concentration of the exchanged species in the chemostats. Hence, they are real-valued, nonfluctuating, and unaffected by the occurrence of exchange reactions. We assume that $[Y]$ can change over time in a way that is encoded in the driving *protocol* π_t . This may describe for instance, the controlled injection of certain molecules across a cell membrane. In such situations the CRN is said to be subjected to a “driving”. In absence of driving the CRNs is instead said to be *autonomous*.

Equilibrium probability distributions are of crucial importance for our discussion. They satisfy the *detailed balance property*

$$w_{\rho}(n) p_n^{\text{eq}} = w_{-\rho}(n + S_{\rho}) p_{n+S_{\rho}}^{\text{eq}}, \quad \text{for all } \rho, n. \quad (14)$$

This means that the probability current of any reaction ρ occurring from any state n vanishes. Stochastic CRNs which admit a steady-state probability distribution satisfying Eq. (14) are referred to as *detailed balanced*. Their stochastic thermodynamics will be analyzed in § V.

Example 2. For the CRN in Fig. 1, the transition rates are

$$\begin{aligned} w_{+1} &= k_{+1} n_A n_E, & w_{-1} &= k_{-1} n_{E^*}, \\ w_{+2} &= k_{+2} n_{E^*}, & w_{-2} &= k_{-2} n_E n_B, \\ w_{+3} &= k_{+3} n_E n_B, & w_{-3} &= k_{-3} n_{E^{**}}, \\ w_{+4} &= k_{+4} n_{E^{**}}, & w_{-4} &= k_{-4} n_E n_A, \\ w_{+a} &= k_{+a} [A_e], & w_{-a} &= k_{-a} n_A, \\ w_{+b} &= k_{+b} [B_e], & w_{-b} &= k_{-b} n_B. \end{aligned} \quad (15)$$

□

C. Stochastic Trajectories

A stochastic trajectory of duration t , n_t , is defined as a set of reactions $\{\rho_i\}$ sequentially occurring at times $\{t_i\}$ starting from n_0 at time t_0 . Such trajectories can be generated by a *Stochastic Simulation Algorithm* [34]. Given the initial state, a trajectory is completely characterized by the counter

$$j_\rho(n, \tau) := \sum_i \delta_{\rho \rho_i} \delta_{n n_{t_i}} \delta(\tau - t_i), \quad (16)$$

that encodes which reaction occurs (ρ_i), from which state it occurs (n_{t_i}), and at which time (t_i). If not otherwise stated, the transition index i runs from $i = 1$ to the last transition prior to time t , N_t , and must not be confused with the label of the internal reactions, “ i ”. The *instantaneous reaction currents*

$$j_\rho(\tau) := \sum_n j_\rho(n, \tau) = \sum_i \delta_{\rho \rho_i} \delta(\tau - t_i). \quad (17)$$

quantify the instantaneous rate of occurrence of each reaction irrespectively of the state from which it occurs. Additionally, we denote the population of the CRN at time $\tau \in [t_0 = 0, t]$ by n_τ .

The probability of a trajectory reads

$$\begin{aligned} \mathcal{P}[n_t] = \prod_{i=0}^{N_t} \exp \left\{ - \int_{t_i}^{t_{i+1}} d\tau \sum_\rho w_\rho(n_\tau, \tau) \right\} \\ \times \prod_{i=1}^{N_t} w_{\rho_i}(n_{t_i}, t_i), \quad (18) \end{aligned}$$

where $t_{N_t+1} := t$ is the final time of the trajectory. The first term accounts for the probability that the system spends $\{t_{i+1} - t_i\}$ time in the state $\{n_{t_i}\}$, while the second accounts for the probability of transitioning. When averaging Eq. (16) over all stochastic trajectories, we obtain the transition rates, Eq. (13),

$$\langle j_\rho(n, \tau) \rangle = w_\rho(n, \tau) p_n(\tau). \quad (19)$$

Changes of state observables $\mathcal{O}(n) \equiv \mathcal{O}(n, t)$ along trajectories can be written as

$$\begin{aligned} \Delta \mathcal{O}[n_t] &= \mathcal{O}(n_t, t) - \mathcal{O}(n_0, 0) \\ &= \int_0^t d\tau \left\{ [\partial_\tau \mathcal{O}(n, \tau)]|_{n_\tau} + \sum_{n, \rho} \Delta_\rho \mathcal{O}(n, \tau) j_\rho(n, \tau) \right\}. \quad (20) \end{aligned}$$

The first term inside the integral accounts for the continuous changes due to the time dependent protocol π_t , while the second accounts for finite changes along reactions, see Fig. 2,

$$\Delta_\rho \mathcal{O}(n, \tau) := \mathcal{O}(n + \mathbf{S}_\rho, \tau) - \mathcal{O}(n, \tau). \quad (21)$$

In contrast, changes of a generic observable read

$$\delta \mathcal{X}[n_t] = \int_0^t d\tau \left\{ [\dot{\mathcal{X}}(n, \tau)]|_{n_\tau} + \sum_{n, \rho} \delta \mathcal{X}_\rho(n, \tau) j_\rho(n, \tau) \right\}. \quad (22)$$

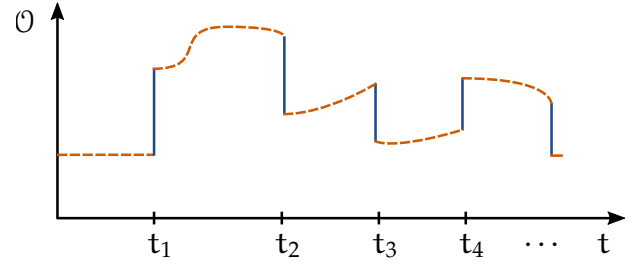


FIG. 2. Pictorial representation of the change of a state variable observable \mathcal{O} along a trajectory. The orange dashed curves represent the changes due to the protocol—first term in Eq. (20)—while vertical blue lines changes due to reactions—second term in Eq. (20).

(22)

where $\dot{\mathcal{X}}(n, \pi_\tau)$ denotes its change due to driving while dwelling in the state n , and $\delta \mathcal{X}_\rho(n, \pi_\tau)$ denotes its change along the reaction ρ occurring from n . Henceforth, we will use the overdot “ \cdot ” to denote rates of change of observable which are not time derivatives.

D. Conservation Laws

The topological properties of CRNs are encoded in the matrices \mathbf{S} and \mathbf{S}^Y and can be identified via their cokernels and kernels. *Conservation laws* ℓ are defined as vectors in $\text{coker } \mathbf{S}$,

$$\ell \cdot \mathbf{S}_\rho = 0, \quad \text{for all } \rho. \quad (23)$$

They identify conserved quantities, called *components* [35]

$$L_n := \ell \cdot n. \quad (24)$$

Despite the fact that L_n depends on the stochastic variable n , the probability of observing any particular value L ,

$$P(L) := \sum_n p_n \delta[L_n, L], \quad (25)$$

is constant over time, *i.e.* $d_t P(L) = 0$. The δ is a Kronecker delta. More generally, any observable of type $\mathcal{O}(L_n)$ does not fluctuate,

$$d_t \sum_n p_n \mathcal{O}(L_n) = 0, \quad (26)$$

as a direct consequence of the fact that $\Delta_\rho \mathcal{O}(L_n) = 0$. Clearly, $P(L)$ can be deduced from the initial conditions $p_n(0)$ and only those states for which $P(L_n, 0)$ is non-vanishing have a finite probability of being observed during the subsequent stochastic dynamics.

In closed CRNs, conservation laws (23) follow from

$$\ell^x \cdot \mathbf{S}_{\rho_i}^x + \ell^y \cdot \mathbf{S}_{\rho_i}^y = 0, \quad \text{for all } \rho_i. \quad (27)$$

We denote a set of linearly independent conservation laws of the closed CRN by $\{\ell_\lambda\}$, and the corresponding components by $\{L_n^\lambda := \ell_\lambda \cdot \mathbf{n}\}$, for $\lambda = 1, \dots, N_\lambda$. The choice of this set is not unique, and different choices have different physical meanings. This set is never empty since the total mass is always conserved. The latter corresponds to a ℓ whose entries are the masses of each species. Physically, the conservation laws of closed CRNs can always be chosen so as to correspond to *moieties*, which are parts of molecules exchanged between species along reactions or subject to isomerization [36].

For open CRNs, the condition identifying conservation laws, Eq. (23), becomes

$$\ell^x \cdot \mathbf{S}_{\rho_i}^x + \ell^y \cdot \mathbf{S}_{\rho_i}^y = 0, \quad \text{for all } \rho_i, \quad (28a)$$

$$\ell^y \cdot \mathbf{S}_{\rho_e}^y = 0, \quad \text{for all } \rho_e. \quad (28b)$$

We now recall that for all ρ_e there is one and only one exchanged species for which the corresponding entry of $\mathbf{S}_{\rho_e}^y$ is different from zero. Hence, Eq. (28b) demands that $\ell^y = 0$ and Eq. (28) become $\ell^x \cdot \mathbf{S}_{\rho_i}^x = 0$ for all ρ_i .

Crucially, any set of independent conservation laws (28), labeled as $\{\ell_{\lambda_u}\}$, for $\lambda_u = 1, \dots, N_{\lambda_u} < N_\lambda$, can be regarded as a subset of the conservation laws of the closed CRN, $\{\ell_\lambda\} \equiv \{\ell_{\lambda_u}\} \cup \{\ell_{\lambda_b}\}$, since they satisfy Eq. (27), too. In view of this, we call them *unbroken conservation laws*. The remaining independent conservation laws, labeled as $\{\ell_{\lambda_b}\}$ and referred to as *broken*, satisfy Eq. (27) while not Eq. (28). They involve exchanged species, $\ell_{\lambda_b}^y \neq 0$, hence $\ell_{\lambda_b}^y \cdot \mathbf{S}_{\rho_e}^y \neq 0$ and the probability distribution of any set $\{L_n^{\lambda_b} \equiv \ell_{\lambda_b} \cdot \mathbf{n}\}$,

$$P(\{L_{\lambda_b}\}) := \sum_{\mathbf{n}} p_{\mathbf{n}} \prod_{\lambda_b} \delta[L_n^{\lambda_b}, L_{\lambda_b}], \quad (29)$$

changes in time.

Summarizing, in open CRNs, the chemostatting breaks a subset of the conservation laws of the corresponding closed CRN, $\{\ell_{\lambda_b}\}$. Only the probability distribution of the *unbroken components* $\{L_n^{\lambda_u} \equiv \ell_{\lambda_u} \cdot \mathbf{n}\}$,

$$P(\{L_{\lambda_u}\}) := \sum_{\mathbf{n}} p_{\mathbf{n}} \prod_{\lambda_u} \delta[L_n^{\lambda_u}, L_{\lambda_u}], \quad (30)$$

is invariant and completely determined by the initial probability distribution $p_{\mathbf{n}}(0)$. The state space identified by one particular set of values for $\{L_{\lambda_u}\}$ is called *stoichiometric compatibility class*.

Example 3. The CRN in Fig. 1 has two conservation laws,

$$\ell_E = \begin{pmatrix} E & E^* & E^{**} & A & B \\ 1 & 1 & 1 & 0 & 0 \end{pmatrix}, \quad (31a)$$

$$\ell_b = \begin{pmatrix} E & E^* & E^{**} & A & B \\ 0 & 1 & 1 & 1 & 1 \end{pmatrix}, \quad (31b)$$

among which the second is broken. The unbroken conservation law identifies the enzyme moiety and corresponds to the total number of enzyme molecules populating the CRN, $L_n^E = n_E + n_{E^*} + n_{E^{**}}$. Instead, the broken one identifies the moiety A—or equivalently B—, $L_n^b = n_{E^*} + n_{E^{**}} + n_A + n_B$. \square

E. Stoichiometric Cycles

We can now set the stage for the thermodynamic description based on a stoichiometric cycle decomposition. This section, as well as the other ones discussing cycles, may be omitted at a first reading.

Additional information about the CRN topology is provided by the *stoichiometric cycles* $\mathbf{c} = \{c_\rho\}$ as they are vectors in $\ker \mathbf{S}$. Equivalently, these satisfy

$$\sum_\rho \mathbf{S}_\rho c_\rho = 0, \quad (32)$$

and at most one entry for each forward–backward transition pair is nonzero. Since \mathbf{S} is integer-valued, any \mathbf{c} can always be chosen non-negative-integer-valued. In this way, its entries denote the number of times each transition occurs along a transformation which overall leaves the state \mathbf{n} unchanged. Alternatively, a stoichiometric cycle can be seen as a set of reactions $\{\rho_{c1}, \rho_{c2}, \dots, \rho_{cN_c}\}$ identifying a closed loop in the state space

$$\mathbf{n} \rightarrow \mathbf{n} + \mathbf{S}_{\rho_{c1}} \rightarrow \dots \rightarrow \mathbf{n} + \sum_{i=1}^{N_c} \mathbf{S}_{\rho_{ci}} = \mathbf{n}, \quad (33)$$

$$\text{where } \sum_{i=1}^{N_c} \mathbf{S}_{\rho_{ci}} = \sum_\rho \mathbf{S}_\rho c_\rho = 0.$$

We now relate cycles of the closed and open CRNs as previously done for conservation laws. In the closed CRN, the stoichiometric cycles are given by

$$\sum_{\rho_i} \mathbf{S}_{\rho_i}^x c_{\rho_i} = 0 \quad (34a)$$

$$\sum_{\rho_i} \mathbf{S}_{\rho_i}^y c_{\rho_i} = 0. \quad (34b)$$

All the entries associated to the exchange reactions are taken equal to 0: $c_{\rho_e} = 0$, for all ρ_e . Let us denote by $\{\mathbf{c}^\alpha\}$, for $\alpha = 1, \dots, N_\alpha$, a set of independent stoichiometric cycles of the closed CRN.

In the open CRN, the condition identifying cycles, Eq. (32), reads

$$\sum_{\rho_i} \mathbf{S}_{\rho_i}^x c_{\rho_i} = 0 \quad (35a)$$

$$\sum_{\rho_i} \mathbf{S}_{\rho_i}^y c_{\rho_i} + \sum_{\rho_e} \mathbf{S}_{\rho_e}^y c_{\rho_e} = 0. \quad (35b)$$

Since the cycles of the closed CRN satisfy Eq. (35), they can be regarded as a subset of an independent set of cycles for the open CRN, $\{\mathbf{c}^\alpha, \mathbf{c}^\eta\}$. We refer to the additional cycles $\{\mathbf{c}^\eta\}$, for $\eta = 1, \dots, N_\eta$, as *emergent*. They are characterized by at least one nonzero entry for $\{\rho_e\}$, and the vectors

$$\mathbf{C}_\eta^Y := \sum_\rho (-\mathbf{S}_\rho^Y) c_\rho^\eta = \sum_{\rho_e} \mathbf{S}_{\rho_e}^Y c_{\rho_e}^\eta \neq 0 \quad (36)$$

quantify the amount of exchanged species flowing in the system from the corresponding chemostats upon completion of \mathbf{c}^η . As the concentrations of the chemostats are unaffected by the exchange of particles with the system, the emergent stoichiometric cycles can be thought of as pathways transferring chemicals across chemostats while leaving the internal state of the CRN unchanged.

As first proved in Ref. [25], by applying the rank-nullity theorem to the stoichiometric matrices of the open and closed CRNs, one can show that

$$N_y = N_{\lambda_b} + N_\eta. \quad (37)$$

In words, for any exchanged species either a conservation law is broken, or an emergent cycle is created.

Example 4. The CRN in Fig. 1 has one cycle

$$\mathbf{c}_{\text{int}} = \begin{pmatrix} +1 & +2 & +3 & +4 & +a & +b \\ 1 & 1 & 1 & 1 & 0 & 0 \end{pmatrix}, \quad (38)$$

and one emergent cycle

$$\mathbf{c}_{\text{ext}} = \begin{pmatrix} +1 & +2 & +3 & +4 & +a & +b \\ 1 & 1 & 0 & 0 & 1 & -1 \end{pmatrix}. \quad (39)$$

Negative entries must be interpreted as reactions occurring in the backward direction. The latter cycle corresponds to the injection of one molecule of A, its conversion into one of B passing via E^* , and its ejection,

$$\mathbf{C}_{\text{ext}} = \begin{pmatrix} A & B \\ 1 & -1 \end{pmatrix}. \quad (40)$$

We can also check the validity of Eq. (37), as the number of chemostats, 2, equals the number of broken conservation laws, 1, see Ex. 3, plus the number of emergent cycles, 1, Eq. (39). \square

Remark Stoichiometric cycles must be distinguished from graph-theoretic cycles, also called *loops* see *e.g.* Ref. [3]. To elucidate this point, we note that the network of transitions of a CRN can be regarded as a semi-infinite graph whose vertices are the accessible states \mathbf{n} , whereas the directed edges are identified by the possible reactions—which are encoded in the stoichiometric matrix, \mathbf{S} . Therefore, loops are recursive appearance of stoichiometric cycles, as in Eq. (33). However, they may not be complete at the boundaries of the graph (low \mathbf{n}) due to peculiar topological properties of the CRN, see *e.g.* Ref. [27]. These observations will be used later to relate different approaches for cycle decomposition of thermodynamic quantities.

III. STOCHASTIC THERMODYNAMICS

We now build a nonequilibrium thermodynamic description on top of the stochastic dynamics. In addition to the elementarity of all reactions, our description

hinges on the hypothesis of *local equilibrium* [37]: if all reactions could be instantaneously shut down, we would observe an equilibrium mixture of inert species at all times. Alternatively, the equilibration of temperature and spatial distributions of molecules is much faster than any reaction time scale. Hence, the nonequilibrium nature of the CRN is solely due to nonequilibrated populations of species.

A. Equilibrium of Closed CRNs

Equilibrium statistical mechanics requires that the equilibrium distribution of a closed CRN with given values of $\{L_\lambda\}$ reads

$$p^{\text{eq}}(\mathbf{n}|\{L_\lambda\}) = \frac{\exp\{-\beta g_{\mathbf{n}}\}}{Z(\{L_\lambda\})} \prod_\lambda \delta[L_{\mathbf{n}}^\lambda, L_\lambda], \quad (41)$$

where

$$g_{\mathbf{n}} = (\mu^\circ - 1k_B T \ln n_s) \cdot \mathbf{n} + k_B T \ln n! \quad (42)$$

is the *Gibbs free energy* of the state \mathbf{n} derived in App. A. The first term quantifies the energetic contribution of each single molecule: $\mu^\circ \equiv \mu^\circ(T)$ is the vector of *standard-state chemical potentials*, whereas $-1k_B T \ln n_s$ is an entropic contribution—constant for all species—since n_s is the population of the solvent. The last term is purely entropic and accounts for the indistinguishability of molecules of the same species. In Eq. (41),

$$Z(\{L_\lambda\}) = \sum_{\mathbf{m}} \exp\{-\beta g_{\mathbf{m}}\} \prod_\lambda \delta[L_{\mathbf{m}}^\lambda, L_\lambda] \quad (43)$$

is the partition function, while $\beta = 1/(k_B T)$. When taking into account an ensemble of components, $P(\{L_\lambda\})$, Eq. (41) allows us to write

$$\begin{aligned} p_{\mathbf{n}}^{\text{eq}} &= \sum_{\{L_\lambda\}} p^{\text{eq}}(\mathbf{n}|\{L_\lambda\}) P(\{L_\lambda\}) \\ &= p^{\text{eq}}(\mathbf{n}|\{L_{\mathbf{n}}^\lambda\}) P(\{L_{\mathbf{n}}^\lambda\}), \end{aligned} \quad (44)$$

which can be regarded as a *constrained* equilibrium distribution. Hence $p^{\text{eq}}(\mathbf{n}|\{L_{\mathbf{n}}^\lambda\})$ is the conditional probability of observing \mathbf{n} given the stoichiometric compatibility class it identifies.

Equation (44) can also be written as

$$p_{\mathbf{n}}^{\text{eq}} = \exp\left\{-\beta [g_{\mathbf{n}} - G_{\text{eq}}(\{L_{\mathbf{n}}^\lambda\})]\right\}, \quad (45)$$

in terms of the *equilibrium Gibbs potential* of the CRN

$$G_{\text{eq}}(\{L_\lambda\}) = k_B T \ln P(\{L_\lambda\}) - k_B T \ln Z(\{L_\lambda\}). \quad (46)$$

It is worth emphasizing that $G_{\text{eq}}(\{L_\lambda\})$ is function solely of the set of components, and that $G_{\text{eq}}(\{L_{\mathbf{n}}^\lambda\})$ needs to be understood as G_{eq} evaluated in $\{L_{\mathbf{n}}^\lambda\}$. Invoking the hypothesis of local equilibrium, we extend G_{eq} to arbitrary

probability distributions p_n , and we call it *stochastic Gibbs potential*,

$$G(n) := k_B T \ln p_n + g_n. \quad (47)$$

For closed CRNs at equilibrium, using Eq. (44), $G(n)$ reduces to G_{eq} in Eq. (46). Also, its average value, the *nonequilibrium Gibbs potential*

$$\langle G \rangle = \sum_n p_n [k_B T \ln p_n + g_n], \quad (48)$$

takes its minimum value at equilibrium

$$\begin{aligned} \langle G \rangle - \sum_{\{L_\lambda\}} P(\{L_\lambda\}) G_{eq}(\{L_\lambda\}) &= \langle G - G_{eq} \rangle \\ &= k_B T \sum_n p_n \ln \frac{p_n}{p_n^{eq}} \\ &\equiv k_B T \mathcal{D}(p \| p^{eq}) \geq 0. \end{aligned} \quad (49)$$

In the first equality, we used

$$\begin{aligned} \sum_{\{L_\lambda\}} P(\{L_\lambda\}) G_{eq}(\{L_\lambda\}) &= \sum_{\{L_\lambda\}} \left[\sum_n p_n \prod_\lambda \delta[L_n^\lambda, L_\lambda] \right] G_{eq}(\{L_\lambda\}) \\ &= \sum_n p_n G_{eq}(\{L_n^\lambda\}). \end{aligned} \quad (50)$$

In the last equality of Eq. (49), $\mathcal{D}(p \| p^{eq})$ is the relative entropy of the transient probability distribution p_n with respect to the equilibrium one p_n^{eq} . It is always positive and vanishes only when $p_n = p_n^{eq}$. We will see later (§ VII) that Eq. (49) quantifies exactly the average dissipation of the relaxation to equilibrium.

B. Local Detailed Balance

The *zero-th of thermodynamics for CRNs* requires that closed CRNs relax to equilibrium. To ensure this, one combines the dynamical requirement for detailed balance, Eq. (14), with the equilibrium distribution, Eq. (44). As a result, the *local detailed balance* ensues

$$\ln \frac{w_{\rho_i}(n)}{w_{-\rho_i}(n + S_{\rho_i})} = -\beta \Delta_{\rho_i} g_n, \quad (51)$$

see Eq. (21). In agreement with deterministic descriptions, see *e.g.* Ref. [26], we recover the relation between the rate constants and the standard-state chemical potentials

$$\ln \frac{k_{\rho_i}}{k_{-\rho_i}} = -\beta (\mu^\circ - k_B T \ln [s]) \cdot S_{\rho_i}, \quad (52)$$

in which $[s] := n_s/V$ denotes the concentration of solvent. The local detailed balance (51) should be regarded as a fundamental property of the stochastic reaction rates of elementary reactions valid beyond closed CRNs. This central concept is well known in stochastic thermodynamics because it provides the connection between

stochastic dynamics and nonequilibrium thermodynamics.

In open CRNs, the local detailed balance

$$\ln \frac{w_\rho(n)}{w_{-\rho}(n + S_\rho)} = -\beta (\Delta_\rho g_n + \mu_Y \cdot S_\rho^Y) \quad (53)$$

generalizes Eq. (51), where

$$\mu_Y = \mu_Y^\circ + k_B T \ln \{[Y]/[s]\} \quad (54)$$

are the chemical potentials of the chemostats. The first contribution accounts for the Gibbs free energy change of the internal species, while the second one for the Gibbs free energy exchanged with the chemostats.

We introduce the *transition affinities* which quantify the force acting along each transition

$$A_\rho(n) = k_B T \ln \frac{w_\rho(n) p_n}{w_{-\rho}(n + S_\rho) p_{n+S_\rho}}. \quad (55)$$

They measure the distance from detailed balance (14), where they all vanish. Using Eq. (53), they can be rewritten in terms of differences of stochastic Gibbs potential (47),

$$A_\rho(n) = -\Delta_\rho G(n) + \mu_Y \cdot (-S_\rho^Y). \quad (56)$$

This fundamental relation reveals the thermodynamic nature of the dynamical forces acting along reaction. Its early formulation for deterministic chemical kinetics is due to de Donder [38].

We will prove in § VII that our theoretical framework based on Eq. (53) guarantees that closed CRNs described by a CME (11) relax to equilibrium, Eq. (44): the average potential $\langle G \rangle$ is minimized by the dynamics during the relaxation and hence plays the role of a Lyapunov function. We now turn our attention to the enthalpy and entropy balance along stochastic trajectories.

C. Enthalpy and Entropy Balance

The *stochastic entropy* of the CRNs follows from the derivative of the stochastic Gibbs potential (47) with respect to the temperature,

$$S(n) = - \left(\frac{\partial G}{\partial T} \right)_n = -k_B \ln p_n + s_n. \quad (57)$$

The last term on the rhs is the entropy of the state n ,

$$s_n = - \left(\frac{\partial g}{\partial T} \right)_n = (s^\circ + k_B \ln n_s) \cdot n - k_B \ln n!. \quad (58)$$

It accounts for both the entropic contribution carried by each species, *i.e.* the *standard entropies of formation*

$$s^\circ = - \left(\frac{\partial \mu^\circ}{\partial T} \right)_n, \quad (59)$$

as well as the entropic contribution due to the multiplicity of indistinguishable states. When averaged, the first term in Eq. (57) gives the Gibbs–Shannon entropy. The enthalpy follows from

$$H(\mathbf{n}) = G(\mathbf{n}) + TS(\mathbf{n}) = g_{\mathbf{n}} + Ts_{\mathbf{n}} = \mathbf{h} \cdot \mathbf{n}, \quad (60)$$

where

$$\mathbf{h} = \mu^\circ + Ts^\circ = \mathbf{h}^\circ \quad (61)$$

denotes the vector of *standard enthalpies of formation*, in agreement with traditional thermodynamics of ideal dilute solutions [35]. Likewise, the chemical potentials of the chemostats, Eq. (54), will be decomposed in terms

$$\Delta_{\rho} H(\mathbf{n}) = \mathbf{h} \cdot \mathbf{S}_{\rho} = \underbrace{\mathbf{h} \cdot \mathbf{S}_{\rho} + \mathbf{h}_Y \cdot \mathbf{S}_{\rho}^Y}_{=: Q_{\rho}^{\text{thr}}} + \underbrace{Ts_Y \cdot (-\mathbf{S}_{\rho}^Y)}_{=: Q_{\rho}^{\text{chm}}} + \underbrace{\mu_Y \cdot (-\mathbf{S}_{\rho}^Y)}_{=: W_{\rho}^c}, \quad \text{for all } \mathbf{n}. \quad (64)$$

We used Eqs. (20), (61) and (62). The first two contributions, Q_{ρ}^{thr} , account for the *heat of reaction*, *i.e.* the heat reversibly flowing from the thermal reservoir (the solvent). The third term characterizes the heat reversibly flowing from the chemostats, Q_{ρ}^{chm} . The first three terms, Q_{ρ} , integrated along the trajectory quantify the total *heat flow*

$$Q[\mathbf{n}_t] = \int_0^t d\tau \left\{ \sum_{\rho} Q_{\rho}^{\text{thr}} J_{\rho}(\tau) + Ts_Y(\tau) \cdot \mathbf{I}^Y(\tau) \right\}, \quad (65)$$

where the *instantaneous external currents*

$$\mathbf{I}^Y(\tau) := \sum_{\rho} (-\mathbf{S}_{\rho}^Y) J_{\rho}(\tau) \quad (66)$$

To recover the entropy balance along stochastic trajectories, we notice that since the entropy is a state function, its change along a trajectory reads,

$$\Delta S[\mathbf{n}_t] = \int_0^t d\tau \left\{ [-\partial_{\tau} k_B \ln p_{\mathbf{n}}(\tau)]|_{\mathbf{n}_{\tau}} + \sum_{\mathbf{n}, \rho} \Delta_{\rho} S(\mathbf{n}) j_{\rho}(\mathbf{n}, \tau) \right\}. \quad (69)$$

as seen in Eq. (20). The changes along transitions can be recast into

$$\begin{aligned} T \Delta_{\rho} S(\mathbf{n}) &= T \Delta_{\rho} s_{\mathbf{n}} - k_B T \ln \frac{p_{\mathbf{n}+\mathbf{s}_{\rho}}}{p_{\mathbf{n}}} \\ &= \underbrace{\mathbf{h} \cdot \mathbf{S}_{\rho} + \mathbf{h}_Y \cdot \mathbf{S}_{\rho}^Y + Ts_Y \cdot (-\mathbf{S}_{\rho}^Y)}_{=: Q_{\rho}} - \underbrace{\left[\Delta_{\rho} g_{\mathbf{n}} + k_B T \ln \frac{p_{\mathbf{n}+\mathbf{s}_{\rho}}}{p_{\mathbf{n}}} \right]}_{=: \Delta_{\rho} G(\mathbf{n})} + \underbrace{\mu_Y \cdot (-\mathbf{S}_{\rho}^Y)}_{=: W_{\rho}^c}, \\ &= A_{\rho}(\mathbf{n}) \end{aligned} \quad (70)$$

where we have used Eq. (60). As highlighted with underbraces, the first three terms are the heat flow along reactions, while the last three correspond to the affinity of transition, Eq. (56). When integrating over the whole trajectory, we

of enthalpic and entropic contributions,

$$\mu_Y = h_Y - Ts_Y, \quad (62)$$

where $h_Y = h_Y^\circ$ and $s_Y = s_Y^\circ - k_B \ln \{[Y]/[s]\}$.

To recover the enthalpy balance along stochastic trajectories, we write the change of enthalpy as the sum of its changes due to reactions,

$$\begin{aligned} \Delta H[\mathbf{n}_t] &= H(\mathbf{n}_t) - H(\mathbf{n}_0) \\ &= \int_0^t d\tau \sum_{\mathbf{n}, \rho} \Delta_{\rho} H(\mathbf{n}) j_{\rho}(\mathbf{n}, \tau), \end{aligned} \quad (63)$$

where

gives the amount of exchanged species injected in the CRN at each time, see Eq. (17).

The last term in Eq. (64), W_{ρ}^c , quantifies the Gibbs free energy exchanged with the chemostats. Once integrated, it gives the *chemical work*

$$W_c[\mathbf{n}_t] = \int_0^t d\tau \mu_Y(\tau) \cdot \mathbf{I}^Y(\tau). \quad (67)$$

From Eqs. (63)–(67), the *enthalpy balance* along a trajectory follows

$$\Delta H[\mathbf{n}_t] = Q[\mathbf{n}_t] + W_c[\mathbf{n}_t]. \quad (68)$$

recover the entropy balance

$$\Delta S[n_t] = \frac{1}{T} Q[n_t] + \Sigma[n_t], \quad (71)$$

where the EP (times the temperature) reads

$$T\Sigma[n_t] = \int_0^t d\tau \left\{ [-\partial_\tau k_B T \ln p_n(\tau)]|_{n_\tau} + \sum_{n,\rho} A_\rho(n, \tau) j_\rho(n, \tau) \right\} \quad (72a)$$

$$= k_B T \ln \frac{p_{n_0}(0)}{p_{n_t}(t)} + \int_0^t d\tau j_\rho(n, \tau) k_B T \ln \frac{w_\rho(n, \tau)}{w_{-\rho}(n + S_\rho, \tau)} \quad (72b)$$

$$= W_c[n_t] - \Delta G[n_t]. \quad (72c)$$

The second equality follows from the definition of affinity, Eq. (55), when integrating the changes of the probability distribution. Instead, the third one readily follows from the relationship between affinity and Gibbs potential, Eq. (56). Mindful of Eq. (18), the EP can be rewritten as the ratio of the probability of observing the trajectory n_t under a forward dynamics driven by a protocol π_t , over the probability of observing the backward trajectory n_t^\dagger under a dynamics driven by the time-reversed protocol π^\dagger such that $\pi_t^\dagger := \pi_{t-\tau}$:

$$T\Sigma[n_t] = k_B T \ln \frac{p_{n_0}(0) \mathcal{P}[n_t]}{p_{n_t}(t) \mathcal{P}[n_t^\dagger, \pi^\dagger]}. \quad (73)$$

This central result in stochastic thermodynamics [12, 39] was formulated for CRNs in Ref. [20] and clearly shows that the EP measures the statistical asymmetry of a trajectory under time reversal. It implies that the EP satisfies the following integral FT

$$\langle \exp\{-\Sigma/k_B\} \rangle = 1, \quad (74)$$

where the *ensamble average* $\langle \cdot \rangle$ runs over all trajectories. It represents a refinement of the second law of thermodynamics at the trajectory level. Using the Jensen's inequality, the second law ensues: $\langle \Sigma \rangle \geq 0$.

Remark Using Eqs. (61) and (62), the local detailed balance, Eq. (53), can be rewritten as

$$\ln \frac{w_\rho(n)}{w_{-\rho}(n + S_\rho)} = -\beta Q_\rho^{\text{thr}} + s_Y \cdot S_\rho^Y + \Delta_\rho s_n. \quad (75)$$

The first term is the entropy change in the thermal bath, the second one the entropy change in the chemostats, whereas the last one the internal entropy change of the CRN.

Remark Chemical work and Gibbs potential are defined up to a gauge, which accounts for the choice of the standard state chemical potentials. Indeed, let us consider the following transformation,

$$\begin{aligned} \mu^\circ &\rightarrow \mu^\circ + \sum_\lambda a_\lambda \ell_\lambda \\ \mu_Y^\circ &\rightarrow \mu_Y^\circ + \sum_\lambda a_\lambda \ell_\lambda^Y, \end{aligned} \quad (76)$$

where the second term is a linear combination of conservation laws. This transformation leaves affinities (56) and EP (73) unchanged, while transforming both the chemical work (68), and the Gibbs potential (47). The former changes as

$$W_c[n_t] \rightarrow W_c[n_t] + \sum_{\lambda_b} a_{\lambda_b} \ell_{\lambda_b}^Y \cdot \mathcal{J}^Y[n_t], \quad (77)$$

where

$$\mathcal{J}^Y[n_t] = \int_0^t d\tau I^Y(\tau), \quad (78)$$

are the integrated currents of exchanged species flowing in the system. Likewise, the Gibbs potential becomes

$$G(n) \rightarrow G(n) + \sum_\lambda a_\lambda L_n^\lambda. \quad (79)$$

Using the properties of conservation laws, § II D, it is easy to verify that

$$\Delta L_{\lambda_u}[n_t] = 0, \quad \Delta L_{\lambda_b}[n_t] = \ell_{\lambda_b}^Y \cdot \mathcal{J}^Y[n_t], \quad (80)$$

which confirms that the gauge terms cancels in the EP, Eq. (72c).

Alternatively, one can apply the transformation (81) to either $(h, h_Y)^\top$ or $(s^\circ, s_Y^\circ)^\top$ and investigate how the terms in the entropy balance (71) change. In the former case, one can easily verify that both $Q[n_t]$ and $S(n)$ are unaltered. In the latter case, instead,

$$\begin{aligned} S(n) &\rightarrow S(n) + \sum_\lambda a_\lambda L_n^\lambda \\ Q[n_t] &\rightarrow Q[n_t] + T \sum_{\lambda_b} a_{\lambda_b} \ell_{\lambda_b}^Y \cdot \mathcal{J}^Y[n_t]. \end{aligned} \quad (81)$$

Further discussions on the gauge arising in the work-potential connection will be given in § V C.

D. FT for the Chemical Work and comparison with previous results

When combining the EP FT (74) with Eq. (72c) we immediately obtain the integral FT for the chemical

work

$$\langle \exp \{-\beta (W_c - \Delta G)\} \rangle = 1. \quad (82)$$

However, a Jarzynski-like integral FTs [40–43] for the chemical work—*i.e.* expressions such as $\langle \exp \{-\beta W_c\} \rangle = \exp \{-\beta \Delta G_{\text{eq}}\}$ —do not ensue. This kind of relation would require ΔG to be a nonfluctuating quantity so that it can be moved out of the average. However, due to broken conservation laws G fluctuates along any trajectory of open CRNs. Let us consider a generic process in which the CRNs is initially closed and at equilibrium, Eq. (44), with a Gibbs free energy $\sum_{\{L_\lambda\}} P(\{L_\lambda\}) G_{\text{eq}}(\{L_\lambda\})$. The CRN is then open and driven according to some time-dependent protocol, π_τ for $\tau \in [0, t]$. At time t the CRN is closed again, and let to relax to a new equilibrium distribution $p_n^{\text{eq}_t}$. Since the chemostatting procedure unavoidably breaks some conservation laws, the accessible state space suddenly increases. The final distribution of broken components, $P(\{L_{\lambda_b}\}; t)$, will thus have a support broader than that of the initial distribution, $P(\{L_{\lambda_b}\}; 0)$, see *e.g.* Fig. 3. This is an instance of *absolute irreversibility* [28]. Namely, when the EP (73) is integrated over all trajectories to obtain the FT (74), there are some backward trajectories whose corresponding forward probability is vanishing. These are the trajectories leading to values of the broken components not in $\text{supp} \{P(\{L_{\lambda_b}\}; 0)\}$. Since the EP of these trajectories diverges negatively the expression of the integral FTs (74), as well as (82), is invalidated, but can be replaced by $\langle \exp \{-\Sigma/k_B\} \rangle = 1 - \lambda_S$, where $0 \leq \lambda_S \leq 1$ measures the probability of those backward trajectories whose forward one has zero probability [28].

Hence, let us assume that $\text{supp} \{P(\{L_{\lambda_b}\}; 0)\}$ spans all possible values of $\{L_{\lambda_b}\}$, so that no absolute irreversibility occurs. By conditioning the average in Eq. (82) upon observation of specific initial and final components $\langle \cdot \rangle_{\{L_\lambda\}, \{L'_\lambda\}}$ we obtain

$$\begin{aligned} & \sum_{\{L_\lambda\}} \sum_{\{L'_\lambda\}} P(\{L_\lambda\}; 0) P(\{L'_\lambda\}, t) \\ & \exp \{ \beta [G_{\text{eq}_t}(\{L'_\lambda\}) - G_{\text{eq}_0}(\{L_\lambda\})] \} \\ & \langle \exp \{-\beta W_c\} \rangle_{\{L_\lambda\}, \{L'_\lambda\}} = 1. \end{aligned} \quad (83)$$

However, this equation cannot be simplified further: since the Gibbs potential depends on the broken components, it fluctuates during the transient dynamics and an average over all components must be taken. As a result, no Jarzynski FT for the chemical work in the Gibbs ensemble can be derived.

We now mention that the Authors of Ref. [20] derive a Jarzynski relation for the chemical work by using the grandcanonical ensemble [20, Eq. (61)]. Translated into our notation, their result reads

$$\langle \exp \{-\beta [W_c - \Delta(\mu^{\text{eq}} \cdot \mathbf{n})]\} \rangle = \exp \{-\beta \Delta \mathfrak{G}_{\text{eq}}\}, \quad (84)$$

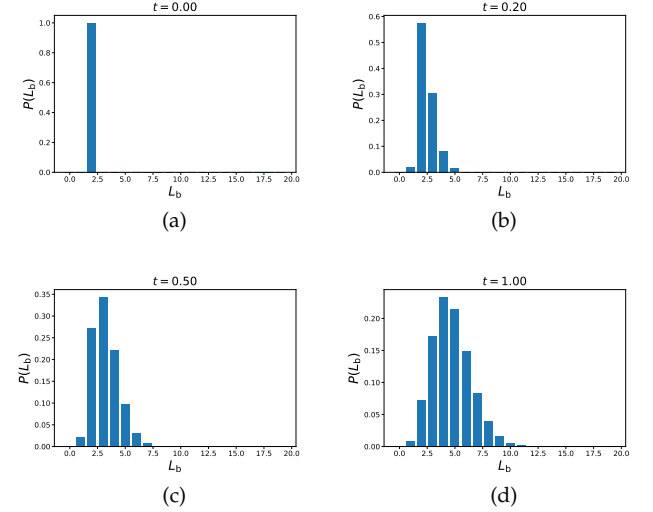


FIG. 3. Illustration of the evolution of the probability distribution of the broken components associated to Eq. (31b) in the CRNs in Fig. 1. As the CRN evolves, the state space enlarges, as the stochastic dynamics explores states corresponding to different broken components, L_b . The four distribution are obtained by means of 10^6 trajectories simulated using the stochastic simulation algorithm. All rate constants are equal to 1, whereas the concentrations of the chemostatted species are $[A_e] = 17$ and $[B_e] = 10$. The value of the enzyme moiety is $L_E = 5$.

where the initial and final equilibrium states are grand-canonical:

$$p_n^{\text{eq}} = \exp \{ \beta [\mathfrak{G}_{\text{eq}} - g_n + \mu^{\text{eq}} \cdot \mathbf{n}] \}. \quad (85)$$

The grand potential is defined as

$$\mathfrak{G} := G - \mu^{\text{eq}} \cdot \mathbf{n}, \quad (86)$$

and μ^{eq} are implicitly defined by

$$\mu_x^{\text{eq}} \cdot S_{\rho_i}^x + \mu_y^{\text{eq}} \cdot S_{\rho_i}^y = 0, \quad \text{for all } \rho_i, \quad (87)$$

[20, Eq. (27)]. The absence of the exchange transition is due to a different form of chemostatting, see remark in § II A. Concerning Eq. (84), we observe that the grand-canonical potential is more suitable to describe CRNs in which all species are chemostatted and μ^{eq} are their chemical potentials. However, in the vast majority of real CRNs, only a restricted set of species needs to be modelled as chemostatted. On top of that, the physical interpretation of the contribution $-\Delta(\mu^{\text{eq}} \cdot \mathbf{n})$ remains unclear. In our next sections we will show that a systematic use of conservation laws leads to the identification of the potential which best describes the equilibrium of CRNs in which not all species are treated as chemostatted. It will also ensue the definition of new work contributions, whose physical interpretation is transparent.

IV. CRN-SPECIFIC STOCHASTIC THERMODYNAMICS

We now proceed with our main results. Making use of the conservation laws identified in section § II D, we decompose the EP into three fundamental contributions: a potential difference, a contribution due to time-dependent driving, and a minimal set of contributions due to nonconservative chemical forces. To do so, we first decompose the local detailed balance and then proceed with the EP.

A. Entropy Production

We start our EP decomposition by partitioning the set of chemostatted species \mathbf{Y} into two groups, denoted by \mathbf{Y}_p and \mathbf{Y}_f . Likewise, the corresponding exchanged species are denoted by \mathbf{y}_p and \mathbf{y}_f , respectively. The former group is composed by a minimal set of chemostatted species which—when starting from the closed CRN—break all broken conservation laws. In other words, each entry of \mathbf{Y}_p breaks exactly one distinct conservation law. The remaining chemostatted species form the latter group. For a given CRN, our partitioning is not unique but the number of \mathbf{y}_p and \mathbf{y}_f is uniquely defined: $N_{\mathbf{y}_p} = N_{\lambda_b}$ and $N_{\mathbf{y}_f} = N_y - N_{\lambda_b}$, respectively, see Ex. 5.

We now notice that the linear independence of $\{\ell_\lambda\}$ implies that the matrix whose rows are $\{\ell_{\lambda_b}^{y_p}\}$ is nonsingular. We will denote by $\{\bar{\ell}_{\lambda_b}^{y_p}\}$ the column vectors of the inverse of the latter matrix. By making use of this crucial property, we can recast the identity

$$\Delta_\rho \mathbf{L}_n^{\lambda_b} \equiv \ell_{\lambda_b} \cdot \mathbf{S}_\rho \equiv \ell_{\lambda_b}^x \cdot \mathbf{S}_\rho^x + \ell_{\lambda_b}^{y_p} \cdot \mathbf{S}_\rho^{y_p} + \ell_{\lambda_b}^{y_f} \cdot \mathbf{S}_\rho^{y_f} \quad (88)$$

into

$$\mathbf{S}_\rho^{y_p} = \Delta_\rho \mathbf{M}_n^{y_p} - \sum_{\lambda_b} \bar{\ell}_{\lambda_b}^{y_p} \left\{ \ell_{\lambda_b}^x \cdot \mathbf{S}_\rho^x + \ell_{\lambda_b}^{y_f} \cdot \mathbf{S}_\rho^{y_f} \right\}, \quad (89)$$

where

$$\mathbf{M}_n^{y_p} := \sum_{\lambda_b} \bar{\ell}_{\lambda_b}^{y_p} \mathbf{L}_n^{\lambda_b}. \quad (90)$$

Mindful that $\mathbf{S}_\rho^Y = -\mathbf{S}_\rho^Y$ and $\ell_{\lambda_b}^x \cdot \mathbf{S}_{\rho_e}^x = 0$ for all ρ_e , one can use Eq. (89) to rewrite the chemical work along reactions as

$$-\mu_Y \cdot \mathbf{S}_\rho^Y = \Delta_\rho \left[\mu_{Y_p} \cdot \mathbf{M}_n^{y_p} \right] - \mathcal{F}_{Y_f} \cdot \mathbf{S}_\rho^{Y_f}, \quad (91)$$

where

$$\mathcal{F}_{Y_f} := \mu_{Y_f} - \mu_{Y_p} \cdot \sum_{\lambda_b} \bar{\ell}_{\lambda_b}^{y_p} \ell_{\lambda_b}^{y_f}. \quad (92)$$

A reformulation of the local detailed balance Eq. (53) readily ensues

$$\ln \frac{w_\rho(\mathbf{n})}{w_{-\rho}(\mathbf{n} + \mathbf{S}_\rho)} = -\beta (\Delta_\rho \mathbf{g}_n + \mathcal{F}_{Y_f} \cdot \mathbf{S}_\rho^{Y_f}), \quad (93)$$

where

$$\mathbf{g}_n := g_n - \mu_{Y_p} \cdot \mathbf{M}_n^{y_p}. \quad (94)$$

We now argue that the expression of the latter potential is reminiscent of a Legendre transform of g_n with respect to $\mathbf{M}_n^{y_p}$, in which μ_{Y_p} are the conjugated intensive fields. To reveal the physical meaning of $\mathbf{M}_n^{y_p}$, let us consider the case in which the broken conservation laws correspond to moieties, see § II D, and hence each species can be thought of as a composition of these. Through \mathbf{y}_p , some combinations of these moieties are exchanged with the environment. The entries of $\mathbf{M}_n^{y_p}$ quantify the total abundance of these combinations in state \mathbf{n} , hence we refer to $\mathbf{M}_n^{y_p}$ as the *moieties population vector*. In view of this and the fact that (in general) not all moieties are exchanged, one can interpret g_n as a *semigrand Gibbs free energy* [35]. Note also that, from the definition of broken conservation law, Eq. (27), it follows that $\Delta_{\rho_i} \mathbf{M}_n^{y_p} = 0$, for all ρ_i —viz. internal reactions never create or destroy moieties—whereas only for ρ_e we have that $\Delta_{\rho_e} \mathbf{M}_n^{y_p} \neq 0$ —viz. exchange reactions introduce or remove moieties. We also mention that an alternative interpretation of g_n can be given once we rewrite it as

$$\mathbf{g}_n := g_n - \sum_{\lambda_b} f_{\lambda_b} \mathbf{L}_n^{\lambda_b}, \quad (95)$$

where

$$f_{\lambda_b} := \mu_{Y_p} \cdot \bar{\ell}_{\lambda_b}^{y_p}. \quad (96)$$

In this form g_n is reminiscent of a Legendre transform with respect to the broken components $\{\mathbf{L}_n^{\lambda_b}\}$, in which $\{f_{\lambda_b}\}$ are the conjugated intensive fields.

In contrast to the first term appearing on the rhs of Eq. (93), the second one is composed by an independent and minimal set of nonconservative terms: if and only if $\mathcal{F}_{Y_f} = 0$, for $y_f = 1, \dots, N_{y_f}$, then the rhs of Eq. (93) is conservative. In this case, the CRN is detailed-balanced since the steady-state probability distribution defined by $p_n^{\text{eq}} \propto \exp\{-\beta g_n\}$ satisfies the detailed balance property, Eq. (14). In physical terms, each \mathcal{F}_{Y_f} identifies a chemical potential gradient imposed by some chemostats on the CRN which prevent the latter from relaxing to equilibrium. Hence we refer to $\{\mathcal{F}_{Y_f}\}$ as *fundamental chemical forces*. Equation (93) is our first major result.

To proceed with our EP decomposition, we combine Eqs. (72b) and (93),

$$\begin{aligned} T \Sigma[\mathbf{n}_t] &= k_B T \ln \frac{p_{\mathbf{n}_0}(0)}{p_{\mathbf{n}_t}(t)} \\ &\quad - \int_0^t d\tau \sum_{\rho, \mathbf{n}} \Delta_\rho \mathbf{g}_n(\tau) \mathbf{j}_\rho(\mathbf{n}, \tau) + \sum_{y_f} W_{y_f}^{\text{nc}}[\mathbf{n}_t], \end{aligned} \quad (97)$$

where

$$W_{y_f}^{\text{nc}}[\mathbf{n}_t] := \int_0^t d\tau \mathcal{F}_{y_f}(\tau) I_{y_f}(\tau). \quad (98)$$

$\{I_{y_f}(\tau)\}$, for $y_f = 1, \dots, N_{y_f}$, denote the entries of the instantaneous external currents corresponding to \mathbf{Y}_f , Eq. (66). We now recall that g_n is a state function, hence

$$\Delta g[n_t] = W_d[n_t] + \int_0^t d\tau \sum_{\rho, n} \Delta_\rho g_n(\tau) j_\rho(n, \tau), \quad (99)$$

where

$$\begin{aligned} W_d[n_t] &:= \int_0^t d\tau [\partial_\tau g_n(\tau)]|_{n_\tau} \\ &= \int_0^t d\tau \left[-\partial_\tau \mu_{Y_p}(\tau) \cdot M_n^{y_p} \right]|_{n_\tau}. \end{aligned} \quad (100)$$

Therefore, combining Eqs. (97) and (99) we obtain

$$T\Sigma[n_t] = -\Delta G[n_t] + W_d[n_t] + \sum_{y_f} W_{y_f}^{nc}[n_t], \quad (101)$$

where the first term is the difference of the *stochastic semigrand Gibbs potential*

$$G(n) := k_B T \ln p_n + g_n. \quad (102)$$

Equation (101) is the main result of our paper. The first term on the rhs constitutes the conservative force contribution of the EP. The second term, Eq. (100), arises in presence of time-dependent driving and quantifies the work spent to manipulate the free energy landscape of the CRN via the chemical potentials μ_{Y_p} . We refer to it as *driving work*. Finally, for each exchanged species \mathbf{Y}_f , a nonconservative force contribution (98) arises. Each $W_{y_f}^{nc}[n_t]$ quantifies the work spent by the chemostats to sustain a flow of chemicals across the CRN, and we refer to them as *nonconservative chemical work contributions*. Equation (101) holds for an arbitrary CRN, yet it is CRN-specific, as it accounts for the topological properties of the CRN, *i.e.* the conservation laws. To gain more intuition, we now focus on specific classes of CRNs, whose resulting decomposition is summarized in Tab. II. In Secs. VI and VII we will further explore the physical consequences of Eq. (101), whereas in Ex. 5 and in § VIII we evaluate W_d and $\{W_{y_f}^{nc}\}$ for specific models.

Autonomous Detailed-Balanced CRNs: The CRN is autonomous and all fundamental forces vanish. The trajectory EP becomes minus a potential difference,

$$T\Sigma[n_t] = -\Delta G[n_t]. \quad (103)$$

We will prove in § VII that this is the class of open CRNs which relax to equilibrium and in which the average potential $\langle G \rangle$ is minimized at equilibrium by the dynamics described by CME (11).

Unconditionally Detailed-Balanced CRNs: The set of species \mathbf{Y}_f is empty—*i.e.* each exchanged species breaks a conservation law—and no force arises. Hence, these CRNs are detailed-balanced irrespective of the values of μ_Y , but the time-dependent driving prevents them from reaching equilibrium, and their EP reads

$$T\Sigma[n_t] = -\Delta G[n_t] + W_d[n_t]. \quad (104)$$

dynamics	$-\Delta G$	W_d	W^{nc}
autonomous detailed-balanced	✓	0	0
unconditionally detailed-balanced	✓	✓	0
autonomous	✓	0	✓
NESS	0	0	✓

TABLE II. Entropy production for specific processes. “0” (resp. “✓”) denotes a vanishing (resp. a finite) contribution. NESS is the acronym for *nonequilibrium steady state*.

Autonomous CRNs: The driving work vanishes and the forces are constant in time. Hence, the EP becomes

$$T\Sigma[n_t] = -\Delta G[n_t] + \sum_{y_f} \mathcal{F}_{y_f} \mathcal{J}_{y_f}[n_t]. \quad (105)$$

The nonconservative chemical work display a typical current–force structure. In the long time limit, $\Delta G[n_t]$ is typically subextensive in time, and we obtain

$$T\Sigma[n_t] \xrightarrow{t \rightarrow \infty} \sum_{y_f} \mathcal{F}_{y_f} \mathcal{J}_{y_f}[n_t]. \quad (106)$$

In other words, the EP is dominated by the dissipative flows of chemicals across the CRN.

Remark For CRN with infinite number of species and reactions—*e.g.* aggregation–fragmentation and polymerization processes [44–46]—the CRN may undergo steady growth regimes in which ΔG is not subextensive in time and cannot be neglected in long-time limit.

Remark Our EP decomposition is not unique and different expressions for g_n and \mathcal{F}_{Y_p} correspond to different choices for the partitioning of \mathbf{Y}_p and \mathbf{Y}_f .

Example 5. For the open CRN in Fig. 1, the chemostatted species can be splitted into \mathbf{Y}_p and \mathbf{Y}_f in two possible—and trivial—ways: either A is regarded as the species breaking the conservation law (31b), or B. We consider the former choice, $y_p = (A)$ and $y_f = (B)$. Since $\ell_A^b = 1$, the only entry of the moiety vector reads,

$$M_n^A = n_{E^*} + n_{E^{**}} + n_A + n_B = L_n^b, \quad (107)$$

which is equal to the total abundance of the A–B moiety. The intensive variable conjugated to the broken conservation law is equal to the chemical potential of A_e ,

$$f_b = \mu_{A_e}. \quad (108)$$

The potential thus readily follows from Eq. (94)—or equivalently Eq. (95)—,

$$g_n = g_n - \mu_{A_e} M_n^A. \quad (109)$$

The instantaneous driving work rate associated to any manipulation of the latter potential is

$$\dot{W}_d(n) = -\partial_t \mu_{A_e} M_n^A. \quad (110)$$

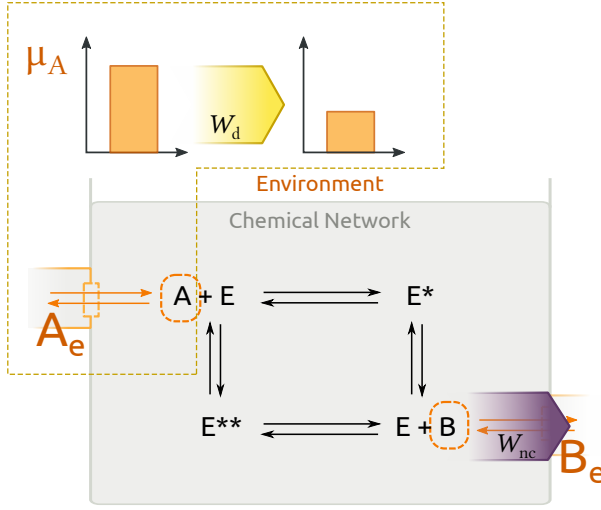


FIG. 4. Pictorial illustration of the work contributions. The driving one arises when the chemical potential of the chemostat A_e changes in time. The nonconservative chemical work, instead, characterizes the sustained conversion of A into B .

Once integrated over a trajectory, it gives the driving work, Eq. (100). Since $y_f = (B)$, the conjugated fundamental chemical force reads

$$\mathcal{F}_{B_e} = \mu_{B_e} - \mu_{A_e}. \quad (111)$$

and the instantaneous dissipative contribution due to this force is

$$\dot{W}_{B_e}^{nc} = \mathcal{F}_{B_e} I_{B_e}, \quad (112)$$

where $I_{B_e} = J_{+b} - J_{-b}$. When integrated over a trajectory, it measures the work spent to sustain a current between A_e and B_e across the CRN. A pictorial illustration of the work contributions is given in Fig. 4. The trajectory EP thus reads

$$\begin{aligned} T\Sigma[n_t] = \int_0^t d\tau & \left[-\partial_\tau \mu_{A_e}(\tau) M_n^A \right] |_{n_\tau} - \Delta G[n_t] \\ & + \int_0^t d\tau \mathcal{F}_{B_e}(\tau) I_{B_e}(\tau). \quad \square \end{aligned} \quad (113)$$

B. Energy Balance

In Eq. (101), the CRN-specific work contributions, W_d and $\{W_{y_f}^{nc}\}$, emerge as dissipative contributions. To strengthen their interpretation as work contributions, we now show that they can also be described as part of an energy balance. For this purpose, let

$$\mathcal{H}(n) := H(n) - \mu_{Y_p} \cdot M_n^{Y_p} = G(n) + TS(n) \quad (114)$$

be the *semigrand enthalpy*, which can be regarded as a CRN-specific form of energy. When combining this potential with the enthalpy and entropy balances, Eqs. (68), (71) and (101), we obtain

$$\Delta H[n_t] = Q[n_t] + W_d[n_t] + \sum_{y_f} W_{y_f}^{nc}[n_t]. \quad (115)$$

Now, we clearly see the role of W_d and $\{W_{y_f}^{nc}\}$ as work contributions, as they are opposed to the heat flow, Q . On the one hand, W_d is the energy spent by an external agent to manipulate the chemostats and does not involve an exchange of any extensive quantity between the CRN and chemostats. On the other hand, $\{W_{y_f}^{nc}\}$ accounts for the energy flowing between different chemostats that is mediated by the CRN.

C. Equilibrium of open CRNs

We have already seen that in absence of fundamental forces, the rhs of the local detailed balance (93) becomes a state function difference. The steady-state probability distribution

$$p_{eq}(n|L_{\lambda_u}) = \frac{\exp\{-\beta g_n\}}{\mathcal{Z}(\{L_{\lambda_u}\})} \prod_{\lambda_u} \delta[L_n^{\lambda_u}, L_{\lambda_u}]. \quad (116)$$

satisfies the detailed balance property (53) and therefore characterizes the equilibrium of open CRNs. Not accidentally, the relationship between the partition function $\mathcal{Z}(\{L_{\lambda_u}\})$ and that of closed CRNs, Eq. (43),

$$\mathcal{Z}(\{L_{\lambda_u}\}) = \sum_m \exp\{-\beta g_m\} \prod_{\lambda_u} \delta[L_m^{\lambda_u}, L_{\lambda_u}] \quad (117)$$

$$= \sum_{\{L_{\lambda_b}\}} \exp\left\{\beta \sum_{\lambda_b} f_{\lambda_b} L_{\lambda_b}\right\} Z(\{L_\lambda\}), \quad (118)$$

is akin to that between canonical and grandcanonical partition functions, see *e.g.* [47]. With an ensemble of unbroken components, $P(\{L_{\lambda_u}\})$, the constrained equilibrium distribution reads

$$\begin{aligned} p_n^{eq} &:= \sum_{\{L_{\lambda_b}\}} p_{eq}(n|L_{\lambda_u}) P(\{L_{\lambda_u}\}) \\ &= p_{eq}(n|L_n^{\lambda_u}) P(\{L_n^{\lambda_u}\}), \end{aligned} \quad (119)$$

where $p_{eq}(n|L_n^{\lambda_u})$ is the probability distribution of observing the state n given its stoichiometric compatibility class. Eq. (119) thus generalizes the equilibrium probability distribution (44) to open CRNs.

Importantly, the average semigrand Gibbs potential (102) takes its minimum value at p_n^{eq} , Eq. (119), where it reduces to the equilibrium semigrand Gibbs potential,

$$g_{eq}(\{L_{\lambda_u}\}) = -k_B T \ln \mathcal{Z}(\{L_{\lambda_u}\}) + k_B T \ln P(\{L_{\lambda_u}\}), \quad (120)$$

averaged over $P(\{L_{\lambda_u}\})$. Indeed,

$$\begin{aligned} \langle g \rangle - \sum_{\{L_{\lambda_u}\}} P(\{L_{\lambda_u}\}) g_{eq}(\{L_{\lambda_u}\}) &= \langle g - g_{eq} \rangle \\ &= k_B T D(p \| p_{eq}) \geq 0. \end{aligned} \quad (121)$$

The first equality follows from the fact that \mathcal{G}_{eq} is non-fluctuating, since it depends solely on the unbroken components. As for the Gibbs free energy in closed CRNs, we will show later (§ VII) that Eq. (121) quantifies the average dissipation during the relaxation to equilibrium.

D. Dissipation Balance along Stoichiometric Cycles

We can now formulate the EP decomposition in term of stoichiometric cycles affinities. These are defined as the sum of the transition affinities along stoichiometric cycles $\{c \equiv \rho_{c1}, \rho_{c2}, \dots, \rho_{cN_c}\}$,

$$\begin{aligned} \mathcal{A} := & \mathcal{A}_{\rho_{c1}}(\mathbf{n}) + \mathcal{A}_{\rho_{c2}}(\mathbf{n} + \mathbf{S}_{\rho_{c1}}) + \dots \\ & \dots + \mathcal{A}_{\rho_{cN_c}}(\mathbf{n} + \sum_{j=1}^{N_c-1} \mathbf{S}_{\rho_{cj}}). \end{aligned} \quad (122)$$

Using Eq. (56), and the fact that $-\Delta_\rho G(\mathbf{n})$ vanishes when summed over the loop c , we obtain

$$\mathcal{A} = -\mu_Y \cdot \sum_{i=1}^{N_c} \mathbf{S}_{\rho_{ci}}^Y = -\mu_Y \cdot \sum_\rho \mathbf{S}_\rho^Y c_\rho. \quad (123)$$

Since $\sum_\rho \mathbf{S}_\rho^Y c_\rho^\alpha = 0$, those evaluated along the stoichiometric cycles of the closed CRN, $\{c^\alpha\}$, always vanish. In contrast, those along the emergent cycles, $\{c^\eta\}$, do not vanish in general,

$$\mathcal{A}_\eta = \mu_Y \cdot \mathbf{C}_\eta^Y, \quad (124)$$

see Eq. (36). These affinities can be thus understood as the chemical potential gradient imposed by the chemostats on the cycle.

To rewrite the EP (101) in terms $\{\mathcal{A}_\eta\}$, let us highlight their relationship with the fundamental forces,

$$\mathcal{A}_\eta = \mathcal{F}_{Y_f} \cdot \mathbf{C}_\eta^{Y_f}, \quad (125)$$

which is obtained when summing the local detailed balance (93) along $\{c^\eta\}$ as in Eq. (122). Since the matrix whose columns are $\{\mathbf{C}_\eta^{Y_f}\}$ is square and nonsingular—as it can be deduced from the linear independence of the set of emergent cycles—, we can invert it and write

$$\mathcal{F}_{Y_f} = \sum_\eta \bar{\mathbf{C}}_\eta^{Y_f} \mathcal{A}_\eta, \quad (126)$$

where $\{\bar{\mathbf{C}}_\eta^{Y_f}\}$ denote the rows of the inverse matrix. This relation clarifies the one-to-one correspondence which lies between $\{\mathcal{F}_{Y_f}\}$ and $\{\mathcal{A}_\eta\}$. Inserting the last expression in the local detailed balance, Eq. (93), we obtain

$$\ln \frac{w_\rho(\mathbf{n})}{w_{-\rho}(\mathbf{n} + \mathbf{S}_\rho)} = -\beta (\Delta_\rho g_\mathbf{n} - \sum_\eta \mathcal{A}_\eta \zeta_{\eta,\rho}), \quad (127)$$

where the coefficients

$$\zeta_{\eta,\rho} := -\bar{\mathbf{C}}_\eta^{Y_f} \cdot \mathbf{S}_\rho^{Y_f} \quad (128)$$

quantify how much each reaction contributes to the emergent cycles. Algebraically, the row vectors $\{\zeta_\eta\}$ are dual to the cycles, $\{c^\eta\}$,

$$\zeta_\eta \cdot c^{\eta'} = -\sum_\rho \bar{\mathbf{C}}_\eta^{Y_f} \cdot \mathbf{S}_\rho^{Y_f} c_\rho^{\eta'} = \bar{\mathbf{C}}_\eta^{Y_f} \cdot \mathbf{C}_{\eta'}^{Y_f} = \delta_{\eta,\eta'}. \quad (129)$$

As previously done for Eq. (101), when integrating the trajectory EP (72b) with the local detailed balance (127) we obtain

$$\mathcal{T}\Sigma[\mathbf{n}_t] = -\Delta\mathcal{G}[\mathbf{n}_t] + W_d[\mathbf{n}_t] + \sum_\eta \Gamma_\eta[\mathbf{n}_t]. \quad (130)$$

The stochastic semigrand Gibbs potential and the driving work read as in Eqs. (102) and (100), respectively. For each emergent stoichiometric cycle,

$$\Gamma_\eta[\mathbf{n}_t] := \int_0^t d\tau \mathcal{A}_\eta(\tau) \sum_\rho \zeta_{\eta,\rho} J_\rho(\tau). \quad (131)$$

quantifies the chemical work spent to sustain the related cyclic flow of chemicals. For autonomous CRNs

$$\mathcal{T}\Sigma[\mathbf{n}_t] = -\Delta\mathcal{G}[\mathbf{n}_t] + \sum_\eta \mathcal{A}_\eta \mathcal{J}_\eta[\mathbf{n}_t], \quad (132)$$

where

$$\mathcal{J}_\eta[\mathbf{n}_t] := \int_0^t d\tau \sum_\rho \zeta_{\eta,\rho} J_\rho(\tau) \quad (133)$$

quantifies the integrated current along the cycle η . In the long-time limit, in which $\Delta\mathcal{G}[\mathbf{n}_t]$ is negligible, we obtain

$$\mathcal{T}\Sigma[\mathbf{n}_t] \xrightarrow{t \rightarrow \infty} \sum_\eta \mathcal{A}_\eta \mathcal{J}_\eta[\mathbf{n}_t]. \quad (134)$$

When all emergent cycle affinities vanish—as well as when no emergent cycle is created—the CRN becomes detailed-balanced, in agreement with the Kolmogorov–Wegscheider condition [48–50].

Remark An alternative approach that can be used for cycle EP decompositions is the graph-theoretic one based on the identification of the loops appearing in the network of transitions [3, 51]. Once these loops are identified, they can be sorted according to the chemostats they are coupled to, as these determine their affinity, see Eq. (122). Equivalently, loops are classified according to the stoichiometric cycle they correspond to. In Ref. [52], a graph-theoretic approach based on loop affinities led to the expression analogous to Eq. (134). In contrast, our cycles EP decomposition is based on a stoichiometric approach: emergent cycles are directly identified by the kernels of S_i and S .

This observation points out the redundancy which is intrinsic in bare graph-theoretic EP decompositions: many loops may be coupled to the same set of reservoirs and thus carry the same affinity, while many others may carry a vanishing affinity—for CRN these latter are those corresponding to stoichiometric cycles of the

closed network, $\{c^\alpha\}$. For generic networks, a systematic way of identifying these so-called *symmetries* was derived in Ref. [53], whereas in Ref. [54] they are used to formulate generic thermodynamic—rather than mere graph-theoretic—EP decompositions.

Example 6. Trivially, the emergent cycle affinity corresponding to the emergent stoichiometric cycle (39) reads

$$\mathcal{A} = \mu_{B_e} - \mu_{A_e} = \mathcal{F}_{B_e}. \quad (135)$$

The contributions to the corresponding cycle current follows from Eq. (128),

$$\zeta^T = \begin{pmatrix} +1 & +2 & +3 & +4 & +a & +b \\ 0 & 0 & 0 & 0 & 0 & -1 \end{pmatrix}. \quad (136)$$

The entries corresponding to the backward reactions are minus those of the forward. Notice that, since the CRN has exactly one emergent cycle, the force and cycle EP decompositions are identical, see Eq. (125).

V. SEMIGRAND GIBBS POTENTIAL

We here further elaborate on equilibrium distributions and semigrand Gibbs potentials by addressing three points: (i) the relationship between Eq. (119), and the equilibrium distributions as expressed in chemical reaction network theory; (ii) the role of conservation laws for characterizing the dissipation of CRNs subject to sequential introduction of exchanged species; (iii) the gauge freedom intrinsic to the definition of driving work. This section can be skipped at a first read.

A. Equilibrium Distributions in Chemical Reaction Network Theory

In Ref. [23] (see also [55]) equilibrium distributions of CRNs are proven to be multi-Poissonian

$$p_{eq}(\mathbf{n}|L_{\lambda_u}) = \frac{\exp\{\mathbf{n} \cdot \ln\{[z]_{eq}V\}\}}{n! \mathcal{Z}(\{L_{\lambda_u}\})} \prod_{\lambda_u} \delta[L_n^{\lambda_u}, L_{\lambda_u}], \quad (137)$$

where $[z]_{eq}$ is the equilibrium concentration distribution of the same CRN described by a set of deterministic rate equations. $\mathcal{Z}(\{L_{\lambda_u}\})$ is again a normalizing factor. To highlight the relationship between this equation and Eqs. (119) and (85), we need to recall that, for deterministic CRNs, thermodynamic equilibrium is defined by the fact that chemical potential differences along all reactions vanish, Eqs. (87) and (A7). As observed in Ref. [26], this entails that

$$\mu^{eq} = \sum_{\lambda} f_{\lambda} \ell_{\lambda}, \quad (138)$$

where $\{f_{\lambda}\}$ are real coefficients depending on μ_Y and $\{L_{\lambda_u}\}$. Those related to the broken components, $\{f_{\lambda_b}\}$, are indeed those appearing in Eq. (96). From Eq. (A7) we therefore have

$$\ln\{[z]_{eq}V\} = -\beta(\mu^\circ - k_B T \ln n_s - \sum_{\lambda} f_{\lambda} \ell_{\lambda}), \quad (139)$$

from which

$$\begin{aligned} \mathbf{n} \cdot \ln\{[z]_{eq}V\} - \ln n! &= -\beta(g_n - \mu^{eq} \cdot \mathbf{n}) \\ &= -\beta(g_n - \sum_{\lambda_u} f_{\lambda_u} L_n^{\lambda_u}) \end{aligned} \quad (140)$$

ensues. At this point, Eqs. (85), (116), and (137) appear identical up to $\sum_{\lambda_u} f_{\lambda_u} L_n^{\lambda_u}$. However, since this term appears both at the nominator of Eq. (137) and in $\mathcal{Z}(\{L_{\lambda_u}\})$, it cancels. This shows the connection between the CRN theoretical and thermodynamic expression of equilibrium distributions.

B. Hierarchies of Equilibria

We here show that when starting from a closed CRN, a sequential introduction of exchange reactions that keep the CRN detailed balanced drives it down in semigrand Gibbs potential by equilibrating previously constrained degrees of freedom: the conservation laws, see Fig. 5. Let us imagine a closed CRN whose initial probability distribution is $p_0(\mathbf{n}|L_{\lambda}) = \sum_{\{L_{\lambda}\}} p_0(\mathbf{n}|L_{\lambda}) P_0(\{L_{\lambda}\})$, where $P_0(\{L_{\lambda}\}) = \prod_{\lambda} P_0^{\lambda}(L_{\lambda})$, i.e. different components are independently distributed. As it relax to equilibrium, $P_0(\{L_{\lambda}\})$ will not change, while $p_0(\mathbf{n}|L_{\lambda})$ will relax to Eq. (41). The average dissipation is

$$T \langle \Sigma \rangle = -\Delta \langle G \rangle = \sum_{\{L_{\lambda}\}} P_0(\{L_{\lambda}\}) \left[k_B T \sum_{\mathbf{n}} p(\mathbf{n}|L_{\lambda}) \ln \frac{p(\mathbf{n}|L_{\lambda})}{p_{eq}(\mathbf{n}|L_{\lambda})} \right] \equiv \sum_{\{L_{\lambda}\}} P_0(\{L_{\lambda}\}) [-\Delta \langle G(\{L_{\lambda}\}) \rangle]. \quad (141)$$

This expression is obtained when combining the properties of the Gibbs potential, Eq. (49), with the equilibrium distribution of closed CRNs, Eq. (44). It shows that the average drop of Gibbs free energy can be expressed as the weighted average of the drops of Gibbs free energy at given components, $-\Delta \langle G(\{L_{\lambda}\}) \rangle$.

We now open the CRN by chemostatting one species. Hence, one conservation law is broken, e.g. the total mass ℓ_{λ_1} , and the CRN relaxes to a new equilibrium, Eq. (119). Clearly, $P_0^{\lambda}(L_{\lambda})$, for $\lambda \neq \lambda_1$, will not change during the

relaxation, and we can rewrite the new equilibrium as

$$p_{\text{eq}}^{(\lambda_1)}(\mathbf{n}) = \frac{\exp\left\{-\beta g_{\mathbf{n}} + \beta f_{\lambda_1} L_{\mathbf{n}}^{\lambda_1}\right\}}{Z_{\lambda_1}(\{L_{\mathbf{n}}^{\lambda}\}_{\lambda \neq \lambda_1})} \prod_{\lambda \neq \lambda_1} P_0^{\lambda}(L_{\mathbf{n}}^{\lambda}) = \underbrace{\frac{\exp\{-\beta g_{\mathbf{n}}\}}{Z(\{L_{\mathbf{n}}^{\lambda}\})}}_{= p_{\text{eq}}(\mathbf{n}|\{L_{\mathbf{n}}^{\lambda}\})} \underbrace{\frac{Z(\{L_{\mathbf{n}}^{\lambda}\}) \exp\{\beta f_{\lambda_1} L_{\mathbf{n}}^{\lambda_1}\}}{Z_{\lambda_1}(\{L_{\mathbf{n}}^{\lambda}\}_{\lambda \neq \lambda_1})}}_{=: P_{\text{eq}}(L_{\mathbf{n}}^{\lambda_1}|\{L_{\mathbf{n}}^{\lambda}\}_{\lambda \neq \lambda_1})} \prod_{\lambda \neq \lambda_1} P_0^{\lambda}(L_{\mathbf{n}}^{\lambda}). \quad (142)$$

The first term is the equilibrium distribution of the closed CRN, while the second can be interpreted as the equilibrium distribution of the broken component, for given unbroken component. In other words, the final equilibrium can be understood as a closed CRN equilibrium with an equilibrium probability distribution over the broken component. Hence, the average amount of semigrand Gibbs free energy, $\mathcal{G}_{\lambda_1}(\mathbf{n}) = G(\mathbf{n}) - f_{\lambda_1} L_{\mathbf{n}}^{\lambda_1}$, dissipated during the relaxation can be written as

$$-\Delta \langle \mathcal{G}_{\lambda_1} \rangle = k_B T \sum_{\mathbf{n}} p_{\text{eq}}(\mathbf{n}|\{L_{\mathbf{n}}^{\lambda}\}) \prod_{\lambda} P_0^{\lambda}(L_{\mathbf{n}}^{\lambda}) \ln \frac{P_0^{\lambda_1}(L_{\mathbf{n}}^{\lambda_1})}{P_{\text{eq}}(L_{\mathbf{n}}^{\lambda_1}|\{L_{\mathbf{n}}^{\lambda}\}_{\lambda \neq \lambda_1})}, \quad (143)$$

upon application of Eqs. (121) with the distributions (44) and (142). When rewriting this expression as a sum over all values of the components and performing the summation over the states of $p_{\text{eq}}(\mathbf{n}|\{L_{\mathbf{n}}^{\lambda}\})$ we finally obtain

$$\begin{aligned} -\Delta \langle \mathcal{G}_{\lambda_1} \rangle &= \sum_{\{L_{\lambda}\}_{\lambda \neq \lambda_1}} P_0^{\lambda}(L_{\lambda}) \left[\sum_{L_{\lambda_1}} P_0^{\lambda_1}(L_{\lambda_1}) k_B T \ln \frac{P_0^{\lambda_1}(L_{\lambda_1})}{P_{\text{eq}}(L_{\lambda_1}|\{L_{\lambda}\}_{\lambda \neq \lambda_1})} \right] \\ &= \sum_{\{L_{\lambda}\}_{\lambda \neq \lambda_1}} P_0^{\lambda}(L_{\lambda}) [-\Delta \langle \mathcal{G}_{\lambda_1}(\{L_{\lambda}\}_{\lambda \neq \lambda_1}) \rangle]. \end{aligned} \quad (144)$$

In the first line we recognize the relative entropy between the initial probability of the broken component, $P_0^{\lambda_1}(L_{\lambda_1})$, and the equilibrium one, $P_{\text{eq}}(L_{\lambda_1}|\{L_{\lambda}\}_{\lambda \neq \lambda_1})$. It is equal to the difference of semigrand Gibbs free energy at given component, as highlighted in the second line. We thus see that the dissipation following the relaxation from one equilibrium to the other is completely characterized by the equilibration of the initially constrained degrees of freedom.

This procedure can of course be repeated when a further species is chemostatted and it breaks another conservation law. The dissipation is quantified by a difference of semigrand Gibbs free energy, which accounts for the relaxation of the degree of freedom which has been released. When the chemostatting breaks all conservation laws without generating fundamental forces, the CRN finally reaches the global minimum of available semigrand Gibbs free energy, Fig. 5. In this case, the potential becomes the grand potential used in Ref. [20] and discussed in § III D, *cf.* Eqs. (86), (138), (102), and (95).

C. W_d - \mathcal{G} Gauge

The driving work and the stochastic semigrand Gibbs potential are defined up to a gauge—distinct from that

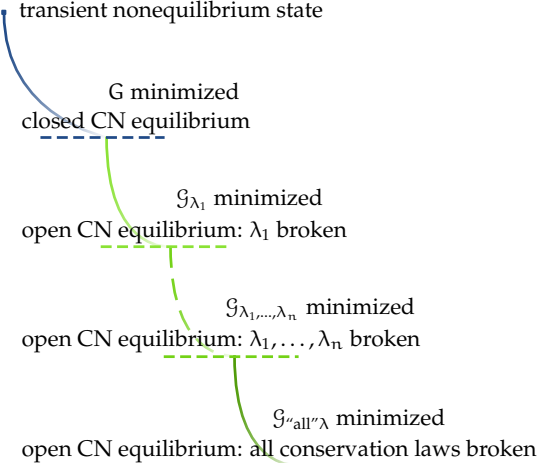


FIG. 5. Pictorial representation of the hierarchy of equilibrium states and the semigrand Gibbs free energy drops following the relaxation to equilibrium when conservation laws are broken.

involving G and W_c , which corresponds to the choice of the components. Let us consider a basis change in the space of conservation laws

$$\ell_{\lambda} \rightarrow \ell'_{\lambda} = \sum_{\lambda'} \Omega_{\lambda \lambda'} \ell_{\lambda'}, \quad (145)$$

with $\Omega_{\lambda_u \lambda_b} = 0$ for all λ_u, λ_b , so that the unbroken ones preserve their properties. Accordingly, the conjugated

intensive variables transform as

$$f_\lambda \rightarrow f'_\lambda = \sum_{\lambda'} f_{\lambda'} \bar{\Omega}_{\lambda' \lambda}, \quad (146)$$

see Eq. (138), where $\bar{\Omega}$ denotes the inverse of Ω . We now notice that when the sum involves only the broken conservation laws, such a bilinear form becomes

$$\sum_{\lambda_b} f_{\lambda_b} \ell_{\lambda_b} \rightarrow \sum_{\lambda_b} f_{\lambda_b} \ell_{\lambda_b} - \sum_{\lambda_u} f_{\lambda_u} \ell_{\lambda_u}, \quad (147)$$

where

$$f_{\lambda_u} := \sum_{\lambda'_u \lambda'_b} f_{\lambda'_b} \bar{\Omega}_{\lambda'_b \lambda'_u} \Omega_{\lambda'_u \lambda_u}. \quad (148)$$

Therefore, the instantaneous driving work rate (the integrand of Eq. (100) rewritten with Eq. (96)), and the semigrand potential, become

$$\dot{W}_d(\mathbf{n}) \rightarrow \dot{W}_d(\mathbf{n}) + \sum_{\lambda_u} \partial_t f_{\lambda_u} L_n^{\lambda_u}, \quad (149)$$

and

$$\mathcal{G}(\mathbf{n}) \rightarrow \mathcal{G}(\mathbf{n}) + \sum_{\lambda_u} f_{\lambda_u} L_n^{\lambda_u}, \quad (150)$$

respectively. In contrast, the nonconservative forces—and thus the nonconconservative work—is left invariant

$$\mathcal{F}_{Y_f} \rightarrow \mathcal{F}_{Y_f} + \sum_{\lambda_u} f_{\lambda_u} \ell_{\lambda_u}^{Y_f} = \mathcal{F}_{Y_f}, \quad (151)$$

since $\ell_{\lambda_u}^{Y_f} = 0$. Crucially, the gauge terms in W_d and $-\Delta \mathcal{G}$ cancel and the EP is unaltered. After all, the physical process is not modified. Notice also that since the gauge term is nonfluctuating, it vanishes for cyclic protocols when integrated over a period.

We thus conclude that driving work and semigrand Gibbs potential are not univocally defined as they are affected by a gauge freedom. The gauge affecting the potential–work connection in stochastic thermodynamics led to debates, see Ref. [56] and references therein. As observed in the latter reference, the problem is rooted in what can be experimentally measured as work, as different experimental set-ups entail different gauge choices. In our chemical framework, different choices of the broken components, involve expressions of the work in which different species appear and whose abundances need to be measured to estimate the work.

Example 7. To illustrate the potential–work gauge we use the CRN in Fig. 1. Let us consider the transformation of the set conservation laws, Eq. (31), identified by the matrix

$$\Omega = \begin{pmatrix} 1 & -1 \\ 0 & 1 \end{pmatrix}, \quad (152)$$

according to which the conservation laws become

$$\ell'_E = \ell_E = \begin{pmatrix} E & E^* & E^{**} & A & B \\ 1 & 1 & 1 & 0 & 0 \end{pmatrix}, \quad (153a)$$

$$\ell'_b = \ell_b - \ell_E = \begin{pmatrix} E & E^* & E^{**} & A & B \\ -1 & 0 & 0 & 1 & 1 \end{pmatrix}. \quad (153b)$$

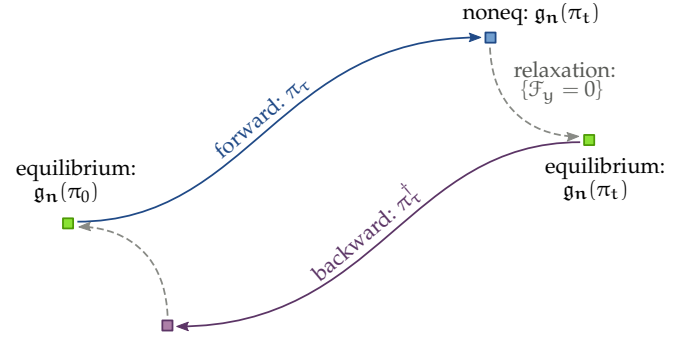


FIG. 6. Schematic representation of the forward and backward processes. The relaxation to the equilibrium obtained by shutting down the driving and turning off the forces at time t (resp. 0) for the forward (resp. backward) process, merely relates the two processes but it is irrelevant for the FT.

Using Eqs. (108), the gauge term reads

$$f_{\lambda_u}(\pi_t) = \mu_A(\pi_t) \quad (154)$$

from which we can easily derive the expression for the new driving work rate

$$\dot{W}_d(\mathbf{n}) = (n_E - n_A - n_B) \partial_t \mu_A. \quad (155)$$

The semigrand Gibbs free energy easily follows. We can now highlight the difference between the two definitions of driving work, Eqs. (110) and (155): while the first entails the measurement of the population of A, B, and of the activated complexes E^* and E^{**} , the latter entails that of A, B, and of the free enzyme E. The values of the two expressions will differ but for cyclic protocols integrated over a period. \square

VI. FLUCTUATION THEOREMS

We now proceed to show that the driving work and the nonconservative chemical work satisfy a finite-time detailed FT. The FT holds for any process, referred to as *forward*, if the open CRN is initially prepared at equilibrium, Eq. (119). For the sake of simplicity, and without loss of generality, we assume that the initial distribution of unbroken components is $P(\{L_n^{\lambda_u}\}) = \prod_{\lambda_u} \delta[L_n^{\lambda_u}, L_{\lambda_u}]$, and we denote by π_0 the initial value of the protocol, which corresponds to equilibrium. At time 0, the driving is activated and the CRN evolves controlled by the protocol π_τ , for $\tau \in [0, t]$. The corresponding *backward* process is again initially prepared at the equilibrium—where all forces vanish—but the chemical potentials μ_{Y_p} must have the same value they have at time t in the forward process. This guarantees that $g_n(t)$ rules the equilibrium distribution. The backward process is driven by the time-reversed protocol, $\pi_\tau^\dagger := \pi_{t-\tau}$, for $\tau \in [0, t]$.

The *finite-time detailed FT* establishes the relationship between the forward and backward process

$$\frac{\mathcal{P}_t(W_d, \{W_{y_f}^{nc}\})}{\mathcal{P}_t^*(-W_d, \{-W_{y_f}^{nc}\})} = \exp \left\{ \beta (W_d + \sum_{y_f} W_{y_f}^{nc} - \Delta \mathcal{G}_{eq}) \right\}, \quad (156)$$

where $\mathcal{P}_t(W_d, \{W_{y_f}^{nc}\})$ is the probability of observing W_d driving work and $\{W_{y_f}^{nc}\}$ nonconservative contributions along the forward process, Eqs. (100) and (98). Instead, $\mathcal{P}_t^*(-W_d, \{-W_{y_f}^{nc}\})$ is the probability of observing $-W_d$ driving work and $\{-W_{y_f}^{nc}\}$ nonconservative contributions along the backward process. Finally,

$$\Delta \mathcal{G}_{eq} = -k_B T \ln \frac{\mathcal{Z}(\pi_t, \{L_{\lambda_u}\})}{\mathcal{Z}(\pi_0, \{L_{\lambda_u}\})}, \quad (157)$$

is the difference of equilibrium semigrand Gibbs potential between the backward and forward initial equilibrium states. When integrating this expression over all possible values of W_d and $\{W_{y_f}^{nc}\}$ we recover a Jarzynski-like integral FT

$$\left\langle \exp \left\{ -\beta (W_d + \sum_{y_f} W_{y_f}^{nc}) \right\} \right\rangle = \exp \left\{ -\beta \Delta \mathcal{G}_{eq} \right\}. \quad (158)$$

The proof of the FT (156) is given in App. B, and it hinges on the generating function techniques presented in Ref. [54].

We now investigate some interesting specific cases of the FT (156). In unconditionally detailed-balance CRNs, the nonconservative work vanish and we obtain the Crooks' FT formulated for CRNs [57–60],

$$\frac{\mathcal{P}_t(W_d)}{\mathcal{P}_t^*(-W_d)} = \exp \left\{ \beta (W_d - \Delta \mathcal{G}_{eq}) \right\}. \quad (159)$$

Instead, for autonomous processes, the FT can be formulated as follows

$$\frac{\mathcal{P}_t(\{J_{y_f}\})}{\mathcal{P}_t(\{-J_{y_f}\})} = \exp \left\{ \beta \sum_{y_f} \mathcal{F}_{y_f} J_{y_f} \right\}. \quad (160)$$

The FT in Eq. (156) is inspired by an analogous result derived in Refs. [54, 61] in the context of generic Markov jump processes. The importance of our result is manifold. It holds for processes of finite duration t , and it is expressed in terms of measurable chemical quantities. Its only constraint is the initial state, which must be equilibrium. It reveals the most appropriate boundary conditions under which Jarzynski–Crooks-like FTs can be formulated for CRNs: equilibrium distribution of open CRNs. Most important, it evidences the merits of our stoichiometric approach based on the identification of conservation laws: it allowed us to characterize the potential describing the equilibrium distribution of open CRNs, and to formulate the decomposition of the EP which supports our FTs, Eq. (101).

Remark A physical interpretation of the argument of the exponential, Eq. (156), follows from the following observation: if, at time t , the driving is stopped and the fundamental forces (92) turned off—*viz.* set to zero by an appropriate choice of $\mu_{Y_f}^* := \mu_{Y_p} \cdot \sum_{\lambda_b} \bar{\ell}_{\lambda_b}^{Y_p} \ell_{\lambda_b}^{Y_f}$ —the CRN relaxes to the initial condition of the backward process. During the relaxation neither W_d nor $\{W_{y_f}^{nc}\}$ are performed and the related EP is $T\Sigma_{\text{relax}} = \mathcal{G}(\mathbf{n}, \pi_t) + k_B T \ln \mathcal{Z}(\pi_t, \{L_{\lambda_u}\})$. The argument of the exponential can thus be interpreted as the EP of the fictitious combined process “forward process + relaxation to the final equilibrium”.

Remark For autonomous CRNs and arbitrary initial conditions, the steady-state FT follows

$$\frac{\mathcal{P}(\{J_{y_f}\})}{\mathcal{P}(\{-J_{y_f}\})} \xrightarrow{t \rightarrow \infty} \exp \left\{ t \beta \sum_{y_f} \mathcal{F}_{y_f} J_{y_f} \right\}, \quad (161)$$

where $\mathcal{P}(\{J_{y_f}\})$ is the probability of observing average rates of fundamental external currents $\{\frac{1}{t} \int_0^t d\tau I_{y_f}(\tau)\}$ equal to $\{J_{y_f}\}$. Eq. (161) can be proved using the large deviation technique used in Ref. [14] in combination with the local detailed balance (93).

FT along Stoichiometric Cycles

An alternative yet equivalent formulation of the FT (156) is that given in terms of nonconservative contributions along emergent stoichiometric cycles, Eq. (131):

$$\frac{\mathcal{P}_t(W_d, \{\Gamma_\eta\})}{\mathcal{P}_t^*(-W_d, \{-\Gamma_\eta\})} = \exp \left\{ \beta (W_d + \sum_\eta \Gamma_\eta - \Delta \mathcal{G}_{eq}) \right\}, \quad (162)$$

where $\mathcal{P}_t(W_d, \{\Gamma_\eta\})$ is the probability of observing W_d driving work and $\{\Gamma_\eta\}$ nonconservative contributions along the forward process. We discuss its proof App. B.

Remark As for the fundamental currents, the local detailed balance (127) can be used to prove a steady-state FT for currents along emergent stoichiometric cycles

$$\frac{\mathcal{P}(\{\dot{J}_\eta\})}{\mathcal{P}(\{-\dot{J}_\eta\})} \xrightarrow{t \rightarrow \infty} \exp \left\{ t \beta \sum_\eta \mathcal{A}_\eta \dot{J}_\eta \right\}, \quad (163)$$

which is valid for autonomous CRNs and arbitrary initial conditions. $\mathcal{P}(\{\dot{J}_\eta\})$ is the probability of observing average rates of emergent cycle currents $\{\frac{1}{t} \int_0^t d\tau \sum_\rho \zeta_{\eta, \rho} J_\rho(\tau)\}$ equal to $\{\dot{J}_\eta\}$. In contrast to the analogous FT obtained in Ref. [15], Eq. (163) is achieved using a stoichiometric approach based on the identification of stoichiometric cycles. For this reason, it accounts for the minimal set of nonzero macroscopic affinities.

VII. ENSEMBLE AVERAGE RATES DESCRIPTION

We now summarize our main results for ensemble average rates and discuss the relaxation to equilibrium of detailed-balanced CRNs. We also highlight the difference between an approach that does and does not take into account the topology of the CRN. We do so by recapitulating the procedure to decompose the EP into its fundamental contributions. We end by formulating a nonequilibrium Landauer's principle.

A. Traditional Description

Enthalpy Balance The enthalpy balance follows from the time derivative of the average enthalpy, Eq. (60),

$$d_t \sum_n p_n (\mathbf{h} \cdot \mathbf{n}) \equiv d_t \langle H \rangle = \langle \dot{Q} \rangle + \langle \dot{W}_c \rangle. \quad (164)$$

It characterizes the average rate of change of enthalpy in the same way Eq. (68) characterizes the enthalpy change along stochastic trajectories. The average heat flow rate is given by

$$\langle \dot{Q} \rangle = \langle \dot{Q}^{\text{thr}} \rangle + \langle \dot{Q}^{\text{chm}} \rangle. \quad (165)$$

The first term quantifies the average rate of heat of reaction,

$$\langle \dot{Q}^{\text{thr}} \rangle = \sum_{\rho} [\mathbf{h} \cdot \mathbf{S}_{\rho} + \mathbf{h}_Y \cdot \mathbf{S}_{\rho}^Y] \langle J_{\rho} \rangle, \quad (166)$$

where $\langle J_{\rho} \rangle = \sum_n w_{\rho}(n)p_n$ is the average reaction current. The second term is the average heat flow in the chemostats,

$$\langle \dot{Q}^{\text{chm}} \rangle = T \mathbf{s}_Y \cdot \langle \mathbf{I}^Y \rangle, \quad (167)$$

where $\langle \mathbf{I}^Y \rangle = \sum_{\rho} (-\mathbf{S}_{\rho}^Y) \langle J_{\rho} \rangle$ are the average external currents, Eq. (19), and the —the second term on the rhs. Instead, the ensemble average chemical work rate,

$$\langle \dot{W}_c \rangle = \mathbf{u}_Y \cdot \langle \mathbf{I}^Y \rangle, \quad (168)$$

quantifies the average rate of exchange of Gibbs free energy with the chemostats.

Entropy Production Rate At the ensemble average level, the second law of thermodynamics manifests itself in the non-negative average EP rate

$$\begin{aligned} \langle \dot{\Sigma} \rangle &= d_t \langle S \rangle - \frac{1}{T} \langle \dot{Q} \rangle \\ &= k_B \sum_{n, \rho} w_{\rho}(n)p_n \ln \frac{w_{\rho}(n)p_n}{w_{\rho}(n + \mathbf{S}_{\rho})p_{n + \mathbf{S}_{\rho}}} \geq 0. \end{aligned} \quad (169)$$

where $\langle S \rangle = \sum_n p_n S(n)$, Eq. (57). Using the expression for the transition affinity, Eq. (56), it can be recast into,

$$T \langle \dot{\Sigma} \rangle = \langle \dot{W}_c \rangle - d_t \langle G \rangle, \quad (170)$$

where the chemical work rate and the average Gibbs potential are given in Eqs. (168) and (48), respectively. Equivalently, Eqs. (164), (169), and (170) can be obtained by directly averaging Eqs. (68), (72a), and (72c), respectively, over all stochastic trajectories.

For closed CRNs, Eq. (170) reduces to $d_t \langle G \rangle = -T \langle \dot{\Sigma} \rangle \leq 0$. This relation, together with Eq. (49), shows that: (i) $\langle G \rangle$ is a Lyapunov function, and hence that closed CRNs relax to equilibrium, Eq. (44); (ii) $\langle G \rangle - \sum_{\{L_{\lambda}\}} P(\{L_{\lambda}\}) G_{\text{eq}}(\{L_{\lambda}\}) = T \langle \dot{\Sigma} \rangle$ is the average dissipation during the relaxation to equilibrium.

B. CRN-specific Description

Entropy Production Rate We now summarize the procedure to recover the EP decomposition (101) at the ensemble average level. (i) Identify the broken and unbroken conservation laws, $\{\ell_{\lambda_u}, \ell_{\lambda_b}\}$, § II D. (ii) Identify a set of N_{λ_b} exchanged species, y_p , for which the matrix whose rows are $\{\ell_{\lambda_b}^{y_p}\}$ is nonsingular. The columns of its inverse are denoted by $\{\bar{\ell}_{\lambda_b}^{y_p}\}$. Physically, each species y_p breaks exactly one conservation law. The remaining exchanged species form the set denoted by y_f . (iii) The *nonequilibrium semigrand Gibbs potential* follows from the average of Eq. (102),

$$\langle \mathcal{G} \rangle = \sum_n p_n [k_B T \ln p_n + g_n]. \quad (171)$$

It depends on the vector $\langle \mathbf{M}^{y_p} \rangle$ which describes the average population of the combination of moieties whose conservation is broken by the chemostats, § II D and Eq. (90). (iv) The change in time of $\langle g \rangle$ due to the time-dependent driving describes the average driving work rate, Eq. (100),

$$\langle \dot{W}_d \rangle = -\partial_t \mathbf{u}_{Y_p} \cdot \langle \mathbf{M}^{y_p} \rangle. \quad (172)$$

It quantifies the average amount of work spent to change the chemical potentials of the chemostats Y_p . (v) The second group of exchanged species, y_f , is used to identify the minimal set of fundamental chemical forces, $\mathcal{F}_{Y_f} \equiv \{\mathcal{F}_{y_f}\}$, Eq. (92). The average nonconservative chemical work rate follows from the product of these forces and their corresponding instantaneous external currents, Eq. (66)

$$\langle \dot{W}_{y_f}^{\text{nc}} \rangle := \mathcal{F}_{y_f} \langle I_{y_f} \rangle. \quad (173)$$

They quantify the average work per unit time spent to sustain a net current of species y_f across the CRN. (vi) The average EP rate decomposed as in Eq. (101) finally follows from Eqs. (171), (172), and (173)

$$T \langle \dot{\Sigma} \rangle = -d_t \langle \mathcal{G} \rangle + \langle \dot{W}_d \rangle + \sum_{y_f} \langle \dot{W}_{y_f}^{\text{nc}} \rangle. \quad (174)$$

Its three fundamental contributions appear: a conservative force contribution, a time-dependent driving contribution, a minimal set of nonconservative terms.

For open autonomous detailed-balanced CRNs, $\mathcal{F}_{Y_f} = 0$, $d_t \mu_{Y_p} = 0$, and hence Eq. (174) reduces to $d_t \langle \mathcal{G} \rangle = -T \langle \dot{\Sigma} \rangle \leq 0$. Mindful of Eq. (121), this relation shows that: (i) $\langle \mathcal{G} \rangle$ is a Lyapunov function, and hence that these CRNs relax to equilibrium, Eq. (119); (ii) $\langle \mathcal{G} \rangle - \sum_{\{L_{\lambda_u}\}} P(\{L_{\lambda_u}\}) G_{eq}(\{L_{\lambda_u}\}) = T \langle \Sigma \rangle$ is the average dissipation during the relaxation to equilibrium.

Enthalpy Balance By averaging Eq. (115), the CRN-specific average enthalpy balance also ensues

$$T \langle \mathcal{H} \rangle = \langle \dot{Q} \rangle + \langle \dot{W}_d \rangle + \sum_{Y_f} \langle \dot{W}_{Y_f}^{nc} \rangle, \quad (175)$$

which strengthen the interpretation of $\langle \dot{W}_d \rangle$ and $\langle \dot{W}_{Y_f}^{nc} \rangle$ as average work rate contributions.

C. Average EP along Stoichiometric Cycles

The average EP decomposition expressed in terms of emergent cycles currents and affinities can be achieved through an analogous recipe. (i) Identify broken and unbroken conservation laws, $\{\ell_{\lambda_u}, \ell_{\lambda_b}\}$, as well as stoichiometric and emergent stoichiometric cycles, $\{c^\alpha, c^\eta\}$ §§ II D and II E. Steps (ii)–(iv) as above. (v) Identify the emergent stoichiometric cycles affinities, Eq. (124), as well as their corresponding average currents $\sum_\rho \zeta_{\eta, \rho} \langle J_\rho \rangle$, Eq. (128). (vi) The average EP rate follows from Eqs. (171), (172), and the emergent stoichiometric cycles currents and affinities,

$$T \langle \dot{\Sigma} \rangle = -d_t \langle \mathcal{G} \rangle + \langle \dot{W}_d \rangle + \sum_\eta \langle \dot{J}_\eta \rangle, \quad (176)$$

where,

$$\langle \dot{J}_\eta \rangle = \mathcal{A}_\eta \sum_\rho \zeta_{\eta, \rho} \langle J_\rho \rangle, \quad (177)$$

as in Eqs. (130) and (131).

D. Nonequilibrium Landauer's Principle

We can now formulate the nonequilibrium Landauer's principle for the driving and nonconservative work. We have already seen that when the driving is stopped and all forces are turned off, the CRN relaxes to equilibrium by minimizing the nonequilibrium semigrand Gibbs potential. Equation (121) can be thus combined with Eq. (174) to give

$$\langle \dot{W}_d^{irr} \rangle + \sum_{Y_f} \langle \dot{W}_{Y_f}^{nc} \rangle = k_B T d_t \mathcal{D}(p \| p_{eq}) + T \langle \dot{\Sigma} \rangle. \quad (178)$$

where

$$\langle \dot{W}_d^{irr} \rangle := \langle \dot{W}_d \rangle - d_t \sum_{\{L_{\lambda_u}\}} P(\{L_{\lambda_u}\}) G_{eq}(\{L_{\lambda_u}\}), \quad (179)$$

is the *irreversible driving work rate*. We emphasize that this work is gauge invariant, see § VC. Integrating over time, we obtain

$$\langle W_d^{irr} \rangle + \sum_{Y_f} \langle W_{Y_f}^{nc} \rangle = k_B T \Delta \mathcal{D}(p \| p_{eq}) + T \langle \Sigma \rangle. \quad (180)$$

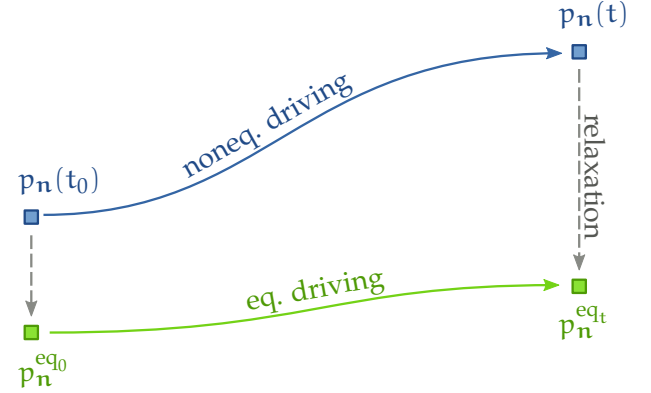


FIG. 7. Pictorial representation of the transformation between two nonequilibrium probability distributions. The nonequilibrium transformation (blue line) is compared with the equilibrium one (green line). The latter is obtained by shutting down the driving and turning off the forces at each time (dashed gray lines).

This fundamental result shows that the minimal cost for transforming a CRN from an arbitrary nonequilibrium state to another is bounded by a difference of relative entropies, as depicted in Fig. 7. The transformation may involve either time-dependent driving, or relaxation to steady states, or both. It generalizes the early result obtained in Refs. [29, 62, 63] to nondetailed balanced CRNs (see also Refs. [54, 64]). For unconditionally detailed-balanced CRNs, we recover the result first obtained in Ref. [26] for deterministic CRNs: $\langle W_d^{irr} \rangle = k_B T \Delta \mathcal{D}(p \| p_{eq}) + T \langle \Sigma \rangle$.

Remark To obtain the Landauer's principle for $\langle \dot{W}_d \rangle$ and $\langle \dot{W}_{Y_f}^{nc} \rangle$, the equilibrium states of the open CRN have been used as reference states, see Fig. 7. Alternatively, one could use the equilibrium states of the closed CRN, which are obtained by shutting down all exchange reactions. If one does so and uses Eq. (170), an analogous Landauer's principle for the chemical work can be derived,

$$\langle W_c^{irr} \rangle = k_B T \Delta \mathcal{D}(p \| p_{eq}) + T \langle \Sigma \rangle, \quad (181)$$

where

$$\langle W_c^{irr} \rangle := \langle W_c \rangle - \Delta \left[\sum_{\{L_\lambda\}} P(\{L_\lambda\}) G_{eq}(\{L_\lambda\}) \right], \quad (182)$$

is the irreversible chemical work. The traditional thermodynamic work relation $\langle W_c^{irr} \rangle \geq 0$ is recovered for processes whose initial and final condition are equilibrium states.

E. Connection with Deterministic Descriptions

For CRNs with very abundant populations of species, a deterministic dynamical description in terms of non-

linear rate equations is justified. The corresponding nonequilibrium thermodynamics was analyzed in Ref. [26], where the counterparts of Eqs. (164), (170), and (104), can be found. Following a procedure similar to that described in this paper, one can also formulate the deterministic analog of the EP decomposition (174).

One can also recover the deterministic thermodynamic description from the stochastic one by performing the limit $n \gg 1$ and assuming that $p_n \simeq \delta_{n,N}$, *i.e.* the distribution is very peaked around the population that is solution of the rate equations, \mathbf{N} , see App. A.

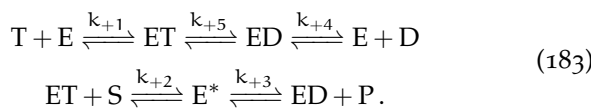
We thus conclude with two remarks.

Remark Not all results valid for stochastic CRNs hold for the deterministic ones. An example is provided by the *adiabatic–nonadiabatic EP decomposition* introduced in Ref. [65] for generic stochastic processes: it is valid for deterministic CRNs only for *complex-balanced* CRNs, see Refs. [26, 66].

Remark As briefly mentioned in § II A, there is an alternative way of modeling open CRNs in which the exchanged species \mathbf{y} are treated as particle *reservoir* with very large population. All main results of our paper—*i.e.* the EP decomposition (101), the finite-time detailed FT (156), and the Landauer’s principle (180)—still hold. The only difference lies in the fact that the different definitions of stoichiometric matrices, Eq. (6), also entail slightly different definitions of broken conservation law. Besides that, the recipe described in § VII B can be followed in the same way.

VIII. APPLICATION

We now illustrate our EP decompositions (101) and (130) on a CRN displaying more than one fundamental force, which thus allows us to introduce the phenomenology of free energy transduction. We consider the following active catalytic mechanism



It describes the T-driven catalysis of S into P, having D as a byproduct, see Fig. 8. All substrates and products are regarded as exchanged species,

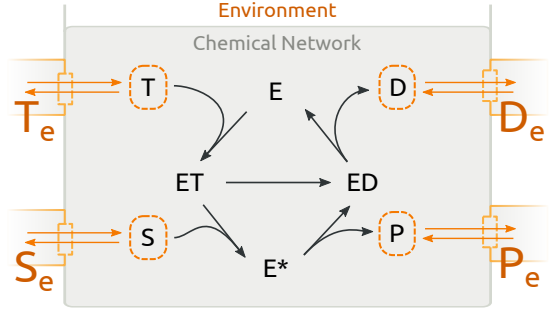
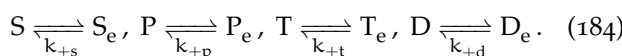


FIG. 8. Pictorial illustration of the open CRN in Eqs. (183) and (184), from which one can see the more clearly the active catalytic mechanism.

The stoichiometric matrix of the open CRN reads

$$\begin{array}{c|ccccc|ccccc} & +1 & +2 & +3 & +4 & +5 & +s & +p & +t & +d \\ \hline E & -1 & 0 & 0 & 1 & 0 & 0 & 0 & 0 & 0 \\ ET & 1 & -1 & 0 & 0 & -1 & 0 & 0 & 0 & 0 \\ E^* & 0 & 1 & -1 & 0 & 0 & 0 & 0 & 0 & 0 \\ ED & 0 & 0 & 1 & -1 & 1 & 0 & 0 & 0 & 0 \\ S & 0 & -1 & 0 & 0 & 0 & 1 & 0 & 0 & 0 \\ P & 0 & 0 & 1 & 0 & 0 & 0 & 1 & 0 & 0 \\ T & -1 & 0 & 0 & 0 & 0 & 0 & 0 & 1 & 0 \\ D & 0 & 0 & 0 & 1 & 0 & 0 & 0 & 0 & 1 \\ \hline S_e & 0 & 0 & 0 & 0 & 0 & -1 & 0 & 0 & 0 \\ P_e & 0 & 0 & 0 & 0 & 0 & 0 & -1 & 0 & 0 \\ T_e & 0 & 0 & 0 & 0 & 0 & 0 & 0 & -1 & 0 \\ D_e & 0 & 0 & 0 & 0 & 0 & 0 & 0 & 0 & -1 \end{array}, \quad (185)$$

in which the stoichiometric matrix of the closed CRN is highlighted.

We now follow the recipe described in § VII, and characterize all terms of Eq. (101). (i) The closed CRN has three independent conservation laws:

$$\ell_E = (1 \ 1 \ 1 \ 1 \ 0 \ 0 \ 0 \ 0 \ 0 \ 0 \ 0 \ 0), \quad (186a)$$

$$\ell_S = (0 \ 0 \ 1 \ 0 \ 1 \ 1 \ 0 \ 0 \ 1 \ 1 \ 0 \ 0), \quad (186b)$$

$$\ell_T = (0 \ 1 \ 1 \ 1 \ 0 \ 0 \ 1 \ 1 \ 0 \ 0 \ 1 \ 1). \quad (186c)$$

The first corresponds to the enzyme moiety and it is unbroken in the open CRN. In contrast, the last two correspond to the moieties S–P and T–D, which are broken in the open CRN. (ii) We choose S_e and T_e as chemostatted species \mathbf{Y}_p , since the entries of ℓ_S and ℓ_T corresponding to these species identify a nonsingular matrix—it is an identity matrix. (iii) The moieties population vector reads

$$\mathbf{M}_n^{Y_p} = \frac{S_e}{T_e} \begin{pmatrix} n_{E^*} + n_S + n_P \\ n_{ET} + n_{E^*} + n_{ED} + n_T + n_D \end{pmatrix}, \quad (187)$$

from which the semigrand Gibbs potential \mathcal{G} follows, Eqs. (102) and (171). (iv) The driving work rate follows from the scalar product of the vector above and

$$-\partial_t \mu_{Y_p} = \frac{S_e}{T_e} \begin{pmatrix} -\partial_t \mu_{S_e} \\ -\partial_t \mu_{T_e} \end{pmatrix}, \quad (188)$$

Eqs. (100) and (172). (v) The chemostatted species P_e and D_e form the set Y_f and determine the fundamental forces,

$$\mathcal{F}_{Y_f} = \begin{pmatrix} \mathcal{F}_{P_e} \\ \mathcal{F}_{D_e} \end{pmatrix} = \begin{pmatrix} P_e \\ D_e \end{pmatrix} \begin{pmatrix} \mu_{P_e} - \mu_{S_e} \\ \mu_{D_e} - \mu_{T_e} \end{pmatrix}, \quad (189)$$

Eq. (92). Together with the instantaneous external currents

$$I_{Y_f} = \begin{pmatrix} I_{P_e} \\ I_{D_e} \end{pmatrix} = \begin{pmatrix} P_e \\ D_e \end{pmatrix} \begin{pmatrix} J_{+p} - J_{-p} \\ J_{+d} - J_{-d} \end{pmatrix}, \quad (190)$$

they identify the nonconservative contributions, Eq. (98). The first one, $\mathcal{F}_{P_e} I_{P_e}$, characterizes the work spent to convert S into P , while the second, $\mathcal{F}_{D_e} I_{D_e}$, that due to the consumption of T . The sum of these terms and the driving work integrated over time contribute to the EP as in Eq. (101).

The similar EP decomposition written in terms of nonconservative contributions along stoichiometric cycles follows when these latter are identified. The kernel of stoichiometric matrix of the closed CRN is empty, while that of the open is spanned by

$$c_1^T = \begin{pmatrix} +1 & +2 & +3 & +4 & +5 & +s & +p & +t & +d \\ 1 & 0 & 0 & 1 & 1 & 0 & 0 & 1 & -1 \end{pmatrix}, \quad (191a)$$

$$c_2^T = \begin{pmatrix} +1 & +2 & +3 & +4 & +5 & +s & +p & +t & +d \\ 1 & 1 & 1 & 1 & 0 & 1 & -1 & 1 & -1 \end{pmatrix}, \quad (191b)$$

which are regarded as emergent stoichiometric cycles. Along the first, the enzyme converts one molecule of T into one of D , while for the second it processes T and S and produces D and P ,

$$C_1^T = \begin{pmatrix} S_e & P_e & T_e & D_e \\ 0 & 0 & 1 & -1 \end{pmatrix}, \quad (192a)$$

$$C_2^T = \begin{pmatrix} S_e & P_e & T_e & D_e \\ 1 & -1 & 1 & -1 \end{pmatrix}. \quad (192b)$$

At this point we can proceed from step (v) and determine the affinities,

$$\mathcal{A}_1 = \mu_{T_e} - \mu_{D_e} \quad (193a)$$

$$\mathcal{A}_2 = \mu_{T_e} + \mu_{S_e} - \mu_{D_e} - \mu_{P_e}, \quad (193b)$$

as well as the related instantaneous reaction currents,

$$\mathcal{J}_1 = J_{+p} - J_{-p} - J_{+d} - J_{-d} \quad (194a)$$

$$\mathcal{J}_2 = J_{-p} - J_{+p}. \quad (194b)$$

The nonconservative work follows from the products $\mathcal{A}_1 \mathcal{J}_1$ and $\mathcal{A}_2 \mathcal{J}_2$, and the decomposition in Eq. (130) can be thus expressed. The former characterizes the dissipation due to the futile consumption of T , since S is not converted into P . The latter, instead, is the work spent to convert T and S into D and P .

This system can be used to illustrate free energy transduction when one considers the autonomous regime where $\mathcal{F}_{D_e} < 0$, $\mathcal{F}_{P_e} > 0$, but $\langle \dot{W}_{D_e}^{nc} \rangle > -\langle \dot{W}_{P_e}^{nc} \rangle > 0$. Namely, the external current of P_e flows towards the chemostat, $\langle I_{P_e} \rangle < 0$ (P_e produced), despite the fact that its force is positive, $\mathcal{F}_{P_e} > 0$. This can happen thanks to the free energy provided by the conversion of T_e into D_e , $\langle \dot{W}_{D_e}^{nc} \rangle > 0$. In Fig. 9 we illustrate the behavior of the average external currents and work contributions as function of time when the transducer in Fig. 8 is smoothly switched from a nontransducing regime to a transduction one. At early times, $\mathcal{F}_{D_e} = 0$, $\mathcal{F}_{P_e} > 0$, and one observes only a consumption of P_e : $\langle I_{P_e} \rangle > 0$ and $\langle I_{D_e} \rangle \simeq 0$ (respectively, orange and blue curves in Fig. 9a). Consequently, the nonconservative work contributions are $\langle \dot{W}_{P_e}^{nc} \rangle > 0$ and $\langle \dot{W}_{D_e}^{nc} \rangle = 0$ (respectively, orange and blue curves in Fig. 9b). In contrast, when the *motive* fundamental force \mathcal{F}_{D_e} is switched on (at large times), the current $\langle I_{P_e} \rangle$ turns negative whereas the *motive* current $\langle I_{P_e} \rangle$ aligns itself with its corresponding force. We thus observe $\langle \dot{W}_{D_e}^{nc} \rangle > -\langle \dot{W}_{P_e}^{nc} \rangle > 0$. At intermediate times, driving work is extracted following the smooth increase of the *motive* force (green curve in Fig. 9b).

IX. CONCLUSIONS AND PERSPECTIVES

In this paper we presented a thorough description of nonequilibrium thermodynamics of stochastic CRNs. The fundamental results of traditional irreversible chemical thermodynamics (*viz.* enthalpy and entropy balance) are formulated at the level of single trajectories, Eqs. (60) and (71). By making use of the CRN topology and by identifying conservation laws we decompose the EP into two fundamental work contributions and a semigrand potential difference, Eqs. (101) and (174). The driving work describes the thermodynamic cost of manipulating the CRN by changing the chemical potentials of its chemostats. Instead, the nonconservative work quantifies the cost of sustaining chemical currents through the CRN. These currents prevent the CRN from reaching equilibrium, but when the related fundamental forces vanish (and the chemical potentials of the reservoirs are kept constant in time), the CRN relaxes to equilibrium by minimizing the semigrand Gibbs potential. We elucidate the relationship between this thermodynamic potential and the dynamical potentials used in chemical reaction network theory. Our EP decomposition written

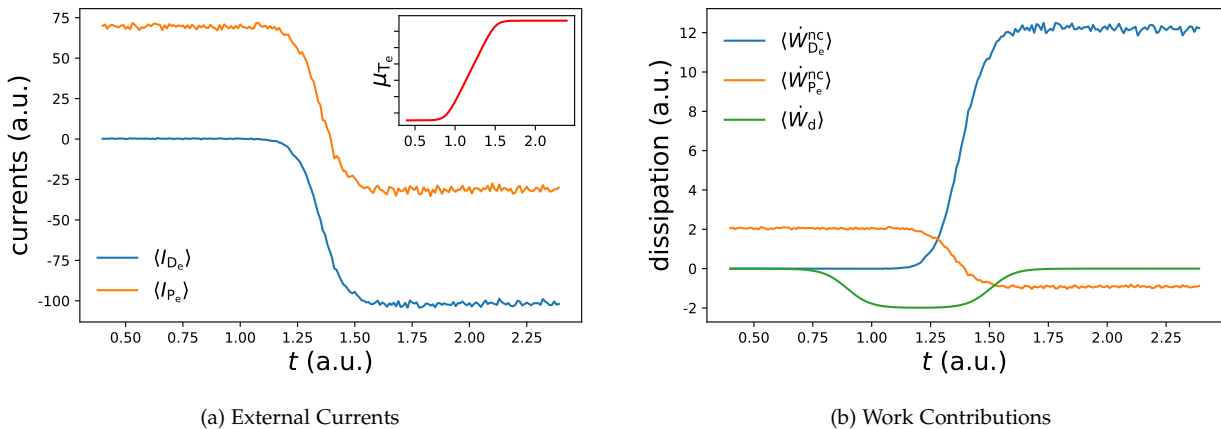


FIG. 9. (a) average external currents and (b) average work rates *vs.* time, for the CRN in Fig. 8. The plots are obtained using 10^4 trajectories generated via the stochastic simulation algorithm. To simplify the illustration, all substrate and products are treated as chemostatted species. The concentrations of S_e , P_e , and D_e are kept constant $[S_e] = 10$, $[P_e] = 70$, and $[D_e] = 10$ whereas that of T_e increases according to a logistic function: $[T_e] = [T_e]_{\max}/(1 + \exp\{-\kappa(t - t_0)\})$ $[T_e]_{\max} = 200$, $\kappa = 20$, $t_0 = 1.5$. This mimics the process in which the force that sustain the active catalysis, \mathcal{F}_{D_e} , is switched on from 0 to a finite value after t_0 . The change of chemical potential μ_{T_e} is plotted in red in the inset. The choice of the rate constants is as follows: $k_{+1} = 10^3$; $k_{+2} = 10^3$; $k_{+3} = 10^3$; $k_{+4} = 10^3$; $k_{+5} = 10^2$; whereas the backward rates are obtained by means of Eq. (52) using the following values for the standard state chemical potentials: $\mu_E^\circ = 1$; $\mu_{ET}^\circ = 3$; $\mu_{ED}^\circ = 2$; $\mu_{S_e}^\circ = 1$; $\mu_{P_e}^\circ = 2$; $\mu_{T_e}^\circ = 10$; $\mu_{D_e}^\circ = 1$. Since reactions are unimolecular the constant term $-k_B T \ln[s]$ is ignored. Finally, $k_B T = 1$ and the value of the enzyme moiety is $L_E = 10$.

in terms of stoichiometric cycles affinities generalizes previous decompositions formulated for linear CRNs or steady-state dynamics.

Two detailed FTs follow from our EP decompositions, Eqs. (156) and (162). They are valid at any time and entirely expressed in terms of physical quantities. Hence, they offer the possibility of validating experimentally our findings, and, from a wider perspective, of validating the foundations of stochastic thermodynamics beyond electronic devices or colloidal particles [67, 68]. Finally, we derive a nonequilibrium Landauer's principle for the work contributions, Eq. (180), which quantifies the minimum thermodynamic cost involved in transformations between arbitrary nonequilibrium states. In contrast to early formulations of the latter principle, we consider not only the cost of external manipulations, but also that related to sustained currents across the system.

Our EP decomposition identifies the fundamental dissipative contributions in CRNs of arbitrary complexity, and it can be thus used to analyze free energy conversion in CRNs beyond single biocatalysts, molecular motors, or sensory systems, which are usually described by linear CRNs [69–72]. The nonconservative work contributions capture Hill's idea of free energy transduction and extend it to nonlinear CRNs with an arbitrary number of chemical forces. [As illustrated in § VIII, transduction occurs whenever one contribution becomes negative, thus requiring the other ones to be positive and larger than the former in absolute value by virtue

of the second law of thermodynamics.] In turn, the driving work contribution allows to generalize transduction to CRNs with reservoirs externally controlled in time. Hence, our framework can be used to analyze pumping in CRNs [73, 74], namely mechanisms whose periodic external control sustains a chemical current against its spontaneous direction.

In biochemical information-handling systems [71, 75, 76] and chemical computing [77–79], information is stored and processed at the molecular level. Early applications of the nonequilibrium Landauer's principle proved successful for characterizing the thermodynamic cost of information processing in simple mechanisms [80, 81]. Our generalization of the work principle could be thus used to analyze biochemical information-handling systems of far greater complexity. This endeavor is important in the light of the current understanding that biological systems have developed by optimizing the gathering and representation of information [82, 83].

Noise is known to play an important role in many biochemical processes. Since a complete stochastic description remains both analytically and computationally demanding, developing hybrid stochastic–deterministic descriptions would be of great importance [26, 84, 85]. Also, many of these processes are regulated by enzymes, thus extending the present theory beyond mass-action kinetics, as already done for deterministic CRNs [86], is also necessary.

ACKNOWLEDGMENTS

R.R. warmly thanks A. Wachtel, A. Lazarescu and M. Polettini for valuable discussions. This work was funded by the National Research Fund of Luxembourg (AFR PhD Grant 2014-2, No. 9114110) and the European Research Council project NanoThermo (ERC-2015-CoG Agreement No. 681456).

Appendix A: Thermodynamic Potentials

Using equilibrium statistical mechanics, we derive the equilibrium Gibbs free energy of a CRN in a given state \mathbf{n} . We refer the reader to Refs. [87–89] for similar approaches.

We regard the reacting species, labelled by $\sigma = 1, \dots, N_z$, as solutes of an ideal dilute solution in a closed vessel. Since the solvent, s , is much more abundant than the solutes, $n_s \gg \sum_\sigma n_\sigma$. As in ideal solutions, interactions among solutes are negligible, and the partition function of the whole solution $\Omega(T, \mathbf{n}, n_s)$ can be written as the product of single species partition functions, $\mathbf{q} \equiv \{q_\sigma(T)\}$ and q_s , [87, Ch. 9],

$$\Omega(T, \mathbf{n}, n_s) = \frac{(n_s + \sum_\sigma n_\sigma)!}{n_s! \prod_\sigma n_\sigma!} q_s(n_s) \prod_\sigma q_\sigma^{n_\sigma}. \quad (\text{A1})$$

$\mathbf{q} \equiv \{q_\sigma(T)\}$ depends on temperature and on solutes–solvent interactions. The combinatorial term counts the different distinguishable configurations of molecules, and can be approximated as

$$\frac{(n_s + \sum_\sigma n_\sigma)!}{n_s! \prod_\sigma n_\sigma!} \simeq \prod_\sigma \frac{n_s^{n_\sigma}}{n_\sigma!} \equiv \frac{n_s^\mathbf{n}}{\mathbf{n}!} \quad (\text{A2})$$

using Stirling’s formula and the high relative abundance of the solvent. Using Eq. (A1), the *Gibbs free energy* of a given state \mathbf{n} is thus given by

$$\begin{aligned} g_{\mathbf{n}} &= -k_B T \ln \Omega(T, \mathbf{n}, n_s) \\ &= (\mu^\circ - 1k_B T \ln n_s) \cdot \mathbf{n} + k_B T \ln \mathbf{n}! + g_s, \end{aligned} \quad (\text{A3})$$

where

$$\mu^\circ := -k_B T \ln \mathbf{q} \quad (\text{A4})$$

can be identified as *standard chemical potentials*. Since the contribution deriving from the solvent, $g_s :=$

$-k_B T \ln q_s(n_s)$, is constant, it can be set to zero without loss of generality. Hence, the Gibbs free energy changes along internal reactions are

$$\begin{aligned} \Delta_{\rho_i} g &= g_{\mathbf{n} + \mathbf{S}_{\rho_i}} - g_{\mathbf{n}} \\ &= (\mu^\circ - 1k_B T \ln n_s) \cdot \mathbf{S}_{\rho_i} + k_B T \ln \{(\mathbf{n} + \mathbf{S}_{\rho_i})! / \mathbf{n}!\}. \end{aligned} \quad (\text{A5})$$

Thermodynamic Limit For $V \gg 1$, $\mathbf{n} \gg 1$, and finite $[\mathbf{z}] = \mathbf{n}/V$, the Gibbs potential (A3) becomes

$$g_{\mathbf{n}}/V \simeq \mu \cdot [\mathbf{z}] - k_B T [\mathbf{z}] \cdot \mathbf{1}, \quad (\text{A6})$$

where

$$\mu = \mu^\circ + k_B T \ln \{[\mathbf{z}] / [\mathbf{s}]\} \quad (\text{A7})$$

are the *chemical potentials* of solutes in an ideal dilute solution, and $[\mathbf{s}] = n_s/V$ is the concentration of solvent. We thus recover the Gibbs free energy density of ideal dilute solutions, see *e.g.* [47, 90].

When applying the same limit to the Gibbs free energy differences, Eq. (A5), we recover the *Gibbs free energies of reaction*,

$$\Delta_{\rho_i} g \simeq \mu \cdot \mathbf{S}_{\rho_i}. \quad (\text{A8})$$

This result also justifies the form of the second term in the local detailed balance of exchange reactions, Eq. (53).

Summarizing, $g_{\mathbf{n}}$ given in Eq. (A3) characterizes the free energy of each CRN state. In the thermodynamic limit, the traditional potentials of ideal dilute solutions are recovered.

Appendix B: Proofs of Detailed Fluctuation Theorems

To prove the finite time detailed FTs (156) we use a moment generating functions and change the notation in favor of a bracket one using operators.

Let $P_t(\mathbf{n}, W_d, \{W_{y_f}^{nc}\})$ be the joint probability of observing a trajectory ending in the state \mathbf{n} along which the driving work is W_d while the nonconservative contributions are $\{W_{y_f}^{nc}\}$. These probabilities, one for each \mathbf{n} , are stacked in the ket $|P_t(W_d, \{W_{y_f}^{nc}\})\rangle$. The time evolution of their moment generating function,

$$|\Lambda_t(\xi_d, \{\xi_{y_f}\})\rangle := \int dW_d \prod_{y_f} dW_{y_f}^{nc} \exp \left\{ -\xi_d W_d - \sum_{y_f} \xi_{y_f} W_{y_f}^{nc} \right\} |P_t(W_d, \{W_{y_f}^{nc}\})\rangle, \quad (\text{B1})$$

is ruled by the biased stochastic dynamics

$$dt |\Lambda_t(\xi_d, \{\xi_{y_f}\})\rangle = \mathcal{W}_t(\xi_d, \{\xi_{y_f}\}) |\Lambda_t(\xi_d, \{\xi_{y_f}\})\rangle, \quad (\text{B2})$$

where the entries of the biased generator are given by

$$\mathcal{W}_{mn,t}(\xi_d, \{\xi_{y_f}\}) = \sum_\rho w_\rho(n) \left\{ \exp \left\{ -\sum_{y_f} \xi_{y_f} \mathcal{F}_{y_f}(-S_\rho^{y_f}) \right\} \delta_{m,n+s_\rho} - \delta_{m,n} \right\} - \xi_d \partial_t g_m \delta_{n,m}. \quad (\text{B3})$$

We denoted the entries of $S_\rho^{y_f}$ as $\{S_\rho^{y_f}\}$. As a consequence of the local detailed balance (93), the stochastic generator satisfies the following symmetry

$$\mathcal{W}_t^T(\xi_d, \{\xi_{y_f}\}) = \mathcal{B}_t^{-1} \mathcal{W}_t(\xi_d, \{1 - \xi_{y_f}\}) \mathcal{B}_t, \quad (\text{B4})$$

where the entries of \mathcal{B}_t are given by

$$\mathcal{B}_{nm,t} := \exp \{-\beta g_m(t)\} \delta_{n,m}. \quad (\text{B5})$$

Introducing the partition function for the generic equilibrium state identified by the protocol at time τ , $\mathcal{Z}_\tau \equiv \mathcal{Z}(\pi_\tau, \{L_{\lambda_u}\}) = \exp\{-\beta \mathcal{G}_{eq_\tau}\}$, the initial condition can be written as

$$|\Lambda_0(\xi_d, \{\xi_{y_f}\})\rangle = |\mathbf{p}_{eq_0}\rangle = \mathcal{B}_0/\mathcal{Z}_0 |1\rangle. \quad (\text{B6})$$

The ket $|1\rangle$ refers to the vector in the state space whose entries are all equal to one.

In order to proceed further, it is convenient to first prove a preliminary result. Let us consider the generic biased dynamics, *e.g.* Eq. (B2),

$$d_t |\Lambda_t(\xi)\rangle = \mathcal{W}_t(\xi) |\Lambda_t(\xi)\rangle, \quad (\text{B7})$$

whose initial condition is $|\Lambda_0(\xi)\rangle = |\mathbf{p}(0)\rangle$. A formal solution of Eq. (B7) is $|\Lambda_t(\xi)\rangle = \mathcal{U}_t(\xi) |\mathbf{p}(0)\rangle$, where the time-evolution operator reads $\mathcal{U}_t(\xi) = \mathcal{T}_+ \exp \left\{ \int_0^t d\tau \mathcal{W}_\tau(\xi) \right\}$, \mathcal{T}_+ being the time-ordering operator. We clearly have $d_t \mathcal{U}_t(\xi) = \mathcal{W}_t(\xi) \mathcal{U}_t(\xi)$. Let us now consider the following transformed evolution operator

$$\tilde{\mathcal{U}}_t(\xi) := \mathcal{X}_t^{-1} \mathcal{U}_t(\xi) \mathcal{X}_0, \quad (\text{B8})$$

\mathcal{X}_t being a generic invertible operator. Its dynamics is ruled by the following biased stochastic dynamics

$$d_t \tilde{\mathcal{U}}_t(\xi) = d_t \mathcal{X}_t^{-1} \mathcal{U}_t(\xi) \mathcal{X}_0 + \mathcal{X}_t^{-1} d_t \mathcal{U}_t(\xi) \mathcal{X}_0 = \left\{ d_t \mathcal{X}_t^{-1} \mathcal{X}_t + \mathcal{X}_t^{-1} \mathcal{W}_t(\xi) \mathcal{X}_t \right\} \tilde{\mathcal{U}}_t(\xi) \equiv \tilde{\mathcal{W}}_t(\xi) \tilde{\mathcal{U}}_t(\xi), \quad (\text{B9})$$

which allows us to conclude that the transformed time-evolution operator is given by

$$\tilde{\mathcal{U}}(\xi) = \mathcal{T}_+ \exp \left\{ \int_0^t d\tau \tilde{\mathcal{W}}_\tau(\xi) \right\}. \quad (\text{B10})$$

From Eqs. (B8), (B9) and (B10) we deduce that

$$\mathcal{X}_t^{-1} \mathcal{U}_t(\xi) \mathcal{X}_0 = \mathcal{T}_+ \exp \left\{ \int_0^t d\tau \left[d_\tau \mathcal{X}_\tau^{-1} \mathcal{X}_\tau + \mathcal{X}_\tau^{-1} \mathcal{W}_\tau(\xi) \mathcal{X}_\tau \right] \right\}. \quad (\text{B11})$$

We can now come back to our specific biased stochastic dynamics (B2). The moment generating function of $P_t(W_d, \{W_{y_f}^{nc}\})$ is given by

$$\Lambda_t(\xi_d, \{\xi_{y_f}\}) = \langle 1 | \Lambda_t(\xi_d, \{\xi_{y_f}\}) \rangle = \langle 1 | \mathcal{U}_t(\xi_d, \{\xi_{y_f}\}) \mathcal{B}_0/\mathcal{Z}_0 | 1 \rangle = \langle 1 | \frac{\mathcal{B}_t}{\mathcal{Z}_t} \mathcal{B}_t^{-1} \mathcal{U}_t(\xi_d, \{\xi_{y_f}\}) \mathcal{B}_0 | 1 \rangle \frac{\mathcal{Z}_t}{\mathcal{Z}_0}, \quad (\text{B12})$$

where $\mathcal{U}_t(\xi_d, \{\xi_{y_f}\})$ is the time-evolution operator of the biased stochastic dynamics (B2). Note that $\langle 1 | \mathcal{B}_t/\mathcal{Z}_t$ is the equilibrium initial distribution of the backward process $\langle \mathbf{p}_{eq_t} |$. Using the relation in Eq. (B11), the last term can be rewritten as

$$= \langle \mathbf{p}_{eq_t} | \mathcal{T}_+ \exp \left\{ \int_0^t d\tau \left[\partial_\tau \mathcal{B}_\tau^{-1} \mathcal{B}_\tau + \mathcal{B}_\tau^{-1} \mathcal{W}_\tau(\xi_d, \{\xi_{y_f}\}) \mathcal{B}_\tau \right] \right\} | 1 \rangle \exp \{ -\beta \Delta \mathcal{G}_{eq} \}, \quad (\text{B13})$$

where $\Delta\mathcal{G}_{\text{eq}}$ is defined in Eq. (157). Since $\partial_\tau \mathcal{B}_\tau^{-1} \mathcal{B}_\tau = \text{diag}\{\partial_\tau g_n\}$ the first term in square bracket can be added to the diagonal entries of the second term, thus giving

$$= \langle p_{\text{eq}_t} | \mathcal{T}_+ \exp \left\{ \int_0^t d\tau \left[\mathcal{B}_\tau^{-1} \mathcal{W}_\tau(\xi_d - 1, \{\xi_{y_f}\}) \mathcal{B}_\tau \right] \right\} | 1 \rangle \exp \{-\beta \Delta \mathcal{G}_{\text{eq}}\}. \quad (\text{B14})$$

The symmetry (B4) allow us to recast the latter into

$$= \langle p_{\text{eq}_t} | \mathcal{T}_+ \exp \left\{ \int_0^t d\tau \mathcal{W}_\tau^T(\xi_d - 1, \{1 - \xi_{y_f}\}) \right\} | 1 \rangle \exp \{-\beta \Delta \mathcal{G}_{\text{eq}}\}. \quad (\text{B15})$$

The crucial step comes as we transform the integration variable from τ to $\tau^\dagger = t - \tau$. Accordingly, the time-ordering operator, \mathcal{T}_+ , becomes an anti-time-ordering one \mathcal{T}_- , while the diagonal entries of the biased generator become

$$\mathcal{W}_{\mathbf{m}, \mathbf{m}, t - \tau^\dagger}(\xi_d, \{\xi_{y_f}\}) = \sum_\rho w_\rho(\mathbf{m}, t - \tau^\dagger) + \xi_d \partial_{\tau^\dagger} g_{\mathbf{m}}(t - \tau^\dagger) \quad (\text{B16})$$

from which we conclude that

$$\mathcal{W}_{\mathbf{n}, \mathbf{m}, t - \tau^\dagger}(\xi_d, \{\xi_{y_f}\}) = \mathcal{W}_{\mathbf{n}, \mathbf{m}, t - \tau^\dagger}(-\xi_d, \{\xi_{y_f}\}) =: \mathcal{W}_{\mathbf{n}, \mathbf{m}, \tau^\dagger}^\dagger(-\xi_d, \{\xi_{y_f}\}). \quad (\text{B17})$$

$\mathcal{W}_{\tau^\dagger}^\dagger(\xi_d, \{\xi_{y_f}\})$ is the biased generator of the dynamics subject to the time-reversed protocol, π^\dagger , *i.e.* the dynamics of the backward process. Equation (B15) thus becomes

$$= \langle p_{\text{eq}_t} | \mathcal{T}_- \exp \left\{ \int_0^t d\tau^\dagger \mathcal{W}_{\tau^\dagger}^\dagger(1 - \xi_d, \{1 - \xi_{y_f}\}) \right\} | 1 \rangle \exp \{-\beta \Delta \mathcal{G}_{\text{eq}}\}. \quad (\text{B18})$$

Upon a global transposition, we can write

$$= \langle 1 | \mathcal{T}_+ \exp \left\{ \int_0^t d\tau^\dagger \mathcal{W}_{\tau^\dagger}^\dagger(1 - \xi_d, \{1 - \xi_{y_f}\}) \right\} | p_{\text{eq}_t} \rangle \exp \{-\beta \Delta \mathcal{G}_{\text{eq}}\}, \quad (\text{B19})$$

where we also used the relationship between transposition and time-ordering

$$\mathcal{T}_+ \left(\prod_i A_{t_i}^T \right) = (\mathcal{T}_- \prod_i A_{t_i})^T, \quad (\text{B20})$$

in which A_t is a generic operator. From the last expression, we readily obtain

$$\begin{aligned} &= \langle 1 | \mathcal{U}_t^\dagger(1 - \xi_d, \{1 - \xi_{y_f}\}) | p_{\text{eq}_t} \rangle \exp \{-\beta \Delta \mathcal{G}_{\text{eq}}\} \\ &= \Lambda_t^\dagger(1 - \xi_d, \{1 - \xi_{y_f}\}) \exp \{-\beta \Delta \mathcal{G}_{\text{eq}}\}, \end{aligned} \quad (\text{B21})$$

where $\Lambda_t^\dagger(\xi_d, \{\xi_{y_f}\})$ is the moment generating function of $P_t^\dagger(W_d, \{W_{y_f}^{\text{nc}}\})$. Summarizing, we have the following symmetry

$$\Lambda_t(\xi_d, \{\xi_{y_f}\}) = \Lambda_t^\dagger(1 - \xi_d, \{1 - \xi_{y_f}\}) \exp \{-\beta \Delta \mathcal{G}_{\text{eq}}\}, \quad (\text{B22})$$

whose inverse Laplace transform gives the FT in Eq. (156).

Fluctuation Theorem for Emergent Stoichiometric Cycles Currents

The finite-time detailed FT for nonconservative contributions along fundamental cycles, Eq. (162), follows the same logic and mathematical steps described above. The moment generating function which now must be taken into account is

$$|\Lambda_t(\xi_d, \{\xi_\eta\})\rangle := \int dW_d \prod_\eta d\Gamma_\eta \exp \left\{ -\xi_d W_d - \sum_\eta \xi_\eta \Gamma_\eta \right\} |P_t(W_d, \{\Gamma_\eta\})\rangle, \quad (\text{B23})$$

which is ruled by the biased generator whose entries are

$$\mathcal{W}_{mn,t}(\xi_d, \{\xi_\eta\}) = \sum_\rho w_\rho(n) \left\{ \exp \left\{ -\sum_\eta \xi_\eta \mathcal{A}_\eta \zeta_{\eta,\rho} \right\} \delta_{m,n+s_\rho} - \delta_{m,n} \right\} - \xi_d \partial_t g_m \delta_{n,m}. \quad (\text{B24})$$

The symmetry of the latter generator—on top of which the proof is constructed—is based on the expression of the local detailed balance given in Eq. (93),

$$\mathcal{W}_t^T(\xi_d, \{\xi_\eta\}) = \mathcal{B}_t^{-1} \mathcal{W}_t(\xi_d, \{1 - \xi_\eta\}) \mathcal{B}_t, \quad (\text{B25})$$

where the entries of \mathcal{B}_t are given in Eq. (B5). Following the steps from Eq. (B12) to Eq. (B22), with the definitions and equations in Eqs. (B23)–(B25), proves the FT in Eq. (162).

[1] T. L. Hill, *Free energy transduction in biology* (Academic Press, New York, 1977).

[2] T. L. Hill, *Free Energy Transduction and Biochemical Cycle Kinetics* (Dover, 2005).

[3] J. Schnakenberg, *Rev. Mod. Phys.* **48**, 571 (1976).

[4] D. A. McQuarrie, *J. Appl. Probab.* **4**, 413 (1967).

[5] D. T. Gillespie, *Physica A* **188**, 404 (1992).

[6] J.-l. Luo, C. Van den Broeck, and G. Nicolis, *Z. Phys. B* **56**, 165 (1984).

[7] C. Y. Mou, J.-l. Luo, and G. Nicolis, *J. Chem. Phys.* **84**, 7011 (1986).

[8] Q. Zheng and J. Ross, *J. Chem. Phys.* **94**, 3644 (1991).

[9] M. O. Vlad and J. Ross, *J. Chem. Phys.* **100**, 7268 (1994).

[10] K. Sekimoto, *Stochastic Energetics*, 1st ed., Lecture Notes in Physics, Vol. 799 (Springer-Verlag Berlin Heidelberg, 2010).

[11] C. Jarzynski, *Annu. Rev. Condens. Matter Phys.* **2**, 329 (2011).

[12] U. Seifert, *Rep. Prog. Phys.* **75**, 126001 (2012).

[13] C. Van den Broeck and M. Esposito, *Physica A* **418**, 6 (2015).

[14] P. Gaspard, *J. Chem. Phys.* **120**, 8898 (2004).

[15] D. Andrieux and P. Gaspard, *J. Chem. Phys.* **121**, 6167 (2004).

[16] D. Andrieux and P. Gaspard, *J. Stat. Phys.* **127**, 107 (2007).

[17] H. Ge and H. Qian, *Phys. Rev. Lett.* **103**, 148103 (2009).

[18] M. Vellela and H. Qian, *J. R. Soc. Interface* **6**, 925 (2009).

[19] H. Qian and L. M. Bishop, *Int. J. Mol. Sci.* **11**, 3472 (2010).

[20] T. Schmiedl and U. Seifert, *J. Chem. Phys.* **126**, 044101 (2007).

[21] F. Horn and R. Jackson, *Arch. Ration. Mech. An.* **47**, 81 (1972).

[22] M. Feinberg, *Arch. Ration. Mech. An.* **49**, 187 (1972).

[23] D. F. Anderson, G. Craciun, and T. G. Kurtz, *Bull. Math. Biol.* **72**, 1947 (2010).

[24] D. Cappelletti and C. Wiuf, *SIAM J. Appl. Math.* **76**, 411 (2016).

[25] M. Polettini and M. Esposito, *J. Chem. Phys.* **141**, 024117 (2014).

[26] R. Rao and M. Esposito, *Phys. Rev. X* **6**, 041064 (2016).

[27] M. Polettini, A. Wachtel, and M. Esposito, *J. Chem. Phys.* **143**, 184103 (2015).

[28] Y. Murashita, K. Funo, and M. Ueda, *Phys. Rev. E* **90**, 042110 (2014).

[29] M. Esposito and C. Van den Broeck, *Europhys. Lett.* **95**, 40004 (2011).

[30] J. M. R. Parrondo, J. M. Horowitz, and T. Sagawa, *Nature Phys.* **11**, 131 (2015).

[31] H. Qian and D. A. Beard, *Biophys. Chem.* **114**, 213 (2005).

[32] G. Nicolis and I. Prigogine, *Self-organization in Nonequilibrium Systems: From Dissipative Structures to Order Through Fluctuations* (Wiley-Blackwell, 1977).

[33] T. G. Kurtz, *J. Chem. Phys.* **57**, 2976 (1972).

[34] D. T. Gillespie, *Ann. Rev. Phys. Chem.* **58**, 35 (2007).

[35] R. A. Alberti, *Thermodynamics of biochemical reactions* (Wiley-Interscience, 2003).

[36] H. S. Haraldsdóttir and R. M. T. Fleming, *PLoS Comput. Biol.* **12**, e1004999 (2016).

[37] D. Kondepudi and I. Prigogine, *Modern Thermodynamics: From Heat Engines to Dissipative Structures*, 2nd ed. (Wiley, 2014), § 15.1. I. Prigogine, *Physica* **15**, 272 (1949).

[38] T. de Donder, *L'affinité*, Mémoires de la Classe des sciences No. vol. 1 (Gauthier-Villars, 1927).

[39] U. Seifert, *Phys. Rev. Lett.* **95**, 040602 (2005).

[40] G. Bochkov and Y. Kuzovlev, *Zh. Eksp. Teor. Fiz.* **72**, 238 (1977).

[41] G. Bochkov and Y. Kuzovlev, *Zh. Eksp. Teor. Fiz.* **76**, 1071 (1979).

[42] C. Jarzynski, *Phys. Rev. Lett.* **78**, 2690 (1997).

[43] J. Horowitz and C. Jarzynski, *J. Stat. Mech. Theor. Exp.* **2007**, P11002 (2007).

[44] P. Krapivsky, S. Redner, and E. Ben-Naim, *A Kinetic View of Statistical Physics* (Cambridge University Press, 2010).

[45] R. Rao, D. Lacoste, and M. Esposito, *J. Chem. Phys.* **143**, 244903 (2015).

[46] D. Andrieux and P. Gaspard, *Proc. Natl. Acad. Sci. U.S.A.* **105**, 9516 (2008).

[47] L. Peliti, *Statistical Mechanics in a Nutshell* (Princeton University Press, 2011), § 3.15.

[48] A. Kolmogoroff, *Math. Ann.* **112**, 155 (1936).

[49] F. P. Kelly, *Reversibility and Stochastic Networks* (John Wiley & Sons Ltd., 1979).

[50] S. Schuster and R. Schuster, *J. Math. Chem.* **3**, 25 (1989).

[51] M. Polettini, *Lett. Math. Phys.* **105**, 89 (2014).

[52] D. Andrieux and P. Gaspard, *J. Stat. Mech. Theor. Exp.* **P02006** (2007).

[53] M. Polettini, G. Bulnes Cuetara, and M. Esposito, *Phys. Rev. E* **94**, 052117 (2016).

[54] R. Rao and M. Esposito, *New J. Phys.* **20**, 023007 (2018).

[55] W. J. Heuett and H. Qian, *J. Chem. Phys.* **124**, 044110 (2006), <https://doi.org/10.1063/1.2165193>.

[56] M. Campisi, P. Hänggi, and P. Talkner, *Rev. Mod. Phys.* **83**, 771 (2011).

[57] G. Bochkov and Y. Kuzovlev, *Physica A* **106**, 443 (1981).

[58] G. Bochkov and Y. Kuzovlev, *Physica A* **106**, 480 (1981).

[59] G. E. Crooks, *J. Stat. Phys.* **90**, 1481 (1998).

[60] G. E. Crooks, *Phys. Rev. E* **60**, 2721 (1999).

[61] G. Bulnes Cuetara, M. Esposito, and A. Imparato, *Phys. Rev. E* **89**, 052119 (2014).

[62] H.-H. Hasegawa, J. Ishikawa, K. Takara, and D. Driebe, *Phys. Lett. A* **374**, 1001 (2010).

[63] K. Takara, H.-H. Hasegawa, and D. Driebe, *Phys. Lett. A* **375**, 88 (2010).

[64] B. Altaner, *J. Phys. A: Math. Theor.* **50**, 454001 (2017).

[65] M. Esposito, U. Harbola, and S. Mukamel, *Phys. Rev. E* **76**, 031132 (2007).

[66] H. Ge and H. Qian, *Chem. Phys.* **472**, 241 (2016).

[67] K. Proesmans, Y. Dreher, M. Gavrilov, J. Bechhoefer, and C. Van den Broeck, *Phys. Rev. X* **6**, 041010 (2016).

[68] S. Ciliberto, *Phys. Rev. X* **7**, 021051 (2017).

[69] U. Seifert, *Eur. Phys. J. E* **34**, 26 (2011).

[70] R. Rao and L. Peliti, *J. Stat. Mech. Theor. Exp.* , P06001 (2015).

[71] S. Bo, M. Del Giudice, and A. Celani, *J. Stat. Mech. Theor. Exp.* , P01014 (2015).

[72] B. Altaner, A. Wachtel, and J. Vollmer, *Phys. Rev. E* **92**, 042133 (2015).

[73] R. D. Astumian, *Annu. Rev. Biophys.* **40**, 289 (2011).

[74] M. Esposito and J. M. R. Parrondo, *Phys. Rev. E* **91** (2015), [10.1103/physreve.91.052114](https://doi.org/10.1103/physreve.91.052114).

[75] J. M. Horowitz and M. Esposito, *Phys. Rev. X* **4**, 031015 (2014).

[76] T. E. Ouldridge, C. C. Govern, and P. R. ten Wolde, *Phys. Rev. X* **7**, 021004 (2017).

[77] D. Soloveichik, M. Cook, E. Winfree, and J. Bruck, *Nat. Comp.* **7**, 615 (2008).

[78] A. Murugan, Z. Zeravcic, M. P. Brenner, and S. Leibler, *Proc. Natl. Acad. Sci. U.S.A.* **112**, 54 (2015).

[79] W. Poole, A. Ortiz-Muñoz, A. Behera, N. S. Jones, T. E. Ouldridge, E. Winfree, and M. Gopalkrishnan, in *DNA Computing and Molecular Programming*, edited by R. Brijder and L. Qian (Springer, Cham, 2017) pp. 210–231.

[80] P. Sartori and S. Pigolotti, *Phys. Rev. X* **5**, 041039 (2015).

[81] T. E. Ouldridge and P. R. ten Wolde, *Phys. Rev. Lett.* **118**, 158103 (2017).

[82] W. Bialek, *Biophysics: Searching for Principles* (Princeton University Press, 2012).

[83] G. Tkačik and W. Bialek, *Annu. Rev. Condens. Matter Phys.* **7**, 1 (2016).

[84] P. C. Bressloff and J. M. Newby, *Phys. Rev. E* **89**, 042701 (2014).

[85] S. Winkelmann and C. Schütte, *J. Chem. Phys.* **147**, 114115 (2017).

[86] A. Wachtel, R. Rao, and M. Esposito, *New J. Phys.* **20**, 042002 (2018).

[87] D. A. McQuarrie, *Statistical Mechanics* (Harper & Row, 1976).

[88] D. A. Beard and H. Qian, *Chemical Biophysics. Quantitative Analysis of Cellular Systems* (Cambridge University Press, 2008).

[89] T. E. Ouldridge, *Nat. Comp.* **17**, 3 (2017).

[90] E. Fermi, *Thermodynamics* (Dover, 1956).

5

DETERMINISTIC DESCRIPTION

In the previous chapter we established a rigorous stochastic thermodynamic description for chemical reaction networks. This description is important for those processes involving low particle numbers, but in those circumstances in which particle numbers are high, *e.g.* metabolic networks, stochastic descriptions are either unfeasible or unnecessary. It might be unfeasible because the CME is both extremely hard to solve analytically and very demanding to compute numerically. It might be unnecessary because high particle numbers— $n \gg 1$ —allow mean field descriptions in terms of rate equations or reaction–diffusion equations for concentration distributions, which are indeed easier to solve, at least numerically.

In this chapter, we introduce the thermodynamic description for two fundamental mean field types of dynamics: rate equations and reaction–diffusion equations, Secs. 5.1 and 5.2. In Sec. 5.3, we introduce a thermodynamically coarse-graining which enable to simplify descriptions of chemical reaction networks involving enzymatic reactions.

5.1 SPATIALLY HOMOGENEOUS PROCESSES

In the following reprinted article, p. 145, we present a nonequilibrium thermodynamic description for deterministic chemical reaction networks described by rate equations. The timeless expression of these equation is exactly as in Eqs. (87) and (87), where $\{N^x\}$ and $\{N^y\}$ need to be regarded as concentrations homogeneously distributed in space, see Eqs. [(9) and (10), p. 148]. We mention that with respect to the description in Ch. 3 the concentrations of the chemostatted species are directly controlled by the chemostats, *i.e.* they can be regarded as chemical reservoirs within the system. Hence, in contrast to the description in Ch. 4 all reactions are *internal*, and those involving chemostatted species also involve a flow of chemostats which restores their concentrations.

Our approach is inspired by stochastic thermodynamics as we build the thermodynamic description on top of the dynamics. The connection between these two lies in the local detailed balance property, which—in a timeless formulation—relates the ratio of forward and backward extent of reactions to the overall Gibbs free energy change, Eqs. (93) and [(48) and (50), p. 153–154].

$$\ln \frac{d\xi_{+\rho}(N)}{d\xi_{-\rho}(N)} = -\beta_r \left[\sum_x \mu_x^s(N^x) S_\rho^x + \sum_y \mu_y(N^y) S_\rho^y \right]. \quad (124)$$

Notice that internal Gibbs free energy changes are quantified as differences of internal species chemical potential. It is a consequence of the *local equilibrium hypothesis*, according to which all spatial and thermal degrees of freedom are at equilibrium except for the overall concentrations. Hence, we can characterize the energetic state of the network using well defined chemical potentials, whose expression follows from the theory of ideal dilute solutions, Eq. [(45), p. 153].

In contrast to previous thermodynamic description of chemical processes, ours is set up on a mathematically rigorous network description. We can thus formalize the energy and entropy balances (Eqs. (90) and (93)) for arbitrary chemical networks, Eqs. [(68) and (65), p. 155], and, using conservation laws, we can characterize the thermodynamics of open networks relaxing to equilibrium in absence of driving, *i.e.* *detailed-balanced networks*, Sec. [V, pp. 158–160]. We also bridge the gap between chemical thermodynamics and (i) chemical reaction network theory and (ii) information processing. Concerning the former, we characterize the thermodynamic properties of *complex-balanced networks* [1–3], which are a class of networks whose specific topological properties completely determine their dynamic behaviour, Sec. [III and IV, pp. 151–153 and 157–158]. Regarding the latter, we for first formulate the nonequilibrium Landauer principle (Eqs. (73) and (75)) for deterministic descriptions, Eqs. [(82) and (101), pp. 156 and 160]. Remarkably, the generalized relative entropy \mathcal{D} , Eq. (72), becomes the Lyapunov function of detailed- and complex-balanced networks introduced by Shear [3, 4],

$$\mathcal{D} \equiv \mathcal{D}(\mathbf{N} \parallel \mathbf{N}_{\text{eq}}) = \sum_{\sigma} \left[N^{\sigma} \ln \frac{N^{\sigma}}{N_{\text{eq}}^{\sigma}} - N^{\sigma} + N_{\text{eq}}^{\sigma} \right] \geq 0, \quad (125)$$

see Eq. [(75), p. 156]. It has the same properties of the relative entropy for probability distributions: it is always positive and vanishes only when $\mathbf{N} = \mathbf{N}_{\text{eq}}$. It thus quantifies the distance from equilibrium, as formalized in Eq. (72).

In the second reprinted article, p. 171, the technique of analysing conservation laws is applied to monomer exchange dynamics [5]. Our aim is to model the action of a class of enzymes, called *disproportionating enzymes*, active in polysaccharides metabolism [6–8]. In these networks the species are polymers, which can be of any size, and hence the chemical reaction network is infinite dimensional. This gives rise to dynamical behaviours usually absent in ordinary chemical reaction networks, like for instance continuous growth. Conservation laws allow us to clearly identify when these behaviours manifest.

5.2 SPATIALLY INHOMOGENEOUS PROCESSES

The cases described so far assumed that the concentrations of reacting species were homogeneously distributed in the reaction vessel. However, this is not always a good approximation, and when it is not, diffusion must be taken into account: the rate equations must be replaced by *reaction–diffusion equations*. These equations may give rise to interesting phenomenologies, like for instance Turing patterns and travelling waves, which are stationary and propagating inhomogeneous spatial distribution of concentrations, respectively [9, Sec. 19.5]. These phenomena appear in several biological processes like organs and tissues formation [10], and cellular rhythms regulations via calcium waves [11].

In the article reprinted at p. 185 we provide a complete nonequilibrium thermodynamic description of reaction–diffusion systems. The connection between the phenomenological and dynamical description is understood once the reaction–diffusion equation, Eq. [(1), p. 185], are formulated in a timeless fashion

$$dN^{\sigma}(\mathbf{r}) = -\nabla \cdot d\Xi^{\sigma}(\mathbf{r}) + \sum_{\rho} S_{\rho}^{\sigma} d\xi_{\rho}(\mathbf{r}) + d_r N^{\sigma}(\mathbf{r}). \quad (126)$$

In this equation, $N^\sigma(\mathbf{r})$ is the local concentration and the first term on the rhs quantifies the rate at which diffusion changes it. The other two terms on the rhs are the reaction and exchange terms already mentioned, where the latter is different from zero solely for the chemostatted species and in those regions of space where the reservoirs are located. The balances of abundances, Eqs. (87) and (89), follows when integrating Eq. (126) over the volume of the reaction vessel V . Indeed, $\{N^\sigma\}$, $\{d\xi_p\}$, and $\{d_r N^\sigma\}$ are the overall abundances, extents of reaction, and exchange terms, respectively,

$$N^\sigma = \int_V d\mathbf{r} N^\sigma(\mathbf{r}), \quad d\xi_p = \int_V d\mathbf{r} d\xi_p(\mathbf{r}), \quad d_r N^\sigma = \int_V d\mathbf{r} d_r N^\sigma(\mathbf{r}). \quad (127)$$

The first therm on the rhs of Eq. (126) vanishes when integrated over all space. We can thus identify conservation laws Eq. [(8), p. 187], and exhibit the entropy production decomposition in terms of conservative, driving, and nonconservative contributions, Eqs. (102) and [(12), p. 187], where the details of the derivation are reported in the supplementary material at p. 191. In this context, the conservative term, $-d\mathcal{G}$, can be interpreted as the cost of structuring spatial distributions of molecules, the driving work, $d\mathcal{H}$, that of manipulating them, and finally the nonconservative chemical works, $\{\mathcal{K}_{y_f} d_r N^{y_f}\}$, that of sustaining them. The minimal costs of structuring, manipulating, and sustaining these distributions is quantified by a nonequilibrium Landauer principle, Eqs. (75) and [(14), p. 187]. In this formulation, the generalized relative entropy becomes

$$\mathcal{D} \equiv \mathcal{D}(\mathbf{N} \parallel \mathbf{N}_{eq}) = \int_V d\mathbf{r} \sum_\sigma \left[N^\sigma(\mathbf{r}) \ln \frac{N^\sigma(\mathbf{r})}{N_{eq}^\sigma} - N^\sigma(\mathbf{r}) + N_{eq}^\sigma \right] \geq 0, \quad (128)$$

which measures how dissimilar a concentration distribution is from an homogeneous equilibrium one, Eq. [(4), p. 186].

5.3 COARSE-GRAINED PROCESSES

Elementary reactions is one the assumption underpinning both the stochastic and the deterministic thermodynamic descriptions introduced thus far. However, it is very well known that the majority of reactions in biochemical systems are catalysed by enzymes. An accurate description of enzyme catalysed reactions in terms of elementary reactions would require a detailed description of each individual step. Unfortunately, this is quite unfeasible for two main reasons. First, all intermediate reaction steps are difficult to identify for each enzyme. Second, biochemical networks, *e.g.* metabolic networks, typically involve a vast number of different enzymes which overall catalyse several hundreds of reactions. Including each intermediate elementary step for each enzymes would enormously raise the complexity of the description. We thus need a thermodynamically consistent way of accounting for enzymatic reactions, *i.e.* a thermodynamically consistent coarse-graining scheme. In the Article reprinted at p. 201 we provide such a procedure.

The idea of this procedure is as follows (Sec. [2, p. 202], and Fig. [1, p. 202]). First, the enzymatic scheme is isolated and treated as a chemical reaction network: all enzyme complexes are regarded as internal species while all substrates and products as chemostatted. At this point, we observe that in the same way reactions create pathways between reservoirs in generic networks, Sec. (3.3), enzymes create pathways transforming substrates into

products. Therefore, the stoichiometry of these transformations must be given by Eq. (105)—this emphasizes once more the importance of conservation laws. These overall transformations determine the coarse-grained reactions which replace the enzymatic steps. Their currents, or extent of reaction, can be obtained by means of the graph-theoretical method first introduced by Kirchhoff [12, 13], whereas their affinity is given by the fundamental forces, Eq. (101). As an important result, we also show that the local detailed balance as written in Eq. (124), is in general invalid at the coarse-grained level: it is valid *solely* for those enzymatic schemes characterized by one fundamental force, *i.e.* one pathway between substrates and products. Importantly, this clarifies previous misconceptions about its validity, *cf.* [14].

REFERENCES FOR CHAPTER 5

- [1] F. HORN, “Necessary and sufficient conditions for complex balancing in chemical kinetics”, *Arch. Ration. Mech. An.* **49**.3 (1972), 172–186.
- [2] M. FEINBERG, “Complex balancing in general kinetic systems”, *Arch. Ration. Mech. An.* **49**.3 (1972), 187–194.
- [3] F. HORN and R. JACKSON, “General mass action kinetics”, *Arch. Ration. Mech. An.* **47**.2 (1972), 81–116.
- [4] D. SHEAR, “An analog of the Boltzmann H-theorem (a Liapunov function) for systems of coupled chemical reactions”, *J. Theor. Biol.* **16**.2 (1967), 212–228.
- [5] P. KRAPIVSKY, S. REDNER and E. BEN-NAIM, *A Kinetic View of Statistical Physics*, Cambridge University Press, 2010.
- [6] G. JONES and W. WHELAN, “The action pattern of d-enzyme, a trans-maltodextrinylase from potato”, *Carbohydr. Res.* **9**.4 (1969), 483–490.
- [7] T. TAKAHASHI and S. M. SMITH, “The functions of 4- α -glucanotransferases and their use for the production of cyclic glucans”, *Biotechnol. Genet. Eng. Rev.* **16**.1 (1999), 257–280.
- [8] Ö. KARTAL et al., “Carbohydrate-active enzymes exemplify entropic principles in metabolism”, *Mol. Syst. Biol.* **7**.1 (2011), 542–542.
- [9] D. KONDEPUDI and I. PRIGOGINE, *Modern Thermodynamics: From Heat Engines to Dissipative Structures*, Wiley, 2014.
- [10] D. IBER and D. MENSHYKAU, “The control of branching morphogenesis”, *Open Biol.* **3**.9 (2013), 130088.
- [11] K. THURLEY et al., “Fundamental properties of Ca²⁺ signals”, *Biochim. Biophys. Acta* **1820**.8 (2012), 1185–1194.
- [12] G. KIRCHHOFF, “Ueber die Auflösung der Gleichungen, auf welche man bei der Untersuchung der linearen Vertheilung galvanischer Ströme geführt wird”, *Ann. Phys.* **148**.12 (1847), 497–508.
- [13] E. L. KING and C. ALTMAN, “A Schematic Method of Deriving the Rate Laws for Enzyme-Catalyzed Reactions”, *J. Phys. Chem.* **60**.10 (1956), 1375–1378.
- [14] D. A. BEARD and H. QIAN, “Relationship between Thermodynamic Driving Force and One-Way Fluxes in Reversible Processes”, *PLoS ONE* **2**.1 (2007), e144.

The following article is reprinted from
[R. RAO and M. ESPOSITO, *Phys. Rev. X* **6**.4 (2016), 041064]
under the conditions of the Creative Commons Attribution 3.0 Unported
Licence¹.

The page numbers placed in the outer margins provide a continuous pagination throughout the thesis.

¹ <https://creativecommons.org/licenses/by/3.0/>

Nonequilibrium Thermodynamics of Chemical Reaction Networks: Wisdom from Stochastic Thermodynamics

Riccardo Rao and Massimiliano Esposito

Complex Systems and Statistical Mechanics, Physics and Materials Science Research Unit,

University of Luxembourg, L-1511 Luxembourg, Luxembourg

(Received 23 February 2016; revised manuscript received 26 October 2016; published 22 December 2016)

We build a rigorous nonequilibrium thermodynamic description for open chemical reaction networks of elementary reactions. Their dynamics is described by deterministic rate equations with mass action kinetics. Our most general framework considers open networks driven by time-dependent chemostats. The energy and entropy balances are established and a nonequilibrium Gibbs free energy is introduced. The difference between this latter and its equilibrium form represents the minimal work done by the chemostats to bring the network to its nonequilibrium state. It is minimized in nondriven detailed-balanced networks (i.e., networks that relax to equilibrium states) and has an interesting information-theoretic interpretation. We further show that the entropy production of complex-balanced networks (i.e., networks that relax to special kinds of nonequilibrium steady states) splits into two non-negative contributions: one characterizing the dissipation of the nonequilibrium steady state and the other the transients due to relaxation and driving. Our theory lays the path to study time-dependent energy and information transduction in biochemical networks.

DOI: 10.1103/PhysRevX.6.041064

Subject Areas: Chemical Physics, Nonlinear Dynamics, Statistical Physics

I. INTRODUCTION

Thermodynamics of chemical reactions has a long history. The second half of the 19th century witnessed the dawn of the modern studies on thermodynamics of chemical mixtures. It is indeed at that time that Gibbs introduced the concept of *chemical potential* and used it to define the thermodynamic potentials of noninteracting mixtures [1]. Several decades later, this enabled de Donder to approach the study of chemical reacting mixtures from a thermodynamic standpoint. He proposed the concept of *affinity* to characterize the chemical force irreversibly driving chemical reactions and related it to the thermodynamic properties of mixtures established by Gibbs [2]. Prigogine, who perpetuated the Brussels School founded by de Donder, introduced the assumption of *local equilibrium* to describe irreversible processes in terms of equilibrium quantities [3,4]. In doing so, he pioneered the connections between thermodynamics and kinetics of chemical reacting mixtures [5].

During the second half of the 20th century, part of the attention moved to systems with small particle numbers which are ill described by “deterministic” rate equations. The Brussels School, as well as other groups, produced various studies on the nonequilibrium thermodynamics of

chemical systems [6–11] using a stochastic description based on the (chemical) master equation [12,13]. These studies played an important role during the first decade of the 21st century for the development of *stochastic thermodynamics*, a theory that systematically establishes a non-equilibrium thermodynamic description for systems obeying stochastic dynamics [14–17], including chemical reaction networks (CRNs) [18–22].

Another significant part of the attention moved to the thermodynamic description of biochemical reactions in terms of deterministic rate equations [23,24]. This is not so surprising since living systems are the paramount example of nonequilibrium processes and they are powered by chemical reactions. The fact that metabolic processes involve thousands of coupled reactions also emphasized the importance of a network description [25–27]. While complex dynamical behaviors such as oscillations were analyzed in small CRNs [28,29], most studies on large biochemical networks focused on the steady-state dynamics. Very few studies considered the thermodynamic properties of CRNs [30–33]. One of the first nonequilibrium thermodynamic descriptions of open biochemical networks was proposed in Ref. [34]. However, it did not take advantage of chemical reaction network theory, which connects the network topology to its dynamical behavior and which was extensively studied by mathematicians during the 1970s [35–37] (this theory was also later extended to stochastic dynamics [38–41]). As far as we know, the first and single study that related the nonequilibrium thermodynamics of CRNs to their topology is Ref. [22], still restricting itself to steady states.

Published by the American Physical Society under the terms of the [Creative Commons Attribution 3.0 License](#). Further distribution of this work must maintain attribution to the author(s) and the published article's title, journal citation, and DOI.

In this paper, we consider the most general setting for the study of CRNs, namely, open networks driven by chemo-statted concentrations that may change over time. To the best of our knowledge, this was never considered before. In this way, steady-state properties as well as transient ones are captured. Hence, in the same way that stochastic thermodynamics is built on top of stochastic dynamics, we systematically build a nonequilibrium thermodynamic description of CRNs on top of deterministic chemical rate equations. In doing so, we establish the energy and entropy balance and introduce the nonequilibrium entropy of the CRN as well as its nonequilibrium Gibbs free energy. We show the latter to bear an information-theoretical interpretation similar to that of stochastic thermodynamics [42–45] and to be related to the dynamical potentials derived by mathematicians. We also show the relation between the minimal chemical work necessary to manipulate the CRNs far from equilibrium and the nonequilibrium Gibbs free energy. Our theory embeds both the Prigoginian approach to thermodynamics of irreversible processes [5] and the thermodynamics of biochemical reactions [23]. Making full use of the mathematical chemical reaction network theory, we further analyze the thermodynamic behavior of two important classes of CRNs: detailed-balanced networks and complex-balanced networks. In the absence of time-dependent driving, the former converges to thermodynamic equilibrium by minimizing their nonequilibrium Gibbs free energy. In contrast, the latter converges to a specific class of nonequilibrium steady states and always allows for an adiabatic–nonadiabatic separation of their entropy production, which is analogous to that found in stochastic thermodynamics [46–50]. Recently, a result similar to the latter was independently found in Ref. [51].

A. Outline and notation

The paper is organized as follows. After introducing the necessary concepts in chemical kinetics and chemical reaction network theory, Sec. II, the nonequilibrium thermodynamic description is established in Sec. III. As in stochastic thermodynamics, we build it on top of the dynamics and formulate the entropy and energy balance, Secs. III D and III E. Chemical work and nonequilibrium Gibbs free energy are also defined, and the information-theoretic content of the latter is discussed. The special properties of detailed-balanced and of complex-balanced networks are considered in Secs. V and IV, respectively. Conclusions and perspectives are drawn in Sec. VI, while some technical derivations are detailed in the appendixes.

We now proceed by fixing the notation. We consider a system composed of reacting *chemical species* X_σ , each of which is identified by an index $\sigma \in \mathcal{S}$, where \mathcal{S} is the set of all indices or species. The species populations change due to *elementary reactions*, i.e., all reacting species and reactions must be resolved (none can be

hidden), and all reactions must be *reversible*, i.e., each forward reaction $+\rho$ has a corresponding backward reaction $-\rho$. Each pair of forward-backward reactions is a *reaction pathway* denoted by $\rho \in \mathcal{R}$. The orientation of the set of reaction pathways \mathcal{R} is arbitrary. Hence, a generic CRN is represented as

$$\sum_{\sigma} \nabla_{+\rho}^{\sigma} X_{\sigma} \xrightleftharpoons[k^{-\rho}]{k^{+\rho}} \sum_{\sigma} \nabla_{-\rho}^{\sigma} X_{\sigma}. \quad (1)$$

The constants $k^{+\rho}$ ($k^{-\rho}$) are the *rate constants* of the forward (backward) reactions. The stoichiometric coefficients $-\nabla_{+\rho}^{\sigma}$ and $\nabla_{-\rho}^{\sigma}$ identify the number of molecules of X_{σ} involved in each forward reaction $+\rho$ (the stoichiometric coefficients of the backward reactions have opposite signs). Once stacked into two non-negative matrices, $\nabla_+ = \{\nabla_{+\rho}^{\sigma}\}$ and $\nabla_- = \{\nabla_{-\rho}^{\sigma}\}$, they define the integer-valued stoichiometric matrix

$$\nabla \equiv \nabla_- - \nabla_+. \quad (2)$$

The reason for the choice of the symbol “ ∇ ” will become clear later.

Example 1.—The stoichiometric matrix of the CRN depicted in Fig. 1 is

$$\nabla = \begin{pmatrix} -1 & 0 \\ 2 & 0 \\ 1 & -1 \\ 0 & -1 \\ 0 & 1 \end{pmatrix}. \quad (3)$$

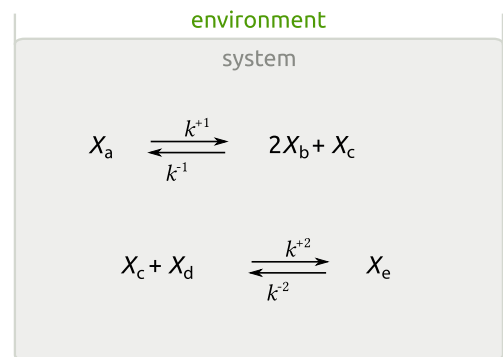


FIG. 1. Representation of a closed CRN. The chemical species are $\{X_a, \dots, X_e\}$. The two reaction pathways are labeled by 1 and 2. The nonzero stoichiometric coefficients are $-\nabla_{+1}^a = -1$, $\nabla_{-1}^b = 2$, and $\nabla_{-1}^c = 1$ for the first forward reaction and $-\nabla_{+2}^c = -1$, $-\nabla_{+2}^d = -1$, and $\nabla_{-2}^e = 1$ for the second one. Since the network is closed, no chemical species is exchanged with the environment.

Physical quantities associated with species and reactions are represented in upper-lower indices vectorial notation. Upper and lower indexed quantities have the same physical values, e.g., $Z^i = Z_i$, $\forall i$. We use the Einstein summation notation: repeated upper-lower indices implies the summation over all the allowed values for those indices—e.g., $\sigma \in \mathcal{S}$ for species and $\rho \in \mathcal{R}$ for reactions. Given two arbitrary vectorial quantities $\mathbf{a} = \{a^i\}$ and $\mathbf{b} = \{b^i\}$, the following notation is used:

$$a^{ib_i} \equiv \prod_i a^{ib_i}.$$

Finally, given the matrix C , whose elements are $\{C_j^i\}$, the elements of the transposed matrix C^T are $\{C_i^j\}$.

The time derivative of a physical quantity A is denoted by $d_t A$, its steady state value by an overbar \bar{A} , and its equilibrium value by A_{eq} or A^{eq} . We reserve the overdot \dot{A} to denote the rate of change of quantities that are *not* exact time derivatives.

II. DYNAMICS OF CRNS

In this section, we formulate the mathematical description of CRNs [52,53] in a suitable way for a thermodynamic analysis. We introduce closed and open CRNs and show how to drive these latter in a time-dependent way. We then define conservation laws and cycles and review the dynamical properties of two important classes of CRNs: detailed-balanced networks and complex-balanced networks.

We consider a chemical system in which the reacting species $\{X_\sigma\}$ are part of a homogeneous and ideal dilute solution: the reactions proceed slowly compared to diffusion and the solvent is much more abundant than the reacting species. Temperature T and pressure p are kept constant. Since the volume of the solution V is overwhelmingly dominated by the solvent, it is assumed constant. The species abundances are large enough so that the molecule's discreteness can be neglected. Thus, at any time t , the system state is well described by the molar concentration distribution $\{Z^\sigma \equiv N^\sigma/V\}$, where N^σ is the molarity of the species X_σ .

The reaction kinetics is controlled by the reaction rate functions $J^{\pm\rho}(\{Z^\sigma\})$, which measure the rate of occurrence of reactions and satisfy the mass action kinetics [52,54,55]:

$$J^{\pm\rho} \equiv J^{\pm\rho}(\{Z^\sigma\}) = k^{\pm\rho} Z^\sigma \nabla_\sigma^{\pm\rho}. \quad (4)$$

The net concentration current along a reaction pathway ρ is thus given by

$$J^\rho \equiv J^{+\rho} - J^{-\rho} = k^{+\rho} Z^\sigma \nabla_\sigma^{+\rho} - k^{-\rho} Z^\sigma \nabla_\sigma^{-\rho}. \quad (5)$$

Example 2.—For the CRN in Fig. 1 the currents are

$$\begin{aligned} J^1 &= k^{+1} Z^a - k^{-1} (Z^b)^2 Z^c, \\ J^2 &= k^{+2} Z^c Z^d - k^{-2} Z^e. \end{aligned} \quad (6)$$

□

A. Closed CRNs

A closed CRN does not exchange any chemical species with the environment. Hence, the species concentrations vary solely due to chemical reactions and satisfy the rate equations

$$d_t Z^\sigma = \nabla_\rho^{\sigma} J^\rho, \quad \forall \sigma \in \mathcal{S}. \quad (7)$$

Since rate equations are nonlinear, complex dynamical behaviors may emerge [29]. The fact that the rate equations [Eq. (7)] can be thought of as a continuity equation for the concentration, where the stoichiometric matrix ∇ [Eq. (2)] acts as a discrete differential operator, explains the choice of the symbol “ ∇ ” for the stoichiometric matrix [56].

B. Driven CRNs

In open CRNs, matter is exchanged with the environment via reservoirs that control the concentrations of some specific species, Fig. 2. These externally controlled species are said to be *chemostatted*, while the reservoirs controlling them are called chemostats. The chemostatting procedure may mimic various types of controls by the environment. For instance, a direct control could be implemented via external reactions (not belonging to the CRN) or via abundant species whose concentrations are negligibly affected by the CRN reactions within relevant time scales. An indirect control may be achieved via semipermeable membranes or by controlled injection of chemicals in continuous stirred-tank reactors.

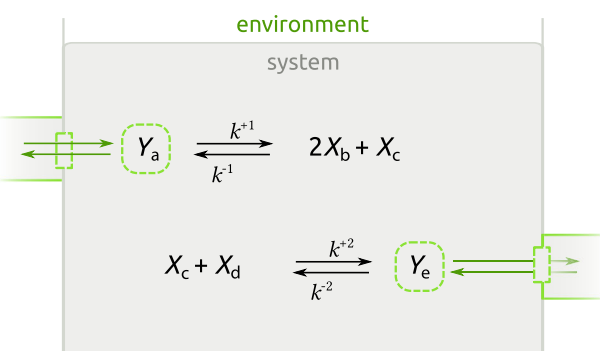


FIG. 2. Representation of an open CRN. With respect to the CRN in Fig. 1, the species X_a and X_e are chemostatted, hence, represented as Y_a and Y_e . The green boxes on the sides represent the reservoirs of chemostatted species.

Among the chemical species, the chemostatted ones are denoted by the indices $\sigma_y \in \mathcal{S}_y$, and the internal ones by $\sigma_x \in \mathcal{S}_x$ ($\mathcal{S} \equiv \mathcal{S}_x \cup \mathcal{S}_y$). Also, the part of the stoichiometric matrix related to the internal (chemostatted) species is denoted by $\nabla^X = \{\nabla_{\rho}^{\sigma_x}\}$ ($\nabla^Y = \{\nabla_{\rho}^{\sigma_y}\}$).

Example 3.—When chemostatting the CRN in Fig. 1 as in Fig. 2 the stoichiometric matrix Eq. (3) splits into

$$\nabla^X = \begin{pmatrix} 2 & 0 \\ 1 & -1 \\ 0 & -1 \end{pmatrix}, \quad \nabla^Y = \begin{pmatrix} -1 & 0 \\ 0 & 1 \end{pmatrix}. \quad (8)$$

□

In nondriven open CRNs, the chemostatted species have constant concentrations, i.e., $\{d_t Z^{\sigma_y} = 0\}$. In driven open CRNs, the chemostatted concentrations change over time according to some time-dependent protocol $\pi(t)$: $\{Z^{\sigma_y} \equiv Z^{\sigma_y}(\pi(t))\}$. The changes of the internal species are solely due to reactions and satisfy the rate equations

$$d_t Z^{\sigma_x} = \nabla_{\rho}^{\sigma_x} J^{\rho}, \quad \forall \sigma_x \in \mathcal{S}_x. \quad (9)$$

Instead, the changes of chemostatted species $\{d_t Z^{\sigma_y}\}$ are not only given by the species formation rates $\{\nabla_{\rho}^{\sigma_y} J^{\rho}\}$ but must in addition contain the external currents $\{I^{\sigma_y}\}$, which quantify the rate at which chemostatted species enter into the CRN (negative if chemostatted species leave the CRN),

$$d_t Z^{\sigma_y} = \nabla_{\rho}^{\sigma_y} J^{\rho} + I^{\sigma_y}, \quad \forall \sigma_y \in \mathcal{S}_y. \quad (10)$$

This latter equation is not a differential equation since the chemostatted concentrations $\{Z^{\sigma_y}\}$ are not dynamical variables. It shows that the external control of the chemostatted concentration is not necessarily direct, via the chemostatted concentrations, but can also be indirectly controlled via the external currents. We note that Eq. (10) is the dynamical expression of the decomposition of changes of species populations in internal-external introduced by de Donder (see Secs. 4.1 and 15.2 of Ref. [57]).

A steady-state distribution $\{\bar{Z}^{\sigma_x}\}$, if it exists, must satisfy

$$\nabla_{\rho}^{\sigma_x} \bar{J}^{\rho} = 0, \quad \forall \sigma_x \in \mathcal{S}_x, \quad (11a)$$

$$\nabla_{\rho}^{\sigma_y} \bar{J}^{\rho} + \bar{I}^{\sigma_y} = 0, \quad \forall \sigma_y \in \mathcal{S}_y, \quad (11b)$$

for given chemostatted concentrations $\{Z^{\sigma_y}\}$.

C. Conservation laws

In a closed CRN, a conservation law $\ell = \{\ell_{\sigma}\}$ is a left null eigenvector of the stoichiometric matrix ∇ [23,25]:

$$\ell_{\sigma} \nabla_{\rho}^{\sigma} = 0, \quad \forall \rho \in \mathcal{R}. \quad (12)$$

Conservation laws identify conserved quantities $L \equiv \ell_{\sigma} Z^{\sigma}$, called components [23,25], which satisfy

$$d_t L = \ell_{\sigma} d_t Z^{\sigma} = 0. \quad (13)$$

We denote a set of independent conservation laws of the closed network by $\{\ell^{\lambda}\}$ and the corresponding components by $\{L^{\lambda} \equiv \ell_{\sigma}^{\lambda} Z^{\sigma}\}$. The choice of this set is not unique, and different choices have different physical meanings. This set is never empty since the total mass is always conserved. Physically, conservation laws are often related to parts of molecules, called moieties [58], which are exchanged between different species and/or subject to isomerization (see Example 4).

In an open CRN, since only $\{Z^{\sigma_x}\}$ are dynamical variables, the conservation laws become the left null eigenvectors of the stoichiometric matrix of the internal species ∇^X . Stated differently, when starting from the closed CRN, the chemostatting procedure may break a subset of the conservation laws of the closed network $\{\ell^{\lambda}\}$ [56]. For example, when the first chemostat is introduced the total mass conservation law is always broken. Within the set $\{\ell^{\lambda}\}$, we label the broken ones by λ_b and the unbroken ones by λ_u . The broken conservation laws are characterized by

$$\underbrace{\ell_{\sigma_x}^{\lambda_b} \nabla_{\rho}^{\sigma_x}}_{\neq 0} + \ell_{\sigma_y}^{\lambda_b} \nabla_{\rho}^{\sigma_y} = 0, \quad \forall \rho \in \mathcal{R}, \quad (14)$$

where the first term is nonvanishing for at least one $\rho \in \mathcal{R}$. The broken components $\{L^{\lambda_b} \equiv \ell_{\sigma}^{\lambda_b} Z^{\sigma}\}$ are no longer constant over time. On the other hand, the unbroken conservation laws are characterized by

$$\underbrace{\ell_{\sigma_x}^{\lambda_u} \nabla_{\rho}^{\sigma_x}}_{=0} + \ell_{\sigma_y}^{\lambda_u} \nabla_{\rho}^{\sigma_y} = 0, \quad \forall \rho \in \mathcal{R}, \quad (15)$$

where the first term vanishes for all $\rho \in \mathcal{R}$. Therefore, the unbroken components $\{L^{\lambda_u} \equiv \ell_{\sigma}^{\lambda_u} Z^{\sigma}\}$ remain constant over time. Without loss of generality, we choose the set $\{\ell^{\lambda}\}$ such that the entries related to the chemostatted species vanish, $\ell_{\sigma_y}^{\lambda_u} = 0, \forall \lambda_u, \sigma_y$.

Example 4.—For the CRN in Fig. 1, an independent set of conservation laws is

$$\begin{aligned} \ell^1 &= (2 \ 1 \ 0 \ 0 \ 0), \\ \ell^2 &= (0 \ 0 \ 0 \ 1 \ 1), \\ \ell^3 &= (0 \ \frac{1}{2} \ -1 \ 1 \ 0). \end{aligned} \quad (16)$$

When chemostatting as in Fig. 2, the first two conservation laws break while the last one remains unbroken. We also

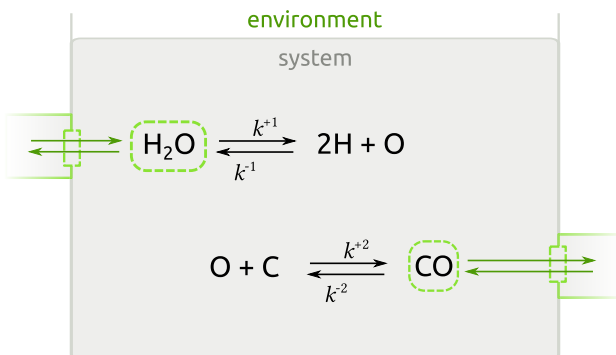


FIG. 3. Specific implementation of the CRN in Fig. 2.

note that this set is chosen so that the unbroken conservation law satisfies $\ell_a^3 = \ell_e^3 = 0$. When considering the specific implementation in Fig. 3 of the CRN in Fig. 2, we see that the first two conservation laws in Eq. (16) represent the conservation of the concentrations of the moiety H and C, respectively. Instead, the third conservation law in Eq. (16) does not have a straightforward interpretation. It is related to the fact that when the species H or C are produced, also O must be produced and vice versa. \square

D. Detailed-balanced networks

A steady state [Eq. (11)] is said to be an equilibrium state $\{Z_{\text{eq}}^\sigma\}$ if it satisfies the detailed-balance property [[57], § 9.4], i.e., all concentration currents Eq. (5) vanish:

$$J_{\text{eq}}^\rho \equiv J^\rho(\{Z_{\text{eq}}^\sigma\}) = 0, \quad \forall \rho \in \mathcal{R}. \quad (17)$$

For open networks, this means that the external currents, Eq. (11b), must also vanish, $\{I_{\text{eq}}^\sigma = 0\}$. By virtue of mass action kinetics, Eq. (4), the detailed-balance property Eq. (17) can be rewritten as

$$\frac{k^{+\rho}}{k^{-\rho}} = Z_{\text{eq}}^\sigma \nabla_\rho^\sigma, \quad \forall \rho \in \mathcal{R}. \quad (18)$$

A CRN is said to be detailed balanced if, for given kinetics $\{k^{\pm\rho}\}$ and chemostatting $\{Z^\sigma\}$, its dynamics exhibits an equilibrium steady state, Eq. (17). For each set of unbroken components $\{L^{\lambda_u}\}$ —which are given by the initial condition and constrain the space where the dynamics dwells—the equilibrium distribution is globally stable [59]. Equivalently, detailed-balanced networks always relax to an equilibrium state, which for a given kinetics and chemostatting is unique and depends on the unbroken components only; see also Sec. V.

Closed CRNs must be detailed balanced. This statement can be seen as the zeroth law for CRNs. Consequently, rather than considering Eq. (18) as a property of the equilibrium distribution, we impose it as a property that

the rate constants must satisfy and call it a local detailed-balance property. It is a universal property of elementary reactions that holds regardless of the network state. Indeed, while the equilibrium distribution depends on the components, the rhs of Eq. (18) does not. This point will become explicit after introducing the thermodynamic structure, Eq. (88) in Sec. V. The local detailed-balance property will be rewritten in a thermodynamic form in Sec. III B, Eq. (50).

In open nondriven CRNs, the chemostatting procedure may prevent the system from reaching an equilibrium state. To express this scenario algebraically, we now introduce the concepts of emergent cycle and cycle affinity.

A cycle $\tilde{\mathbf{c}} = \{\tilde{c}^\rho\}$ is a right null eigenvector of the stoichiometric matrix [56], namely,

$$\nabla_\rho^\sigma \tilde{c}^\rho = 0, \quad \forall \sigma \in \mathcal{S}. \quad (19)$$

Since ∇ is integer valued, $\tilde{\mathbf{c}}$ can always be rescaled to only contain integer coefficients. In this representation, its entries denote the number of times each reaction occurs (negative signs identify reactions occurring in backward direction) along a transformation that overall leaves the concentration distributions $\{Z^\sigma\}$ unchanged; see Example 5. We denote by $\{\tilde{\mathbf{c}}_a\}$ a set of linearly independent cycles. An emergent cycle $\mathbf{c} = \{c^\rho\}$ is defined algebraically as [56]

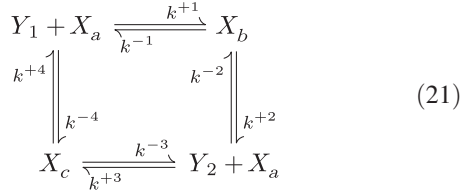
$$\begin{aligned} \nabla_\rho^{\sigma_x} c^\rho &= 0, \quad \forall \sigma_x \in \mathcal{S}_x, \\ \nabla_\rho^{\sigma_y} c^\rho &\neq 0, \quad \text{for at least one } \sigma_y \in \mathcal{S}_y. \end{aligned} \quad (20)$$

In its integer-valued representation, the entries of \mathbf{c} denote the number of times each reaction occurs along a transformation that overall leaves the concentrations of the internal species $\{Z^{\sigma_x}\}$ unchanged while changing the concentrations of the chemostatted species by an amount $\nabla_\rho^{\sigma_y} c^\rho$. These latter are, however, immediately restored to their prior values due to the injection of $-\nabla_\rho^{\sigma_y} c^\rho$ molecules of X_{σ_y} performed by the chemostats. Emergent cycles are, thus, pathways transferring chemicals across chemostats while leaving the internal state of the CRN unchanged. We denote by $\{\mathbf{c}_e\}$ a set of linearly independent emergent cycles.

When chemostatting an initially closed CRN, for each species that is chemostatted, either a conservation law breaks—as mentioned in Sec. II C—or an independent emergent cycle arises [56]. This follows from the rank nullity theorem for the stoichiometric matrices ∇ and ∇^X , which ensures that the number of chemostatted species $|\mathcal{S}_y|$ equals the number of broken conservation laws $|\lambda_b|$ plus the number of independent emergent cycles $|\mathbf{c}_e|$: $|\mathcal{S}_y| = |\lambda_b| + |\mathbf{c}_e|$. Importantly, the rise of emergent cycles is a topological feature: it depends on the species that are chemostatted, but not on the chemostatted concentrations.

We also note that emergent cycles are modeled as “flux modes” in the context of metabolic networks [60–62].

Example 5.—To illustrate the concepts of cycles and emergent cycles, we use the following CRN [56]:



whose Y_1 and Y_2 species are chemostatted. The stoichiometric matrix decomposes as

$$\begin{aligned}
 \nabla^X &= \begin{pmatrix} -1 & 1 & -1 & 1 \\ 1 & -1 & 0 & 0 \\ 0 & 0 & 1 & -1 \end{pmatrix}, \\
 \nabla^Y &= \begin{pmatrix} -1 & 0 & 0 & 1 \\ 0 & 1 & -1 & 0 \end{pmatrix}.
 \end{aligned} \quad (22)$$

The set of linearly independent cycles, Eq. (19), consists of only one cycle, which can be written as

$$\tilde{\mathbf{c}} = (1 \ 1 \ 1 \ 1)^T. \quad (23)$$

As the CRN is chemostatted, one linearly independent emergent cycle Eq. (20) arises:

$$\mathbf{c} = (1 \ 1 \ -1 \ -1)^T. \quad (24)$$

We now see that if each reaction occurs a number of times given by the entry of the cycle Eq. (23), the CRN goes back to the initial state, no matter which one it is. On the other hand, when the emergent cycle Eq. (24) is performed, the state of the internal species does not change, while two molecules of Y_1 are annihilated and two of Y_2 are created. However, since the chemostats restore their initial values, the overall result of \mathbf{c} is to transfer two Y_1 , transformed in Y_2 , from the first to the second chemostat.

The closed version of this CRN has two independent conservation laws,

$$\begin{aligned}
 \ell^1 &= (0 \ 1 \ 1 \ 1 \ 1), \\
 \ell^2 &= (1 \ 1 \ 1 \ 0 \ 0),
 \end{aligned} \quad (25)$$

the first of which, ℓ^1 , is broken following the chemostatting of any of the two species Y_1 or Y_2 . The other chemostatted species, instead, gives rise to the emergent cycle Eq. (24), so that the relationship $|\mathcal{S}_y| = |\lambda_b| + |\varepsilon|$ is satisfied. \square

Any cycle $\tilde{\mathbf{c}}_\alpha$ and emergent cycle \mathbf{c}_e bears a cycle affinity [56],

$$\tilde{\mathcal{A}}_\alpha = \tilde{c}_\alpha^\rho RT \ln \frac{J_{+\rho}}{J_{-\rho}}, \quad (26)$$

$$\mathcal{A}_e = c_e^\rho RT \ln \frac{J_{+\rho}}{J_{-\rho}}. \quad (27)$$

From the definition of cycle, Eq. (19), and current, Eq. (5), and the local detailed balance, Eq. (18), it follows that the cycle affinities along the cycles Eq. (19) vanish, $\{\tilde{\mathcal{A}}_\alpha = 0\}$, and that the cycle affinities along the emergent cycles depend on only the chemostatted concentrations

$$\mathcal{A}_e = c_e^\rho RT \ln \frac{k_{+\rho}}{k_{-\rho}} Z_{\sigma_y}^{-\nabla_\rho^{\sigma_y}}. \quad (28)$$

Since emergent cycles are pathways connecting different chemostats, the emergent affinities quantify the chemical forces acting along the cycles. This point will become clearer later, when the thermodynamic expressions of the emergent cycle affinities $\{\mathcal{A}_e\}$ is given, Eq. (49).

A CRN is detailed balanced if and only if all the emergent cycle affinities $\{\mathcal{A}_e\}$ vanish. This condition is equivalent to the Wegscheider condition [59]. This happens when the chemostatted concentrations fit an equilibrium distribution. As a special case, unconditionally detailed-balanced networks are open CRNs with no emergent cycle. Therefore, they are detailed balanced for any choice of the chemostatted concentrations. Consequently, even when a time-dependent driving acts on such a CRN and prevents it from reaching an equilibrium state, a well-defined equilibrium state exists at any time: the equilibrium state to which the CRN would relax if the time-dependent driving were stopped.

Example 6.—Any CRN with one chemostatted species only ($|\mathcal{S}_y| = 1$) is unconditionally detailed balanced. Indeed, as mentioned in Sec. II C, the first chemostatted species always breaks the mass conservation law $|\lambda_b| = 1$, and, thus, no emergent cycle arises, $|\varepsilon| = |\mathcal{S}_y| - |\lambda_b| = 0$.

The open CRN in Fig. 2 is an example of an unconditionally detailed-balanced network with two chemostatted species, since the chemostatting breaks two conservation laws; see Example 4. Indeed, a nonequilibrium steady state would require a continuous injection of Y_a and ejection of Y_e (or vice versa). But this would necessarily result in a continuous production of X_b and consumption of X_d , which is in contradiction with the steady-state assumption. \square

Finally, a tacit assumption in the above discussion is that the network involves a finite number of species and reactions, i.e., the CRN is finite dimensional. Infinite-dimensional CRNs can exhibit long-time behaviors

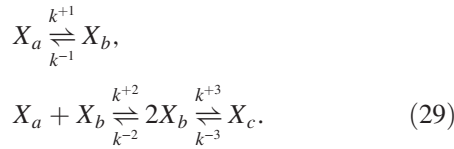
different from equilibrium even in the absence of emergent cycles [63].

E. Complex-balanced networks

To discuss complex-balanced networks and complex-balanced distributions, we first introduce the notion of complex in open CRNs.

A *complex* is a group of species that combines in a reaction as products or as reactants. Each side of Eq. (1) defines a complex, but different reactions might involve the same complex. We label complexes by $\gamma \in \mathcal{C}$, where \mathcal{C} is the set of complexes.

Example 7.—Let us consider the following CRN [64]



The set of complexes is $\mathcal{C} = \{X_a, X_b, X_a + X_b, 2X_b, X_c\}$, and the complex $2X_b$ is involved in both the second and third reaction. \square

The notion of complex allows us to decompose the stoichiometric matrix ∇ as

$$\nabla_\rho^\sigma = \Gamma_\gamma^\sigma \partial_\rho^\gamma. \quad (30)$$

We call $\Gamma = \{\Gamma_\gamma^\sigma\}$ the composition matrix [35,37]. Its entries Γ_γ^σ are the stoichiometric number of species X_σ in the complex γ . The composition matrix encodes the structure of each complex in terms of species; see Example 8. The matrix $\partial = \{\partial_\rho^\gamma\}$ denotes the incidence matrix of the CRN, whose entries are given by

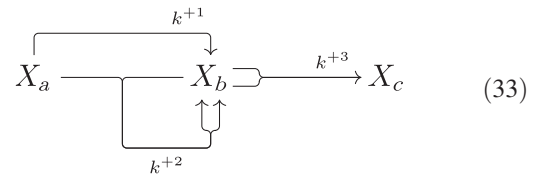
$$\partial_\rho^\gamma = \begin{cases} 1 & \text{if } \gamma \text{ is the product complex of } +\rho \\ -1 & \text{if } \gamma \text{ is the reactant complex of } +\rho \\ 0 & \text{otherwise.} \end{cases} \quad (31)$$

The incidence matrix encodes the structure of the network at the level of complexes, i.e., how complexes are connected by reactions. If we think of complexes as network nodes, the incidence matrix associates an edge to each reaction pathway and the resulting topological structure is a reaction graph, see, e.g., Fig. 1 and Eqs. (21) and (29). The stoichiometric matrix instead encodes the structure of the network at the level of species. If we think of species as the network nodes, the stoichiometric matrix does not define a graph, since reaction connects more than a pair of species, in general. The structure originating is rather a hypergraph [56,65] or, equivalently, a Petri net [66,67].

Example 8.—The composition matrix and the incidence matrix of the CRN in Eq. (29) are

$$\Gamma = \begin{pmatrix} 1 & 0 & 1 & 0 & 0 \\ 0 & 1 & 1 & 2 & 0 \\ 0 & 0 & 0 & 0 & 1 \end{pmatrix}, \quad \partial = \begin{pmatrix} -1 & 0 & 0 \\ 1 & 0 & 0 \\ 0 & -1 & 0 \\ 0 & 1 & -1 \\ 0 & 0 & 1 \end{pmatrix}, \quad (32)$$

where the complexes are ordered as in Example 7. The corresponding reaction hypergraph is



where only the forward reactions are depicted. \square

In an open CRN, we regroup all complexes $\gamma \in \mathcal{C}$ of the closed CRN that have the same stoichiometry for the internal species (i.e., all complexes with the same internal part of the composition matrix Γ_γ^X regardless of the chemostatted part Γ_γ^Y) in sets denoted by \mathcal{C}_j , for $j = 1, 2, \dots$. Complexes of the closed network made solely of chemostatted species in the open CRN are all regrouped in the same complex \mathcal{C}_0 . This allows one to decompose the internal species stoichiometric matrix as

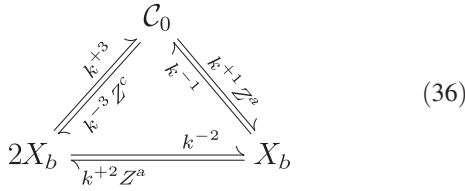
$$\nabla_\rho^{\sigma_s} = \Gamma_j^{\sigma_s} \partial_\rho^j. \quad (34)$$

where $\{\Gamma_j^{\sigma_s} \equiv \Gamma_\gamma^{\sigma_s} \text{ for } \gamma \in \mathcal{C}_j\}$ are the entries of the composition matrix corresponding to the internal species, and $\{\partial_\rho^j \equiv \sum_{\gamma \in \mathcal{C}_j} \partial_\rho^\gamma\}$ are the entries of the incidence matrix describing the network of regrouped complexes. This regrouping corresponds to the—equivalent—CRN made of only internal species with the effective rate constant $\{k^{\pm\rho} Z^{\sigma_s} \nabla_{\sigma_s}^{\pm\rho}\}$ ruling each reaction.

Example 9.—Let us consider the CRN Eq. (29) where the species X_a and X_c are chemostatted. The five complexes of the closed network, see Example 7, are regrouped as $\mathcal{C}_0 = \{X_a, X_c\}$, $\mathcal{C}_1 = \{X_b, X_b + X_a\}$, and $\mathcal{C}_2 = \{2X_b\}$. In terms of these groups of complexes, the composition matrix and incidence matrix are

$$\Gamma^X = (0 \ 1 \ 2), \quad \partial^C = \begin{pmatrix} -1 & 0 & 1 \\ 1 & -1 & 0 \\ 0 & 1 & -1 \end{pmatrix}, \quad (35)$$

which corresponds to the effective representation



A steady-state distribution $\{\bar{Z}^{\sigma_x}\}$ (11) is said to be complex balanced if the net current flowing in each group of complexes \mathcal{C}_j vanishes, i.e., if the currents $\{\bar{J}^\rho\}$ satisfy

$$\partial_\rho^j \bar{J}^\rho \equiv \sum_{\gamma \in \mathcal{C}_j} \partial_\rho^\gamma \bar{J}^\rho = 0, \quad \forall j. \quad (37)$$

Complex-balanced steady states are, therefore, a subclass of steady states Eq. (11a) that include equilibrium ones, Eq. (17), as a special case:

$$\begin{aligned} \Gamma_j^{\sigma_x} \partial_\rho^j & \quad \underbrace{\bar{J}^\rho}_{\substack{=0 \text{ iff Detailed-Balanced Steady State} \\ =0 \text{ iff Complex-Balanced Steady State} \\ =0 \text{ for generic steady states}}} \\ \end{aligned} \quad . \quad (38)$$

While for generic steady states only the internal species formation rates vanish, for complex-balanced ones the complex formation rates also vanish.

For a fixed kinetics ($\{k^{\pm\rho}\}$) and chemostatting (\mathcal{S}_y and $\{Z^{\sigma_y}\}$), a CRN is complex balanced if its dynamics exhibits a complex-balanced steady state, Eq. (37) [35,36]. The complex-balanced distribution Eq. (37) depends on the unbroken components $\{L^{\lambda_u}\}$, which can be inferred from the initial conditions, and is always globally stable [68]. Hence, complex-balanced networks always relax to a—complex-balanced—steady state. Detailed-balanced networks are a subclass of complex-balanced networks.

Whether or not a CRN is complex balanced depends on the network topology (∇), the kinetics ($\{k^{\pm\rho}\}$), and the chemostatting (\mathcal{S}_y and $\{Z^{\sigma_y}\}$). For any given network topology and set of chemostatted species \mathcal{S}_y , one can always find a set of effective rate constants $\{k^{\pm\rho} Z^{\sigma_y} \nabla_{\sigma_y}^{\pm\rho}\}$ that makes that CRN complex balanced [37]. However, for some CRNs, this set coincides with the one that makes the CRN detailed balanced [69]. A characterization of the set of effective rate constants that make a CRN complex balanced is reported in Refs. [37,69].

Deficiency-zero CRNs are a class of CRNs that are complex balanced irrespective of the effective kinetics $\{k^{\pm\rho} Z^{\sigma_y} \nabla_{\sigma_y}^{\pm\rho}\}$ [35–37]. The network deficiency is a topological property of the CRN, which we briefly discuss in Appendix D; see Refs. [22,52,53] for more details. Consequently, regardless of the way in which a deficiency-zero CRN is driven in time, it will always remain

complex balanced. Throughout this paper, we refer to these CRNs as unconditionally complex balanced, as in the seminal work [35].

Example 10.—The open CRN, Eq. (36), has a single steady state \bar{Z}^b for any given set of rate constants and chemostatted concentrations Z^a and Z^c [64], defined by Eq. (11a):

$$\begin{aligned} d_t \bar{Z}^b &= \bar{J}^1 + \bar{J}^2 - 2\bar{J}^3 \\ &= k^{+1}Z^a - k^{-1}\bar{Z}^b + k^{+2}Z^a\bar{Z}^b - k^{-2}(\bar{Z}^b)^2 \\ &\quad + 2k^{-3}Z^c - 2k^{+3}(\bar{Z}^b)^2 = 0. \end{aligned} \quad (39)$$

If the stronger condition Eq. (37) holds,

$$\begin{aligned} \bar{J}^3 - \bar{J}^1 &= 0 \quad (\text{group } \mathcal{C}_0), \\ \bar{J}^1 - \bar{J}^2 &= 0 \quad (\text{group } \mathcal{C}_1), \\ \bar{J}^2 - \bar{J}^3 &= 0 \quad (\text{group } \mathcal{C}_2), \end{aligned} \quad (40)$$

which is equivalent to

$$\begin{aligned} k^{+1}Z^a - k^{-1}\bar{Z}^b &= k^{+2}Z^a\bar{Z}^b - k^{-2}(\bar{Z}^b)^2 \\ &= k^{+3}(\bar{Z}^b)^2 - k^{-3}Z^c, \end{aligned} \quad (41)$$

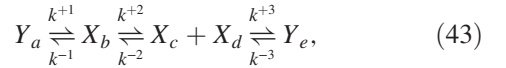
the steady state is complex balanced. Yet, if the steady-state currents are all independently vanishing,

$$\bar{J}^1 = \bar{J}^2 = \bar{J}^3 = 0, \quad (42)$$

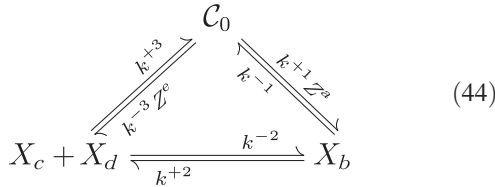
i.e., Eq. (41) is equal to zero, then the steady state is detailed balanced.

When, for simplicity, all rate constants are taken as 1, the complex-balanced set of quadratic equations, Eq. (41), admits a positive solution \bar{Z}^b only if $Z^a = 2 - Z^c$ ($0 < Z^c < 2$) or $Z^a = \sqrt{Z^c}$. The former case corresponds to a genuine complex-balanced state, $\bar{Z}^b = 1$ with currents $\bar{J}^1 = \bar{J}^2 = \bar{J}^3 = 1 - Z^c$, while the second corresponds to a detailed-balance state, $\bar{Z}^b = \sqrt{Z^c}$ with vanishing currents. When, for example, $Z^a = 1$ and $Z^c = 4$, neither of the two previous conditions holds: the nonequilibrium steady state is $\bar{Z}^b = \sqrt{3}$ with currents $\bar{J}^1 = 1 - \sqrt{3}$, $\bar{J}^2 = -3 + \sqrt{3}$, and $\bar{J}^3 = -1$. \square

Example 11.—Let us now consider the following open CRN [22]:



where the species Y_a and Y_e are chemostatted. Out of the four complexes of the closed network, $\{Y_a, X_b, X_c + X_d, Y_e\}$, two are grouped into $\mathcal{C}_0 = \{Y_a, Y_e\}$ and the other two remain $\mathcal{C}_1 = \{X_b\}$ and $\mathcal{C}_2 = \{X_c + X_d\}$. The effective representation of this open CRN is



This network is deficiency zero and, hence, unconditionally complex balanced [22]. Therefore, given any set of rate constants $k^{\pm 1}$, $k^{\pm 2}$, and $k^{\pm 3}$, and the chemostatted concentrations Z^a and Z^e , the steady state of this CRN is complex balanced, i.e., the steady state always satisfies a set of condition like those in Eq. (40). Indeed, contrary to Example 10, steady-state currents $\{\bar{J}^1, \bar{J}^2, \bar{J}^3\}$ different from each other cannot exist since they would induce a growth or decrease of some concentrations. \square

III. THERMODYNAMICS OF CHEMICAL NETWORKS

Using local equilibrium, here we build the connection between the dynamics and the nonequilibrium thermodynamics for arbitrary CRNs. In the spirit of stochastic thermodynamics, we derive an energy and entropy balance, and express the dissipation of the CRN as the difference between the chemical work done by the reservoirs on the CRN and its change in nonequilibrium free energy. We, finally, discuss the information-theoretical content of the nonequilibrium free energy and its relation to the dynamical potentials used in chemical reaction network theory.

A. Local equilibrium

Since we consider homogeneous reaction mixtures in ideal dilute solutions, the assumption of local equilibrium (Ref. [57], Sec. 15.1, and Ref. [70]) means that the equilibration following any reaction event is much faster than any reaction time scale. Thus, what is assumed is that the nonequilibrium nature of the thermodynamic description is solely due to the reaction mechanisms. If all reactions could be instantaneously shut down, the state of the whole CRN would immediately become an equilibrated ideal mixture of species. As a result, all the intensive thermodynamic variables are well defined and equal everywhere in the system. The temperature T is set by the solvent, which acts as a thermal bath, while the pressure p is set by the environment the solution is exposed to. As a result, each chemical species is characterized by a chemical potential (Ref. [23], Sec. III. 1),

$$\mu_\sigma = \mu_\sigma^\circ + RT \ln \frac{Z_\sigma}{Z_{\text{tot}}}, \quad \forall \sigma \in \mathcal{S}, \quad (45)$$

where R denotes the gas constant and $\{\mu_\sigma^\circ \equiv \mu_\sigma^\circ(T)\}$ are the standard-state chemical potentials, which depend on the temperature and on the nature of the solvent. The total

concentration of the solution is denoted by $Z_{\text{tot}} = \sum_\sigma Z^\sigma + Z^0$, where Z^0 is the concentration of the solvent. We assume for simplicity that the solvent does not react with the solutes. In case it does, our results still hold provided one treats the solvent as a nondriven chemostatted species, as discussed in Appendix A. Since the solvent is much more abundant than the solutes, the total concentration is almost equal to that of the solvent which is a constant, $Z_{\text{tot}} \simeq Z^0$. Without loss of generality, the constant term $-RT \ln Z_{\text{tot}} \simeq -RT \ln Z^0$ in Eq. (45) is absorbed in the standard-state chemical potentials. Consequently, many equations appear with nonmatching dimensions. We also emphasize that standard-state quantities, denoted with “ \circ ”, are defined as those measured in ideal conditions, at standard pressure ($p^\circ = 100$ kPa) and molar concentration ($Z_\sigma^\circ = 1$ mol/dm³), but not at a standard temperature (Ref. [71], p. 61).

Because of the assumption of local equilibrium and homogeneous reaction mixture, the densities of all extensive thermodynamic quantities are well defined and equal everywhere in the system. With a slight abuse of notation, we use the same symbol and name for densities as for their corresponding extensive quantity. For example, S is the molar entropy divided by the volume of the solution, but we denote it as *entropy*. We apply the same logic to rates of change. For example, we call entropy production rate the molar entropy production density rate.

B. Affinities, emergent affinities, and local detailed balance

The thermodynamic forces driving reactions are given by differences of chemical potential [Eq. (45)],

$$\Delta_r G_\rho \equiv \nabla_\rho^\sigma \mu_\sigma, \quad (46)$$

also called Gibbs free energies of reaction (Ref. [23], Sec. III. 2, and Ref. [57], Sec. IX.3). Since these must all vanish at equilibrium, $\nabla_\rho^\sigma \mu_\sigma^{\text{eq}} = 0$, $\forall \rho$, we have

$$\Delta_r G_\rho = -RT \nabla_\rho^\sigma \ln \frac{Z_\sigma}{Z_\sigma^{\text{eq}}}. \quad (47)$$

The local detailed balance, Eq. (18)] allows us to express these thermodynamic forces in terms of reaction affinities,

$$A_\rho \equiv RT \ln \frac{J_{+\rho}}{J_{-\rho}} = -\Delta_r G_\rho, \quad (48)$$

which quantify the kinetic force acting along each reaction pathway (Ref. [57], Sec. IV.1.3).

The change of Gibbs free energy along emergent cycles,

$$\mathcal{A}_e = -c_e^\rho \Delta_r G_\rho = -c_e^\rho \nabla_\rho^{\sigma_y} \mu_{\sigma_y}, \quad (49)$$

gives the external thermodynamic forces the network is coupled to, as we see in Eq. (61), and thus provides a thermodynamic meaning to the cycle affinities Eq. (28).

Combining the detailed-balance property Eq. (18) and the equilibrium condition on the affinities $A_\rho^{\text{eq}} = 0$ [Eq. (46)], we can relate the Gibbs free energies of reaction to the rate constants

$$\frac{k^{+\rho}}{k^{-\rho}} = \exp \left\{ -\frac{\Delta_r G_\rho^\circ}{RT} \right\}, \quad (50)$$

where $\Delta_r G_\rho^\circ \equiv \nabla_\rho^\sigma \mu_\sigma^\circ$. This relation is the thermodynamic counterpart of the local detailed balance Eq. (18). It plays the same role as in stochastic thermodynamics, namely, connecting the thermodynamic description to the stochastic dynamics. We emphasize that the local detailed-balance property as well as the local equilibrium assumption by no mean imply that the CRN operates close to equilibrium. Their importance is to assign well-defined equilibrium potentials to the states of the CRN, which are then connected by the nonequilibrium mechanisms, i.e., reactions.

C. Enthalpies and entropies of reaction

To identify the heat produced by the CRN, we need to distinguish the enthalpic change produced by each reaction from the entropic one. We consider the decomposition of the standard-state chemical potentials (Ref. [23], Sec. III. 2):

$$\mu_\sigma^\circ = h_\sigma^\circ - T s_\sigma^\circ. \quad (51)$$

The standard enthalpies of formation $\{h_\sigma^\circ\}$ take into account the enthalpic contributions carried by each species (Ref. [23], Sec. III. 2, and Ref. [72], Sec. X.4.2). Enthalpy changes caused by reactions give the enthalpies of reaction (Ref. [23], Sec. III. 2, and Ref. [57], Sec. II. 4),

$$\Delta_r H_\rho = \nabla_\rho^\sigma h_\sigma^\circ, \quad (52)$$

which at constant pressure measure the heat of reaction. This is the content of the Hess law (see, e.g., Ref. [72], Sec. X.4.1). The standard entropies of formation $\{s_\sigma^\circ\}$ take into account the internal entropic contribution carried by each species under standard-state conditions (Ref. [23], Sec. III. 2). Using Eq. (51), the chemical potentials Eq. (45) can be rewritten as

$$\mu_\sigma = h_\sigma^\circ - T \underbrace{(s_\sigma^\circ - R \ln Z_\sigma)}_{\equiv s_\sigma}. \quad (53)$$

The entropies of formation $\{s_\sigma \equiv s_\sigma^\circ - R \ln Z_\sigma\}$ account for the entropic contribution of each species in the CRN (Ref. [23], Sec. III. 2). Entropy changes along reactions are given by

$$\Delta_r S_\rho = \nabla_\rho^\sigma s_\sigma, \quad (54)$$

called entropies of reaction [23] § 3.2].

D. Entropy balance

1. Entropy production rate

The entropy production rate is a non-negative measure of the break of detailed balance in each chemical reaction. Its typical form is given by (Ref. [8] and Ref. [57], Sec. IX.5)

$$T \dot{S}_i \equiv RT(J_{+\rho} - J_{-\rho}) \ln \frac{J_{+\rho}}{J_{-\rho}} \geq 0, \quad (55)$$

because (1) it is non-negative and vanishes only at equilibrium, i.e., when the detailed-balance property Eq. (17) is satisfied, and (2) it vanishes to first order around equilibrium, thus allowing for quasistatic reversible transformations. Indeed, defining

$$\frac{Z^\sigma - Z_{\text{eq}}^\sigma}{Z_{\text{eq}}^\sigma} = \epsilon^\sigma, \quad |\epsilon^\sigma| \ll 1, \quad \forall \sigma \in \mathcal{S}, \quad (56)$$

we find that

$$\dot{S}_i = E_\sigma^\sigma \epsilon^\sigma \epsilon_\sigma + O(\epsilon^3), \quad (57)$$

where $E \equiv \{E_\sigma^\sigma\}$ is a positive semidefinite symmetric matrix.

Furthermore, it can be rewritten in a thermodynamically appealing way using [Eq. (48)]

$$T \dot{S}_i = -J^\rho \Delta_r G_\rho. \quad (58)$$

It can be further expressed as the sum of two distinct contributions [56]:

$$T \dot{S}_i = \underbrace{-\mu_{\sigma_x} d_t Z^{\sigma_x}}_{\equiv T \dot{S}_x} - \underbrace{\mu_{\sigma_y} (d_t Z^{\sigma_y} - I^{\sigma_y})}_{\equiv T \dot{S}_y}. \quad (59)$$

The first term is due to changes in the internal species and thus vanishes at steady state. The second term is due to the chemostats. It takes into account both the exchange of chemostatted species and the time-dependent driving of their concentration. If the system reaches a nonequilibrium steady state, the external currents $\{\bar{I}^{\sigma_y}\}$ do not vanish and the entropy production reads

$$T \bar{\dot{S}}_i = \bar{I}^{\sigma_y} \mu_{\sigma_y}. \quad (60)$$

This expression can be rewritten as a bilinear form of emergent cycle affinities $\{\mathcal{A}_e\}$ Eq. (49) and currents along the emergent cycle $\{\bar{\mathcal{J}}^e \equiv c_\rho^\varepsilon \bar{J}^\rho\}$ [56]

$$T\dot{S}_i = \bar{\mathcal{J}}^e \mathcal{A}_e, \quad (61)$$

which clearly emphasizes the crucial role of emergent cycles in steady-state dissipation.

2. Entropy flow rate

The entropy flow rate measures the reversible entropy changes in the environment due to exchange processes with the system [57]. Using the expressions for the enthalpy of reaction Eq. (52) and entropy of formation Eq. (53), we express the entropy flow rate as

$$T\dot{S}_e \equiv \underbrace{J^p \Delta_r H_p}_{\equiv \dot{Q}} + I^{\sigma_y} T s_{\sigma_y}. \quad (62)$$

The first contribution is the heat flow rate (positive if heat is absorbed by the system). When divided by temperature, it measures minus the entropy changes in the thermal bath. The second contribution accounts for minus the entropy change in the chemostats.

3. System entropy

The entropy of the ideal dilute solution constituting the CRN is given by (see Appendix A)

$$S = Z^\sigma s_\sigma + RZ^S + S_0. \quad (63)$$

The total concentration term,

$$Z^S \equiv \sum_{\sigma \in \mathcal{S}} Z^\sigma, \quad (64)$$

and the constant S_0 together represent the entropic contribution of the solvent. S_0 may also account for the entropy of chemical species not involved in the reactions. We also prove in Appendix B that the entropy [Eq. (63)] can be obtained as a large particle limit of the stochastic entropy of CRNs.

S would be an equilibrium entropy if the reactions could all be shut down. But in the presence of reactions, it becomes the nonequilibrium entropy of the CRN. Indeed, Using eqs. (53), (58), and (62), we find that its change can be expressed as

$$\begin{aligned} d_t S &= s_\sigma d_t Z^\sigma + Z^\sigma d_t s_\sigma + R d_t Z^S \\ &= s_\sigma d_t Z^\sigma \\ &= J^p \Delta_r S_p + I^{\sigma_y} s_{\sigma_y} \\ &= \dot{S}_i + \dot{S}_e. \end{aligned} \quad (65)$$

This relation is the nonequilibrium formulation of the second law of thermodynamics for CRNs. It demonstrates that the non-negative entropy production Eq. (55) measures

the entropy changes in the system plus those in the reservoirs (thermal and chemostats) [57].

E. Energy balance

1. First law of thermodynamics

Since the CRN is kept at constant pressure p , its enthalpy

$$H = Z^\sigma h_\sigma^\circ + H_0 \quad (66)$$

is equal to the CRN internal energy, up to a constant. Indeed, the enthalpy H is a density which, when written in terms of the internal energy (density) U , reads $H = U + p$.

Using the rate equations (9) and (10), the enthalpy rate of change can be expressed as the sum of the heat flow rate, defined in Eq. (62), and the enthalpy of formation exchange rate:

$$d_t H = h_\sigma^\circ d_t Z^\sigma = \dot{Q} + I^{\sigma_y} h_{\sigma_y}^\circ. \quad (67)$$

Equivalently, it can be rewritten in terms of the entropy flow rate Eq. (62) as (Ref. [57], Sec. IV.1.2)

$$d_t H = T\dot{S}_e + I^{\sigma_y} \mu_{\sigma_y}. \quad (68)$$

The last term on the rhs of Eq. (68) is the free energy exchanged with the chemostats. It represents the chemical work rate performed by the chemostats on the CRN [21,23]:

$$\dot{W}_c \equiv I^{\sigma_y} \mu_{\sigma_y}. \quad (69)$$

Either Eq. (67) or (68) may be considered as the non-equilibrium formulation of the first law of thermodynamics for CRNs. The former has the advantage to solely focus on energy exchanges. The latter contains entropic contributions but is appealing because it involves the chemical work Eq. (69).

2. Nonequilibrium Gibbs free energy

We are now in the position to introduce the thermodynamic potential regulating CRNs. The Gibbs free energy of ideal dilute solutions reads

$$G \equiv H - TS = Z^\sigma \mu_\sigma - RTZ^S + G_0. \quad (70)$$

As for entropy, the total concentration term $-RTZ^S$ and the constant G_0 represent the contribution of the solvent (see Appendix A). Furthermore, in the presence of reactions, G becomes the nonequilibrium Gibbs free energy of CRNs.

We now show that the nonequilibrium Gibbs free energy of a closed CRN is always greater than or equal to its corresponding equilibrium form. A generic non-equilibrium concentration distribution $\{Z^\sigma\}$ is characterized by the set of components $\{L^\lambda = \ell_\sigma^\lambda Z^\sigma\}$. Let $\{Z_{eq}^\sigma\}$ be

the corresponding equilibrium distribution defined by the detailed-balance property Eq. (18) and characterized by the same set of components $\{L^\lambda\}$ [a formal expression for the equilibrium distribution is given in Eq. (88)]. At equilibrium, the Gibbs free energy Eq. (70) reads

$$G_{\text{eq}} = Z_{\text{eq}}^\sigma \mu_\sigma^{\text{eq}} - RT Z_{\text{eq}}^S + G_0. \quad (71)$$

As we discuss in Sec. III B, the equilibrium chemical potentials must satisfy $\nabla_\rho^\sigma \mu_\sigma^{\text{eq}} = 0$. We deduce that μ_σ^{eq} must be a linear combination of the closed system conservation laws Eq. (12),

$$\mu_\sigma^{\text{eq}} = f_\lambda \ell_\sigma^\lambda, \quad (72)$$

where $\{f_\lambda\}$ are real coefficients. Thus, we can write the equilibrium Gibbs free energy as

$$G_{\text{eq}} = f_\lambda L^\lambda - RT Z_{\text{eq}}^S + G_0. \quad (73)$$

In this form, the first term of the Gibbs free energy appears as a bilinear form of components $\{L^\lambda\}$ and conjugated generalized forces $\{f_\lambda\}$ (Ref. [23], Sec. III. 3), which can be thought of as chemical potentials of the components. From Eq. (72) and the properties of components Eq. (13), the equality $Z_{\text{eq}}^\sigma \mu_\sigma^{\text{eq}} = Z^\sigma \mu_\sigma^{\text{eq}}$ follows. Hence, using the definition of chemical potential Eq. (45), the nonequilibrium Gibbs free energy G of the generic distribution $\{Z^\sigma\}$ defined above is related to G_{eq} [Eq. (73)] by

$$G = G_{\text{eq}} + RT \mathcal{L}(\{Z^\sigma\} | \{Z_{\text{eq}}^\sigma\}), \quad (74)$$

where we introduce the relative entropy for non-normalized concentration distributions, also called the Shear Lyapunov function or the pseudo-Helmholtz function [35,73,74]:

$$\mathcal{L}(\{Z^\sigma\} | \{Z'^\sigma\}) \equiv Z^\sigma \ln \frac{Z_\sigma}{Z'_\sigma} - (Z^S - Z'^S) \geq 0. \quad (75)$$

This quantity is a natural generalization of the relative entropy, or Kullback-Leibler divergence, used to compare two normalized probability distributions [75]. For simplicity, we still refer to it as relative entropy. It quantifies the distance between two distributions: it is always positive and vanishes only if the two distributions are identical: $\{Z^\sigma\} = \{Z'^\sigma\}$. Hence, Eq. (74) proves that the nonequilibrium Gibbs free energy of a closed CRN is always greater than or equal to its corresponding equilibrium form, $G \geq G_{\text{eq}}$.

We now proceed to show that the nonequilibrium Gibbs free energy is minimized by the dynamics in closed CRNs; viz., G —or, equivalently, $\mathcal{L}(\{Z^\sigma\} | \{Z_{\text{eq}}^\sigma\})$ [59,76]—acts as a Lyapunov function in closed CRNs. Indeed, the time derivative of G Eq. (70) always reads

$$\begin{aligned} d_t G &= \mu_\sigma d_t Z^\sigma + Z^\sigma d_t \mu_\sigma + R d_t Z^S \\ &= \mu_\sigma d_t Z^\sigma. \end{aligned} \quad (76)$$

When using the rate equation for closed CRNs Eq. (7), we find that $d_t G = -J^\rho \nabla_\rho^\sigma \mu_\sigma$. Using Eq. (74) together with Eqs. (46) and (58), we get

$$d_t G = RT d_t \mathcal{L}(\{Z^\sigma\} | \{Z_{\text{eq}}^\sigma\}) = -T \dot{S}_i \leq 0, \quad (77)$$

which proves the aforementioned result.

3. Chemical work

In arbitrary CRNs, the rate of change of nonequilibrium Gibbs free energy, Eq. (76), can be related to the entropy production rate, Eq. (59), using the rate equations of open CRN, Eqs. (9) and (10), and the chemical work rate, Eq. (69):

$$T \dot{S}_i = \dot{W}_c - d_t G \geq 0. \quad (78)$$

This important result shows that the positivity of the entropy production sets an intrinsic limit on the chemical work that the chemostats must perform on the CRN to change its concentration distribution. The equality sign is achieved for quasistatic transformations ($\dot{S}_i \approx 0$).

If we now integrate Eq. (78) along a transformation generated by an arbitrary time-dependent protocol $\pi(t)$, which drives the CRN from an initial concentration distribution $\{Z_i^\sigma\}$ to a final one $\{Z_f^\sigma\}$, we find

$$T \Delta_i S = W_c - \Delta G \geq 0, \quad (79)$$

where $\Delta G = G_f - G_i$ is the difference of nonequilibrium Gibbs free energies between the final and the initial state. Let us also consider the equilibrium state $\{Z_{\text{eqf}}^\sigma\}$ ($\{Z_{\text{eqf}}^\sigma\}$) obtained from $\{Z_i^\sigma\}$ ($\{Z_f^\sigma\}$) if one closes the network (i.e., interrupts the chemostatting procedure) and lets it relax to equilibrium, as illustrated in Fig. 4. The Gibbs free energy difference between these two equilibrium distributions, $\Delta G_{\text{eq}} = G_{\text{eqf}} - G_{\text{eqi}}$, is related to ΔG via the difference of relative entropies, Eq. (74):

$$\Delta G = \Delta G_{\text{eq}} + RT \Delta \mathcal{L}, \quad (80)$$

where

$$\Delta \mathcal{L} \equiv \mathcal{L}(\{Z_f^\sigma\} | \{Z_{\text{eqf}}^\sigma\}) - \mathcal{L}(\{Z_i^\sigma\} | \{Z_{\text{eqi}}^\sigma\}). \quad (81)$$

Thus, the chemical work Eq. (79) can be rewritten as

$$W_c - \Delta G_{\text{eq}} = RT \Delta \mathcal{L} + T \Delta_i S, \quad (82)$$

which is a key result of our paper. ΔG_{eq} represents the reversible work needed to reversibly transform the CRN

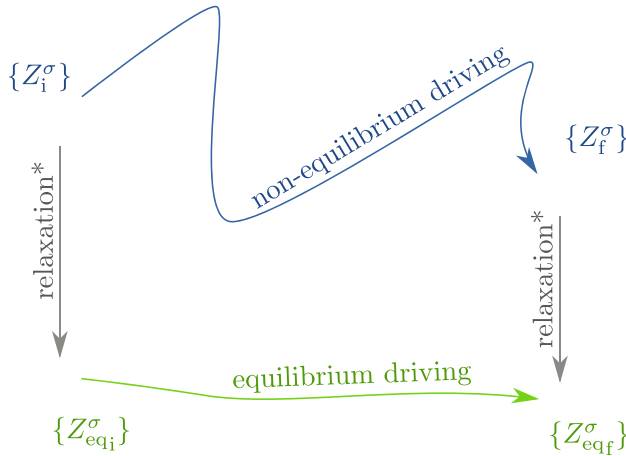


FIG. 4. Pictorial representation of the transformation between two nonequilibrium concentration distributions. The nonequilibrium transformation (blue line) is compared with the equilibrium one (green line). The equilibrium transformation depends on the equilibrium states corresponding to the initial and final concentration distributions. In Sec. III E 3, for an arbitrary CRN, these equilibrium states are obtained by first closing the network and then letting it relax to equilibrium. Instead, in Sec. V, for a detailed balance CRN, the equilibrium states are obtained by simply stopping the time-dependent driving and letting the system spontaneously relax to equilibrium.

from $\{Z_{\text{eqi}}^{\sigma}\}$ to $\{Z_{\text{eqf}}^{\sigma}\}$. Implementing such a reversible transformation may be difficult to achieve in practice. However, it allows us to interpret the difference $W_c^{\text{irr}} \equiv W_c - \Delta G_{\text{eq}}$ in Eq. (82) as the chemical work dissipated during the nonequilibrium transformation, i.e., the irreversible chemical work. The positivity of the entropy production implies that

$$W_c^{\text{irr}} \geq RT\Delta\mathcal{L}. \quad (83)$$

This relation sets limits on the irreversible chemical work involved in arbitrary far-from-equilibrium transformations. For transformations connecting two equilibrium distributions, we get the expected inequality $W_c^{\text{irr}} \geq 0$. More interestingly, Eq. (83) tells us how much chemical work the chemostat needs to provide to create a nonequilibrium distribution from an equilibrium one. It also tells us how much chemical work can be extracted from a CRN relaxing to equilibrium.

The conceptual analogue of Eq. (82) in stochastic thermodynamics (where probability distributions replace non-normalized concentration distributions) is called the nonequilibrium Landauer principle [42,43] (see also Refs. [77–79]). It has been shown to play a crucial role in analyzing the thermodynamic cost of information processing (e.g., for Maxwell demons, feedback control, or proofreading). The inequality Eq. (83) is, therefore, a nonequilibrium Landauer principle for CRN.

IV. THERMODYNAMICS OF COMPLEX-BALANCED NETWORKS

In this section, we focus on unconditionally complex-balanced networks. We see that the thermodynamics of these networks bears remarkable similarities to stochastic thermodynamics.

Let us first observe that whenever a CRN displays a well-defined steady-state distribution $\{\bar{Z}^{\sigma_x}\}$, the entropy production rate Eq. (55) can be formally decomposed as the sum of an adiabatic and a nonadiabatic contribution,

$$T\dot{S}_i = \underbrace{J^{\rho}RT \ln \frac{\bar{J}^{\rho}}{\bar{J}^{-\rho}}}_{\equiv T\dot{S}_a} - d_i Z^{\sigma_x} RT \ln \frac{Z^{\sigma_x}}{\bar{Z}^{\sigma_x}}, \quad (84)$$

$$\equiv T\dot{S}_{\text{na}}$$

in analogy with what was done in stochastic thermodynamics [46–50]. As we discuss in Sec. II E, unconditionally complex-balanced networks have a unique steady-state distribution, $\{\bar{Z}^{\sigma_x} \equiv \bar{Z}^{\sigma_x}(\pi(t))\}$, Eq. (37), for any value of the chemostatted concentrations, $\{Z^{\sigma_y} \equiv Z^{\sigma_y}(\pi(t))\}$, and of the fixed unbroken components $\{L^{\lambda_u}\}$. The decomposition Eq. (84) is thus well defined at any time, for any protocol $\pi(t)$. As a central result, we prove in Appendix C that the adiabatic and nonadiabatic contribution are non-negative for unconditionally complex-balanced networks as well as for complex-balanced networks without time-dependent driving.

The adiabatic entropy production rate encodes the dissipation of the steady state $\{\bar{Z}^{\sigma_x}\}$. It can be rewritten in terms of the steady-state Gibbs free energy of reaction $\{\Delta_r \bar{G}_{\rho}\}$ Eq. (48) as

$$T\dot{S}_a = -J^{\rho} \Delta_r \bar{G}_{\rho} \geq 0. \quad (85)$$

This inequality highlights the fact that the transient dynamics—generating the currents $\{J^{\rho}\}$ —is constrained by the thermodynamics of the complex-balanced steady state, i.e., by $\{\Delta_r \bar{G}_{\rho}\}$.

The nonadiabatic entropy production rate characterizes the dissipation of the transient dynamics. It can be decomposed as

$$T\dot{S}_{\text{na}} = -RT d_i \mathcal{L}(\{Z^{\sigma_x}\} | \{\bar{Z}^{\sigma_x}\}) + \underbrace{RT d_i \bar{Z}^{\mathcal{S}_x} - Z^{\sigma_x} d_i \bar{\mu}_{\sigma_x}}_{\equiv T\dot{S}_d} \geq 0, \quad (86)$$

where $\bar{Z}^{\mathcal{S}_x} = \sum_{\sigma_x \in \mathcal{S}_x} \bar{Z}^{\sigma_x}$ (see Refs. [46,48] for the analogous decomposition in the stochastic context). The first term is proportional to the time derivative of the relative entropy Eq. (75) between the nonequilibrium concentration distribution at time t and the corresponding complex-balanced steady-state distribution. Hence, it describes the dissipation of the relaxation towards the steady state. The

second term, $T\dot{S}_d$, is related to the time-dependent driving performed via the chemostatted species and thus denoted the driving entropy production rate [46]. It vanishes in nondriven networks where we obtain

$$\dot{S}_{\text{na}} = -Rd_t \mathcal{L}(\{Z^{\sigma_x}\}|\{\bar{Z}^{\sigma_x}\}) \geq 0. \quad (87)$$

This result shows the role of the relative entropy $\mathcal{L}(\{Z^{\sigma_x}\}|\{\bar{Z}^{\sigma_x}\})$ as a Lyapunov function in nondriven complex-balanced networks with mass action kinetics. It was known in the mathematical literature [35,80], but we provide a clear thermodynamic interpretation to this result by demonstrating that it derives from the nonadiabatic entropy production rate.

We mention that an alternative derivation of the adiabatic–nonadiabatic decomposition for nondriven complex-balanced networks with mass action kinetics was very recently found in Ref. [51].

V. THERMODYNAMICS OF OPEN DETAILED-BALANCED NETWORKS

We finish our study by considering detailed-balanced networks. We discuss the equilibrium distribution, introduce a new class of nonequilibrium potentials, and derive a new work inequality.

Let us also emphasize that open detailed-balanced CRNs are a special class of open complex-balanced CRNs for which the adiabatic entropy production rate vanishes (since the steady state is detailed balanced) and thus the nonadiabatic entropy production characterizes the entire dissipation.

A. Equilibrium distribution

As we discuss in Sec. II D, for given kinetics $\{k^{\pm\rho}\}$, chemostatting $\{Z^{\sigma_y}\}$ and unbroken components $\{L^{\lambda_u}\}$, detailed-balanced networks always relax to a unique equilibrium distribution. Since the equilibrium chemical potentials can be expressed as a linear combination of conservation laws, Eq. (72), we can express the equilibrium distribution as

$$Z_\sigma^{\text{eq}} = \exp \left\{ -\frac{\mu_\sigma^\circ - f_{\lambda_b} \ell_\sigma^{\lambda_b}}{RT} \right\}, \quad (88)$$

inverting the expression for the chemical potentials Eq. (45). Since the independent set of unbroken conservation laws $\{\ell^{\lambda_u}\}$ is such that $\ell_{\sigma_y}^{\lambda_u} = 0, \forall \lambda_u, \sigma_y$, see Sec. II C, we have that

$$\mu_{\sigma_y}^{\text{eq}} = f_{\lambda_b} \ell_{\sigma_y}^{\lambda_b}, \quad \forall \sigma_y \in \mathcal{S}_y. \quad (89)$$

We thus conclude that the $|\lambda_b|$ broken generalized forces $\{f_{\lambda_b}\}$ depend on only the chemostatted concentrations $\{Z^{\sigma_y}\}$. Instead, the remaining $|\lambda_u|$ unbroken generalized

forces f_{λ_u} can be determined by inverting the nonlinear set of equations $L^{\lambda_u} = \ell_{\sigma_x}^{\lambda_u} Z_{\text{eq}}^{\sigma_x}$. They, therefore, depend on both $\{Z^{\sigma_y}\}$ and $\{L^{\lambda_u}\}$.

One can easily recover the local detailed-balanced property [Eqs. (50) and (18)] using Eq. (88).

B. Open nondriven networks

As a consequence of the break of conservation laws, the nonequilibrium Gibbs free energy G Eq. (70) is no longer minimized at equilibrium in open detailed-balanced networks. In analogy to equilibrium thermodynamics [23], the proper thermodynamic potential is obtained from G by subtracting the energetic contribution of the broken conservation laws. This transformed nonequilibrium Gibbs free energy reads

$$\begin{aligned} \mathcal{G} &\equiv G - f_{\lambda_b} L^{\lambda_b} \\ &= Z^\sigma (\mu_\sigma - f_{\lambda_b} \ell_\sigma^{\lambda_b}) - RTZ^S + G_0. \end{aligned} \quad (90)$$

We proceed to show that \mathcal{G} is minimized by the dynamics in nondriven open detailed-balanced networks. Let $\{Z^{\sigma_x}\}$ be a generic concentration distribution in a detailed-balanced network characterized by $\{L^{\lambda_u}\}$ and $\{Z^{\sigma_y}\}$, and let $\{Z_{\text{eq}}^{\sigma_x}\}$ be its corresponding equilibrium. Using the relation between equilibrium chemical potentials and conservation laws Eq. (72), the transformed Gibbs free energy Eq. (90) at equilibrium reads

$$\mathcal{G}_{\text{eq}} = f_{\lambda_u} L^{\lambda_u} - RTZ_{\text{eq}}^S + G_0. \quad (91)$$

Yet, combining Eq. (72) and the properties of unbroken components, one can readily show that $Z_{\text{eq}}^{\sigma_x} (\mu_\sigma^{\text{eq}} - f_{\lambda_b} \ell_\sigma^{\lambda_b}) = Z^\sigma (\mu_\sigma^{\text{eq}} - f_{\lambda_b} \ell_\sigma^{\lambda_b})$. The relation between the nonequilibrium \mathcal{G} and the corresponding equilibrium value thus follows

$$\mathcal{G} = \mathcal{G}_{\text{eq}} + RT\mathcal{L}(\{Z^{\sigma_x}\}|\{Z_{\text{eq}}^{\sigma_x}\}) \quad (92)$$

(we show in Appendix A the derivation of the latter in the presence of a reacting solvent). The non-negativity of the relative entropy for concentration distributions $\mathcal{L}(\{Z^{\sigma_x}\}|\{Z_{\text{eq}}^{\sigma_x}\})$ ensures that the nonequilibrium transformed Gibbs free energy is always greater than or equal to its equilibrium value, $\mathcal{G} \geq \mathcal{G}_{\text{eq}}$. Since entropy production and nonadiabatic entropy production coincide, using Eqs. (87) and (92), we obtain

$$d_t \mathcal{G} = RT d_t \mathcal{L}(\{Z^{\sigma_x}\}|\{Z_{\text{eq}}^{\sigma_x}\}) = -T\dot{S}_i \leq 0, \quad (93)$$

which demonstrates the role of \mathcal{G} as a Lyapunov function. The relative entropy $\mathcal{L}(\{Z^{\sigma_x}\}|\{Z^{\sigma_x}\})$ was known to be a Lyapunov function for detailed-balanced networks [76,81], but we provide its clear connection to the transformed nonequilibrium Gibbs free energy. To summarize, instead

of minimizing the nonequilibrium Gibbs free energy G Eq. (70) as in closed CRNs, the dynamics minimizes the transformed nonequilibrium Gibbs free energy \mathcal{G} in open nondriven detailed-balanced CRNs.

C. Open driven networks

We now consider unconditionally detailed-balanced CRNs. As we discuss in Sec. II D, they are characterized by a unique equilibrium distribution $\{Z_{\text{eq}}^{\sigma_x} \equiv Z_{\text{eq}}^{\sigma_x}(\pi(t))\}$, defined by Eq. (18), for any value of the chemostatted concentrations $\{Z^{\sigma_y} = Z^{\sigma_y}(\pi(t))\}$.

We start by showing that the external fluxes $\{I^{\sigma_y}\}$ can be expressed as the influx rate of moieties. Since the CRN is open and unconditionally detailed balanced, each chemostatted species breaks a conservation law (no emergent cycle is created, Sec. II D). Therefore, the matrix whose entries are $\{\ell_{\sigma_y}^{\lambda_b}\}$ in Eq. (89) is square and also nonsingular [82]. We can thus invert Eq. (89) to get

$$f_{\lambda_b} = \mu_{\sigma_y}^{\text{eq}} \hat{\ell}_{\lambda_b}^{\sigma_y}, \quad (94)$$

where $\{\hat{\ell}_{\lambda_b}^{\sigma_y}\}$ denote the entries of the inverse matrix of that with entries $\{\ell_{\sigma_y}^{\lambda_b}\}$. Hence, using the definition of a broken component, $\{L^{\lambda_b} \equiv \ell_{\sigma_y}^{\lambda_b} Z^{\sigma_y}\}$, we obtain that

$$f_{\lambda_b} L^{\lambda_b} = \mu_{\sigma_y}^{\text{eq}} \underbrace{\hat{\ell}_{\lambda_b}^{\sigma_y} \ell_{\sigma_y}^{\lambda_b} Z^{\sigma_y}}_{\equiv M^{\sigma_y}}. \quad (95)$$

From the rate equations for the chemostatted concentrations Eq. (10), we find that

$$d_t M^{\sigma_y} = I^{\sigma_y}, \quad \forall \sigma_y \in \mathcal{S}_y. \quad (96)$$

We can thus interpret M^{σ_y} as the concentration of a moiety that is exchanged with the environment only through the chemostatted species X_{σ_y} . Equation (95) shows that the energetic contribution of the broken components can be expressed as the Gibbs free energy carried by these specific moieties.

Example 12.—A simple implementation of this scenario is the thermodynamic description of CRNs at constant pH (Ref. [23], Chap. 4), where the chemostatted species becomes the ion H^+ and M^{H^+} is the total amount of H^+ ions in the system. The transformed Gibbs potential thus becomes $G' = G - \mu_{H^+} M^{H^+}$ and the transformed chemical potentials can be written in our formalism as $\mu'_{\sigma_x} = \mu_{\sigma_x} - \mu_{H^+} \hat{\ell}_b^{\text{H}^+} \ell_{\sigma_x}^b$, where $\ell_{\sigma_x}^b$ is the conservation law broken by chemostatting H^+ . \square

Example 13.—For the CRN in Fig. 2, whose conservation laws are given in example 4, the concentrations of the exchanged moieties are

$$\begin{aligned} M^1 &= Z^a + \frac{1}{2} Z^b, \\ M^2 &= Z^d + Z^e. \end{aligned} \quad (97)$$

For the specific implementation of that CRN, Fig. 3, the first term (second term) is the total number of moiety 2H (C) in the system, which can be exchanged with the environment only via the chemostatted species H_2O (CO). \square

We now turn to the new work relation. From the general work relation Eq. (78), using Eqs. (90) and (95), we find

$$T \dot{S}_i = \dot{W}_d - d_t \mathcal{G} \geq 0, \quad (98)$$

where the driving work due to the time-dependent driving of the chemostatted species is obtained using the chemical work rate Eq. (69) together with Eqs. (95) and (96):

$$\begin{aligned} \dot{W}_d &\equiv \dot{W}_c - d_t (f_{\lambda_b} L^{\lambda_b}) \\ &= \mu_{\sigma_y}^{\text{eq}} d_t M^{\sigma_y} - d_t (\mu_{\sigma_y}^{\text{eq}} M^{\sigma_y}) \\ &= -d_t \mu_{\sigma_y}^{\text{eq}} M^{\sigma_y}. \end{aligned} \quad (99)$$

Equivalently, the driving work rate Eq. (99) can be defined as the rate of change of the transformed Gibbs free energy Eq. (90) due to the time-dependent driving only; i.e.,

$$\dot{W}_d \equiv \frac{\partial \mathcal{G}}{\partial t} \equiv d_t \mu_{\sigma_y}^{\text{eq}} \frac{\partial \mathcal{G}}{\partial \mu_{\sigma_y}^{\text{eq}}}. \quad (100)$$

To relate this alternative definition to Eq. (99), all $\{Z^{\sigma_y}\}$ must be expressed in terms of $\{\mu_{\sigma_y}^{\text{eq}}\}$ using the definition of chemical potential Eq. (45).

The driving work rate \dot{W}_d vanishes in nondriven CRNs, where Eq. (98) reduces to Eq. (93). After demonstrating that the entropy production rate is always proportional to the difference between the chemical work rate and the change of nonequilibrium Gibbs free energy in Eq. (79), we show that, for unconditionally detailed-balanced CRNs, it is also proportional to the difference between the driving work rate and the change in transformed nonequilibrium Gibbs free energy, Eq. (98).

We end by formulating a nonequilibrium Landauer principle for the driving work instead of the chemical work done in Sec. III E 3. We consider a time-dependent transformation driving the unconditionally detailed-balanced CRN from $\{Z_i^{\sigma}\}$ to $\{Z_f^{\sigma}\}$. The distribution $\{Z_{\text{eq}}^{\sigma}\}$ ($\{Z_{\text{eq}}^{\sigma}\}$) denotes the equilibrium distribution obtained from $\{Z_i^{\sigma}\}$ ($\{Z_f^{\sigma}\}$) by stopping the time-dependent driving and letting the system relax towards the equilibrium, Fig. 4. Note that this reference equilibrium state is different from the one obtained by closing the network in Sec. III E 3. Integrating Eq. (98) over time and using Eq. (92), we get

$$W_d - \Delta\mathcal{G}_{eq} = RT\Delta\mathcal{L} + T\Delta_i S, \quad (101)$$

where

$$\Delta\mathcal{L} \equiv \mathcal{L}(\{Z_f^{\sigma_x}\}|\{Z_{eqf}^{\sigma_x}\}) - \mathcal{L}(\{Z_i^{\sigma_x}\}|\{Z_{eqi}^{\sigma_x}\}). \quad (102)$$

$\Delta\mathcal{G}_{eq}$ represents the reversible driving work, and the irreversible driving work satisfies the inequality

$$W_d^{irr} \equiv W_d - \Delta\mathcal{G}_{eq} \geq RT\Delta\mathcal{L}. \quad (103)$$

This central relation sets limits on the irreversible work spent to manipulate nonequilibrium distributions. It is a nonequilibrium Landauer principle for the driving work by the same reasons that inequality Eq. (83) is a nonequilibrium Landauer principle for the chemical work. The key difference is that the choice of the reference equilibrium state is different in the two cases. The above discussed inequality Eq. (103) holds only for unconditionally detailed-balanced CRNs, while Eq. (83) is valid for any CRNs.

VI. CONCLUSIONS AND PERSPECTIVES

Following a strategy reminiscent of stochastic thermodynamics, we systematically build a nonequilibrium thermodynamic description for open driven CRNs made of elementary reactions in homogeneous ideal dilute solutions. The dynamics is described by deterministic rate equations whose kinetics satisfies mass action law. Our framework is not restricted to steady states and allows us to treat transients as well as time-dependent drivings performed by externally controlled chemostatted concentrations. Our theory embeds the nonequilibrium thermodynamic framework of irreversible processes established by the Brussels School of Thermodynamics.

We now summarize our results. Starting from the expression for the entropy production rate, we establish a nonequilibrium formulation of the first and second law of thermodynamics for CRNs. The resulting expression for the system entropy is that of an ideal dilute solution. The clear separation between chemostatted and internal species allows us to identify the chemical work done by the chemostats on the CRN and to relate it to the nonequilibrium Gibbs potential. We are also able to express the minimal chemical work necessary to change the nonequilibrium distribution of species in the CRN as a difference of relative entropies for non-normalized distributions. The latter measure the distance of the initial and final concentration distributions from their corresponding equilibrium ones, obtained by closing the network. This result is reminiscent of the nonequilibrium Landauer principle derived in stochastic thermodynamics [43] and which prove very useful to study the energetic cost of information processing [45]. We also highlight the deep relationship between the topology of CRNs, their dynamics, and their

thermodynamics. Closed CRNs (nondriven open detailed-balanced networks) always relax to a unique equilibrium by minimizing their nonequilibrium Gibbs free energy (transformed nonequilibrium Gibbs free energy). This latter is given, up to a constant, by the relative entropy between the nonequilibrium and equilibrium concentration distribution. Nondriven complex-balanced networks relax to complex-balanced nonequilibrium steady states by minimizing the relative entropy between the nonequilibrium and steady-state concentration distribution. In all these cases, even in the presence of driving, we show how the rate of change of the relative entropy relates to the CRN dissipation. For complex-balanced networks, we also demonstrate that the entropy production rate can be decomposed, as in stochastic thermodynamics, in its adiabatic and nonadiabatic contributions quantifying, respectively, the dissipation of the steady state and of the transient dynamics.

Our framework could be used to shed new light on a broad range of problems. We mention only a few.

Stochastic thermodynamics has been successfully used to study the thermodynamics cost of information processing in various synthetic and biological systems [44,83–87]. However, most of these are modeled as few state systems or linear networks [8,9]—e.g., quantum dots [88], molecular motors [89,90], and single enzyme mechanisms [91,92]—while biochemical networks involve more-complex descriptions. The present work overcomes this limitation. It could be used to study biological information-handling processes, such as kinetic proofreading [93–99] or enzyme-assisted copolymerization [92,100–105], which have currently only been studied as single enzyme mechanisms.

Our theory could also be used to study metabolic networks. However, these require some care, since complex enzymatic reaction mechanisms are involved [106]. Nevertheless, our framework provides a basis to build effective coarse-graining procedures for enzymatic reactions [107]. For instance, proofreading mechanisms operating in metabolic processes could be considered [108]. We foresee an increasing use of thermodynamics to improve the modeling of metabolic networks, as recently shown in Refs. [30,32,33].

Since our framework accounts for time-dependent drivings and transient dynamics, it could be used to represent the transmission of signals through CRNs or their response to external modulations in the environment. These features become crucial when considering problems such as signal transduction and biochemical switches [24,109,110], biochemical oscillations [28,111], growth and self-organization in evolving biosystems [112,113], or sensory mechanisms [85,87,114–117]. Also, since transient signals in CRNs can be used for computation [118] and have been shown to display Turing universality [119–122], one should be able to study the thermodynamic cost of chemical computing [123].

Finally, one could use our framework to study any process that can be described as nucleation or reversible polymerization [124–129] (see also Ref. [130], Chaps. 5 ad 6) since these processes can be described as CRNs [63].

As closing words, we believe that our results constitute an important contribution to the theoretical study of CRNs. It does for nonlinear chemical kinetics what stochastic thermodynamics has done for stochastic dynamics, namely, build a systematic nonequilibrium thermodynamics on top of the dynamics. It also opens many new perspectives and builds bridges between approaches from different communities studying CRNs: mathematicians who study CRNs as dynamical systems, physicists who study them as nonequilibrium complex systems, and biochemists as well as bioengineers who aim for accurate models of metabolic networks.

ACKNOWLEDGMENTS

The present project was supported by the Luxembourg National Research Fund (Project No. FNR/A11/02 and AFR Ph.D. Grant 2014-2, No. 9114110) as well as by the European Research Council (Project No. 681456).

APPENDIX A: THERMODYNAMICS OF IDEAL DILUTE SOLUTIONS

We show that the nonequilibrium Gibbs free energy Eq. (70) is the Gibbs free energy of an ideal dilute solution (Ref. [131], Chap. 7) (see also Ref. [51]). We also show that in open detailed-balanced networks in which the solvent reacts with the solutes, the expression of the transformed Gibbs free energy Eq. (92) is recovered by treating the solvent as a special chemostatted species.

The Gibbs free energy (density) of an ideal dilute mixture of chemical compounds kept at constant temperature and pressure reads

$$G = Z^\sigma \mu_\sigma + Z_0 \mu_0 \quad (\text{A1})$$

where the labels $\sigma \in \mathcal{S}$ refer to the solutes and 0 to the solvent. The chemical potentials of each species Eq. (45) read

$$\begin{aligned} \mu_\sigma &= \mu_\sigma^\circ + RT \ln \frac{Z_\sigma}{Z_{\text{tot}}}, \quad \forall \sigma \in \mathcal{S}, \\ \mu_0 &= \mu_0^\circ + RT \ln \frac{Z_0}{Z_{\text{tot}}}. \end{aligned} \quad (\text{A2})$$

Since the solution is dilute, $Z_{\text{tot}} = \sum_{\sigma \in \mathcal{S}} Z^\sigma + Z_0 \simeq Z_0$ and the standard-state chemical potentials $\{\mu_\sigma^\circ\}$ depend on the nature of the solvent. Hence, the chemical potentials of the solutes read

$$\mu_\sigma \simeq \mu_\sigma^\circ + RT \ln \frac{Z_\sigma}{Z_0}, \quad \forall \sigma \in \mathcal{S}, \quad (\text{A3})$$

while that of the solvent reads

$$\mu_0 \simeq \mu_0^\circ - RT \frac{Z^S}{Z_0}, \quad (\text{A4})$$

where $Z^S \equiv \sum_{\sigma \in \mathcal{S}} Z^\sigma$. Therefore, the Gibbs free energy Eq. (A1) reads

$$G \simeq Z^\sigma \mu_\sigma + Z_0 \mu_0^\circ - RT Z^S, \quad (\text{A5})$$

which is Eq. (70), where G_0 is equal to $Z_0 \mu_0^\circ$ plus possibly the Gibbs free energy of solutes that do not react.

We now consider the case where the solvent reacts with the solutes. We assume that both the solutes and the solvent react according to the stoichiometric matrix

$$\nabla = \begin{pmatrix} \nabla^0 \\ \nabla^X \\ \nabla^Y \end{pmatrix}, \quad (\text{A6})$$

where the first row refers to the solvent, the second block of rows to the internal species, and the last one to the chemostatted species. The solvent is treated as a chemostatted species such that $d_i Z_0 = 0$.

In order to recover the expression for the transformed Gibbs free energy Eq. (92) in unconditionally detailed-balanced networks, we observe that, at equilibrium,

$$\nabla_\rho^\sigma \mu_\sigma^{\text{eq}} + \nabla_\rho^0 \mu_0^{\text{eq}} = 0. \quad (\text{A7})$$

Therefore, the equilibrium chemical potentials are a linear combination of the conservation laws of ∇ [Eq. (A6)],

$$\begin{aligned} \mu_\sigma^{\text{eq}} &= f_\lambda \ell_\sigma^\lambda, \\ \mu_0^{\text{eq}} &= f_\lambda \ell_0^\lambda. \end{aligned} \quad (\text{A8})$$

As mentioned Sec. II C, the chemostatting procedure breaks some conservation laws, which are labeled by λ_b . The unbroken ones are labeled by λ_u .

The transformed Gibbs free energy is defined as in Eq. (90), reported here for convenience,

$$\mathcal{G} \equiv G - f_{\lambda_b} L^{\lambda_b}, \quad (\text{A9})$$

where G reads as in Eq. (A1), $\{L^{\lambda_b}\}$ are the broken components, and $\{f_{\lambda_b}\}$ are here interpreted as the conjugated generalized forces. Adding and subtracting the term $Z^\sigma \mu_\sigma^{\text{eq}} + Z_0 \mu_0^{\text{eq}}$ from the last equation and using Eq. (A8), we obtain

$$\mathcal{G} = \mathcal{G}_{\text{eq}} + Z^\sigma (\mu_\sigma - \mu_\sigma^{\text{eq}}) + Z_0 (\mu_0 - \mu_0^{\text{eq}}), \quad (\text{A10})$$

where

$$\mathcal{G}_{\text{eq}} = f_{\lambda_u} L^{\lambda_u}. \quad (\text{A11})$$

From Eqs. (A3) and (A4) and the fact that $Z^{\sigma_y} = Z_{\text{eq}}^{\sigma_y}$ and $Z_0 = Z_0^{\text{eq}}$, we obtain

$$\begin{aligned} \mathcal{G} &\simeq \mathcal{G}_{\text{eq}} + Z^{\sigma_x}(\mu_{\sigma_x} - \mu_{\sigma_x}^{\text{eq}}) - RT(Z^{\mathcal{S}_x} - Z_{\text{eq}}^{\mathcal{S}_x}) \\ &= \mathcal{G}_{\text{eq}} + Z^{\sigma_x}RT \ln \frac{Z^{\sigma_x}}{Z_{\text{eq}}^{\sigma_x}} - RT(Z^{\mathcal{S}_x} - Z_{\text{eq}}^{\mathcal{S}_x}) \\ &\equiv \mathcal{G}_{\text{eq}} + RT\mathcal{L}(\{Z^{\sigma_x}\}|\{Z_{\text{eq}}^{\sigma_x}\}), \end{aligned} \quad (\text{A12})$$

in agreement with the expression derived in the main text, Eq. (92).

APPENDIX B: ENTROPY OF CRNs

We show how the nonequilibrium entropy Eq. (63) can be obtained as a large particle limit of the stochastic entropy. We point out that very recently similar derivations for other thermodynamic quantities have been obtained in Refs. [51,132].

In the stochastic description of CRNs, the state is characterized by the population vector $\mathbf{n} = \{n^\sigma\}$. The probability to find the network is in state \mathbf{n} at time t is denoted $p_t(\mathbf{n})$. The stochastic entropy of that state reads [21,107], up to constants,

$$S(\mathbf{n}) = -k_B \ln p_t(\mathbf{n}) + s(\mathbf{n}). \quad (\text{B1})$$

The first term is a Shannon-like contribution, while the second term is the configurational entropy,

$$s(\mathbf{n}) \equiv n^\sigma \tilde{s}_\sigma^\circ - k_B \sum_\sigma \ln \frac{n^\sigma!}{n_0^{n^\sigma}}. \quad (\text{B2})$$

\tilde{s}_σ° is the standard entropy of one single X_σ molecule, and n_0 is the very large number of solvent molecules.

We now assume that the probability becomes very narrow in the large particle limit $n^\sigma \gg 1$ and behaves as a discrete delta function $p_t(\mathbf{n}) \simeq \delta[\mathbf{n} - \hat{\mathbf{n}}(t)]$. The vector $\hat{\mathbf{n}}(t) \equiv \{\hat{n}^\sigma\}$ denotes the most probable and macroscopic amount of chemical species, such that $Z^\sigma = \hat{n}^\sigma/(VN_A)$. Hence, the average entropy becomes

$$\langle S \rangle = \sum_{\mathbf{n}} p_t(\mathbf{n}) S(\mathbf{n}) \simeq s(\hat{\mathbf{n}}). \quad (\text{B3})$$

When using the Stirling approximation ($\ln m! \simeq m \ln m - m$ for $m \gg 1$), we obtain

$$\begin{aligned} s(\hat{\mathbf{n}}) &\simeq \hat{n}^\sigma \tilde{s}_\sigma^\circ - \hat{n}^\sigma k_B \ln \frac{\hat{n}^\sigma}{n_0} + k_B \sum_\sigma \hat{n}^\sigma \\ &= \hat{n}^\sigma \left(\tilde{s}_\sigma^\circ + k_B \ln \frac{n_0}{VN_A} \right) \\ &\quad + -\hat{n}^\sigma k_B \ln \frac{\hat{n}^\sigma}{VN_A} + k_B \sum_\sigma \hat{n}^\sigma \\ &\equiv \hat{n}^\sigma (\tilde{s}_\sigma^\circ + k_B \ln Z_0) \\ &\quad + -\hat{n}^\sigma k_B \ln Z^\sigma + k_B \sum_\sigma \hat{n}^\sigma. \end{aligned} \quad (\text{B4})$$

Dividing by V and using the relation $R = N_A k_B$, we finally get the macroscopic entropy density Eq. (63)

$$\langle S \rangle / V \simeq Z^\sigma s_\sigma^\circ - Z^\sigma R \ln Z_\sigma + RZ^\sigma, \quad (\text{B5})$$

where the (molar) standard entropies of formation s_σ° reads

$$s_\sigma^\circ = N_A (\tilde{s}_\sigma^\circ + k_B \ln Z_0). \quad (\text{B6})$$

Mindful of the information-theoretical interpretation of the entropy [133], we note that the uncertainty due to the stochasticity of the state disappears [the first term on the rhs of Eq. (B1)]. However, the uncertainty due to the indistinguishability of the molecules of the same species—quantified by the configurational entropy Eq. (B2)—remains and contributes to the whole deterministic entropy function Eq. (63).

APPENDIX C: ADIABATIC-NONADIABATIC DECOMPOSITION

We prove the positivity of the adiabatic and nonadiabatic entropy production rates Eq. (84) using the theory of complex-balanced networks; see Sec. II E.

We first rewrite the mass action kinetics currents Eq. (5) as [53,81] $J^\rho = K_\gamma^\rho \psi^\gamma$, where $\psi^\gamma \equiv Z^{\sigma \Gamma_\gamma^\rho}$ and $K = \{K_\gamma^\rho \equiv K_\gamma^{+\rho} - K_\gamma^{-\rho}\}$ is the rate constants matrix whose entries are defined by

$$K_\gamma^\rho = \begin{cases} k^{+\rho} & \text{if } \gamma \text{ is the reactant complex of } +\rho \\ -k^{-\rho} & \text{if } \gamma \text{ is the product complex of } +\rho \\ 0 & \text{otherwise.} \end{cases} \quad (\text{C1})$$

Hence, the definition of a complex-balanced network Eq. (37) reads

$$\sum_{\gamma \in \mathcal{C}_j} \mathcal{W}_\gamma^\gamma \bar{\psi}^\gamma = 0, \quad \forall j, \quad (\text{C2})$$

where $\mathcal{W} \equiv \partial K = \{\partial_\rho^\gamma K_\gamma^\rho\} \equiv \{\mathcal{W}_\gamma^\rho\}$ is the so-called kinetic matrix [35], and $\bar{\psi}^\gamma \equiv \bar{Z}^{\sigma \Gamma_\gamma^\rho}$.

The kinetic matrix \mathcal{W} is a Laplacian matrix [76,81]: any off-diagonal term is equal to the rate constant of the reaction having γ' as a reactant and γ as a product if the reaction exists, and it is zero otherwise. Also, it satisfies

$$\sum_{\gamma \in \mathcal{C}} \mathcal{W}_\gamma^\gamma = 0, \quad (\text{C3})$$

which is a consequence of the fact that the diagonal terms are equal to minus the sum of the off-diagonal terms along the columns. The detailed balanced property Eq. (18) implies that

$$\mathcal{W}_\gamma^\gamma \psi_\gamma^{\text{eq}} = \mathcal{W}_{\gamma'}^{\gamma'} \psi_{\gamma'}^{\text{eq}}, \quad \forall \gamma, \gamma', \quad (\text{C4})$$

where $\psi_\gamma^{\text{eq}} \equiv Z_\sigma^{\text{eq} \Gamma_\sigma^\sigma}$.

In order to prove the non-negativity of the adiabatic term Eq. (84), we rewrite it as

$$\begin{aligned} \dot{S}_a &\equiv J^\rho \ln \frac{\bar{J}_{+\rho}}{\bar{J}_{-\rho}} = K_{\gamma'}^\rho \psi_{\gamma'}^{\text{eq}} \ln \left(\frac{\bar{Z}_\sigma}{Z_\sigma^{\text{eq}}} \right)^{-\nabla_\rho^\sigma} \\ &= -\mathcal{W}_{\gamma'}^{\gamma'} \psi_{\gamma'}^{\text{eq}} \ln \frac{\bar{\psi}_{\gamma'}^{\text{eq}}}{\bar{\psi}_{\gamma'}^{\text{eq}}}. \end{aligned} \quad (\text{C5})$$

The detailed balance property is used in the first equality, and the decomposition of the stoichiometric matrix Eq. (30) in the second one. Also, the constant RT is taken equal to 1. Using Eq. (C3), Eq. (C5) can be rewritten as

$$\dot{S}_a = -\mathcal{W}_{\gamma'}^{\gamma'} \psi_{\gamma'}^{\text{eq}} \ln \frac{\bar{\psi}_{\gamma'}^{\text{eq}}}{\bar{\psi}_{\gamma'}^{\text{eq}}}. \quad (\text{C6})$$

From the log inequality $-\ln x \geq 1 - x$ and the detailed balance property Eq. (C4), we obtain

$$\begin{aligned} \dot{S}_a &\geq \mathcal{W}_{\gamma'}^{\gamma'} \left(1 - \frac{\bar{\psi}_{\gamma'}^{\text{eq}}}{\bar{\psi}_{\gamma'}^{\text{eq}}} \right) \\ &= -\mathcal{W}_{\gamma'}^{\gamma'} \frac{\bar{\psi}_{\gamma'}^{\text{eq}}}{\bar{\psi}_{\gamma'}^{\text{eq}}} = -\mathcal{W}_{\gamma'}^{\gamma'} \frac{\psi_{\gamma'}^{\text{eq}}}{\psi_{\gamma'}^{\text{eq}}} = 0. \end{aligned} \quad (\text{C7})$$

The last equality follows from the assumption of a complex-balanced steady state Eq. (C2), the properties of the groups of complexes $\{\mathcal{C}_j\}$ (Sec. II E), and the fact that $\{Z_{\sigma_y} = \bar{Z}_{\sigma_y}\}$. Indeed,

$$\begin{aligned} \mathcal{W}_{\gamma'}^{\gamma'} \frac{\psi_{\gamma'}^{\text{eq}}}{\bar{\psi}_{\gamma'}^{\text{eq}}} &= \sum_j \sum_{\gamma' \in \mathcal{C}_j} \mathcal{W}_{\gamma'}^{\gamma'} \bar{\psi}_{\gamma'}^{\text{eq}} \left(\frac{Z_{\sigma_x}}{\bar{Z}_{\sigma_x}} \right)^{\Gamma_{\gamma'}^{\sigma_x}} \\ &= \sum_j \left(\frac{Z_{\sigma_x}}{\bar{Z}_{\sigma_x}} \right)^{\Gamma_j^{\sigma_x}} \sum_{\gamma' \in \mathcal{C}_j} \mathcal{W}_{\gamma'}^{\gamma'} \bar{\psi}_{\gamma'}^{\text{eq}} = 0. \end{aligned} \quad (\text{C8})$$

Concerning the nonadiabatic term Eq. (84), using the rate equations (9) and the fact that $\{Z_{\sigma_y} = \bar{Z}_{\sigma_y}\}$, we can rewrite it as

$$\dot{S}_{\text{na}} \equiv -d_t Z^\sigma \ln \frac{Z_\sigma}{\bar{Z}_\sigma} = -\mathcal{W}_\gamma^\gamma \psi_\gamma^{\text{eq}} \ln \frac{\psi_\gamma^{\text{eq}}}{\bar{\psi}_\gamma^{\text{eq}}}. \quad (\text{C9})$$

Because of Eq. (C3), we further get that

$$\dot{S}_{\text{na}} = -\mathcal{W}_{\gamma'}^{\gamma'} \psi_{\gamma'}^{\text{eq}} \ln \frac{\psi_{\gamma'}^{\text{eq}}}{\bar{\psi}_{\gamma'}^{\text{eq}}}. \quad (\text{C10})$$

From the log inequality $-\ln x \geq 1 - x$ and from Eq. (C4),

$$\dot{S}_{\text{na}} \geq \mathcal{W}_{\gamma'}^{\gamma'} \left(1 - \frac{\psi_{\gamma'}^{\text{eq}}}{\bar{\psi}_{\gamma'}^{\text{eq}}} \right) = -\mathcal{W}_{\gamma'}^{\gamma'} \bar{\psi}_{\gamma'}^{\text{eq}} \frac{\psi_{\gamma'}^{\text{eq}}}{\bar{\psi}_{\gamma'}^{\text{eq}}} = 0. \quad (\text{C11})$$

The last equality again follows from the assumption of a complex-balance steady state Eq. (C2) as in Eq. (C8).

APPENDIX D: DEFICIENCY OF CRNs

The deficiency of an open CRN is defined as [22]

$$\delta = \dim \ker \nabla^X - \dim \ker \partial^C \geq 0, \quad (\text{D1})$$

where $\partial^C = \{\partial_\rho^j \equiv \sum_{\gamma \in \mathcal{C}_j} \partial_\rho^\gamma\}$. Other equivalent definitions can be found in Refs. [52,53]. The kernel of ∇^X identifies the set of cycles, Eqs. (19) and (20), while the kernel of the incidence matrix $\hat{\partial}$ identifies the set of cycles of the reaction graph. Hence, the deficiency measures the difference between the number of cyclic transformations on chemical species and how many of them can be represented as cycles on the reaction graph. Deficiency-zero networks are defined by $\delta = 0$; i.e., they exhibit a one-to-one correspondence between the two. This topological property has many dynamical consequences, the most important of which is that deficiency-zero networks are unconditionally complex balanced [36,37]. As shown in Ref. [22], deficiency also has implications on the stochastic thermodynamic description of networks: the stochastic entropy production of a deficiency-zero network converges to the deterministic entropy production in the long-time limit. Linear networks are the simplest class of deficiency-zero networks. Since only one internal species appears in each complex with a stoichiometric coefficient equal to 1, $\nabla^X \equiv \partial^C$, and thus $\delta = 0$.

[1] J. W. Gibbs, *The Scientific Papers of J. Willard Gibbs, Vol. 1: Thermodynamics* (Dover, New York, 1961).
[2] T. de Donder, *L'affinité*, Mémoires de la Classe des Sciences (Gauthier-Villars, Paris, 1927), Vol. 1.

[3] I. Prigogine, *Etude Thermodynamique des Phénomènes Irréversibles* (Desoer, Liège, 1947).

[4] I. Prigogine, *Introduction to Thermodynamics of Irreversible Processes* (John Wiley & Sons, New York, 1967).

[5] I. Prigogine and R. Defay, *Chemical Thermodynamics* (Longmans, Green & Co., New York, 1954).

[6] G. F. Oster, A. S. Perelson, and A. Katchalsky, *Network Thermodynamics: Dynamic Modelling of Biophysical Systems*, *Q. Rev. Biophys.* **6**, 1 (1973).

[7] M. Malek-Mansour and G. Nicolis, *A Master Equation Description of Local Fluctuations*, *J. Stat. Phys.* **13**, 197 (1975).

[8] J. Schnakenberg, *Network Theory of Microscopic and Macroscopic Behavior of Master Equation Systems*, *Rev. Mod. Phys.* **48**, 571 (1976).

[9] T. L. Hill, *Free Energy Transduction in Biology* (Academic Press, New York, 1977).

[10] C. Y. Mou, J. Luo, and G. Nicolis, *Stochastic Thermodynamics of Nonequilibrium Steady States in Chemical Reaction Systems*, *J. Chem. Phys.* **84**, 7011 (1986).

[11] J. Ross, *Thermodynamics and Fluctuations Far from Equilibrium* (Springer, New York, 2008).

[12] D. A. McQuarrie, *Stochastic Approach to Chemical Kinetics*, *J. Appl. Probab.* **4**, 413 (1967).

[13] D. T. Gillespie, *A Rigorous Derivation of the Chemical Master Equation*, *Physica A* **188**, 404 (1992).

[14] K. Sekimoto, in *Stochastic Energetics*, 1st ed., Lecture Notes in Physics (Springer-Verlag, Berlin, 2010), Vol. 799.

[15] C. Jarzynski, *Equalities and Inequalities: Irreversibility and the Second Law of Thermodynamics at the Nanoscale*, *Annu. Rev. Condens. Matter Phys.* **2**, 329 (2011).

[16] U. Seifert, *Stochastic Thermodynamics, Fluctuation Theorems and Molecular Machines*, *Rep. Prog. Phys.* **75**, 126001 (2012).

[17] C. Van den Broeck and M. Esposito, *Ensemble and Trajectory Thermodynamics: A Brief Introduction*, *Physica A* **418**, 6 (2015).

[18] P. Gaspard, *Fluctuation Theorem for Nonequilibrium Reactions*, *J. Chem. Phys.* **120**, 8898 (2004).

[19] D. Andrieux and P. Gaspard, *Fluctuation Theorem and Onsager Reciprocity Relations*, *J. Chem. Phys.* **121**, 6167 (2004).

[20] T. Schmiedl, T. Speck, and U. Seifert, *Entropy Production for Mechanically or Chemically Driven Biomolecules*, *J. Stat. Phys.* **128**, 77 (2007).

[21] T. Schmiedl and U. Seifert, *Stochastic Thermodynamics of Chemical Reaction Networks*, *J. Chem. Phys.* **126**, 044101 (2007).

[22] M. Polettini, A. Wachtel, and M. Esposito, *Dissipation in Noisy Chemical Networks: The Role of Deficiency*, *J. Chem. Phys.* **143**, 184103 (2015).

[23] R. A. Alberti, *Thermodynamics of Biochemical Reactions* (Wiley-Interscience, New York, 2003).

[24] D. A. Beard and H. Qian, *Chemical Biophysics. Quantitative Analysis of Cellular Systems* (Cambridge University Press, Cambridge, England, 2008).

[25] B. Ø. Palsson, *Systems Biology: Properties of Reconstructed Networks* (Cambridge University Press, Cambridge, England, 2006).

[26] B. Ø. Palsson, *Systems Biology: Simulation of Dynamic Network States* (Cambridge University Press, Cambridge, England, 2011).

[27] B. Ø. Palsson, *Systems Biology: Constraint-Based Network Reconstruction and Analysis* (Cambridge University Press, Cambridge, England, 2015).

[28] A. Goldbeter, *Biochemical Oscillations and Cellular Rhythms* (Cambridge University Press, Cambridge, England, 1996).

[29] I. R. Epstein and J. A. Pojman, in *An Introduction to Nonlinear Chemical Dynamics: Oscillations, Waves, Patterns, and Chaos*, Topics in Physical Chemistry (Oxford University Press, New York, 1998).

[30] D. A. Beard, S.-d. Liang, and H. Qian, *Energy Balance for Analysis of Complex Metabolic Networks*, *Biophys. J.* **83**, 79 (2002).

[31] H. Qian, D. A. Beard, and S.-d. Liang, *Stoichiometric Network Theory for Nonequilibrium Biochemical Systems*, *Eur. J. Biochem.* **270**, 415 (2003).

[32] D. A. Beard, E. Babson, E. Curtis, and H. Qian, *Thermodynamic Constraints for Biochemical Networks*, *J. Theor. Biol.* **228**, 327 (2004).

[33] A. Chakrabarti, L. Miskovic, K. C. Soh, and V. Hatzimanikatis, *Towards Kinetic Modeling of Genome-Scale Metabolic Networks without Sacrificing Stoichiometric, Thermodynamic and Physiological Constraints*, *Biotechnol. J.* **8**, 1043 (2013).

[34] H. Qian and D. A. Beard, *Thermodynamics of Stoichiometric Biochemical Networks in Living Systems Far from Equilibrium*, *Biophys. Chem.* **114**, 213 (2005).

[35] F. Horn and R. Jackson, *General Mass Action Kinetics*, *Arch. Ration. Mech. Anal.* **47**, 81 (1972).

[36] M. Feinberg, *Complex Balancing in General Kinetic Systems*, *Arch. Ration. Mech. Anal.* **49**, 187 (1972).

[37] F. Horn, *Necessary and Sufficient Conditions for Complex Balancing in Chemical Kinetics*, *Arch. Ration. Mech. Anal.* **49**, 172 (1972).

[38] T. G. Kurtz, *The Relationship between Stochastic and Deterministic Models for Chemical Reactions*, *J. Chem. Phys.* **57**, 2976 (1972).

[39] D. F. Anderson, G. Craciun, and T. G. Kurtz, *Product-Form Stationary Distributions for Deficiency Zero Chemical Reaction Networks*, *Bull. Math. Biol.* **72**, 1947 (2010).

[40] D. F. Anderson, G. Craciun, M. Gopalkrishnan, and C. Wiuf, *Lyapunov Functions, Stationary Distributions, and Non-Equilibrium Potential for Reaction Networks*, *Bull. Math. Biol.* **77**, 1744 (2015).

[41] D. Cappelletti and C. Wiuf, *Product-Form Poisson-like Distributions and Complex Balanced Reaction Systems*, *SIAM J. Appl. Math.* **76**, 411 (2016).

[42] K. Takara, H.-H. Hasegawa, and D. J. Driebe, *Generalization of the Second Law for a Transition between Non-equilibrium States*, *Phys. Lett. A* **375**, 88 (2010).

[43] M. Esposito and C. Van den Broeck, *Second Law and Landauer Principle Far from Equilibrium*, *Europhys. Lett.* **95**, 40004 (2011).

[44] T. Sagawa, *Thermodynamics of Information Processing in Small Systems* (Springer, Japan, 2013).

[45] J. M. R. Parrondo, J. M. Horowitz, and T. Sagawa, *Thermodynamics of Information*, *Nat. Phys.* **11**, 131 (2015).

[46] M. Esposito, U. Harbola, and S. Mukamel, *Entropy Fluctuation Theorems in Driven Open Systems: Application to Electron Counting Statistics*, *Phys. Rev. E* **76**, 031132 (2007).

[47] R. J. Harris and G. M. Schütz, *Fluctuation Theorems for Stochastic Dynamics*, *J. Stat. Mech.* (2007) P07020.

[48] M. Esposito and C. Van den Broeck, *Three Faces of the Second Law. I. Master Equation Formulation*, *Phys. Rev. E* **82**, 011143 (2010).

[49] C. Van den Broeck and M. Esposito, *Three Faces of the Second Law. II. Fokker-Planck Formulation*, *Phys. Rev. E* **82**, 011144 (2010).

[50] H. Ge and H. Qian, *Physical Origins of Entropy Production, Free Energy Dissipation, and Their Mathematical Representations*, *Phys. Rev. E* **81**, 051133 (2010).

[51] H. Ge and H. Qian, *Nonequilibrium Thermodynamic Formalism of Nonlinear Chemical Reaction Systems with Waage-Guldberg's Law of Mass Action*, *Chem. Phys.* **472**, 241 (2016).

[52] M. Feinberg, "Lecture on Chemical Reaction Networks" (unpublished).

[53] J. Gunawardena, "Chemical Reaction Network Theory for In Silico Biologists Contents" (unpublished).

[54] S. R. de Groot and P. Mazur, *Non-Equilibrium Thermodynamics* (Dover, New York, 1984).

[55] M. Pekar, *Thermodynamics and Foundations of Mass-Action Kinetics*, *Prog. React. Kinet. Mech.* **30**, 3 (2005).

[56] M. Polettini and M. Esposito, *Irreversible Thermodynamics of Open Chemical Networks. I. Emergent Cycles and Broken Conservation Laws*, *J. Chem. Phys.* **141**, 024117 (2014).

[57] D. Kondepudi and I. Prigogine, *Modern Thermodynamics: From Heat Engines to Dissipative Structures*, 2nd ed. (Wiley, New York, 2014).

[58] A. D. McNaught and A. Wilkinson, *Compendium of Chemical Terminology*, 2nd ed. (Blackwell Science, 1997).

[59] S. Schuster and R. Schuster, *A Generalization of Wegscheider's Condition. Implications for Properties of Steady States and for Quasi-Steady-State Approximation*, *J. Math. Chem.* **3**, 25 (1989).

[60] J. Leiser and J. J. Blum, *On the Analysis of Substrate Cycles in Large Metabolic Systems*, *Cell Biophysics* **11**, 123 (1987).

[61] S. Schuster and C. Hilgetag, *On Elementary Flux Modes in Biochemical Reaction Systems at Steady State*, *J. Biol. Syst.* **02**, 165 (1994).

[62] S. Klamt and J. Stelling, *Two Approaches for Metabolic Pathway Analysis?*, *Trends Biotechnol.* **21**, 64 (2003).

[63] R. Rao, D. Lacoste, and M. Esposito, *Glucans Monomer-Exchange Dynamics as an Open Chemical Network*, *J. Chem. Phys.* **143**, 244903 (2015).

[64] F. Horn, *Stability and Complex Balancing in Mass-Action Systems with Three Short Complexes*, *Proc. R. Soc. A* **334**, 331 (1973).

[65] S. Klamt, U.-U. Haus, and F. Theis, *Hypergraphs and Cellular Networks*, *PLoS Comput. Biol.* **5**, e1000385 (2009).

[66] C. A. Petri and W. Reisig, *Petri Net*, *Scholarpedia* **3**, 6477 (2008), revision 91646.

[67] J. C. Baez and B. Fong, *Quantum Techniques for Studying Equilibrium in Reaction Networks*, *J. Complex Netw.* **3**, 22 (2015).

[68] G. Craciun, *Toric Differential Inclusions and a Proof of the Global Attractor Conjecture*, *arXiv:1501.02860*.

[69] A. Dickenstein and M. P. Millán, *How Far is Complex Balancing from Detailed Balancing?*, *Bull. Math. Biol.* **73**, 811 (2011).

[70] I. Prigogine, *Le Domaine de Validité de la Thermodynamique des Phénomènes Irréversibles*, *Physica A* **15**, 272 (1949).

[71] E. R. Cohen, T. Cvitas, J. G. Frey, B. Holmström, K. Kuchitsu, R. Marquardt, I. Mills, F. Pavese, M. Quack, J. Stohner, H. L. Strauss, M. Takami, and A. J. Thor, *Quantities, Units and Symbols in Physical Chemistry*, 3rd ed. (IUPAC and RSC Publishing, 2008).

[72] R. Holyst and A. Poniewierski, *Thermodynamics for Chemists, Physicists and Engineers* (Springer, New York, 2012).

[73] D. Shear, *An Analog of the Boltzmann H-Theorem (a Liapunov Function) for Systems of Coupled Chemical Reactions*, *J. Theor. Biol.* **16**, 212 (1967).

[74] J. Higgins, *Some Remarks on Shear's Liapunov Function for Systems of Chemical Reactions*, *J. Theor. Biol.* **21**, 293 (1968).

[75] T. M. Cover and J. A. Thomas, *Elements of Information Theory*, 2nd ed. (Wiley-Interscience, New York, 2006).

[76] A. van der Schaft, S. Rao, and B. Jayawardhana, *On the Mathematical Structure of Balanced Chemical Reaction Networks Governed by Mass Action Kinetics*, *SIAM J. Appl. Math.* **73**, 953 (2013).

[77] I. Procaccia and R. D. Levine, *Potential Work: A Statistical-Mechanical Approach for Systems in Disequilibrium*, *J. Chem. Phys.* **65**, 3357 (1976).

[78] S. Vaikuntanathan and C. Jarzynski, *Dissipation and Lag in Irreversible Processes*, *Europhys. Lett.* **87**, 60005 (2009).

[79] H.-H. Hasegawa, J. Ishikawa, K. Takara, and D. J. Driebe, *Generalization of the Second Law for a Nonequilibrium Initial State*, *Phys. Lett. A* **374**, 1001 (2010).

[80] M. Gopalkrishnan, *On the Lyapunov Function for Complex-Balanced Mass-Action Systems*, *arXiv:1312.3043*.

[81] A. van der Schaft, S. Rao, and B. Jayawardhana, *Complex and Detailed Balancing of Chemical Reaction Networks Revisited*, *J. Math. Chem.* **53**, 1445 (2015).

[82] The fact that the matrix whose entries are $\{\ell_{\alpha_j}^{\lambda_u}\}$ is nonsingular follows from $\ell^{\lambda_u} \in \ker \nabla$, $\forall \lambda_u$, and from the linear independence of $\{\ell^{\lambda}\}$.

[83] M. Esposito and G. Schaller, *Stochastic Thermodynamics for "Maxwell Demon" Feedbacks*, *Europhys. Lett.* **99**, 30003 (2012).

[84] G. Diana, G. B. Bagci, and M. Esposito, *Finite-Time Erasing of Information Stored in Fermionic Bits*, *Phys. Rev. E* **87**, 012111 (2013).

[85] J. M. Horowitz and M. Esposito, *Thermodynamics with Continuous Information Flow*, *Phys. Rev. X* **4**, 031015 (2014).

[86] A. C. Barato and U. Seifert, *Unifying Three Perspectives on Information Processing in Stochastic Thermodynamics*, *Phys. Rev. Lett.* **112**, 090601 (2014).

[87] S. Bo, M. Del Giudice, and A. Celani, *Thermodynamic Limits to Information Harvesting by Sensory Systems*, *J. Stat. Mech.* (2015) P01014.

[88] P. Strasberg, G. Schaller, T. Brandes, and M. Esposito, *Thermodynamics of a Physical Model Implementing a Maxwell Demon*, *Phys. Rev. Lett.* **110**, 040601 (2013).

[89] N. Golubeva and A. Imparato, *Efficiency at Maximum Power of Interacting Molecular Machines*, *Phys. Rev. Lett.* **109**, 190602 (2012).

[90] B. Altaner, A. Wachtel, and J. Vollmer, *Fluctuating Currents in Stochastic Thermodynamics. II. Energy Conversion and Nonequilibrium Response in Kinesin Models*, *Phys. Rev. E* **92**, 042133 (2015).

[91] U. Seifert, *Stochastic Thermodynamics of Single Enzymes and Molecular Motors*, *Eur. Phys. J. E* **34**, 26 (2011).

[92] R. Rao and L. Peliti, *Thermodynamics of Accuracy in Kinetic Proofreading: Dissipation and Efficiency Trade-Offs*, *J. Stat. Mech.* (2015) P06001.

[93] J. J. Hopfield, *Kinetic Proofreading: A New Mechanism for Reducing Errors in Biosynthetic Processes Requiring High Specificity*, *Proc. Natl. Acad. Sci. U.S.A.* **71**, 4135 (1974).

[94] J. Ninio, *Kinetic Amplification of Enzyme Discrimination*, *Biochimie* **57**, 587 (1975).

[95] J. J. Hopfield, *The Energy Relay: A Proofreading Scheme Based on Dynamic Cooperativity and Lacking All Characteristic Symptoms of Kinetic Proofreading in DNA Replication and Protein Synthesis*, *Proc. Natl. Acad. Sci. U.S.A.* **77**, 5248 (1980).

[96] E. D. Sontag, *Structure and Stability of Certain Chemical Networks and Applications to the Kinetic Proofreading Model of T-Cell Receptor Signal Transduction*, *IEEE Trans. Autom. Control* **46**, 1028 (2001).

[97] H. Ge, M. Qian, and H. Qian, *Stochastic Theory of Nonequilibrium Steady States. Part II: Applications in Chemical Biophysics*, *Phys. Rep.* **510**, 87 (2012).

[98] A. Murugan, D. H. Huse, and S. Leibler, *Speed, Dissipation, and Error in Kinetic Proofreading*, *Proc. Natl. Acad. Sci. U.S.A.* **109**, 12034 (2012).

[99] A. Murugan, D. H. Huse, and S. Leibler, *Discriminatory Regimes in Non-Equilibrium Systems*, *Phys. Rev. X* **4**, 021016 (2014).

[100] C. H. Bennett, *Dissipation-Error Tradeoff in Proofreading*, *BioSystems* **11**, 85 (1979).

[101] D. Andrieux and P. Gaspard, *Nonequilibrium Generation of Information in Copolymerization Processes*, *Proc. Natl. Acad. Sci. U.S.A.* **105**, 9516 (2008).

[102] D. Andrieux and P. Gaspard, *Molecular Information Processing in Nonequilibrium Copolymerizations*, *J. Chem. Phys.* **130**, 014901 (2009).

[103] J. R. Arias-Gonzalez, *Entropy Involved in Fidelity of DNA Replication*, *PLoS One* **7**, e42272 (2012).

[104] P. Sartori and S. Pigolotti, *Kinetic versus Energetic Discrimination in Biological Copying*, *Phys. Rev. Lett.* **110**, 188101 (2013).

[105] P. Sartori and S. Pigolotti, *Thermodynamics of Error Correction*, *Phys. Rev. X* **5**, 041039 (2015).

[106] A. Cornish-Bowden, *Fundamentals of Enzyme Kinetics*, 4th ed. (Wiley-Blackwell, 2012).

[107] M. Esposito, *Stochastic Thermodynamics under Coarse Graining*, *Phys. Rev. E* **85**, 041125 (2012).

[108] C. L. Linster, E. van Schaftingen, and A. D. Hanson, *Metabolite Damage and Its Repair or Pre-emption*, *Nat. Chem. Biol.* **9**, 72 (2013).

[109] H. Qian and T. C. Reluga, *Nonequilibrium Thermodynamics and Nonlinear Kinetics in a Cellular Signaling Switch*, *Phys. Rev. Lett.* **94**, 028101 (2005).

[110] H. Qian and S. Roy, *An Information Theoretical Analysis of Kinase Activated Phosphorylation Dephosphorylation Cycle*, *IEEE Trans. Nanobiosci.* **11**, 289 (2012).

[111] J. M. G. Vilar, H. Y. Kueh, N. Barkai, and S. Leibler, *Mechanisms of Noise-Resistance in Genetic Oscillators*, *Proc. Natl. Acad. Sci. U.S.A.* **99**, 5988 (2002).

[112] G. Nicolis and I. Prigogine, *Self-Organization in Nonequilibrium Systems: From Dissipative Structures to Order Through Fluctuations* (Wiley-Blackwell, 1977).

[113] R. Feistel and W. Ebeling, *Physics of Self-Organization and Evolution* (Wiley VCH, 2011).

[114] P. Mehta and D. J. Schwab, *Energetic Costs of Cellular Computation*, *Proc. Natl. Acad. Sci. U.S.A.* **109**, 17978 (2012).

[115] P. Sartori, L. Granger, C. F. Lee, and J. M. Horowitz, *Thermodynamic Costs of Information Processing in Sensory Adaptation*, *PLoS Comput. Biol.* **10**, e1003974 (2014).

[116] D. Hartich, A. C. Barato, and U. Seifert, *Nonequilibrium Sensing and Its Analogy to Kinetic Proofreading*, *New J. Phys.* **17**, 055026 (2015).

[117] S.-W. Wang, Y. Lan, and L.-H. Tang, *Energy Dissipation in an Adaptive Molecular Circuit*, *J. Stat. Mech.* (2015) P07025.

[118] *DNA Computing and Molecular Programming*, edited by Y. Sakakibara and Y. Y. Mi (Springer, Berlin, 2011); *DNA Computing and Molecular Programming*, edited by Luca Cardelli and W. Shih (Springer, Berlin, 2011); *DNA Computing and Molecular Programming*, edited by D. Stefanovic and A. Turberfields (Springer, Berlin, 2012); *DNA Computing and Molecular Programming*, edited by D. Soloveichik and B. Yurke (Springer International Publishing, 2013); *DNA Computing and Molecular Programming*, edited by S. Murata and S. Kobayashi (Springer International Publishing, 2014); *DNA Computing and Molecular Programming*, edited by A. Phillips and P. Yin (Springer International Publishing, 2015).

[119] A. Hjelmfelt, E. D. Weinberger, and J. Ross, *Chemical Implementation of Neural Networks and Turing Machines*, *Proc. Natl. Acad. Sci. U.S.A.* **88**, 10983 (1991).

[120] A. Hjelmfelt, E. D. Weinberger, and J. Ross, *Chemical Implementation of Finite-State Machines*, *Proc. Natl. Acad. Sci. U.S.A.* **89**, 383 (1992).

[121] M. O. Magnasco, *Chemical Kinetics is Turing Universal*, *Phys. Rev. Lett.* **78**, 1190 (1997).

[122] D. Soloveichik, M. Cook, E. Winfree, and J. Bruck, *Computation with Finite Stochastic Chemical Reaction Networks*, *Nat. Comput.* **7**, 615 (2008).

[123] C. H. Bennett, *The Thermodynamics of Computation—A Review*, *Int. J. Theor. Phys.* **21**, 905 (1982).

[124] T. P. J. Knowles, W. Shu, G. L. Devlin, S. Meehan, S. Auer, C. M. Dobson, and M. E. Welland, *Kinetics and Thermodynamics of Amyloid Formation from Direct Measurements of Fluctuations in Fibril Mass*, *Proc. Natl. Acad. Sci. U.S.A.* **104**, 10016 (2007).

[125] T. P. J. Knowles, C. A. Waudby, G. L. Devlin, S. I. A. Cohen, A. Aguzzi, M. Vendruscolo, E. M. Terentjev, M. E. Welland, and C. M. Dobson, *An Analytical Solution to the Kinetics of Breakable Filament Assembly*, *Science* **326**, 1533 (2009).

[126] S. I. A. Cohen, S. Linse, L. M. Luheshi, E. Hellstrand, D. A. White, L. Rajah, D. E. Otzen, M. Vendruscolo, C. M. Dobson, and T. P. J. Knowles, *Proliferation of Amyloid- β 42 Aggregates Occurs through a Secondary Nucleation Mechanism*, *Proc. Natl. Acad. Sci. U.S.A.* **110**, 9758 (2013).

[127] Z. Budrikis, G. Costantini, C. A. M. La Porta, and S. Zapperi, *Protein Accumulation in the Endoplasmic Reticulum as a Non-Equilibrium Phase Transition*, *Nat. Commun.* **5**, 3620 (2014).

[128] Ö. Kartal, S. Mahlow, A. Skupin, and O. Ebenhöh, *Carbohydrate-Active Enzymes Exemplify Entropic Principles in Metabolism*, *Mol. Syst. Biol.* **7**, 542 (2011).

[129] S. Lahiri, Y. Wang, M. Esposito, and D. Lacoste, *Kinetics and Thermodynamics of Reversible Polymerization in Closed Systems*, *New J. Phys.* **17**, 085008 (2015).

[130] P. Krapivsky, S. Redner, and E. Ben-Naim, *A Kinetic View of Statistical Physics* (Cambridge University Press, Cambridge, England, 2010).

[131] Enrico Fermi, *Thermodynamics* (Dover, New York, 1956).

[132] H. Ge and H. Qian, *Mesoscopic Kinetic Basis of Macroscopic Chemical Thermodynamics: A Mathematical Theory*, *Phys. Rev. E* **94**, 052150 (2016).

[133] E. T. Jaynes, *Information Theory and Statistical Mechanics*, *Phys. Rev.* **106**, 620 (1957).

The following article is reprinted from
[R. RAO, D. LACOSTE and M. ESPOSITO, *J. Chem. Phys.* **143**.24 (2015), 244903]
with the permission of AIP Publishing.

The page numbers placed in the outer margins provide a continuous pagination throughout the thesis.

Glucans monomer-exchange dynamics as an open chemical network

Riccardo Rao,^{1,a)} David Lacoste,² and Massimiliano Esposito^{1,b)}

¹*Complex Systems and Statistical Mechanics, Physics and Materials Science Research Unit, University of Luxembourg, L-1511 Luxembourg, Luxembourg*

²*Laboratoire de Physico-Chimie Théorique, UMR CNRS Gulliver 7083, ESPCI - 10 rue Vauquelin, F-75231 Paris, France*

(Received 25 September 2015; accepted 3 December 2015; published online 23 December 2015)

We describe the oligosaccharides-exchange dynamics performed by the so-called D-enzymes on polysaccharides. To mimic physiological conditions, we treat this process as an open chemical network by assuming some of the polymer concentrations fixed (chemostatting). We show that three different long-time behaviors may ensue: equilibrium states, nonequilibrium steady states, and continuous growth states. We dynamically and thermodynamically characterize these states and emphasize the crucial role of conservation laws in identifying the chemostatting conditions inducing them. © 2015 AIP Publishing LLC. [<http://dx.doi.org/10.1063/1.4938009>]

I. INTRODUCTION

Biological systems use large and branched chains of basic sugars, called polysaccharides, to store energy.¹ *Glucans* such as *glycogen* and starch are polysaccharides whose building blocks are *D-glucose* monosaccharides. Despite the apparent simplicity of their constituents, their metabolism involves several chemical steps, each performed by a specific set of enzymes.² Interestingly, some of these catalysts lack specificity regarding the reaction they catalyze or the substrates they act on.^{3,23–32} An example is provided by (1 → 4)-*alpha-D-glucans*^{2,4–6} (EC 2.4.1.25), also called *D-enzymes*, which act on pairs of glucans regardless of their size.⁷ Specifically, D-enzymes catalyze the transfer of groups of glycosyl residues from a donor glucan to an acceptor glucan.^{4,5} Experimental evidences highlight the presence of bonds between glycosyl residues which are not cleaved by D-enzymes⁴—at least not over physiological time scales.⁷ These bonds are called *forbidden linkages*.⁴ In this way, D-enzymes transfer segments of glucan chains containing one or more forbidden linkages, and the transfer of segments containing one forbidden linkage are the most probable.⁴ Also, each glucan chain is characterized by a reducing-end glucose which is not transferred by D-enzymes.^{4,7} Hence, glucans made of just the reducing end can act only as acceptor in the transfer.

Qualitatively, D-enzymes process medium-size glucans by disproportionating them into unit-size and big-size glucans.⁵ Since their transfers reactions are neutral energetically,^{7,8} entropy is the main driving force in this system. In closed conditions, this system evolves towards an equilibrium state maximizing the entropy.^{7,9}

In this paper we consider a simplified kinetic description of the D-enzyme's action on glucans, which we treat as a chemical network. Since metabolic processes should be thought of as part of an open system continuously fed from

the environment, we mimic these physiological conditions by introducing *chemostats* (i.e., species whose concentrations are kept constant by the environment). Our goal is to characterize the dynamical and thermodynamical implications of treating the action of the D-enzymes on glucans as an open chemical network. In the framework of deterministic chemical networks endowed with *mass action kinetics*, we prove that chemostatting can induce three different types of long-time behaviors: equilibrium, non-equilibrium steady state, and continuous growth. The equilibrium state corresponds to the stationary concentration distribution in which the concentration currents along each reaction pathway vanishes (detailed balance property¹⁰). Non-equilibrium steady states refer to stationary distributions violating detailed balance. Hence, contrary to equilibrium states, a continuous and steady flow of mass circulates across the network. Finally, the continuous growth regime we observed corresponds to a non-stationary state characterized by continuous and steady flow of mass entering the network and resulting in its continuous growth. We emphasize the dynamical and thermodynamical roles of conservation laws and emergent cycles in identifying the chemostatting conditions leading to these states. We are thus able to confirm the general relation between the number of chemostatted species and the number of independent thermodynamical forces—or *affinities*—found in Ref. 11. Despite the simplicity of our description, the closed system results found in Ref. 7 are reproduced and the qualitative disproportionating behavior of D-enzymes⁵ is captured by our (chemostatted) open system description.

The plan of the paper is as follows: in Sec. II, the kinetic model is established and the related rate equation description for the concentration of polysaccharides is introduced. In Sec. III, the chemostatting conditions leading to non-equilibrium steady states rather than equilibrium ones are found. For this purpose, both the conservation laws of the dynamics and the emergent cycles of the network are analyzed. The dissipation of the non-equilibrium steady state is also studied. The network's conservation laws identified in Sec. III A are used in Sec. IV to derive the steady-state concentration

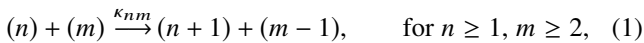
^{a)}riccardo.rao@uni.lu

^{b)}massimiliano.esposito@uni.lu

distributions for different numbers of chemostats. The explosive asymptotic behavior is described in Sec. V. Conclusions are drawn in Sec. VI. Some technical derivations and proofs are provided in Appendices.

II. THE KINETIC MODEL

The action of D-enzymes is modeled as follows (see also Fig. 1). Glucans are treated as polymers whose monomers represent single transferable segments. Hence, each glucan is identified by its number of monomers, or equivalently by its monomeric mass. The enzymatic steps performed by the D-enzymes in order to achieve the transfer are not explicitly described—they are coarse-grained—and we describe the interaction between two polymers of mass n and m as a *mass-exchange process*.¹²



where κ_{nm} denotes the related coarse-grained rate constant. Transfers of oligosaccharides longer than one monomeric unit are less probable⁴ and are not considered in our description. We take into account the presence of non-transferable units by imposing the size of the donor glucan (m) to be greater than one.^{4,7}

Let us note that each reaction is reversible because the backward path is already included in (1) (it is realized by replacing $n \rightarrow m-1$ and $m \rightarrow n+1$ in the above expression). Furthermore, the constraint on the minimal size of the donor molecules imposes that $m \geq 2$. Since we describe the glucans as linear polymers, and since D-enzymes do not discriminate the size of the polymers, we assume a constant kernel for the reactions: $\kappa_{mn} = \kappa$, $\forall n \geq 1, \forall m \geq 2$. This assumption is based on the evidence that the free-enthalpy release resulting from any reaction is almost vanishing.^{7,8} Indeed, for any bond cleaved, a new one of the same kind will be formed.

Assuming a large and well stirred pool of interacting polymers, the evolution of the system is well described by reaction rate equations.¹² According to this mean-field description, the molar concentration of polymers of mass k at time t , $Z^k = Z^k(t)$, satisfies the following first order differential equations:

$$\dot{Z}^k = \frac{1}{2} \sum_{\substack{n \geq 1 \\ m \geq 2}} \nabla_{nm}^k \underbrace{(J^{+nm} - J^{-nm})}_{\equiv J^{nm}}, \quad \text{for } k \geq 1. \quad (2)$$

The $\frac{1}{2}$ factor in front of the summation takes into account that summing over all $n \geq 1$ and $m \geq 2$ includes every

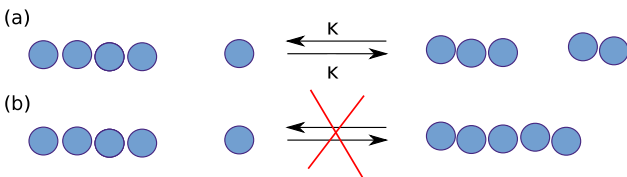


FIG. 1. (a) The typical monomer-exchange reaction describing the action of D-enzymes on glucan chains. (b) The attachment of free monomers to other species is not allowed.

reaction pathway twice.¹³ ∇_{nm}^k represents the element of the *stoichiometric matrix* related to the species of mass k and to the reaction involving an acceptor and a donor polymer of mass n and m , respectively. The reaction scheme in (1) implies that

$$\nabla_{nm}^k = \delta_{n+1}^k + \delta_{m-1}^k - \delta_n^k - \delta_m^k, \quad (3)$$

where δ_i^j represents the Kronecker delta. Assuming a *mass action kinetics*, the forward (denoted by +) and the backward fluxes (−) can be written as

$$J^{+nm} = \kappa Z^n Z^m, \quad J^{-nm} = \kappa Z^{n+1} Z^{m-1}, \quad (4)$$

where Z^n denotes the concentrations of the polymers of size n . To simplify the following discussion, we will use the Einstein summation notation: upper indexed quantities represent vectors, lower indexed ones covectors, and repeated indexes imply the summation over all the allowed values for those indexes ($1 \leq n \leq n_{\max}$ and $2 \leq m \leq m_{\max}$, or $1 \leq k \leq k_{\max}$, where n_{\max} , m_{\max} , and k_{\max} are finite in closed systems but infinite in open ones). To avoid confusion, exponents will always act on parentheses (e.g., $(a)^n$ denotes the quantity a to the power n).

The rate equations (2) assume the following form when the expressions for both stoichiometric matrix (3) and fluxes (4) are considered

$$\begin{aligned} \dot{Z}^1 &= \kappa Z (Z^2 - Z^1) + \kappa Z^1 Z^1, \\ \dot{Z}^k &= \kappa Z (Z^{k+1} - 2Z^k + Z^{k-1}) \\ &\quad + \kappa Z^1 (Z^k - Z^{k-1}), \quad \text{for } k \geq 2, \end{aligned} \quad (5)$$

where $Z \equiv \sum_{k=1}^{k_{\max}} Z^k$ denotes the total concentration. The second term in the right hand side of (5) arises from the constraint that the donor species cannot be monomers¹⁴ (see Fig. 1(b)).

To model the open system we now assume that the environment keeps the concentrations of some species constant by refilling the consumed ones and eliminating the produced ones, see Fig. 2. We call these species *chemostats*¹⁵ and we denote them with the indices $k_y \in \Omega_Y$, where $\Omega_Y \subset \mathbb{N}$ represents a subset of all species. The remaining (variable) species are explicitly denoted by k_x .

By definition, the chemostats' concentrations must remain constant, $\dot{Z}^{k_y} = 0$. The rate of chemostatted molecules consumed by the reactions in the network must therefore be balanced by the rate of chemostatted molecules injected/rejected from the system. The rate of injection/rejection

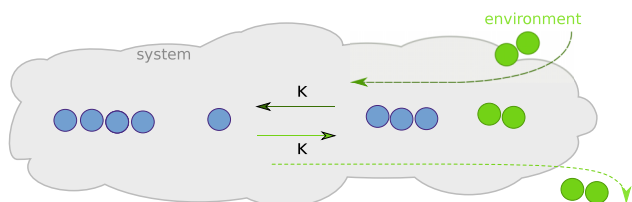


FIG. 2. Pictorial representation of a reaction involving a chemostat. When a reaction produces a chemostat (here a dimer), the environment extracts one molecule of this species from the system (dotted light green reaction). On the other hand, when a chemostat reacts, a new molecule is injected into the system (dashed dark green reaction).

of the k_y th chemostat is quantified by the external currents, ¹¹ whose expression is

$$\begin{aligned} I^{ky} &= \frac{1}{2} \nabla_{nm}^{ky} (J^{+nm} - J^{-nm}) \\ &= \kappa Z (Z^2 - Z^1) + \kappa Z^1 Z^1 \quad \text{if } k_y = 1 \\ &= \kappa Z (Z^{ky+1} - 2Z^{ky} + Z^{ky-1}) \\ &\quad + \kappa Z^1 (Z^{ky} - Z^{ky-1}) \quad \text{if } k_y \geq 2. \end{aligned} \quad (6)$$

III. STEADY STATES: CONSERVATION LAWS, CYCLES, AND DISSIPATION

Three different types of long-time behaviors have been identified for our kinetic model: equilibrium, non-equilibrium steady state and continuous growth. We start by focusing on the chemostatting conditions leading to equilibrium or non-equilibrium steady states. The existence and uniqueness of the steady state are currently *a priori* assumed.

Closed systems always reach an equilibrium steady state ¹⁶ defined by $\dot{Z}_{\text{eq}}^{k_x} = 0, \forall k_x$ and $J_{\text{eq}}^{nm} = 0, \forall n, m$. Their dynamics is constrained by *conservation laws*, ^{11,17,18} which fully characterize the equilibrium concentration distribution. Chemostatting generic chemical species may break these conservation laws and may create chemical forces—also called *affinities*. ¹¹ The appearance of affinities is directly related to that of so-called *emergent cycles*, through which the external chemical forces can act. In finite chemical networks, if no emergent affinity arises from the chemostatting procedure, the system will always relax to a unique equilibrium state compatible with the chemostats and the non-broken conservation laws. ^{11,16} When emergent cycles—or equivalently affinities—are generated, the system may evolve towards a non-equilibrium steady state defined by $\dot{Z}^{k_x} = 0, \forall k_x$ and $\dot{J}^{nm} \neq 0$ (non-equilibrium steady state quantities are denoted by an overbar in the text). In Subsections III A–III C, we analyze how the closed system's conservation laws and emergent cycles are modified by the gradual increase of the number of chemostatted chemical species. In Subsection III C, we relate these to the dissipation in the system.

A. Conservation Laws

Conservation laws denote the presence of physical quantities which are conserved during the evolution of the system, the so-called *components*. In general, they can be identified from the cokernel space of the stoichiometric matrix. ^{11,17,18} Indeed, if $l_k \in \text{coker} \nabla$, namely, if $l_k \nabla_{nm}^k = 0$, the scalar $l_k Z^k$ is conserved

$$\begin{aligned} \frac{d}{dt} (l_k Z^k) &= l_k \dot{Z}^k \\ &= \frac{1}{2} l_k \nabla_{nm}^k (J^{+nm} - J^{-nm}) = 0. \end{aligned} \quad (7)$$

For the closed system, the equation leading to the conservation laws is $l_{n+1}^k - l_n^k = l_m^k - l_{m-1}^k$, for $1 \leq n \leq n_{\max} = k_{\max} - 1$ and $2 \leq m \leq m_{\max} = k_{\max}$. It exhibits the following solutions: $l_k^{(1)} = \alpha$ and $l_k^{(2)} = \alpha \cdot k$ (where α is an arbitrary constant, which is taken as one when expressing the components), which correspond to the conservations of

the total concentration $Z \equiv \sum_{k=1}^{k_{\max}} Z^k$ and the total mass $M \equiv \sum_{k=1}^{k_{\max}} k Z^k$, respectively. Hence, $k_{\max} = M - Z + 1$.

However, when the system is opened by setting chemostats, the relevant stoichiometric matrix becomes the stoichiometric submatrix of the variable species: $\nabla_{nm}^{k_x}$. Also, $k_{\max} = \infty$. No matter what the sizes of the chemostatted glucans are, neither the total concentration conservation law $l_{k_x} = \alpha$ nor the total mass conservation law $l_{k_x} = \alpha k_x$ survives (i.e., they are not anymore elements of the cokernel space of $\nabla_{nm}^{k_x}$). We therefore say that the total mass and the total concentration are *broken conservation laws*. Nevertheless, when just one chemostat is present, $\Omega_Y \equiv \{k_y\}$, a new conservation law emerges,

$$l_{k_x}^{(3)} = \alpha (k_x - k_y). \quad (8)$$

Hence, the system exhibits just one (net) broken conservation law. It corresponds to the component

$$q = M - k_y Z, \quad (9)$$

which can assume any value in \mathbb{R} and takes into account that the total mass can change in the system only by multiples of the chemostat mass, k_y . In presence of more than one chemostat, no conservation law survives.

The components derived in this section— M and Z for the closed system and q for the network with one chemostat—will be used to characterize the steady state distribution in Sec. IV.

B. Emergent cycles

A cycle represents a finite set of reactions which leave the state of the network unchanged. Algebraically they are represented as vectors c^{nm} and they belong by definition to the kernel space of the stoichiometric matrix ($c^{nm} \in \ker \nabla$): $\frac{1}{2} \nabla_{nm}^k c^{nm} = 0$.

The steady-state currents satisfy $\nabla_{nm}^k \bar{J}^{nm} = 0$ and can always be written as linear combinations of cycles. The cycle space of our polymers system is however infinite dimensional and its complete characterization is of little use. However, in order to characterize non-equilibrium steady states only the *emergent cycles*—those cycles that may appear when chemostatted species are introduced—are needed. ¹¹ Physically, they represent cyclic transformations leaving the variable species k_x unchanged, but which would change the concentrations of the chemostats k_y if they were not kept constant and contribute to the external currents.

An emergent cycle (γ^{nm}) is thus defined by

$$\begin{cases} \frac{1}{2} \nabla_{nm}^{k_x} \gamma^{nm} = 0, \\ \frac{1}{2} \nabla_{nm}^{k_y} \gamma^{nm} = v_y^{k_y} \neq 0 \text{ for at least one } k_y, \end{cases} \quad (10)$$

where $\left\{ v_y^{k_y} \right\}_{k_y \in \Omega_Y}$ denotes the amount of chemostats of mass k_y injected (minus sign) or rejected (plus sign) from the chemical network during the transformation γ^{nm} . These quantities cannot take arbitrary values, due to the constraints imposed by the conservation laws of ∇_{nm}^k . Indeed, for any conservation law, $l_k^{(i)}$, a constraint of the following form holds:

$$l_{k_y}^{(i)} v_y^{k_y} = l_{k_y}^{(i)} \frac{1}{2} \nabla_{nm}^{k_y} \gamma^{nm} = 0. \quad (11)$$

Taking into account the total concentration $l_k^{(1)} = \alpha$ and total mass $l_k^{(2)} = \alpha k$ conservation laws, derived in Sec. III A (the emergent conservation law $l_k^{(3)}$ is a linear combination of the first two on the whole set of species indexes), we obtain the following constraints:

$$\begin{cases} \sum_{k_y} v_\gamma^{k_y} = 0 \\ \sum_{k_y} k_y v_\gamma^{k_y} = 0 \end{cases} \quad (12)$$

Non-trivial solutions of this set of equations signal the presence of emergent cycles, and thus of independent affinities, which read¹¹

$$A_\gamma = \frac{1}{2} \sum_{nm} \gamma^{nm} \ln \prod_{k_y} (Z^{k_y})^{-\nabla_{k_y}^{nm}}. \quad (13)$$

The set of linearly independent solutions of (12) gives the number of independent emergent cycles in the chemostatted chemical network. If we normalize this set so to have the smallest non-vanishing integer values for $v_\gamma^{k_y}$, these values indicate the number of chemostatted species which are introduced in or rejected from the system in precisely one (emergent) cyclic transformation.

For less than three chemostats, only trivial solutions of (12) exist and therefore no emergent cycle appears. For three chemostats, we obtain one emergent cycle characterized by the following normalized values for v^{k_y} :

$$\begin{aligned} v^{k_y 1} &= k_{y3} - k_{y2}, \\ v^{k_y 2} &= k_{y1} - k_{y3}, \\ v^{k_y 3} &= k_{y2} - k_{y1}, \end{aligned} \quad (14)$$

where k_{y1} , k_{y2} , and k_{y3} represent the masses of the chemostats. For any additional chemostat, we obtain an additional emergent cycle, each characterized by its value for the coefficients v^{k_y} .

C. External currents and dissipation

We now show that at steady state, the emergent cycles determine the external currents \bar{I}^{k_y} and the entropy production rate Σ .

We first observe that the steady-state external currents \bar{I}^{k_y} are in general linear combination of the coefficients $v^{k_y}_i$ and must satisfy the same constraints (Eq. (12)). Indeed, the steady-state equations in presence of chemostats,

$$\begin{cases} \frac{1}{2} \nabla_{nm}^k \bar{J}^{nm} = 0, \\ \frac{1}{2} \nabla_{nm}^k \bar{J}^{nm} = \bar{I}^{k_y}, \end{cases} \quad (15)$$

are equivalent to Eq. (10): the emergent cycles γ^{nm} are substituted by the steady state currents \bar{J}^{nm} and the coefficients v^{k_y} by the steady-state external currents \bar{I}^{k_y} . Thereby, if no cycle emerges due to the chemostats, the steady-state external currents \bar{I}^{k_y} are vanishing, provided that the steady state exists. The system is then at equilibrium.

The dissipation at steady state is intimately related to the external currents.¹¹ Indeed, the (non-negative) entropy production rate for our chemical reaction network can be

TABLE I. Summary of the behaviors of our model for different numbers of chemostats (ES stands for “equilibrium state” whereas NESS for “non-equilibrium steady state”). The number of broken conservation laws and independent affinities are also reported. The growth state occurs whenever the concentration of the largest chemostat is larger than the concentration of the smallest one: $(Z^{k_y \text{ larger}} \geq Z^{k_y \text{ 1}})$.

Number of chemostats, s^Y	Broken c. laws, b	Independent affinities, a	Asymptotic behavior
0	0	0	ES
1	1	0	ES
2	2	0	ES/growth
3	2	1	NESS/growth
4	2	2	NESS/growth

written as

$$\begin{aligned} \Sigma &\equiv \frac{1}{2} \sum_{nm} J^{nm} R \ln \frac{J^{+nm}}{J^{-nm}} \\ &= - \underbrace{\sum_{k_x} \dot{Z}^{k_x} R \ln \frac{Z^{k_x}}{Z_{\text{eq}}^{k_x}}}_{\equiv \Sigma_X} - \underbrace{\sum_{k_y} I^{k_y} R \ln \frac{Z^{k_y}}{Z_{\text{eq}}^{k_y}}}_{\equiv \Sigma_Y}, \end{aligned} \quad (16)$$

where R is the gas constant. At the steady state, the internal species’ contribution Σ_X always vanishes. Hence, the dissipation is characterized by the contribution due to the chemostats Σ_Y , which is non-vanishing if the set of steady-state external currents \bar{I}^{k_y} is also non-vanishing. We also mention that the steady state entropy production can be expressed as the sum along a set of independent emergent cycles of products of affinities (13) and emergent cycle currents¹¹ \mathcal{J}_γ : $\bar{\Sigma} = \sum_\gamma A_\gamma \mathcal{J}_\gamma$.

Summarizing, the conservation laws provide us with both the components—which are useful for expressing the steady state distributions—and the constraints (Eq. (12)) on the emergent cycles of the network (Eq. (10)). Due to these constraints, the first emergent cycle appears in the system with three chemostats. For any additional chemostat an additional independent cycle emerges. Through these cycles the environment exerts chemical forces, which are generated by the chemostats concentrations. The external currents analyzed in Subsection III C result from these forces and characterize the dissipation.

We emphasize that the relation between the number of chemostats s^Y , of net broken conservation laws b , and of emergent cycles a , is in perfect agreement with the general result obtained for finite-dimensional phase space in Ref. 11 stating that

$$s^Y = b + a. \quad (17)$$

These results are summarized in Table I.

IV. THE STATIONARY DISTRIBUTIONS

We now use the components introduced in Subsection III A to derive the steady-state concentration distribution for different number of chemostats. The conditions on the

chemostats' concentrations not leading to the steady state solution are also identified.

From the steady-state equations corresponding to (5) and from the equations for external currents (6), we can write a general expression for the steady-state concentrations as a function of the concentration of monomers, \bar{Z}^1 , the fraction of polymers larger than monomers, $\bar{r} \equiv 1 - \bar{Z}^1/\bar{Z}$, and the chemostats fluxes, \bar{I}^{k_y} , as follows:

$$\bar{Z}^k = \bar{Z}^1(\bar{r})^{k-1} + \sum_{k_y \in \Omega_Y} \frac{\bar{I}^{k_y}}{\kappa} \frac{1 - (\bar{r})^{k-k_y}}{1 - \bar{r}} \Theta(k - k_y - 1), \quad (18)$$

where $\Theta(\cdot)$ represents the discrete step function (we refer the reader to [Appendix A](#) for details). Here, the number of chemostats is arbitrary, and since the external currents at steady state satisfy the same constraints as in (12), only $s^Y - 2$ of them are independent. In the next paragraphs, we will discuss in detail the above expression for zero, one, two, and three chemostats, and the variables \bar{Z}^1 , \bar{r} , and \bar{I}^{k_y} will be expressed in terms of the components and of the chemostats' concentrations.

A. Closed system

As previously discussed, the closed system exhibits the following components: $Z = \sum_{k=1}^{k_{\max}} Z^k$ and $M = \sum_{k=1}^{k_{\max}} k Z^k$. In order to express the equilibrium distribution algebraically as function of Z and M we consider the following limit $M \gg Z$. In this way $k_{\max} \sim \infty$ and imposing $Z = \sum_{k=1}^{\infty} Z^k$ and $M = \sum_{k=1}^{\infty} k Z^k$ on expression (18) we can write \bar{Z}^1 and \bar{r} as functions of Z and M . Hence

$$\bar{Z}^k = \frac{(Z)^2}{M} \left(1 - \frac{Z}{M}\right)^{k-1}. \quad (19)$$

Fig. 3 shows the behavior of this distribution for different values of Z and M . As expected, the higher the ratio between the mass and the concentration $M \gg Z$, the broader the distribution.

Remark. The equilibrium distribution we obtained from our dynamical description is equivalent to the result obtained

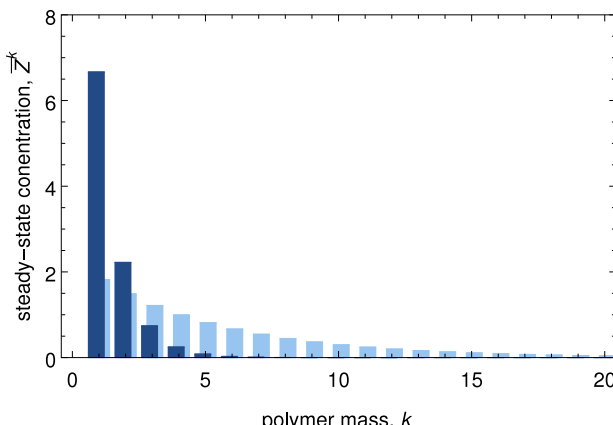


FIG. 3. Equilibrium concentration distribution for the closed system of monomers-exchanging polymers at different values of the total concentration Z and total mass M . The dark blue bar plot refers to the choice $Z = 10$ and $M = 15$, while the light blue one to $Z = 10$ and $M = 55$.

using maximum entropy approaches and is consistent with experimental observations.⁷ The equivalence is inferred by comparing Eq. (19) with Eqs. (1), (3), and (4) in Ref. 7.

B. Open system: 1 chemostat

Introducing a chemostat breaks the concentration and mass conservation laws, but a new one arises (8). As a result, no affinity appears ($s^Y = 1$, $b = 1$, and $a = 0$) and the system evolves towards an equilibrium state compatible with the chemostat concentration Z^{k_y} and the value of the component q (9) (the steady-state external current vanishes, $\bar{I}^{k_y} = 0$). Also, since the system is now open, k_{\max} is infinite.

Imposing the constraints on the expression for the steady state (18), namely,

$$\begin{cases} q = \bar{Z}^1 \frac{1 - k_y(1 - \bar{r})}{(1 - \bar{r})^2}, \\ Z^{k_y} = \bar{Z}^1(\bar{r})^{k_y-1} \end{cases} \quad (20)$$

we can express the variables \bar{Z}^1 and \bar{r} numerically as functions of q and Z^{k_y} and obtain the equilibrium—exponential—distribution as a function of q and Z^{k_y} .

C. Open system: 2 chemostats

From two chemostats on, the infinite dimension of the system starts to play a role. As discussed in Sec. III, two chemostats are not enough to drive the network towards a non-equilibrium steady state ($s^Y = 2$, $b = 2$, and $a = 0$): $I^{k_{y1}} = 0$ and $I^{k_{y2}} = 0$, where k_{y1} and k_{y2} represent the masses of the two chemostats ($k_{y1} < k_{y2}$). Thus, imposing the known values of the chemostat concentrations on expression (18) leads to

$$\begin{cases} Z^{k_{y1}} = \bar{Z}^1(\bar{r})^{k_{y1}-1} \\ Z^{k_{y2}} = \bar{Z}^1(\bar{r})^{k_{y2}-1}, \end{cases} \quad (21)$$

which only admits physical solutions if $Z^{k_{y1}} > Z^{k_{y2}}$. In this case, from (21) we obtain the equilibrium distribution

$$\bar{Z}^k = Z^{k_{y1}} \left(\frac{Z^{k_{y2}}}{Z^{k_{y1}}} \right)^{\frac{k-k_{y1}}{k_{y2}-k_{y1}}}, \quad (22)$$

which is broader the smaller $Z^{k_{y1}} - Z^{k_{y2}}$ is or the larger $k_{y2} - k_{y1}$ is. When $Z^{k_{y1}} \leq Z^{k_{y2}}$ the equilibrium concentration distribution becomes an increasing exponential which cannot be reached. As a result the system will enter a regime of continuous growth aimed at reaching that state (which we analyze in Sec. V).

D. Open system: 3 chemostats

Three is the minimum number of chemostats able to drive the system in a non-equilibrium steady state (Sec. III B). Indeed, a class of emergent cycles appears ($s^Y = 3$, $b = 2$, and $a = 1$) and the system exhibits a set of non-vanishing external currents. If we impose the values for the chemostats' concentrations on the general expression for the steady state

(18), we obtain

$$\left\{ \begin{array}{l} \bar{Z}^{k_{y1}} = \bar{Z}^1(\bar{r})^{k_{y1}-1}, \\ \bar{Z}^{k_{y2}} = \bar{Z}^1(\bar{r})^{k_{y2}-1} + \frac{\bar{I}^{k_{y1}}}{\kappa} \frac{1 - (\bar{r})^{k_{y2}-k_{y1}}}{1 - \bar{r}}, \\ \bar{Z}^{k_{y3}} = \bar{Z}^1(\bar{r})^{k_{y3}-1} + \frac{\bar{I}^{k_{y1}}}{\kappa} \frac{1 - (\bar{r})^{k_{y3}-k_{y1}}}{1 - \bar{r}} \\ \quad + \frac{\bar{I}^{k_{y2}}}{\kappa} \frac{1 - (\bar{r})^{k_{y3}-k_{y2}}}{1 - \bar{r}}. \end{array} \right. \quad (23)$$

As discussed in Sec. III C, the external currents \bar{I}^{k_y} are subject to the same constraints as the emergent cycles and can be written as linear combinations of them. Since we have one class of emergent cycles, characterized by the ν^{k_y} values in (14), we have that

$$\bar{I}^{k_{yi}} = \bar{I} \nu^{k_{yi}}, \quad i = 1, 2, 3, \quad (24)$$

where $\bar{I} \in \mathbb{R}$ determines the exact value of the fluxes. As for two chemostats, the set of equations in (23), in the variables \bar{Z}^1 , \bar{r} , and \bar{I} , does not exhibit physical solutions if the concentration of the largest chemostat is higher than the one of the smallest one, i.e., $Z^{k_{y1}} \leq Z^{k_{y3}}$. On the other hand, whenever the above condition is not fulfilled, the stationary solution is unique and stable (Appendix B). Solving the system (23) numerically, we obtain the values of \bar{Z}^1 , \bar{r} , and \bar{I} given $Z^{k_{y1}}$, $Z^{k_{y2}}$, and $Z^{k_{y3}}$. In Fig. 4, the distribution is shown for different values of these concentrations.

The chemostat concentrations also determine the sign of the related fluxes: if the concentration of the second chemostat lies above the equilibrium distribution obtained by the first and third one, we have a continuous flow of mass from the intermediate chemostat towards the external ones ($\bar{I} > 0$, Fig. 4(a)). Vice versa, if the concentration of the second chemostat lies below the equilibrium distribution obtained by the first and the third one, we have a continuous flow of mass from the smallest and largest chemostats towards the intermediate one ($\bar{I} < 0$, Fig. 4(b)). Importantly, whatever physical value $Z^{k_{y1}}$, $Z^{k_{y2}}$, and $Z^{k_{y3}}$ assume, the system cannot exhibit a condition in which a net flux of matter from the largest species to the smallest one occurs. This is clear by looking at the ν^{k_y} -values in (14) used to express $\bar{I}^{k_{yi}}$, Eq. (24): the sign of $\nu^{k_{y1}}$ and $\nu^{k_{y3}}$ is always the same, and opposite to the one of $\nu^{k_{y2}}$.

E. Open system: More chemostats

Going on adding chemostats, new independent classes of emergent cycles appear. The procedure for determining the steady-state distribution is equivalent to that discussed in Subsections IV C and IV D. In these two cases we proved that when the largest chemostat has a concentration greater or equal to that of the smallest one, the system does not reach a steady state. The same exact behavior has been observed numerically for more chemostats, hence we speculate that this property holds for an arbitrary number of chemostats.

As a final remark, we point out that the steady-state distributions do not depend on the value of the rate constant κ . Indeed, solving Equations (20), (21), and (23) for \bar{Z}^1 , \bar{r} ,

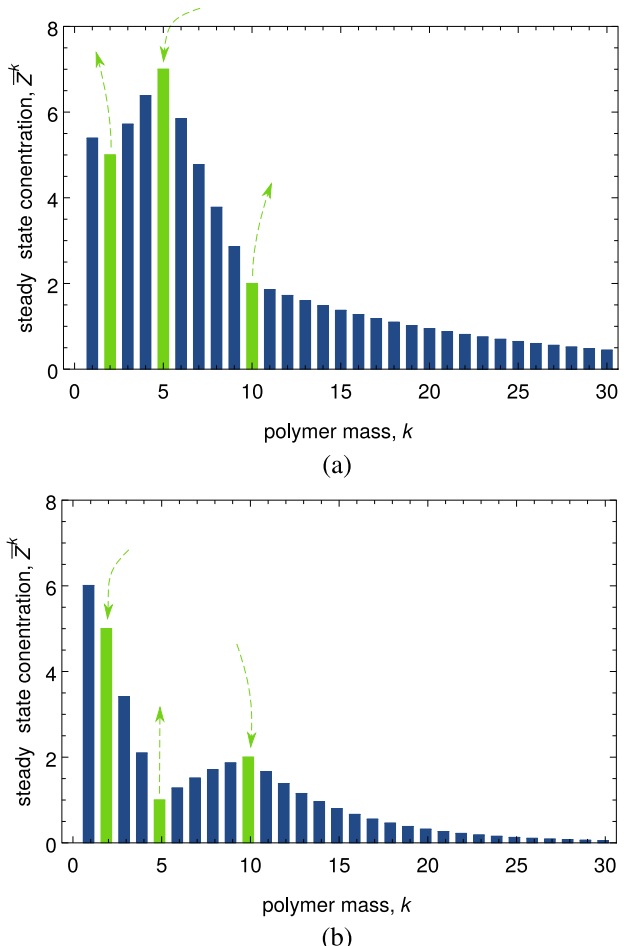


FIG. 4. Non-equilibrium steady-state distributions for the system of monomer-exchanging polymers with three chemostatted species. In both of the plots, the chemostats—highlighted in green and by the arrows—are $k_{y1} = 2$, $k_{y2} = 5$, and $k_{y3} = 10$. The orientation of the arrows denotes the sign of the external fluxes of chemostats: arrows pointing up means chemostats leaving the system, i.e., $\bar{I}^{k_y} > 0$. The chosen chemostat's concentrations are: plot (a) $Z^{k_{y1}} = 5$, $Z^{k_{y2}} = 7$, and $Z^{k_{y3}} = 2$; plot (b) $Z^{k_{y1}} = 5$, $Z^{k_{y2}} = 1$, and $Z^{k_{y3}} = 2$.

and \bar{I}^{k_y}/κ , we obtain them as functions of the components and the chemostats' concentrations. Since the latter do not depend on κ , the same holds for \bar{Z}^1 , \bar{r} , and \bar{I}^{k_y}/κ . As a corollary \bar{I}^{k_y} is proportional to κ and the same holds true for entropy production (16).

V. ASYMPTOTIC GROWTH REGIME

We mentioned in the previous section that the system does not exhibit a steady state when the concentration of the largest chemostat exceeds that of the smallest one, $Z^{k_{y1}} \leq Z^{k_{y3}}$ —we refer in the text to this configuration of chemostats leading to continuous growth as “unbalanced.” The dynamical fixed point moves outside the region of physical solutions—namely, to $\bar{r} \geq 1$, see Appendix B—and the system approaches the limit $\bar{r} \rightarrow 1$. This indicates that the concentration of the single monomer species becomes negligible compared to the rest of the species. Hence the system grows towards an unreachable steady state with an exponentially increasing concentration distribution.

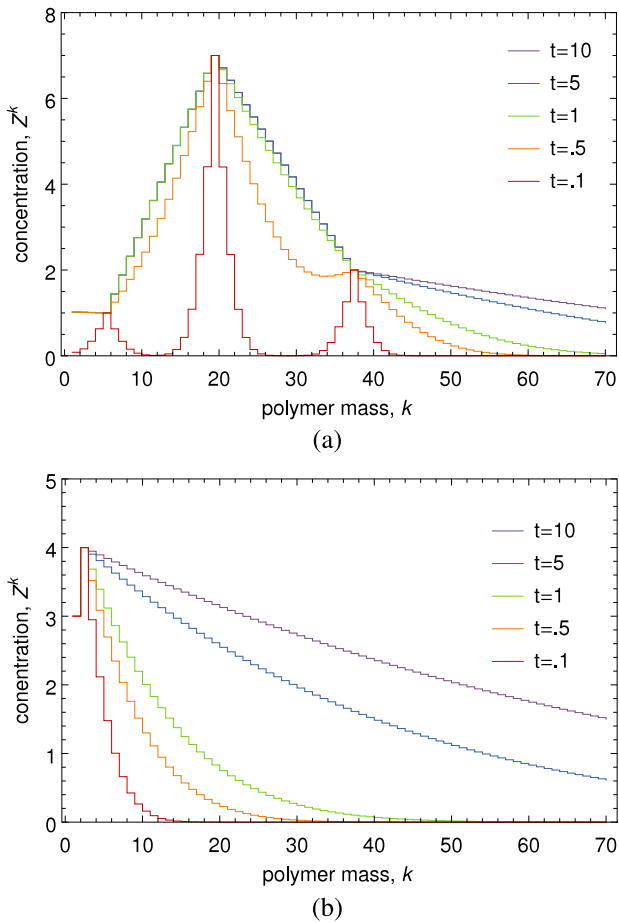


FIG. 5. Concentration distributions at different times are shown for system in unbalanced conditions. Different colors from red to violet correspond to exponentially increasing times. The set of plots is obtained by numerical solution of differential equation (5). Absorbing boundary conditions have been chosen, meaning that the concentration at the cutoff—here set to $k_{\text{cutoff}} = 1000$ —is zero. We point out that this prescription is safe before the cutoff is reached. In plot (a) we report a system with three chemostats. The chemostat's masses and the related concentrations chosen are: $Z^5 = 1$, $Z^{19} = 7$, and $Z^{37} = 2$. The concentrations of the species between the chemostats basically overlap at times $t \gtrsim 1$ and become steady. Beyond this time the growth only involves the species larger than the biggest chemostat. In plot (b) we consider a system with monomers and dimers chemostatted: $Z^1 = 3$ and $Z^2 = 4$.

Fig. 5(a) shows the concentration distributions of an unbalanced system at different times before the numerical cutoff (more details are given in the related caption) is reached. These different distributions show that while the concentrations of the species between two chemostats stabilize to steady values, the concentrations of the species larger than the biggest chemostat do not. Hence, the system continuously grows trying to populate the infinite size polymer. This behavior has been observed taking into account different number of chemostats and chemostats' concentrations.

In order to characterize this growth algebraically, we consider a system with monomer and dimer chemostats ($k_{y1} = 1$ and $k_{y2} = 2$) such that $Z^{k_{y1}} \leq Z^{k_{y2}}$. (The typical growth obtained numerically in this scenario is shown in Fig. 5(b).) Since the growth dynamics cannot be solved exactly, we assume that the asymptotic concentration distribution can be parametrized by (equilibrium) steady state expression (18)

with time dependent parameters, i.e.,

$$Z^k(t) \simeq A(t)(a(t))^{k-3}, \quad \text{for } k \geq 3, \quad (25)$$

where $A(t)$ and $a(t)$ are unknown real functions of time. To simplify the notation, let us denote the concentrations of the chemostats by $Y^1 \equiv Z^{k_{y1}}$ and $Y^2 \equiv Z^{k_{y2}}$. The functions $A(t)$ and $a(t)$ can be determined by means of the differential equations for the total concentration Z and the total mass M ,

$$\begin{aligned} \dot{Z} &= -I^1 - I^2 = -\kappa Z(Z^3 - Y^2) - \kappa Y^2 Y^1, \\ \dot{M} &= -I^1 - 2I^2 \\ &= -\kappa Z(2Z^3 - 3Y^2 + Y^1) - \kappa 2Y^2 Y^1 + \kappa Y^1 Y^1, \end{aligned} \quad (26)$$

where Z , M and the concentration of trimers Z^3 assume the following form when ansatz (25) is taken into account,

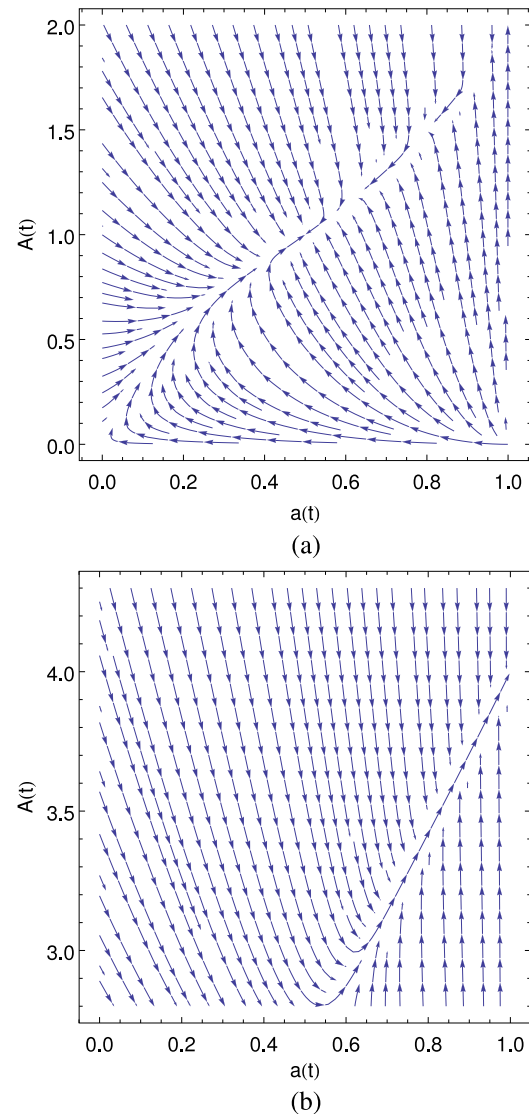


FIG. 6. Stream plot of the differential equations (26) expressed in terms of the ansatz functions $a(t)$ (abscissa) and $A(t)$ (ordinate). When balanced chemostat concentrations are used, the fixed point takes values of $a(t)$ in $[0, 1]$: plot (a). The chemostats chosen for this plot are $Y^1 = 4$ and $Y^2 = 2$. Vice versa, when the chemostats are unbalanced ($Y^1 = 2$ and $Y^2 = 4$) the fixed point moves outside from the physical region ($a(t) > 1$): plot (b).

$$\begin{aligned} Z(t) &\simeq \frac{A(t)}{1-a(t)} + Y^1 + Y^2, \\ M(t) &\simeq \frac{3-2a(t)}{(1-a(t))^2} A(t) + Y^1 + 2Y^2, \\ Z^3(t) &\simeq A(t). \end{aligned} \quad (27)$$

When the equations are expressed in terms of $A(t)$ and $a(t)$, the stream plots for different values of the chemostats' concentrations show that the ansatz captures the non-equilibrium phase transition occurring when the chemostats become unbalanced, see Fig. 6. Indeed, for balanced chemostats, the system evolves towards a fixed point with a lying in $[0, 1]$, Fig. 6(a). On the other hand, when the chemostats are unbalanced the fixed point lies beyond $a = 1$ signaling an asymptotic growth regime, Fig. 6(b).

The numerical solution for $A(t)$ and $a(t)$ obtained using (26) and (27) accurately characterizes the asymptotic growth. Indeed, as seen in Fig. 7, when comparing the evolution of Z and M obtained from $A(t)$ and $a(t)$ with that obtained by numerically solving the rate equations, the former solution overlaps with the latter before the cutoff used in the numerics

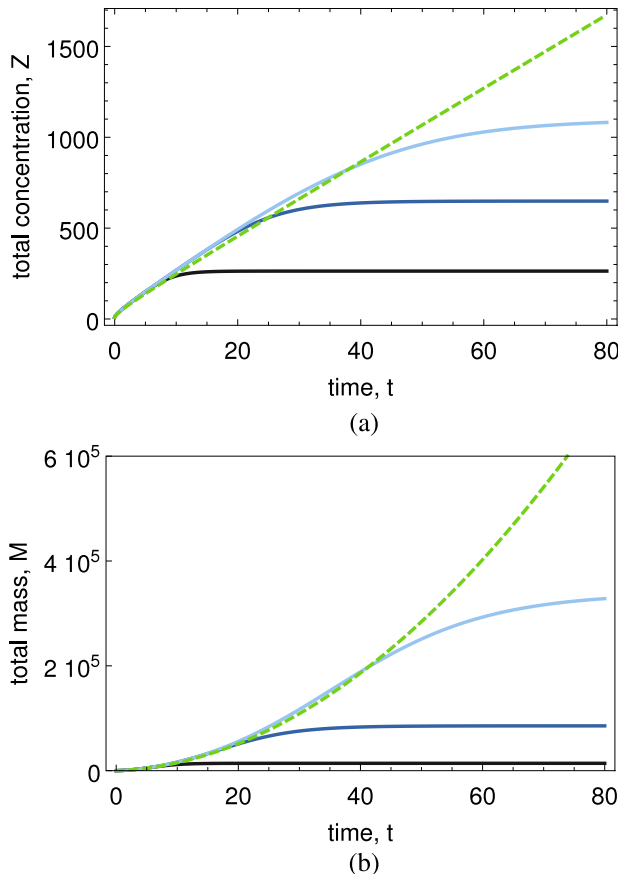


FIG. 7. Total concentration (a) and total mass (b) as functions of time in the asymptotic growth regime. The numerical solution obtained using ansatz (25) is plotted in green (dashed). These plots are compared with numerical solutions of the system of differential equations (5) with different cutoffs (blue curves). The chosen chemostat concentrations are: $Y^1 = 3$ and $Y^2 = 4$ while the initial condition imposed is $Z^k(t=0) = \frac{2}{5}(\frac{2}{3})^k$. Finally, the chosen cutoff concentrations are: $k_c = 200$ (dark blue curve), $k_c = 500$ (blue curve) and $k_c = 1000$ (light blue curve).

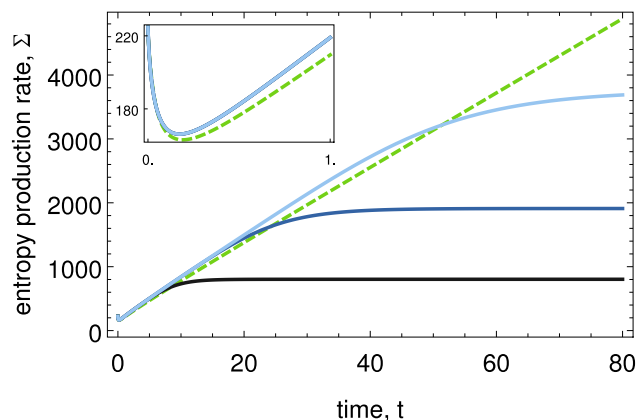


FIG. 8. Entropy production rate as a function of time in the asymptotic growth regime. The numerical solution obtained using ansatz (25) is plotted in green (dashed). This plot is compared with numerical solutions of the system of differential equations (5) with different cutoffs (blue curves). In all the plot, the entropy production rate is given in units of R . The chosen chemostat concentrations are: $Y^1 = 3$ and $Y^2 = 4$ while the initial condition imposed is $Z^k(t=0) = \frac{2}{5}(\frac{2}{3})^k$. The chosen cutoffs k_c are: 200 (dark blue curve), 500 (blue curve) and 1000 (light blue curve). Also, the inset shows in greater details the initial transient relaxation stage.

is reached. We find that the total concentration grows linearly with time whereas the mass quadratically.

Taking into account ansatz (25), entropy production rate (16) becomes

$$\Sigma \simeq RI^1 \ln \frac{A(t)}{Y^1(a(t))^2} + RI^2 \ln \frac{A(t)}{Y^2 a(t)}, \quad (28)$$

where I^1 and I^2 can be written in terms of Y^1 , Y^2 , $A(t)$, and $a(t)$ using Eq. (26). The latter is plotted in Fig. 8, where it is compared with the numerical solutions for different cutoffs. The agreement with the numerical solution is not perfect but captures the linear asymptotic growth of the entropy production rate reasonably well. Also, we point out that the unbalanced dynamics shown in Fig. 8 exhibits an initial transient relaxation stage shown in the inset.

We conclude mentioning that the same ansatz could be used for systems characterized by more chemostats with unbalanced concentrations. Indeed, the growth always involves the species larger than the biggest chemostat, whereas the species between chemostats converge faster to proper steady values. Hence, fixing the concentration of these latter species, we could assume a growth like (25) for the species larger than the biggest chemostat and perform the same analysis.

VI. CONCLUSIONS

This paper provides a kinetic description of systems made of glucans and processed by the class of enzymes known as D-enzymes. The action of the enzyme induces a monomer-exchange process¹² between pairs of glucans which are distinguished by their mass or degree of polymerization. Free monomers are not allowed to attach to other polymers⁴ implying that the total concentration and the total mass are conserved when the system is closed. The system's dynamics is ruled by rate equations for the polymer

concentrations endowed with mass action kinetics. We mimic physiological conditions by introducing *chemostats* which effectively describe the action of the environment by fixing the concentrations of certain glucans. In this scenario, chemostats represent species processed by the environment. For example, they may represent species which need to be processed and injected by the environment in the system; analogously, they may represent final products of the metabolic processes which are taken out of the system. Importantly, chemostatting the system amounts to open it and introduce driving forces on the non-chemostatted species.

Our main results are summarized in Table I. We identified three types of different long-time behaviors depending on the chemostatting conditions: equilibrium state, non-equilibrium steady state, and continuous growth of the system. The closed system as well as the open system with a single chemostat always relax to an equilibrium state. In presence of two chemostats the system will either relax to equilibrium or turn into a state of continuous growth depending on whether or not the concentration of the largest chemostat is lower than the concentration of the smallest one. We proved that this latter condition for growth holds true for up to three chemostats and conjectured that it is generally true based on numerical evidence. For more than two chemostats, if the concentration of the largest chemostat is lower than that of the smallest one, the system will reach a nonequilibrium steady state where the chemostats continuously exchange matter across the system. Our results confirm that, even in the infinite-dimensional chemical network considered here, the number of chemostats equals to the number of broken conservation laws plus the number of emergent cycles (see Table I). A proof of this equality for finite dimensional chemical networks is provided in Ref. 11. We also emphasized the role of the emergent cycles in driving the chemostatted chemical networks towards nonequilibrium steady states rather than equilibrium states.¹¹

The metabolism of polysaccharides is a complex process involving many steps and several enzymes² and its complete dynamical characterization is beyond the scope of the present paper. We focused on the dynamical characterization of the disproportionating action of D-enzymes in the breakdown and synthesis processes of glucans.⁵ Under physiological conditions, it has been pointed out that one of the possible role of D-enzymes in these processes is to produce glucans of large sizes (which are then processed by other enzymes) starting from medium sized ones.⁵ Importantly, a production of glucose (monomers in our descriptions) is expected too.⁵ This disproportionating behavior can be reproduced in a (nonequilibrium) steady state by the three chemostats system depicted in Figure 4(a). The intermediate high concentration chemostatted glucans represent the species to be processed, while the low concentration chemostatted glucans represent the species to be produced—in this case the small and large glucans. In this scenario, a continuous flow of intermediate glucans enters the system and consequently both the smaller and the larger glucans are steadily produced and expelled from the system (Sec. IV D). We stress that the production of the small glucans follows from the total concentration conservation law (Sec. III A), i.e., the fact that free monomers

cannot attach to other glucans. As seen in Sec. IV C, two chemostats are not sufficient to reproduce a nonequilibrium steady state.

Also, under closed in vitro conditions, the equilibrium distribution (which has also been analyzed in Ref. 9 and can be equivalently obtained by means of maximum entropy methods⁷) agrees with experiments.⁷ This means that if chemostatting conditions could be implemented in vitro, our predictions could be verified experimentally. Such a procedure would also enable to engineer different polymer concentration distributions.

The approach we developed could be easily extended to describe the behavior of more sophisticated forms of D-enzymes⁷ embedding further conservation laws. It is also relevant to study any type of exchange process or aggregation-fragmentation dynamics¹² in an open system framework,^{19–22} emphasizing the importance of conservation laws and providing more insights into the mechanisms driving these processes out of equilibrium.

ACKNOWLEDGMENTS

R.R. is grateful to A. Wachtel for valuable discussions and suggestions. The present project was supported by the National Research Found, Luxembourg, in the frame of Project No. FNR/A11/02 and of the AFR Ph.D. Grant 2014-2, No. 9114110.

APPENDIX A: STEADY-STATE DISTRIBUTIONS

The generic expression for steady-state distribution (18) can be obtained as follows. The steady-state equations can be expressed as

$$\begin{aligned} \bar{Z} \{ \bar{Z}^2 - \bar{Z}^1 \} + \bar{Z}^1 \bar{Z}^1 &= 0, \\ \bar{Z} \{ \bar{Z}^{k+1} - 2\bar{Z}^k + \bar{Z}^{k-1} \} + \bar{Z}^1 \{ \bar{Z}^k - \bar{Z}^{k-1} \} &= 0, \\ &= \frac{\bar{I}^k}{\kappa} \delta_{k, k_y \in \Omega_Y}, \quad \text{for } k \geq 2. \end{aligned} \quad (\text{A1})$$

Defining the variable $\Delta\bar{Z}^k \equiv \bar{Z}^k - \bar{Z}^{k-1}$, they become

$$\begin{aligned} \bar{Z} \Delta\bar{Z}^2 + \bar{Z}^1 \bar{Z}^1 &= 0, \\ \bar{Z} \{ \Delta\bar{Z}^{k+1} - \Delta\bar{Z}^k \} + \bar{Z}^1 \Delta\bar{Z}^k &= \frac{\bar{I}^k}{\kappa} \delta_{k, k_y \in \Omega_Y}, \quad \text{for } k \geq 2. \end{aligned} \quad (\text{A2})$$

Hence, by hierarchically substituting these expression one into the other and using the variable $\bar{r} \equiv 1 - \bar{Z}^1/\bar{Z}$, we obtain

$$\begin{aligned} \Delta\bar{Z}^k &= -(1 - \bar{r}) \bar{Z}^1 \bar{r}^{k-2} + \\ &+ \sum_{k_y \in \Omega_Y} \frac{\bar{I}^{k_y}}{\kappa} \bar{r}^{k-k_y-1} \Theta(k - k_y - 1), \end{aligned} \quad (\text{A3})$$

where $\Theta(\cdot)$ represents the discrete step function,

$$\Theta(k) = \begin{cases} 0 & \text{if } k < 0, \\ 1 & \text{if } k \geq 0. \end{cases} \quad (\text{A4})$$

Finally,

$$\bar{Z}^k = \sum_{i=1}^k \Delta \bar{Z}^i = \bar{Z}^1(\bar{r})^{k-1} + \sum_{k_y \in \Omega_Y} \frac{\bar{I}^{k_y}}{\kappa} \frac{1 - (\bar{r})^{k-k_y}}{1 - \bar{r}} \Theta(k - k_y - 1), \quad (A5)$$

which corresponds to Equation (18) in the main text.

APPENDIX B: THREE CHEMOSTATS STEADY STATE

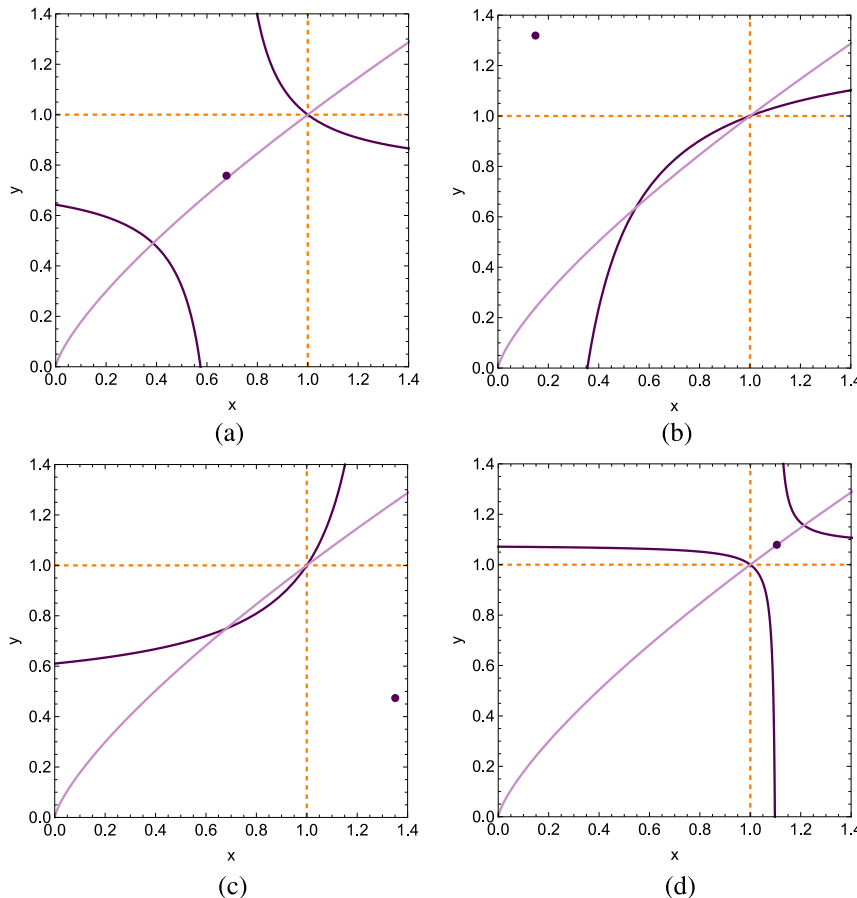
We discuss the uniqueness and stability conditions for the steady state when three chemostats are present.

From the constraints on the steady state (23) and from the condition for external currents (24), we can write a single steady state condition involving just \bar{r} as variable,

$$\begin{aligned} & (\nu^{k_{y3}} \bar{Z}^{k_{y1}} + \nu^{k_{y1}} \bar{Z}^{k_{y2}})(\bar{r})^{\nu^{k_{y1}} + \nu^{k_{y3}}} - (\nu^{k_{y1}} + \nu^{k_{y3}}) \bar{Z}^{k_{y2}}(\bar{r})^{\nu^{k_{y1}}} \\ & - (\nu^{k_{y3}} \bar{Z}^{k_{y1}} + \nu^{k_{y1}} \bar{Z}^{k_{y3}})(\bar{r})^{\nu^{k_{y3}}} \\ & + (\nu^{k_{y3}} \bar{Z}^{k_{y2}} + \nu^{k_{y1}} \bar{Z}^{k_{y3}}) = 0. \end{aligned} \quad (B1)$$

Let us define the variables $x \equiv (\bar{r})^{\nu^{k_{y3}}}$ and $y \equiv (\bar{r})^{\nu^{k_{y1}}}$, so that the above-expressed steady-state condition can be written as the intersection of two curves: a rectangular hyperbola and a power law function

$$\begin{cases} y_h = y_0 - \frac{z_0}{x - x_0}, \\ y_p = (x)^{\nu^{k_{y1}}/\nu^{k_{y3}}}, \end{cases} \quad (B2)$$



where the coefficients are given by

$$\begin{aligned} x_0 &= \frac{(\nu^{k_{y1}} + \nu^{k_{y3}}) \bar{Z}^{k_{y2}}}{\nu^{k_{y3}} \bar{Z}^{k_{y1}} + \nu^{k_{y1}} \bar{Z}^{k_{y2}}}, \\ y_0 &= \frac{\nu^{k_{y3}} \bar{Z}^{k_{y1}} + \nu^{k_{y1}} \bar{Z}^{k_{y3}}}{\nu^{k_{y3}} \bar{Z}^{k_{y1}} + \nu^{k_{y1}} \bar{Z}^{k_{y2}}}, \\ z_0 &= \frac{\nu^{k_{y1}} \nu^{k_{y3}} (\bar{Z}^{k_{y2}} - \bar{Z}^{k_{y1}}) (\bar{Z}^{k_{y2}} - \bar{Z}^{k_{y3}})}{(\nu^{k_{y3}} \bar{Z}^{k_{y1}} + \nu^{k_{y1}} \bar{Z}^{k_{y2}})^2}. \end{aligned} \quad (B3)$$

[The subscripts h and p simply help us to distinguish the two functions.] From a geometrical point of view, physical solutions are represented by those intersection points lying in $(x, y) \in (0, 1) \times (0, 1)$. In order to prove that this happens whenever $\bar{Z}^{k_{y1}} > \bar{Z}^{k_{y3}}$ we observe that all of the possible configurations of chemostat concentrations are described by the following four cases for the parameters x_0 and y_0 .

- $x_0 < 1$ and $y_0 < 1$ ($z_0 < 0$). This condition implies the following configuration for the chemostats: $\bar{Z}^{k_{y1}} > \bar{Z}^{k_{y2}} > \bar{Z}^{k_{y3}}$.

In this case we have always one and only one solution. Indeed, the center of the hyperbola (x_0, y_0) lies in $(0, 1) \times (0, 1)$, and the upper right branch of the hyperbola always intersects the power law in $x = 1$ (which is non-physical). The left lower one, instead, always intersects the power law for values in $(0, 1) \times (0, 1)$ since $y_h(x = 0) > 0$ (Fig. 9(a)).

- $x_0 < 1$ and $y_0 > 1$ ($z_0 > 0$). This condition corresponds to $\bar{Z}^{k_{y1}} > \bar{Z}^{k_{y2}}$ and $\bar{Z}^{k_{y3}} > \bar{Z}^{k_{y2}}$.

FIG. 9. Plots of the hyperbola (dark purple curve) and power law (light purple curve) in (B2) for different configurations of parameters. The center of the hyperbola is highlighted by a dark purple dot, while the physical region by the dashed orange lines. (a) $x_0 < 1$ and $y_0 < 1$, (b) $x_0 < 1$ and $y_0 > 1$, (c) $x_0 > 1$ and $y_0 < 1$ and (d) $x_0 > 1$, and $y_0 > 1$.

In this case we have one solution if and only if $\bar{Z}^{k_{y1}} > \bar{Z}^{k_{y3}}$. The center of the hyperbola lies in $(0, 1) \times (1, \infty)$ and the upper left branch of the hyperbola never intersects the power law. The right lower one, instead, always intersects the power law in $x = 1, y = 1$ (Fig. 9(b)). We have a further intersection in the physical region if and only if $\frac{dy_p}{dx} \Big|_{x=1} > \frac{dy_p}{dx} \Big|_{x=1}$, which holds iff $\bar{Z}^{k_{y1}} > \bar{Z}^{k_{y3}}$ —indeed, $x^* : y_h(x^*) = 0$ is such that $x^* > 0$, for any choice of the chemostats.

- $x_0 > 1$ and $y_0 < 1$ ($z_0 > 0$). This condition corresponds to: $\bar{Z}^{k_{y1}} < \bar{Z}^{k_{y2}}$ and $\bar{Z}^{k_{y3}} < \bar{Z}^{k_{y2}}$.

Once again, we have one solution if and only if $\bar{Z}^{k_{y1}} > \bar{Z}^{k_{y3}}$. The center of the hyperbola lies in $(1, \infty) \times (0, 1)$ and the right lower branch of the hyperbola never intersects the power law. The upper left one, instead, always intersects the power law in $x = 1, y = 1$ (Fig. 9(c)). We have a further intersection in the physical region if and only if $\frac{dy_p}{dx} \Big|_{x=1} > \frac{dy_p}{dx} \Big|_{x=1}$, which holds iff $\bar{Z}^{k_{y1}} > \bar{Z}^{k_{y3}}$ —indeed, $y_h(0) > 0$ for any choice of the chemostats.

- $x_0 > 1$ and $y_0 > 1$ ($z_0 < 0$). This condition implies the following configuration for the chemostats: $\bar{Z}^{k_{y1}} < \bar{Z}^{k_{y2}} < \bar{Z}^{k_{y3}}$.

In this case we have no solutions. Indeed, the center of the hyperbola lies in $(x, y) \in (1, \infty) \times (1, \infty)$ and neither the upper right nor the lower left branch of the hyperbola intersects the power law in the physical region. The left lower one, indeed, always intersects the power law in $(1, 1)$ which is non-physical (Fig. 9(c)).

Summarizing, we have a unique steady state whenever the concentration of the largest chemostat is higher than the concentration of the smallest one: $\bar{Z}^{k_{y1}} > \bar{Z}^{k_{y3}}$.

Stability. In order to prove the stability of the fixed point we resort to the following Lyapunov function:

$$L = \sum_k Z^k \ln \frac{Z^k}{Z_s^k} - (Z - Z_s). \quad (B4)$$

It is easy to prove that this function is always positive and vanishes only for $Z^k = Z_s^k$, where Z_s^k represents the steady-state solution. If the steady-state solution exists, namely, if exists $Z_s^k : \dot{Z}_s^k = 0$, the time derivative of the Lyapunov function (B4) can be written as

$$\frac{dL}{dt} = \sum_{k_x} \dot{Z}^{k_x} \ln \frac{Z^{k_x}}{Z_s^{k_x}}. \quad (B5)$$

Close to the steady state the above derivative is negative. Spanning the phase space with small perturbations on every concentration, we always obtain $\frac{dL}{dt} \leq 0$, where the equal sign is reached only at the steady state. Disregarding the infinite dimension of the phase space, we consider the independent set of perturbations labeled with the index k'_x and quantified by the small real value ϵ

$$Z^{k_x} = Z_s^{k_x} + \epsilon \delta^{k'_x k_x}, \quad |\epsilon| \ll \min_k Z_s^k. \quad (B6)$$

Embedding these perturbation in (B5) and using rate equations (5) we obtain

$$\begin{aligned} \frac{dL}{dt} &\simeq -\frac{\kappa}{Z_s^1} (Z_s - Z_s^1 - Z_s^2) \epsilon^2, \quad \text{for } k'_x = 1, \\ \frac{dL}{dt} &\simeq -\frac{\kappa}{Z_s^{k'_x}} (2Z_s + 2Z_s^{k'_x} \\ &\quad - Z_s^{k'_x+1} - Z_s^{k'_x-1} - Z_s^1) \epsilon^2, \quad \text{for } k'_x \neq 1, \end{aligned} \quad (B7)$$

which are always negative, no matter the sign of the perturbation.

¹D. Nelson and M. Cox, *Lehninger Principles of Biochemistry* (W. H. Freeman, 2008), pp. 244–246.

²S. G. Ball and M. K. Morell, *Annu. Rev. Plant Biol.* **54**, 207 (2003).

³Enzymes' lack of specificity is nowadays getting increased attention. The most notorious examples are enzymes involved in genetic processes and which are unspecific because they need to act on different substrates, e.g., polymerases and synthetases acting on the four nucleo-bases.²³ More recently, enzymes involved in metabolic processes have also been shown to lack specificity.²⁴ These observations have led to various theoretical studies on the thermodynamical cost of error correction.^{25–32}

⁴G. Jones and W. Whelan, *Carbohydr. Res.* **9**, 483 (1969).

⁵T. Takaha and S. M. Smith, *Biotechnol. Genet. Eng. Rev.* **16**, 257 (1999).

⁶C. Colleoni, D. Dauvillée, G. Mouille, M. Morell, M. Samuel, M.-C. Slomany, L. Liénard, F. Wattebled, C. d'Hulst, and S. Ball, *Plant Physiol.* **120**, 1005 (1999).

⁷Ö. Kartal, S. Mahlow, A. Skupin, and O. Ebenhöh, *Mol. Syst. Biol.* **7**, 542 (2011).

⁸R. N. Goldberg, D. Bell, Y. B. Tewari, and M. A. McLaughlin, *Biophys. Chem.* **40**, 69 (1991).

⁹S. Lahiri, Y. Wang, M. Esposito, and D. Lacoste, *New J. Phys.* **17**, 085008 (2015).

¹⁰See for instance: D. Kondepudi, and I. Prigogine, *Modern Thermodynamics: From Heat Engines to Dissipative Structures* (Wiley, 2014), Sec. 9.4.

¹¹M. Pollettini and M. Esposito, *J. Chem. Phys.* **141**, 024117 (2014).

¹²P. Krapivsky, S. Redner, and E. Ben-Naim, *A Kinetic View of Statistical Physics* (Cambridge University Press, 2010), Chap. 5.

¹³Indeed, the symmetry of the reaction scheme (1) is inherited by the stoichiometric matrix, which satisfies $\nabla_{nm}^k = -\nabla_{m-1, n+1}^k$.

¹⁴We refer to Eq. (5.99) in Ref. 12 for the monomers-exchange processes without constraints.

¹⁵To be precise, chemostats represent reservoirs of particles to whom the system is connected. However, in order to simplify the nomenclature we refer to the chemical species exchanged by the reservoirs as chemostat, as well.

¹⁶S. Schuster and R. Schuster, *J. Math. Chem.* **3**, 25 (1989).

¹⁷R. A. Alberti, *Thermodynamics of Biochemical Reactions* (John Wiley & Sons, 2003).

¹⁸B. O. Palsson, *Systems Biology: Properties of Reconstructed Networks* (Cambridge University Press, 2006).

¹⁹Z. Budrikis, G. Costantini, C. La Porta, and S. Zapperi, *Nat. Commun.* **5**, 3620 (2014).

²⁰T. P. J. Knowles, W. Shu, G. L. Devlin, S. Meehan, S. Auer, C. M. Dobson, and M. E. Welland, *Proc. Natl. Acad. Sci. U. S. A.* **104**, 10016 (2007).

²¹T. P. J. Knowles, C. A. Waudby, G. L. Devlin, S. I. A. Cohen, A. Aguzzi, M. Vendruscolo, E. M. Terentjev, M. E. Welland, and C. M. Dobson, *Science* **326**, 1533 (2009).

²²S. I. A. Cohen, S. Linse, L. M. Luheshi, E. Hellstrand, D. A. White, L. Rajah, D. E. Otzen, M. Vendruscolo, C. M. Dobson, and T. P. J. Knowles, *Proc. Natl. Acad. Sci. U. S. A.* **110**, 9758 (2013).

²³W. Bialek, *Biophysics: Searching for Principles* (Princeton University Press, 2012), Sec. 4.5.

²⁴C. L. Linster, E. van Schaftingen, and A. D. Hanson, *Nat. Chem. Biol.* **9**, 72 (2013).

²⁵J. J. Hopfield, *Proc. Natl. Acad. Sci. U. S. A.* **71**, 4135 (1974).

²⁶J. Ninio, *Biochimie* **57**, 587 (1975).

²⁷C. H. Bennett, *Biosystems* **11**, 85 (1979).

²⁸D. Andrieux and P. Gaspard, *Proc. Natl. Acad. Sci. U. S. A.* **105**, 9516 (2008).

²⁹G. Bel, B. Munsky, and I. Nemenman, *Phys. Biol.* **7**, 016003 (2010).

³⁰A. Murugan, D. H. Huse, and S. Leibler, *Proc. Natl. Acad. Sci. U. S. A.* **109**, 12034 (2012).

³¹P. Sartori and S. Pigolotti, *Phys. Rev. Lett.* **110**, 188101 (2013).

³²R. Rao and L. Peliti, *J. Stat. Mech.: Theory Exp.* **2015**, P06001.

The following article is reprinted with permission from
[G. FALASCO, R. RAO and M. ESPOSITO, *Phys. Rev. Lett.* **121**.10 (2018), 108301].
Copyright (2018) by the American Physical Society.

Supplementary Material follows.

The page numbers placed in the outer margins provide a continuous pagination throughout the thesis.

Information Thermodynamics of Turing Patterns

Gianmaria Falasco, Riccardo Rao, and Massimiliano Esposito

Complex Systems and Statistical Mechanics, Physics and Materials Science Research Unit, University of Luxembourg,
L-1511 Luxembourg



(Received 14 March 2018; revised manuscript received 15 June 2018; published 4 September 2018)

We set up a rigorous thermodynamic description of reaction-diffusion systems driven out of equilibrium by time-dependent space-distributed chemostats. Building on the assumption of local equilibrium, nonequilibrium thermodynamic potentials are constructed exploiting the symmetries of the chemical network topology. It is shown that the canonical (resp. semigrand canonical) nonequilibrium free energy works as a Lyapunov function in the relaxation to equilibrium of a closed (resp. open) system, and its variation provides the minimum amount of work needed to manipulate the species concentrations. The theory is used to study analytically the Turing pattern formation in a prototypical reaction-diffusion system, the one-dimensional Brusselator model, and to classify it as a genuine thermodynamic nonequilibrium phase transition.

DOI: 10.1103/PhysRevLett.121.108301

Introduction.—Reaction-diffusion systems (RDSs) are ubiquitous in nature. When nonlinear feedback effects within the chemical reactions are locally destabilized by diffusion, complex spatiotemporal phenomena emerge. These latter ranging from stationary Turing patterns [1,2] to traveling waves [3,4] play a critical role in the aggregation and structuring of hard matter [5] as well as living systems [6]. In biology, striking examples are embryogenesis determined by the prepatterning of morphogens [7–9] and cellular rhythms regulated by calcium waves [10,11].

Nonequilibrium conditions consisting in a continual influx of chemicals and energy are required to create and maintain these dissipative structures. Since the original work of Prigogine and Nicolis [12,13], which made clear how order can emerge spontaneously at the expense of continuous dissipation, much work has been dedicated to better understanding the chaotic and nonequilibrium dynamics of RDSs [14]. Most of it has focused on searching for general extremum principles, e.g., in selecting the relative stability of competing patterns [15]. Nevertheless, a complete framework is still lacking that models RDSs as proper thermodynamic systems in contact with nonequilibrium chemical reservoirs subject to external work and entropy changes. Such a theory is all the more necessary nowadays, when promising technological applications, such as biomimetics [16,17] and chemical computing [18], are envisaged that deliberately exploit the self-organized structures of RDSs. In this respect, the work needed to manipulate a Turing pattern and the efficiency with which information exchanges through traveling waves can occur are thermodynamic questions of crucial importance.

In this Letter, we lay the basis to address these questions by presenting a rigorous thermodynamic theory of RDSs far from equilibrium. We take the viewpoint of stochastic

thermodynamics [19,20] and carry over its systematic way to define thermodynamic quantities (such as work and entropy), anchoring them to the (herein deterministic) dynamics of the RDSs. Stochastic thermodynamics has recently emerged as a comprehensive framework for describing *small* systems arbitrarily far from equilibrium, as it allows one to study the efficiency of thermal micro-engines [21], rationalize the fluctuation theorems [22], and connect information processing to work [23]. We supplement this well-established approach with a novel yet pivotal element, which is the inclusion of the conservation laws [24–26] of the underlying chemical network (CN) for constructing thermodynamic potentials under general non-equilibrium conditions. Moreover, viewing the RDS as the *large size limit* of stochastically reacting and diffusing chemicals, we can study Turing patterns as instances of thermodynamic nonequilibrium phase transitions [27–32].

Theory.—The description of Ref. [33] is extended to CNs endowed with a spatial structure. We consider a dilute ideal mixture of chemical species σ that diffuse within a vessel $\mathcal{V} \ni \mathbf{r}$ with impermeable walls and undergo elementary reactions ρ . The abundance of some species is possibly controlled by the coupling with external chemostats (if not, the system is called closed). Hence, the concentration $Z_\sigma(\mathbf{r}, t)$ of internal and chemostatted species, respectively denoted x and y follows the reaction-diffusion equations

$$\partial_t Z_\sigma = -\nabla \cdot \mathbf{J}_\sigma + \sum_\rho \mathbb{S}_\rho^\sigma j_\rho + I_\sigma. \quad (1)$$

Fick's diffusion currents $\mathbf{J}_\sigma = -D_\sigma \nabla Z_\sigma$ are responsible for the transport of chemicals across space and vanish at the boundaries of \mathcal{V} ; the external currents $I_\sigma \neq 0 \forall \sigma$ describe the rate at which the controlled species are injected into the

(open) system by the chemostats; $\mathbb{S}_\rho^\sigma j_\rho$ gives the concentration variation upon reaction ρ . Here, $\mathbb{S}_\rho^\sigma = \nu_{-\rho}^\sigma - \nu_{+\rho}^\sigma$ is the stoichiometric matrix, i.e., the negative difference between the number of species σ involved in the forward ($+\rho$) and backward ($-\rho$) reaction and $j_\rho = j_{+\rho} - j_{-\rho}$ is the net reaction current. While the former specifies the CN topology, the latter determines its kinetics. By virtue of the mass-action kinetics assumption [34], each reaction current is proportional to the product of the reacting species concentrations, $j_{\pm\rho} = k_{\pm\rho} \prod_\sigma Z_\sigma^{\nu_{\pm\rho}^\sigma}$. For example, the net current associated with the autocatalytic reaction

$2X_1 + X_2 \xrightleftharpoons[k_-]{k_+} 3X_1$ (the core of the Brusselator model discussed later) is $j_\rho = k_+ Z_{X_1}^2 Z_{X_2} - k_- Z_{X_1}^3$, where $\nu_{+\rho}^{X_1} = 2$, $\nu_{+\rho}^{X_2} = 1$, and $\nu_{-\rho}^{X_1} = 3$. Thermodynamic equilibrium characterized by homogeneous concentrations Z_σ^{eq} is reached when all external and reaction currents vanish identically, $j_\rho = I_\sigma = 0$. It implies for the rate constants the *local detailed balance* condition $k_{+\rho}/k_{-\rho} = \prod_\sigma (Z_\sigma^{\text{eq}})^{\mathbb{S}_\rho^\sigma}$. Such a relation is taken to be valid irrespective of the system's state. The CN instead may be in a *global* nonequilibrium state characterized by space-dependent concentrations $Z_\sigma(\mathbf{r}, t)$ as a result of inhomogeneous initial conditions or because of nonvanishing external currents I_σ . Yet, we assume it to be kept by the solvent in *local* thermal equilibrium at a given temperature T . Therefore, the species can be assigned thermodynamic state functions, which have the known equilibrium form valid for dilute ideal mixtures but are a function of the nonequilibrium concentrations $Z_\sigma(\mathbf{r}, t)$ (Ref. [35], Chap. 15).

A central role is played by the nonequilibrium chemical potential $\mu_\sigma(\mathbf{r}) := \mu_\sigma^\circ + \ln Z_\sigma(\mathbf{r})$ (given in units of temperature T times the gas constant R , as any other quantity hereafter). It renders the local detailed balance in the form $k_{+\rho}/k_{-\rho} = \exp(-\sum_\sigma \mathbb{S}_\rho^\sigma \mu_\sigma^\circ)$ involving only the difference between the energy of formation of reactants and products. Moreover, its variation across space and between species gives the local diffusion and reaction affinity [34]

$$\mathbf{F}_\sigma(\mathbf{r}) := -\nabla \mu_\sigma(\mathbf{r}), \quad f_\rho(\mathbf{r}) := -\sum_\sigma \mathbb{S}_\rho^\sigma \mu_\sigma(\mathbf{r}), \quad (2)$$

which are the thermodynamic forces driving the system.

We introduce as nonequilibrium potential the “canonical” Gibbs free energy of the system $G := \int_V d\mathbf{r} \sum_\sigma (\mu_\sigma Z_\sigma - Z_\sigma)$ (given up to a constant). It can be expressed in terms of the equilibrium free energy $G^{\text{eq}} = G(Z_\sigma^{\text{eq}})$ as

$$G = G^{\text{eq}} + \mathcal{L}(Z_\sigma \| Z_\sigma^{\text{eq}}) \quad (3)$$

introducing the *relative entropy* for non-normalized concentration distributions

$$\mathcal{L}(Z_\sigma \| Z_\sigma^{\text{eq}}) := \int_V d\mathbf{r} \sum_\sigma \left(Z_\sigma \ln \frac{Z_\sigma}{Z_\sigma^{\text{eq}}} - (Z_\sigma - Z_\sigma^{\text{eq}}) \right). \quad (4)$$

Akin to the Kullback–Leibler divergence for probability densities [36], Eq. (4) quantifies the dissimilarity between two concentrations: Being positive for all $Z_\sigma \neq Z_\sigma^{\text{eq}}$, it implies that G is always larger than its equilibrium counterpart G^{eq} . Most importantly, it is minimized by the relaxation dynamics of *closed* systems. This is shown by evaluating the time derivative of Eq. (3) with the aid of Eq. (1) at $I_\sigma = 0$ and Eq. (2),

$$d_t \mathcal{L} = d_t G = -\dot{\Sigma}_{\text{dff}} - \dot{\Sigma}_{\text{ret}} =: -\dot{\Sigma} \leq 0, \quad (5)$$

and recognizing the standard form of the total entropy production rate (EPR) $\dot{\Sigma}$ split into its diffusion and reaction parts [34]:

$$\dot{\Sigma}_{\text{dff}} := \int_V d\mathbf{r} \sum_\sigma \mathbf{J}_\sigma \cdot \mathbf{F}_\sigma, \quad \dot{\Sigma}_{\text{ret}} := \int_V d\mathbf{r} \sum_\rho j_\rho f_\rho. \quad (6)$$

The relative entropy (4) possesses some important physical features. First, in the absence of reactions, it gives the total entropy produced by the diffusive expansion of concentrations. For example, consider n_A and n_B moles of inert chemicals A and B initially placed in the volume fractions V_A and V_B , respectively. They relax to homogeneous concentrations with an entropy production $-\mathcal{L} = n_A \log V_A + n_B \log V_B$ that is exactly the *entropy of mixing* of the two species [37]. It is remarkable that diffusive dissipation and mixing entropy are, thus, fully described in a purely information theoretic fashion, namely, as a relative entropy between concentrations. Second, the relative entropy between reacting concentrations $Z_\sigma(\mathbf{r}, t) = \bar{Z}_\sigma(t) \phi_\sigma(\mathbf{r}, t) \mathcal{V}$ and arbitrary reference homogeneous concentrations Z_σ^h can be split into the relative entropy between space-averaged concentrations $\bar{Z}_\sigma(t) = \int_V d\mathbf{r} Z_\sigma(\mathbf{r}, t) / \mathcal{V}$ and equilibrium ones Z_σ^{eq} plus the relative entropy of the normalized local modulations $\phi_\sigma(\mathbf{r})$ around \bar{Z}_σ and the flat distribution $1/\mathcal{V}$:

$$\mathcal{L}(Z_\sigma \| Z_\sigma^h) = \mathcal{L}(\bar{Z}_\sigma \| Z_\sigma^h) + \sum_\sigma \bar{Z}_\sigma \mathcal{L}(\phi_\sigma \| 1/\mathcal{V}). \quad (7)$$

The positivity of relative entropy implies $\mathcal{L}(Z_\sigma \| Z_\sigma^h) \geq \mathcal{L}(\bar{Z}_\sigma \| Z_\sigma^h)$; i.e., the free energy of a patterned system is always larger than its homogeneous counterpart. Third, different patterns may have the same relative entropy (see Fig. 1) indicating that morphology and thermodynamics need not be correlated [38].

The conservation laws of the CN play a central role in building the nonequilibrium thermodynamics of the system, i.e., in the derivation of Eqs. (3) and (4). The left null vectors of \mathbb{S}_ρ^σ , i.e., $\sum_\sigma \ell_\sigma^\lambda \mathbb{S}_\rho^\sigma = 0$, define the components

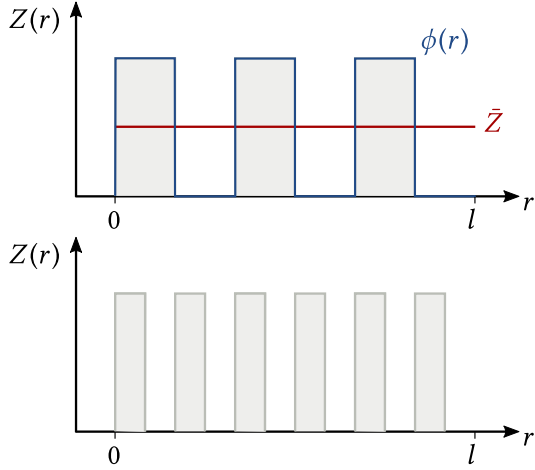


FIG. 1. Sketch of two patterns with equal relative entropy. Any transformation $\phi(r) \rightarrow \phi'(r) = \phi(r')$ with $|\partial r / \partial r'| = 1$ corresponding to a simple rearrangement of the local concentrations leaves $\mathcal{L}(Z|Z^{\text{eq}})$ unchanged. This is rooted in the lack of interactions between chemicals at the scale of the RDS.

$L_\lambda = \sum_\sigma \ell_\sigma^\lambda Z_\sigma$, which are the global conserved quantities of the closed system: $d_t \int_V d\mathbf{r} L_\lambda = 0$. For this reason, ℓ_σ^λ are called conservation laws. Physically, they identify parts of molecules called moieties exchanged between species [39]. When the system is opened by chemostatting, ℓ_σ^λ differentiate into the $\ell_\sigma^{\lambda_u}$'s that are left null vectors of the submatrix of internal species \mathbb{S}_ρ^x and the $\ell_\sigma^{\lambda_b}$'s that are not, namely,

$$\sum_x \ell_x^{\lambda_u} \mathbb{S}_\rho^x = 0, \quad \sum_x \ell_x^{\lambda_b} \mathbb{S}_\rho^x \neq 0. \quad (8)$$

Accordingly, the unbroken components $L_{\lambda_u} = \sum_\sigma \ell_\sigma^{\lambda_u} Z_\sigma$ remain global conserved quantities of the system, $d_t \int_V d\mathbf{r} L_{\lambda_u} = 0$, while the broken ones $L_{\lambda_b} = \sum_\sigma \ell_\sigma^{\lambda_b} Z_\sigma$ change over time, $d_t \int_V d\mathbf{r} L_{\lambda_b} = \sum_y \ell_y^{\lambda_b} \int_V d\mathbf{r} I_y \neq 0$.

In light of that, the equilibrium condition $\sum_\sigma \mathbb{S}_\rho^\sigma \mu_\sigma^{\text{eq}} = 0$ corresponding to null reaction affinities $f_\rho = 0$ implies that μ_σ^{eq} is a linear combination of the conservation laws ℓ_σ^λ . This entails $\int_V d\mathbf{r} \sum_\sigma \mu_\sigma^{\text{eq}} \partial_t Z_\sigma = 0$, which yields, in turn, the decomposition (3) when integrating along a relaxation dynamics that leads from Z_σ to Z_σ^{eq} [40].

Moreover, the conservation laws are the passkey to construct the correct nonequilibrium thermodynamic potential for *open* systems. For the latter, an additional term appears when taking the time derivative of G due to the external current in Eq. (1),

$$\dot{W}_{\text{chem}} := \int_V d\mathbf{r} \sum_y \mu_y(\mathbf{r}) I_y(\mathbf{r}), \quad (9)$$

which defines the chemical work performed by the chemostats. The second law (5) thus attains the new form

$$\dot{W}_{\text{chem}} - d_t G = \dot{\Sigma} \geq 0, \quad (10)$$

where the EPR $\dot{\Sigma}$ is still given by the two contributions of Eq. (6) even for $I_\sigma \neq 0$. Consequently, G is no longer minimized due to the break of conservation laws. Similar to equilibrium thermodynamics when passing from canonical to grand canonical ensembles, one needs to transform the free-energy G subtracting the energetic contributions of matter exchanged with the reservoirs [41]. This amounts to the moieties of the broken components $M_{y_p} := \sum_{\lambda_b} \ell_{y_p}^{\lambda_b - 1} \int d\mathbf{r} L_{\lambda_b}(\mathbf{r})$ entering those chemostats y_p that break all conservation laws, times the reference values of their chemical potential $\mu_{y_p}^{\text{ref}}$ (which simplifies to μ_{y_p} for homogeneous chemostats). The so-obtained semi-grand Gibbs free energy

$$\mathcal{G} := G - \sum_{y_p} \mu_{y_p}^{\text{ref}} M_{y_p} \quad (11)$$

encodes CN-specific topological and spatial features thanks to the freedom in the choice of y_p and $\mu_{y_p}^{\text{ref}}$. This allows one to split the EPR

$$\dot{W}_{\text{driv}} + \dot{W}_{\text{nc}} - d_t \mathcal{G} = \dot{\Sigma}, \quad (12)$$

in terms of the driving and the nonconservative chemical work rate, respectively,

$$\dot{W}_{\text{driv}} := - \sum_{y_p} d_t \mu_{y_p}^{\text{ref}} M_{y_p}, \quad \dot{W}_{\text{nc}} := \sum_y \int_V d\mathbf{r} I_y \mathcal{F}_y. \quad (13)$$

The former results from time-dependent manipulations of the reference chemostats y_p , while the latter gives the cost of sustaining chemical flows by means of the forces $\mathcal{F}_y(\mathbf{r}) = \mu_y(\mathbf{r}) - \sum_{y_p} \mu_{y_p}^{\text{ref}} \sum_{\lambda_b} \ell_{y_p}^{\lambda_b - 1} \ell_y^{\lambda_b}$ measured with respect to the reference chemical potentials $\mu_{y_p}^{\text{ref}}$ [40]. Equation (12) is a major result of this Letter and can be verified by direct substitution. It quantifies exactly the energy needed to manipulate, sustain, and create chemical patterns. In the absence of driving ($d_t \mu_{y_p}^{\text{ref}} = 0$) and nonconservative forcing ($\mathcal{F}_y = 0$), it simplifies to $d_t \mathcal{G} = -\dot{\Sigma} \leq 0$, which proves that the CN, despite being *open*, relaxes to equilibrium by minimizing the free energy \mathcal{G} . Moreover, for a generic open CN, the decomposition of \mathcal{G} corresponding to Eq. (3), i.e., $\mathcal{G} - \mathcal{G}^{\text{eq}} = \mathcal{L}(Z_\sigma \| Z_\sigma^{\text{eq}}) \geq 0$, and a time integral between two nonequilibrium states connected by an arbitrary manipulation turn Eq. (12) into a *non-equilibrium Landauer principle* [36] for RDS,

$$W_{\text{driv}} + W_{\text{nc}} - \Delta \mathcal{G}_{\text{eq}} \geq \Delta \mathcal{L}(Z_\sigma \| Z_\sigma^{\text{eq}}). \quad (14)$$

The latter states that the dissipative work spent to manipulate the CN is bounded by the variation in relative entropy between the boundary states and their respective equilibria attained by stopping the driving and zeroing the forcing.

Turing pattern in the Brusselator model.—As first proposed by Turing in his seminal paper [42], RDSs

undergo a spatial symmetry breaking leading to a stationary pattern when at least two chemical species react nonlinearly and their diffusivities differ substantially. A minimal system that captures these essential features is the Brusselator model [43] in one spatial dimension. Here, the concentrations of two chemical species, an activator $Z_{X_1} = x_1(r, t)$ and an inhibitor $Z_{X_2} = x_2(r, t)$, evolve in time and space $r \in [0, l]$ according to the RDS (1) for the chemical equations in Fig. 2, namely,

$$\partial_t \begin{pmatrix} x_1 \\ x_2 \end{pmatrix} = \underbrace{\begin{pmatrix} k_1 y_1 - k_{-1} x_1 - k_2 y_2 x_1 + k_{-2} y_3 x_2 + k_3 x_1^2 x_2 - k_{-3} x_1^3 - k_4 x_1 + k_{-4} y_4 + D_{x_1} \partial_r^2 x_1, \\ k_2 y_2 x_1 - k_{-2} y_3 x_2 - k_3 x_1^2 x_2 + k_{-3} x_1^3 + D_{x_2} \partial_r^2 x_2 \end{pmatrix}}_{= \mathcal{J}(x_1, x_2)}. \quad (15)$$

The y_1 , y_2 , y_3 , and y_4 are the homogeneous concentrations of the chemostatted species, and the diffusivities satisfy the Turing condition $D_{x_1} \ll D_{x_2}$. Equation (15) admits a homogeneous stationary solution $(x_1^h, x_2^h)^\top$ that becomes unstable for $y_2 \geq y_2^c$ so that a sinusoidal pattern with wave number q_c and amplitude proportional to the (in general complex) function $A(r, t)$ starts developing around the space-averaged concentrations $\bar{x}(t)$ [35]:

$$\begin{pmatrix} x_1(r, t) \\ x_2(r, t) \end{pmatrix} = \begin{pmatrix} \bar{x}_1(t) \\ \bar{x}_2(t) \end{pmatrix} + \begin{pmatrix} 1 \\ u_{x_2} \end{pmatrix} [A(r, t) e^{i q_c r} + \text{c.c.}]. \quad (16)$$

The critical values y_2^c and q_c are determined by the condition of marginal stability of the homogeneous state: They are the smaller values for which the matrix $\partial_x \mathcal{J}(x_1^h, x_2^h)$ (evolving linearized perturbations) acquires a zero eigenvalue, the corresponding eigenvector being $(1, u_{x_2})^\top$. Near the onset of instability, one can treat $\epsilon = (y_2 - y_2^c)/y_2^c \ll 1$ as a small parameter and carry out a perturbation expansion in powers of ϵ . This leads to the amplitude equation for $A(r, t)$ [44],

$$\tau \partial_t A = \epsilon A - \alpha |A|^2 A + \xi \partial_r^2 A, \quad (17)$$

which describes an exponential growth from an initial small perturbation $A(r, 0) \simeq 0$ followed by a late-time saturation due to the nonlinear terms in Eq. (15). Amplitude equations provide a general quantitative description of pattern formation in several systems near the onset of instability [45], irrespective of the details of the underlying physical process that is subsumed into the effective coefficients τ , α , and ξ . Since Eq. (17) can be seen as a gradient flow in a complex Ginzburg-Landau potential involving a bifurcation as ϵ turns positive, pattern formation is usually considered a *dynamical* phase transition [46]. Here, using an analytical

approximate solution to Eq. (15) valid for $\epsilon \ll 1$, we show that the phenomenon is, in fact, a genuine *thermodynamic* phase transition identified by the appearance of a kink singularity at y_2^c in the nonequilibrium free energy $\mathcal{G}(y_2)$. The semigrand canonical free energy of Fig. 2 is calculated [40] taking the stationary stable solution corresponding to a given value of y_2 , i.e., the homogenous one for $y_2 \leq y_2^c$ and the patterned one for $y_2 > y_2^c$, namely,

$$\begin{pmatrix} x_1^p(r) \\ x_2^p(r) \end{pmatrix} \sim \begin{pmatrix} 1 \\ u_{x_2} \end{pmatrix} \sqrt{\frac{\epsilon}{\alpha}} 2 \cos(q_c r). \quad (18)$$

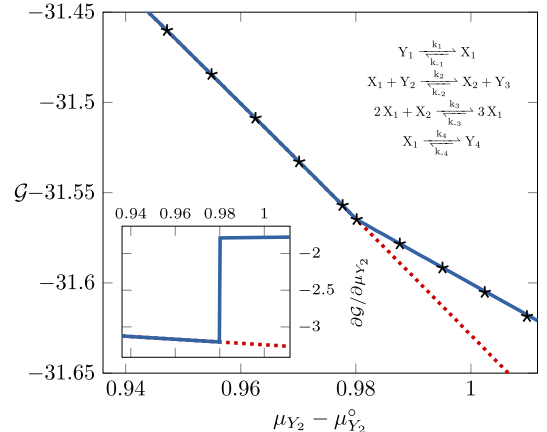


FIG. 2. Nonequilibrium semigrand Gibbs free energy \mathcal{G} for the Brusselator model as a function of the chemical potential of the chemostatted species Z_{Y_2} obtained by the analytic stationary solution of the amplitude equation. To define \mathcal{G} , we choose y_1 and y_2 as the reference chemostats breaking the two components $L_1 = x_1 + x_2 + y_1 + y_4$ and $L_2 = y_2 + y_3$. The dotted line represents the free energy \mathcal{G} in the unstable homogeneous system before the pattern growth. Symbols (\star) result from numerical integration of Eq. (15). Inset: The derivative $\partial \mathcal{G} / \partial \mu_{Y_2}$ displays a discontinuity at $y_2^c \simeq 2.66$.

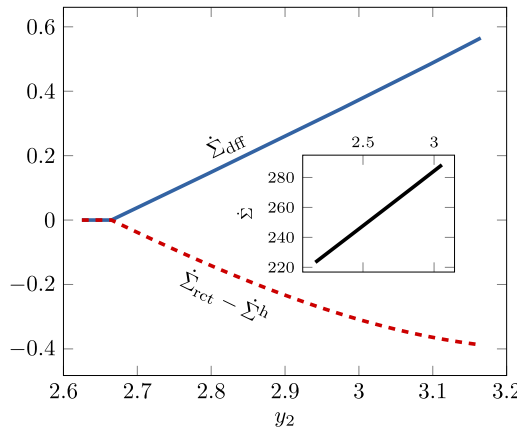


FIG. 3. Analytical result for the EPR of reaction $\dot{\Sigma}_{\text{ret}}$ (dashed) and diffusion $\dot{\Sigma}_{\text{dff}}$ (solid) in the stable stationary state as function of the concentration y_2 . The EPR of the (unstable for $y_2 > y_2^c$) homogeneous state $\dot{\Sigma}^h$ is subtracted from the former to show the effect of the pattern formation, i.e., decreasing reaction dissipation at the expense of diffusion dissipation. Inset: The total entropy production shows no singularity at the phase transition. All results correspond to the weakly reversible case $k_{-\rho} = 10^{-4} \ll k_{+\rho} = 1$, and $y_3 = y_4 = 10^{-4}$, $y_1 = 2$, $D_{x_1} = 1$, $D_{x_2} = 10$.

The physical meaning of the kink at $y_2 = y_2^c$ is best understood noticing that the quantity $\partial \mathcal{G} / \partial \mu_{Y_2} = \dot{W}_{\text{driv}} / d_t \mu_{Y_2}$ is the driving work upon a quasistatic manipulation of the chemical potential μ_{Y_2} . In particular, for $y_2 > y_2^c$ it represents the minimum work needed to vary the wave number q_c of the Turing pattern (18). Interestingly, the total EPR shows no singularity at the transition (cf. Fig. 3): Moving across y_2^c , the EPR of reaction $\dot{\Sigma}_{\text{ret}}$ decreases with respect to the homogeneous state value $\dot{\Sigma}^h$, while a nonzero EPR of diffusion appears, their sum being continuous. This is different from what has been observed in some previous studies of non-equilibrium phase transition [27–31].

Conclusion.—We presented the nonequilibrium thermodynamics of RDSs and exemplified the theory with the application to the Brusselator model. We went beyond the conventional treatment of classical nonequilibrium thermodynamics [47] in two respects: avoiding to linearize the chemistry, i.e., to oversimplify reaction affinities to currents times Onsager coefficients; explicitly building thermodynamic potentials that act as Lyapunov functions in the relaxation to equilibrium provide minimum work principles and reveal the existence of nonequilibrium phase transitions. As demonstrated by the paradigmatic case of the Brusselator model, the framework can be directly applied to quantify the energy cost of pattern manipulations in complex biochemical systems [48–50] and paves the way to study information transmission in signal transduction [51], quorum sensing [52], and chemotaxis [53].

We acknowledge funding from the National Research Fund of Luxembourg (AFR Ph.D. Grant 2014-2, No. 9114110) and the European Research Council project NanoThermo (ERC-2015-CoG Agreement No. 681456).

- [1] V. Castets, E. Dulos, J. Boissonade, and P. De Kepper, *Phys. Rev. Lett.* **64**, 2953 (1990).
- [2] Q. Ouyang and H. L. Swinney, *Nature (London)* **352**, 610 (1991).
- [3] A. N. Zaikin and A. M. Zhabotinsky, *Nature (London)* **225**, 535 (1970).
- [4] A. T. Winfree, *Science* **175**, 634 (1972).
- [5] P. J. Ortoleva, *Geochemical Self-Organization* (Oxford University Press, New York, 1994).
- [6] J. D. Murray, *Mathematical Biology. II Spatial Models and Biomedical Applications*, 3rd ed. (Springer-Verlag, Berlin 2001).
- [7] S. Kondo and T. Miura, *Science* **329**, 1616 (2010).
- [8] D. Iber and D. Menshykau, *Open Biol.* **3**, 130088 (2013).
- [9] S. Kretschmer and P. Schwille, *Curr. Opin. Cell Biol.* **38**, 52 (2016).
- [10] M. Falcke, *Adv. Phys.* **53**, 255 (2004).
- [11] K. Thurley, A. Skupin, R. Thul, and M. Falcke, *Biochim. Biophys. Acta* **1820**, 1185 (2012).
- [12] I. Prigogine and G. Nicolis, *Q. Rev. Biophys.* **4**, 107 (1971).
- [13] G. Nicolis and I. Prigogine, *Self-Organization in Non-equilibrium Systems: From Dissipative Structures to Order Through Fluctuations* (Wiley-Blackwell, New York, 1977).
- [14] M. C. Cross and P. C. Hohenberg, *Rev. Mod. Phys.* **65**, 851 (1993).
- [15] J. Ross, *Thermodynamics and Fluctuations Far from Equilibrium* (Springer, New York, 2008), Chap. 5.
- [16] F. Rossi, S. Ristori, M. Rustici, N. Marchettini, and E. Tiezzi, *J. Theor. Biol.* **255**, 404 (2008).
- [17] B. A. Grzybowski and W. T. Huck, *Nat. Nanotechnol.* **11**, 585 (2016).
- [18] A. Adamatzky, B. De Lacy Costello, and T. Asai, *Reaction-Diffusion Computers* (Elsevier, New York, 2005).
- [19] C. Jarzynski, *Annu. Rev. Condens. Matter Phys.* **2**, 329 (2011).
- [20] C. Van den Broeck and M. Esposito, *Physica (Amsterdam)* **418A**, 6 (2015).
- [21] G. Verley, M. Esposito, T. Willaert, and C. Van den Broeck, *Nat. Commun.* **5**, 4721 (2014).
- [22] U. Seifert, *Rep. Prog. Phys.* **75**, 126001 (2012).
- [23] J. M. R. Parrondo, J. M. Horowitz, and T. Sagawa, *Nat. Phys.* **11**, 131 (2015).
- [24] M. Polettini and M. Esposito, *J. Chem. Phys.* **141**, 024117 (2014).
- [25] M. Polettini, G. Bulnes-Cuetara, and M. Esposito, *Phys. Rev. E* **94**, 052117 (2016).
- [26] R. Rao and M. Esposito, *New J. Phys.* **20**, 023007 (2018).
- [27] P. Gaspard, *J. Chem. Phys.* **120**, 8898 (2004).
- [28] T. Tomé and M. J. de Oliveira, *Phys. Rev. Lett.* **108**, 020601 (2012).
- [29] Y. Zhang and A. C. Barato, *J. Stat. Mech.* (2016) 113207.
- [30] E. Crosato, R. E. Spinney, R. Nigmatullin, J. T. Lizier, and M. Prokopenko, *Phys. Rev. E* **97**, 012120 (2018).

[31] H. Vroylandt, M. Esposito, and G. Verley, *Europhys. Lett.* **120**, 30009 (2018).

[32] T. Herpich, J. Thingna, and M. Esposito, arXiv:1802.00461 [Phys. Rev. X (to be published)].

[33] R. Rao and M. Esposito, *Phys. Rev. X* **6**, 041064 (2016).

[34] S. R. de Groot and P. Mazur, *Non-Equilibrium Thermodynamics* (Dover, New York, 1984).

[35] D. Kondepudi and I. Prigogine, *Modern Thermodynamics: From Heat Engines to Dissipative Structures*, 2nd ed. (Wiley, New York, 2014).

[36] M. Esposito and C. Van den Broeck, *Europhys. Lett.* **95**, 40004 (2011).

[37] A. Ben-Naim, *A Farewell to Entropy: Statistical Thermodynamics Based on Information* (World Scientific Publishing Company, Singapore, 2008), Chap. 6.

[38] H. Serna, A. P. Muñozuri, and D. Barragán, *Phys. Chem. Chem. Phys.* **19**, 14401 (2017).

[39] H. S. Haraldsdóttir and R. M. T. Fleming, *PLoS Comput. Biol.* **12**, e1004999 (2016).

[40] See Supplemental Material at <http://link.aps.org/supplemental/10.1103/PhysRevLett.121.108301> for details on mathematical demonstrations.

[41] R. A. Alberti, *Thermodynamics of Biochemical Reactions* (Wiley-Interscience, New York, 2003).

[42] A. Turing, *Bull. Math. Biol.* **52**, 153 (1990).

[43] I. Prigogine and R. Lefever, *J. Chem. Phys.* **48**, 1695 (1968).

[44] B. Peña and C. Pérez-García, *Phys. Rev. E* **64**, 056213 (2001).

[45] M. Cross and H. Greenside, *Pattern Formation and Dynamics in Nonequilibrium Systems* (Cambridge University Press, Cambridge, England, 2009).

[46] I. S. Aranson and L. Kramer, *Rev. Mod. Phys.* **74**, 99 (2002).

[47] S. Kjelstrup and D. Bedeaux, *Non-Equilibrium Thermodynamics of Heterogeneous Systems*, Vol. 16, (World Scientific, Singapore, 2008).

[48] A. S. Zadorin, Y. Rondelez, J.-C. Galas, and A. Estevez-Torres, *Phys. Rev. Lett.* **114**, 068301 (2015).

[49] I. R. Epstein and B. Xu, *Nat. Nanotechnol.* **11**, 312 (2016).

[50] J. Halatek and E. Frey, *Nat. Phys.* **14**, 507 (2018).

[51] S. Ito and T. Sagawa, *Nat. Commun.* **6**, 7498 (2015).

[52] A. F. Taylor, M. R. Tinsley, F. Wang, Z. Huang, and K. Showalter, *Science* **323**, 614 (2009).

[53] G. Micali and R. G. Endres, *Curr. Opin. Microbiol.* **30**, 8 (2016).

Supplementary Material of “Information Thermodynamics of Turing Patterns”

Gianmaria Falasco, Riccardo Rao, and Massimiliano Esposito
*Complex Systems and Statistical Mechanics, Physics and Materials Science
Research Unit, University of Luxembourg, L-1511 Luxembourg, G.D. Luxembourg*
(Dated: August 27, 2018. Rev. b867f6e)

We here recall the basic ingredients underlying the dynamics and thermodynamics of reaction–diffusion systems (RDS). In the following sections, the algebraic details underlying our main results are explained.

The evolution in time of the concentration of each chemical species σ is ruled by a reaction–diffusion equation

$$\partial_t Z_\sigma(\mathbf{r}) = -\nabla \cdot \mathbf{J}_\sigma(\mathbf{r}) + \sum_\rho \mathbb{S}_\rho^\sigma j_\rho(\mathbf{r}) + I_\sigma(\mathbf{r}). \quad (1)$$

The diffusion currents (null at the boundaries of the system) follow from *Fick’s first law*

$$\mathbf{J}_\sigma(\mathbf{r}) = -D_\sigma \nabla Z_\sigma(\mathbf{r}), \quad (2)$$

whereas the reaction ones satisfy the mass-action kinetics

$$j_\rho(\mathbf{r}) = k_{+\rho} \prod_\sigma [Z_\sigma(\mathbf{r})]^{\nu_{+\rho}^\sigma} - k_{-\rho} \prod_\sigma [Z_\sigma(\mathbf{r})]^{\nu_{-\rho}^\sigma}. \quad (3)$$

The currents $I_\sigma(\mathbf{r})$ are non zero only for the chemostatted species y , and only at the points where the chemostats are located.

Enforcing the hypothesis of local equilibrium [1], we prescribe that each point in space is characterized by a well-defined Gibbs free energy density

$$g(\mathbf{r}) = \sum_\sigma [\mu_\sigma(\mathbf{r}) - RT] Z_\sigma(\mathbf{r}), \quad (4)$$

where the chemical potential of the species is that of a dilute ideal gas

$$\mu_\sigma(\mathbf{r}) = \mu_\sigma^\circ + RT \ln \{Z_\sigma(\mathbf{r})/Z_0\}. \quad (5)$$

As discussed in Refs. [2], the term proportional to the total concentration, $-RT \sum_\sigma Z_\sigma(\mathbf{r})$, is due to the solvent. Z_0 is the concentration of the solvent. Dynamics and thermodynamics are connected by the *local detailed balance*,

$$\frac{k_{+\rho}}{k_{-\rho}} = \prod_\sigma (Z_\sigma^{\text{eq}})^{\mathbb{S}_\rho^\sigma} = \exp \left\{ -\sum_\sigma [\mu_\sigma^\circ - RT \ln Z_0] \mathbb{S}_\rho^\sigma \right\}, \quad (6)$$

which relates the ratio of forward and backward reaction rates to the difference of *standard-state* chemical potentials, μ_σ° . Since Z_0 is constant, the term $-RT \ln Z_0$ is absorbed in μ_σ° in the main text. Integrating Eq. (4) over all volume \mathcal{V} , we obtain the Gibbs free energy of RDS,

$$G = \int_{\mathcal{V}} d\mathbf{r} [\mu_\sigma(\mathbf{r}) Z_\sigma(\mathbf{r}) - RT \sum_\sigma Z_\sigma(\mathbf{r})]. \quad (7)$$

We finally recall that the forces which act on RDS are related to either spatial gradients of concentrations

$$\mathbf{F}_\sigma(\mathbf{r}) := -\nabla \mu_\sigma(\mathbf{r}), \quad (8)$$

or to chemical reactions

$$\mathbf{f}_\rho(\mathbf{r}) := -\sum_\sigma \mu_\sigma(\mathbf{r}) \mathbb{S}_\rho^\sigma. \quad (9)$$

These forces are called *affinities* and they vanish only at thermodynamic equilibrium: for each point of space \mathbf{r} , $\mathbf{J}_\sigma(\mathbf{r}) = \mathbf{0}$ for all σ and $j_\rho(\mathbf{r}) = 0$ for all ρ .

DYNAMICS AND THERMODYNAMICS OF CLOSED RDS

We now discuss the minimization of the Gibbs free energy as closed RDS relax to equilibrium, and show how this minimization is related to the entropy production rate (EPR).

In closed CNs $I_\sigma(\mathbf{r}) = 0$ for all σ , namely there is no exchange of matter with the chemostats. We also assume that closed RDS always relax to thermodynamic equilibrium. At equilibrium, Z_σ^{eq} must be homogeneous, i.e. $\nabla Z_\sigma^{\text{eq}} = 0$ for all σ , as a consequence of $\mathbf{F}_\sigma^{\text{eq}} = 0$ for all σ . All affinities related to chemical reactions must also vanish

$$f_\rho^{\text{eq}} = \sum_\sigma \mu_\sigma^{\text{eq}} \mathbb{S}_\rho^\sigma = 0, \quad \text{for all } \rho, \quad (10)$$

which implies that the chemical potentials can be written as a linear combination of conservation laws

$$\mu_\sigma^{\text{eq}} = \sum_\lambda \psi_\lambda \ell_\sigma^\lambda. \quad (11)$$

The conservation laws are left null vectors of the stoichiometric matrix \mathbb{S} . They identify components, $L_\lambda(\mathbf{r}) := \sum_\sigma \ell_\sigma^\lambda Z_\sigma(\mathbf{r})$, namely global conserved quantities in closed RDS. Indeed,

$$d_t \int_V d\mathbf{r} L_\lambda(\mathbf{r}) = \int_V d\mathbf{r} \sum_\sigma \ell_\sigma^\lambda d_t Z_\sigma(\mathbf{r}) = \int_V d\mathbf{r} \sum_\sigma \ell_\sigma^\lambda \left[-\nabla \cdot \mathbf{J}_\sigma(\mathbf{r}) + \sum_\rho \mathbb{S}_\rho^\sigma j_\rho(\mathbf{r}) \right] = 0, \quad (12)$$

where the first term vanish because $\mathbf{J}_\sigma(\mathbf{r})$ vanishes at the boundaries, whereas the second one because of the definition of ℓ_σ^λ .

We can now show that the Gibbs free energy can be expressed in terms of a relative entropy for non-normalized concentrations distribution, i.e. Eq. (4) of the main text. We first observe that the difference between G of a generic state $Z_\sigma(\mathbf{r})$ and that of a reference homogeneous state, Z_σ^h , can be written as

$$G - G^h = \int_V d\mathbf{r} \sum_\sigma [(\mu_\sigma(\mathbf{r}) - \mu_\sigma^h) Z_\sigma(\mathbf{r}) - RT(Z_\sigma(\mathbf{r}) - Z_\sigma^h)] + \sum_\sigma \mu_\sigma^h \int_V d\mathbf{r} [Z_\sigma(\mathbf{r}) - Z_\sigma^h]. \quad (13)$$

We now notice that using the definition of chemical potential, Eq. (5), the first term on the rhs can be recast into (up to a global factor equal to RT)

$$\mathcal{L}(Z_\sigma \| Z_\sigma^h) := \int_V d\mathbf{r} \sum_\sigma \left\{ Z_\sigma(\mathbf{r}) \ln \frac{Z_\sigma(\mathbf{r})}{Z_\sigma^h} - [Z_\sigma(\mathbf{r}) - Z_\sigma^h] \right\} \geq 0, \quad (14)$$

which is akin to a relative entropy for non-normalized distributions. It is indeed always non-negative and vanish only when $Z_\sigma = Z_\sigma^h$. The second term in Eq. (13) is in general different from zero, but when the homogeneous reference state is the equilibrium one, $Z_\sigma^h = Z_\sigma^{\text{eq}}$, then it vanishes. The latter fact is due to the properties of equilibrium chemical potentials, Eq. (11), and the properties of conservation laws, Eq. (12). Therefore,

$$G - G^h = RT \mathcal{L}(Z_\sigma \| Z_\sigma^h) + \sum_\sigma \mu_\sigma^h \int_V d\mathbf{r} [Z_\sigma(\mathbf{r}) - Z_\sigma^h] \quad (15)$$

holds in general, but when the equilibrium state is chosen as a reference, one has

$$G - G_{\text{eq}} = RT \mathcal{L}(Z_\sigma \| Z_\sigma^{\text{eq}}) \geq 0. \quad (16)$$

Crucially, the last equation tells us that G takes its minimum value at equilibrium, where it becomes

$$G_{\text{eq}} = \sum_\lambda \psi_\lambda L_\lambda - RT V \sum_\sigma Z_\sigma^{\text{eq}}. \quad (17)$$

We now relate the changes of G to the EPR when the RDS relaxes to equilibrium. By taking the time derivative of the Gibbs free energy (7), we obtain

$$d_t G = \int_V d\mathbf{r} \sum_\sigma \mu_\sigma(\mathbf{r}) \left\{ -\nabla \cdot \mathbf{J}_\sigma(\mathbf{r}) + \sum_\rho \mathbb{S}_\rho^\sigma j_\rho(\mathbf{r}) \right\}. \quad (18)$$

Notice that the first term in curly brackets can be written as

$$-\int_V d\mathbf{r} \sum_\sigma \mu_\sigma(\mathbf{r}) \nabla \cdot \mathbf{J}_\sigma(\mathbf{r}) = \int_V d\mathbf{r} \sum_\sigma \{-\nabla \cdot [\mathbf{J}_\sigma(\mathbf{r}) \mu_\sigma(\mathbf{r})] + \mathbf{J}_\sigma(\mathbf{r}) \cdot \nabla \mu_\sigma(\mathbf{r})\}. \quad (19)$$

The divergence theorem, together with the fact that the currents vanish at the boundaries, implies that the first term on the rhs vanishes. The second term, instead, is minus the EPR due to diffusion

$$T\dot{\Sigma}_{\text{dff}} := \int_{\mathcal{V}} d\mathbf{r} \sum_{\sigma} \mathbf{J}_{\sigma}(\mathbf{r}) \cdot \mathbf{F}_{\sigma}(\mathbf{r}) = RT \int_{\mathcal{V}} d\mathbf{r} \sum_{\sigma} D_{\sigma} \frac{\|\nabla Z_{\sigma}(\mathbf{r})\|^2}{Z_{\sigma}(\mathbf{r})} \geq 0, \quad (20)$$

where we used the definition of diffusion affinity given in Eq. (8).

The second term in curly brackets of Eq. (18) is easily recognized as minus the EPR due to the reactions

$$T\dot{\Sigma}_{\text{rct}} := \int_{\mathcal{V}} d\mathbf{r} \sum_{\rho} j_{\rho}(\mathbf{r}) f_{\rho}(\mathbf{r}) = RT \int_{\mathcal{V}} d\mathbf{r} \sum_{\rho} j_{\rho}(\mathbf{r}) \ln \frac{j_{+\rho}(\mathbf{r})}{j_{-\rho}(\mathbf{r})} \geq 0, \quad (21)$$

where we used the definition of reaction affinity given in Eq. (9). The last equality in Eq. (21) is sometimes called *reaction isotherm* or *flux-force relation* and follows from the assumption of elementary reactions (mass-action kinetics) and the local detailed balance, Eq. (6). We can thus conclude that

$$d_t G = -T\dot{\Sigma}_{\text{dff}} - T\dot{\Sigma}_{\text{rct}} \equiv -T\dot{\Sigma} \leq 0, \quad (22)$$

which, together with Eq. (16), also demonstrates that G is a Lyapunov function in closed RDS.

DYNAMICS AND THERMODYNAMICS OF OPEN RDS

Open RDS are characterized by nonvanishing currents $I_{\sigma}(\mathbf{r})$ for the species y which are chemostatted. As a consequence, the time derivative of the Gibbs free energy reads

$$d_t G = \dot{W}_{\text{chem}} - T\dot{\Sigma}, \quad (23)$$

where

$$W_{\text{chem}} = \int_{\mathcal{V}} d\mathbf{r} \sum_y \mu_y(\mathbf{r}) I_y(\mathbf{r}), \quad (24)$$

is the chemical work, namely the free energy exchanged with the chemostats. Crucially, even if the open RDS is prepared in such a way to relax to an equilibrium concentration distribution (more about these conditions will be given later), G is not minimized anymore. The reason is that G_{eq} depends on all conservation laws, Eq. (17), but in open RDS some conservation laws are broken. Broken conservation laws, labeled by λ_b , are those minimal subset of conservation laws such that $\sum_x \ell_x^{\lambda_b} \mathbb{S}_{\rho}^x \neq 0$ for at least one ρ . As a consequence, the related components change due to the exchange of chemostatted species with the environment

$$d_t \int_{\mathcal{V}} d\mathbf{r} L_{\lambda_b}(\mathbf{r}) = \sum_y \ell_y^{\lambda_b} \int_{\mathcal{V}} d\mathbf{r} I_y(\mathbf{r}) \neq 0. \quad (25)$$

The subset of conservation laws which are not broken by the exchange of mass are labeled by λ_u . They are characterized by the fact that $\sum_x \ell_x^{\lambda_u} \mathbb{S}_{\rho}^x = 0$ for all ρ , and as a consequence $d_t \int_{\mathcal{V}} d\mathbf{r} L_{\lambda_u}(\mathbf{r}) = 0$.

In order to find the potential which is minimized at equilibrium in open RDS, we need an expression for the EPR which, in contrast to Eq. (23), accounts for the broken conservation laws.

EPR Decomposition

We will now derive Eq. (12) of the main text, namely an EPR decomposition which accounts for those RDS-specific topological properties encoded in conservation laws.

We start by partitioning the set of chemostatted species y into two disjoint groups, to which belong species denoted y_p and y_f . The first group is composed by a minimal set of chemostats that break all broken conservation laws when starting from the closed CN. Clearly, the number of species y_p equals that of λ_b . All other chemostatted species fall into the second group. From the fact that the set of conservation laws is linearly independent, it follows that the matrix whose entries are $\ell_{y_p}^{\lambda_b}$ is square and nonsingular. The entries of the inverse matrix are denoted by $\ell_{\lambda_b}^{y_p-1}$.

We now observe that this partitioning allows us to recast Eq. (25) as

$$d_t M_{y_p} = \int_{\mathcal{V}} d\mathbf{r} I_{y_p}(\mathbf{r}) + \sum_{\lambda_b} \ell_{\lambda_b}^{y_p-1} \sum_{y_f} \ell_{y_f}^{\lambda_b} \int_{\mathcal{V}} d\mathbf{r} I_{y_f}(\mathbf{r}), \quad (26)$$

where

$$M_{y_p} := \sum_{\lambda_b} \ell_{\lambda_b}^{y_p-1} \int_{\mathcal{V}} d\mathbf{r} L_{\lambda_b}(\mathbf{r}), \quad (27)$$

are defined as the moiety concentrations.

At this point we choose some reference values $\mu_{y_p}^{\text{ref}}$ for the chemical potentials of the species y_p . These can be chosen arbitrarily among the values of $\mu_{y_p}(\mathbf{r})$ where $Z_{y_p}(\mathbf{r})$ are controlled by the chemostats. With this prescription, we can rewrite Eq. (26) as

$$\mu_{y_p}^{\text{ref}} d_t M_{y_p} = d_t \left[\mu_{y_p}^{\text{ref}} M_{y_p} \right] + d_t \mu_{y_p}^{\text{ref}} M_{y_p} = \mu_{y_p}^{\text{ref}} \int_{\mathcal{V}} d\mathbf{r} I_{y_p}(\mathbf{r}) + \mu_{y_p}^{\text{ref}} \sum_{\lambda_b} \ell_{\lambda_b}^{y_p-1} \sum_{y_f} \ell_{y_f}^{\lambda_b} \int_{\mathcal{V}} d\mathbf{r} I_{y_f}(\mathbf{r}). \quad (28)$$

When inserting the above identity in the definition of chemical work, Eq. (24), we obtain

$$\dot{W}_{\text{chem}} = d_t \left[\sum_{y_p} \mu_{y_p}^{\text{ref}} M_{y_p} \right] - \sum_{y_p} d_t \mu_{y_p}^{\text{ref}} M_{y_p} + \sum_y \int_{\mathcal{V}} d\mathbf{r} I_y(\mathbf{r}) \mathcal{F}_y(\mathbf{r}), \quad (29)$$

where the fundamental chemical forces are defined as

$$\mathcal{F}_y(\mathbf{r}) := \mu_y(\mathbf{r}) - \sum_{y_p} \mu_{y_p}^{\text{ref}} \sum_{\lambda_b} \ell_{\lambda_b}^{y_p-1} \ell_y^{\lambda_b}. \quad (30)$$

Overall, the EP can be written as

$$T \dot{\Sigma} = \dot{W}_{\text{driv}} + \dot{W}_{\text{nc}} - d_t \mathcal{G} \quad (31)$$

(Eq. (12) in the main text) where

$$\dot{W}_{\text{driv}} = - \sum_{y_p} d_t \mu_{y_p}^{\text{ref}} M_{y_p} \quad (32)$$

is defined as the driving work rate,

$$\dot{W}_{\text{nc}} = \sum_y \int_{\mathcal{V}} d\mathbf{r} I_y(\mathbf{r}) \mathcal{F}_y(\mathbf{r}) \quad (33)$$

as the nonconservative chemical work, and finally

$$\mathcal{G} = G - \sum_{y_p} \mu_{y_p}^{\text{ref}} M_{y_p} \quad (34)$$

is the semigrand Gibbs free energy. These three terms reflect the three fundamental forms of dissipation occurring in RDS. \dot{W}_{driv} involves the time derivative of $\mu_{y_p}^{\text{ref}}$, hence it accounts for external manipulation via time-dependently driven chemostats and vanishes for autonomous RDS. \dot{W}_{nc} is the sum of a minimal number of current-force terms. It describes the thermodynamic cost of sustaining currents of chemicals across the system and vanishes in detailed-balanced RDS, see next section. Finally, $-d_t \mathcal{G}$ is the conservative contribution which quantifies the dissipation during transient dynamics and vanishes at steady states.

We now briefly linger on the definition of fundamental force, Eq. (30). For the chemostatted species y_p , the forces read $\mathcal{F}_{y_p}(\mathbf{r}) = \mu_{y_p}(\mathbf{r}) - \mu_{y_p}^{\text{ref}}$. Therefore, they simply accounts for differences of chemical potential of the same species in different points of the boundaries. They originate steady currents of chemicals across the RDS which not necessarily involve reactions. In contrast, $\mathcal{F}_{y_f}(\mathbf{r}) = \mu_{y_f}(\mathbf{r}) - \sum_{y_p} \mu_{y_p}^{\text{ref}} \sum_{\lambda_b} \ell_{\lambda_b}^{y_p-1} \ell_{y_f}^{\lambda_b}$ also accounts for chemical potential differences of different species which are coupled by reactions. Therefore, they originate steady currents of chemicals which involve reactions.

Open Detailed-Balanced RDS

Open detailed-balanced RDS can relax to equilibrium despite the fact that they exchange matter with the environment. As we now show, this happens when all fundamental forces vanishing and the time-dependent driving is stopped.

Let us assume that the open RDS relaxes to equilibrium. From Eq. (11), it follows that

$$\sum_{\lambda_b} \psi_{\lambda_b} \ell_{y_p}^{\lambda_b} = \mu_{y_p}^{\text{ref}}, \quad (35)$$

where we have used the fact that $\ell_{y_p}^{\lambda_u} = 0$, for all λ_u , by definition of unbroken conservation law. In words, Eq. (35) tells us that the equilibrium distribution must be shaped by the reference chemical potentials. We can thus rewrite the semigrand Gibbs potential as

$$\mathcal{G} = G - \sum_{\lambda_b} \psi_{\lambda_b} \int_{\mathcal{V}} d\mathbf{r} L_{\lambda_b}(\mathbf{r}), \quad (36)$$

whose expression is reminiscent of a Legendre transform of G with respect to the broken components. Using the equilibrium expression of G , Eq. (17), one can write the equilibrium semigrand potential as

$$\mathcal{G}_{\text{eq}} = \sum_{\lambda_u} \psi_{\lambda_u} \int_{\mathcal{V}} d\mathbf{r} L_{\lambda_u}(\mathbf{r}) - RT\mathcal{V} \sum_{\sigma} Z_{\sigma}^{\text{eq}}. \quad (37)$$

We thus readily get that

$$\mathcal{G} - \mathcal{G}_{\text{eq}} = G - \sum_{\lambda} \psi_{\lambda} \int_{\mathcal{V}} d\mathbf{r} L_{\lambda}(\mathbf{r}) - RT\mathcal{V} \sum_{\sigma} Z_{\sigma}^{\text{eq}} = RT\mathcal{L}(Z_{\sigma} \| Z_{\sigma}^{\text{eq}}) \geq 0. \quad (38)$$

holds far from equilibrium.

Equation (38) tells us that \mathcal{G} takes its minimum value at the equilibrium distribution identified by the reference chemical potentials, Eq. (35). However, \mathcal{G} may not be effectively minimized by the dynamics, namely $d_t \mathcal{G} \not\leq 0$. This happens only when all fundamental forces vanish and the time-dependent driving is stopped. Then, Eq. (31) becomes

$$d_t \mathcal{G} = -T \dot{\Sigma} \leq 0, \quad (39)$$

which, in combination with Eq. (38), demonstrates the role of \mathcal{G} as a Lyapunov function in open detailed-balanced RDS.

Some comments are in order regarding the requirements that all fundamental forces vanish. First, $\mathcal{F}_{y_p}^* = 0$ if and only if $\mu_{y_p}^*(\mathbf{r}) = \mu_{y_p}^{\text{ref}}$ wherever exchange with the chemostats is allowed. Physically, this means that there cannot develop steady diffusion currents of y_p due to gradients of $\mu_{y_p}(\mathbf{r})$ imposed by the chemostats. Second, $\mathcal{F}_{y_f}^* = 0$ if and only if the chemical potentials of y_f at the points where exchange is allowed are constant and equal to

$$\mu_{y_f}^*(\mathbf{r}) = \sum_{y_p} \mu_{y_p}^{\text{ref}} \sum_{\lambda_b} \ell_{\lambda_b}^{y_p} \ell_{y_f}^{\lambda_b}. \quad (40)$$

Hence, steady diffusion currents of y_f and steady currents of chemical reactions across the RDS are prevented.

Nonequilibrium Landauer's Principle

In absolute generality, Eqs. (31) and (38) can be combined in the form

$$\dot{W}_{\text{nc}} + \dot{W}_{\text{driv}} - d_t \mathcal{G}_{\text{eq}} = RT d_t \mathcal{L}(Z_{\sigma} \| Z_{\sigma}^{\text{eq}}) + T \dot{\Sigma}. \quad (41)$$

where Z_{σ}^{eq} must be understood as the equilibrium concentration distribution identified by $\mu_{y_p}^{\text{ref}}$, Eq. (35). Clearly, the latter distribution is achieved when stopping the driving and turning off the fundamental forces, so that Eq. (39) is recovered. When integrating over time between two arbitrary nonequilibrium concentration distributions we obtain

$$W_{\text{nc}} + W_{\text{driv}} - \Delta \mathcal{G}_{\text{eq}} = RT \Delta \mathcal{L}(Z_{\sigma} \| Z_{\sigma}^{\text{eq}}) + T \Sigma. \quad (42)$$

(Eq. (14) in the main text). The positivity of the EP thus bounds the overall work, $W_{\text{nc}} + W_{\text{driv}} - \Delta \mathcal{G}_{\text{eq}}$, to be greater than the difference of relative entropies, which measure the distance from equilibrium of the initial and final distribution.

Homogeneous Chemostatted Species Limit

We now discuss the case of homogeneous chemostatting used in the second part our Letter. It can be seen as the limit of fast-diffusing chemostatted species. In this limit $\mathbf{J}_y(\mathbf{r}) = 0$, or equivalently $\nabla\mu_y = 0$, for time scales comparable to those of reactions. Therefore, the reaction–diffusion equation for the concentrations of chemostatted species become balance equations of the form

$$dt Z_y = \sum_{\rho} \mathbb{S}_{\rho}^y j_{\rho}(\mathbf{r}) + I_y(\mathbf{r}), \quad (43)$$

with external currents in general different from zero everywhere in the vessel. In this limit, the chemical work (24) becomes

$$\dot{W}_{\text{chem}} = \sum_y \mu_y \int_{\mathcal{V}} d\mathbf{r} I_y(\mathbf{r}). \quad (44)$$

One can as well determine the EPR decomposition (31) in this limit. First, one has that $\mu_{y_p} = \mu_{y_p}^{\text{ref}}$ for all \mathbf{r} . Hence, the expressions of semigrand Gibbs free energy and driving work reads identical as in Eqs. (34) and (32). Instead, there cannot be fundamental forces $\mathcal{F}_{y_p} = 0$ due to differences of chemical potentials of y_p . The other fundamental forces are instead homogeneous, and can be expressed as

$$\mathcal{F}_{y_f} := \mu_{y_f} - \sum_{y_p} \mu_{y_p} \sum_{\lambda_b} \ell_{\lambda_b}^{y_p} \ell_{y_f}^{\lambda_b}, \quad (45)$$

so that the related nonconservative contributions read $\dot{W}_{\text{nc}} = \mathcal{F}_{y_f} \int_{\mathcal{V}} d\mathbf{r} I_{y_f}(\mathbf{r})$.

BRUSSELATOR MODEL

We study the Brusselator model as an open CN constituted of two dynamical species X_1, X_2 and four homogeneously chemostatted species Y_1, \dots, Y_4 . Their concentrations are denoted by $x_1(r, t), x_2(r, t)$ and y_1, \dots, y_4 , respectively. The chemical equations governing the CN are depicted in the upper left corner of Fig. 2 in the main text. Their main feature is the autocatalytic reaction $\rho = 3$ that is responsible of the nonlinear effects at the basis of patter formation. The stoichiometric matrix of the closed CN

$$\mathbb{S}_{\rho}^{\sigma} = \begin{pmatrix} 1 & -1 & 1 & -1 \\ 0 & 1 & -1 & 0 \\ -1 & 0 & 0 & 0 \\ 0 & -1 & 0 & 0 \\ 0 & 1 & 0 & 0 \\ 0 & 0 & 0 & 1 \end{pmatrix} \quad (46)$$

possesses two conservation laws $\ell_{\sigma}^1 = (1 1 1 0 0 1)$ and $\ell_{\sigma}^2 = (0 0 0 1 1 0)$ that are both broken by chemostatting. The species Y_1 and Y_2 are chosen to be the reference chemostats y_p . Other choices do not change qualitatively our results.

The reaction-diffusion equations for the Brusselator model in one spatial dimension $[0, \ell] \ni r$ read, in vector form,

$$\partial_t \begin{pmatrix} x_1 \\ x_2 \end{pmatrix} = \begin{pmatrix} k_1 y_1 - k_{-1} x_1 - k_2 y_2 x_1 + k_{-2} y_3 x_2 + k_3 x_1^2 x_2 - k_{-3} x_1^3 - k_4 x_1 + k_{-4} y_4 + D_{x_1} \partial_r^2 x_1 \\ k_2 y_2 x_1 - k_{-2} y_3 x_2 - k_3 x_1^2 x_2 + k_{-3} x_1^3 + D_{x_2} \partial_r^2 x_2 \end{pmatrix} := \mathcal{J}(x_1, x_2). \quad (47)$$

Setting all partial derivatives to zero in Eq. (47), one finds the unique stationary homogeneous solution

$$(x_1^h, x_2^h)^T = \left(\frac{k_1 y_1 + k_{-4} y_4}{k_{-1} + k_4}, \frac{(k_2 y_2 + k_3 x_1^h) x_1^h}{k_{-2} y_3 + k_3 x_1^h} \right)^T. \quad (48)$$

Its linear stability against small perturbations is analyzed by applying to (47) a Fourier transform $x(q, t) := \int d\mathbf{r} x(r, t) e^{iqr}$ and considering its Jacobian matrix evaluated in the homogeneous state $(x_1^h, x_2^h)^T$:

$$\partial_x \mathcal{J}(x_1^h, x_2^h) = \begin{pmatrix} -(k_{-1} + k_4) - k_2 y_2 - 3k_{-3} x_1^{h2} - D_{x_1} q^2 & k_{-2} y_3 + k_3 x_1^{h2} \\ k_2 y_2 - 2k_3 x_1^h x_2^h + 3k_{-3} x_1^{h2} & -k_{-2} y_3 - k_3 x_1^{h2} - D_{x_2} q^2 \end{pmatrix}. \quad (49)$$

The eigenvalues $\lambda_{\pm}(q)$ of (49) are most easily expressed by means of the Jacobian's trace and determinant:

$$\mathcal{T}(q) := \text{Tr}\{\partial_x \mathcal{J}(x_1^h, x_2^h)\}, \quad \mathcal{D}(q) := \text{Det}\{\partial_x \mathcal{J}(x_1^h, x_2^h)\}, \quad \lambda_{\pm}(q) = \frac{1}{2} \left[\mathcal{T}(q) \pm \sqrt{\mathcal{T}^2(q) - 4\mathcal{D}(q)} \right]. \quad (50)$$

The homogeneous solution is stable if both eigenvalues are negative, while it is unstable if at least one eigenvalue is positive. The Turing mechanism requires the homogeneous state to be stable in the absence of diffusion, i.e. $\lambda_{\pm}(0) \leq 0$, and to turn unstable for some finite value of q . In view of (50), these two conditions correspond to, respectively,

$$\mathcal{T}(0) < 0 \text{ and } \mathcal{D}(0) > 0, \quad \mathcal{D}(q) \leq 0 \text{ for some } q. \quad (51)$$

Since \mathcal{D} is an upward parabola in q^2 , the critical wavelength q_c of the Turing pattern is determined by looking for the value of q which first makes \mathcal{D} negative:

$$\frac{1}{2q} \frac{\partial \mathcal{D}}{\partial q} \Big|_{q=q_c} = 0, \text{ i.e. } q_c = \sqrt{\frac{D_{x_1}(k_3 x_1^{h^2} - k_{-2} y_3) + D_{x_2}(2k_3 x_1^h x_2^h - k_2 y_2 - k_4 - 3k_{-3} x_1^{h^2} - k_{-1})}{2D_{x_1} D_{x_2}}}. \quad (52)$$

The critical value of the chemostat concentration y_2^c is fixed by setting $\mathcal{D}(q_c) = 0$, which corresponds to the condition of marginal stability of the homogeneous state, i.e. $\lambda_+(q_c) = 0$. We call $(1, u_{x_2})^T$ the corresponding eigenvector.

The above linear stability analysis suggests that sufficiently close to the threshold value y_2^c the concentrations are well described by

$$\begin{pmatrix} x_1(r, t) \\ x_2(r, t) \end{pmatrix} = \begin{pmatrix} \bar{x}_1(t) \\ \bar{x}_2(t) \end{pmatrix} + \begin{pmatrix} 1 \\ u_{x_2} \end{pmatrix} (A(r, t) e^{iq_c r} + c.c.), \quad (53)$$

with $A(r, t)$ following the so-called amplitude equation

$$\tau \partial_t A = \epsilon A - \alpha |A|^2 A + \xi \partial_r^2 A. \quad (54)$$

The latter can be derived by a multiple scale expansion based on the replacements $\partial_r \rightarrow \partial_r + \sqrt{\epsilon} \partial_r$ and $\partial_t \rightarrow \epsilon \partial_t$ together with the expansion of $(x_1, x_2)^T$ in powers of the small reduced parameter $\sqrt{\epsilon} := \sqrt{(y_2 - y_2^c)/y_2^c}$ [3]. This formalizes the intuitive idea that the amplitude $A(r, t)$ describes slow modulations of the pattern around its leading critical mode. Thus, it changes sizeably only over long distances $r' = \sqrt{\epsilon} r$ and large times $t' = \epsilon t$, related by the diffusive scaling $x'^2 \sim t'$. Truncating the expansion at lowest order gives (54), whose effective coefficients are expressible in closed form if the backward reactions are neglected [4]:

$$\tau := \frac{1 + \epsilon y_1}{1 - \epsilon^2}, \quad \eta := \frac{D_{x_1}}{D_{x_2}}, \quad \alpha := \frac{-8 + 38y_1\eta + 5y_1^2\eta^2 - 8y_1^3\eta^3}{9y_1^3\eta(1 + y_1\eta)}, \quad \xi := \frac{2}{1 + y_1\eta}. \quad (55)$$

Hence, hereafter we focus on the weakly reversible case $k_{+\rho} = 1 \gg k_{-\rho} = 10^{-4}$, and to obtain analytic results we approximate $k_{-\rho} = 0$ as far as purely dynamical expressions are concerned. From here on, we also make use of the no-flux boundary conditions of Eq. (47): they restrict the spectrum of Fourier modes $x(q, t) \sim \cos(qr)$, and impose that the critical wavenumber q_c is a multiple of $2\pi/\ell$.

First, we look for an analytic solution of the amplitude equation (54). Very close to the critical point inhomogeneous solutions of (54) may be just small modulations with wavelength close to q_c . Though, such solutions do not conform with the no-flux conditions at the boundaries $r = \{0, \ell\}$ and thus must be excluded. Therefore, (54) admits only a real-valued homogeneous solution

$$A(t) = \sqrt{\frac{\epsilon}{\alpha - \exp[-\frac{2\epsilon}{\tau}(t - t_0)]}}, \quad (56)$$

that for long times relaxes to the pattern maximum amplitude $\sqrt{\epsilon/\alpha}$. Second, we focus on the space-averaged concentrations. Integrating Eqs. (47) over space and adding them up we obtain,

$$d_t \bar{x}_1 + d_t \bar{x}_2 = y_1 - \bar{x}_1, \quad (57)$$

which shows that \bar{x}_1 attains the same value in the homogeneous and patterned stationary state, i.e. $\bar{x}_1^h = \bar{x}_1^p = y_1$. In fact, the numerical solution of (47) shows that $\bar{x}_1(t)$ varies very little during the formation of the pattern (e.g. a

relative variation smaller than 10^{-4} is observed at $\epsilon = 0.05$) so that the approximation $\bar{x}_1(t) \simeq y_1$ is legitimate at all times. Then, an approximate solution for $\bar{x}_2(t)$ is found by using (56) together with (53), namely,

$$\begin{pmatrix} x_1(r, t) \\ x_2(r, t) \end{pmatrix} = \begin{pmatrix} y_1 \\ \bar{x}_2(t) \end{pmatrix} + \begin{pmatrix} 1 \\ u_{x_2} \end{pmatrix} 2A(t) \cos(q_c r), \quad (58)$$

plugging it into (47) and averaging over space. We arrive at

$$d_t \bar{x}_2 = y_1 y_2 - \overline{x_1^2 x_2} = y_1 y_2 - 4A^2(t) u_{x_2} - (y_1^2 + 2A^2(t) u_{x_2}) \bar{x}_2, \quad (59)$$

whose solution

$$\bar{x}_2(t) = \frac{1}{\gamma(t)} \left[y_2 + y_1 \int_{t_0}^t dt' \gamma(t') (y_2 - 4A^2(t') u_{x_2}) \right] \quad \text{with} \quad \gamma(t) = e^{y_1^2 t} \left[\frac{\frac{\alpha}{\tau} + \exp(-2\frac{\epsilon}{\tau}(t - t_0))}{\frac{\alpha}{\tau} + \exp(-2\frac{\epsilon}{\tau}t_0)} \right]^{\frac{\tau}{\alpha}} \quad (60)$$

can be given explicitly in terms of hypergeometric functions (being cumbersome we avoid to present it here). The dynamics of the pattern formation is thus fully characterized for $\epsilon \ll 1$. The long time solution (58) and (60), i.e.

$$\begin{pmatrix} x_1^p(r) \\ x_2^p(r) \end{pmatrix} = \begin{pmatrix} y_1 \\ \bar{x}_2^p \end{pmatrix} + \begin{pmatrix} 1 \\ u_{x_2} \end{pmatrix} \sqrt{\frac{\epsilon}{\alpha}} 2 \cos(q_c r), \quad (61)$$

is employed to evaluate the Gibbs free energy and the EPR of the pattern.

[1] D. Kondepudi and I. Prigogine, *Modern Thermodynamics: From Heat Engines to Dissipative Structures*, 2nd ed. (Wiley, 2014).
[2] E. Fermi, *Thermodynamics* (Dover, 1956).
[3] M. Cross and H. Greenside, *Pattern formation and dynamics in nonequilibrium systems* (Cambridge University Press, 2009).
[4] B. Peña and C. Pérez-García, *Phys. Rev. E* **64**, 056213 (2001).

The following article is reprinted from
[A. WACHTEL, R. RAO and M. ESPOSITO, *New J. Phys.* **20**.4 (2018), 042002]
under the conditions of the Creative Commons Attribution 3.0 Unported
Licence².

The page numbers placed in the outer margins provide a continuous pagination throughout the thesis.

² <https://creativecommons.org/licenses/by/3.0/>

New Journal of Physics

The open access journal at the forefront of physics

Deutsche Physikalische Gesellschaft 

IOP Institute of Physics

Published in partnership
with: Deutsche Physikalische
Gesellschaft and the Institute
of Physics



OPEN ACCESS

RECEIVED
23 November 2017

REVISED
22 February 2018

ACCEPTED FOR PUBLICATION
12 March 2018

PUBLISHED
12 April 2018

FAST TRACK COMMUNICATION

Thermodynamically consistent coarse graining of biocatalysts beyond Michaelis–Menten

Artur Wachtel , Riccardo Rao  and Massimiliano Esposito 

Complex Systems and Statistical Mechanics, Physics and Materials Science Research Unit, University of Luxembourg, 162a, Avenue de la Faïencerie, 1511 Luxembourg, Luxembourg

E-mail: artur.wachtel@uni.lu

Keywords: coarse graining, biochemical reaction networks, thermodynamics, enzyme kinetics

Original content from this work may be used under the terms of the [Creative Commons Attribution 3.0 licence](#).

Any further distribution of this work must maintain attribution to the author(s) and the title of the work, journal citation and DOI.



Abstract

Starting from the detailed catalytic mechanism of a biocatalyst we provide a coarse-graining procedure which, by construction, is thermodynamically consistent. This procedure provides stoichiometries, reaction fluxes (rate laws), and reaction forces (Gibbs energies of reaction) for the coarse-grained level. It can treat active transporters and molecular machines, and thus extends the applicability of ideas that originated in enzyme kinetics. Our results lay the foundations for systematic studies of the thermodynamics of large-scale biochemical reaction networks. Moreover, we identify the conditions under which a relation between one-way fluxes and forces holds at the coarse-grained level as it holds at the detailed level. In doing so, we clarify the speculations and broad claims made in the literature about such a general flux–force relation. As a further consequence we show that, in contrast to common belief, the second law of thermodynamics does not require the currents and the forces of biochemical reaction networks to be always aligned.

1. Introduction

Catalytic processes are ubiquitous in cellular physiology. Biocatalysts are involved in metabolism, cell signaling, transcription and translation of genetic information, as well as replication. All these processes and pathways involve not only a few but rather dozens to hundreds, sometimes thousands of different enzymes. Finding the actual catalytic mechanism of a single enzyme is difficult and time consuming work. To date, for many enzymes the catalytic mechanisms are not known. Even if such detailed information was at hand, including detailed catalytic mechanisms into a large scale model is typically unfeasable for numerical simulations. Therefore, larger biochemical reaction networks contain the enzymes as single reactions following enzymatic kinetics. This simplified description captures only the essential dynamical features of the catalytic action, condensed into a single reaction.

The history of enzyme kinetics [1] stretches back more than a hundred years. After the pioneering work of Brown [2] and Henri [3], Michaelis and Menten [4] laid the foundation for the systematic coarse graining of a detailed enzymatic mechanism into a single reaction. Since then, a lot of different types of mechanisms have been found and systematically classified [5]. Arguably, the most important catalysts in biochemical processes are enzymes—which are catalytically active proteins. However, other types of catalytic molecules are also known, some of them occur naturally like catalytic RNA (ribozymes) or catalytic anti-bodies (abzymes), some of them are synthetic (synzymes) [5]. For our purposes it does not matter which kind of biocatalyst is being described by a catalytic mechanism—we treat all of the above in the same way.

From a more general perspective, other scientific fields are concerned with the question of how to properly coarse grain a process as well. While in most applications the focus lies on the dynamics, or kinetics, of a process, it turned out that thermodynamics plays an intricate role in this question [6]. For processes occurring at thermodynamic equilibrium, every choice of coarse graining can be made thermodynamically consistent—after all, the very foundation of equilibrium thermodynamics is concerned with reduced descriptions of physical

phenomena [7]. Instead, biological systems are open systems exchanging particles with reservoirs and as such they are inherently out of equilibrium. Nonequilibrium processes, in general, do not have a natural coarse graining.

When the particle numbers in a reaction network are small, it needs to be described stochastically with the chemical master equation. Indeed, there is increased interest in the correct thermodynamic treatment of stochastic processes [8, 9]. With stochastic processes it is possible to investigate energy-conversion in molecular motors [10–13], error correction via kinetic proofreading [14–16], as well as information processing in small sensing networks [17–19]. In this field, different suggestions arose for coarse grainings motivated by thermodynamic consistency [20–22]. In these cases, the dissipation in a nonequilibrium process is typically underestimated—although also overestimations may occur [23]. For a general overview of coarse-graining in Markov processes, see [24] and references therein.

For large-scale networks however, a stochastic treatment is unfeasable. On the one hand, stochastic simulations quickly become computationally so demanding that they are effectively untractable. On the other hand, when species appear in large abundances (e.g. metabolic networks) the stochastic noise is negligible. This paper is exclusively concerned with this latter case. The dynamics is governed by deterministic differential equations: the nonlinear rate equations of chemical kinetics. Assuming a separation of time scales in these equations, model reduction approaches have been developed [25–27]. However, they do not address the question of thermodynamic consistency. Remarkably, recent development in the thermodynamics of chemical reaction networks [28, 29] highlighted the strong connection between the thermodynamics of deterministic rate equations and of stochastic processes, including the relation between energy, work, and information. Unfortunately, these studies were limited to elementary reactions with mass-action kinetics. The present paper addresses this constraint, thus extending the theory to kinetics of coarse-grained catalysts.

Understanding the nonequilibrium thermodynamics of catalysts is a crucial step towards incorporating thermodynamics into large-scale reaction networks. There is ongoing effort in the latter [30–32] which very often is based on the connection between thermodynamics and kinetics [33–35].

In this paper we show how to coarse grain the deterministic description of any biocatalyst in a thermodynamically consistent way—extending the applicability of such simplifications even to molecular motors [10, 36] and active membrane transport [37]. The starting point is the catalytic mechanism described as a reversible chemical reaction network where each of the M reaction steps ρ is an elementary transition representing a conformational change of a molecule or an elementary chemical reaction with mass-action kinetics. The corresponding rates are given by the fluxes (kinetic rate laws), ϕ_ρ^\pm , that incorporate the reaction rate constants and the dependence on the concentration of the reactant molecules. The mass-action reaction forces (negative Gibbs free energies of reaction) are $-\Delta_\rho G = RT \ln \phi_\rho^+ / \phi_\rho^-$ [38]. At this level, the reaction currents, $J_\rho = \phi_\rho^+ - \phi_\rho^-$, of these elementary steps are aligned with their respective reaction forces [39]: when one is positive, so is the other. From here we construct a reduced set of C reactions with effective reaction fluxes ψ_α^\pm and net forces $-\Delta_\alpha G$. As we will see later, there is a limited freedom to choose the exact set of reduced reactions. Nonetheless, the number of reduced reactions is independent of this choice.

By construction, our coarse graining procedure captures the entropy-production rate (EPR) [39, 40] of the underlying catalytic mechanism,

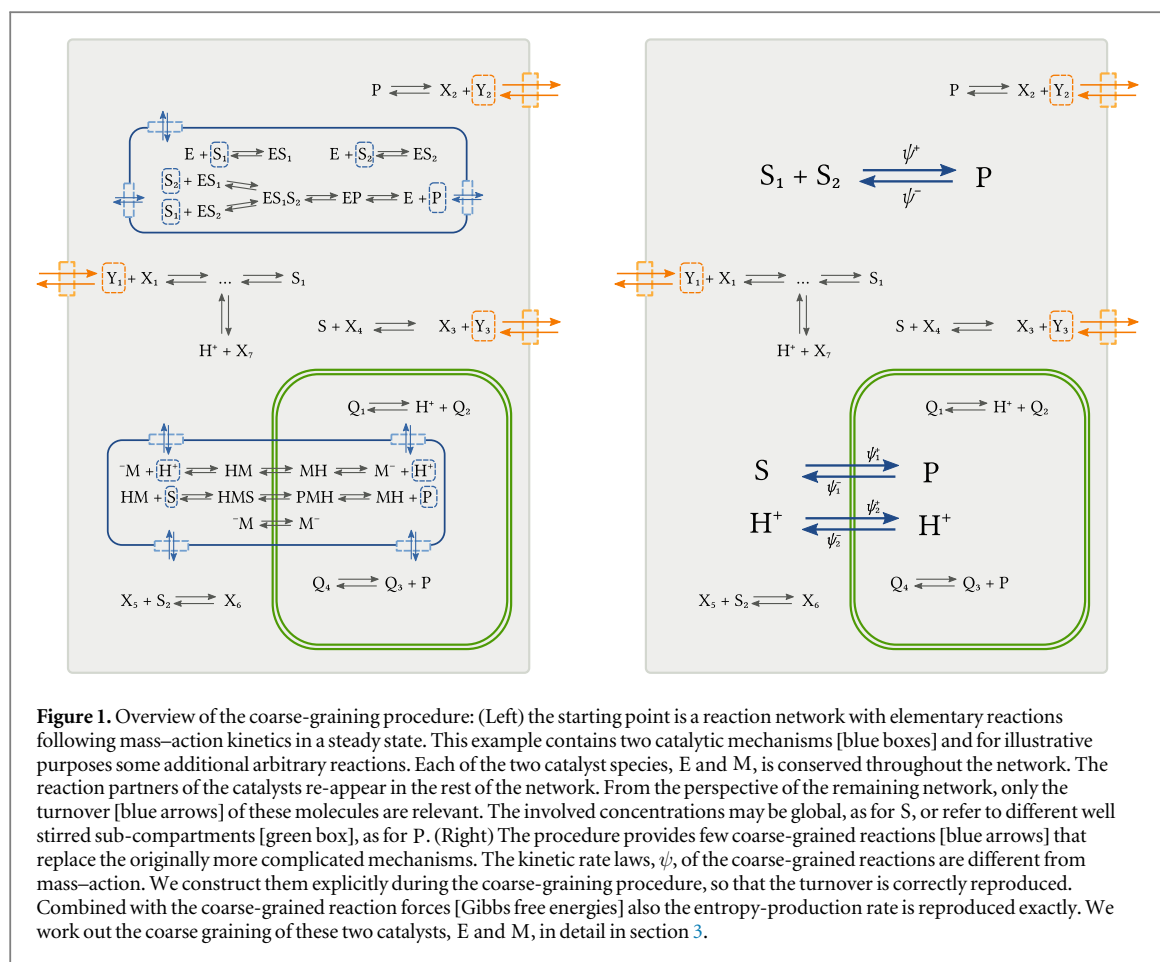
$$T\sigma := -\sum_\rho^M (\phi_\rho^+ - \phi_\rho^-) \Delta_\rho G = -\sum_\alpha^C (\psi_\alpha^+ - \psi_\alpha^-) \Delta_\alpha G \geq 0,$$

even though the number C of effective reactions α is much smaller than the number M of original reaction steps ρ . Therefore, our procedure is applicable in nonequilibrium situations, such as biological systems. In fact, the above equation is exact under steady-state conditions. In transient and other time-dependent situations the coarse graining can be a reasonable approximation. We elaborate this point further in the discussion.

Secondly, we work out the condition for this coarse graining to reduce to a single reaction α . In this case, we prove that the following flux–force relation holds true for this coarse-grained reaction:

$$-\Delta_\alpha G = RT \ln \frac{\psi_\alpha^+}{\psi_\alpha^-}.$$

A trivial consequence is that the coarse-grained reaction current, $J_\alpha = \psi_\alpha^+ - \psi_\alpha^-$, is aligned with the net force, $-\Delta_\alpha G$. In the past, such a flux–force relation has been used in the literature [41, 42] after its general validity was claimed [33] and later questioned [31, 34]. From here the belief arises that in every biochemical reaction network with any type of kinetics the currents and the forces of each reaction individually need to be aligned, a constraint used especially in flux balance analysis [43–45]. However, as we show in this paper, this relation does not hold when the coarse-graining reduces the biocatalyst to two or more coupled reactions.



This paper is structured as follows: first we present our results. Then, we illustrate our findings with two examples: the first is enzymatic catalysis of two substrates into one product. This can be reduced to a single reaction, for which we verify the flux–force relation at the coarse-grained level. The second example is a model of active membrane transport of protons, which is a prototype of a biocatalyst that cannot be reduced to a single reaction. Afterwards, we sketch the proofs for our general claims. Finally, we discuss our results and their implications. Rigorous proofs are provided in the [appendix](#).

2. Results

Our main result is a systematic procedure for a thermodynamically consistent coarse graining of catalytic processes. These processes may involve several substrates, products, modifiers (e.g. activators, inhibitors) that bind to or are released from a single molecule—the catalyst. The coarse graining involves only a few steps and is exemplified graphically in figure 1:

- (1) Consider the catalytic mechanism in a closed box and identify the internal stoichiometric cycles of the system. An internal stoichiometric cycle is a sequence of reactions leaving the state of the system invariant. Formally, internal stoichiometric cycles constitute the nullspace of the full stoichiometric matrix, \mathbb{S} .
- (2) Consider the concentrations of all substrates, modifiers, and products (summarized as Y) constant in time—therefore reduce the stoichiometric matrix by exactly those species. The remaining species, X , represent N different states of the catalyst. As a consequence, the reduced stoichiometric matrix, \mathbb{S}^X , has a larger nullspace: new stoichiometric cycles emerge in the system. These emergent cycles cause a turnover in the substrates/products while leaving the internal species invariant. Choose a basis, C_α , of emergent stoichiometric cycles that are linearly independent from the internal cycles.
- (3) Identify the net stoichiometry, $\mathbb{S}^Y C_\alpha$, together with the sum, $-\Delta_\alpha G$, of the forces along each emergent cycle α .
- (4) Calculate the apparent fluxes ψ_α^\pm along the emergent cycles at steady state.

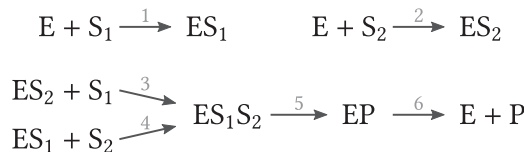


Figure 2. An enzymatic scheme turning two substrates into one product. The substrates can bind in arbitrary order. We adopt a reference direction for the individual reactions: forward is from left to right, as indicated by the arrows. The backward reactions are from right to left, thus every single reaction step is reversible. This scheme has a clear interpretation as a graph: the reactions are edges, reactants/products are vertices, where different combinations of reactants/products are considered different vertices. This graph has three disconnected components and contains no circuit.

For each emergent stoichiometric cycle α this procedure provides a new reversible reaction with net stoichiometry $\mathbb{S}^Y C_\alpha$, net force $-\Delta_\alpha G$, and net fluxes ψ_α^\pm . Furthermore, it preserves the EPR and, therefore, is thermodynamically consistent.

Our second result is a consequence of the main result: we prove that the flux–force relation is satisfied at the coarse-grained level by any catalytic mechanism for which only one single cycle emerges in step 2 of the presented procedure, as in example 3.1. When more cycles emerge, the flux–force relation does not hold as we show in the explicit counter-example 3.2.

3. Examples

3.1. Enzymatic catalysis

Let us consider the enzyme E that we introduced in figure 1. It is capable of catalyzing a reaction of two substrates, S_1 and S_2 , into a single product molecule, P. The binding order of the two substrates does not matter. Every single one of these reaction steps is assumed to be reversible and to follow mass–action kinetics. For every reaction we adopt a reference forward direction. Overall, the enzymatic catalysis can be represented by the reaction network in figure 2.

We apply our main result to this enzymatic scheme and thus construct a coarse-grained description for the net catalytic action. We furthermore explicitly verify our second result by showing that the derived enzymatic reaction fluxes satisfy the flux–force relation.

3.1.1. Closed system—internal cycles

When this system is contained in a closed box, no molecule can leave or enter the reaction volume. The dynamics is then described by the following rate equations:

$$\frac{d}{dt}z = \mathbb{S}J(z), \quad (1)$$

where we introduced the concentration vector z , the current vector $J(z)$, as well as the stoichiometric matrix \mathbb{S} :

$$z = \begin{pmatrix} [E] \\ [ES_1] \\ [ES_2] \\ [ES_1S_2] \\ [EP] \\ [S_1] \\ [S_2] \\ [P] \end{pmatrix}, \quad J(z) = \begin{pmatrix} k_1[E][S_1] - k_{-1}[ES_1] \\ k_2[E][S_2] - k_{-2}[ES_2] \\ k_3[ES_2][S_1] - k_{-3}[ES_1S_2] \\ k_4[ES_1][S_2] - k_{-4}[ES_1S_2] \\ k_5[ES_1S_2] - k_{-5}[EP] \\ k_6[EP] - k_{-6}[E][P] \end{pmatrix}, \quad \mathbb{S} = \begin{pmatrix} -1 & -1 & 0 & 0 & 0 & 1 \\ 1 & 0 & 0 & -1 & 0 & 0 \\ 0 & 1 & -1 & 0 & 0 & 0 \\ 0 & 0 & 1 & 1 & -1 & 0 \\ 0 & 0 & 0 & 0 & 1 & -1 \\ -1 & 0 & -1 & 0 & 0 & 0 \\ 0 & -1 & 0 & -1 & 0 & 0 \\ 0 & 0 & 0 & 0 & 0 & 1 \end{pmatrix}.$$

In the dynamical equations, only the currents $J(z)$ depend on the concentrations, whereas the stoichiometric matrix \mathbb{S} does not. The stoichiometric matrix thus imposes constraints on the possible steady-state concentrations that can be analyzed with mere stoichiometry: at steady state the current has to satisfy $0 = \mathbb{S}J(z_{ss})$ or, equivalently, $J(z_{ss}) \in \ker \mathbb{S}$. In our example, the nullspace $\ker \mathbb{S}$ is one-dimensional and spanned by $C_{\text{int}} = (1 \ -1 \ -1 \ 1 \ 0 \ 0)^\top$. Hence, the steady-state current is fully described by a single scalar value, $J(z_{ss}) = J_{\text{int}} C_{\text{int}}$. The vector C_{int} represents a series of reactions that leave the system state unchanged: the two substrates are bound along reactions 1 and 4 and released again along reactions -3 and -2 . In the end, the system returns to the exact same state as before these reactions. Therefore, we call this vector *internal stoichiometric cycle*. Having identified this internal cycle renders the first step complete.

Note that this stoichiometric cycle does not correspond to a self-avoiding closed path, or *circuit*, in the reaction graph in figure 2. This is due to the fact that *combinations* of species serve as vertices. If instead each species individually is a vertex, then also each cycle corresponds to a circuit.

In the following we explain why the first step of the procedure is important. The closed system has to satisfy a constraint that comes from physics: a closed system necessarily has to relax to a thermodynamic equilibrium state—which is characterized by the absence of currents of extensive quantities on any scale. Thus thermodynamic equilibrium is satisfied if $J_{\text{int}} = 0$. One can show that this requirement is equivalent to Wegscheider's condition [46]: the product of the forward rate constants along the internal cycle equals that of the backward rate constants,

$$k_1 k_4 k_{-3} k_{-2} = k_{-1} k_{-4} k_3 k_2. \quad (2)$$

Furthermore, irrespective of thermodynamic equilibrium, the steady state has to be stoichiometrically compatible with the initial condition: there are three linearly independent vectors in the cokernel of \mathbb{S} :

$$\mathcal{C}_E = \begin{pmatrix} E \\ ES_1 \\ ES_2 \\ ES_1 S_2 \\ EP \\ S_1 \\ S_2 \\ P \end{pmatrix}, \quad \mathcal{C}_1 = \begin{pmatrix} 0 \\ ES_1 \\ ES_2 \\ ES_1 S_2 \\ EP \\ S_1 \\ S_2 \\ P \end{pmatrix}, \quad \mathcal{C}_2 = \begin{pmatrix} 0 \\ ES_1 \\ ES_2 \\ ES_1 S_2 \\ EP \\ S_1 \\ S_2 \\ P \end{pmatrix}.$$

For each such vector, the scalar $L \equiv \mathcal{C} \cdot z$ evolves according to $\frac{\partial}{\partial t} \mathcal{C} \cdot z = \mathcal{C} \cdot \mathbb{S} J(z) = 0$, and thus is a *conserved quantity*. We deliberately chose linearly independent vectors with a clear physical interpretation. These vectors represent conserved moieties, i.e. a part of (or an entire) molecule that remains intact in all reactions. The total concentration of the enzyme moiety in the system is given by L_E . The other two conservation laws, L_1 and L_2 , are the total concentrations of moieties of the substrates, S_1 and S_2 , respectively.

Given a set of values for the conserved quantities from the initial condition, Wegscheider's condition on the rate constants ensures uniqueness of the equilibrium solution [46].

3.1.2. Open system—emergent cycles

So far we only discussed the system in a closed box that will necessarily relax to a thermodynamic equilibrium.

We now open the box and assume that there is a mechanism capable of fixing the concentrations of S_1 , S_2 and P to some given levels. These three species therefore no longer take part in the dynamics. Formally, we divide the set of species into two disjoint sets:

$$\underbrace{\{E, ES_1, ES_2, ES_1 S_2, EP\}}_X \cup \underbrace{\{S_1, S_2, P\}}_Y.$$

The first are the *internal species*, X , which are subject to the dynamics. The second are the *chemostatted species*, Y , which are exchanged with the environment. We apply this splitting to the stoichiometric matrix,

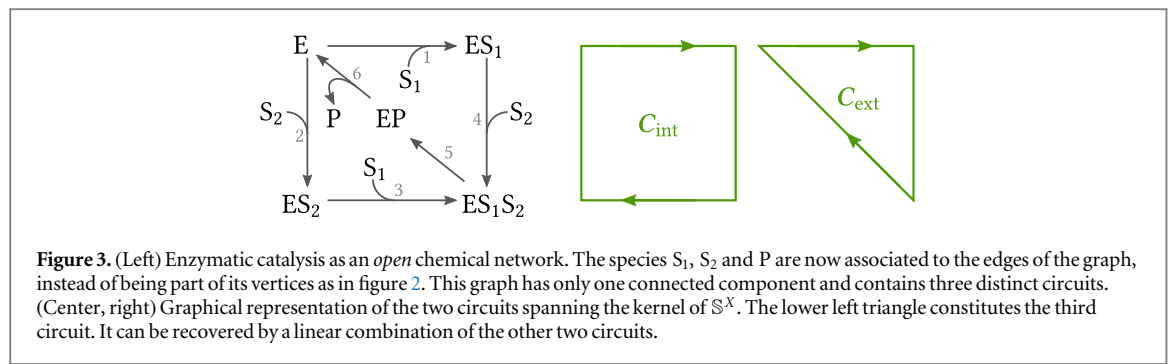
$$\mathbb{S} = \begin{pmatrix} \mathbb{S}^X \\ \mathbb{S}^Y \end{pmatrix},$$

and the vector of concentrations, $z = (x, y)$. Analogously, the rate equations for this open reaction system split into

$$\frac{\partial}{\partial t} x = \mathbb{S}^X J(x, y), \quad (3)$$

$$0 \equiv \frac{\partial}{\partial t} y = \mathbb{S}^Y J(x, y) + I(x, y). \quad (4)$$

The equation (4) is merely a definition for the exchange current I , keeping the species Y at constant concentrations. Note that the exchange currents I quantify the substrate/product turnover. The actual dynamical rate equations, the equation (3), are a subset of the original equations for the closed system, treating the chemostats as constant parameters. Absorbing these latter concentrations into the rate constants, we arrive at a linear ODE system with new *pseudo-first-order rate constants* $\tilde{k}(y)$. For these rate equations, one needs to reconsider the graphical representation of this reaction network: since the chemostatted species now are merely parameters for the reactions, we have to remove the chemostatted species from the former vertices of the network representation and associate them to the edges. The resulting graph representing the open network is drawn in figure 3.



The steady-state current $J_{ss} = J(x_{ss}, y)$ of equation (3) needs to be in the kernel of the internal stoichiometric matrix \mathbb{S}^X only. This opens up new possibilities. It is obvious that $\ker \mathbb{S}$ is a subset of $\ker \mathbb{S}^X$, but $\ker \mathbb{S}^X$ is in fact bigger. In our example we now have two *stoichiometric cycles*,

$$C_{\text{int}} = \begin{pmatrix} 1 & 1 \\ 2 & -1 \\ 3 & -1 \\ 4 & 1 \\ 5 & 0 \\ 6 & 0 \end{pmatrix} \quad \text{and} \quad C_{\text{ext}} = \begin{pmatrix} 1 & 1 \\ 2 & 0 \\ 3 & 0 \\ 4 & 1 \\ 5 & 1 \\ 6 & 1 \end{pmatrix}. \quad (5)$$

The first cycle is the internal cycle we identified in the closed system already: it only involves reactions that leave the closed system invariant, thus upon completion of this cycle not a single molecule is being exchanged. The second cycle is different: upon completion it leaves the internal species unchanged but chemostatted species are exchanged with the environment. Since this type of cycle appears only upon chemostatting, we call them *emergent stoichiometric cycles*. Overall, the steady-state current is a linear combination of these two cycles: $J_{ss} = J_{\text{int}} C_{\text{int}} + J_{\text{ext}} C_{\text{ext}}$. This completes step 2.

These two stoichiometric cycles correspond to circuits in the open reaction graph. We give a visual representation on the right of figure 3. As a consequence of working with catalysts, the vertices of the reaction graph for the open system coincide with the internal species X . Therefore, for all catalysts the cycles of the open system correspond to circuits in the corresponding graph.

The cycles are not the only structural object affected by the chemostatting procedure: the conservation laws change as well. In the enzyme example we have merely one conservation law left—that of the enzyme moiety, L_E . The substrate moieties are being exchanged with the environment, which renders L_1 and L_2 *broken conservation laws*. Overall, upon adding three chemostats two conservation laws were broken and one cycle emerged. In fact, the number of chemostatted species always equals the number of broken conservation laws plus the number of emergent cycles [47].

3.1.3. Net stoichiometries and net forces

The net stoichiometry of the emergent cycle is $S_1 + S_2 \rightleftharpoons P$. This represents a single reversible reaction describing the net catalytic action of the enzyme. For a complete coarse graining, we still need to identify the fluxes and the net force along this reaction. Its net force is given by the sum of the forces along the emergent cycle. Collecting the Gibbs energies of reaction in a vector, $\Delta_r G := (\Delta_1 G, \dots, \Delta_6 G)^\top$, this sum is concisely written as

$$-\Delta_{\text{ext}} G := -C_{\text{ext}} \cdot \Delta_r G = RT \ln \frac{k_1 k_4 k_5 k_6 [S_1][S_2]}{k_{-1} k_{-4} k_{-5} k_{-6} [P]}. \quad (6)$$

One could also ask about the net stoichiometry and net force along the internal cycle. However, we have $C_{\text{int}} \cdot \Delta_r G = 0$ since the internal cycle does not interact with the chemostats. Moreover, the net force along the internal cycle is

$$-\Delta_{\text{int}} G := -C_{\text{int}} \cdot \Delta_r G = RT \ln \frac{k_1 k_4 k_{-3} k_{-2}}{k_{-1} k_{-4} k_3 k_2} = 0 \quad (7)$$

by virtue of Wegscheider's condition.

3.1.4. Apparent fluxes

We now determine the apparent fluxes along the two cycles of the system. To that end, we first solve the linear rate equations to calculate the steady-state concentrations and the steady-state currents. For the steady-state

concentrations we use a diagrammatic method popularized by King and Altman [48] that we summarize in appendix A.

As derived in step 2 of the procedure, the steady-state current vector is

$$\mathbf{J}_{ss} = \begin{pmatrix} 1 & J_{int} + J_{ext} \\ 2 & -J_{int} \\ 3 & -J_{int} \\ 4 & J_{int} + J_{ext} \\ 5 & J_{ext} \\ 6 & J_{ext} \end{pmatrix}.$$

Hence the two cycle currents are

$$J_{int} = -J_2 = k_{-2}[ES_2] - k_2[E][S_2], \quad J_{ext} = J_6 = k_6[EP] - k_{-6}[E][P].$$

With the explicit steady-state concentrations given in appendix A.1, we find (see appendix B.1 for details):

$$J_{int} = k_{-2}[ES_2] - k_2[E][S_2] = \frac{L_E k_2 k_3}{N_E(\mathbf{y}) k_1} \left(\frac{k_{-1}}{k_4} + [S_2] \right) (k_{-1} k_{-4} k_{-5} k_{-6}[P] - k_1 k_4 k_5 k_6 [S_1][S_2]).$$

and

$$J_{ext} = k_6[EP] - k_{-6}[E][P] = \frac{L_E \xi(\mathbf{y})}{N_E(\mathbf{y})} (k_1 k_4 k_5 k_6 [S_1][S_2] - k_{-1} k_{-4} k_{-5} k_{-6}[P]). \quad (8)$$

Here, L_E is the total amount of available enzyme, $N_E(\mathbf{y})$ is a positive quantity that depends on the chemostat concentrations as well as all rate constants, and

$$\xi(\mathbf{y}) = k_3[S_1] + \frac{k_2 k_3 [S_2]}{k_1} + k_{-2} + \frac{k_{-2} k_{-3}}{k_{-4}}.$$

As expected, the current along the emergent cycle J_{ext} is not zero, provided that its net force is not zero. However, note that the current along the internal cycle does *not* vanish either, even though its own net force is zero. Both currents vanish only when the net force, $-\Delta_{ext} G$, vanishes—which is at thermodynamic equilibrium.

Finally, we decompose the current $J_{ext} = \psi^+ - \psi^-$ into the apparent fluxes

$$\psi^+ = \frac{L_E \xi(\mathbf{y})}{N_E(\mathbf{y})} k_1 k_4 k_5 k_6 [S_1][S_2] > 0, \quad \psi^- = \frac{L_E \xi(\mathbf{y})}{N_E(\mathbf{y})} k_{-1} k_{-4} k_{-5} k_{-6}[P] > 0. \quad (9)$$

Here, it is important to note that while

$$\psi^+ - \psi^- = k_6[EP] - k_{-6}[E][P],$$

there are several cancellations happening in the derivation of equation (8) implying that

$$\psi^+ \neq k_6[EP], \quad \psi^- \neq k_{-6}[E][P].$$

We elaborate on these cancellations in this special case in appendix B.1 as well as for the general case in appendix B.3.

3.1.5. Flux–force relation

With the explicit expressions for the net force, equation (6), and the apparent fluxes, equation (9), of the emergent cycle we explicitly verify the flux–force relation at the coarse-grained level:

$$RT \ln \frac{\psi^+}{\psi^-} = RT \ln \frac{k_1 k_4 k_5 k_6 [S_1][S_2]}{k_{-1} k_{-4} k_{-5} k_{-6}[P]} = -\Delta_{ext} G.$$

This flux–force relation implies that the reaction current is always aligned with the net force along this reaction: $J_{ext} > 0 \Leftrightarrow -\Delta_{ext} G > 0$. In other words, the reaction current directly follows the force acting on this reaction.

In fact, in this case we can connect the flux–force relation to the second law of thermodynamics. The EPR reads

$$\begin{aligned} T\sigma(\mathbf{x}_{ss}, \mathbf{y}) &= -\mathbf{J}_{ss} \cdot \Delta_r \mathbf{G} = -J_{int} \mathbf{C}_{int} \cdot \Delta_r \mathbf{G} - J_{ext} \mathbf{C}_{ext} \cdot \Delta_r \mathbf{G} \\ &= -J_{ext} \Delta_{ext} G = RT(\psi^+ - \psi^-) \ln \frac{\psi^+}{\psi^-} \geq 0. \end{aligned}$$

With this representation, it is evident that the flux–force relation ensures the second law: $\sigma \geq 0$. Moreover, we see explicitly that the EPR is faithfully reproduced at the coarse-grained level. This shows the thermodynamic consistency of our coarse-graining procedure.

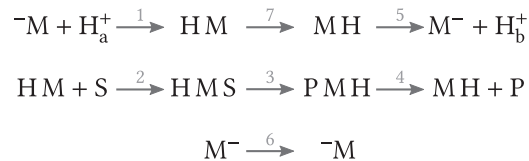


Figure 4. Reaction graph for the mechanism modeling the active transport of protons from one side of a membrane, H_a^+ , to the other side, H_b^+ . The transport is coupled to the catalysis of a substrate, S, to a product, P. The free transporter itself exists in two different conformations $\neg M$ and M^- , respectively. Again, all reactions are considered reversible and to follow mass-action kinetics. A reference forward direction is indicated as arrows from left to right.

3.2. Active membrane transport

We now turn to the second example introduced in figure 1: a membrane protein, M, that models a proton pump similar to the one presented in [37]. It transports protons from one side of the membrane (side a) to the other (side b). The membrane protein itself is assumed to be charged to facilitate binding of the protons and to have different conformations M^- and $\neg M$ where it exposes the binding site to the two different sides of the membrane. Furthermore, when a proton is bound, it can either bind another substrate S when exposing the proton to side a—or the respective product P when the proton is exposed to side b. The latter could be some other ion concentrations on either side of the membrane—or an energy rich compound (ATP) and its energy poor counterpart (ADP). The reactions modeling this mechanism are summarized in the reaction graph in figure 4.

In order to find a coarse-grained description for this transporter we apply our result. Since the procedure is already detailed in example 3.1, we omit some repetitive explanations in this example.

3.2.1. Closed system—internal cycles

This closed system has no cycle, therefore Wegscheider's conditions do not impose any relation between the reaction rate constants. There are three conservation laws in the closed system,

$$\mathcal{C}_M = \begin{pmatrix} \neg M \\ HM \\ HMS \\ PMH \\ MH \\ M^- \\ H_a^+ \\ H_b^+ \\ S \\ P \end{pmatrix}, \quad \mathcal{C}_H = \begin{pmatrix} \neg M \\ HM \\ HMS \\ PMH \\ MH \\ M^- \\ H_a^+ \\ H_b^+ \\ S \\ P \end{pmatrix}, \quad \mathcal{C}_S = \begin{pmatrix} \neg M \\ HM \\ HMS \\ PMH \\ MH \\ M^- \\ H_a^+ \\ H_b^+ \\ S \\ P \end{pmatrix}.$$

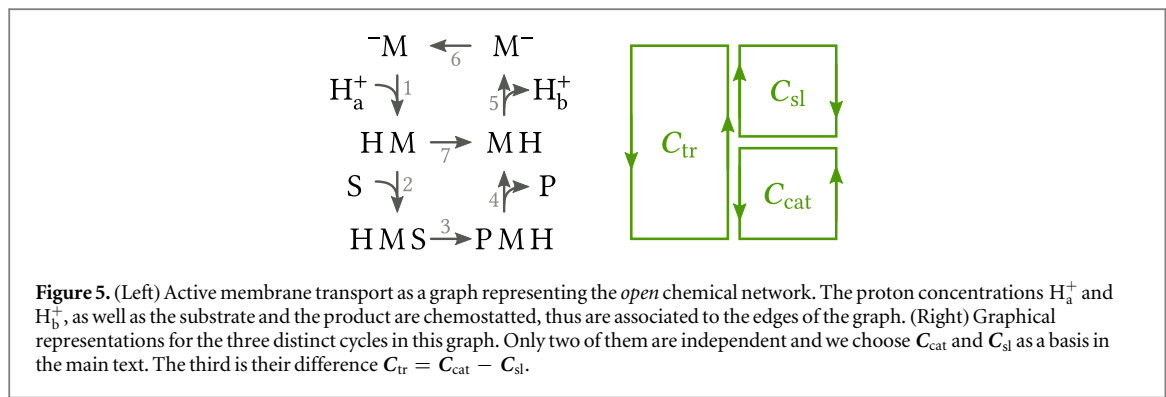
They represent the conservation of membrane protein (L_M), proton (L_H), and substrate moieties (L_S), respectively, showing that these three are conserved independently. For any initial condition, the corresponding rate equations will relax to a unique steady-state solution satisfying thermodynamic equilibrium, $J(z) = 0$.

3.2.2. Open system—emergent cycles

We now fix the concentrations of the protons H_a^+ and H_b^+ in the two reservoirs, as well as the substrate and the product concentrations. The reaction network for this open system is depicted in figure 5. The open system still has a conserved membrane protein moiety while the conservation laws of protons and substrate are broken upon chemostatting. Furthermore, there are two emergent cycles now,

$$C_{\text{cat}} = \begin{pmatrix} 1 \\ 2 \\ 3 \\ 4 \\ 5 \\ 6 \\ 7 \end{pmatrix} \quad \text{and} \quad C_{\text{sl}} = \begin{pmatrix} -1 \\ 0 \\ 0 \\ 0 \\ -1 \\ -1 \\ -1 \end{pmatrix}. \quad (10)$$

Their visual representation as circuits is given on the right of figure 5.



3.2.3. Net stoichiometry and net forces

The first emergent cycle has the net stoichiometry $S \rightleftharpoons P$, which represents pure catalysis with net force

$$-\Delta_{\text{cat}}G = RT \ln \frac{k_1 k_2 k_3 k_4 k_{-7}[S]}{k_{-2} k_{-3} k_{-4} k_7[P]}. \quad (11)$$

The second cycle has net stoichiometry $H_b^+ \rightleftharpoons H_a^+$. This represents the slip of one proton from side b back to side a with net force

$$-\Delta_{\text{sl}}G = RT \ln \frac{k_{-1} k_{-5} k_{-6} k_{-7}[H_b^+]}{k_1 k_5 k_6 k_7[H_a^+]}. \quad (12)$$

For later reference, we note that the difference $C_{\text{tr}} = C_{\text{cat}} - C_{\text{sl}}$ has net stoichiometry $H_a^+ + S \rightleftharpoons H_b^+ + P$. This is the active transport of a proton from side a to side b, under catalysis of one substrate into one product. The net force of this reaction is

$$-\Delta_{\text{tr}}G = -\Delta_{\text{cat}}G + \Delta_{\text{sl}}G = RT \ln \frac{k_1 k_2 k_3 k_4 k_5 k_6[H_a^+][S]}{k_{-1} k_{-2} k_{-3} k_{-4} k_{-5} k_{-6}[H_b^+][P]}. \quad (13)$$

3.2.4. Apparent fluxes

Solving the linear rate equations (see appendix A), we have a solution for the steady-state concentrations. The exact expressions are given in appendix A.2. With the steady-state concentrations, we calculate the contributions of both cycles to the steady-state current: $J(\mathbf{x}_{\text{ss}}, \mathbf{y}) = J_{\text{cat}} C_{\text{cat}} + J_{\text{sl}} C_{\text{sl}}$. Each current contribution is given by a single reaction:

$$J_{\text{cat}} = J_2 =: \psi_{\text{cat}}^+ - \psi_{\text{cat}}^-, \quad J_{\text{sl}} = -J_1 =: \psi_{\text{sl}}^+ - \psi_{\text{sl}}^-.$$

With the abbreviations

$$\xi_{\text{cat}} := k_{-6} k_{-5}[H_b^+] + k_1 k_{-5}[H_a^+][H_b^+] + k_6 k_1[H_a^+], \quad \xi_{\text{sl}} := k_3 k_4 + k_{-2} k_4 + k_{-3} k_{-2},$$

we can express the apparent fluxes as

$$\begin{aligned} \frac{N_M}{L_M} \psi_{\text{cat}}^+ &= k_1 k_2 k_3 k_4 k_5 k_6[H_a^+][S] + \xi_{\text{cat}} k_{-7} k_2 k_3 k_4[S], \\ \frac{N_M}{L_M} \psi_{\text{cat}}^- &= k_{-1} k_{-2} k_{-3} k_{-4} k_{-5} k_{-6}[H_b^+][P] + \xi_{\text{cat}} k_7 k_{-2} k_{-3} k_{-4}[P], \\ \frac{N_M}{L_M} \psi_{\text{sl}}^+ &= k_{-1} k_{-2} k_{-3} k_{-4} k_{-5} k_{-6}[H_b^+][P] + \xi_{\text{sl}} k_{-1} k_{-5} k_{-6} k_{-7}[H_b^+], \\ \frac{N_M}{L_M} \psi_{\text{sl}}^- &= k_1 k_2 k_3 k_4 k_5 k_6[H_a^+][S] + \xi_{\text{sl}} k_1 k_5 k_6 k_7[H_a^+]. \end{aligned}$$

The derivation for these equations is detailed in appendix B.2. Note that N_M depends on all rate constants and all chemostat concentrations.

3.2.5. Breakdown of the flux–force relation

We see that the abbreviated terms ξ appear symmetrically in the forward and backward fluxes. Therefore, when the net forces are zero, necessarily the currents vanish and the system is at thermodynamic equilibrium. However, in general, the currents do not vanish. Moreover, the concentrations of the chemostats appear in the four different fluxes in different combinations—indicating that both net forces couple to both coarse-grained reactions. Due to this coupling, it is impossible to find nice flux–force relations for the two reactions

independently:

$$-\Delta_{\text{cat}}G \neq RT \ln \frac{\psi_{\text{cat}}^+}{\psi_{\text{cat}}^-}, \quad -\Delta_{\text{sl}}G \neq RT \ln \frac{\psi_{\text{sl}}^+}{\psi_{\text{sl}}^-}. \quad (14)$$

To the contrary, it is easy to find concentrations for the four chemostats where the catalytic force is so strong that it drives the slip current against its natural direction—giving rise to a negative contribution in the EPR. Nonetheless, the overall EPR is correctly reproduced at the coarse-grained level:

$$T\sigma = -\mathbf{J}_{\text{ss}} \cdot \Delta_{\text{r}}\mathbf{G} = -J_{\text{cat}} \Delta_{\text{cat}}G - J_{\text{sl}} \Delta_{\text{sl}}G \geq 0.$$

Since this is, by construction, the correct EPR of the full system at steady state, we know that it is always non-negative—and that the coarse-graining procedure is thermodynamically consistent. This example shows explicitly that biochemical reaction networks need not satisfy the flux–force relation, nor need their currents and forces be aligned to comply with the second law. After all, the function of this membrane protein is to transport protons from side a to side b against the natural concentration gradient.

4. Cycle-based coarse graining

From the perspective of a single biocatalyst, the rest of the cell (or cellular compartment) serves as its environment, providing a reservoir for different chemical species. Our coarse graining exploits this perspective to disentangle the interaction of the catalyst with its environment—in the form of emergent cycles—from the behavior of the catalyst in a (hypothetical) closed box at thermodynamic equilibrium—in the form of the internal cycles. From the perspective of the environment, only the interactions with the catalyst matter, i.e. the particle exchange currents: they prescribe the substrate/product turnover and when combined with the reservoir's concentrations (chemical potentials) also the dissipation. Our coarse graining respects the reservoir's concentrations and incorporates all the emergent cycles that exchange particles with the reservoir. It thus correctly reproduces the exchange currents: this is the fundamental reason why we can replace the actual detailed mechanism of the catalyst with a set of coarse-grained reactions in a thermodynamically exact way. A formal version of this reasoning, including all necessary rigor and a constructive prescription to find the apparent fluxes, is provided in appendix B.

In our examples we illustrated the fundamental difference between the case where a catalyst can be replaced with a single coarse-grained reaction and the case where this is not possible. In the first case, such a catalyst interacts with substrate and product molecules that are coupled via exchange of mass in a specific stoichiometric ratio. This is known as tight coupling. Whether or not the catalysis is additionally modified by activators or inhibitors, does not interfere with this condition. After all, the modifiers are neither consumed nor produced. Thus they appear only in the normalizing denominators of the steady-state concentrations and affect the kinetics while leaving the thermodynamics untouched. Furthermore, if there is only one single emergent cycle in a catalytic mechanism, any product of pseudo-first-order rate constants along any circuit in the network will either (i) satisfy Wegscheider's conditions or (ii) reproduce (up to sign) the net force, $-\Delta_{\text{a}}G$, of the emergent cycle. Ultimately, this is why the flux–force relation holds in this tightly coupled case. A formal version of this proof, including all necessary rigor, is provided in appendix C.

In the case where we have to provide two or more coarse-grained reactions, the catalytic mechanism couples several processes that are not tightly coupled via exchange of mass. To the contrary: the turnover of different substrates/products need not have fixed stoichiometric ratios. In fact, their ratios will depend on the environment's concentrations. In this case the flux–force relation does not hold in general, as we proved with our counter-example. After all, when several processes are coupled, the force of one process can overcome the force of the second process to drive the second current against its natural direction. This transduction of energy [12, 49] would not be possible at a coarse-grained level, if the flux–force relation was always true.

We now assess the reduction provided by our procedure: the number C of coarse-grained reactions α is always lower than the number M of reaction steps ρ in the original mechanism. This can be understood from the graph representation of the open system: the number B of circuits in a connected graph is related to its number N of vertices (catalyst states) and the number M of edges (reaction steps) by $B = M - N + 1$ [50]. Some of the circuits represent internal cycles, rendering B an upper bound to the number of emergent cycles C . Since the number N of catalyst states is at least two, these numbers are ordered: $M > B \geq C$. This proves that our coarse graining always reduces the number of reactions.

5. Discussion

The original work of Michaelis and Menten [4] was based on a specific enzyme that converts a single substrate into a single product assuming a totally irreversible step. Their goal was to determine the rate of production of product molecule. Later progress in enzyme kinetics extended their method to deal with fully reversible mechanisms, as well as many substrates, many products and modifiers [1]. The focus on the turnover led many people to identify the net effect of the enzyme with a *single* effective reaction, describing its kinetics with the Michaelis–Menten equation (or one of its generalizations). Our coarse-graining indeed incorporates all these special cases: the Michaelis–Menten equation arises from coarse graining a mechanism of the form



and assuming that the last reaction step, the release of the product, is much faster than the other steps. Then the coarse-grained reaction current is identical to the substrate/product turnover. Importantly, our procedure highlights that there is no direct correspondence between the number of required net reactions and the number of circuits in the reaction graph—even of the open system. Some circuits correspond to *internal cycles* that play a kinetic role, not leaving a trace in the thermodynamic forces. Only the *emergent cycles* need to be taken into account for the coarse graining. Thus the net effect of a multi-cyclic catalyst might be consistently expressed as a single effective reaction, as seen in the example 3.1.

Likewise, in theoretical studies of biochemical systems, effective unimolecular reactions of the form



are frequently used, where the reaction rate constants satisfy

$$\frac{k^+}{k^-} = \exp \left[\frac{\mu_A^\circ - \mu_B^\circ + \mu_X - \mu_Y}{RT} \right].$$

Here, the chemical potentials, μ , account for the thermodynamic force exerted by X and Y. Even when the actual effective reaction does not follow mass-action kinetics, this equation is assumed, implying that the effective reaction fluxes are $k^+[A] = \psi^+$ and $k^-[B] = \psi^-$, and the ‘constants’ k indeed depend on some concentrations. This is only consistent if the implicit conversion mechanism is tightly coupled by exchange of mass: when tightly coupled, the differences of the chemical potentials represent the Gibbs free energy change along the reaction $A + X \rightleftharpoons B + Y$. In this case, the above equation is the flux–force relation. Otherwise, our coarse-graining procedure reveals that this is thermodynamically inconsistent: if the implicitly modeled catalysis is not tightly coupled via the exchange of mass, there is a hidden thermodynamic driving force that is independent of the concentrations of A and B, while the turnover of X/Y is not in a stoichiometric ratio to the turnover of A/B. We have seen in example 3.2 that the flux–force relation indeed does not hold in this case.

The failure of the flux–force relation in the nontightly coupled case does not imply inconsistent thermodynamics. Our coarse-graining procedure indeed deals with this case very easily. The resulting fluxes and forces reproduce the EPR while sacrificing the flux–force relation. The key difference to the original ideas in enzyme kinetics is that the substrate/product turnover is split into *several* effective reactions with their own reaction fluxes and forces, reproducing the EPR. This is especially important for complex catalysts: many models for molecular motors and active transporters are not tightly coupled. These free-energy transducers often display slippage via futile cycles. While some enzymes also show signs of slippage, many simple enzymes are modeled as tightly coupled—which implies they satisfy the flux–force relation. Our coarse graining deals with all these cases and in that sense goes far beyond Michaelis–Menten.

Our procedure greatly reduces the number of species and reactions involved in a network while reproducing the EPR. This comes at the cost of complicated effective fluxes (rate laws). They are rational functions of the involved concentrations and thus more complicated than simple mass-action kinetics. Nonetheless, our procedure is constructive by giving these complicated expressions explicitly. With the explicit solutions at hand, further assumptions can be made to simplify the effective fluxes—as in the case of the original Michaelis–Menten equation. Note that these additional simplifications may have an impact on the EPR, in the worst case breaking the thermodynamic consistency. This trade-off between simplicity and thermodynamic correctness needs to be evaluated case by case.

We now discuss the limitations of our approach. The presented coarse-graining procedure is exact in *steady-state* situations, arbitrarily far from equilibrium. When the surrounding reaction network is not in a steady state, the coarse graining can still be used: then the coarse-grained reaction fluxes and forces have to be considered *instantaneous*—they change in time due to the changing substrate/product (or modifier) concentrations. Underlying this point of view is a separation of time scales: when the abundance of substrates and products is very large, as compared to the abundance of catalyst, then the concentrations of the latter change much more quickly. This results in a quasi-steady state for the catalyst-containing species. Consequently, our coarse graining

cannot capture the contribution to dissipation that arises in this fast relaxation dynamics. It only captures the dissipation due to the conversion of substrate into product. This reasoning can be made more rigorous: there are time-scale separation techniques for deterministic rate equations [25, 51] frequently used in biochemical contexts [26], furthermore stochastic corrections due to small copy-numbers [52] and even effective memory effects [27, 53] can be incorporated. However, these techniques do not explicitly address the question of thermodynamic consistency and we think that combining our coarse-graining with these techniques is a promising endeavor for the future.

We restricted the entire reasoning in this paper to catalysts. They follow linear rate equations when their reaction partners have constant concentrations. This linearity allowed us to give explicit solutions for general catalysts. Focusing on the emergent cycles to reproduce the correct thermodynamics paves the way to apply a similar procedure beyond catalysts: reaction networks that remain nonlinear after chemostatting still have emergent cycles [28]. They can be calculated algebraically from bases for the nullspaces of the full and the reduced stoichiometric matrices, \mathbb{S} and \mathbb{S}^X . The cycles in nonlinear networks may not have a representation as circuits in the reaction graph, as we have seen with the internal cycle of the enzyme in a closed box. Nonetheless, each of the emergent cycles \mathbf{C}_α can serve as an effective reaction: it has a well defined stoichiometry, $\mathbb{S}^Y \mathbf{C}_\alpha$, and a well defined net force, $-\Delta_r \mathbf{G} \cdot \mathbf{C}_\alpha$. The steady state concentrations as well as the fluxes, however, need to be determined case by case. Nonlinear differential equations can be multi-stable, where our coarse graining applies to each stable steady state. Some nonlinear ODEs exhibit limit cycles, thus never reaching a steady state. In this case our procedure is no longer applicable.

6. Summary

We have presented a coarse-graining procedure for biocatalysts and have shown that it is thermodynamically consistent. During this coarse graining procedure, a detailed catalytic mechanism is replaced by a few net reactions. The stoichiometry, deterministic kinetic rate laws and net forces for the coarse-grained reactions are calculated explicitly from the detailed mechanism—ensuring that at steady state the detailed mechanism and the net reactions have both the same substrate/product turnover and the same EPR.

Furthermore, we have shown that in the tightly coupled case where a detailed mechanism is replaced by a single reaction, this net reaction satisfies a flux–force relation. In the case where a detailed mechanism has to be replaced with several net reactions, the flux–force relation does not hold for the net reactions due to cross-coupling of independent thermodynamic forces. Ultimately, this cross-coupling allows the currents and forces not to be aligned—while complying with the second law of thermodynamics.

Overall, we have shown that coarse-graining schemes which preserve the correct thermodynamics far from equilibrium are not out of reach.

Acknowledgments

This work is financially supported by the National Research Fund of Luxembourg in the frame of AFR PhD Grants No. 7865466 and No. 9114110. Furthermore, this research is funded by the European Research Council project NanoThermo (ERC-2015-CoG Agreement No. 681456).

Conflict of interest

The authors declare that they have no conflict of interest.

Appendix A. Diagrammatic method for explicit steady states of linear reaction networks

We consider a catalytic mechanism with a catalyst and several substrates, products, inhibitors or activators. The mechanism is resolved down to elementary reactions following mass–action kinetics.

Upon chemostatting all the substrates, products, inhibitors and activators—summarized as \mathbf{y} —we are left with rate equations that are linear in the catalyst-containing species—summarized as \mathbf{x} . While the steady-state equations alone, $0 = \mathbb{S}^X \mathbf{J}(\mathbf{x}, \mathbf{y})$, are under-determined and linearly dependent, the open system still has a conservation law for the total catalyst-moiety concentration $L = \sum_i x_i$, which again is a linear equation. We can replace the first line of the steady-state equations with this constraint to arrive at linear equations $L \mathbf{e}_1 = \mathbb{M}(\mathbf{y}) \mathbf{x}$, where $\mathbf{e}_1 = (1, 0, \dots)$ is the first Cartesian unit vector and $\mathbb{M}(\mathbf{y})$ is an invertible square matrix that depends on the chemostat concentrations. According to Cramer’s rule the unique solution to this problem is given by

$$\frac{x_i^*}{L} = \frac{\det \mathbb{M}_i(\mathbf{y})}{\det \mathbb{M}(\mathbf{y})}, \quad (\text{A1})$$

where $\mathbb{M}_i(\mathbf{y})$ is identical to $\mathbb{M}(\mathbf{y})$ just with the i th column replaced by \mathbf{e}_1 . We now provide a diagrammatic method to represent this solution. This diagrammatic method is frequently attributed to King and Altman [48] or Hill [54], while an equivalent approach was already employed by Kirchhoff [55] to solve problems in electric networks. We give the diagrammatic method in the language of graph theory [50, 56], for which we need some definitions.

The open pseudo-first-order reaction network has a simple representation as a connected graph \mathcal{G} where all the catalyst-containing species i form the vertices \mathcal{V} and the reactions $\rho \cup -\rho$ form bidirectional edges \mathcal{R} . The reduced stoichiometric matrix \mathbb{S}^X is the *incidence matrix* for this graph.

A closed self-avoiding path in a graph is a *circuit* and can be identified with a vector $\mathbf{c} \in \mathbb{R}^{\mathcal{R}}$ over the edges, whose entries are in fact restricted to $\{-1, 0, 1\}$. Since a circuit is a closed path, it satisfies $\mathbb{S}^X \mathbf{c} = 0$ and reaches as many vertices as it contains edges. A graph not containing any circuit is called *forest*, a connected forest is called *tree*.

A connected subgraph $\tau \subset \mathcal{G}$ is called *spanning tree* if it spans all the vertices but contains no circuit. The set \mathcal{T} of spanning trees of a finite graph is always finite. A *rooted spanning tree* is a tree where all the edges are oriented along the tree towards one and the same vertex, called the *root*.

With these notions set, the determinants in equation (A1) can be written as

$$\det \mathbb{M}_i(\mathbf{y}) = \sum_{\tau \in \mathcal{T}_i} \prod_{\rho \in \tau} \tilde{k}_\rho(\mathbf{y}), \quad \det \mathbb{M}(\mathbf{y}) = \sum_i \sum_{\tau \in \mathcal{T}_i} \prod_{\rho \in \tau} \tilde{k}_\rho(\mathbf{y}) =: N(\mathbf{y}).$$

Here, \mathcal{T}_i is the set of spanning trees rooted in vertex i , and $\tilde{k}_\rho(\mathbf{y})$ is the pseudo-first-order rate constant of reaction ρ . Overall, Kirchhoff's formula for the solution to the linear problem is

$$\frac{x_i^*}{L} = \frac{1}{N(\mathbf{y})} \sum_{\tau \in \mathcal{T}_i} \prod_{\rho \in \tau} \tilde{k}_\rho(\mathbf{y}). \quad (\text{A2})$$

From this result it is easy to confirm that the solution exists and is always unique as long as the chemostat concentrations are finite and positive. Furthermore, the steady-state concentrations are expressed as sums of products of positive quantities, thus themselves are always positive.

While this formula is very compact and abstract, it is not obviously convenient for practical calculations. However, the rooted spanning trees appearing in this formula can be visually represented as diagrams, as we will see in the following examples. These diagrams are intuitive enough to make practical calculations with this formula feasible.

A.1. Steady-state concentrations for the enzymatic catalysis

The enzymatic catalysis example in the main text, when open, is represented by the graph in figure 3. This graph has five vertices and six edges. It contains three distinct circuits and twelve different spanning trees.

A visual representation of Kirchhoff's formula (A2) for its steady-state concentrations is given by the following diagrams:

$$\begin{aligned} \frac{[E]}{L_E} &= \frac{1}{N_E} \left[\begin{array}{c} \text{Diagram 1} \\ \text{Diagram 2} \\ \text{Diagram 3} \\ \text{Diagram 4} \\ \text{Diagram 5} \\ \text{Diagram 6} \\ \text{Diagram 7} \\ \text{Diagram 8} \\ \text{Diagram 9} \\ \text{Diagram 10} \\ \text{Diagram 11} \\ \text{Diagram 12} \end{array} \right] \\ \frac{[ES_2]}{L_E} &= \frac{1}{N_E} \left[\begin{array}{c} \text{Diagram 1} \\ \text{Diagram 2} \\ \text{Diagram 3} \\ \text{Diagram 4} \\ \text{Diagram 5} \\ \text{Diagram 6} \\ \text{Diagram 7} \\ \text{Diagram 8} \\ \text{Diagram 9} \\ \text{Diagram 10} \\ \text{Diagram 11} \\ \text{Diagram 12} \end{array} \right] \\ \frac{[EP]}{L_E} &= \frac{1}{N_E} \left[\begin{array}{c} \text{Diagram 1} \\ \text{Diagram 2} \\ \text{Diagram 3} \\ \text{Diagram 4} \\ \text{Diagram 5} \\ \text{Diagram 6} \\ \text{Diagram 7} \\ \text{Diagram 8} \\ \text{Diagram 9} \\ \text{Diagram 10} \\ \text{Diagram 11} \\ \text{Diagram 12} \end{array} \right] \\ \frac{[ES_1]}{L_E} &= \frac{1}{N_E} \left[\begin{array}{c} \text{Diagram 1} \\ \text{Diagram 2} \\ \text{Diagram 3} \\ \text{Diagram 4} \\ \text{Diagram 5} \\ \text{Diagram 6} \\ \text{Diagram 7} \\ \text{Diagram 8} \\ \text{Diagram 9} \\ \text{Diagram 10} \\ \text{Diagram 11} \\ \text{Diagram 12} \end{array} \right] \\ \frac{[ES_1S_2]}{L_E} &= \frac{1}{N_E} \left[\begin{array}{c} \text{Diagram 1} \\ \text{Diagram 2} \\ \text{Diagram 3} \\ \text{Diagram 4} \\ \text{Diagram 5} \\ \text{Diagram 6} \\ \text{Diagram 7} \\ \text{Diagram 8} \\ \text{Diagram 9} \\ \text{Diagram 10} \\ \text{Diagram 11} \\ \text{Diagram 12} \end{array} \right] \end{aligned}$$

Here, each diagram represents a product of pseudo-first-order rate constants over a spanning tree that is rooted in the (circled) vertex associated with the species we want to solve for (left-hand side). Thus, the concentrations are sums of twelve diagrams each, normalized by a denominator N_E that equals the sum of all the 60 diagrams given above.

A.2. Steady-state concentrations for the active transporter

The active membrane transporter example in the main text, when open, is represented by the graph in figure 5. This graph has six vertices and seven edges. It contains three distinct circuits and 15 different spanning trees.

A visual representation of Kirchhoff's formula (A2) for its steady-state concentrations is given by the following diagrams:

$$\begin{aligned} \frac{[M^-]}{L_M} &= \frac{1}{N_M} \left[\begin{array}{c} \text{Diagram 1} \\ \text{Diagram 2} \\ \vdots \\ \text{Diagram 15} \end{array} \right] \\ \frac{[HM]}{L_M} &= \frac{1}{N_M} \left[\begin{array}{c} \text{Diagram 1} \\ \text{Diagram 2} \\ \vdots \\ \text{Diagram 15} \end{array} \right] \\ \frac{[HMS]}{L_M} &= \frac{1}{N_M} \left[\begin{array}{c} \text{Diagram 1} \\ \text{Diagram 2} \\ \vdots \\ \text{Diagram 15} \end{array} \right] \\ \frac{[M^-]}{L_M} &= \frac{1}{N_M} \left[\begin{array}{c} \text{Diagram 1} \\ \text{Diagram 2} \\ \vdots \\ \text{Diagram 15} \end{array} \right] \\ \frac{[MH]}{L_M} &= \frac{1}{N_M} \left[\begin{array}{c} \text{Diagram 1} \\ \text{Diagram 2} \\ \vdots \\ \text{Diagram 15} \end{array} \right] \\ \frac{[PMH]}{L_M} &= \frac{1}{N_M} \left[\begin{array}{c} \text{Diagram 1} \\ \text{Diagram 2} \\ \vdots \\ \text{Diagram 15} \end{array} \right] \end{aligned}$$

Here, each diagram represents a product of pseudo-first-order rate constants over a spanning tree that is rooted in the (circled) vertex associated with the species we want to solve for (left-hand side). Thus, the concentrations are sums of 15 diagrams each, normalized by a denominator N_M that equals the sum of all the 90 diagrams given above.

Appendix B. Kinetic rate laws for the coarse-grained reactions

We now explicitly construct the kinetic rate laws as apparent cycle fluxes. First, we make use of the diagrammatic method to derive the coarse-grained kinetic rate laws for the two example systems of the main text. Then we generalize these examples to generic catalysts.

B.1. Kinetic rate laws for the enzymatic catalysis

As shown in the main text, the cycle currents are

$$J_{\text{int}} = -J_2 = k_{-2}[\text{ES}_2] - k_2[\text{E}][\text{S}_2], \quad J_{\text{ext}} = J_6 = k_6[\text{EP}] - k_{-6}[\text{E}][\text{P}].$$

Plugging in the diagrams (appendix A.1) for the steady-state concentrations of the enzyme-containing species we arrive at

$$\begin{aligned} \frac{N_E}{L_E} J_{\text{int}} &= k_{-2} \left[\begin{array}{c} \text{Diagram 1} \\ \text{Diagram 2} \\ \vdots \\ \text{Diagram 15} \end{array} \right] - k_2[\text{S}_2] \left[\begin{array}{c} \text{Diagram 1} \\ \text{Diagram 2} \\ \vdots \\ \text{Diagram 15} \end{array} \right], \\ \frac{N_E}{L_E} J_{\text{ext}} &= k_6 \left[\begin{array}{c} \text{Diagram 1} \\ \text{Diagram 2} \\ \vdots \\ \text{Diagram 15} \end{array} \right] - k_{-6}[\text{P}] \left[\begin{array}{c} \text{Diagram 1} \\ \text{Diagram 2} \\ \vdots \\ \text{Diagram 15} \end{array} \right]. \end{aligned}$$

Next, we multiply the remaining pseudo-first-order rate constants into the diagrams and highlight them in blue. This leads us to

$$\begin{aligned} \frac{N_E}{L_E} J_{\text{int}} &= \left[\begin{array}{c} \text{Diagram 1} \\ \text{Diagram 2} \\ \vdots \\ \text{Diagram 15} \end{array} \right] - \left[\begin{array}{c} \text{Diagram 1} \\ \text{Diagram 2} \\ \vdots \\ \text{Diagram 15} \end{array} \right], \\ \frac{N_E}{L_E} J_{\text{ext}} &= \left[\begin{array}{c} \text{Diagram 1} \\ \text{Diagram 2} \\ \vdots \\ \text{Diagram 15} \end{array} \right] - \left[\begin{array}{c} \text{Diagram 1} \\ \text{Diagram 2} \\ \vdots \\ \text{Diagram 15} \end{array} \right]. \end{aligned}$$

Note how some of the diagrams did not contain that edge before, leading to a circuit in the new diagrams. The new pseudo-first-order rate constant carries an arrowhead to highlight the orientation of that edge. The black edges remain oriented along the other black edges towards the circled vertex. The remaining diagrams already contained the reverse pseudo-first-order rate constant for the newly incorporated edge. The product of these forward and backward pseudo-first-order rate constants is highlighted as a dashed blue edge without arrowhead. The latter tree diagrams appear on both sides of the minus signs and can be canceled. Thus the currents are

$$\begin{aligned} \frac{N_E}{L_E} J_{\text{int}} &= \left[\begin{array}{c} \text{Diagram 1} \\ \text{Diagram 2} \\ \vdots \\ \text{Diagram 15} \end{array} \right] - \left[\begin{array}{c} \text{Diagram 1} \\ \text{Diagram 2} \\ \vdots \\ \text{Diagram 15} \end{array} \right], \\ \frac{N_E}{L_E} J_{\text{ext}} &= \left[\begin{array}{c} \text{Diagram 1} \\ \text{Diagram 2} \\ \vdots \\ \text{Diagram 15} \end{array} \right] - \left[\begin{array}{c} \text{Diagram 1} \\ \text{Diagram 2} \\ \vdots \\ \text{Diagram 15} \end{array} \right]. \end{aligned}$$

Here, we highlight the entire circuits in blue to emphasize the common factors in the remaining terms. Note that the square representing the internal cycle remained in the internal cycle current on both sides of the minus sign. However, Wegscheider's conditions, equation (2), ensure that these terms cancel as well. Furthermore, Wegscheider's conditions allow us to express the diagrams containing the lower triangle with the upper triangle:

$$\text{Diagram 1} = \text{Diagram 2} \times \frac{\text{Diagram 3}}{\text{Diagram 4}} = \text{Diagram 5} \times \frac{k_{-2}k_{-3}}{k_{-1}k_{-4}}, \quad \text{Diagram 6} = \text{Diagram 7} \times \frac{\text{Diagram 8}}{\text{Diagram 9}} = \text{Diagram 10} \times \frac{k_2k_3}{k_1k_4}.$$

Overall, the currents expressed with rate constants and concentrations are

$$J_{\text{int}} = \frac{L_E k_2 k_3}{N_E k_1} \left(\frac{k_{-1}}{k_4} + [S_2] \right) (k_{-1} k_{-4} k_{-5} k_{-6} [P] - k_1 k_4 k_5 k_6 [S_1] [S_2]),$$

$$J_{\text{ext}} = \frac{L_E}{N_E} \left(k_3 [S_1] + \frac{k_2 k_3 [S_2]}{k_1} + k_{-2} + \frac{k_{-2} k_{-3}}{k_{-4}} \right) (k_1 k_4 k_5 k_6 [S_1] [S_2] - k_{-1} k_{-4} k_{-5} k_{-6} [P]).$$

B.2. Kinetic rate laws for the active transporter

We proceed analogously to the previous calculation for the enzymatic catalysis: plug the tree diagrams from appendix A.2 into

$$J_{\text{cat}} = J_2 = k_2 [S] [HM] - k_{-2} [HMS],$$

$$J_{\text{sl}} = -J_1 = k_{-1} [HM] - k_1 [H_a^+] [M],$$

and cancel all diagrams that do not contain a circuit. This leads us to

$$\frac{N_M}{L_M} J_{\text{cat}} = \left[\text{Diagram 11} \right] - \left[\text{Diagram 12} \right],$$

$$\frac{N_M}{L_M} J_{\text{sl}} = \left[\text{Diagram 13} \right] - \left[\text{Diagram 14} \right].$$

Since this membrane transporter mechanism does not have an internal cycle, we cannot exploit Wegscheider's conditions to cancel more terms. Nonetheless, we see that we can factor the circuits out of some of the terms.

Overall, we arrive at the cycle currents

$$J_{\text{cat}} =: \psi_{\text{cat}}^+ - \psi_{\text{cat}}^-, \quad J_{\text{sl}} =: \psi_{\text{sl}}^+ - \psi_{\text{sl}}^-.$$

with the fluxes

$$\frac{N_M}{L_M} \psi_{\text{cat}}^+ = k_1 k_2 k_3 k_4 k_5 k_6 [H_a^+] [S] + \xi_{\text{cat}} k_{-7} k_2 k_3 k_4 [S],$$

$$\frac{N_M}{L_M} \psi_{\text{cat}}^- = k_{-1} k_{-2} k_{-3} k_{-4} k_{-5} k_{-6} [H_b^+] [P] + \xi_{\text{cat}} k_7 k_{-2} k_{-3} k_{-4} [P],$$

$$\frac{N_M}{L_M} \psi_{\text{sl}}^+ = k_{-1} k_{-2} k_{-3} k_{-4} k_{-5} k_{-6} [H_b^+] [P] + \xi_{\text{sl}} k_{-1} k_{-5} k_{-6} k_{-7} [H_b^+],$$

$$\frac{N_M}{L_M} \psi_{\text{sl}}^- = k_1 k_2 k_3 k_4 k_5 k_6 [H_a^+] [S] + \xi_{\text{sl}} k_1 k_5 k_6 k_7 [H_a^+],$$

where we used the abbreviations

$$\xi_{\text{cat}} := k_{-6} k_{-5} [H_b^+] + k_1 k_{-5} [H_a^+] [H_b^+] + k_6 k_1 [H_a^+], \quad \xi_{\text{sl}} := k_3 k_4 + k_{-2} k_4 + k_{-3} k_{-2}.$$

B.3. Kinetic rate laws for generic catalysts

By making use of the graph theory notation introduced in appendix A, we can generalize the above calculations to generic catalysts.

Before proceeding with calculations, we need a general method to determine the cycle currents from individual reaction currents. To that end, we construct a special spanning tree τ^* for the graph \mathcal{G} of the open system: (1) we start with the *closed* system and determine its internal cycles $\text{ker } \mathbb{S}$. We take the set $\mathcal{I} \subset \mathcal{R}$ of edges that the internal cycles are supported on. (2) Consider this set of edges $\mathcal{I} \subset \mathcal{G}$ as a subgraph of the *open* network. Choose a spanning tree $\tau_{\mathcal{I}}$ for this subgraph. (3) Complete $\tau_{\mathcal{I}}$ to a spanning tree τ^* of \mathcal{G} . All the edges not contained in the spanning tree are the *chords*.

There is a special connection between chords and circuits first highlighted by Schnakenberg [57]: the spanning tree alone, by definition, does not contain any circuit. Adding a chord to the spanning tree gives rise to a circuit composed of the chord together with edges from the spanning tree. Furthermore, by construction every chord gives rise to a *different* circuit and the set of these circuits form a basis of the cycle space $\text{ker } \mathbb{S}^X$. In this

context the circuits associated to chords are also called *fundamental cycles*. The currents on the chords then are identical to the steady-state currents along the fundamental cycles of the chords [57].

The special spanning tree τ^* that we constructed is separating the chords into two sets: each chord in \mathcal{I} gives rise to an *internal cycle*, while the chords not in \mathcal{I} give rise to the emergent cycles. This construction provides a basis for the entire cycle space, yet keeps the internal cycles and the emergent cycles separated. Therefore we call it a *separating spanning tree*.

It is worth noting that not every basis of circuits can be expressed as fundamental cycles of a spanning tree. This technical detail, however, has no impact on our results. Different bases are just different representations of the same space. In the following we assume a spanning tree mainly for convenience.

Let $j \rightarrow i$ be the chord of an emergent cycle. Then the current through that chord is

$$J_{ij} = \tilde{k}_{ij}(\mathbf{y})x_j - \tilde{k}_{ji}(\mathbf{y})x_i = \frac{L}{N(\mathbf{y})} \left[\tilde{k}_{ij}(\mathbf{y}) \sum_{\tau \in \mathcal{T}_j} \prod_{\rho \in \tau} \tilde{k}_\rho(\mathbf{y}) - \tilde{k}_{ji}(\mathbf{y}) \sum_{\tau \in \mathcal{T}_i} \prod_{\rho \in \tau} \tilde{k}_\rho(\mathbf{y}) \right].$$

Next, we note that a lot of terms cancel by taking this difference. All the spanning trees that contain the edge $i \rightarrow j$ or $j \rightarrow i$, respectively, appear with both plus and minus sign:

$$\begin{aligned} J_{ij} &= \frac{L}{N(\mathbf{y})} \underbrace{\left[\tilde{k}_{ij}(\mathbf{y}) \sum_{\substack{\tau \in \mathcal{T}_j \\ i \rightarrow j \in \tau}} \prod_{\rho \in \tau} \tilde{k}_\rho(\mathbf{y}) - \tilde{k}_{ji}(\mathbf{y}) \sum_{\substack{\tau \in \mathcal{T}_i \\ j \rightarrow i \in \tau}} \prod_{\rho \in \tau} \tilde{k}_\rho(\mathbf{y}) \right]}_{=0} \\ &\quad + \frac{L}{N(\mathbf{y})} \left[\tilde{k}_{ij}(\mathbf{y}) \sum_{\substack{\tau \in \mathcal{T}_j \\ i \rightarrow j \notin \tau}} \prod_{\rho \in \tau} \tilde{k}_\rho(\mathbf{y}) - \tilde{k}_{ji}(\mathbf{y}) \sum_{\substack{\tau \in \mathcal{T}_i \\ j \rightarrow i \notin \tau}} \prod_{\rho \in \tau} \tilde{k}_\rho(\mathbf{y}) \right]. \end{aligned}$$

After canceling these spanning tree contributions, we define the *apparent cycle fluxes* as

$$\psi_{ij} := \frac{L}{N(\mathbf{y})} \tilde{k}_{ij}(\mathbf{y}) \sum_{\substack{\tau \in \mathcal{T}_j \\ i \rightarrow j \notin \tau}} \prod_{\rho \in \tau} \tilde{k}_\rho(\mathbf{y}). \quad (\text{B1})$$

We obviously have $J_{ij} = \psi_{ij} - \psi_{ji}$. Thus the apparent cycle fluxes serve as kinetic rate laws for the coarse-grained reactions.

There is, technically speaking, no strict necessity to cancel the spanning tree contributions in order to arrive at expressions that can serve as coarse-grained kinetic rate laws. Keeping the spanning tree contributions results in the apparent fluxes of the substrates/products that are being produced/consumed along the chord. This is a natural choice for dealing with data from isotope labeling experiments. With this definition for kinetic rate laws, however, the flux–force relation is not satisfied—even in the case of a single emergent cycle [34]. In contrast, our definition of apparent fluxes resembles the apparent *cycle fluxes*, rather than apparent exchange fluxes. Comparing the apparent cycle fluxes with the net force along the emergent cycle, we do have a flux–force relation, as shown in the next section.

Appendix C. Proof of the flux–force relation

Before we prove the flux–force relation, we rewrite the apparent fluxes for the emergent cycles derived in equation (B1). This simplifies the final proof considerably. To that end, we observe that adding a chord to a spanning tree not containing this chord always creates a circuit. Since in equation (B1) we sum over all possible spanning trees, the same circuits re-appear in several summands. We now re-sort the sums to first run over distinct circuits, and then sum over the remainders of the spanning trees. For that we need some notation.

For any circuit c we abbreviate the product of pseudo-first-order rate constants along it as $w(c) = \prod_{\rho \in c} \tilde{k}_\rho(\mathbf{y})$. The net force along a circuit thus is concisely written as

$$-\Delta_c G = RT \sum_{\rho \in c} \ln \frac{\tilde{k}_\rho(\mathbf{y})}{\tilde{k}_{-c}(\mathbf{y})} = RT \ln \frac{w(c)}{w(-c)}. \quad (\text{C1})$$

Here, $-c$ refers to traversing the circuit c with reversed orientation. For any circuit, c , we furthermore define $\mathcal{F}(c)$ to be the set of subforests of \mathcal{G} that (i) do not contain any edge of c , (ii) span the rest of the graph, and (iii) are directed towards the circuit c . Analogously to the product of rate constants along a circuit, for this set of subforests we denote the sum of products of rate constants as

$$\xi(c) := \sum_{f \in \mathcal{F}(c)} \prod_{\rho \in f} \tilde{k}_\rho(\mathbf{y}).$$

By construction, $\xi(c) = \xi(-c)$ since the set $\mathcal{F}(c)$ does not depend on the orientation of c . Let \mathcal{C}_{ij} be the set of circuits traversing the edge $j \rightarrow i$. Note that these circuits are exactly the ones appearing in equation (B1).

With this notation we rewrite the apparent cycle fluxes in the following way:

$$\psi_{ij} = \frac{L}{N(\mathbf{y})} \sum_{c \in \mathcal{C}_{ij}} w(c) \xi(c).$$

This rewriting is not limited to the case of a single emergent cycle. In fact, we used this form to express the apparent cycle fluxes of the active membrane transporter in appendix B.2.

We now prove the flux–force relation—under the assumption that there is exactly one emergent cycle c_η with chord $\eta = j \rightarrow i$. Let $-\Delta_\eta G$ be the net force along this cycle and let J_η be its current at steady state. Let furthermore τ^* be a separating spanning tree, as we defined in appendix B.3.

Having only one emergent cycle means that for every circuit $c \in \mathcal{C}_{ij}$ we have one of the following cases:

- The circuit is formed by following the separating spanning tree from vertex i back to j , in which case it is exactly the emergent cycle: $c = c_\eta$.
- The circuit is formed by traversing more chords, in which case it can be written as $c = c_\eta + \gamma$ where $\gamma \in \ker \mathbb{S}$ is an internal cycle. In this case we have $\frac{w(c)}{w(-c)} = \frac{w(\gamma)}{w(-\gamma)} \frac{w(c_\eta)}{w(-c_\eta)} = \frac{w(c_\eta)}{w(-c_\eta)}$ due to Wegscheider's conditions.

In any case we can write $w(\pm c) = \zeta(c)w(\pm c_\eta)$ where $\zeta(c) = \zeta(-c)$ is a symmetric factor. Overall, the apparent fluxes for the emergent cycle are

$$\psi_{ij} = \frac{L}{N(\mathbf{y})} \sum_{c \in \mathcal{C}_{ij}} w(c) \xi(c) = \frac{L}{N(\mathbf{y})} \left[\sum_{c \in \mathcal{C}_{ij}} \xi(c) \zeta(c) \right] w(c_\eta).$$

By construction, ξ and ζ are symmetric and also any sum over these terms is symmetric. Consequently, the apparent forward and backward fluxes of the emergent cycle satisfy

$$\frac{\psi_{ij}}{\psi_{ji}} = \frac{\frac{L}{N(\mathbf{y})} \left[\sum_{c \in \mathcal{C}_{ij}} \xi(c) \zeta(c) \right] w(c_\eta)}{\frac{L}{N(\mathbf{y})} \left[\sum_{c \in \mathcal{C}_{ji}} \xi(-c) \zeta(-c) \right] w(-c_\eta)} = \frac{w(c_\eta)}{w(-c_\eta)}$$

which, together with equation (C1), concludes the proof.

From this proof it is evident, why the flux–force relation breaks down once there are several emergent cycles with nonzero forces: in the case where a circuit $c \in \mathcal{C}_{ij}$ is not identical to the emergent cycle c_η , we can still write it as $c = c_\eta + \gamma$. However, now γ need not be an internal but might be another emergent cycle. Therefore, Wegscheider's condition does not apply to it, thus $w(\gamma)$ and hence $\zeta(c)$ need not be symmetric. As a consequence, the ratio of apparent forward and backward cycle fluxes cannot be expressed by the force of the emergent cycle $-\Delta_\eta G$ alone.

The proof also shows why the choice of a separating spanning tree is mainly for convenience. In the case of a single emergent cycle, the exact basis for the internal cycles does not matter and you can always find an appropriate separating spanning tree. In the case of several emergent cycles, there is no simple and direct relation between the force and the fluxes of a cycle. The only consistency requirement is the EPR. However, the EPR is a scalar and thus invariant under change of basis. Furthermore, it involves only the forces and the currents of the cycles. This imposes no restrictions on the individual forward and backward fluxes.

ORCID iDs

Artur Wachtel  <https://orcid.org/0000-0002-6194-6938>

Riccardo Rao  <https://orcid.org/0000-0003-0040-6783>

Massimiliano Esposito  <https://orcid.org/0000-0002-2249-4035>

References

- [1] Cornish-Bowden A 2013 *FEBS Lett.* **587** 2725
- [2] Brown AJ 1902 *J. Chem. Soc. Trans.* **81** 373
- [3] Henri V 1902 *C. R. Hebd. Acad. Sci.* **135** 916
- [4] Michaelis L and Menten M L 1913 *Biochem. Z.* **49** 333

- [5] Cornish-Bowden A 2012 *Fundamentals of Enzyme Kinetics* 4th edn (Weinheim: Wiley-VCH)
- [6] Puglisi A, Pigolotti S, Rondoni L and Vulpiani A 2010 *J. Stat. Mech.* **P05015**
- [7] Callen H B 1985 *Thermodynamics and an Introduction to Thermostatistics* 2nd edn (New York: Wiley)
- [8] Seifert U 2012 *Rep. Prog. Phys.* **75** 126001
- [9] Van den Broeck C and Esposito M 2015 *Proc. 13th Int. Summer School on Fundamental Problems in Statistical Physics; Physica A* **418** 6
- [10] Jülicher F, Ajdari A and Prost J 1997 *Rev. Mod. Phys.* **69** 1269
- [11] Seifert U 2011 *Eur. Phys. J. E* **34** 26
- [12] Altaner B, Wachtel A and Vollmer J 2015 *Phys. Rev. E* **92** 042133
- [13] Astumian R D, Mukherjee S and Warshel A 2016 *ChemPhysChem* **17** 1719
- [14] Murugan A, Huse D H and Leibler S 2012 *Proc. Natl Acad. Sci. USA* **109** 12034
- [15] Rao R and Peliti L 2015 *J. Stat. Mech.* **P06001**
- [16] Sartori P and Pigolotti S 2015 *Phys. Rev. X* **5** 041039
- [17] Barato A C, Hartich D and Seifert U 2014 *New J. Phys.* **16** 103024
- [18] Bo S and Celani A 2016 *J. Stat. Phys.* **162** 1365
- [19] Ouldridge T E, Govern C C and ten Wolde P R 2017 *Phys. Rev. X* **7** 021004
- [20] Esposito M 2012 *Phys. Rev. E* **85** 041125
- [21] Altaner B and Vollmer J 2012 *Phys. Rev. Lett.* **108** 228101
- [22] Knoch F and Speck T 2015 *New J. Phys.* **17** 115004
- [23] Esposito M and Parrondo J M R 2015 *Phys. Rev. E* **91** 052114
- [24] Bo S and Celani A 2017 *Phys. Rep.* **670** 1
- [25] Segel L A and Slemrod M 1989 *SIAM Rev.* **31** 446
- [26] Gunawardena J 2014 *FEBS J.* **281** 473
- [27] Rubin K J, Lawler K, Sollich P and Ng T 2014 *J. Theor. Biol.* **357** 245
- [28] Polettini M and Esposito M 2014 *J. Chem. Phys.* **141** 024117
- [29] Rao R and Esposito M 2016 *Phys. Rev. X* **6** 041064
- [30] Beard D A, dan Liang S and Qian H 2002 *Biophys. J.* **83** 79
- [31] Fleming R, Thiele I, Provan G and Nasheuer H 2010 *J. Theor. Biol.* **264** 683
- [32] Soh K C and Hatzimanikatis V 2010 *Curr. Opin. Microbiol.* **13** 350
- [33] Beard D A and Qian H 2007 *PLoS One* **2** 1
- [34] Wiechert W 2007 *Biophys. J.* **93** 2255
- [35] Noor E, Flamholz A, Liebermeister W, Bar-Even A and Milo R 2013 *FEBS Lett.* **587** 2772
- [36] Liepelt S and Lipowsky R 2007 *Phys. Rev. Lett.* **98** 258102
- [37] Pietrobon D and Caplan S R 1985 *Biochemistry* **24** 5764
- [38] Alberts R A 2003 *Thermodynamics of Biochemical Reactions* (New York: Wiley)
- [39] Kondepudi D and Prigogine I 2015 *Modern Thermodynamics: From Heat Engines to Dissipative Structures* 2nd edn (New York: Wiley)
- [40] de Groot S and Mazur P 1984 *Non-equilibrium Thermodynamics*, Dover Books on Physics Series (New York: Dover)
- [41] Flamholz A, Noor E, Bar-Even A, Liebermeister W and Milo R 2013 *Proc. Natl Acad. Sci. USA* **110** 10039
- [42] Noor E, Bar-Even A, Flamholz A, Reznik E, Liebermeister W and Milo R 2014 *PLoS Comput. Biol.* **10** 1
- [43] Henry C S, Broadbelt L J and Hatzimanikatis V 2007 *Biophys. J.* **92** 1792
- [44] Orth J D, Thiele I and Palsson B Ø 2010 *Nat. Biotechnol.* **28** 245
- [45] Chakrabarti A, Miskovic L, Soh K C and Hatzimanikatis V 2013 *Biotechnol. J.* **8** 1043
- [46] Schuster S and Schuster R 1989 *J. Math. Chem.* **3** 25
- [47] Polettini M, Wachtel A and Esposito M 2015 *J. Chem. Phys.* **143** 184103
- [48] King E L and Altman C 1956 *J. Phys. Chem.* **60** 1375
- [49] Hill T L 1977 *Free Energy Transduction in Biology: The Steady-State Kinetic and Thermodynamic Formalism* (New York: Academic)
- [50] Tutte W 2001 *Graph Theory (Cambridge Mathematical Library)* (Cambridge: Cambridge University Press)
- [51] Lee C H and Othmer H G 2009 *J. Math. Biol.* **60** 387
- [52] Thomas P, Grima R and Straube A V 2012 *Phys. Rev. E* **86** 041110
- [53] Rubin K J and Sollich P 2016 *J. Chem. Phys.* **144** 174114
- [54] Hill T L 1966 *J. Theor. Biol.* **10** 442
- [55] Kirchhoff G 1847 *Ann. Phys., NY* **148** 497
- [56] Knauer U 2011 *Algebraic Graph Theory: Morphisms, Monoids and Matrices De Gruyter Studies in Mathematics* (Berlin: de Gruyter & Co)
- [57] Schnakenberg J 1976 *Rev. Mod. Phys.* **48** 571

CONCLUSIONS

Starting from a phenomenological description of nonequilibrium thermodynamics, we introduced a systematic way of determining broken conservation laws, Sec. 1.5.1. These laws identify conserved quantities whose changes in the systems are always matched by an opposite change in the environment, Eq. (52). In this way, these quantities carry the information about the way the system *globally* exchanges system quantities with the reservoirs. By combining the balance equations of broken conserved quantities with the laws of thermodynamics, we find that energy and entropy balance can be decomposed in terms of three fundamental types of energetic and dissipative contributions, Secs. 1.5 and 3.3: those due to external driving, which vanish in processes which are not manipulated; those due to nonconservative forces created by the coupling with multiple reservoirs, which are responsible for sustaining currents of system quantities across the system; and those conservative contributions which account for overall changes of system quantities within the systems, and which characterize the relaxation to equilibrium states.

Our phenomenological description is generic, yet it formally accounts for features that are specific for any system. In this way, it can be applied to any process, regardless of its dynamics. We specialized it to Markov jump processes and chemical reaction networks, Sec. 2 and Part ii. Regarding the former, conservation laws enabled us to provide the first complete thermodynamic description. But the importance of our formulation is not only theoretical. On a practical level, it provides a systematic procedure to analyse the thermodynamics of specific systems. For a large variety of these, we demonstrated how easy the identification of their dissipative mechanisms is, Sec. [6, p. 51].

Regarding chemical reaction networks we established a rigorous thermodynamic description for different types of dynamics: chemical master equation, which describes the evolution in time of the probability distributions of molecules numbers, Eqs. (119) and [(11), p. 113]; rate equations, which describe concentrations, Eqs. (87), (89), and [(9) and (10), p. 148]; and reaction-diffusion equations for space-inhomogeneous concentration distributions, Eqs. (126) and [(1), p. 185]. For the last two types of dynamics, our approach is inspired by stochastic thermodynamics, as we build the thermodynamics on top of the dynamics. Conservation laws, thus enabled us to identify the thermodynamic potentials which are minimized at equilibrium, and to establish the connection with the potentials identified by mathematicians in the context of chemical reaction network theory.

We also introduced a formulation of the nonequilibrium Landauer principle that is valid for arbitrary isothermal processes, Sec. 1.6. This principle relates the minimal thermodynamic cost of transforming a given system from two arbitrary nonequilibrium states, to their distance from equilibrium. Its early formulation for mechanically driven processes, Ref. [1, 2], played a major role for the formulation of *thermodynamics of information* [3]. Indeed, since information processing is physical and can be regarded as the transformation of nonequilibrium states, this principle allows to quantify the minimal cost of this processing, *i.e.* the minimal cost of computation. Importantly, this principle also proved useful for assessing the cost of information pro-

cessing in simple biochemical mechanisms, like copolymerization processes inspired by DNA replication and RNA transcription [4, 5]. The formulation that we derived generalizes these earlier ones in two regards. First, it is formulated for arbitrary isothermal systems—not just mechanically driven ones—and in particular for systems prevented from reaching equilibrium due to nonconservative forces. Second, our formulation is valid for arbitrary dynamics—not just stochastic ones—and in particular for chemical reaction networks described by rate equation and reaction-diffusion equations. For each of these types of dynamics the generalized relative entropy introduced in Eq. (72) assumes a specific form (Eqs. (83), (125), and (128)), but all these forms share the same properties. In this respect, we find fascinating how thermodynamics imposes a clear theoretical structure which assumes different forms depending on the class of processes to which it is applied. Our generalized nonequilibrium Landauer principle can hence be used to analyse biochemical information-handling systems whose complexity goes beyond simple mechanisms. This endeavour is important in the light of the current understanding that biological systems have developed by optimizing the gathering and representation of information [6, 7].

In the context of chemical reaction networks, our description lays the foundations for thermodynamic analysis of metabolic networks. Metabolisms is indeed the core thermodynamic process of living organism, which allows them to manage the energy required for their functioning. Quantifying the thermodynamic performance of these process is therefore important as it might reveal crucial features of these organisms.

REFERENCES

- [1] K. TAKARA, H.-H. HASEGAWA and D. DRIEBE, “Generalization of the second law for a transition between nonequilibrium states”, *Phys. Lett. A* **375**.2 (2010), 88–92.
- [2] M. ESPOSITO and C. VAN DEN BROECK, “Second law and Landauer principle far from equilibrium”, *Europhys. Lett.* **95**.4 (2011), 40004.
- [3] J. M. R. PARRONDO, J. M. HOROWITZ and T. SAGAWA, “Thermodynamics of information”, *Nature Phys.* **11**. (2015), 131–139.
- [4] P. SARTORI and S. PIGOLOTTI, “Thermodynamics of Error Correction”, *Phys. Rev. X* **5**.4 (2015), 041039.
- [5] T. E. OULDIDGE and P. R. ten WOLDE, “Fundamental Costs in the Production and Destruction of Persistent Polymer Copies”, *Phys. Rev. Lett.* **118**.15 (2017), 158103.
- [6] W. BIALEK, *Biophysics: Searching for Principles*, Princeton University Press, 2012.
- [7] G. TKAČIK and W. BIALEK, “Information Processing in Living Systems”, *Annu. Rev. Condens. Matter Phys.* **7**.1 (2016), 1.

AUTHOR CONTRIBUTIONS

All articles presented in my thesis are the outcome of my research activity within the group of M. Esposito at the University of Luxembourg.

The project on dynamics of glucans, resulting in Ref. [1], originated from a collaboration between M. Esposito and D. Lacoste. When I started my PhD, I took the lead of the project: Guided by M. Esposito, I performed all calculations, the numerical simulations, and wrote the paper. While working on it, I realized that a rigorous and complete thermodynamic description of chemical reaction networks was lacking. This initiated the project on thermodynamics of chemical reaction networks, which resulted in Ref. [2]. Under the constant supervision of M. Esposito, I developed the mathematical formulation, performed all calculations, and wrote the paper.

Afterwards, M. Esposito suggested to connect the results of Ref. [2] with previously derived fluctuation theorems. I thus worked on conservation laws in stochastic thermodynamics of both generic Markov jump processes and stochastic chemical reaction networks, Refs. [3, 4]. For these works, I contributed to designing the research, I performed all calculations and wrote the papers with the help of M. Esposito.

At the same time, the need for a thermodynamic description applicable to chemical reaction networks with enzymatic reactions triggered the project leading to Ref. [5]. The key result of this work was conceived together with A. Wachtel. I then followed the development of the project at all its subsequent stages.

The paper on thermodynamics of reaction-diffusion systems, Ref. [6], arose from the interest of extending the results of Ref. [2] to space-inhomogeneous chemical processes. I developed the main theory, performed the related calculations, and discussed its application to the Brusselator model with G. Falasco, who performed the analysis.

Finally, several discussions with M. Esposito lead him to conceive a unifying perspective on a class of fluctuation relations, Ref. [7]. For this work, I developed the mathematical formulations, the performed all calculations, and wrote the paper, benefiting of M. Esposito support and guidance.

PUBLICATIONS

- [1] R. RAO, D. LACOSTE and M. ESPOSITO, “Glucans monomer-exchange dynamics as an open chemical network”, *J. Chem. Phys.* **143**.24 (2015), 244903.
- [2] R. RAO and M. ESPOSITO, “Nonequilibrium Thermodynamics of Chemical Reaction Networks: Wisdom from Stochastic Thermodynamics”, *Phys. Rev. X* **6**.4 (2016), 041064.
- [3] R. RAO and M. ESPOSITO, “Conservation laws shape dissipation”, *New J. Phys.* **20**.2 (2018), 023007.
- [4] R. RAO and M. ESPOSITO, “Conservation Laws and Work Fluctuation Relations in Chemical Reaction Networks” (arXiv 1805.12077).

- [5] A. WACHTEL, R. RAO and M. ESPOSITO, “Thermodynamically Consistent Coarse Graining of Biocatalysts beyond Michaelis–Menten”, *New J. Phys.* **20**.4 (2018), 042002.
- [6] G. FALASCO, R. RAO and M. ESPOSITO, “Information Thermodynamics of Turing Patterns”, *Phys. Rev. Lett.* **121**.10 (2018), 108301.
- [7] R. RAO and M. ESPOSITO, “Detailed Fluctuation Theorems: A Unifying Perspective”, *Entropy* **20**.9 (2018), 635.

ACKNOWLEDGEMENTS

I am extremely grateful to Massimiliano Esposito, for his tireless support, unlimited patience, and for raising me as a researcher during the four years of my PhD. I felt enthusiastic of working with him, and I feel privileged for having been his student. I am especially thankful for the very exciting and friendly working environment he contributed to create. In this respect, I am also grateful to my group members (*tFoLSoT*), and long-term visitors of our group: Kamran Shayanfar, Gregory Bulnes Cuetara, Alexandre Lazarescu, Bernard Altaner, Tim Herpich, Juzar Thingna, Philipp Strasberg, Tommaso Cossetto, Samuel Jacob, Danilo Forastiere, Emanuele Penocchio, Matteo Polettini, Gianmaria Falasco, Artur Wachtel, Yûto Murashita, Shiqi Sheng, Francesco Avanzini, Jean-Charles Delvenne, and John Bechhoefer, who were a constant and diversified source of inspiration. Special respect is due to Artur, whose unbelievably broad knowledge and wisdom *converted* me to *The Right Thing*™ in many circumstances.

I am also thankful to Frédérique Bertrand, and Yoanna Koleva, who helped me to deal with the most difficult part of my PhD: bureaucracy. I thank the *FNR* for financing my PhD. I am grateful to Luca Peliti—without whom my adventure would have not taken place—and Alexander Skupin for their encouragement and support, and Biagio Buonaura, for providing me with important bibliographic resources.

I thank the external members of my dissertation defence committee, Pierre Gaspard and Thomas Ouldridge, for carefully reading my thesis, and for their valuable feedback and constructive comments.

I express my gratitude for the many people who enriched my stay in Luxembourg, in particular Martine, Petra, Jonathon, Ricardo, Winnie, and Joëlle. I thank my best friends, Davide, Claudio, GianMarco, and Carlo, whose friendship survived despite the time and the distance. I thank my parents and brothers for their everlasting and unconditioned support. And finally, I thank Annarita—to whom this work is dedicated—for her love, for holding my hand tight everyday, despite the distance, and ... for patiently bearing my wild commitment to work.

Luxembourg, 23rd October 2018

Riccardo Rao

FUNDING

This work was funded by *Luxembourg National Research Fund: AFR PhD Grant 2014-2*, No. 9114110.